

21st International
Symposium on

Rarefied Gas
Dynamics

Marseille (France)
26-31 July 1998



Book of Abstracts Volume I

Oral Sessions

DISTRIBUTION STATEMENT A

Approved for public release;
Distribution Unlimited

19990115 047

AQ F99-04-0639

REPORT DOCUMENTATION PAGE

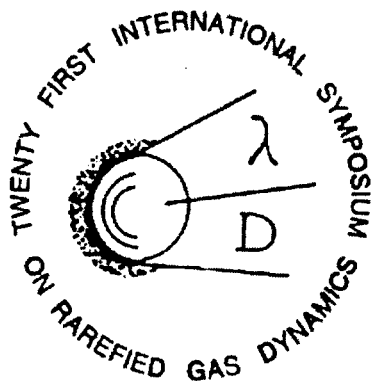
Form Approved OMB No. 0704-0188

Public reporting burden for this collection of information is estimated to average 1 hour per response, including the time for reviewing instructions, searching existing data sources, gathering and maintaining the data needed, and completing and reviewing the collection of information. Send comments regarding this burden estimate or any other aspect of this collection of information, including suggestions for reducing this burden to Washington Headquarters Services, Directorate for Information Operations and Reports, 1215 Jefferson Davis Highway, Suite 1204, Arlington, VA 22202-4302, and to the Office of Management and Budget, Paperwork Reduction Project (0704-0188), Washington, DC 20503.

1. AGENCY USE ONLY (Leave blank)		2. REPORT DATE 30 July 1998		3. REPORT TYPE AND DATES COVERED Conference Proceedings	
4. TITLE AND SUBTITLE 21st International Symposium on Rarefied Gas Dynamics , Vol 1				5. FUNDING NUMBERS F6170898W0021	
6. AUTHOR(S) Conference Committee					
7. PERFORMING ORGANIZATION NAME(S) AND ADDRESS(ES) I.U.S.T.I. Technopole de Chateau-Gombert; 5 Rue Enrico Fermi Marseille 13453 France				8. PERFORMING ORGANIZATION REPORT NUMBER N/A	
9. SPONSORING/MONITORING AGENCY NAME(S) AND ADDRESS(ES) EOARD PSC 802 BOX 14 FPO 09499-0200				10. SPONSORING/MONITORING AGENCY REPORT NUMBER CSP 98-1024	
11. SUPPLEMENTARY NOTES 3 Volumes - Oral sessions, Poster sessions, and Special Session					
12a. DISTRIBUTION/AVAILABILITY STATEMENT Approved for public release; distribution is unlimited.				12b. DISTRIBUTION CODE A	
13. ABSTRACT (Maximum 200 words) The Final Proceedings for 21st International Symposium on Rarefied Gas Dynamics, 26 July 1998 - 31 July 1998 This is an interdisciplinary conference. Topics include Boltzman equation and kinetic theory; Mathematical methods and models; Flow in transitional and rarefied regimes; Numerical simulations of RGD flows; Instrumentation and diagnostics in RGD flows; Free jets and molecular beams; Elementary collisional processes; Transport and relaxation phenomena; Chemical processes; Shock waves; Low density plasmas and ionized gases; Gas-surface interactions; Molecular beams; Clusters; Aerosols; Phase change; Aerodynamics and aerothermochemistry of space vehicles; Industrial applications I (vacuum technology, thin film, microengines...); Industrial applications II (beams, jets, lasers, reactors...); Astrophysics; Environmental aspects.					
14. SUBJECT TERMS EOARD, Rarefied Gas Dynamics, Low Density Plasma				15. NUMBER OF PAGES 875	
				16. PRICE CODE N/A	
17. SECURITY CLASSIFICATION OF REPORT UNCLASSIFIED	18. SECURITY CLASSIFICATION OF THIS PAGE UNCLASSIFIED	19. SECURITY CLASSIFICATION OF ABSTRACT UNCLASSIFIED	20. LIMITATION OF ABSTRACT UL		

NSN 7540-01-280-5500

Standard Form 298 (Rev. 2-89)
Prescribed by ANSI Std. Z39-18
298-102



21st International
Symposium on

Rarefied Gas
Dynamics

Marseille (France)
26-31 July 1998



Book of Abstracts Volume I

Oral Sessions

Invited Lectures

Kinetic Theory and Models (KTM)

Gas-Surface interaction (GS)

Monte Carlo Methodology (MCM)

Industrial Processes (IP)

Ionization and Radiation (IR)

Molecular Properties and Transport (MPT)

Numerical Simulation (NS)

Two-Phase flows (TP)

Rarefied Flows (RF)

Non-Equilibrium Processes (NE)

Aerospace Applications (AA)

Astrophysics and Environment (AE)

INVITED LECTURES

PLENARY LECTURES GRAND AMPHITHÉÂTRE

H. GRAD memorial lecture

Monday, July 27, 1998, 9:00

P.L. LIONS: *Mathematical state of the art for Boltzmann equations*
(abstract not available)

L. THOMAS memorial lecture

Friday, July 31, 1998, 8:30

E.P. MUNTZ: *Surface dominated rarefied flows and the potential of surface nanomanipulation*

Additional plenary lecture

Tuesday, July 28, 1998, 8:30

A. ASPECT: *Laser cooling of Atoms beyond the Limits*, (abstract not available)

ROOM MARION

ROOM PÉRÈS

Monday, July 27, 1998 14:00	S. KAWASHIMA: <i>Survey on the initial-boundary value problems for the discrete Boltzmann equation</i>	R. G. LORD: <i>Modelling of gas-surface interactions and inelastic intermolecular collisions in DSMC calculations</i>
Tuesday, July 28, 1998 14:00	A.V. BOBYLEV: <i>Relationships between continuous and discrete kinetic theories</i>	J.P. BŒUF et al.: <i>Physics and modeling of the stationary plasma thruster</i>
Wednesday, July 29, 1998 8:30	I. WYSONG: <i>Molecular models for reacting flows: should variable collision diameters for internal states be used in DSMC simulations ?</i>	D.S. SCHRAM: <i>Electronic relaxation in free jet expansions, as generated from arcs, RF, or laser heated plasma sources</i>
Thursday, July 30, 1998 8:30	A.E. BEYLICH: <i>Structure and applications of jets</i>	M. CAPITELLI et al.: <i>Non-equilibrium vibrational kinetics and dissociation-recombination processes</i>
Friday, July 31, 1998 14:00	D. GILLET: <i>On the structure of radiative shock waves in stellar atmospheres</i>	R.C. BLANCHARD: <i>Review of entry flight measurements during transition from rarefied flow into the hypersonic continuum (presented by R. WILMOTH)</i>

Surface Dominated Rarefied Flows and the Potential of Surface Nanomanipulations*

E.P. Muntz

University of Southern California, Department of Aerospace Engineering
Los Angeles, California, USA

The typical stay time of nitrogen or oxygen molecules on surfaces at room temperature is around $\tau = 10^{-10}s^{(1)}$. Water molecules will stay about $3 \times 10^{-6}s^{(1)}$. In macroscopic gas driven systems at normal pressures the reservoir of adsorbed molecules statistically stored on the system's surfaces is extremely small compared to the mass of working gas in the system. On the other hand in micron size micromechanical systems the mass stored as 2-D gas on the surfaces can equal the mass of the working 3-D gas because of dramatically increased surface to volume ratios. In this situation it is interesting and entertaining to consider the practical implications of actively manipulating the surface gas to produce work for a range of possible microdevices related purposes. One possibility is the release of the stored mass by rapid surface heating to produce significant surface pressures for brief periods.

The steady state fractional surface coverage by the 2-D gas can be expressed as^(1,3)

$$\Theta = \left[1 + \left(\tau n_g (kT_g / 2\pi m_g)^{1/2} \sigma^0 \right)^{-1} \right]^{-1} \quad (1)$$

The nomenclature is standard with $()_g$ referring to the 3-D gas and σ^0 the area occupied by a molecule on the surface ($16.2 \times 10^{-20} \text{ m}^2$ for N_2). For nitrogen at 300K and 10^5 N/m^2 , $\Theta = (1 + 17.3)^{-1} = 0.055$.

For small coverages eq. (1) is fairly realistic but generally fails as $\Theta \rightarrow 1$, which in this case would happen at higher gas number densities n_g . Note that for a typical macroscopic scale (say $3 \times 10^{-1} \text{ m}$) rarefied gas dynamic experiment n_g might be 10^{-5} atm. and Θ becomes very small ($\Theta = (1 + 17.3 \times 10^5)^{-1}$). For the same Knudsen number a microscale experiment with a characteristic dimension of $3 \times 10^{-6} \text{ m}$ would operate at atmo-

spheric density and a coverage $\Theta = 0.055$. Surfaces frequently have adsorption areas greatly in excess of their projected areas (10^2 and higher is not uncommon^(2,3)). For a surface with 10^2 greater adsorption area the microscale gas dynamic experiment mentioned above would hold a somewhat larger number of molecules on its surface than in the 3-D gas. As is well known by the RGD community the maintenance of a constant Kn in the experiment scaling described above maintains the ratio of the surface area to the mass of the working gas constant. The gas dynamic scaling is preserved, but only if the change in the relative amount of adsorbed gas does not affect surface reflection significantly.

In the presentation and the full paper several possibilities associated with the relatively large store of adsorbed gas in microscale gaseous systems will be discussed. This includes release mechanisms and the potential presented by manipulating surface nanotextures to alter both the quantity of adsorbed gas and the timing of its release and readsorption. Rapid transient studies of adsorbed gas release have been the subject of active research over the past decade by the physical chemistry community^(4,5,6) and others⁽⁷⁾.

References

- [1] J.H., De Boer, The Dynamical Character of Adsorption, Clarendon Press, Oxford, 1968.
- [2] A.W., Adamson, Physical Chemistry of Surfaces, John Wiley & Sons, New York, 1990.
- [3] S. Dushman, Scientific Foundation of Vacuum Technique, John Wiley & Sons, New York, 1962.
- [4] D.S., King, R.R., Cavanagh, Molecular Desorption From Solid Surfaces: Laser Diagnostics

*Abstract of invited paper 6216 presented to the 21st International Symposium on Rarefied Gas Dynamics, Marseille, France, July 26-31, 1998

INVITED LECTURES

and Chemical Dynamics, *Advances in Chemical Physics*, ed. K.P. Lawley, pp. 45-89, John Wiley & Sons, 1989.

- [5] A.C., Tam, H., Schroeder, Laser Induced Desorption of Moisture from a Surface in Atmospheric Conditions, *J. Appl. Phys.* 64(7), pp. 3667-3671, Oct. 1988.
- [6] C.R., Maechling, S.J., Clemett, F. Engelke, R.N., Zare, Evidence for Thermalization of Surface-Desorbed Molecules at Heating Rates of 10^8 K/s, *J. Chem. Phys.* 104(21), June 1996.
- [7] G. Pham-Van-Diep, E.P., Muntz, D.C., Wadsworth, Transient Normal Forces on Rapidly Heated Surfaces with Application to Micromechanical Devices, in *Rarefied Gas Dynamics 19*, eds. J. Harvey, G. Lord, V1, pp. 701-707. Oxford University Press, Oxford, 1995.

Survey on the initial-boundary value problems for the discrete Boltzmann equation *

Shuichi KAWASHIMA

Graduate School of Mathematics, Kyushu University, Fukuoka 812-0053, Japan

This talk gives a survey on the initial-boundary value problems and the corresponding stationary problems for the discrete Boltzmann equation in one- space dimension.

The discrete Boltzmann equation describes the motion of gas particles with a finite number of velocities, we consider the case of binary collisions only, so that the collision term contained in the equation is quadratic. We study this discrete Boltzmann equation in a one-dimensional region, which is either the half space (half line) or a bounded domain (finite interval). The boundary condition imposed is either the diffuse boundary condition (abbreviated by (D)) or the reflection boundary condition (abbreviated by (R)). Thus we have 5 different initial-boundary value problems; 2 for the half space and 3 for the bounded domain. For these initial-boundary value problems we discuss :

- Global existence and uniqueness of nonstationary solutions,
- Existence and uniqueness of stationary solutions,
- Asymptotic stability of stationary solutions, i.e., asymptotic convergence of nonstationary conditions to the corresponding stationary solutions.

We have satisfactory results on the global existence and uniqueness of nonstationary solutions. The key to the proof is to obtain the a priori estimate of solutions and it is based on the conservation of mass and momentum and also on the Boltzmann H - theorem. Stationary problems are more difficult. We know the existence (without uniqueness) of stationary solutions for the problems in the bounded domain with (D)-(D) and (D)-(R) boundary conditions, respectively. This existence result was proved by the Browder-Potter fixed point theorem of Leray-

Schauder type and the key estimate in the proof is again based on the conservation of mass and momentum. The uniqueness and the asymptotic stability of these stationary solutions are shown under "smallness" assumptions. The stability condition introduced by Y. Shizuta and S. K. Playon a crucial role in the proof. On the other hand, the stationary problems in the bounded domain with (R)-(R) boundary condition and in the half space with (R) boundary condition remain unsolved.

Very recently, an important progress has been made by S. Ukai for the stationary problem in the half-space with (D) boundary condition. He proved the existence and uniqueness of stationary solutions to that problem under "smallness" condition and several structural assumptions. The asymptotic stability of Ukai's stationary solution is also discussed in this talk. It seems interesting to apply Ukai's idea to the stationary problem in the half space with (R) boundary condition.

*Abstract of invited paper 6911 presented to the 21st International Symposium on Rarefied Gas Dynamics, Marseille, France, July 26-31, 1998

Modelling of Gas-Surface Interactions and Inelastic Intermolecular Collisions in DSMC calculations. *

R.G. Lord

Department of Engineering Science, Oxford University, England

1 Introduction

The paper will survey some developments in direct simulation Monte Carlo (DSMC) modelling of gas-surface interactions and energy exchange in inelastic intermolecular collisions which have taken place since the previous review paper by Harvey [1]. The survey will be by no means exhaustive and the emphasis will inevitably be on the author's own, and closely related, work. For many years gas-surface interaction were modelled almost exclusively by the so-called Maxwell model [2] and energy exchange in inelastic intermolecular collisions by the Borgnakke-Larsen (B-L) model [3]. While both models are highly efficient from a computational point of view and satisfy detailed balance at equilibrium, both are patently unrealistic in that they assume complementary probabilities of either completely elastic scattering or complete equilibration in each collision; in reality, partial equilibration will occur in every collision. Recent increases in computing speeds have meant that the penalties incurred by the use of more complicated, but more realistic, models are now much less serious.

2 Gas-surface Interactions

A significant development was the DSMC implementation of the Cercignani-Lampis (C-L) model [4], some 20 years after its conception, and the simultaneous extension to classical internal degrees of freedom [5]. Since then a number of extensions of the C-L model have been devised to include diffuse scattering with partial energy accommodation [6], partially diffuse scattering [7], vibrational energy exchange for both harmonic [6] and anharmonic [7] oscillator models and energy exchange between translational and internal degrees of freedom [8].

An alternative approach to modelling of gas-surface interactions is based on the model of Nocilla [9], in which the distribution of molecules leaving the surface is represented by a "drifting Maxwellian" distribution whose parameters depend on the velocity and direction of the incident molecule. This model was developed by Hurlbut and Sherman [10] for DSMC calculations but does not describe internal energy exchange nor does it satisfy detailed balance at equilibrium. An recent extension of Nocilla's model by Cercignani and his co-workers [11] overcomes the latter problem but has not so far been used in DSMC calculations.

3 Inelastic Collisions

An attempt to extend the basic B-L model to partial equilibration was made by the original authors [12]. This consisted of restricting the amount of energy taking part in the exchange process to a certain fraction of the total collision energy. Unfortunately, this "restricted exchange" model fails to satisfy detailed balance at equilibrium and therefore does not preserve an equilibrium distribution. A more satisfactory method has been devised by Pullin [13], in which the number of degrees of freedom of each molecule involved in the exchange, rather than the energy itself, is restricted. Pullin's model does satisfy detailed balance but does not appear to have been much used. The extension of the basic classical B-L model to the case of quantized vibrational energy levels has been achieved by Bergemann and Boyd [14] (the B-B model).

A somewhat different approach to the modelling of partial equilibration in inelastic collisions, which is applicable to both classical and quantized energy levels, has been devised by Lord [15]. Although the model itself is perhaps inferior the Pullin extension of the B-L model, the method of formulation, in terms of cumulative probability functions rather than probability density functions, proves to have certain advantages. The idea has been used

*Abstract of invited paper 5621 presented to the 21st International Symposium on Rarefied Gas Dynamics, Marseille, France, July 26-31, 1998

subsequently to extend the C-L model to the case of the unequally spaced vibrational energy levels of an anharmonic oscillator [7] and to combine the B-B and Pullin inelastic collision models to allow partial equilibration in the case of quantized energy levels. Very recently, a modification of the B-B/Pullin combined model has been devised by Lord [16], in which only the kinetic part of vibrational energy of the molecule is exchanged in inelastic collisions. This model was developed in order to achieve compatibility with a model of collisional dissociation by the same author [17].

References

- [1] Harvey J.K., *Inelastic Collision Models for Monte Carlo Simulation Computation*, in Rarefied Gas Dynamics: Physical Phenomena, ed E.P. Muntz, D.P. Weaver and D.H. Campbell, AIAA, Washington, pp.3-24, 1989.
- [2] Maxwell J.C., *On Stresses in Rarefied Gases arising from Inequalities of Temperature*, Phil. Trans. Roy. Soc. 170, pp 231-256, 1879.
- [3] Borgnakke C. and Larsen P.L., *Statistical Collision Models for Monte Carlo Simulation of Polyatomic Gas Mixtures*, Journal of Computational Physics, 18, pp.405-420, 1975.
- [4] Cercignani C. and Lampis M., *Kinetic Models for Gas-surface Interactions*, Transport Theory and Statistical Physics, 1, pp101- 104, 1971.
- [5] Lord R.G., *Application of the C-L scattering kernel to DSMC Calculations*, in Rarefied Gas Dynamics 17, ed A.E. Beylich, VCH, Weinheim, pp.1427-1433, 1991.
- [6] Lord R.G., *Some Extensions to the Cercignani-Lampis Scattering Kernel*, Phys. Fluids A 3, pp.706-710, 1991.
- [7] Lord R.G., *Some Further Extensions of the Cercignani-Lampis Gas-Surface Interaction Model*, Phys. Fluids 7, pp.1159- 1161, 1995.
- [8] Lord R.G., *Gas-Surface Interactions Models for Monte Carlo Calculations*, in Aerothermochemistry of Spacecraft and Associated Hypersonic Flows, ed R. Brun and A.A. Chikhaoui, IUTAM, Marseille, pp79-84, 1992.
- [9] Nocilla S., *On the Interactions between Stream and Body in Free-Molecule Flow* in Rarefied Gas Dynamics, ed L. Talbot, Academic Press, New York, pp.169-208, 1961.
- [10] Hurlbut F.C. and Sherman F.S. *Application of the Nocilla Wall Reflection Model to Free-Molecule Kinetic Theory* Phys. Fluids 11, pp.486-496, 1968.
- [11] Cercignani C. *New Scattering Kernel for Gas-Surface Interaction* AIAA J. 35, pp.1000-1011, 1997.
- [12] Larsen P.L. and Borgnakke C. *Statistical Model for Simulating Polyatomic Gas with Restricted Energy Exchange* in Rarefied Gas Dynamics, ed M. Becker and M. Fiebig, DFVLR, Portz-Wahn, pp.A.7-1-A.7-7, 1974.
- [13] Pullin D.I. *Kinetic Models for Polyatomic Molecules with Phenomenological Exchange*, Phys. Fluids 21, pp.209-216, 1978.
- [14] Bergemann F. and Boyd I.D. *New Discrete Vibrational Energy Model for the Direct Simulation Monte Carlo Method* in Rarefied Gas Dynamics: Experimental Techniques and Physical Systems, ed B.D. Shizgal and D.P. Weaver, AIAA, Washington, pp.174-183, 1994.
- [15] Lord R.G., *A New Model of Energy Exchange in Inelastic Collisions*, in Rarefied Gas Dynamics 19, ed J.K. Harvey and R.G. Lord, OUP, Oxford, pp.563-570, 1995.
- [16] Lord R.G., *Modeling Vibrational Energy Exchange of Diatomic Molecules using the Morse Interatomic Potential*, Phys. Fluids 10,3, pp.742-746, 1998.
- [17] Lord R.G., *Modelling Dissociation of Diatomic Molecules using the Morse Potential*, in Rarefied Gas Dynamics 20, ed Ching Shen, Peking University Press, Beijing, pp.180-185, 1997.

Relationships between Discrete and Continuous Kinetic Theories *

A.V. Bobylev^{1,2},

¹ Keldysh Institute of Applied Mathematics, Moscow, Russia

² Department of Mathematics, University of Saarlandes, Germany

We present a review of some new results in the theory of discrete velocity models (DVM) of the Boltzmann equation in connection with general problems of kinetic theory and rarefied gas dynamics. Our goal is to consider all aspects (physical, mathematical, and computational) of the relationship between DVM and continuous kinetic equations.

Despite the fact that the first DVM were proposed with the aim to understand better some properties of the Boltzmann equation, the discrete and continuous kinetic theories became almost completely separated in the subsequent history [1, 2]. The situation however changed significantly during the last decade. One of main reasons for that was a development of computer methods which need in principle some sort of discretization of the continuous kinetic equations. As a result, we obtain by using ideas of discrete kinetic theory some new numerical methods in fluid mechanics (lattice gases, lattice Boltzmann equation) and in rarefied gas dynamics. What more can we learn from discrete velocity models? Our discussion is concentrated on the following problems:

1. Approximation of the Boltzmann equation by discrete velocity models. Three different approaches to discretization [3 – 8]. DVM and number-theoretical methods. 2d and 3d models. Symmetry properties and Galilei invariance. What is the "best" DVM for the Boltzmann equation? Countable DVM and tails of distribution functions.

2. Efficiency of deterministic numerical schemes for DVM and BE. Estimates of computational work. Fast Fourier Transform methods [9].

3. New exact solutions of multidimensional stationary problems for the Broadwell model [10 – 14]. Two dimensional stationary flows - comparison with "true" rarefied gases. Non-uniqueness of solutions to well - posed (in continuous kinetic

theory) problems. . Physical and non-physical properties of discrete velocity models.

4. Stationary plane problems in unbounded domains (evaporation, condensation, shock waves). Qualitative analysis and phase portrait. Topological indecies of singular points for DVM and for the Boltzmann equation. How many degrees of freedom are needed to reproduce a correct behaviour of solutions to the Boltzmann equation ? DVM and other methods of discretization (Navier - Stokes equations, moment methods) [15].

5. Hydrodynamics and thermodynamics of DVM. Properties of the stationary Navier - Stokes equations for the Broadwell model . A role of temperature in the discrete kinetic theory [16-17].

6. Non-Markowian effects for discrete and continuous kinetic systems. Uchiyama's example. What is a correct kinetic equation for the Broadwell model? [18-19]

7. Generalizations and new directions [20].

The review is based on papers of different authors as well as on papers of the present author published in 1995-98. Some new unpublished results are also included.

References

- [1] Gatignol, R., *Théorie Cinétique des Gaz à Répartition Discrète de Vitesses*, Lecture Notes in Physics, 36, Springer, Berlin, 1975.
- [2] Cabannes, H., *The Discrete Boltzmann Equation*, Lecture Notes, University of California, Berkeley, 1980.
- [3] Goldstein, D., Sturtevant, B. and Broadwell, J.E. , *Investigations of the motion of discrete-velocity gases*, in "Rarefied Gas Dynamics: Theoretical and Computational Techniques",

*Abstract of invited paper 1871 presented to the 21st International Symposium on Rarefied Gas Dynamics, Marseille, France, July 26-31, 1998

INVITED LECTURES

- Edited by E.P. Muntz, D.P. Weaver and D. H. Campbell, pp. 110-117, AIAA Washington, 1989.
- [4] Bobylev, A.V., Palczewski, A. and Schneider, J., *Discretization of the Boltzmann equation and discrete velocity models*, in "Rarefied Gas Dynamics 19", J. Harvey and G. Lord, eds., Vol. II, pp. 857-863, Oxford University Press, Oxford, 1995.
 - [5] Bobylev, A.V., Palczewski, A. and Schneider, J., *On approximation of the Boltzmann equation by discrete velocity models*, C.R. Acad.Sci. Paris, Série 1, 320, pp. 639 - 644, 1995.
 - [6] Palczewski, A., Schneider, J. and Bobylev A.V., *A consistency result for a discrete velocity model of the Boltzmann equation*, SIAM J. Numer. Anal., 34, pp. 1865 - 1883, 1997.
 - [7] Rogier, F., Schneider, J., *A direct method for solving the Boltzmann equation*, Transp. Theory and Stat. Phys., 23, pp. 313-338, 1994.
 - [8] Panferov, V., *Convergence of Discrete Velocity Models to the Boltzmann equation*, Preprint, Goteborg University, 1997.
 - [9] Bobylev, A.V. and Rjasanow, S., *Difference scheme for the Boltzmann equation based on the Fast Fourier Transform*, Eur. J. Mech., B/Fluids, 16, pp. 293-306, 1997.
 - [10] Bobylev, A.V., *Exact solutions of discrete kinetic models and stationary problems for the plane Broadwell model*, Math.Meth.Appl.Sci., 19, pp.825 - 845, 1996.
 - [11] Bobylev, A.V. and Spiga, G., *On a class of exact two-dimensional solutions for the Broadwell model of the Boltzmann equation*, J.Phys.A:Math.Gen., 27, pp.7451 - 7459, 1994.
 - [12] Bobylev, A.V. and Toscani, G., *Two dimensional half-space problems for the Broadwell discrete velocity model*, Continuum Mech. Thermodyn.,8, pp. 257 - 274, 1996.
 - [13] Cabannes, H., *New analytic solutions for the Broadwell equations on discrete kinetic theory*, Eur. J. Mech., B/Fluids, 16, pp.1 - 15, 1997.
 - [14] Cabannes, H., *Evaporation and condensation problems in discrete kinetic theory*, Eur. J. Mech., B/Fluids, 13, pp. 685 - 699, 1994.
 - [15] Bobylev, A.V., Ostmo, S. and Ytrehus, T., *Qualitative analysis of the Navier-Stokes equations for evaporation-condensation problems*, Phys. Fluids, 8, pp. 1764 - 1773, 1996.
 - [16] Cercignani, C., *On the thermodynamics of a discrete velocity gas*, Transp. Theory and Stat. Phys., 23, pp. 1 - 8, 1995.
 - [17] Cercignani, C., *Temperature, entropy and kinetic theory*, J. Stat. Phys., 87, pp. 1097 - 1109, 1997.
 - [18] Uchiyama, K., *On the Boltzmann-Grad limit for the Broadwell model of the Boltzmann equation*, J. Stat. Phys., 52, pp. 331 - 335, 1988.
 - [19] Bobylev, A.V., Maaß, F., Hansen, A. and Hauge E.H., *What more can we learn from the Lorentz model*, J. Stat. Phys., 87, pp. 1205 - 1228, 1997.
 - [20] Bobylev, A.V., Cercignani, C., *Discrete velocity models for mixtures*, to appear in J. Stat. Phys. in 1998.

Physics and Modeling of Stationary Plasma Thrusters *

J.P. Boeuf, L. Garrigues

CPAT, Universit P. Sabatier, Toulouse, France

Stationary Plasma Thrusters are ion thrusters whose properties make them especially suitable for satellite station-keeping or orbit transfer. In these thrusters, the plasma is confined between two concentric dielectric cylinders (typical dimensions: radii 3 and 5 cm, length 4 cm). The anode is at one end of the channel formed by the two cylinders. A flow of xenon is injected into the cylinders through the anode and is ionized by electron impact. The resulting positive ions are ejected at the other end of the channel (exhaust). The cathode is outside the system of concentric cylinders. Since the gas density is rather low (the xenon mass flow rate is on the order of 5 mg/s, which corresponds to gas densities on the order of $10(13) \text{ cm}^{-3}$), the electron mean free path is much larger the channel length. In order to increase the total path length of the electrons from the exhaust to the anode, a system of coils is used in order to create a magnetic field inside the plasma column. The magnetic field is radial in the exhaust region. The resulting decrease of the axial electron drift velocity leads to an increase of the electron ionization coefficient and a plasma can be sustained in the channel.

In normal operating conditions, more than 90% of the gas flow is ionized. The voltage across the plasma column is between 200 and 300 V and the current is on the order of 5 A. The radial magnetic field is on the order of 200 G at the exhaust and decreases to zero at the anode. Due to the low electron conductivity in the exhaust region the electric field is large in this region in order to ensure current continuity. The large electric field in the exhaust region provides the ion acceleration (the ions are practically collisionless and insensitive to the magnetic field). The impulse and thrust of the SPT are on the order of 2000 s (i.e. the ion velocity is about 20000 m/s at exhaust) and 100 mN respectively. Since the ions are accelerated by a self-consistent electric field, there is no need to use electrostatic grids to extract the ions from the plasma as in elec-

trostatic ion thrusters. Another interesting feature of the SPT is that the current is not space charge limited since the accelerating field is not a space charge field but is due to the presence of a large radial magnetic field (and thus a low electron conductivity) in the exhaust region.

In this this lecture we present a simple model which has been developped in order to clarify the electrical properties of these thrusters and the low frequency oscillation regime which has been observed experimentally. The model is based on the assumption of quasi-neutrality of the plasma column and on a 1D transient hybrid treatment of electron and ion transport in the device. Electrons are considered as a fluid and ions are described with a collisionless kinetic equation. This model provides reasonable estimates of the plasma properties and is able to give a clear picture of the low frequency oscillations, qualitatively close to the experimental observations.

*Abstract of invited paper 1226 presented to the 21st International Symposium on Rarefied Gas Dynamics, Marseille, France, July 26-31, 1998

Molecular Models for Reacting Flows: Should Variable Collision Diameters for Internal States be used in DSMC Simulations? *

Ingrid J. Wysong
Raytheon STX, AFRL, Edwards AFB, CA, USA

The formulation of expressions for transport properties in nonequilibrium flows has been an active research field for many years [1]. One powerful feature of particle simulation methods such as direct simulation Monte Carlo (DSMC) is that they do not require transport properties as input parameters. Rather, given a sufficiently realistic model of the intermolecular potential and energy transfer, transport properties emerge naturally as a statistical consequence of many collisions along with boundary conditions [2]. Thus, a physically realistic yet computationally tractable model for molecular collisions is of primary importance for DSMC methods.

In a DSMC simulation, collision pairs are selected based on the local density and the velocity-dependent collision cross section. For any given reaction (or relaxation) model, the number of reactions produced in a given calculation (the local reaction rate) will be controlled by the local total collision frequency. Therefore, any increase or decrease in a molecule collision cross section can directly affect its effective reaction rate.

Gorbachev *et al.* [3] have presented a derivation of analytical expressions for the average internuclear distance $R(v,J)$ of a diatomic molecule as a function of vibration and rotation level, based on an accurate internuclear potential. Gimelshein *et al.* [4] have presented an implementation of these expressions in a DSMC code as an addition to the variable soft sphere (VSS) collision model. This intriguing proposal will produce significantly increased collision cross sections for particles with high levels of internal excitation, thus increasing their rates of reaction. Although the expressions for average internuclear distance $R(v,J)$ may be expected to be quite accurate, the effect on intermolecular collision cross section may not be straightforward. The goal of the present discussion is to examine the feasibility

of validating the realism of this approach.

Transport properties are an important source of information on intermolecular potentials. The following discussion refers to viscosity, but most of the same arguments apply to diffusion. The viscosity is typically dominated by elastic collisions, so that, in a first approximation, molecules may be viewed as atom-like. If we consider higher-order effects, we must include inelastic collisions. The effect of inelastic collisions on the transport collision integral (for viscosity) is expected to be small (Mason-Monchick approximation), but has not been thoroughly investigated for high temperatures. The other effect specific to molecules is the subject of this paper: that is, higher rovibrational (v,J) states will increase $R(v,J)$, which may in turn increase the collision cross section. Since the population of high (v,J) states will become significant at high temperatures, one might expect that the viscosity at high temperatures may reflect this effect [5]. However, in addition to the difficulty in obtaining accurate viscosity data at very high temperatures, any examination of these data to glean insight into the effect of $R(v,J)$ would need also to disentangle the effect of inelastic collisions.

To estimate the feasibility of validating the effect of increasing $R(v,J)$ at higher temperatures from viscosity data, some estimates are provided for a simple gas of pure molecular hydrogen. The (v,J) populations are in equilibrium and the viscosity collision cross section is given by the VSS cross section where each (v,J) state has a different reference diameter as defined in [4]. Fig. 1 shows that the assumed effect of $R(v,J)$ will begin to significantly decrease the viscosity compared with the VSS model for very high temperatures. However, the effects of dissociation and ionization at these high temperatures in a real gas are expected to be of greater importance to the measurable viscosity than the diameter effect. The calculation indicates that the effect of (v,J) excitation on collision cross section due solely to the diameter as proposed in [4] is likely im-

*Abstract of invited paper 6507 presented to the 21st International Symposium on Rarefied Gas Dynamics, Marseille, France, July 26-31, 1998

possible to verify through viscosity data. However, other effects such as a change in the attractive well depth or inelastic collisions may contribute in reality.

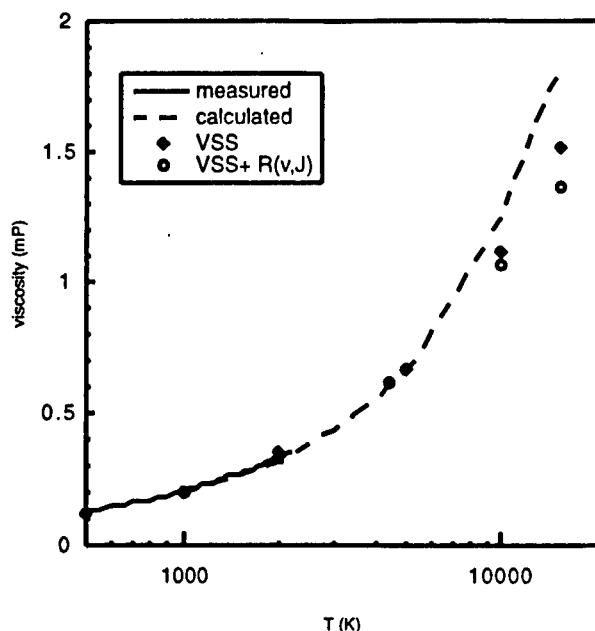


Figure 1: Variation in viscosity due to addition of rovibrational diameters to VSS model

The viscosity effect shown above may seem to indicate that including collision diameters based on (v, J) level is of no importance. This conclusion is not necessarily true for highly nonequilibrium gases, which are naturally the regime of interest for DSMC simulations. Certain nonequilibrium gases have highly excited vibrational distributions and, in these cases, an increase in collision diameter for the molecules with high vibrational quantum number could change the chemistry prediction for a DSMC simulation.

A number of experiments using light-induced drift (LID) have been performed which can directly measure the effect of changing (v, J) on the diffusion cross section of certain molecules [6]. These measurements show that the diffusion collision frequency, and thus the collision cross section, typically increases a small amount when v is increased from 0 to 1. On the other hand, these molecules show a decrease in collision frequency by a few percent as J increases. It is not clear how similar the results would be for other molecules. It is also difficult to assess how the results for a small range of (v, J) values would change for very high v or J levels. These results do demonstrate, however, that

even though $R(v, J)$ increases in a predictable way with increasing internal energy, the effect on the intermolecular collision cross section is difficult to predict and is influenced by subtle details of the intermolecular potential.

The proposal to include increased collision cross sections for high (v, J) states in DSMC simulations is worthy of examination. It is based on a first-principles approach to fundamental molecular properties. While the majority of flowfields, where the populations of very high internal energy states are insignificant, need not consider such an effect, there are certain nonequilibrium cases where this effect could potentially be important. It seems, however, that the collision cross section may not always increase with (v, J) in the straightforward manner proposed. Details of specific characteristics of the applicable intermolecular potential may need to be considered. Some validation of the relationship between internuclear diameter and intermolecular collision cross section is recommended before it is widely applied in DSMC codes.

References

- [1] Brun R., *Transport properties of nonequilibrium gas flows*, in *Molecular Physics and Hypersonic Flows*, p. 361, ed. M. Capitelli, Kluwer Academic, Netherlands, 1996.
- [2] Bird G.A., *Molecular Gas Dynamics*, Oxford Univ Press, Oxford, 1994.
- [3] Gorbachev Yu.E., Gordillo-Vasquez F.J., and Kunc J.A., *Diameters of rotationally and vibrationally excited diatomic molecules*, *Physica A: Statistical and Theoretical Physics*, Vol. 247, p.108, 1997.
- [4] Gimelshein S.F., Ivanov M.S., Markelov, G.N. and Gorbachev Yu.E., *Quasiclassical VRT transition models in the DSMC computations of reacting rarefied flows*, in *Rarefied Gas Dynamics 20*, p. 711, ed. C. Shen, Peking Univ. Press, Beijing, 1997.
- [5] Kang S.H. and Kunc J.A., *Viscosity of high-temperature iodine*, *Phys. Rev. A*, Vol. 44, p. 3596, 1991.
- [6] van Duijn E.J., Nokhai R.N., Hermans L.J.F., *Experimental investigation of the rotational- and vibrational-state dependence of the HF-Rg interactions*, *J. Chem. Phys*, Vol. 105, p. 6375, 1996.

Electronic Relaxation in Free Jet Expansions, as Generated from Arcs, RF, Laser Heated Plasma Sources *

D.C. Shram

Department of Applied Physics, Eindhoven University of Technology, The Netherlands

Expanding plasmas from upstream plasma sources are media which are very interesting from the point of physics in terms of flow properties, electromagnetic phenomena and excitation characteristics. At the same time expanding plasmas are widely used in new technologies as remote plasma processing, laser induced ablation, and in vacuum arc spots. The subject is also of interest for astrophysical objects. In the review the basic physical mechanisms, as dissipation, pressure enhancement in the source, the expansion cooling, flow properties, and the generation of electric and magnetic fields, will be described, together with a comparison with expansion of a hot gas. The similarities of and differences between the expansion of the various sources will be discussed. At the hand of detailed experimental information on the expansion from a thermal plasma source, obtained by various diagnostic techniques, as CARS, TALIF, Thomson, Rayleigh, and Raman scattering the physics will be illustrated. The contribution will be concluded with a critical discussion of the technological implications and possible large scale use of expanding plasmas for chemical conversion, deposition and surface modification.

*Abstract of invited paper 6906 presented to the 21st International Symposium on Rarefied Gas Dynamics, Marseille, France, July 26-31, 1998

Structure and Applications of Jets *

Alfred E. Beylich

Technische Hochschule Aachen, Aachen, Germany

The purpose of this paper is to review, discuss, and evaluate some of those aspects of jets which might have some relation to the field of rarefied gas dynamics (RGD); if possible, applications will be shown; jets with charged particles will not be included.

Jets are among the most often used devices in fluid flow and they are one of the most simple energy conversion machines that exists: In an internal flow, by means of specially shaped cross-sections, internal energy is converted into directed kinetic energy. There exist some properties which are common for most of the jet structures and the large number of applications: Starting from a stagnation state, $\Pi_0 = (p_0, T_0)$, flow is accelerated to sonic condition by shaping some guiding device in such a way that stream-lines are converging; downstream of the sonic region there may exist a further guided expansion, such as in a Laval nozzle, or there may not be a further guidance, such as in a free jet expansion; sometimes we may find a combination of guided and free expansion or a guidance by fluid elements.

One of the most important applications of jets is that for thrust producing engines, such as rocket nozzles or arc-jets used for propulsion; recent concepts of space-plane propulsion use air-frame integrated structures such as single expansion ramp nozzles (SERN); for off-design situations, active and passive devices for thrust-vector control are needed but still at the research level. Jets are also needed for fluid acceleration by transfer of impulse, such as in diffusion-, booster-, and jet-pumps, or for thrust augmentation in air-breathing engines.

In RGD, the supersonic low-density free jet, issued from an orifice or a sonic nozzle, has been widely studied: This type of jet allows for the fastest possible expansion and, therefore, suffers from little losses due to boundary/shear layers. Inside the (first) supersonic cell (the shock barrel), along the axis, a rather simple source-like expansion flow exists that allows a simple modelling; in the expand-

ing flow it is possible to have a transition from a collision dominated ("continuum") to a (near) free-molecular flow and, therefore, it is well suited for basic research on several phenomena like relaxation of translational, rotational, and vibrational degrees of freedom. Furthermore, in the isentropic expansion, the saturation line will be crossed (in the case of "normal" fluids); thus, the free jet, which also allows to vary the expansion speed by changing the parameter $p_0 D$ (D is the orifice diameter), is an excellent tool to study the onset of condensation due to (homogeneous) nucleation and its freezing at low densities. In connection with basic studies for laser isotope-separation, gas mixture expansions had to be studied; in this case non-equipartition of thermal energies as well as onset of condensation can destroy the effect of cooling. In another application, in "seeded" jets as used in molecular beam studies, incomplete momentum transfer (slip) due to less collisions may limit the final kinetic energy of molecules.

Reducing the background pressure p_∞ , when in the region near the shock surfaces (the shock barrel or the Mach disc) the local Knudsen number will become of order one, the shocks will broaden into a very diffuse zone and, eventually, they disappear; in this case we speak of a jet plume. For instance in space applications (where the background pressure $p_\infty \rightarrow 0$), there exists a great interest in contamination due to the action of thrusters (gas-surface interaction problem), and in the perturbation of the thrust vector due to plume-surface interaction.

For plumes with higher background pressures p_∞ , the background gas can penetrate into the jet plume, and, when gas mixtures are expanded in the jet, the different cross sections may cause a separation.

Reducing the stagnation pressure p_0 , we eventually meet the situation that the local Knudsen number at the orifice becomes of order one. This has a profound influence on the mass flux through the orifice and, eventually, the limiting case of a free molecular flow (effusion) is reached.

* Abstract of invited paper 1628 presented to the 21st International Symposium on Rarefied Gas Dynamics, Marseille, France, July 26-31, 1998

INVITED LECTURES

Numerous studies have been made using shapes of orifices that are not round; in this case, general features like the cell structure and the properties of the expanding gas state are of interest. For some applications, like laser isotope-separation or gas dynamic lasers, planar guided/free-jet expansions are needed and, in practice, often jets issued from linear slits or (underexpanded) nozzles are used. Concerning the lateral extent of the shock cells, there exists a "reciprocal" behavior with respect to the corresponding length of the orifice (i.e. in the plane of the slit height the cell diameter is large, and it is small in the plane of the slit length). In this context one must also mention the interference problem of clustered jets (two or more jets, up to the limit of a "porous" orifice).

Whereas considerable work was invested in the study of the interior of the jet cell, relatively little attention has been paid to the "outside", i.e. the region downstream of the shock surfaces. The reason for this might be that the interior flow is more easily accessible to any theoretical modelling, whereas the outer region consists of a rather complex (shear) layer. However, this region is of fundamental interest for all pumping applications that are based on momentum transfer. Some studies indicate an onset of instabilities and secondary flow; we may look at this as being first steps towards the evolution of a "turbulent" structure; its understanding can help to improve the mixing process.

A considerable part of jet studies is experimental, and therefore the development and application of diagnostic tools is useful. For higher densities, the classical devices like Pitot probes, (laser-) Schlieren, etc. can be applied. For low densities, however, these tools usually fail and, additionally, the increasing degree of non-equilibrium of the local state makes it necessary to measure an increasing number of observables. Besides the famous Patterson probe, a very useful device has been the electron beam probe; it permits to measure density, velocity, components of translational temperature as well as populations of rotational or vibrational levels. For not too low densities lasers have become an extremely useful tool to measure similar moments, again by means of spectroscopic methods (Raman, IR absorption, LIF, REMPI, etc.). For the study of nucleation in condensing flows, useful diagnostic tools have been laser (Rayleigh) scattering, electron-beam diffraction, and molecular-beam mass-spectroscopy.

Concluding we may remark that, until today, the study of numerous modifications of jets as well as

using the jet as a vehicle to understand fundamental properties of kinetic phenomena has provided a rather detailed picture of the physics that is involved. Present and new applications of jets (remaining to be one of the fundamental fluid devices) will direct our interest to new phenomena that have not been understood or neglected until now.

Non-Equilibrium Vibrational Kinetics and Dissociation-Recombination Processes *

M.Capitelli, F.Esposito, C.Gorse

Centro di Studio per la Chimica dei Plasmi del CNR

Department of Chemistry- University of Bari(Italy)

Non equilibrium vibrational kinetics is a topics interesting different disciplines including plasma chemistry, laser physics and hypersonic flows. Sophisticated state to state models including dissociation-recombination reactions have been developed to explain the reactivity of simple molecules under strong non-equilibrium conditions. These models have been then inserted in 1D fluidodynamic codes to obtain informations about vibrational distribution and atomic species profiles. In this paper we will present results obtained under different non-equilibrium conditions (plasma, hypersonic boundary layer, nozzle flows). First we will consider a cold plasma i.e. a non-equilibrium system composed by neutral and ionized species including free electrons [1]. Under many experimental conditions both the electron energy distribution function (eedf) and the molecular distribution functions of internal degrees of freedom of molecules (in particular the vibrational one vdf) are far from equilibrium, so that an appropriate Boltzmann equation for free electrons and a system of vibrational master equations must be solved to obtain the relevant distributions. Several examples of this kind of kinetics have been presented in the literature, nitrogen being one of the most studied systems. For typical plasma conditions (few torr pressure, ionization degree in the range $10^{-4} < \alpha < 10^{-6}$, average electron energy less than 2eV) both eedf and vdf present large deviations from equilibrium. In particular eedf presents structures due to second kind collisions between cold electrons and vibrationally and electronically excited states, while vdf presents long plateaux in the intermediate vibrational quantum number range due to the interplay of V-V(vibration-vibration) and V-T(vibration-translation) energy exchange processes.

At the same time the non-equilibrium vibrational distributions generates a non-equilibrium behaviour in the dissociation rates due to the fact that the plateaux tend to disappear with the increasing of gas temperature. Moreover the dissociation by electron impact strongly increases when the state to state transitions are taken into account: the rate coefficients in fact increase with increasing vibrational quantum number due to the corresponding decreasing of the threshold energy of the process.

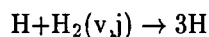
As far we have discussed a zerodimensional kinetics which can be introduced in dimensional codes. Examples in this direction can be considered the study of the vibrational kinetics of nitrogen in RF parallel plate reactors where a particle in cell with Monte Carlo collisions (PIC-MCC) has been used for studying the coupling of state to state kinetics with the dynamics of charged (ions and electrons) particles. Another example is the introduction of vibrational kinetics under expanding flows either in the case of the kinetics occurring in the boundary layer of reentering bodies or in the kinetics occurring in the expansion of high temperature gas through nozzles. In the last cases the introduction of vibrational energy occurs on the top of vibrational ladder because of the preferential pumping of higher vibrational levels by the atomic recombination process. This source of vibrational energy is such to keep non-equilibrium vibrational distributions in the boundary layer of reentering body [2] as well as along the axis of nozzle [3]. In both cases we can note an assisted dissociation recombination process. The final result is a non-Arrhenius behaviour of the dissociation constant along the boundary layer as well as along the x-axis of nozzle flow.

The results as far discussed have been obtained by describing the dissociation-recombination process through the so called ladder climbing model, i.e. we consider a pseudo level located above the last bound vibrational level through which passes all the dissociation-recombination elementary pro-

*Abstract of invited paper 1776 presented to the 21st International Symposium on Rarefied Gas Dynamics, Marseille, France, July 26-31, 1998

cesses. Practically the last bound level controls the dissociation-recombination. This of course is an approximation: in fact heavy particle collisions with the whole vibrational manifold are responsible of the dissociation process. To check this point we present cross sections and rate coefficients for reactions involving dissociation in atom-diatom (rotovibrationally excited) calculated by means of quasi-classical trajectory method with histogram (QCTH), modified by using an original technique that allows to decrease the computational effort due to the calculation of several cross sections from rotational states [4].

A complete set of cross sections for the system



is now available allowing us to compare the dissociation of H_2 by direct impact or through the ladder climbing model.

References

- [1] Capitelli M. et al., *Non-equilibrium vibrational kinetics under discharge and hypersonic flow conditions: a comparison*, AIAA paper 97-2528
- [2] Armenise I. et al, *Nitrogen non-equilibrium vibrational distributions and non-Arrhenius dissociation constants in hypersonic boundary layers*, J. Thermophysics and Heat Transf., 12 (1998)
- [3] Colonna G. et al., *Influence on dissociation rates of the state-to-state vibrational kinetics of nitrogen in nozzle expansion*, this meeting
- [4] Esposito F., work in progress.

On the Structure of Radiative Shock Waves in Stellar Atmospheres *

D. Gillet

Observatoire de Haute- Provence, France

When the shock wave velocity increase, the internal degrees of freedom of atoms are more and more excited and consequently a radiative flux is produced into the de- excitation region of the shock wake. Because the gas between this region and the shock front is optically thin and the shock velocity is quite smaller than the light velocity, a large part of incoming flux is absorbed by the unperturbed cooler gas located in front of the shock. This simple and natural phenomenon dramatically complicates the calculation of the structure of radiative shock waves because the hydrodynamical equations are coupled with the transfer equation which is nonlocal. A direct consequence of the presence of a noticeable radiative field induced by the shock passage, is a strong compression effect which can reach several hundreds. Moreover this last effect provokes a significant amplification of the turbulence level of the unperturbed gas.

The aime of this talk is to give a review of our present understanding of the structure of radiative shock waves. Although hypersonic shocks are very common in stellar atmospheres, similar shocks also occur in shock tube experiments and during the reentry of space vehicles into Earth atmosphere.

*Abstract 3041 invited to the 21st International Symposium on Rarefied Gas Dynamics, Marseille, France, July 26-31, 1998

Review of Entry Flight Aerodynamic Measurements During Rarefied-Flow Transition *

Robert C. Blanchard

NASA Langley Research Center, Hampton, Virginia 23681- 0001 USA

1 Introduction

A flight research effort was initiated by NASA in the late 1970's to create a flight aerothermodynamic database for the Shuttle Orbiter in the rarefied-flow flight regime. The flight program included the development of techniques needed to make insitu rarefied flow aerodynamic measurements during initial reentry into the atmosphere. In parallel, development of computational flow simulation techniques was initiated¹ to support the further development of the database and to supplement the scant wind tunnel performance data². At that time, winged-vehicle reentry aerodynamic performance in this flight regime had not been adequately measured, analytically modeled, or simulated in wind tunnels. Although the lack of detailed information in the rarefied-flow flight regime did not pose a threat to the safety or success of the Shuttle Orbiter mission, it was deemed prudent by NASA to gather flight data in this regime for future applications. The Shuttle Orbiter flight database in the rarefied flow regime provided a validation source for code development. More reliance can now be placed on prediction of rarefied-flow performance via simulation codes for missions utilizing direct entry, aerobraking, and aerocapture.

Flight measurements of entry vehicle aerodynamics in the region from free-molecule flow to the hypersonic continuum, i.e. the rarefied-flow transition region, have been analyzed recently by several investigators. The 20th International Symposium on Rarefied Gas Dynamics included several presentations on measurements in the rarefied-flow regime. For example, DSMC simulations are compared to data from the Japanese OREX (1994) mission³ (a blunt-body 50° half-angle cone entry vehicle), and Russian measurements from the Soyuz reentry vehicle⁴ are used in conjunction with DSMC to establish local bridging methodology for the rarefied-flow transition.

NASA rarefied-flow measurements span a wide variety of shapes ranging from delta-winged vehicles, like the Shuttle Orbiter (from 1983), moderately blunt entry shapes like the Pioneer Venus probes into the planet Venus (1978) and the Galileo probe(1996) into the planet Jupiter, to blunt entry vehicles like the Viking(1976) and Pathfinder(1997) probes into the planet Mars. This review will concentrate on the flight aerodynamic measurements in the rarefied-flow regime acquired on NASA missions spanning a period 20 years and including a variety of flight experiments and vehicle shapes.

2 Flight Experiments

The first NASA experiment specifically designed to provide insitu rarefied-flow entry measurements was the High Resolution Acceleration Package (HiRAP) which had its maiden flight on the Shuttle Orbiter in April, 1983 and

results from 12 successful flights have been analyzed and reported^{5,6,7}. The initial flight data from the HiRAP experiment provided the first flight measurements of performance coefficients for a winged entry vehicle in the rarefied-flow regime^{8,9}.

HiRAP is specifically designed to measure the aerodynamic performance characteristics (e.g. C_N/C_A) of the Shuttle Orbiter during descent through the rarefied flow flight regime. The HiRAP equipment is an orthogonal, tri-axial set of linear, pendulous, gas-damped accelerometers each with a resolution of 1×10^{-6} g (1 mg) and a range of ± 8000 mg. The package is 8.89 cm x 12.7 cm x 10.16 cm and weighs about 1.134 kg; data is taken at 174 samples/s. The experiment is mounted in the wing box of the Shuttle Orbiter with the accelerometer input axes aligned with the Shuttle Orbiter body axes. Fig. 1 provides a sketch of the HiRAP experiment equipment installed on the Shuttle Orbiter.

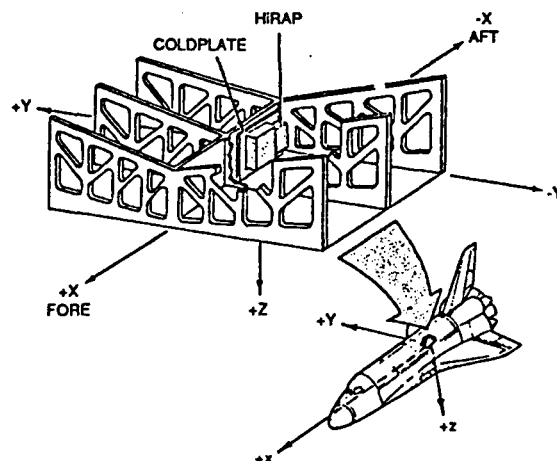


Fig. 1 HiRAP experiment installation on the Shuttle Orbiter.

The post-flight analyses of HiRAP data produce a calibrated measurement of low frequency, low level (e.g. aerodynamic) accelerations exerted on the Shuttle Orbiter during reentry. A collection of flight data from the HiRAP experiment taken during 12 Shuttle Orbiter reentries is given in Fig. 2. The development of this normal-to-axial coefficient database, along with the experiment instrumentation, the flight conditions, the data extraction techniques and the empirical flight model developed from the data¹⁰ will be presented in the full paper.

*Abstract 2351 invited to the 21st International Symposium on Rarefied Gas Dynamics, Marseille, France, July 26-31, 1998

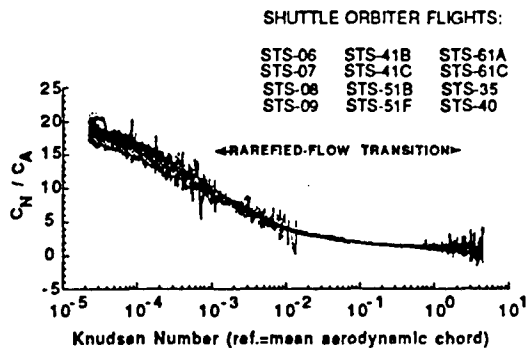


Fig. 2 HiRAP flight C_N/C_A measurements in the rarefied-flow transition regime.

The second significant NASA flight experiment to measure insitu the rarefied-flow aerodynamic parameters was also conducted on the Shuttle Orbiter and is called the Orbital Acceleration Research Experiment¹¹ (OARE). This experiment was an out-growth of the HiRAP flight experiment in an attempt to remove some of the major obstacles encountered during flights with the HiRAP (e.g. laboratory calibration factors, instrument sensitivity, etc.).

The OARE contains a tri-axial accelerometer which uses a single free-floating (non-pendulous) electrostatically suspended cylindrical proofmass. The accelerometer sensor assembly is mounted to a microprocessor-controlled, dual-gimbal platform in order to perform in-flight calibrations (both bias and scale factor). Acceleration measurements are processed and stored in the OARE flight computer memory and, simultaneously, the unprocessed data are recorded on the Shuttle Orbiter payload tape recorder. These payload tape recorder data are telemetered periodically to ground stations during flight while the computer stored data is retrieved after landing. The OARE system layout showing the components of the experimental equipment is shown in the following sketch.

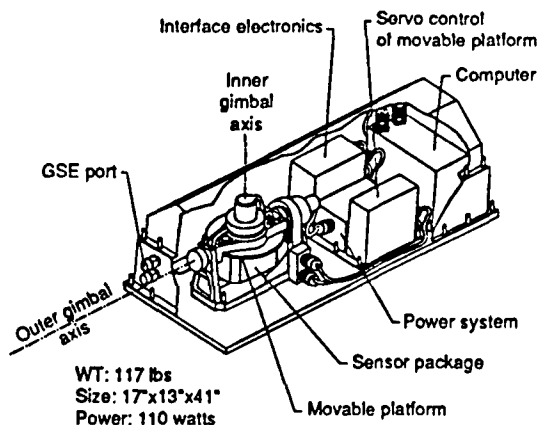


Fig. 3 OARE flight instrument package.

The accelerometer sensor (labeled "sensor package" in Fig. 3) is attached to a moveable platform. The platform is moveable about two axes, the inner-gimbal and the outer-gimbal axis. There are 3 sensor ranges which correspond to acceleration scales of $\pm 10,000$, ± 1000 and $\pm 100 \mu g$ respectively for the X-axis and $\pm 25,000$, ± 1970 and $\pm 150 \mu g$ respectively for the Y- and Z-axes. The best sensor resolution is 3.05 ng ($1 \times 10^{-9} \text{ g}$) which is along the X-axis. The Y- and Z- axes have a slightly larger sensor resolution value of 4.6 ng .

The initial developmental flight of the OARE equipment was on Shuttle Orbiter mission STS-40 in June 1991^{12,13}. This was followed by other developmental flights: STS-50 (July- August, 1992¹⁴), and STS-58 (August, 1993¹⁵). The first reentry measurements using insitu calibration factors were conducted on STS-62 (Mar., 1994¹⁶). The reentry data include the flight regime from orbital altitudes down to about 90 km which covers the free-molecule-flow regime and the upper altitude fringes of the rarefied-flow transition into the hypersonic continuum. Ancillary flight data on Shuttle Orbiter position, orientation, velocity, and rotation rates have been used in models to transform the measured accelerations to the Shuttle Orbiter center of gravity, from which aerodynamic accelerations along the Shuttle Orbiter body axes have been calculated. The resulting aerodynamic acceleration measurements along the Shuttle Orbiter's body axis and the normal-to-axial acceleration ratio were measured and compared with numerical simulations from three direct simulation Monte Carlo (DSMC) codes. Fig. 4 shows a comparison between DSMC simulations and flight measured normal-to-axial coefficient obtained during STS-62.

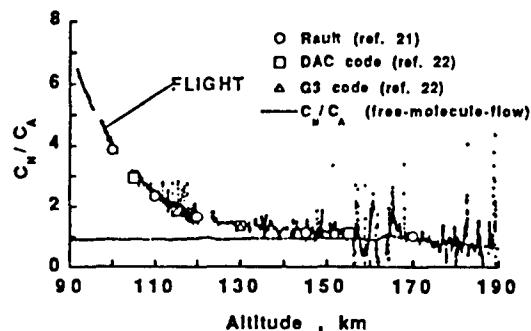


Fig. 4 Comparison of DSMC simulations with flight measured normal-to-axial coefficient during STS-62 reentry.

The full paper will discuss the flight conditions under which the data were obtained, the calibration and data reduction techniques used to extract the aerodynamic parameters, and the DSMC simulation conditions. Also, a direct comparison was made between the OARE experiment flight data and HiRAP data which also was obtained on this same flight.

In addition to the Shuttle Orbiter experiments, other aerodynamic flight data in the rarefied-flow regime have been

collected on blunt body entry vehicles into the planets (e.g. spherically blunted 70° half-cone angle forebodies of the NASA-Mars probes). These include the Mars Viking entry vehicle^{17,18} and the recent Mars Pathfinder entry vehicle^{19,20}. During entry, both vehicles traversed all speed regimes going from orbital velocities under near vacuum conditions, i.e. the free-molecule flow regime, through the hypersonic non-continuum and continuum regimes, down to zero velocity on the planet's surface where the pressure of the CO_2 atmosphere is less than 1% of the Earth's surface pressure. Measurements are available in the rarefied-flow regime from these missions. These landing missions, as well as future aerobraking missions to Mars rely upon knowledge of the entry vehicle aerodynamic characteristics as it transitions from the free-molecule flow regime into the hypersonic continuum regime and knowledge of the properties of the upper atmosphere. Typically, ground-based measurements of aerodynamic characteristics in the rarefied regime are not available so that designers rely heavily on computational results. Confidence in computational techniques can be greatly enhanced by comparing predictions to flight data. Fortunately, for Mars missions, the wealth of data collected by the Viking missions provides confidence to design future missions. This presentation compares recent DSMC simulations with Viking 1 flight aerodynamic extraction results within the rarefied-flow regime (Fig. 5).

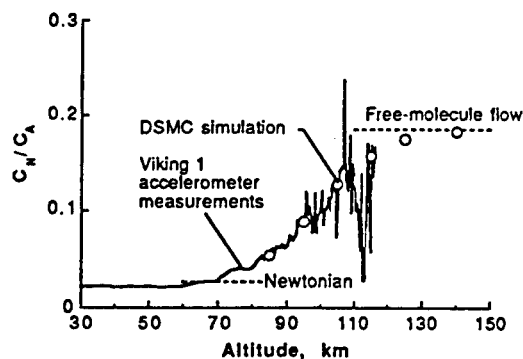


Fig. 5 Normal-to-axial coefficient measurements from Viking 1 compared to DSMC simulations.

The Pathfinder vehicle (also, a spherically blunted 70° half-cone angle forebody vehicle) was targeted to enter the Martian atmosphere at zero deg. angle-of-attack. The vehicle was passively controlled using a spin rate of 2.0 rpm. The entry attitude goal was nearly achieved, thus providing little signal in the normal-to-axial measurements. Figure 6 shows the Pathfinder flight measurements in the rarefied-flow flight regime.

The final paper will discuss the recent flight results of the Mars Pathfinder entry into the planet. Also, there will be a brief discussion of future Mars missions which are relevant to the present studies, including Mars Surveyor Program (MSP)-98 (a Lander mission at $\alpha \sim 0$ deg.), MSP-01 (a Lander at $\alpha \sim 11$ deg.), and MSP-01 (an Orbiter using

aerocapture at $\alpha \sim 11$ deg.). These entry/aerobraking vehicles will contain comprehensive and better resolution instrumentation and are expected to provide more accurate data to complement the existing database.

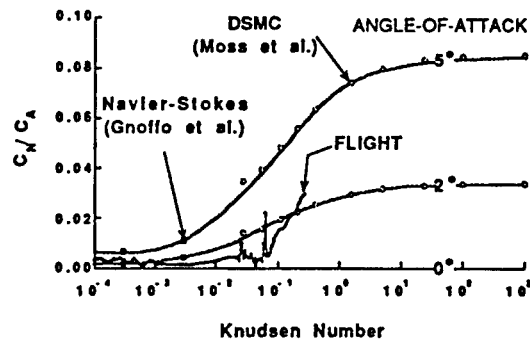


Fig. 6 Comparison of Pathfinder DSMC and Navier-Stokes simulations with normal-to axial measurements.

References

1. Moss, J.N. and Bird, G.A., "Direct Simulation of Transitional Flow for Hypersonic Reentry Conditions," *Thermal Design of Aeroassisted Orbital Transfer Vehicles*, Progress in Astronautics and Aeronautics, edited by H. F. Nelson, AIAA, 1985, pp. 113-139.
2. "Aerodynamics Design Substantiation Report-Vol. I: Orbiter Vehicle", Rockwell International, Space Division, Downey, CA SD74-SH0206-1H, January 1986
3. Moss, J.N. and Price, J.M., "DSMC Simulations of OREX Entry Conditions", *Rarefied Gas Dynamics 20*, edited by Ching Shen, Peking Univ. Press, Beijing, China, 1997, pp. 459-462.
4. Ivanov, M.S., Markelov, G.N., Gimelshein, S.F., and Antonov, S.G., "DSMC Studies of High-Altitude Aerodynamics of Reentry Capsules", *Rarefied Gas Dynamics 20*, edited by Ching Shen, Peking Univ. Press, Beijing, China, 1997, pp. 455-459.
5. Blanchard, R. C.; and Rutherford, J. F.: Shuttle Orbiter High Resolution Accelerometer Package Experiment: Preliminary Flight Results. *Journal of Spacecraft and Rockets*, vol. 22, no. 4, July-August 1985, pp. 474-480.
6. Blanchard, R. C.; and Buck, G. M.: Rarefied-Flow Aerodynamics and Thermosphere Structure From Shuttle Flight Measurements. *Journal of Spacecraft and Rockets*, vol. 24, no. 6, November-December 1987, pp. 504-507.

7. Blanchard, R. C., Larman, K. T. and Barret, M., "The High Resolution Accelerometer Package Flight Experiment Summary for the First 10 Flights," NASA Reference Publication 1267, April 1992.
8. Blanchard, R.C.: Rarefied Flow Lift-to-Drag Measurements of the Shuttle Orbiter. ICAS Paper 86-2.10.2, London, United Kingdom, September 1986.
9. Blanchard, R.C.; and Hinson, E.W.: Hypersonic Rarefied-Flow Aerodynamics Inferred from Shuttle Orbiter Acceleration Measurements. Paper No. 7 presented at the International Congress on Hypersonic Aerodynamics, Manchester, England, September 4-6, 1989.
10. Blanchard, R.C., Larman, K.T., Moats, C.D.; Rarefied-Flow Shuttle Aerodynamics Model, NASA TM 107698, February, 1993.
11. Blanchard, R.C., Hendrix, M.K., Fox, J.C., Thomas, D.J., and Nicholson, J.Y., "The Orbital Acceleration Research Experiment," Journal of Spacecraft and Rockets, vol. 24, no. 6, Nov.-Dec. 1987, pp. 504-511.
12. Blanchard, R.C., Nicholson, J.Y., and Ritter, J.R., "STS-40 Orbital Acceleration Research Experiment Flight Results During a Typical Sleep Period," Microgravity Science and Technology: International Journal of Microgravity Research and Applications, vol. 2, 1992, pp. 86-93.
13. Rogers, M.J.B.; Baugher, C.R.; Blanchard, R.C.; DeLombard, R.; Durgin, W.W.; Matthheisen, D.H.; Neupert, W.; and Roussel, P.: Low Gravity Environment On-board Columbia During STS-40. AIAA 93-0833, January 1993.
14. Blanchard, R. C.; Nicholson, J. Y.; and Ritter, J. R.: Absolute Acceleration Measurements on STS-50 from the Orbital Acceleration Research Experiment (OARE), Microgravity Science and Technology: International Journal of Microgravity Research and Applications, VII/1, March 1994, pp. 60-67.
15. Blanchard, R. C.; Nicholson, J. Y.; Ritter, J. R.; and Larman, K. T.: Orbital Acceleration Research Experiment Calibration Measurements, Journal of Spacecraft and Rockets, Vol. 32, No. 4, July-August, 1995, pp. 619-626.
16. Blanchard, R. C.; Wilmoth, R. G.; and LeBeau, G. J.: Rarefied-Flow Transition Regime Orbiter Aerodynamic Acceleration Flight Measurements. Journal of Spacecraft and Rockets, vol. 34, no. 1, Jan.-Feb. 1997, pp. 8-15.
17. Blanchard, R. C.; and Walberg, G. D.: Determination of the Hypersonic-Continuum/Rarefied-Flow Drag Coefficient of the Viking Lander Capsule I Aeroshell from Flight Data. NASA TP 1793, December 1980.
18. Blanchard, R. C.; Wilmoth, R. G.; and Moss, J. N.: Atmospheric Flight Measurements and Rarefied-Flow Simulations of Mars Entry Vehicles. Journal of Spacecraft and Rockets, vol. 34, no. 5, Sept.-Oct., 1997, pp. 687-690.
19. Spencer, D. A.; Blanchard, R. C.; Braun, R. D.; and Thurman, S. W.: Mars Pathfinder Atmospheric Entry Reconstruction. AAS Paper 98-146, AAS/AIAA Space Flight Mechanics Meeting, Monterey, CA, Feb. 9-11, 1998.
20. Moss, J. N.; Blanchard, R. C.; Wilmoth, R. G.; and Braun, R. D.: Mars Pathfinder Rarefied Aerodynamics: Computations and Measurements. AIAA Paper 98-0298, AIAA Aerospace Sciences Meeting, Reno, NV, Jan. 12-15, 1998.
21. Rault, D.F.G., "Aerodynamics of the Shuttle Orbiter at High Altitudes," Journal of Spacecraft and Rockets, vol. 31, no. 6, Nov.-Dec. 1994, pp. 944-952.
22. Wilmoth, R. G., LeBeau, G. J., and Carlson A. B., "DSMC Grid Methodologies for Computing Low-Density Hypersonic Flows About Reusable Launch Vehicles," AIAA Paper 96-1812, June 1996.

KINETIC THEORY AND MODELS - KTM 1

ROOM MARION

MONDAY, JULY 27, 1998

9:45

Initial Boundary Value Problem for the Boltzmann Equation in a Bounded Convex Domain *

K. Asano

Graduate School of Human and Environmental Studies
Kyoto University, Kyoto 606-8501, Japan

The density distribution of the rarefied gas particles is governed by the Boltzmann equation. We consider the initial boundary value problem for the Boltzmann equation with an external potential force in a bounded and strictly convex domain Ω in \mathbb{R}^3 (or $\mathbb{R}^n, n \geq 3$). We assume :

(A.1) The boundary $S = \partial\Omega$ is of class C^2 and the curvature tensor $\kappa(x)$ is positive definite at each $x \in S$.

(A.2) The external force $a(x) = -\nabla b(x)$ satisfies : $b(x) \in C^3(\bar{\Omega}), b(x) \geq 1$ and $\langle a(x), n(x) \rangle = 0$ at $x \in S$, where $n(x)$ is the inner unit normal at $x \in S$.

(A.3) The boundary condition is the specular reflection i.e. $\gamma^+ f(x, \xi) = \gamma^- f(x, \xi - 2 \langle n(x), \xi \rangle n(x)) =: C\gamma^- f(x, \xi)$. Here $\gamma^\pm f(x, \xi)$ describes the trace of f at $(x, \xi) \in S \times \mathbb{R}^3$ with $\langle n(x), \xi \rangle > 0 (< 0)$.

(A.4) The initial data $f_0(x, \xi)$ is a small fluctuation from an absolute Maxwellian $g_0(\xi) = (2\pi)^{-3/2} e^{-|\xi|^2/2}$ or from $g(x, \xi) = g_0(\xi) e^{-b(x)}$, $f_0(x, \xi) = g(x, \xi) + g(x, \xi)^{1/2} u_0(x, \xi), \|u_0\| \ll 1$.

We apply the Grad scheme and obtain the modified Boltzmann equation (B):

$$\partial_t u + \xi \cdot \nabla_x u + a(x) \cdot \nabla_\xi u = Lu + \Gamma[u, u],$$

$$\gamma^+ u = C\gamma^- u,$$

$$u|_{t=0} = u_0(x, \xi).$$

Then we have

THEOREM Under the assumptions (A.1)-(A.4), there exists a unique global solution $u(t, x, \xi) \in B([0, \infty); B(\Omega \times \mathbb{R}^3))$ of (B).

*Abstract 1831 submitted to the 21st International Symposium on Rarefied Gas Dynamics, Marseille, France, July 26-31, 1998

On the Smoothing Properties of a Model Boltzmann Equation Without Grad's Cutoff Assumption. *

L. Desvillettes¹, F. Golse²

¹ Département de Mathématiques, Université d'Orléans, France

² Université Paris 7 & Ecole Normale Supérieure, DMI, Paris, France

1 Introduction

It is well known that the cross section entering Boltzmann's collision integral is not integrable in the angular variable measuring the deviation of relative velocities before and after collisions when the interparticle force is proportional to r^{-s} (with r denoting the interparticle distance). In Ref. [8], Grad proposed to truncate this cross section in a way that corresponds physically to neglect grazing collisions. Most of the existing mathematical results on the Boltzmann equation are obtained under Grad's cutoff assumption or variants of it.

The space homogeneous Boltzmann equation without Grad's cutoff assumption (or closely related models such as the Kac model) has been considered in some recent publications: see Refs. [3], [4], [5], [13]. These papers show that the evolution semigroup associated to the space homogeneous Boltzmann equation is a smoothing operator for any positive time (just as, for example, the semigroup associated to the heat equation).

On the contrary, under Grad's cutoff assumption, the same semigroup never is a smoothing operator, for any positive time. Indeed, in the cutoff case, the evolution semigroup can be split into gain and loss part, and P.-L. Lions recently proved in [10] that the gain term has some regularizing properties; the remark above concerning the space homogeneous Boltzmann evolution semigroup follows easily from considering the integral formulation of the Boltzmann equation obtained by solving for the number density in terms of the gain part of the collision integral and the initial data: see Refs. [10], [14], [1].

To this date, no analogous result is known for the space inhomogeneous Boltzmann equation. In addition, the method used on the space homogeneous problem (Fourier transforming the equation in the

velocity variable) seems hopeless on the space inhomogeneous case.

In the present paper, we propose a different method that might help in attacking the space inhomogeneous case:

- 1] use the entropy production (estimated by the H theorem) to control fractional derivatives of the number density in the velocity variable;
- 2] apply the Velocity Averaging method (see Refs. [7], [6]) to obtain smoothness in (t, x, v) on quantities of the form

$$\int f(t, x, w) \chi(v, w) dw$$

for any smooth test function χ ; moreover, estimate the norm (in some Sobolev or Besov space) of such velocity average in terms of χ ;

- 3] replace χ by a suitable approximation of the identity and use the results of steps 1 and 2 above to finally obtain some regularity on f itself in the variables (t, x, v) .

This method is somewhat reminiscent of the work of P.-L. Lions [11] on the Landau-Fokker-Planck equation, except that one is looking for regularity estimates and not just compactness as in [11].

2 Main Result

In the present paper, we test the above method on the following very simple model Boltzmann equation:

$$\partial_t f + \cos(2\pi v) \partial_x f = Q(f), \quad t > 0, \quad x, v \in \mathbf{T}^1; \quad (1)$$

where $\mathbf{T}^1 = \mathbf{R}/2\pi\mathbf{Z}$, with collision operator

$$Q(f)(v) =$$

$$\int_{-1/2}^{1/2} \int_{\mathbf{T}^1} [f(v + \theta) f(w - \theta) - f(v) f(w)] b(\theta) dw d\theta \quad (2)$$

*Abstract 4532 submitted to the 21st International Symposium on Rarefied Gas Dynamics, Marseille, France, July 26-31, 1998

and where b is an even function on $[-1/2, 1/2]$ such that

$$C_0|\theta|^{-\gamma} \leq b(\theta) \leq C_1|\theta|^{-\gamma} \text{ for all } \theta \in [-1/2, 1/2] \quad (3)$$

with $0 < C_0 < C_1$ and $1 < \gamma < 3$.

This model is vaguely reminiscent of the well-known Kac model (see Ref.[9]), and also of a model recently considered by Cabannes and Sibgatullin (see Ref. [2]).

Next consider the Cauchy problem for (1) with the initial condition

$$f(0, x, v) = f_0(x, v), \quad (x, v) \in \mathbf{T}^1 \times \mathbf{T}^1. \quad (4)$$

Our main result is

Theorem. *Let b be an even function on $[-1/2, 1/2]$ satisfying (3) and let $f_0 \in L^\infty(\mathbf{T}^1 \times \mathbf{T}^1)$, with $f_0 \geq 0$ a.e.. Then the Cauchy problem (1)-(4) has a solution f in the Sobolev space $H^s(\mathbf{R}_+^* \times \mathbf{T}^1 \times \mathbf{T}^1)$ for all s such that*

$$0 \leq s < \frac{\gamma - 1}{2(\gamma + 1)(\gamma + 3)}.$$

If moreover $f_0 \geq R$ a.e. for some $R > 0$, then the same existence holds with the slightly better Sobolev regularity index s as follows:

$$0 \leq s < \frac{\gamma - 1}{2(\gamma + 1)^2}.$$

In particular, $f(t, \cdot, \cdot) \in H^s(\mathbf{T}^1 \times \mathbf{T}^1)$ for a.e. $t > 0$. However, we do not know whether the strategy outlined above can be iterated to prove that $f \in C^\infty$. It could be that this program applies to the Boltzmann equation after some suitable modifications (recently P.-L. Lions announced in Ref. [12] that step 1 can be achieved for the Boltzmann equation).

References

- [1] Bouchut F., Desvillettes L., A proof of the smoothing properties of the positive part of Boltzmann's kernel, to appear in Rev. Mat. Iberoam.
- [2] Cabannes H., Sibgatullin N., Math. Models and Methods Appl. Sci. **5**, (1995), no. 8, 1129-1138
- [3] Desvillettes L., Comm. Math. Phys., **168**, (1995), no. 2, 417-440.
- [4] Desvillettes L., Transport Theory Statist. Phys., **25**, (1996), no. 3-5, 383-394.

- [5] Desvillettes L., Transport Theory Statist. Phys., **26**, (1997), no. 3, 341-357.
- [6] DiPerna R., Lions P.-L., Comm. Pure Appl. Math., **42**, (1989), no. 6, 729-757.
- [7] Golse F., Lions P.-L., Perthame B., Sentis R., J. Funct. Anal., **76**, (1988), no. 1, 110-125.
- [8] Grad, H., *Principles of the kinetic theory of gases*, Flügge's Handbuch der Physik, **12**, (1958), 205-294.
- [9] Kac M., Foundations of Kinetic Theory; Proceedings of the 3rd Berkeley Symposium on Mathematical Statistics and Probability 1954-55, vol. III, pp. 171-197, U. of California Press, Berkeley and Los Angeles (1956).
- [10] Lions P.-L., I and II, J. Math. Kyoto Univ., **34**, (1994), no. 2, 391-427, 429-461. III, J. Math. Kyoto Univ., **34**, (1994), no. 3, 539-584.
- [11] Lions P.-L., Philos. Trans. Roy. Soc. London Ser. A, **346**, (1994), 191-204.
- [12] Lions P.-L., Régularité et compacité pour des noyaux de collision de Boltzmann sans troncature angulaire, preprint.
- [13] Proutière A., New results of regularization for weak solutions of Boltzmann equation, preprint.
- [14] Wennberg B., Comm. Part. Diff. Eq., **19**, no. 11-12, (1994), 2057-2074.

On Stationary and Timedependent Solutions to the Linear Boltzmann Equation *

R. Pettersson

Department of Mathematics, Chalmers University of Technology,
S-412 96 Göteborg, Sweden

Introduction

The linear Boltzmann equation is frequently used for mathematical modelling in physics, (e.g. for describing the neutron distribution in reactor physics), cf. refs. [1]-[4].

One fundamental question concerns the longtime behavior of the function $f(x, v, t)$ representing the distribution of particles, in particular the problem of convergence to a stationary equilibrium solution, when time goes to infinity.

In our earlier papers, cf. [5]-[7], we have studied such convergence to equilibrium for the space-dependent linear Boltzmann equation with general boundary conditions and general initial data, under the assumption of existence of a corresponding stationary solution. For the proofs we use iterate functions, defined by an exponential form of the equation together with the boundary conditions, and we also use a general relative entropy functional for the quotient of the timedependent and the stationary solutions.

Problems and Results

One fundamental question in Kinetics concern existence and uniqueness of stationary solutions to the space-dependent transport equation, with given (general) distribution function for the host particles and (general) collision mechanism (including the case of inverse power forces), together with (general) boundary conditions (including the periodic, specular and diffuse cases). We will study this problem, using our earlier methods with iterate functions f_n (representing the distribution of particles having undergone at most n collisions), together with our general relative entropy functional, cf. ref. [8]. Cf. also the methods in ref. [9].

References

- [1] Bellomo, N. Palczewski, A., and Toscani, G., *Mathematical topics in nonlinear Kinetic theory*, World Scientific, (1989).
- [2] Cercignani, C., *The Boltzmann equation and its applications*, Springer-Verlag, (1988).
- [3] Greenberg, W., van der Mec, C., and Protopopescue, V., *Boundary value problems in abstract Kinetic theory*, Birkhauser-Verlag, (1987).
- [4] Truessedell, C., and Muncaster, R. G., *Fundamentals of Maxwell's Kinetic theory of a simple monoatomic gas*, Academic Press, (1980).
- [5] Pettersson, R., *On solutions to the linear Boltzmann equation with general boundary conditions and infinite range forces*, J. Stat. Phys., 59, 403-440(1990).
- [6] Pettersson, R., *On weak and strong convergence to equilibrium for solutions to the linear Boltzmann equation*, J. Stat. Phys., 72, 355-380(1993).
- [7] Pettersson, R., *On convergence to equilibrium for the linear Boltzmann equation without detailed balance assumptions*, Proc. 19th RGD, Oxford, 107-113(1994).
- [8] Pettersson, R., *On stationary solutions to the linear Boltzmann equation with general boundary conditions*, (in preparation), (1998).
- [9] Lasota, A., and Mackey, M., *Chaos, fractals and noise, Stochastic aspects of dynamics*, Springer, (1994).

*Abstract 5386 submitted to the 21st International Symposium on Rarefied Gas Dynamics, Marseille, France, July 26-31, 1998

KINETIC THEORY AND MODELS - KTM 2

ROOM MARION

MONDAY, JULY 27, 1998

11:00

"Eternal" Solutions for a Semi-Continuous Model of the Two-Dimensional Boltzmann Equation *

H. Cabannes

Lab. de Modélisation en Mécanique, Université P. et M. Curie, Paris, France

We study the following model of the Boltzmann equation:

$$\frac{\partial N(t; \theta)}{\partial t} = \frac{1}{2\pi} \int_0^{2\pi} \{N^2(t; \varphi) - N^2(t; \theta)\} d\varphi \quad (1)$$

where $N(t; \theta)$, a density, is a π -periodic function of the angle θ . We have obtained the following results.

1 °) To equation (1) is associated the classical $H(t)$ Boltzmann function, but also an infinite number of "entropy functions", $G_{2n+1}(t)$, that means decreasing functions of the time.

$$H(t) = \frac{1}{2\pi} \int_0^{2\pi} N(t; \theta) \text{Log}[N(t; \theta)] d\theta, \\ \text{with } N(t; \theta) > 0,$$

$$G_{2n+1}(t) = \frac{1}{2\pi} \int_0^{2\pi} N^{2n+1}(t; \theta) d\theta, \\ \text{with } n \text{ integer.}$$

2 °) The integration of equation 1, a **nonlinear** integro-differential equation, has been reduced to the integration of a **linear** ordinary differential equation. Then we have been able to obtain the general solution on a parametric form: $t = \bar{t}(x)$, $N(t; \theta) = \bar{N}(x; \theta)$.

3 °) Studying the initial value problem to the future, we recognize if the solution blows up, or exists for all positive times. The last case corresponds to a positive initial density $N(0; \theta)$, and in some cases to a partially negative initial density. The conditions for global existence to the future concern only the minimum of the initial density.

4 °) Studying the initial value problem to the past, we recognize if the solution blows up (to the past) or exists for all negative times. The conditions of global existence to the past concern only the maximum of the initial density.

5 °) Using the former results we have built an family of "eternal" solutions (solutions valid for all positive and negative times). A conjecture says that the only "eternal" solutions of the Boltzmann equation are the maxwellian solutions. Our work is a contribution to the study of this conjecture, but also for equation 1 the problem is still open.

*Abstract 1301 submitted to the 21st International Symposium on Rarefied Gas Dynamics, Marseille, France, July 26-31, 1998

Gradient Expansions for Distribution Functions and Derivation of Moment Equations *

T.G. Elizarova¹, J.C. Lengrand², I.A. Graur¹

¹ Institute of Mathematical Modeling, Russian Academy of Sciences, Moscow, Russia

² Lab. d'Aérodynamique du CNRS, Meudon, France

1 Moment equations

To obtain the equations for viscous gas flows (Navier-Stokes (NS) equations), one retains the first order terms in a series expansion of the distribution function. The form of this approximation (function f^{NS}) was obtained as a result of the Chapman-Enskog procedure. The formal change

$$f \rightarrow f^{NS}$$

in the convective term of Boltzmann equation (BE)

$$\frac{\partial f}{\partial t} + (\xi \nabla) f = \mathcal{I}$$

results in the approximation

$$\frac{\partial f}{\partial t} + (\xi \nabla) f^{NS} = \mathcal{I},$$

and finally in NS equation system after multiplication by collisional invariants and averaging over velocity space.

In place of f^{NS} the authors propose to use other variants of series expansions, namely gradient expansions, that are very similar to NS ones and result in a family of systems of momentum equations.

The first variant (QGD gradient expansion) is

$$f^{QGD} = f_0 - \tau(\xi \nabla) f_0,$$

where f_0 is the local maxwellian distribution function and τ is the maxwellian relaxation time. The formal change

$$f \rightarrow f^{QGD}$$

in the convective term of BE results in

$$\frac{\partial f}{\partial t} + (\xi \nabla) f_0 - (\xi \nabla) \tau (\xi \nabla) f_0 = \mathcal{I}.$$

Averaging this approximation after multiplication by collisional invariants (and introducing Prandtl number Pr and specific heat ratio γ for generalization purpose) results in a system of moment equations that describes viscous and heat conductive flows: quasigasdynamic (QGD) equations. This model was used successfully to describe gas flows, including rarefied ones and it presented some advantages compared with NS one [1].

Another gradient expansion (QGD 3T) allows to generalize QGD equations to flows of monoatomic gas with translational nonequilibrium, i.e., with anisotropy of the distribution function. We use the approximation

$$f \rightarrow f^{QGD3T} \text{ where } f^{QGD3T} = f_e - \tau(\xi \nabla) f_e$$

and f_e is an ellipsoidal distribution function, built with different translational temperatures in different directions. Now the approximation of BE is

$$\frac{\partial f}{\partial t} + (\xi \nabla) f_e - (\xi \nabla) \tau (\xi \nabla) f_e = \mathcal{I}.$$

This equation is multiplied successively by $1, \xi, \xi_i^2/2$ and averaged over the velocity space to yield the QGD 3T equations. Because the ξ_i^2 are not collisional invariants, exchange terms appear in the equations that govern the evolution of energy in the different directions. It was shown that accounting for temperature nonequilibrium results in a better description of, e.g., shock-wave structure [2].

To model rarefied flows with nonequilibrium between translational and rotational temperatures a so-called QGDR approximation was used

$$f \rightarrow f^{QGDR},$$

where a new gradient expansion is introduced

$$f^{QGDR} = f_{0r} - \tau(\xi \nabla) f_{0r}.$$

*Abstract 2057 submitted to the 21st International Symposium on Rarefied Gas Dynamics, Marseille, France, July 26-31, 1998

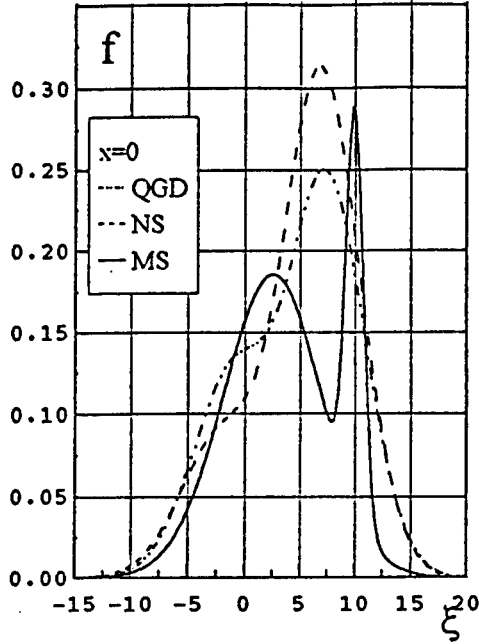


Figure 1: Distribution function in the center of shock wave for $Ma = 10$

$f_{0r} = f_0 \times f_r$, and f_r is the Hinshelwood distribution function for rotational energy in di- or polyatomic molecules [3]. The approximation for BE becomes

$$\frac{\partial f}{\partial t} + (\xi \nabla) f_{0r} - (\xi \nabla) \tau (\xi \nabla) f_{0r} = \mathcal{I}$$

that results finally in QGDR moment equations. QGDR equations for a 1D plane flow of a gas with 2 rotational degrees of freedom are presented in [4]. The flow parameters obtained for the shock wave problem are closed to those computed by kinetic models.

2 QGD and NS distribution functions

Differentiating function f_0 with respect to x_i , f^{QGD} writes

$$f^{QGD} = f_0(1 + \tau \mathcal{P}_3^{QGD}(\xi_i)),$$

where \mathcal{P}_3^{QGD} is a polynomial of degree 3 in ξ_i . Similarly, the NS distribution function writes

$$f^{NS} = f_0(1 + \tau \mathcal{P}_3^{NS}(\xi_i))$$

where the viscosity coefficient is identified as $\mu = p\tau$.

Thus NS and QGD distribution functions can both be written as a series expansion in τ . In the par-

ticular case $\gamma = 5/3$, $Pr = 1$, the coefficient for the terms containing ξ_i^3 are identical

$$a_{QGD}^{(3)} = \frac{-1}{2RT^2} \frac{\partial T}{\partial x_i} \text{ and } a_{NS}^{(3)} = \frac{-\gamma}{5Pr(\gamma-1)} \frac{1}{RT^2} \frac{\partial T}{\partial x_i}.$$

Thus functions f^{NS} and f^{QGD} have the same asymptotic behavior along the axes for large values of ξ_i . Most other coefficients are identical except for the numerical factors.

The comparison of QGD, NS and MS (Mott-Smith) distribution functions in the "center" of a shock wave (where $\rho = (\rho_1 + \rho_2)/2$) is shown in Fig.1 for a gas of Maxwell molecules. The distribution functions are plotted against ξ_x for $\xi_y = \xi_z = 0$.

3 Results and conclusions

The comparison of distribution functions confirms that f^{QGD} is a reasonable approximation of the actual distribution function f . In a shock wave, it is close to (for small Mach numbers) or better than (for large Mach numbers) f^{NS} . Approximations of the distribution function in the form of gradient expansions allow to derive moment equations that describe not only viscous (QGD) flows, but also flows with translational (QGD 3T) or rotational (QGDR) nonequilibrium.

The full paper will include comparisons with DSMC results for this and other problems.

References

- [1] Elizarova T.G, Graur I.A, Lengrand J.C, Chpoun A., *Rarefied Gas Flow Simulation Based on Quasigasdynamic Equations*, AIAA J., 1995, V.33, No.12, pp.2316-2324.
- [2] Graur I.A., Elizarova T.G, Lengrand J.C., *Calculation of Shock Wave Structure Based on QGD Model with Multiple Translational Temperatures*, Proc. 21th Intern. Symp. on Shock Waves, Great Keppel, Australia, July 23-28, 1997 (to be published).
- [3] Bird G.A., *Molecular Gas Dynamics and the Direct Simulation of Gas Flows*, Clarendon Press. Oxford, 1994.
- [4] Chirokov I.A., Elizarova T.G., Lengrand J.C., *Numerical Study of Shock Wave Structure Based on Quasigasdynamic Equations with Rotational Nonequilibrium*, this symposium.

Anomalous Sound Dispersion in Two-Component Systems *

B.D. Shizgal, D.G. Napier
University of British Columbia, Vancouver, Canada

1 Introduction

Recent experimental studies of sound propagation in mixtures of gases have demonstrated a new set of dispersion behaviours that are not described by conventional hydrodynamic treatments [1-8]. These anomalous properties have been measured in mixtures of gases of disparate mass. Some experiments have shown the existence of sound modes with propagation velocities and attenuation rates that exhibit significantly different characteristics than hydrodynamic modes. This phenomenon is attributed to the decoupling of the light and heavy components when the frequency of sound approaches the order of the collisional frequency of the gas mixture. Related phenomena, such as sound mode degeneracies and propagation gaps at critical frequencies and gas composition have also been studied in these systems [1, 8].

Huck and Johnson [9] were the first to suggest the possibility of measuring fast and slow sound propagation modes in a gas mixtures. They termed this 'double sound propagation'. The term 'fast sound' describes the mode that propagates exclusively through the light component was coined by Bosse et al. [11]. Campa and Cohen [12] later predicted the existence of fast sound modes in mixtures of dilute binary fluids using a BGK model of a modified Enskog fluid. Their calculations indicated the existence of fast sound modes that propagate only through the light component at much higher velocity than ordinary sound. Experimental data has since revealed the existence of analogous slow sound modes.

The first experimental measurement of fast-propagating free sound waves was in He-Ne mixtures using neutron scattering [3]. Rayleigh-Brillouin light scattering revealed slow sound in He-Xe mixtures [5]. Both fast and slow sound modes were then later observed through light scattering in H₂-Xe and H₂-Ar mixtures [4, 6, 7]. Other studies reported fast sound in H₂-Ar and slow sound in

H₂-SF₆ [2]. All theoretical analyses of experimental data has so far used two-temperature hydrodynamics [1, 4, 10] based on Burger's representation of a homogeneous multi-component fluid [13].

Recent experimental data obtained from Rayleigh-Brillouin scattering has shown anomalous sound dispersion behaviour in multicomponent gases at large Knudsen number, Kn . All current theoretical approaches provide only qualitative agreement with experiment for small Kn . The treatment of Cohen and Campa has only been applied to simple model systems (BGK treatment of hard-sphere Enskog fluids) [12]. Gas kinetic approaches are an obvious method for exploring anomalous sound dispersion phenomena since anomalous sound behaviour is frequently observed near the limits of the hydrodynamic region [1, 4].

The purpose of this work is to apply a gas kinetic theory of mixtures to small-amplitude oscillations near or in the Knudsen region of a gas. Experimental data suggests that oscillatory disturbances in gases exhibit complicated behaviour in this region [1-8]. This work attempts to examine and interpret non-hydrodynamic behaviour observed in real systems using methods of gas kinetic theory. The method used here has been used to successfully reproduce the behaviour of simple gas systems but the present work is the first known application to mixtures gases of disparate mass.

2 Method

Consider a dilute mixture of gases labeled 1 and 2 where the distribution functions are given by two coupled Boltzmann equations

$$\left(\frac{\partial}{\partial t} + \mathbf{c} \cdot \nabla\right) f_1 = J_{11}(f_1) + J_{12}(f_1, f_2) \quad (1)$$

$$\left(\frac{\partial}{\partial t} + \mathbf{c} \cdot \nabla\right) f_2 = J_{22}(f_2) + J_{21}(f_1, f_2) \quad (2)$$

where $J_{\eta\gamma}$ is the Boltzmann cross collision term. The velocity distribution functions, f_η are close to a Maxwellian distribution, characterized by the number density n_γ and a common temperature T .

* Abstract 2776 submitted to the 21st International Symposium on Rarefied Gas Dynamics, Marseille, France, July 26-31, 1998

The distribution function for species η is written as a Maxwellian perturbed by a small term h_η , $f_\eta(\mathbf{c}, \mathbf{r}, t) = f_\eta^{(0)}(\mathbf{c})[1 + h_\eta(\mathbf{c}, \mathbf{r}, t)]$. The linearized Boltzmann equation is

$$\left(\frac{\partial}{\partial t} + \mathbf{c} \cdot \nabla\right) h_\eta = [\kappa_\eta K_{\eta\eta} + \kappa_{\eta\gamma} L_{\eta\gamma}] h_\eta + L_{\gamma\gamma} h_\gamma \quad (3)$$

where the $K_{\eta\eta}$ operator corresponds to the linearized self-collision while linearized cross collision terms are given by $L_{\eta\gamma}$ and $L_{\gamma\eta}$. A pressure fluctuation propagating as a plane wave perturbs the system in the manner $h(\mathbf{c}_\eta, \mathbf{r}, t) = h_\eta(\mathbf{c}_\eta) e^{i(\mathbf{k} \cdot \mathbf{r} - \omega t)}$ where $\hat{\mathbf{k}}$ defines the direction of propagation and ω is the frequency of the oscillation.

The perturbation h_η is written as an expansion in axially-symmetric Burnett functions $\psi_{nl}^{(\eta)}(\xi_\eta, \theta)$

$$h_\eta(\xi_\eta, \mu) = \sum_{n,l=0}^{\infty} a_{nl}^{(\eta)} \psi_{nl}^{(\eta)}(\xi_\eta, \theta) \quad (4)$$

and substituted into the linearized Boltzmann equation, Eq. (3). Multiplying the Boltzmann equation by each basis function and integrating over the reduced velocities, ξ_η , gives an infinite set of coupled homogeneous linear equations in $a_{nl}^{(\eta)}$. A series truncation scheme using an extension to the Gross-Jackson method suggested by Sirovich and Thurber [14] was used to reduce the set of linear equations to a matrix. The secular determinant of the matrix gave a dispersion relation for sound propagation in a two-component mixture. The roots of the dispersion relation were computed for some physical systems using the simple model of Maxwell molecules. Sound phase velocities and attenuations were calculated using masses and collision cross sections corresponding to He-Xe mixtures for which experimental data is available [1]. The calculations performed on the He-Xe system show that it is feasible to apply the above method to a real system.

3 Conclusions

In spite of the overall success in modelling the acoustical properties of gases, there are some major defects common to gas kinetic treatments. In hydrodynamic calculations, any thermodynamic and transport coefficients for any system can be obtained from empirical data and inserted into the equations. In gas kinetic theory, one cannot do this without modifying the transport properties. Internal degrees of freedom can also be incorporated into

hydrodynamic equations through phenomenological data and should, in principle, be modelled using inelastic Boltzmann collision terms. Another deficiency arises from the effects of modelling interatomic potentials. Phase velocities and attenuation coefficients provide only a simple check of the validity of the present model. Comparisons with light-scattering data should provide a more comprehensive test in the future.

References

- [1] J. R. Bowler and E. A. Johnson, Proc. R. Soc. Lond. A, **408**, 79 (1986).
- [2] M.J. Clouter, H. Luo, H. Kieft and J. A. Zollweg, Phys. Rev. A, **41**, 2239 (1990).
- [3] M. Montfrooij, P. Westerhuijs, V. O. de Haan, I. M. de Schepper, Phys. Rev. Lett., **63**, 544 (1989).
- [4] R.P.C. Schram and G.H. Wegdam Physica A, **203**, 33 (1994).
- [5] G.H. Wegdam and H. M. Schaink, Phys. Rev. A, **41**, 3419 (1990).
- [6] G.H. Wegdam, A. Bot, R.P.C. Schram and H. M. Schaink, Phys. Rev. Lett., **63**, 2697 (1989).
- [7] G.H. Wegdam and H. M. Schaink, Phys. Rev. A, **41**, 3419 (1990).
- [8] R.P.C. Schram, G.H. Wegdam and A. Bot, Phys. Rev. A, **44**, 8062 (1991).
- [9] R. J. Huck and E.A. Johnson, Phys Rev. Lett, **44**, 142 (1980).
- [10] E. A. Johnson, J. Stat. Phys., **57**, 3, 647 (1989).
- [11] J. Bosse, J. Jacucci, M. Ronchetti and W. Schirmacher, Phys Rev. Lett, **57**, 3277 (1986).
- [12] A. Campa and E. G. D. Cohen, Phys. Rev. Lett., **61**, 853
- [13] J. M. Burgers, *Flow Equations for Composite Gases*, Academic Press, New York (1969). (1988).
- [14] L. Sirovich and J.K. Thurber, J. Acoustical Soc. Amer., **38**, 3, 1 (1965).

KINETIC THEORY AND MODELS - KTM 3

ROOM MARION

MONDAY, JULY 27, 1998

14:40

Levermore's Moment Closure of Discrete Boltzmann Equations for Non-Equilibrium Kinetic Flows *

P. Charrier¹, B. Dubroca,² J.L. Feugeas^{1,2}

¹ Mathématiques Appliquées, Université Bordeaux I, France

² CEA/CESTA, Le Barp, France

1 Introduction

Computation of high altitude flows in the transitional regime between the kinetic and continuum limit are known to be difficult. Indeed, the flow is far from kinetic equilibrium and the Navier-Stokes equations are not enough accurate in boundary layers or across shock fronts. On the other hand, usual numerical methods for Boltzmann equations (like Monte Carlo method for example) are quite expensive in the transitional regime where the free mean path is small.

H. Grad proposed in [3] to increase the number of unknowns by considering anisotropic pressure and heat flux for example. The additional equations are obtained by closure of Boltzmann equations and involve some source terms that include moments of collision operator. Unfortunately, The Grad's system loses its hyperbolicity property for Mach greater than 1, 5.

To overcome this problem, D. Levermore in [4] proposed a closure based on a distribution function of the form $f(x, v, t) = \exp(\alpha(x, t) \cdot m(v))$. Every system derived is hyperbolic and possesses a locally dissipated entropy. However, these systems are not explicitly known. Indeed the physical fluxes are defined as the integral of exponential of polynomial of order 4 or more, and cannot be expressed explicitly. Moreover, the model does not possess the property of the realizability of its predicted moments.

To solve these problems, we proposed in [2] to apply the Levermore's closure at the discrete BGK Boltzmann equations. We obtain systems with the same properties (hyperbolicity, dissipation of entropy). But, these systems are explicitly known and hence can be used for numerical computation. Moreover, our discrete model possesses the property of the realizability of its predicted moments which guaran-

tees that it cannot break down for some time.

A short summary about the construction of our model will be given in section 2. Some numerical examples are showed in section 3.

2 Discrete 14-moment closure

In what follows, V denotes a finite mesh of velocity space. If we note $f = (f_k)_{k \in V}$ a function defined on V then $\langle f \rangle = \sum_{k \in V} f_k$ is the average of f over the space of velocity. We can write now the discrete Boltzmann BGK equations:

$$\frac{\partial f_k}{\partial t} + \vec{v}_k \cdot \nabla_x f_k = \frac{1}{\tau} (\mathcal{E}(f)_k - f_k) \quad (1)$$

$\mathcal{E}(f)$ is the discrete equilibrium function which verifies the *minimum entropy principle*:

$$\begin{aligned} \mathcal{E}(f) &= \min_{g \in \mathcal{A}(f)} \langle g \ln g \rangle \\ \mathcal{A}(f) &= \{g \geq 0 / \langle g \vec{m}_e \rangle = \langle f \vec{m}_e \rangle\} \end{aligned}$$

where $\vec{m}_e = (1, \vec{v}, |\vec{v}|^2)$ denotes the vector of collisional invariants. Indeed, $\mathcal{A}(f)$ is the set of admissible functions which realize the moments of f over the space of collisional invariants.

As in [4], we close the system of moment based on (1) by introducing a function which verifies an *generalized minimum entropy principle*. For this goal, we take into account the anisotropic pressure and heat flux as new unknowns by setting $\vec{m} = (1, \vec{v}, \vec{v} \wedge \vec{v}, |\vec{v}|^2, |\vec{v}|^4)$. If $\vec{\rho}$ is a vector of admissible moments (obtained from a positive discrete distribution function) then we search a function solution of the following problem:

$$f = \min_{g \in \mathcal{A}(\vec{\rho})} \langle g \ln g \rangle \quad (2)$$

$$\mathcal{A}(\vec{\rho}) = \{g \geq 0 / \langle g \vec{m} \rangle = \vec{\rho}\} \quad (3)$$

With this choice, the problem (2,3) has a unique solution. Moreover if there exists $g > 0 \in \mathcal{A}(\vec{\rho})$ the

*Abstract 1521 submitted to the 21st International Symposium on Rarefied Gas Dynamics, Marseille, France, July 26-31, 1998

	14 discrete moments [2]	DSMC (Bird) [1]	14 quadrature moments [4]
Slip velocity	3.8 m/s	5 m/s	6.2 m/s
Slip temperature	1.4 K	1.4 k	2 K
Steady pressure	0.55 Nm ²	0.549 Nm ²	0.5497 Nm ²
Density extent	9.13 10 ⁻⁶ kg/m ³	9.1 10 ⁻⁶ kg/m ³	9.1 10 ⁻⁶ kg/m ³
Temperature extent	293.4 K	290 K	290 K

Table 1: Transitional Couette flow computation by different methods

solution of (2,3) takes the form $f = \exp(\vec{\alpha} \cdot \vec{m})$ where the vector $\vec{\alpha}$ depends only on vector $\vec{\rho}$. Indeed, this property implies that our model possesses the property of the realizability of its predicted moments. Now, we can write our moment closure:

$$\frac{\partial \vec{\rho}}{\partial t} + \nabla_x \cdot \vec{j}(\vec{\rho}) = \frac{1}{\tau} (\mathcal{E}(\vec{\rho}) - \vec{\rho}) \quad (4)$$

with $\vec{j}(\vec{\rho}) = \langle \vec{v} \wedge \vec{m} f \rangle$ where f is the solution of (2,3) and $\mathcal{E}(\vec{\rho}) = \langle \vec{m} \mathcal{E}(f) \rangle$ where $\mathcal{E}(f)$ is the discrete equilibrium Maxwellian associated with f .

Finally we can state our main result which insures that our system is well posed:

Theorem. *the system (4) is hyperbolic and has an entropy which is locally dissipated. Moreover the system possesses the property of the realizability of its predicted moments and cannot break down in finite time.*

To compute steady solution, we use a linearized time implicit scheme. This scheme improves the convergence and moreover the linearization with respect to $\vec{\alpha}$ avoids solving non linear problems to compute $\vec{\alpha}$ from $\vec{\rho}$ at each time step and each mesh point.

3 Numerical Results

The numerical results of table 1 show results obtained for one dimensional Couette flow computation ($T_{\text{wall}} = 273$ K, $V_{\text{wall}} = 0$ and 300 m/s). We compare our results with other contributions issued from [1, 5]. Temperature and velocity jumps at the wall are predicted by Knudsen Layer theory. Moreover the strength of these jumps are in good ad-equation with other papers.

Now we consider a two dimensional computation around a flat plane: the infinity Mach number is 4. Figure 1 shows a cross section profile of pressure at $x = 0.45$ m. We can observe the linear decrease of pressure near the wall. This effect characterizes the Knudsen layer and shows the capability of our model to compute transitional flows.

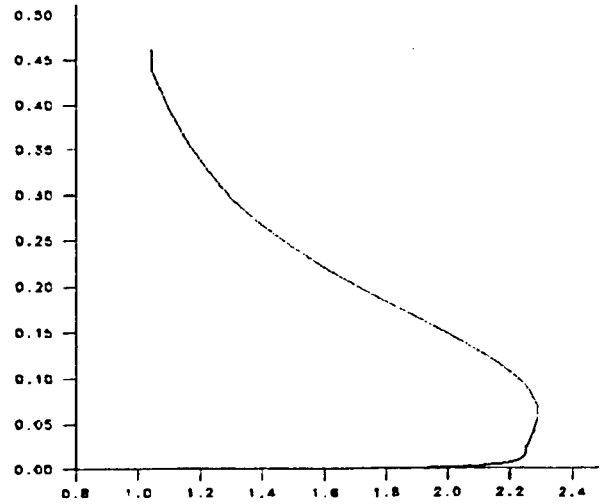


Figure 1: Pressure profile normal to the ramp

References

- [1] G.A. BIRD. *Molecular Gas Dynamics and The Direct Simulation of Gas Flows*, volume 42 of *Oxford Engineering Science Series*. Oxford Science Publications.
- [2] J.L. FEUGEAS. *Etude Numérique des Systèmes aux Moments de Levermore pour la Modélisation d'Écoulements Bidimensionnels Hors Équilibre Cinétique*. PhD thesis, University of Bordeaux I, November 1997.
- [3] H. GRAD. *On the Kinetic Theory of the Rarefied Gases*, *Comm. Pure & Appl. Math.*, Vol. II, pp. 331-407, 1949.
- [4] D. LEVERMORE. *Moment Closure Hierarchies for Kinetic Theories*, *J. Stat. Phys.*, Vol. 83, 1996.
- [5] P. LE TALLEC and J.P. PERLAT. *Numerical Analysis of the Levermore's Moment System*, INRIA Research Report 3124, 1997.

The Moment Method and Non-Equilibrium Thermodynamics of Rarefied Gases *

V.I. Roldughin¹, V.M. Zhdanov²

¹ Institute of Physical Chemistry, Moscow, Russia

² Moscow Engineering Physics Inst., Moscow, Russia

The methods of kinetic theory are often used to verify the ranges of the applicability of the phenomenological non-equilibrium thermodynamics. In the papers [1] the widely distributed opinion was refuted on the inapplicability of non-equilibrium thermodynamics methods to the problems, in which Navier-Stokes hydrodynamics gives unsatisfactory description of transport processes. It was shown that linearized version The linearized version of the Chapman-Enskog theory in any approximation completely coincides with the principles of non-equilibrium thermodynamics. In particular, this is true for the linearized Burnett approximation. For this approximation, the local entropy production contains the terms proportional to the second derivatives of the gas velocity and temperature. There are "nonphysical" terms providing the Onsager relations feasibility in the entropy production.

Grad was the first to mention the possibility for application of the non-equilibrium thermodynamics to the non-equilibrium uniform gases under the conditions when gas state is determined not only by the local gas density and temperature but any additional state parameters (the moments of distribution function). This idea was later developed in the framework of so-called Extended Irreversible Thermodynamics (EIT). The EIT uses as additional state parameters the heat flux and stress tensor.

The EIT deals with the situations when the characteristic time of the problem under consideration is comparable with the time of relaxation due to molecular collisions. This requires to use the non-stationary moment equations. But the space derivatives of the fluxes (moments) of different tensor ranks were not taken into account. These derivatives give contribution to the heat flux and the stress tensor leading them out of the framework of the standard linear transfer equations of the non-

equilibrium thermodynamics. However, one can show that the generalization mentioned is not in contradiction with non-equilibrium thermodynamics, while the thermodynamic forces are complicated, the entropy production has the classical form of bilinear combination of generalized thermodynamic forces and fluxes. The system of phenomenological equations expands due to taking into account additional moments of the distribution function, but the cross coefficients for the fluxes of the same tensor rank obey the Onsager relations.

In this work we generalize the non-equilibrium thermodynamics in the manner outlined above. In this way, the entropy production was derived on the basis of distribution function of non-equilibrium gas. The distribution function is expanded in a series in orthogonal tensor polynomials. The polynomials are productions of Sonin polynomials by the tensor spherical harmonics. The linearized moment equations derived by the kinetic theory were also used. Using the perturbation theory with respect to the small Knudsen number we deduced the phenomenological equations of non-equilibrium thermodynamics corresponding to the Burnett approximation of the kinetic theory. The required kinetic coefficients were calculated.

References

- [1] Roldughin V.I., *The Chapman-Enskog Theory and Non-equilibrium Thermodynamics*, J. of Non-Equilib. Thermodyn., Vol.9, No.1, pp.71-80, 1984.

* Abstract 5131 submitted to the 21st International Symposium on Rarefied Gas Dynamics, Marseille, France, July 26-31, 1998

Moment Equations Based on the First Order Chapman-Enskog Solution II -Relativistic Gas- *

L.H. Söderholm, N. Yoshida

Department of Mechanics, Royal Institute of Technology, Stockholm, Sweden

1 Introduction

In 1963 Cercignani [1] improved the moment theory of the kinetic layer in pure shear flow and showed the first order Chapman-Enskog [2] solution, rather than the corresponding Hermite polynomials, to be suitable for the analysis. In the same way, Söderholm [3] derived new 13 moments equations correct to first order in the Knudsen number, with the same general form as Grad's [4], but with correct values of viscosity and heat conductivity.

The Grad 13 moments method gives the Navier-Stokes equations with Fourier's expression for the heat current but with lowest order values only for viscosity and heat conductivity in terms of Sonine polynomials. In ref [3] the corresponding values for the relaxation times and the couplings between heat current and viscous pressure were also calculated.

In this work we apply a similar method to relativistic gas dynamics. In the case of flow in the relativistic regime there is a non-vanishing volume viscosity also for particles with no inner degrees of freedom. The simplest truncation thus leads to 14 rather than 13 moments. The full first order Chapman-Enskog solution is used as a basis to analyze a flow of two length scales.

2 Relativistic Gas

In the early sixties several authors, see de Groot et al [5] and references cited there, extended the classical methods of Chapman and Enskog and of Grad to the domain of relativity. See also Israel [6], Stewart [7], and Hiscock and Lindblom [8]. In the relativistic regime moment equations have

attracted particular attention as they solve the problem with causality. The diffusive kind of equations, like (the relativistic extension of) the Navier-Stokes equations, give an infinite speed of propagation of some disturbances in the rest frame of the fluid, which relativistically means a violation of causality.

Because of the complex form of the Jüttner function, which is the relativistic local equilibrium distribution function, we cannot make use of classical orthogonal polynomials such as the Sonine polynomials employed in the determination of the transport coefficients in the classical theory. As an alternative, de Groot et al [5] used an infinite series in powers of a dimensionless variable related to the particle energy. The coefficient functions are approximated to any desired degree of accuracy by the polynomials. We take the same approach in this work.

3 14 Moment Equations

The flow is assumed basically to have a length scale, which is large compared to the mean free path. From this length scale the Knudsen number is formed. The flow also has a small perturbation, the size of which is given by the Knudsen number, but with a length scale, which is allowed to approach the mean free path.

$$f = f^{(0)}(1 + \phi).$$

$f^{(0)}$ is shown to be the Maxwell-Jüttner function. The function ϕ satisfies the linearized Boltzmann equation. To obtain a solution for ϕ , the deviation function, we formulate our Ansatz as

$$\phi = \frac{1}{nk_B T} \left(\hat{A}\Pi + \frac{3}{c}\hat{B}_\mu q^\mu + 5\hat{C}^{\mu\nu}\check{\Pi}_{\mu\nu} \right).$$

$\Pi^{\mu\nu}$ is the viscous pressure tensor, $\check{\Pi}^{\mu\nu}$ its traceless

*Abstract 5396 submitted to the 21st International Symposium on Rarefied Gas Dynamics, Marseille, France, July 26-31, 1998

part, and Π its trace. \hat{A} , \hat{B}_μ , $\hat{C}^{\mu\nu}$ are, up to normalizing factors, the scalar, vector and tensor contributions of the first-order Chapman-Enskog solution. If Π , q^μ , $\check{\Pi}_{\mu\nu}$ are given their values for the relativistic Navier-Stokes-Fourier equations, this Ansatz reduces precisely to the first-order Chapman-Enskog solution. Here, however, the moments Π , q^μ , $\check{\Pi}_{\mu\nu}$ are in the Ansatz arbitrary functions of space and time. Inserting this Ansatz into the linearized Boltzmann equation and applying a symmetric Galerkin method, we obtain the appropriate 14 moments equations for Π , q^μ , $\check{\Pi}_{\mu\nu}$.

If we truncate the above-mentioned expansions in the dimensionless energy of the Chapman-Enskog functions \hat{A} , \hat{B}_μ , $\hat{C}^{\mu\nu}$ after the first non-trivial terms, our Ansatz reduces to that of the 14 moment approximation, see de Groot et al [5]. The corresponding equations are of the form

$$\frac{1}{\eta_\nu} \Pi + \frac{1}{nk_B T} (\varphi_p \mathbf{D} \Pi - \varphi_q \nabla_\mu q^\mu) + \nabla_\mu U^\mu = 0$$

$$\frac{1}{\lambda T} q^\mu + \frac{1}{nk_B T} (\vartheta_q \mathbf{D} q^\mu + \vartheta_\nu \nabla_\nu \check{\Pi}^{\mu\nu} + \vartheta_p \nabla^\mu \Pi) - \frac{\nabla^\mu T}{T} + \frac{\nabla^\mu p}{h n} = 0$$

$$\frac{1}{2\eta} \check{\Pi}^{\mu\nu} + \frac{1}{nk_B T} (\varrho_\nu \mathbf{D} \check{\Pi}^{\mu\nu} - \varrho_q \nabla^{<\mu} q^{\nu>}) - \nabla^{<\mu} U^{\nu>} = 0$$

U^μ is the four-velocity of the gas and \mathbf{D} the substantial derivative. $\langle \dots \rangle$ denotes symmetric traceless part. Coefficients such as φ , ϑ , ϱ are purely thermodynamic functions. We are here largely following the notation of [5]. As is well known, the Grad moment equations give only the first approximation for the viscosities and heat conductivity.

As, however, our Ansatz, for flows of just the one, large length scale, precisely reduces to the first-order Chapman Enskog solution, our moments equations should have the correct values of viscosities and heat conductivity, i.e., be correct to first order in the Knudsen number, just as in the corresponding non-relativistic case. Work is here in progress.

References

- [1] Cercignani C., *Shear flow for gas molecules interacting with an arbitrary force*, Nuovo Cimento, 27, p1240, 1963.
- [2] Chapman S. and Cowling T.G., *The Mathematical Theory of Non-uniform Gases*, Cambridge 1958.
- [3] Söderholm L.H., *19 moments equations based on first order Chapman-Enskog solution*, Proceeding of the 20th Rarefied Gas Dynamics 1996
- [4] Grad H., *Principles of the Kinetic Theory of Gases*, Handbuch der Physik XII, 205, Berlin 1958.
- [5] de Groot S.R., van Leeuwen W.A., and van Weert Ch.G., *Relativistic Kinetic Theory*, North Holland, Amsterdam 1980.
- [6] Israel W., *Non stationary irreversible thermodynamics: a causal relativistic theory*, Ann. Phys. (N.Y.), 100, p310, 1976.
- [7] Stewart J.M., *On transient relativistic thermodynamics and kinetic theory*, Proc.R.Soc.Lond., A 357, p59, 1977.
- [8] Hiscock W.A. and Lindblom L., *Stability and Causality in Dissipative Relativistic Fluids*, Ann. Phys., 151, p466, 1983.

Polynomial Expansions for Isotropic Boltzmann Equation and Invariance of the Collision Integral with Respect to the Choice of Basis Functions *

A. Ya. Ender ¹, I. A. Ender ²,

¹ A.F. Ioffe Physico-Technical Institute, St. Petersburg 194021, Russia

² St. Petersburg State University, St. Petersburg 199034, Russia

Principal mathematical results obtained in solving the Boltzmann equation refer to the case of a linearized equation and weak departure from equilibrium. These are well known methods of Chapman-Enskog, Barnett, and Grad. Analytical solutions of the nonlinear Boltzmann equation are only known for a very limited number of cases. The existing numerical solution methods (mainly variations of the Monte-Carlo technique) give only a crude notion of the behavior of the distribution function at high velocities. At the same time the behavior of the distribution function at high energies plays a key role in a number of physicochemical processes.

In 1982 appeared a paper by Turchetti and Paolili [1] who calculated systematically for the first time the distribution function for the isotropic Boltzmann equation at high velocities by means of the nonlinear moment method. The distribution function was represented by a truncated series in Sonine polynomials, and higher moments were used for describing the tails of the distribution function. The central problem with this method consists in calculating the interaction matrix corresponding to the moments of the nonlinear collision integral. Even in the case of an isotropic (with respect to velocities) Boltzmann equation the problem is rather complicated; for example, in the above-mentioned work, which considers power potentials on the assumption that the scattering cross section is angle-independent, the analytical formulas derived for matrix elements contain six embedded sums. The computational difficulties build-up dramatically with increasing number of moments taken into account, which gives no way of going beyond the 13th moment.

Previously the authors of the present work have developed a method for integral transformation of the

nonlinear Boltzmann equation in which the distribution function and the collision integral are represented as a superposition of Maxwell distributions, and an equation (α -representation of the Boltzmann equation) equivalent to the Boltzmann equation in the v -space [2], is constructed for the weight function. We also considered [3] a moment method identical to that used in [1], using the mathematical apparatus developed for deriving the α -representation enabled us to obtain formulas for matrix elements applicable to the case of arbitrary power potentials, including the Coulomb interaction of particles, with the resulting formulas being much simpler (4 embedded sums). This made possible calculating up to 30 moments with the same accuracy as before.

In a previous work [4] we proposed to use in analyzing the matrix elements the invariance of the collision integral of the Maxwell distribution function with respect to the choice of basis functions. As these were considered Sonine polynomials with different temperatures of Maxwellians characterizing the decomposition. As a result, relations between the matrix elements were obtained and used as criteria of whether or not are correct of calculations. It was particularly stressed that at arbitrary interaction cross sections the matrix elements are not independent, with some relations existing between them.

In the present work the concept of invariance of the collision integral with respect to the choice of basis is generalized to the case of an arbitrary distribution function and most detailed relations are derived which enable nonlinear matrix elements to be expressed in terms of the linear ones. These relations make possible tracing how the main properties of the linear elements affect those of the nonlinear elements. Also, these more detailed relations can be used for checking the correctness of calculations.

*Abstract 6837 submitted to the 21st International Symposium on Rarefied Gas Dynamics, Marseille, France, July 26-31, 1998

And finally, these relations can be considered as recurrent formulas for calculating nonlinear matrix elements in terms of the linear ones.

This new approach to constructing the isotropic interaction matrix significantly improves the accuracy and reduces by many orders the time necessary for computing matrix elements. This, on the one hand, increases the number of terms N ($N = 128$ and more) in the expansion of the distribution function for isotropic problems by an order of magnitude, and, on the other, opens up a possibility to generalize the approach to more complicated cases. Using recurrence relations we calculated some problems of isotropic relaxation for various interaction models.

The principle of invariance of the collision integral with respect to the choice of basis functions may prove fairly effective in calculating matrix elements in the case of nonisotropic relaxation. Correspondingly, the expansion of the distribution function is to be performed, in this case, in Hermite polynomials $H_{r,l,m}$ which are products of spherical harmonics and Sonine polynomials with a weighting Maxwellian depending on temperature and mean velocity. Relations between matrix elements will be found in this case on passing to a basis with a Maxwellian distribution characterized not only by a different temperature, but by some other shear velocity as well.

Up to now the moment method was poorly developed for the nonisotropic case because of severe difficulties encountered both in deriving the necessary formulas and in calculating nonlinear matrix elements. The formulas known from the transport theory were obtained only for linear elements and $l \leq 2$. However, in nonisotropic problems too, the apparatus of $\alpha - u$ transformations, developed in [2], provides a possibility to obtain simple relations between matrix elements, similar to those derived in the present report. As a result, a major advance toward higher velocities can be achieved in constructing the distribution function for the case of nonisotropic problems. This is particularly important for tackling with problems of physicochemical kinetics and describing transport processes at large departures from equilibrium. Particular emphasis should be placed on the necessity of taking into account higher-order moments and matrix elements with larger indices in describing neoclassical electron transport in thermonuclear plasma.

References

- [1] Turchetti G. and Paolilli M., *The relaxation to equilibrium from a Boltzmann equation with isotropic cross section*, Phys. Lett. **90** A, 123, 1982.
- [2] Ender A.Ya. and Ender I.A., *On a representation of the Boltzmann equation*, Dokl. Akad. Nauk SSSR **193**, 61, 1970. [Sov. Phys. Dokl. **15**, 633, 1971].
- [3] Ender A.Ya. and Ender I.A., *Moment method for the isotropic Boltzmann equation*, Zh. Tekh. Fiz. **64**, 38, 1994. [Tech. Phys. **39**(10), 997, 1994].
- [4] Ender A.Ya. and Ender I.A., *Relaxation of a hard-sphere gas and criteria of the correctness of calculations*, Zh. Tekh. Fiz., to be published, 1998. [Tech. Phys.].

KINETIC THEORY AND MODELS - KTM 4

ROOM MARION

MONDAY, JULY 27, 1998

16:20

A Numerical Method for Rarefied Flow Computation Using a Discrete Velocity BGK Model *

P. Charrier¹, B. Dubroca², L. Mieussens^{1,2}

¹ Mathématiques Appliquées de Bordeaux, Université Bordeaux I, France

² CEA-CESTA/DEV/SIS, Le Barp, France

1 Introduction

The most commonly used numerical methods for the computations of rarefied gas flows are of probabilistic type like direct simulation Monte Carlo (DSMC) method. But recently, deterministic methods regained attention like the one introduced by Rogier and Schneider [1]. They are based on discrete velocity models of the Boltzmann equation, that have stimulated many fundamental studies in kinetic theory (see the book by Gatignol [2]). These methods work very well but are of explicit type and therefore too much expensive for steady flows.

In this work, we study the simpler BGK model, in order to get a source term less expensive (roughly speaking, the cost of an evaluation of the BGK operator is of order $O(n)$, whereas it is $O(n^2)$ for the Boltzmann operator). Despite its simplicity, the BGK model is known to be very good in near equilibrium regions, and some recent studies [3] have suggested its relevance for computing transport properties far from equilibrium.

Therefore, we follow an approach similar to [1] to construct a discrete velocity approximation of BGK equation, and we introduce a discrete equilibrium function such that conservation of moments and non-increasing entropy still hold for the discrete velocity model.

Our numerical method consists then in approximating in space and time the discrete velocity model by a classical finite volume scheme. This scheme may be of explicit type, but we particularly investigate an implicit version for fast computing steady flows, whereas these flows are generally very expensive with the over mentioned methods. At last, numerical results in one and two dimensions will be provided, including comparisons with DSMC.

2 A discrete velocity model for the BGK equation

The BGK equation describes the evolution of the distribution function $f(t, x, v)$

$$\partial_t f + v \cdot \nabla_x f = \frac{1}{\tau} (M[f] - f), \quad (1)$$

where τ is a relaxation time and $M[f]$ is the local equilibrium distribution called maxwellian distribution.

We now define a discrete velocity grid of step Δv by $\mathcal{V} = \{v_k = k\Delta v + a, k \in \mathcal{K}\} \subset \mathbb{R}^3$, where $\mathcal{K} = \{k = (k^{(1)}, k^{(2)}, k^{(3)}) \in \mathbb{N}^3, k^{(i)} \leq K^{(i)}, K^{(i)} \geq 2\}$ is a multi-indices set of \mathbb{N}^3 . The distribution function f is approximated by $f_k \approx f(v_k)$, and we denote by $f_{\mathcal{K}}$ the vector $(f_k)_{k \in \mathcal{K}}$. We also define $\tilde{m}_k = (1, v_k, \frac{1}{2}|v_k|^2)^T$ and the 5 first "discrete" moments of $f_{\mathcal{K}}$ by $\tilde{\rho}_{\mathcal{K}} = \sum_{k \in \mathcal{K}} f_k \tilde{m}_k \Delta v^3$. The discrete velocity model for (1) is then a finite set of transport equations coupled by a source term

$$\partial_t f_k + v_k \cdot \nabla_x f_k = \frac{1}{\tau} (\mathcal{E}_k - f_k) \quad \forall k \in \mathcal{K}, \quad (2)$$

where $\mathcal{E}_{\mathcal{K}} = (\mathcal{E}_k)_{k \in \mathcal{K}}$ is the discrete equilibrium distribution function defined by the following result [4]: **Proposition:** *There exists a unique $\tilde{a} \in \mathbb{R}^5$ such that $\mathcal{E}_k = \exp(\tilde{a}^T \tilde{m}_k)$ satisfies the non-linear system of equations $\sum_{k \in \mathcal{K}} \mathcal{E}_k \tilde{m}_k \Delta v^3 = \tilde{\rho}_{\mathcal{K}}$, if and only if there exists at least one $g \in \mathbb{R}^{|\mathcal{V}|}$ strictly positive such that $\sum_{k \in \mathcal{K}} g_k \tilde{m}_k \Delta v^3 = \tilde{\rho}_{\mathcal{K}}$.*

That gives a consistent approximation of the source term with the BGK equation in the sense that the discrete moments and the discrete entropy of $f_{\mathcal{K}}$ satisfy the same properties as in the continuous case.

* Abstract 3301 submitted to the 21st International Symposium on Rarefied Gas Dynamics, Marseille, France, July 26-31, 1998

3 Discretization in space and time

Equation (2) is approximated in space and time using a classical finite volume scheme on a 2-D curvilinear mesh

$$\begin{aligned} f_{k,I}^{n+1} &= f_{k,I}^n - \frac{\Delta t}{\Delta x} \Delta_i Flux_k^n - \frac{\Delta t}{\Delta y} \Delta_j Flux_k^n \\ &+ \frac{\Delta t}{\tau_f^n} (\mathcal{E}_{k,I}^n - f_{k,I}^n), \end{aligned} \quad (3)$$

where $f_{k,I}^n$ is an approximation of $f_k(n\Delta t, x_I, y_I)$ and $\Delta_i Flux_k^n$ denotes the difference of numerical fluxes across the edges $i - \frac{1}{2}$ and $i + \frac{1}{2}$. The computation of $\mathcal{E}_{k,I}^n$ is carried out by a Newton type algorithm.

It can be proved [4] that the scheme is positive, conservative, and that the discrete entropy is non increasing, under a CFL type condition on the time step, implying in particular that Δt is smaller than the relaxation time. These conditions are therefore too much restrictive for steady computations. We thus propose a linearized implicit version of (3). A linearization of the discrete equilibrium function $\mathcal{E}_{k,I}^{n+1}$ and an implicitation of the numerical fluxes lead to the following δ -form of our implicit scheme

$$\left(\frac{Id}{\Delta t} + T^n + R^n \right) \delta f^n = RHS^n, \quad (4)$$

where $\delta f^n = f^{n+1} - f^n$, Id is the unit matrix, T^n is the transport matrix resulting from the implicitation of the numerical fluxes, $R^n = (-\frac{1}{\tau_f^n} (Id - \frac{\partial \mathcal{E}_k^n}{\partial f_k^n}))$, and RHS^n is the explicit part of the scheme (numerical fluxes and relaxation). Thanks to the special structure of T^n and R^n , a cheap iterative resolution of (4) has been used. The previous schemes can easily be extended to second order accuracy in space. Boundary conditions of specular and diffuse types are implemented using a ghost cell technique.

4 Numerical results

The implicit scheme has been tested on classical 1-D flows like normal shock wave or couette flow. The results are in good agreement with DSMC. Our method has also been tested on various 2-D flows. A supersonic flow past a compression ramp of 10° is presented in Fig.1. The steady state is reached after 500 iterations, with $8 \times 8 \times 6$ discrete velocities and 70×70 cells, and a CFL of 10000. Finally, a supersonic flow past a cylinder is presented in Fig.2. The steady state is reached after 500 iterations with

$12 \times 12 \times 6$ discrete velocities and 20×40 cells, and a CFL of 10000. One can note the velocity slip at the boundary.

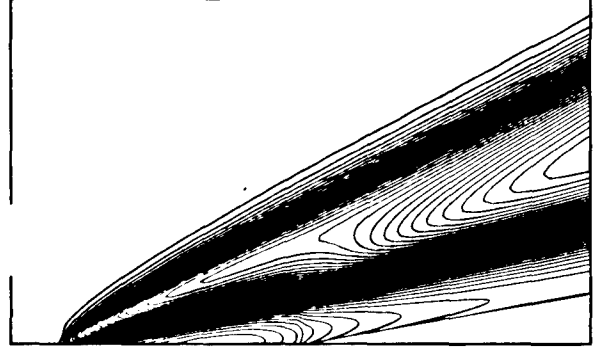


Figure 1: Density countours past a compression ramp ($M_\infty = 4$, $Kn = 0.04$).

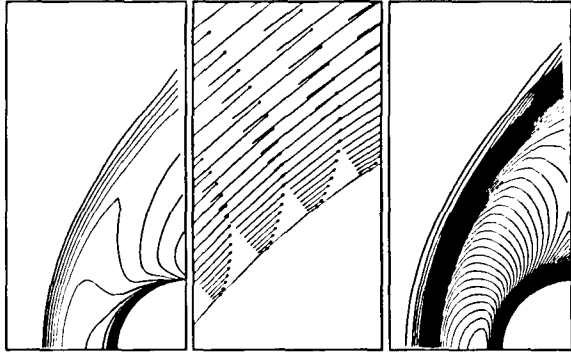


Figure 2: Supersonic flow past a cylinder: density, velocity, temperature ($M_\infty = 4$, $Kn = 0.03$).

References

- [1] Rogier F. and Schneider J., *A Direct Method For Solving the Boltzmann Equation*, Transp. Th. Stat. Phys., Vol. 23, No. 1-3, pp.313-338, 1994.
- [2] Gatignol R., *Théorie cinétique des gaz à répartition discrète de vitesses*, Lecture Notes in Physics, Vol. 36, Springer Verlag, 1975.
- [3] Garzó V. and Santos A., *Comparison Between the Boltzmann and BGK Equations for Uniform Shear Flows*, Physica A, Vol. 213, pp.426-434, 1995.
- [4] Mieussens L., *Une méthode numérique déterministe pour un modèle discret en vitesses de l'équation BGK*, preprint, MAB, Université Bordeaux I.

Discrete Velocity Models for Mixtures *

A.V. Bobylev¹, C. Cercignani²,

¹ Keldysh Institute of Applied Mathematics, Moscow, Russia

² Dipartimento di Matematica, Politecnico di Milano, Milano, Italy

1 Introduction

In the last twenty years research on discrete models of the Boltzmann equation has flourished. The renewed interest for DVM and their potential use as tools to produce approximate solutions to the Boltzmann equation makes it necessary to cover the area of mixtures as well. The extension of DVM to mixtures seems impossible when the ratio of masses is irrational, but poses no special problems for the case of a rational ratio (this limitation is, of course, irrelevant in practice). Yet, the fact that only trivial models have appeared so far, stimulated us to investigate this matter.

2 DVM for mixtures

According to standard definitions, a discrete velocity model of a gas is a system of partial differential equations of hyperbolic type (discrete Boltzmann equation), having the following form:

$$\partial f_{\mathbf{n}}/\partial t + \mathbf{v}_{\mathbf{n}} \cdot \partial f_{\mathbf{n}}/\partial \mathbf{x} = Q_{\mathbf{n}}(f, f) \quad (1)$$

$$Q_{\mathbf{n}}(f, f) = \sum_{\mathbf{l}, \mathbf{k}} c_{\mathbf{n}, \mathbf{l}, \mathbf{k}} f_{\mathbf{l}} f_{\mathbf{k}} - \sum_{\mathbf{m}} k_{\mathbf{n}, \mathbf{m}} f_{\mathbf{n}} f_{\mathbf{m}} \quad (2)$$

where $\mathbf{v}_{\mathbf{n}}$ are the discrete velocities (vectors of \mathbb{R}^d) belonging to a pre-arranged discrete set, $c_{\mathbf{n}, \mathbf{l}, \mathbf{k}}$ and $k_{\mathbf{n}, \mathbf{m}}$ are positive constants and the vector indices run from $-\mathbf{p}$ to \mathbf{p} (\mathbf{p} being a vector with integer components, possibly infinity), whereas $f_{\mathbf{n}}$ are the probabilities (per unit volume) of finding a molecule at time t at position \mathbf{x} with velocity $\mathbf{v}_{\mathbf{n}} = h\mathbf{n}$. We occasionally write f , as done in (2.1b), for the collection $\{f_{\mathbf{n}}\}$.

The coefficients $A_{\mathbf{l}, \mathbf{k}}^{\mathbf{m}, \mathbf{n}}$ must vanish if the following conservation equations are not satisfied:

$$\mathbf{l} + \mathbf{k} = \mathbf{m} + \mathbf{n} \quad (3)$$

$$|\mathbf{l}|^2 + |\mathbf{k}|^2 = |\mathbf{m}|^2 + |\mathbf{n}|^2 \quad (4)$$

* Abstract 4111 submitted to the 21st International Symposium on Rarefied Gas Dynamics, Marseille, France, July 26-31, 1998

The most natural and popular model was first proposed by Goldstein, Sturtevant and Broadwell in 1989 [1]. The proof of consistency for this model was provided in [2].

Let us consider a mixture with integer masses m_1, m_2, \dots, m_s where s is the number of species.

Let us consider any pair of molecules with masses m_i, m_j and let us put $m_i = m, m_j = M$ ($m < M$). The usual Boltzmann for mixtures (with continuous velocities) has the following form

$$\partial f_i/\partial t + \mathbf{v} \cdot \partial f_i/\partial \mathbf{x} = \sum_j Q_{ij} \quad (5)$$

where

$$Q_{ij} = \int d\mathbf{v} d\boldsymbol{\omega} |\mathbf{u}| \sigma(\mu |\mathbf{u}|^2/2, \mathbf{u} \cdot \boldsymbol{\omega}/|\mathbf{u}|) \times [f(\mathbf{v}')F(\mathbf{w}') - f(\mathbf{v})F(\mathbf{w})] \quad (6)$$

where $f(\mathbf{v}) = f_i(\mathbf{v})$, $F(\mathbf{v}) = f_j(\mathbf{w})$, and

$$\mathbf{u} = \mathbf{v} - \mathbf{w}, \quad \mu = \frac{mM}{m+M} \quad (7)$$

$$\mathbf{v}' = \frac{m\mathbf{v} + M\mathbf{w}}{m+M} + |\mathbf{u}| \boldsymbol{\omega} \frac{\mu}{m} \quad (8)$$

$$\mathbf{w}' = \frac{m\mathbf{v} + M\mathbf{w}}{m+M} - |\mathbf{u}| \boldsymbol{\omega} \frac{\mu}{M} \quad (9)$$

The first step toward obtaining a form of the collision term suitable for arriving at a discrete velocity model is to adopt $\mathbf{u} = \mathbf{v} - \mathbf{w}$ as an integration variable. We obtain:

$$Q_{ij} = \int d\mathbf{u} d\boldsymbol{\omega} |\mathbf{u}| \sigma(\mu |\mathbf{u}|^2/2, \mathbf{u} \cdot \boldsymbol{\omega}/|\mathbf{u}|) \times [f(\mathbf{v}')F(\mathbf{w}') - f(\mathbf{v})F(\mathbf{v} - \mathbf{u})] \quad (10)$$

where the primed variables must be expressed according to

$$\mathbf{v}' = \mathbf{v} + \frac{M}{m+M} (|\mathbf{u}| \boldsymbol{\omega} - \mathbf{u}) \quad (11)$$

$$\mathbf{w}' = \mathbf{v} - \mathbf{u} - \frac{m}{m+M} (|\mathbf{u}| \boldsymbol{\omega} - \mathbf{u}) \quad (12)$$

We change again the variables by letting $\mathbf{u} = m + M\tilde{\mathbf{u}}$ and then omitting the tilda. We have:

$$Q_{ij} = (m + M)^{d+1} \int d\mathbf{u} d\omega |\mathbf{u}| \sigma(mM(m + M)|\mathbf{u}|^2/2, \mathbf{u} \cdot \omega/|\mathbf{u}|) \times [f(\mathbf{v} - M\mathbf{u} + M|\mathbf{u}|\omega)F(\mathbf{v} - M\mathbf{u} - m|\mathbf{u}|\omega) - f(\mathbf{v})F(\mathbf{v} - (M + m)\mathbf{u})] \quad (13)$$

It will be useful, for any vector \mathbf{u}' , to write:

$$\Psi(\mathbf{u}, \mathbf{u}') = |\mathbf{u}| \sigma(mM(m + M)|\mathbf{u}|^2/2, \mathbf{u} \cdot \mathbf{u}'/|\mathbf{u}|^2) [f(\mathbf{v} - M\mathbf{u} + M\mathbf{u}')F(\mathbf{v} - M\mathbf{u} - m\mathbf{u}') - f(\mathbf{v})F(\mathbf{v} - (M + m)\mathbf{u})] \quad (14)$$

A modification of [2] yields the following:

Lemma. Let $\Psi(\mathbf{u}, \mathbf{u}') : \mathbb{R}^d \times \mathbb{R}^d \Rightarrow \mathbb{R}$ be continuous and have a compact support. Let, for any $d \geq 3$:

$$S_h(\Psi) = \sum_{\mathbf{n} \in \mathbb{Z}^d} h^d \frac{|\Omega_{d-1}|}{r_d(|\mathbf{n}|^2)} \sum_{|\mathbf{m}|^2 = |\mathbf{n}|^2} \Psi(\mathbf{n}h, \mathbf{m}h) \quad (15)$$

where $|\Omega_{d-1}|$ is the area of the unit sphere in d dimensions and $r_d(|\mathbf{n}|^2)$ denotes the number of the roots of the equation $|\mathbf{m}|^2 = |\mathbf{n}|^2$ where the vectors with integer components \mathbf{m} and \mathbf{n} denote, respectively an unknown and a given vector. Then

$$S_h(\Psi) \rightarrow \int d\mathbf{u} d\omega \Psi(\mathbf{u}, |\mathbf{u}\omega|) \quad \text{as } h \rightarrow 0 \quad (16)$$

This lemma provides the desired approximation and hence a rule to construct discrete velocity models for mixtures with arbitrarily many velocities.

3 Models with a finite number of velocities

In order to obtain nontrivial models with a finite number of velocities, we found that we must have at least 5+8 and 9+16 velocities, respectively. The velocities of these models are illustrated in Figs. 1 and 2.

A drawback of the first model is that it becomes "unreasonable" in the limiting case of two non-interacting species. The resulting DVM are unsatisfactory because we obtain two independent Broadwell models for light particles, and a Broadwell model plus the non-interacting particles with zero velocity for heavy particles.

The main idea behind the second model is to allow some new collisions between the identical particles of the previous model, with the consequence of constructing a "reasonable" model for each component

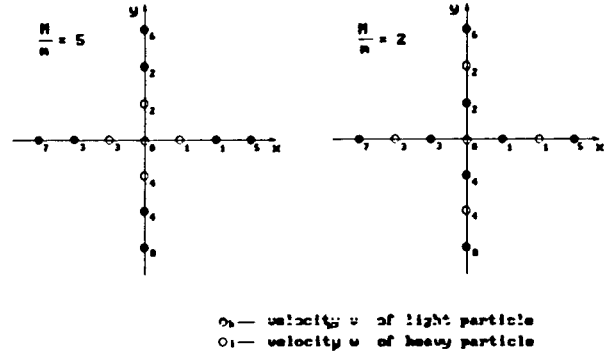


Figure 1: The discrete velocities for the first non-trivial model.

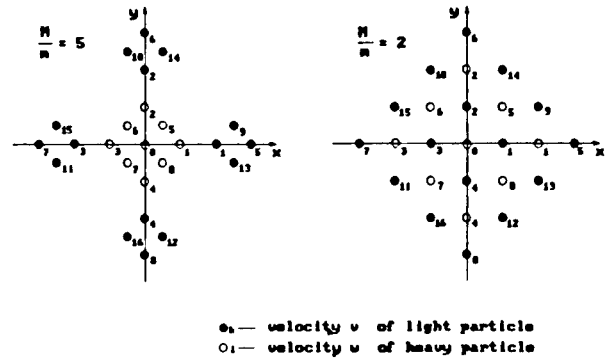


Figure 2: The discrete velocities for the second non-trivial model.

of the mixture even in the limiting case discussed above. A price to be paid is that the new model has 9+16 velocities.

In the paper to be presented at the Symposium we shall briefly describe the equations for the second non-trivial model (which includes the first one as a limiting case) and present some applications.

References

- [1] Goldstein, D., Sturtevant, B. and Broadwell, J.E., "Investigations of the motion of discrete-velocity gases", in "Rarefied Gas Dynamics: Theoretical and Computational Techniques", Edited by E.P. Muntz, D.P. Weaver and D. H. Campbell, pp. 110-117, AIAA Washington, 1989.
- [2] Bobylev, A.V., Palczewski, A. and Schneider, J., "Discretization of the Boltzmann equation and discrete velocity models", in "Rarefied Gas Dynamics 19", J. Harvey and G. Lord, eds., Vol. II, pp. 857-863, Oxford University Press, Oxford, 1995.

Excessive Invariants of Discrete Kinetic Equations *

Y.Y. Arkhipov

The Keldysh Institute of Applied Mathematics,
Russian Academy of Sciences, Moscow, Russia

1 Introduction

In this paper one of the aspects of the relation between discrete velocity models (DVMs) and the Boltzmann equation is investigated concerning existence of excessive invariants (decreasing functionals). As an attempt to clarify it, the spaces of decreasing functionals for some particular DVMs are compared with the analogous space for the Boltzmann equation. It is shown that these DVMs have the infinite number of linearly independent invariants and, hence, they possess many invariants which have no analogues for the Boltzmann equation. However there exists a model, introduced by S. Harris, which has a finite collection of linearly independent invariants. Since the H -functional is the unique actually decreasing functional, the problem of finding decreasing functionals can be reduced to the problem of finding linear invariants. The latter reduces to solving one or more functional equations which are transformed by acting of linear translational operators into first-order quasi-linear equations not connected with each other. To find invariants (decreasing functionals), we use a method based on the technique developed in [3], where the uniqueness of the H -functional was proved.

2 Formulation of problem

The DVMs investigated in the present paper can be represented by the following set of first-order quasi-linear equations

$$\frac{\partial f_i}{\partial t} + v_i \frac{\partial f_i}{\partial x} = Q_i(f_1, \dots, f_N), i = \overline{1, N}, \quad (1)$$

where $Q_i \in C^1(R^N)$, $i = \overline{1, N}$ - given functions, v_i - given points in the space R^N , and the functions $f_i(x, t)$, where $x \in R^n$, $t \in R$, are unknown. In the connection with the set (1) we will consider func-

tionals of the form

$$G[f, t] \equiv \int_{R^n} \sum_{i=1}^N \varphi_i(x - v_i t, f_i) dx. \quad (2)$$

The arguments of such functionals are pairs $[f, t]$, where $f = f(x)$ is a vector-function with the components $f(x) = \langle f_1(x), \dots, f_N(x) \rangle$, t is some real number. In the case of

$$\begin{aligned} n = 2, N = 4, \\ v_1 \equiv -v_2 \equiv (1, 0), v_3 \equiv -v_4 \equiv (0, 1), \\ Q_1 \equiv Q_2 \equiv -Q_3 \equiv -Q_4 \equiv f_3 f_4 - f_1 f_2 \end{aligned} \quad (3)$$

the set (1) coincides with the two-dimensional four-velocity Broadwell model. If

$$\begin{aligned} n = 3, N = 6, \\ v_1 \equiv -v_2 \equiv (1, 0, 0), v_3 \equiv -v_4 \equiv (0, 1, 0), \\ v_5 \equiv -v_6 \equiv (0, 0, 1), \\ Q_1 \equiv Q_2 \equiv f_3 f_4 + f_5 f_6 - 2f_1 f_2, \\ Q_3 \equiv Q_4 \equiv f_1 f_2 + f_5 f_6 - 2f_3 f_4, \\ Q_5 \equiv Q_6 \equiv f_1 f_2 + f_3 f_4 - 2f_5 f_6 \end{aligned} \quad (4)$$

the set (1) coincides with the three-dimensional six-velocity Broadwell model. If

$$\begin{aligned} n = 2, N = 6, \\ v_1 \equiv -v_4 \equiv (-1, 0), \\ v_2 \equiv -v_5 \equiv (-1/2, -\sqrt{3}/2), \\ v_3 \equiv -v_6 \equiv (1/2, -\sqrt{3}/2), \\ Q_1 \equiv Q_4 \equiv f_2 f_5 + f_3 f_6 - 2f_1 f_4, \\ Q_2 \equiv Q_5 \equiv f_3 f_6 + f_1 f_4 - 2f_2 f_5, \\ Q_3 \equiv Q_6 \equiv f_1 f_4 + f_2 f_5 - 2f_3 f_6 \end{aligned} \quad (5)$$

the set (1) coincides with the two-dimensional six-velocity model.

The problem is to find functionals which have the form (2) and decrease on all solutions of the models (3)-(5). Note that any functional (2) (independently of functions φ_i) is conserved on the solutions to the free motion equations which are obtained if the right hand sides in (1) are set equal

*Abstract 4286 submitted to the 21st International Symposium on Rarefied Gas Dynamics, Marseille, France, July 26-31, 1998

to zero. Thus the formulated problem is the problem of finding the decreasing functionals of DVMs in the classes of invariants of the free motion equations associated with these models.

3 Results

The main result consists in providing the general form of decreasing functionals for the models (3)–(5) in the class of free motion invariants. The obtained results may be applied, first of all, to the excessive invariants problem. In order to identify the excessive invariants the general form of decreasing functionals for the Boltzmann equation has also been provided (in the analogous class of free motion invariants). Because of the enormous size of the formulae we avoid writing them here. See [1], [2] for details. We will just list some qualitative results. Any decreasing functional of both the Boltzmann equation and the DVMs (3)–(5) can be represented by the sum of the H -functional and some invariant which linearly depends on f . Moreover,

- every element in the family of the Boltzmann equation invariants is uniquely determined by the collection of four scalar and three vector parameters;
- every element in the family of the four-velocity Broadwell model invariants is uniquely determined by six arbitrary functions of one variable;
- every element in the family of the six-velocity Broadwell model invariants is uniquely determined by eight arbitrary functions of one variable and three arbitrary functions of two variables;
- every element in the family of the planar six-velocity model invariants is uniquely determined by eight scalar constants and eight arbitrary functions of one variable.

The problem of finding the general form of decreasing functionals was considered in [3], but in a class narrower than (2). Using such an approach excessive invariants didn't arise, since both the Boltzmann equation and the Broadwell models had only one decreasing functional (H -functional) and mass, momentum and energy invariants. Extending the class of search to (2) was stimulated by [4], in which linear conservation laws for the Boltzmann equation were found. Though the method which is used in this paper appears to be more general, but being applied to the Boltzmann equation it doesn't discover

any new conservation laws as compared with [4]. It has been applied to the Boltzmann equation just to give an exact answer to the following question: which of the invariants of the investigated DVMs are excessive.

When discussing the general form of decreasing functionals of the above models, Harris's model (which is derived from (5) by adding triple collisions) should also be mentioned

$$\frac{\partial f_i}{\partial t} + v_i \frac{\partial f_i}{\partial x} = Q_i + G_i, i = \overline{1, 6}. \quad (6)$$

In this formula the quantities Q_i , the velocities v_i and the unknown functions f_i are the same as in the two-dimensional six-velocity model (5) and $G_i \equiv (-1)^i (f_2 f_4 f_6 - f_1 f_3 f_5)$, $i = \overline{1, 6}$. The formula which provides the general form of decreasing functionals for the model (5) is a starting point for studying other two-dimensional six-velocity models containing higher order collisions. As a matter of fact, using this formula the explicit form of the decreasing functionals for Harris's model (6) can be easily obtained which will be done in the near future. One of the direct consequences of the formula is that any decreasing functional for (6) is always the sum of the H -functional and several linear invariants. And, moreover, the dimension of the space of the linear invariants for the set of equations (6) is finite and less than 10 (i.e. it doesn't exceed the number of the linearly independent invariants of the two-dimensional Boltzmann equation). In contrast, as it has already been mentioned, the dimension of the space of the invariants for the DVMs (3)–(5) is infinite.

References

- [1] Y.Arhipov, A.Klar, O.Mingalyov and V.Vedenyapin, *A class of invariants for the Boltzmann equation and the Broadwell model*, Eur. J. Mech., B/Fluids, Vol.16, No.3, pp.387–399, 1997
- [2] Y.Y.Arhipov, *On the Connection of the Stationary Distributions and Entropy. Decreasing Functionals of Kinetic Equations*, (Russian), Ph.D. Thesis, KIAM, Moscow, 1997
- [3] V.Vedenyapin, *Differential forms in space without a norm. A theorem on the uniqueness of Boltzmann's H-function*, Russian Math. Surveys, Vol.43, No.1, p.193–219, 1988
- [4] V.A.Rykov, *Macroscopic conservational laws in kinetic theory*, J. Comp. Math. and Math. Phys., Vol.25, No.12, 1985

Spline Function Approximation Method for Discrete Boltzmann Equation *

M. Hatakeyama, A. Takaada, H. Ishikawa
Ibaraki University, Hitachi-city, Japan

1 Introduction

In the past, various kinds of approximate methods for the solution of the Boltzmann equation have been proposed, solved and compared. We have also proposed a method of solution [1][2][3]. In the preceding paper [1][2], we have already developed the direct simulation method for the discrete Boltzmann equation. We have called the method the Discrete Velocity Ordinate (DVO, hereafter) method. This method has already been applied to the spatially 0-dimensional problem [1][2], 1-dimensional flow problem [2], and 2-dimensional, unsteady flow problem [2], and the results are rather good when comparing with other results of approximate solutions [2][3].

In the present paper, we propose a new, accurate computing scheme in the velocity space for this DVO method.

2 Modified DVO Scheme

In the present paper, a kind of the function approximation has been adopted for the distribution function F_i of the Discrete Boltzmann (here after, abbreviated to DB) equation.

$$\frac{\partial F_i}{\partial t} + \mathbf{V}_i \cdot \frac{\partial F_i}{\partial \mathbf{x}} = \frac{1}{K_n} \sum_{j=1}^R \frac{|\mathbf{V}_i - \mathbf{V}_j|}{m_0} \sum_{(k,l)}^{m_0} (F_k F_l - F_i F_j)$$

where R is the total mesh numbers in the velocity space.

The function approximation method directly provide the function values at any points like l , and k in the velocity space in Fig. 1.

The Fig.1 shows the 2-dimensional view of the 3-dimensional velocity space. A simple numerical integration (= summation) method is adopted to compute the collision term of the DB equation in

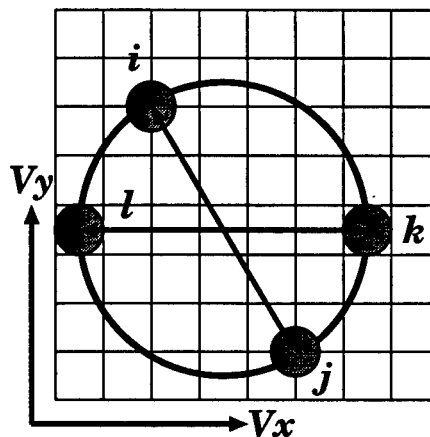


Figure 1: DVO intermolecular collision in the velocity space

Fq.(1). Then, collision term integrations of the DB equation concerning the points i and j can be performed by making use of a simple numerical integration scheme along the 3-dimensional spherical shell in Fig.1.

This computing scheme may become rather accurate than the previous computing schemes like the usual DVO method in the preceding paper [2]. Because, in the previous scheme [2], the integration calculations have been replaced by only one or several collision example calculations. In the present scheme, the collision integrations are performed overall the 3-dimensional spherical shell. Therefore, we can get the more accurate integration results of the collision term for point "i" in Fig.1.

3 Numerical Computing Method for Collision Term

In the present paper, the approximate function we have adopted is a kind of the Spline function. That is the B-spline function [4]. We have already used in the preceding paper [2][3]. We have newly intro-

* Abstract 3830 submitted to the 21st International Symposium on Rarefied Gas Dynamics, Marseille, France, July 26-31, 1998

duced this Spline function to calculate the numerical collision integral accurately. The B-spline function for 3-dimensional velocity space $S(V_x, V_y, V_z)$ is defined as follows [4];

$$S(V_x, V_y, V_z) = \sum_{k=1}^{n+m} \sum_{j=1}^{n+m} \sum_{i=1}^{n+m} c_{ijk} N_{mi}(V_x) N_{mj}(V_y) N_{mk}(V_z)$$

where "m" is the order of the spline function, and m=4 in the present paper. The "n" is the degree of the spline function. $n = N - 3$.

To solve the 3-dimensional B-spline function approximation problem, the following first-order simultaneous equations must be solved;

$$\sum_{k=1}^{n+m} \sum_{j=1}^{n+m} \sum_{i=1}^{n+m} c_{ijk} N_{mi}(V_{x_r}) N_{mj}(V_{y_s}) N_{mk}(V_{z_t}) = F_{rst}$$

where, $r, s, t = 0, 1, \dots, N$.

The F_{rst} is the data of the distribution function F . To solve for the c_{ijk} in this equations, N^3 order of coefficient of data matrix must be stored and computed. The magnitude of the total data c_{ijk} is an huge order, say one or several Giga-bytes.

4 Distributed DVO Computing Scheme over Network

The magnitude of the computing data of this modified DVO scheme is too large. For example, about Giga-bytes order of memories are required for $33 \times 33 \times 33$ meshes in the velocity space. Then we have planned to compute these problems by making use of many distributed WorkStations (WS) over the networks [3]. Some advanced PVM network communication system that is developed in our distributed virtual computing system is made use of [3][5].

We have established an automatic distributed network computing system for the direct simulation of the DB equation by the Network-DVO scheme [3]. We have already tested and succeeded in computing on the 10 WS scale automatic distributed network computings.

5 Results and Present Status

At present, since some bugs may be included in our program, the numerical calculation results are not

necessarily complete. Then, all the results are not yet obtained. We have obtained only the result concerning the accuracy of the B-spline function approximation method. For the sufficient numbers of meshes ($m = 4, n = 33$), we have performed one trial. The calculation is applied for the spatially homogeneous relaxation problem that has already been solved by Krook and Wu [6], and compared. The accuracy comparison with that of the analytic solution by Krook and Wu [6] are revised when comparing with the old ones [2][3], and then the relaxation time has become rather long.

As for the computing efficiency, since our computing is not yet perfect, the computing efficiency has not yet correctly be evaluated. But the computing efficiency will be able to expected. The automatic distributed computing system we have developed shows some good results [3]. If the 100 times of higher efficiency than the present schemes are obtained, then the DVO scheme for the DB equation will be applied and made use of to the various flow problems as one of the most accurate methodology for the Boltzmann equation.

References

- [1] H.Oguchi, M.Hatakeyama, and H.Honma, "Computational Aspects on Discrete-Ordinate-Velocity Description of Rarefied Gases", submitted to the 19th RGD, vol.2, pp.815-821, Oxford, England, 1995.
- [2] M. Hatakeyama, S. Sugano, A. Takaada, "Applications of A Family of Function Approximation Methods to Computational Schemes for Boltzmann Equation", 19th RGD, vol.1, pp.64-70, Oxford, England, 1995.
- [3] M. Hatakeyama, Yuuki Shindou, Minoru Shishido, "Network-DVO Scheme for for Discrete Boltzmann Equation", Proceedings of the 10th CFD Symposium, the Japan Society of CFD, pp.278-279, Dec. 1996.
- [4] Charles, K.C. "Multivariate Splines", Society for Industrial and Applied Mathematics, Philadelphia, PS, USA, 1988.
- [5] Janusz Kowalik. PVM: Parallel Virtual Machine. MIT Press, London, 1994.
- [6] M.Krook, and T.T.Wu, "Exact Solutions of the Boltzmann Equation", Physics of Fluids, Vol. 20, pp.1589-1595, 1977.

A Simplified and Cheaper Discrete Velocity Scheme for Gas Mixtures *

C. Buet¹, S. Cordier²

¹ CEA, Bruyères Le Châtel, France

² Laboratoire d'analyse numérique

Université Pierre et Marie Curie, Paris, France

1 Introduction

For rarefied gas, the collisions can be simulated efficiently using discrete velocity method ([3],[4],[5]). In the case of gas mixtures, such method can be used provided that the mass ratio can be approximated by a ratio of small integers. In particular, a mixture of O_2/N_2 which is of primarily practical importance requires an amount of storage and calculations which is not available on actual computer since it needs a very fine velocity grid, see [1]. In the case of the air, a possible solution should be to simplify the collision process by assuming that O_2/N_2 have the same mass. Such hypothesis leads to non physical conservation laws and steady states.

We present a multispecies Boltzmann operator that performs such modifications for the collision process without modifying the macroscopic conservation laws and the real equilibrium states.

Then we define a new discrete velocity scheme which allows, in the case of O-N mixture, to take the same velocity grid for the two species. Therefore the grid can be coarser, which is the interest of the our model and numerical method.

2 A modified Boltzmann operator for gas mixtures

We consider a collision operator given for each species α and β in a weak form by:

$$\begin{aligned} & \int_{\mathbf{R}^3} \tilde{Q}^{\alpha,\beta}(f_\alpha, f_\beta)(v^\alpha) \Psi_\alpha(v^\alpha) dv^\alpha \\ &= \frac{1}{2} \frac{\tilde{m}_\alpha}{m_\alpha} \int_{(\mathbf{R}^3)^2 \times S_+^2} \left(\Psi_\alpha(v^\alpha) - \Psi_\alpha(\tilde{v}'^\alpha) \right) B \\ & \quad (\delta'^\alpha \beta \tilde{f}'^\alpha \tilde{f}'^\beta - \delta^\alpha \beta f^\alpha f^\beta) d\Omega dv^\beta dv^\alpha, \quad (1) \end{aligned}$$

where Ψ_α is a test function, f_α and f_β are the distribution functions of particles with respective mass m_α, m_β , \tilde{v}'_α and \tilde{v}'_β are the post collisionnal velocities of particles with virtual mass \tilde{m}_α

$$\tilde{v}'^\alpha = v^\alpha - 2 \frac{\tilde{\mu}_{\alpha,\beta}}{\tilde{m}_\alpha} (v^\alpha - v^\beta, \Omega) \Omega,$$

$$\tilde{v}'^\beta = v^\beta + 2 \frac{\tilde{\mu}_{\alpha,\beta}}{\tilde{m}_\beta} (v^\alpha - v^\beta, \Omega) \Omega,$$

where $\Omega \in S^2$, $\tilde{\mu}_{\alpha,\beta} = \frac{\tilde{m}_\alpha + \tilde{m}_\beta}{\tilde{m}_\alpha \tilde{m}_\beta}$ is the modified reduced mass and

$B = \sigma \left(\|v^\alpha - v^\beta\|, \frac{(v^\alpha - v^\beta, \Omega)}{\|v^\alpha - v^\beta\|} \right) \|v^\alpha - v^\beta\|$, σ is the cross section.

The functions $\delta^{\alpha\beta}$ and $\delta'^{\alpha\beta}$ are given by

$$\delta^{\alpha\beta} = \tilde{M}_\alpha(v^\alpha) \tilde{M}_\beta(v^\beta) \quad \delta'^{\alpha\beta} = \tilde{M}_\alpha(\tilde{v}'^\alpha) \tilde{M}_\beta(\tilde{v}'^\beta). \quad (2)$$

where

$$\tilde{M}_i(v) = \exp \left(\frac{-(m_i - \tilde{m}_i)|v - u|^2}{2T} \right)$$

where u and T are the common mean velocity and temperature of the mixture at thermodynamical equilibrium. For this model we can prove the following theorem

Theorem 1 *The collision operator defined by (1) satisfies the conservation of mass momentum and energy,*

$$\int_{\mathbf{R}^3} \tilde{Q}^{\alpha,\beta} \Psi_\alpha(v^\alpha) dv^\alpha + \int_{\mathbf{R}^3} \tilde{Q}^{\beta,\alpha} \Psi_\beta(v^\beta) dv^\beta = 0$$

for

$$\Psi_i(v_i) = \begin{pmatrix} m_i v_i \\ m_i |v_i|^2 \end{pmatrix}, \quad i = \alpha, \beta$$

the decay of entropy

$$\frac{d}{dt} \frac{m_i}{\tilde{m}_i} \sum_{i=\alpha,\beta} \int_{\mathbf{R}^3} f^i(v^i) \ln(f^i(v^i)/M_i(v^i)) dv^i \leq 0,$$

*Abstract 1431 submitted to the 21st International Symposium on Rarefied Gas Dynamics, Marseille, France, July 26-31, 1998

and allows the Maxwellians to be steady states

$$\tilde{Q}^{\alpha,\beta}(M_\alpha, M_\beta) = 0$$

for

$$M_i(v) = \rho_i \exp\left(\frac{-m_i|v-u|^2}{2T}\right), \quad i = \alpha, \beta.$$

3 The discrete velocity scheme in the case of a two species mixture O-N

The modified discrete operator 1 can be used for a mixture of gases which have masses which are close together like, O and N for example. In this case we take $\tilde{m}_\alpha = \tilde{m}_\beta$, they can be fixed to $(m_\alpha + m_\beta)/2$ for example, so that we make collision as if the two species have the same mass. The discrete velocity operator is defined like in [3]. We take a cubic lattice $\Delta v \mathbb{Z}^3$ for each of the species. Then the discrete Boltzmann operator is obtained easily by discretizing the weak form (1) and have the generic form

$$\begin{aligned} & \sum_{i \in \mathbb{Z}^3} Q_i^{\alpha\beta} \Psi_i^\alpha \\ &= \frac{1}{2} \frac{\tilde{m}_\alpha}{m_\alpha} \sum_{i,j,k,l \in (\mathbb{Z}^3)^4} (\Psi_i^\alpha - \Psi_k^\alpha) B_{ijkl} \\ & (\delta_{kl}^{\alpha\beta} \tilde{f}_k^\alpha \tilde{f}_l^\beta - \delta_{ij}^{\alpha\beta} f_i^\alpha f_j^\beta) \end{aligned}$$

for a specie α and the notation g_i for a function g stands for $g(v_i)$ with $v_i = (\Delta v)i$, $i \in \mathbb{Z}^3$. The coefficients B_{ijkl} represent the physics, are invariant under permutation of the indices i, j, k, l and are non null if only if $i+j = k+l$ and $(i-j)^2 = (k-l)^2$, that is, when (i, j) and (k, l) are diameters of the same sphere.

We have an analogous of theorem 1 i.e. standard conservation laws H-theorem and Maxwellians as steady state. The resulting discrete Boltzmann equation is

$$\begin{aligned} \frac{df_i^\alpha}{dt} &= Q_i^{\alpha\beta} \\ \frac{df_i^\beta}{dt} &= Q_i^{\beta\alpha}, \end{aligned}$$

$i \in \mathbb{Z}^3$.

The time discretization of this differential system is like the single monoatomic case which is described in [3]: we use sub-lattice to break the naturally $O(N^2)$ cost of the method and splitting method to decompose the discrete operator in four velocities

model of Broadwell type. The differential equations which correspond to these four velocities model are of the form

$$\begin{cases} \frac{d}{dt} X_1 = (\alpha X_2 X_4 - \beta X_1 X_3) \\ \frac{d}{dt} X_2 = -(\alpha X_2 X_4 - \beta X_1 X_3) \\ \frac{d}{dt} X_3 = (\alpha X_2 X_4 - \beta X_1 X_3) \\ \frac{d}{dt} X_4 = -(\alpha X_2 X_4 - \beta X_1 X_3) \end{cases}$$

and can solved exactly. A consequence and an advantage of solving exactly such differential equations is that the resulting scheme is inconditionnaly stable and entropy decreasing.

4 Conclusion

This technic of artificial mass during the collision process would allow numerical computation of rarefied mixtures of gas to be possible at a reasonable cost, that is the cost of the single specie case. It would be generalized without problems to the case of polyatomic gases using a Larsen-Borgnakke model

References

- [1] D.B. Goldstein, *Discrete velocity collision dynamics for polyatomic molecules.*, Phys. Fluids, A, 4 (8), 1992.
- [2] R. Gatignol, *Théorie cinétique des gaz à répartition discrète de vitesses*, Lecture Notes in Physics, Springer Verlag, Vol 36, Berlin, 1975.
- [3] C. Buet, *A discrete-velocity scheme for the boltzmann operator of rarefied gas dynamics*, Transp. Th. Stat. Phys, (1996).
- [4] D. Goldstein, B. Sturtevant and J. E. Broadwell, *Investigations of the Motion of Discrete-Velocity Gases*, in "Rarefied Gas Dynamics: Theoretical and Computational Techniques", 1991
- [5] F. ROGIER and J. SCHNEIDER, *A direct Method for solving the Boltzmann Equation*, Transp. Th. Stat. Phys, (1994).

KINETIC THEORY AND MODELS - KTM 5

ROOM MARION

TUESDAY, JULY 28, 1998

9:15

Kinetic Model Equation By Discrete-Velocity-Ordinate Method *

H. Oguchi

Inst. of Space and Astronaut. Science, Sagami-hara C., Kanagawa, Japan

1 Introduction

In the previous paper[1], we showed that the discrete Boltzmann description reduces a set of closed analytic formulae by incorporating the thirteen-moment approximation for the velocity distribution function. The motivation of the work primarily was to deal with the problem of the rarefied gases flows at near-equilibrium state. As one of the results, for the pseudo-Maxwellian molecules it is shown that the set of closed discrete formulae reduce to a single kinetic model equation quite similar to the so-called S-model proposed by Shakov [2]. For the rigid-sphere molecules also, the similar description is derived. In this paper, kinetic model equations are derived for the molecular gases under general power-law interaction potential, underlying the same approximation as made in the previous paper.

2 Discrete-Velocity-Ordinate Method

In the velocity distribution function F_i is specified at a grid point \vec{I} in a thermal velocity space \vec{V} . A set of discrete Boltzmann equations are written as (detail explanation of the symbols should refer to the previous paper [1])

$$DF_i/Dt = \sum_{j=1}^m \sigma_T g_{ij} (S_{ij} - F_i F_j). \quad (1)$$

where S_{ij} is given as the integral over the sphere having the relative speed g_{ij} as its diameter, for a specific collision partner (\vec{I}, \vec{J}) as follows:

$$S_{ij} = \sigma_T^{-1} \int \int \sigma F(\vec{V}) F(\vec{V}^*) \sin \chi d\chi d\epsilon$$

where σ is the differential cross section, χ is the deflection angle and ϵ the azimuthal angle. We deal with the gases of the monatomic molecules which

obey the elastic collisions with inverse power law of interaction potential defined by

$$U = Kr^{-s}$$

where r is the distance between molecules and K and s are the parameters pertinent to the potential. According to molecular kinetics we have for inverse power-law molecules

$$\sigma_T = A(s)g^{-4/s}, A(s) = 2\pi(4sK/m)^{2/s} A^{(0)}(s)$$

$$A^* = 2\pi(4sK/m)^{2/3} A^{(0)}(s)$$

In S_{ij} , (\vec{V}, \vec{V}^*) represent the respective velocities of post- or inverse collision pair for a fixed pre-collision pair (\vec{V}_i, \vec{V}_j) . With half a relative velocity \vec{r} and the center-of-mass velocity $\vec{G}_{ij} = (\vec{V}_i + \vec{V}_j)/2$, we have

$$\vec{V} = \vec{r} + \vec{G}_{ij}$$

$$\vec{V}^* = -\vec{r} + \vec{G}_{ij}$$

the integral S_{ij} is performed over a sphere whose center is at \vec{G}_{ij} with the diameter g_{ij} or the radius r_{ij} .

Equation 1 becomes

$$DF_i/Dt = \sum_{j=1}^m A(s)g_{ij}^{(s-4)/s} (S_{ij} - F_i F_j). \quad (2)$$

Our basic assumption is that the velocity distribution function is expressed by the 13-moment approximation as

$$F = F_0 [1 + (p_{mn}/2RTp)V_m V_n - (q_m/5RTp)(5 - V^2/RT)V_m].$$

F_0 is an equilibrium distribution function, n the number density, T the temperature, p the pressure, p_{mn} stress tensor component, q_m the heat flux vector component and R the gas constant. The subscripts (m, n) take either of the spatial Cartesian coordinates (x, y, z) . With this approximation, the integral S_{ij} reduces to the following in truncation of the terms of higher order

$$S_{ij} = F_0 F_0^* [1 + (p_{mn}/RTp)G_{ij,m} G_{ij,n} - (2q_m G_{ij,m}/5(RT)^2 p)(5RT - G_{ij}^2 - 5r_{ij}^2/3) + (1 - 3A^*/2A)B^*]. \quad (3)$$

*Abstract 4516 submitted to the 21st International Symposium on Rarefied Gas Dynamics, Marseille, France, July 26-31, 1998

where B^* represents non-isotropic scattering. The most complicated term in Eq.3 is rewritten as

$$\sum_{j=1}^m A(s) g_{ij}^{(s-4)/s} S_{ij} \Delta V_j \rightarrow \int A(s) (2r_{ij})^{(s-4)/s} S_{ij} dV_{jx} dV_{jy} dV_{jz}. \quad (4)$$

3 Kinetic Model Construction

The integral of Eq.4 is carried out over the whole velocity space \vec{V}_j for a fixed \vec{V}_i . This integral is conveniently rewritten in the polar coordinates (r_{ij}, κ, ω) relevant to the spatial Cartesian coordinates (x, y, z) , with the origin at \vec{V}_i

$$\int A(s) (2r_{ij})^{(s-4)/s} S_{ij} r_{ij}^2 \sin \kappa dr_{ij} d\kappa d\omega. \quad (5)$$

The variables involved in S_{ij} of Eq.3 are given as

$$\begin{aligned} G_{ij,m} &= V_{im} - r_{ij,m} \\ r_{ij,x} &= r_{ij} \sin \kappa \cos \omega \\ r_{ij,y} &= r_{ij} \sin \kappa \sin \omega \\ r_{ij,z} &= r_{ij} \cos \omega. \end{aligned}$$

and also we have

$$F_0 F_0^* = n^2 (2\pi RT)^{-1} \times \exp\{-(2r_{ij}^2 - 2r_{ij,m} V_{im} + V_i^2)/2\}. \quad (6)$$

Regarding (V_i, V_{im}) , the terms of higher order may be ignored in taking account into the present approximation. If this is the case, we have from Eq.6

$$F_0 F_0^* \approx n^2 (2\pi RT)^{-1} \exp\{-(2r_{ij}^2 + V_i^2)/RT\} \times \{1 + 2r_{ij,m} V_{im}/RT + 2r_{ij,m}^2 V_{im}^2/(RT)^2\}. \quad (7)$$

As the most simple case, in the previous paper the pseudo-Maxwellian molecules ($s = 4$) was dealt with and the kinetic model equation quite similar to the so-called S-model was derived as follows:

$$DF_i/Dt = An(F_i^+ - F_i). \quad (8)$$

where

$$\begin{aligned} F_i^+/F_{0,i} &= 1 + (1 - 3A^*/4A)(p_{mn}/p) \times \\ &\quad (V_{im} V_{in}/2RT) - (1 - A^*/2A) \times \\ &\quad (q_m V_{im}/pRT)(1 - V_i^2/5RT). \end{aligned}$$

The above equation only depends upon the velocities \vec{V}_i and thus the subscript i may entirely be omitted. For the molecules with the potential exponent $s \neq 4$, the procedure of the derivation is

nearby the same. The S_{ij} of Eq.6 is expressed in terms of $(r_{ij,m}, \kappa, \omega)$. The elementary calculus leads the expression of a bit length, similar to Eq.7. The extended kinetic model equation thus obtained involves the parameters in terms of s , which are expressed by the second kind of Euler integrals:

$$\int_0^\infty r_{ij}^{n(s)} \exp(-r_{ij}^2) dr_{ij}$$

where $n(s)$ is a function of the potential exponent s . Here the outline of the derivation of the extended kinetic model has been prescribed.

4 Conclusion

The kinetic model equation for molecules obeying the power-law interaction potential has much advantage for the computational analyses of various rarefied gas problems, because the computational scheme for the S-model of the pseudo-Maxwellian molecules has already been well established. For example, the reader may refer to the reference [3]. In the meeting the computational results on the typical rarefied gas flows will be presented.

References

- [1] Oguchi H. and Soga T., *Computation of Rarefied Gas Flows at Near-Equilibrium State by Discrete-Velocity-Ordinate Method*, in "Rarefied Gas Dynamics", ed. C. Shen, Peking Univ. Press, Beijing, China, pp.287-290, 1997.
- [2] Shakov E.M., *Generalization of the Krook Kinetic Equation*, J.Fluid Dynamics, 3:95, 1968.
- [3] Oguchi H., Morinishi K. and Satofuka N., *Time-Dependent Approach to Kinetic Analyses of Two-Dimensional Rarefied Gas Flows*, in "Rarefied Gas Dynamics", ed. Reberov et al, Plenum Pub. Co., New York, pp.293-302, 1985.

Unified Theory of the Eigenvalue and Memory-Function Approaches in Electron Thermalization in Gases - II *

T. Nishigori, K. Nagata
Kibi International University
8 Igamachi, Takahashi-shi, Okayama, 716-0018 Japan

1 Introduction

For the analysis of the transient behavior of high-energy electrons in a gas, the Boltzmann equation reduces to a Fokker-Planck (FP) equation. A successful eigenvalue approach to the solution of this FP equation has been developed by Shizgal and his co-workers [1]. They proposed a quadrature discretization method for an efficient calculation of the eigenvalues and eigenfunctions. This eigenvalue approach shows, however, a slow convergence at an initial, short-time domain [2] [3]. Nishigori, on the other hand, proposed a memory-function approach [2] [3], which is based on the short-time expansion, and accurate at small times. The difficulty in this approach is the evaluation of the short-time expansion coefficients. In Ref. 2, a simple polynomial cross section was assumed for e-He scattering.

It is shown in the present paper that the FP operator introduced by Shizgal, *et al.* [1] [4] is just the adjoint to the original FP operator, and useful for evaluation of the short-time expansion coefficients. The aim of the present paper is thus to develop a unified theory in which a matrix used in the eigenvalue calculation is used also to evaluate the coefficients in the memory-function approach. The difficulty in the memory-function approach can then be resolved. A preliminary account was reported in a previous Symposium [5], where the coefficients show small, irregular oscillations with increasing dimension of the matrix. This error is removed in the present paper.

2 Theory

A transient transport property of interest at time t' is expressed by

$$H(t') = \int_0^\infty h(x)\phi(x, t')dx \quad (1)$$

in terms of the electron distribution function $\phi(x, t')$ at speed x , which evolves in time according to

$$\frac{\partial}{\partial t'}\phi(x, t') = L\phi(x, t'). \quad (2)$$

Here, L is a FP operator [5]. Shizgal introduced a new operator \tilde{L} for the distribution function $g(x, t')$ defined by the relation $\phi(x, t') = w(x)g(x, t')$, where $w(x)$ is the equilibrium distribution function. The coefficients in the short-time expansion,

$$H(t') = \sum_{k=0}^{\infty} H_k t'^k, \quad (3)$$

are given by

$$H_k = \frac{1}{k!} H^{(k)}(0) = \frac{1}{k!} [L^{\dagger k} h(x)]_{x=x_0}, \quad (4)$$

where L^{\dagger} is the adjoint to the original FP operator. It is easily seen that Shizgal's operator, \tilde{L} , coincides with the adjoint operator L^{\dagger} . By applying the quadrature discretization method of Shizgal, we obtain a matrix representation, L^{\dagger} , of L^{\dagger} , with which we can evaluate the coefficients by

$$H_k = \frac{1}{k!} [L^{\dagger k} \mathbf{h}]_{i_0\text{-component}}, \quad (5)$$

where the column vector \mathbf{h} is the quadrature discretization representation of the function $h(x)$, and where i_0 is a sequence number of the quadrature point x_{i_0} , which is made to agree with the initial speed. The formula (5) does not require any analytical cross section, and can apply to a variety of electron thermalization problems.

*Abstract 4501 submitted to the 21st International Symposium on Rarefied Gas Dynamics, Marseille, France, July 26-31, 1998

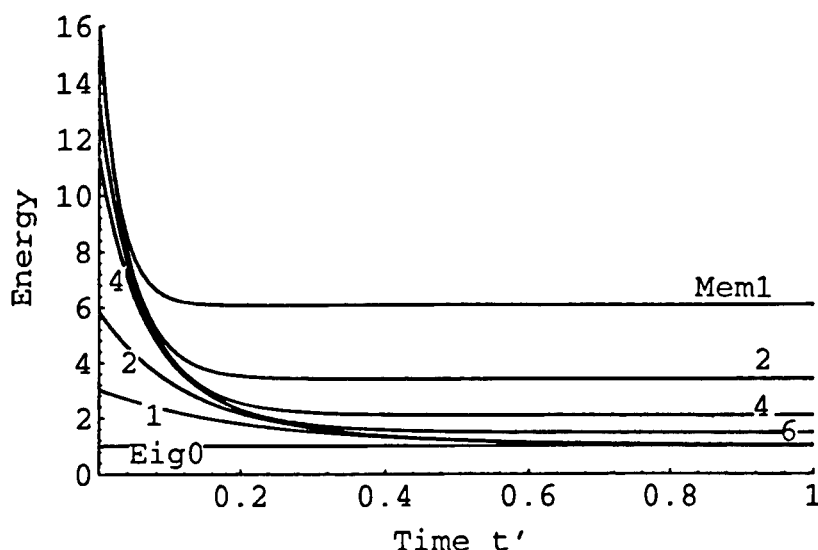


Figure 1: Results of the two approaches. Mem n refers to the result of the n -th order memory-function approach, while Eig n is that of the eigenvalue approach with n eigenmodes.

3 Energy Relaxation in Helium

The present unified theory has been applied to the energy relaxation of electrons in a helium gas at 290.1K without electric field. The initial electron energy has been chosen to be sixteen times the thermal energy. The Shizgal quadrature has been used to obtain the matrix L^\dagger of dimension up to 64. It was found that the small, irregular oscillations of the coefficients H_k are due to small matrix elements of order 10^{-8} or less located far from the diagonal position. We have omitted these small, unphysical elements to obtain the convergence in six significant figures up to the 21st-order coefficient, H_{21} . The validity of this prescription has been confirmed by the fact that all the 64 eigenvalues of the matrix $L^{\dagger 21}$ are correct in six significant figures. With the coefficients H_0, \dots, H_{21} , we can calculate the energy relaxation in the memory-function method up to the 10th order. On the other hand, the eigenvalues and eigenfunctions of the matrix L^\dagger were calculated to compare the two approaches. The results are shown in Figure 1. It is seen that

- the two approaches are complementary to each other; the memory-function method is good at small times, while the eigenvalue method shows a rapid convergence at large times.

- a combination of the two methods gives an efficient way of calculating the relaxation properties over the entire time domain. In the case shown in Figure 1, the result of the memory-function method of order 4 (Mem 4) and that of the eigenvalue method with 4 eigenmodes (Eig 4) can be connected around $t' = 0.15$ to obtain a good result over the entire time domain.

Results on other relaxation properties such as the mobility in other moderator gases with an electric field and/or an attaching gas will be presented in the Symposium.

References

- [1] B. Shizgal, *et al.*, Radiat. Phys. Chem., Vol. 34, pp. 35-50, 1989.
- [2] T. Nishigori and B. Shizgal, J. Chem. Phys., Vol. 89, pp. 3275-3278, 1988.
- [3] T. Nishigori, J. Chem Phys., Vol. 82, pp. 2106-2109, 1985.
- [4] R. Blackmore and B. Shizgal, Phys. Rev. A, Vol. 32, pp. 1855-1868, 1985.
- [5] T. Nishigori, Rarefied Gas Dynamics 20, Ed. by Ching Shen, pp. 85-90, Peking Univ. Press, Beijing, 1997.

Discrete-Velocity Kinetic BGK Models with High-Order Symmetries of Velocity Tensors *

Y.H. Qian¹, R. Gatignol²

¹ Dept. of Applied Physics and Applied Mathem., Columbia Univ., New York, USA

² Lab. de Modélisation en Mécanique, Université Pierre et Marie Curie, Paris, France

In this presentation, we are interested in investigating discrete kinetic Bhatnagar-Gross-Krook (BGK) models which have isotropic 6-order velocity tensors in two and three dimensions. Due to the simplicity of BGK approximation, we are able to derive equations up to third order of Knudsen number ϵ . The importance of each term will be estimated. In the following, the basic procedure and main results will be outlined.

The traditional Chapman-Enskog expansion is used to derive large-scale dynamical equations. Assuming that the distribution function of particle with discrete velocity \vec{c}_i can be developed with power series of ϵ around an equilibrium distribution N_i^ϵ ,

$$N_i = N_i^\epsilon + \epsilon N_i^{(1)} + \epsilon^2 N_i^{(2)} + \epsilon^3 N_i^{(3)} + O(\epsilon^4) \quad (1)$$

where $N_i^{(n)}$ are corrections due to space gradients. Using three time scales, we have: $\partial_t \rightarrow \epsilon \partial_{t_1} + \epsilon^2 \partial_{t_2} + \epsilon^3 \partial_{t_3}$, $\partial_x \rightarrow \epsilon \partial_x$. Inserting the above relations into the starting time evolution equation,

$$\partial_t N_i + \vec{c}_i \cdot \vec{\nabla} N_i = \omega [N_i^\epsilon(t, \vec{x}) - N_i(t, \vec{x})] \quad (2)$$

where ω is the relaxation parameter and the equilibrium distribution N_i^ϵ is chosen as,

$$N_i^\epsilon = t_p \rho \left[1 + \frac{c_{i\alpha} u_\alpha}{c_s^2} + \frac{u_\alpha u_\beta}{2c_s^4} (c_{i\alpha} c_{i\beta} - c_s^2 \delta_{\alpha\beta}) \right] \quad (3)$$

where ρ and \vec{u} are hydrodynamic density and velocity, they are defined as: $\rho = \sum_i N_i = \sum_i N_i^\epsilon$ and $\rho \vec{u} = \sum_i N_i \vec{c}_i = \sum_i N_i^\epsilon \vec{c}_i$. c_s is the sound speed and t_p the weighting factor with $p = c_i^2$. Up to three order ϵ^3 , we obtain,

$$\begin{aligned} & \epsilon (\partial_{t_1} N_i^\epsilon + \vec{c}_i \cdot \text{vec} \nabla N_i^\epsilon) + \epsilon^2 (\partial_{t_1} N_i^{(1)} + \partial_{t_2} N_i^\epsilon + \vec{c}_i \cdot \vec{\nabla} N_i^{(1)}) + \\ & \epsilon^3 (\partial_{t_1} N_i^{(2)} + \partial_{t_2} N_i^{(1)} + \partial_{t_3} N_i^\epsilon + \vec{c}_i \cdot \vec{\nabla} N_i^{(2)}) = -\omega (\epsilon N_i^{(1)} + \epsilon^2 N_i^{(2)} + \epsilon^3 N_i^{(3)}) \end{aligned} \quad (4)$$

The leading order terms give the Euler equation after summation,

$$\partial_{t_1} (\rho u_\alpha) + \partial_\beta \left(\frac{\rho}{2c_s^4} T_{\alpha\beta\gamma\delta} u_\gamma u_\delta - \frac{\rho u^2}{2} \delta_{\alpha\beta} \right) = -\partial_\alpha (c_s^2 \rho) \quad (5)$$

$$\text{where} \quad T_{\alpha\beta\gamma\delta} = \sum_i t_p c_{i\alpha} c_{i\beta} c_{i\gamma} c_{i\delta}$$

This 4th-order tensor $T_{\alpha\beta\gamma\delta}$ should be isotropic. An additional constraint is the Galilean invariance. Therefore, $T_{\alpha\beta\gamma\delta}$ should take the following form in order to yield the above constraints,

$$T_{\alpha\beta\gamma\delta} = c_s^4 (\delta_{\alpha\beta} \delta_{\gamma\delta} + \delta_{\delta\beta} \delta_{\alpha\gamma} + \delta_{\gamma\beta} \delta_{\alpha\delta}) \quad (6)$$

* Abstract 3002 submitted to the 21st Internat. Symp. on Rarefied Gas Dynamics, Marseille, France, July 26-31, 1998

We rewrite the momentum equation in usual form,

$$\partial_t(\rho u_\alpha) + \partial_\beta(\rho u_\alpha u_\beta) = -\partial_\alpha(c_s^2 \rho) \quad (7)$$

The second order equation is the Navier-Stokes equation,

$$\partial_t(\rho u_\alpha) + \partial_\beta(\rho u_\alpha u_\beta) = -\partial_\alpha(\rho c_s^2) + \nu \partial_\beta [\partial_\alpha(\rho u_\beta) + \partial_\beta(\rho u_\alpha)] \quad \text{with } \nu = \frac{c_s^2}{\omega} \quad (8)$$

where ν is the shear viscosity.

The third order equation leads to a dispersive third order term,

$$\partial_t(\rho u_\alpha) + \partial_\beta(\rho u_\alpha u_\beta) = -\partial_\alpha(c_s^2 \rho) + \nu \partial_\beta [\partial_\alpha(\rho u_\beta) + \partial_\beta(\rho u_\alpha)] + \theta \partial_{\beta\beta\alpha} \rho \quad \text{with } \theta = \frac{2c_s^4}{\omega^2} \quad (9)$$

If we consider the nonlinear correction to transport coefficients, we have to make the following 6th-order velocity tensor $K_{\alpha\beta\gamma abc}$ isotropic: $K_{\alpha\beta\gamma abc} = \sum_{pi} t_p c_{pi\alpha} c_{pi\beta} c_{pi\gamma} c_{pia} c_{pib} c_{pic}$, together with the isotropic $T_{\alpha\beta\gamma\delta}$, we obtain a model in two dimensions with 13 discrete velocities (D2Q13) and a model in three dimensions with 33 velocities (D3Q33). We summarize the parameters of these two models in the following table,

Modèle	t_0	t_1	t_2	t_3	t_4	c_s	g_0
D2Q13	$\frac{2}{5}$	$\frac{8}{75}$	$\frac{1}{25}$	/	$\frac{1}{300}$	$\frac{\sqrt{10}}{5}$	$\frac{4}{75}$
D3Q33	$\frac{43}{150}$	$\frac{4}{75}$	$\frac{2}{75}$	$\frac{1}{150}$	$\frac{1}{300}$	$\frac{\sqrt{10}}{5}$	$\frac{16}{75}$

And the final equation of momentum is derived as,

$$\begin{aligned}
 \partial_t(\rho u_\alpha) + \partial_\beta(\rho u_\alpha u_\beta) = & -\partial_\alpha(c_s^2 \rho) + \nu \partial_\beta [\rho(\partial_\alpha u_\beta + \partial_\beta u_\alpha)] \\
 & + \frac{2c_s^4}{\omega^2} \partial_{\beta\beta\alpha}(\rho) \\
 & - \sigma \partial_{\beta\gamma}(\rho u_\alpha u_\beta u_\gamma) \\
 & - \frac{2c_s^2}{\omega^2} \partial_\beta [\rho(\partial_\gamma u_\alpha)(\partial_\gamma u_\beta) + \frac{c_s^2}{\rho}(\partial_\alpha \rho)(\partial_\beta \rho)] \\
 & - \frac{2c_s^2}{\omega^2} \partial_{\beta\gamma} [u_\alpha u_\beta \partial_\gamma(\rho) + u_\alpha u_\gamma \partial_\beta(\rho) + u_\beta u_\gamma \partial_\alpha(\rho)] \\
 & + \frac{3(c_s^6 - g_0)}{2\omega^2 c_s^4} [\partial_{\alpha\beta\beta}(\rho u^2) + 2\partial_{\alpha\beta\gamma}(\rho u_\beta u_\gamma) + 2\partial_{\beta\beta\gamma}(\rho u_\alpha u_\gamma)] \\
 & - \frac{1}{\omega^2} \partial_\beta [u_\beta \partial_{\gamma\delta}(\rho u_\alpha u_\gamma u_\delta) + u_\alpha \partial_{\gamma\delta}(\rho u_\beta u_\gamma u_\delta) + \partial_{\gamma\delta}(\rho u_\alpha u_\beta u_\gamma u_\delta)] \quad (10)
 \end{aligned}$$

In terms of Reynolds number R_e and Mach number M_a , we can estimate the orders of each term involved in the right-hand-side of the above equation:

pressure is order of $\sim 1/M_a^2$

viscous term is $\sim 1/R_e$

dispersive term is $\sim 1/R_e^2$

cubic nonlinear term is $\sim M_a^2/R_e$

dispersive nonlinear terms are $\sim M_a^2/R_e^2$

the last terms are $\sim M_a^4/R_e^2$.

In this communication, discrete kinetic models with 6th-order isotropic velocity tensor have been obtained. Large scale dynamical equation is derived. Modifications to the Navier-Stokes are thus estimated in terms of Reynolds and Mach numbers. In rarefied gas regimes, for example, the micro-electronic mechanical systems, the Knudsen number may not be small and these modifications may play important role. Direct numerical simulations will be used in the future to test the validity of the present models.

On The Boundary Conditions of the Advanced Fluid Dynamic Equations *

T. Soga

Department Aerospace Engineering, Nagoya University, Nagoya, Japan

1 Introduction

The method of Chapman-Enskog expansion is one of the fundamental approaches to the Boltzmann equation. Recently, Zhong [1] demonstrated the applicability of the partially linearized super-Burnett equation, i.e., augmented Burnett equation to the numerical analysis of rarefied hypersonic flows, while Wang-Chang[2] had obtained the structure of weak shock wave using almost same equation systems. Adding linear terms with the third order derivatives to the Burnett equation, they obtained non-oscillating shock-wave structure of high Mach number. So long as the shock-wave structure is concerned, boundary conditions for the basic equations, are self-evident. However, relevant boundary conditions for the equations on the solid boundaries still remain to be determined. Zhong derived one more boundary condition of the shear stress on the wall in addition to the Schamberg's second order boundary conditions(See Zhong[1]). These conditions were derived only using lower moments of the distribution function. Since, however, Schamberg's boundary conditions can be derived using the Grad's method, certain additional relations between the shear stress and higher order moments of the distribution function must be necessary. Present paper yields these relations for the augmented Burnett equation. An application of the conditions to the Couette flow problem is presented.

2 Boundary Conditions

Grad's flux vector: Assuming that α of the impinged molecule on the wall reflect specularly and $(1-\alpha)$ suffer diffuse reflection, the distribution function of the reflected molecules is given by

$$f^+(C_1, C_2, C_3) = \alpha f^-(-C_1, C_2, C_3) + k \exp\left(-\frac{C_w^2}{2RT_w}\right)$$

where the suffix 1 denotes the direction normal to the wall and 2 and 3 denote the directions parallel to the wall, while the suffix w denotes the values pertinent to the wall. $C_w^2 = (\bar{c} - \bar{v}_w)^2$ where \bar{v}_w is the velocity of the wall. $k = (1-\alpha)n_w(2\pi RT_w)^{-3/2}$ where notations are conventional ones. We define the moment of the distribution function f by

$$Qm = \int_{-\infty}^{\infty} \int_{-\infty}^{\infty} \int_{-\infty}^0 Y_{Qm}(\bar{c}) f(C_1, C_2, C_3) d\bar{c}$$

where Y_{Qm} 's are any combination of the Ikenberry's [3] irreducible tensor $Y_{ijk\dots}$ and Sonine polynomials $S_m^{(n)}(C^2)$, for example, $Y_{11} = (c_1^2 - C^2/3)$. Defining $(Qm)^-, (Qm)_w$ by

$$(Qm)^- = \int_{-\infty}^{\infty} \int_{-\infty}^{\infty} \int_{-\infty}^0 Y_{Qm}(\bar{c}) f^-(C_1, C_2, C_3) d\bar{c}$$

$$(Qm)_w = \int_{-\infty}^{\infty} \int_{-\infty}^{\infty} \int_0^{\infty} Y_{Qm}(\bar{c}) k \exp\left(-\frac{C_w^2}{2RT_w}\right) d\bar{c}$$

fluxes normal to the wall (those are expressed by the odd moment on C_1) are given by

$$Qm = (Qm)_w + (1-\alpha)(Qm)^-. \quad (1)$$

For Y_{12} we obtain $p_{12} = (p_{12})_w + (1-\alpha)(p_{12})^-$ where p_{12} denotes the shear stress on the wall.

Burnett's distribution function: Burnett and partially linearized super-Burnett distribution functions are expressed by

$$f_{\text{Burnett}} = f^{(0)}[1 + \Phi^{(1)} + \Phi^{(2)} + \Phi_{\text{linear}}^{(3)}] \quad (2)$$

where $f^{(0)}$ is the Maxwellian and $\Phi^{(1)}$ is the first order Chapman-Enskog solution. $\Phi^{(2)*} = \Phi^{(2)} + \Phi_{\text{linear}}^{(3)}$ can be expressed as (Shavariyev[4]),

$$\Phi^{(2)*} = a_{R0}R_0S_{1/2}^{(2)} + a_{T0}T_0S_{1/2}^{(3)} + a_{Qi}Q_i^{(2)}Y_iS_{3/2}^{(1)}$$

$$+ a_{Si}S_iY_iS_{3/2}^{(2)} + a_{pij}p_{ij}^{(2)}Y_{ij} + a_{Rij}R_{ij}Y_{ij}S_{5/2}^{(1)}$$

$$+ a_{Tij}T_{ij}Y_{ij}S_{5/2}^{(2)} + a_{Qijk}Q_{ijk}Y_{ijk}$$

*Abstract 4520 submitted to the 21st International Symposium on Rarefied Gas Dynamics, Marseille, France, July 26-31, 1998

$$+a_{Sijk}S_{ijk}Y_{ijk}S_{7/2}^{(1)} + a_{Rijk}R_{ijk}Y_{ijk},$$

where Q_{ijk} 's, R_{ijk} ., S_{ijk} ., and T_{ijk} ., are the 3rd, 4th, 5th and 6th order moment of the distribution function, respectively. Substituting Eq. (2) into Eq. (1), we obtain boundary conditions in terms of ρ , \bar{v} , T , p_{ij} , Q_i , Q_{ijk} , and so on, while each moment is express by the derivatives and/or higher derivatives of ρ , \bar{v} , T . Neglecting higher terms of slip velocity, v_s , boundary conditions for odd moments (like the heat flux on the wall) and the condition for the even moments (like the shear stress) are separately obtained. Here, we show the boundary conditions pertinent to the Couette flow,

$$\sqrt{\pi} \frac{(1+\alpha)}{2} \begin{pmatrix} \hat{P}_{12} \\ \hat{R}_{12} \\ \hat{R}_{1112} \\ \hat{R}_{2212} \\ \hat{T}_{12} \end{pmatrix} = (1-\alpha)\hat{n}_w \hat{v}_s$$

$$\times \begin{pmatrix} -\frac{1}{2}(\frac{T_w}{T_0})^{\frac{1}{2}} \\ \frac{3}{2}(\frac{T_w}{T_0})^{\frac{1}{2}} - \frac{7}{4}(\frac{T_w}{T_0})^{\frac{1}{2}} \\ \frac{1}{7}(\frac{T_w}{T_0})^{\frac{1}{2}} \\ -\frac{3}{28}(\frac{T_w}{T_0})^{\frac{1}{2}} \\ -3(\frac{T_w}{T_0})^{\frac{1}{2}} + \frac{27}{4}(\frac{T_w}{T_0})^{\frac{1}{2}} - \frac{63}{16}(\frac{T_w}{T_0})^{\frac{1}{2}} \end{pmatrix}$$

$$+ \begin{pmatrix} \frac{1}{10} & -\frac{1}{2} & 0 & \frac{8}{525} & -\frac{1}{18} & 0 \\ -\frac{11}{20} & \frac{1}{4} & 0 & \frac{5}{28} & -\frac{5}{12} & 0 \\ -\frac{3}{35} & -\frac{9}{14} & 0 & \frac{245}{3} & \frac{1}{12} & 0 \\ \frac{9}{140} & \frac{14}{28} & -\frac{1}{2} & -\frac{9}{980} & -\frac{41}{420} & \frac{1}{18} \\ -\frac{21}{80} & \frac{1}{16} & 0 & -\frac{333}{560} & \frac{157}{720} & 0 \end{pmatrix} \begin{pmatrix} \hat{Q}_2 \\ \hat{Q}_{112} \\ \hat{Q}_{222} \\ \hat{S}_2 \\ \hat{S}_{112} \\ \hat{S}_{222} \end{pmatrix}$$

The values with hat in Eq. (3) denote the nondimensionalized values by ρC_m^n where the C_m is the most probable speed and n is a value relevant to the moment.

3 Application to Couette Flow

We consider the plane Couette flow, where the upper and lower walls moving with the velocity U_0 and $-U_0$, respectively. In the case for $U_0/C_m \ll 1$ Navier-Stokes, Burnett, and augmented Burnett equations are expressed as,

$$p_{12} = \text{const.} \quad (4)$$

A general solution for the flow velocity v of Eq. (4) is given by

$$v = v_0 + ay + \beta^- e^{-\omega y} + \beta^+ e^{\omega y}. \quad (5)$$

where $2 \rightarrow y$, $a = -p_{12}/\mu$, μ the shear viscosity, and $\omega = \sqrt{3\pi}/\lambda$ where λ denotes the mean free path. For the cases of Navier-Stokes and Burnett equations $\beta^\pm = 0$ and $v_0 = v_s$. The first line of the Eq. (3) yields the Schamberg's slip velocity condition, while the second line yields,

$$0 = \frac{\lambda}{C_m} \frac{\partial v}{\partial y} + \frac{6\lambda^2}{\pi C_m} \frac{\partial^2 v}{\partial y^2}, \quad (6)$$

which relevantly supplements the Schamberg's condition. Thus, unknown parameter β^\pm are specified; since, however, R_{12} and Q_{112} in Eq.(3) were calculated using $\Phi^{(2)*} = \Phi^{(2)}$, more precise condition can be obtained using the solution $\Phi_{linear}^{(3)}$. On the other hand, Zhon's new condition yields $p_{12}^{Burnett} = p_{12}^{N-S}$ under the condition $\text{div} \cdot \bar{v} = 0$. Thus, values of β^\pm remain undetermined.

4 Conclusion

Boundary conditions for the moment equations and advanced fluid dynamic equations were derived using the Grad's method. It is found that so long as the slip velocity is small, $v_s/C_m \ll 1$, boundary conditions for the odd order moment of the distribution function and the conditions for the even moments are separable. The obtained boundary condition were applied to the plane Couette flow problem and the validity of the boundary conditions were demonstrated.

(3)

References

- [1] Zhong X., *On Numerical Solutions of Burnett Equations for Hypersonic Flow Past 2-D Circular Blunted Leading Edges in Continuum Transition Regime*, AIAA-93-3092, 1993.
- [2] Wang-Chang C.S., *On the Theory of the Thickness of Weak Shock waves, in Studies in Statistical Mechanics*, V, pp. 27-42, North-Holland Pub, 1970.
- [3] Ikenberry E., *A System of Homogeneous Spherical Harmonics*, Am. Math. Monthly, December, pp. 719-721, 1955.
- [4] Shavariev M.Sh., *The Burnett Approximation of the Distribution Function and the Super-Burnett Contributions to the Shear Tensor and the Heat Flux*, J. Applied Math. Mech. 42(4), pp.698-702, 1978.

KINETIC THEORY AND MODELS - KTM 6

ROOM MARION

TUESDAY, JULY 28, 1998

10:50

Motion of Dispersed Bubbles in a Potential Flow *

B. Lucquin-Desreux

Lab. d'Analyse Numérique, Univ. P. et M. Curie, France

1 Introduction

We here study a two-phase flow. In collaboration with H. Herrero and B. Perthame, we obtain in [1] a kinetic model to describe the motion of dispersed bubbles in an incompressible and irrotational flow. This work follows that of G. Russo and P. Smereka [2]. We go however further, showing that the exact kinetic equation, of Vlasov type, for the dispersed phase can be exactly derived and no further approximation is needed to write the mean field equation. This model preserves the energetic structure of the departing dynamical system. This has effects on the solution computed by numerical simulation. We also show that the fluid limit derived from our kinetic model has nicer mathematical properties than those of the fluid model obtained in [3].

2 The mean field equation

Let us consider a large number N of bubbles which are all rigid balls of fixed radius a . The aim here is to derive a mean field limit equation for the dispersed phase, when simultaneously $N \rightarrow +\infty$ and $a \rightarrow 0$. The parameter λ which naturally appears in this asymptotic is $\lambda = Na^3\tau$. The coefficient τ is given by $\tau = 6\pi\rho_f/(\rho_f + 2\rho_p)$, where ρ_f and ρ_p are the respective densities of the fluid and of the particles. Its expression is connected to the added mass. Following [2], the external fluid is represented as a dipole approximation of a potential flow, which allows an explicit computation. The motion of the bubbles is only created by the pressure forces exerted on their boundary.

We start with the Lagrangian system

$$\frac{d}{dt}X_i(t) = V_i(t), \quad \frac{d}{dt}\left(\frac{\partial \mathcal{L}_N(t)}{\partial v_i}\right) = \frac{\partial \mathcal{L}_N(t)}{\partial x_i}$$

which describes the motion of the bubbles in scaled variables. This Lagrangian is defined by

$$\mathcal{L}_N(t) = \mathcal{L}_N(X_1(t), \dots, X_N(t); V_1(t), \dots, V_N(t)),$$

with

$$\mathcal{L}_N(x_1, \dots, x_N; v_1, \dots, v_N) = \frac{1}{2} \mathcal{V}_N \cdot \mathcal{A}_N \cdot \mathcal{V}_N,$$

where \mathcal{V}_N denotes the $3N$ vector with components $v_i \in \mathbb{R}^3$, while the $3N \times 3N$ matrix $\mathcal{A}_N = \mathcal{A}_N(x_1, x_2, \dots, x_N)$ writes $\mathcal{A}_N = \mathcal{I}_N - a^3\tau B_N$, $B_N = (B_{i,j})_{1 \leq i,j \leq N}$ being of the form: $B_{i,j} = B(x_i - x_j)$ for $i \neq j$ and $B_{i,i} = 0$. In the particular case of the dipole approximation of a potential flow, the 3×3 matrix B is exactly $B = \underline{B}$, with $\underline{B}(x) = D_x^2(1/4\pi|x|)$ for $x \in \mathbb{R}^3 - \{0\}$. We thus have to regularize it, without changing the dynamics of the bubbles.

We introduce the density function of the bubbles defined by

$$f_N(t, x, v) = \frac{1}{N} \sum_{1 \leq i \leq N} \delta(x - X_i(t)) \otimes \delta(v - V_i(t)).$$

This function satisfies the following equation, of Vlasov type ($t > 0$, $x \in \mathbb{R}^3$, $v \in \mathbb{R}^3$),

$$\begin{aligned} \frac{\partial f_N}{\partial t} + v \cdot \nabla_x f_N + F_N \cdot \nabla_v f_N &= 0, \\ F_N(t, x) &= \lambda (B * \partial_t j_N(t, \cdot))(x), \end{aligned}$$

where $j_N(t, x) = \int_{\mathbb{R}^3} v f_N(t, x, v) dv$ (resp. $\rho_N(t, x) = \int_{\mathbb{R}^3} f_N(t, x, v) dv$) is the courant (resp. the density). It is possible to eliminate the time derivative of the courant by introducing the tensor E_N defined by: $E_N = \int_{\mathbb{R}^3} v \otimes v f_N(t, x, v) dv$. Finally, in the potential case with the dipole approximation, we formally have the following mean field limit, when $N \rightarrow +\infty$, $a \rightarrow 0$ with fixed λ ($t > 0$, $x \in \mathbb{R}^3$, $v \in \mathbb{R}^3$):

$$\begin{aligned} \frac{\partial f}{\partial t} + v \cdot \nabla_x f + F \cdot \nabla_v f &= 0, \\ F(t, x) &= \nabla_x U(t, x), \\ -\operatorname{div}_x((1 + \lambda\rho)\nabla_x U) &= -\lambda D_x^2 : E, \end{aligned}$$

where $D_x^2 : E$ means the contracted product $\sum_{k,l} D_{x_k x_l}^2 E_{kl}$, E being a matrix with entries E_{kl} .

*Abstract 3256 submitted to the 21st International Symposium on Rarefied Gas Dynamics, Marseille, France, July 26-31, 1998

We also have $U = \partial_t \varphi$, where φ satisfies $-\Delta_x \varphi = \lambda \operatorname{div} j$. The conserved energy is thus given by:

$$\frac{1}{2} \int_{\mathbb{R}^s} |v|^2 f(t, x, v) dx dv + \frac{1}{2\lambda} \int_{\mathbb{R}^s} |\nabla_x \varphi(t, x)|^2 dx,$$

where: $-\Delta_x \varphi = \lambda \operatorname{div}_x j$. It is a non negative quantity which splits into the kinetic energy and the potential one. Moreover, under some suitable hypothesis on the product λB , each of these two energies is controlled by the total initial one.

3 The Hamiltonian structure

By change of variables, the same analysis can be done starting with the Hamiltonian system:

$$\dot{X}_i(t) = \frac{\partial \mathcal{H}_N(t)}{\partial p_i}, \quad \dot{P}_i(t) = -\frac{\partial \mathcal{H}_N(t)}{\partial x_i}.$$

In these equations, $\mathcal{H}_N(t)$ is the Hamiltonian derived from the Lagrangian $\mathcal{L}_N(t)$ by the Legendre transform. The new variable $P_i(t)$ is the scaled general impulse of the particle with index i (in physical variables, this impulse is the sum of the bubble impulse, proportional to the particle density ρ_p , and of the Kelvin impulse; the latter is proportional to the virtual mass, which writes in terms of the fluid density). The density measure

$$g_N(t, x, p) = \frac{1}{N} \sum_{1 \leq i \leq N} \delta(x - X_i(t)) \otimes \delta(p - P_i(t))$$

satisfies the following kinetic equation ($t > 0, x \in \mathbb{R}^3, p \in \mathbb{R}^3$):

$$\frac{\partial g_N}{\partial t} + \operatorname{div}_x (H_p g_N) - \operatorname{div}_p (H_x g_N) = 0,$$

$$H(t, x, p) = \frac{1}{2} |p + \Phi_N(t, x)|^2,$$

$$\Phi_N(t, x) = \lambda \left[B * (J_N + \rho_N \Phi_N)(t, \cdot) \right](x),$$

where $J_N = j_N - \rho_N \Phi_N$. Let us note that ρ_n and J_N are the density and courant associated with g_N .

4 Approximated models

In view of numerical applications, approximated models are proposed. The idea is to split Φ_N as an infinite series, in terms of λ (supposed small enough), and then to truncate this series. Russo-Smerek's model corresponds, very roughly speaking, to the first order truncation; the energy may

be negative. We propose a second order truncation model, for which the energy is non negative.

Numerical tests are done, by particle method, in order to compare the two models. They confirm that our model is more stable. The simulations also show the appearance of clusters of stratified geometry.

5 Some further remarks

Other comparisons can also be done between Russo-Smerek's model and the full non linear one we have obtained in paragraph 2. Following [2], a stability analysis for the linearized problem shows that our model is stable for a wider range of initial conditions. Moreover, if we look for the fluid dynamic limit of the disperse phase, we find Euler equations which always form an hyperbolic system: we thus improve the results obtained in [3].

References

- [1] H. Herrero, B. Lucquin-Desreux, B. Perthame, *On the motion of a dispersed phase in a potential flow*, Publication du Labo. d'Analyse Numérique de Paris 6 No. 97021, 1997; submitted.
- [2] G. Russo and P. Smereka, *Kinetic theory for bubbly flow I: collisionless case*, SIAM J. Appl. Math., Vol. 56, No.2, pp. 327-357, 1996.
- [3] G. Russo and P. Smereka, *Kinetic theory for bubbly flow II: fluid dynamic limit*, SIAM J. Appl. Math., Vol. 56, No.2, pp. 358-371, 1996.

The Kinetic Equations of Rarefied Gas Suspensions *

V.Ya. Rudyak

Novosibirsk State University of Civil Engineering, Novosibirsk, Russia

1 Introduction

Dynamics of aerosols and gas suspensions has not known the universal approaches. In some cases a dispersed medium can be described on hydrodynamic level of description and in other ones we have to use the kinetic level of description. There are no sufficiently rigorous approaches which should be allowed to formulate the hydrodynamic and kinetic models. One of the reasons of a such situation is the variety of possible dispersed media. Usually these media are classified on an aggregate state. Such a classification is absolutely insufficient and does not permit to select the media classes described by the same models. Really, in many cases the gas-hard particles and liquid-hard particles mixtures conduct themselves equally but in other cases the behavior of the dispersed media of even one class can sharply differ. Therefore before the models describing the dispersed media dynamics will be constructed it is necessary to develop the respective classification of such media. This classification has to permit to pick out the media groups which are described by means of the common similarity parameters. The construction of such classification is the first aim of the present paper.

On the basis of the developed classification the kinetic equations for rarefied fine and middle dispersed gas suspensions are derived.

2 Classification principles

To develop an adequate classification it is necessary to take into account that the dispersed media have the complicated internal structure. Therefore the relation between the scales of medium internal structural elements is one of the most considerable classification features. At last the properties of the heterogeneous medium will be changed depending on the density of the dispersed phase. Thus it is proposed to pick out the next triad classifying the

heterogeneous media [1].

1. Classification on an aggregate state.
2. Classification on the relation of the medium internal structural elements.
3. Classification on the density of a dispersed phase.

Following these principles we can pick out for example four classes of gas suspensions. (i) Molecular gas suspension for which $r_0 \leq R_0$ and $m/M \ll 1$, where r_0 is the radius of the carrier gas molecule and m is its mass, R_0 is radius of the dispersed particles with mass is equal to M . (ii) Fine dispersed gas suspension for which $R_0 \sim \sqrt{\varepsilon_0} \lambda_g$. Here $\lambda_g \sim 1/n_g r_0^2$ is the free path length of the gas molecules and $\varepsilon_0 \sim n_g r_0^3$. (iii) Middle dispersed gas suspension for which $R_0 \geq \lambda_g$. (iv) Coarse dispersed gas suspension for which $\lambda_g \ll R_0 \leq r_h$, where r_h is the hydrodynamically infinitesimal scale $r_h \sim \sqrt{\lambda_g L}$ [2], L is the characteristic length scale of a flow.

On the other hand, depending on the dispersed particles density the gas suspensions are subdivided into four classes too. (j) Ultra rarefied gas suspensions satisfy the conditions $l_{mp} \sim n_p^{-1/3} \leq \varepsilon_p L$ and $\varepsilon_p \sim n_p R_0^3 \ll 1$. Here n_p is the density of the dispersed particle "gas". We can neglect the particles interactions for such a gas suspension. (jj) Rarefied gas suspension is a suspension in which only binary particles collisions are taken into account. For such medium $\varepsilon_p \ll 1$, $R_0/l_{mp} \sim \varepsilon_p^{1/3}$. (jjj) Moderately dense gas suspensions for which $\varepsilon_p \ll 1$, $R_0 < l_{mp}$. (jv) Dense gas suspension is determined by the following relations $\varepsilon_p \leq 1$, $R_0 \sim l_{mp}$.

3 Kinetic equations

The starting point of the kinetic equation derivation of gas suspensions is the Liouville equation for the N -particle distribution function. For the ultra rarefied molecular gas suspension we obtain the system of two Boltzmann equations for the one-particle distribution functions of molecules f_{1g} and dispersed particles f_{1p} .

*Abstract 5136 submitted to the 21st International Symposium on Rarefied Gas Dynamics, Marseille, France, July 26-31, 1998

For the fine dispersed gas suspension for which $R_0 \sim \sqrt{\epsilon_0} \lambda_g$ the following system of kinetic equations are obtained

$$\begin{aligned} \frac{\partial f_{1g}}{\partial t} + \vec{v}_g \cdot \frac{\partial f_g}{\partial \vec{r}} &= J_B^{gg} + J_B^{gp} + J_1^{gp}, \\ \frac{\partial f_{1p}}{\partial t} + \vec{V}_p \cdot \frac{\partial f_p}{\partial \vec{R}} &= J_B^{pp} + J_1^{pp} + J_B^{pg} + J_1^{pg}, \end{aligned} \quad (1)$$

where J^{gg} and J^{pp} are intermolecular and interparticles collision integral respectively and J^{gp} and J^{pg} are the molecule-particle collision integrals. All the collision integrals denoted by the subscript B have the form of the Boltzmann collision integrals. The collision integrals J_1^{gp} , J_1^{pp} and J_1^{pg} , define the corrections to the Boltzmann integrals of the order of $\epsilon_g^{1/4}$ and $\epsilon_g^{1/2}$. These additional terms determine many-particles collision integrals. The three-particle (molecule-particle-molecule or particle-molecule-particle) interactions are the most important contributions.

The kinetic theory of middle and course dispersed gas suspensions is more complicated as compared with the case of the fine one. It is impossible to construct any perturbation theory which permit to obtain the kinetic equations for a one-particle distribution function. The physical reason of this is "the continuity" of the molecular-particle collisions. In other words there are many such collisions during the molecule-particle interaction time. Therefore we are able to obtain only the generalized kinetic equation for middle and course dispersed gas suspensions. For example the generalized kinetic equation of dispersed particles for the ultra dispersed gas suspension in first approximation on small parameter $\mu = m/M \ll 1$ has the following form

$$\begin{aligned} \frac{\partial f_{1p}}{\partial t} + \vec{V}_p \cdot \frac{\partial f_p}{\partial \vec{R}} &= \int d\Gamma \Pi \{ S_- f_N f_p - \\ &- \mu \int_{t_0}^t dt_1 \Omega_{-(t-t_1)} f_N f_p \}, \end{aligned} \quad (2)$$

$$\Pi = \sum_{i,j} \vec{f}_{ij} \cdot \left(\frac{\partial}{\partial \vec{p}_i} - \frac{\partial}{\partial \vec{p}_j} \right),$$

where S_- and Ω_t are certain evolution operators of the system. These operators were defined for an isolated dispersed particle earlier [3]. v_g and V_p are the velocities of molecules and particles, respectively. $d\Gamma$ is the volume element of molecules phase space. \vec{f}_{ij} is the interaction force of molecules and particles. In a general case this force can be conservative or not conservative. For example molecule-particle interaction can be described by means of the diffuse reflection law.

4 Discussion and conclusion

The classification of the dispersed media developed here permits to construct the kinetic and hydrodynamic models of the dispersed fluids. It is important to emphasize that classification features are the certain similarity parameters. In particular it is meant that the particles of the same sizes can be components of a fine or course gas suspension depending on the density of a carrier gas.

The kinetics of gas suspensions is described by the system of the Boltzmann equations only for the ultra-rarefied carrier gas. The additional collision integrals will determine corrections to the dissipative characteristics of a medium of the order of tens of percent. On the other hand, these collision integrals contain many-particles operators. The existence of such operators does not principally permit to solve the obtained rigorous kinetic equations. Therefore we have to construct the model kinetic equations on the basis of the rigorous ones. Such equations for hard spheres model have been derived and discussed in the present paper. It is necessary to keep in mind that this model is singular. The hard spheres have zero time of interaction. All molecule-particle collisions are separated for this model but in reality we have no such time collision separation.

References

- [1] Rudyak V.Ya., *Classification principles of dispersed media*, J. Aerosol Sci., Vol.27, Suppl.1, pp.S271-S272, 1996.
- [2] Rudyak V.Ya., *Nonlocal Solution of the Boltzmann equations*, Rarefied Gas Dynamics 19, Oxford Science Publication, pp.223-229, 1995.
- [3] Rudyak V.Ya., Ershov I.V., *Kinetic equations of Brownian particle*, Sov. Tech. Phys. (USA), Vol.65, No.11, pp.65-76, 1995.

Kinetic Approaches to the Milne-Chandrasekhar Problem *

F. Hanser¹, R. Monaco², A. Rossani², F. Schürer¹

¹ Institut für Theoretische Physik, Technische Universität Graz, Graz, Austria

² Dipartimento di Matematica, Politecnico di Torino, Torino, Italy

1 Introduction

In a recent paper [1], Rossani et al. have proposed a kinetic model for the study of a physical system constituted by two-level atoms and monochromatic photons. Such a model incorporates the basic feature that allows a good description of the problem, namely the interplay of inelastic collisions between atoms, on one hand, and interaction between gas and radiation, on the other. The most remarkable result of such a modelling is that under thermodynamical equilibrium conditions, Planck's law of radiation is recovered selfconsistently without resorting to additional hypotheses.

Moreover, a discretized version of this model has been constructed by Hanser [2] in view of a simpler numerical treatment at a kinetic level of physically meaningful cases. The discretization has been introduced only for atom velocities, according to well known techniques of the Discrete Kinetic Theory [3]. No simplifications have been introduced for the description of the radiation field.

An interesting application for these kinetic models is the Milne-Chandrasekhar problem [4]. We consider a slab filled with a gas and illuminated from one side. The problem consists in the study of the evolution of the radiation field, the excited atom density and the gas temperature within the slab.

Such a problem has been treated by Monaco et al. [5] by means of an hybrid continuum-kinetic approach. Atoms within the slab are described by moment equations, while the radiation field is studied by resorting to the kinetic equation for photons.

In the present work, our aim is to face the Milne-Chandrasekhar problem at a kinetic level by means of the discretized model and to compare such results with those obtained by resorting to the hybrid continuum-kinetic approach.

2 Kinetic Equations

We consider the following physical system:

- A gas of atoms A_1 and A_2 of mass m endowed, respectively, with only two internal energy levels E_1 and E_2 , $E_1 < E_2$.
- A radiation field of photons p at a fixed frequency $\nu = \Delta E/h$, $\Delta E = E_2 - E_1$, h being the Planck constant, interacting with the above gas particles.

The following interactions between particles and between particles and photons take place:

1. Elastic interactions between particles with the same or different energy levels.
2. Inelastic exchange between the internal energy levels: $A_1 + A_1 \rightleftharpoons A_2 + A_1$
3. Interactions between gas-particles and photons:
 - Absorption: $A_1 + p \rightarrow A_2$
 - Spontaneous emission: $A_2 \rightarrow A_1 + p$
 - Stimulated emission: $A_2 + p \rightarrow A_1 + 2p$, where the photons involved in the last process have the same velocity $c\Omega$.

In the non-discretized model, we introduce the distribution functions $f_1 = f_1(t, \mathbf{x}, \mathbf{v})$ of particles A_1 and $f_2 = f_2(t, \mathbf{x}, \mathbf{v})$ of particles A_2 , \mathbf{v} being the atom velocity in \mathcal{R}^3 . The kinetic Boltzmann-like equations for the two particle species A_1 and A_2 have the form

$$\frac{\partial f_k}{\partial t} + \mathbf{v} \cdot \nabla f_k = \mathcal{J}_k^e + \mathcal{J}_k^i + \mathcal{J}_k^r = \mathcal{J}_k, \quad (1)$$

where the $\mathcal{J}_k^l = \mathcal{J}_k^l(t, \mathbf{x}, \mathbf{v})$, $l = e, i, r$ are the collision integrals corresponding to the interaction classes (1), (2), and (3), respectively.

* Abstract 2601 submitted to the 21st International Symposium on Rarefied Gas Dynamics, Marseille, France, July 26-31, 1998

We denote by $F(t, \mathbf{x}, \Omega) d\mathbf{x} d\Omega$ the mean number of photons at time t that belong to the volume element $d\mathbf{x}$ about \mathbf{x} and the direction element $d\Omega$ about Ω . From now on, we shall consider the radiation intensity $I(t, \mathbf{x}, \Omega)$ related to F by $I(t, \mathbf{x}, \Omega) = c h \nu F(t, \mathbf{x}, \Omega)$. The evolution equation for $I(t, \mathbf{x}, \Omega)$ is well-known [4] and it is given by

$$\frac{1}{c} \frac{\partial I}{\partial t} + \Omega \cdot \nabla I = h \nu [n_2(\alpha + \beta I) - n_1 \beta I] = h \nu \mathcal{J}_p, \quad (2)$$

where n_1 and n_2 are the number densities of particles A_1 and A_2 , respectively.

In the discretized model both atoms A_1 and A_2 are allowed to move in the xy -plane with two speeds a and $2a$ in six directions (see Figure 1), according to the following rule:

$$\mathbf{v}_i = \begin{cases} a \mathbf{e}_k & : i = 2k - 1 \\ 2a \mathbf{e}_k & : i = 2k \end{cases} \quad k = 1, \dots, 6,$$

where $\mathbf{e}_k = \mathbf{i} \cos[(k-1)\pi/3] + \mathbf{j} \sin[(k-1)\pi/3]$.

Photons p can move in any direction in the xy plane, so that their velocity is given by $\mathbf{v} = c\Omega$, where $\Omega = \mathbf{i} \cos \theta + \mathbf{j} \sin \theta$, $\theta \in [0, 2\pi)$.

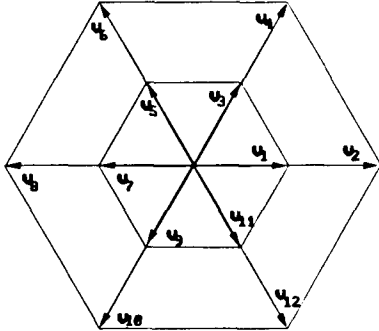


Figure 1: Planar 2×6 discrete velocity model

For atoms A_1 and A_2 , we define the distributions $f_i(x, y, t)$ and $f_i^*(x, y, t)$, respectively, joined to each velocity \mathbf{v}_i . The discretized equations look like Eq.(1), where the collision integrals are now replaced by sums over all the events allowed by momentum and total energy conservation.

Photons are described by means of the intensity $I(x, y, \theta, t)$, $\theta \in [0, 2\pi)$. Their kinetic equation is exactly the two-dimensional version of Eq.(2).

3 Results

The discrete kinetic equations for the atoms and the evolution equation for the radiation intensity were solved numerically on the basis of the *Fractional*

Step Method. Figure 2 shows the thermodynamical equilibrium state of the one dimensional version of the Milne-Chandrasekhar problem: Light energy transport and particle diffusion. The following initial and boundary conditions have been chosen: Thermodynamical equilibrium at time $t = 0$ and specular reflection on the boundaries for both atoms and photons, at time $t = 0^+$ specular reflection for atoms only, constant illumination on the right boundary and total absorption on the left one. The total number density of excited atoms has been multiplied by 10 for a better representation.

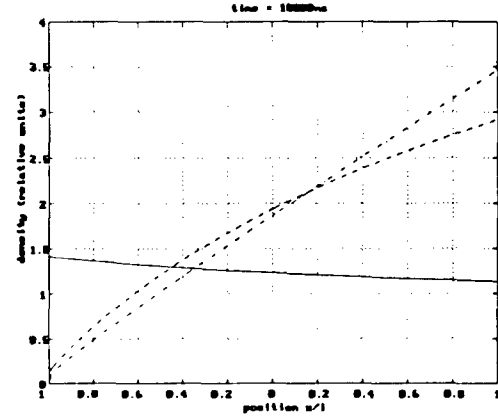


Figure 2: Total number densities of particles A (solid) and A^* (dashed) and total radiation intensity (dashdot) versus space.

References

- [1] A. Rossani, G. Spiga, and R. Monaco, *Kinetic approach for two-level atoms interacting with monochromatic photons*, Mech. Research Comm. **24** (1997), 237-242.
- [2] F. Hanser, *On the discrete kinetic theory of two-level atoms interacting with monochromatic photons*, Diplomarbeit, Technische Universität Graz, 1997.
- [3] R. Monaco, L. Preziosi, *Fluid Dynamic Applications of the Discrete Boltzmann Equation*. World Scientific, Singapore 1991.
- [4] S. Chandrasekhar, *Radiative Transfer*, Dover Pubs., New York 1960.
- [5] R. Monaco, J. Polewczak, A. Rossani, *Kinetic theory of atoms and photons: moment equations and their application to the Milne-Chandrasekhar problem*, Report No.18, Dip. Mat. Politecn. Torino, 1997.

Smoothing of Boundary Conditions for Boltzmann Equation on Grained/Rough Surface*

A.I. Erofeev, O.G. Friedlander

Central Aerohydrodynamics Institute (TsAGI), Zhukovsky, Russia

1 Introduction

The grained/rough surface structure (fine structure) has an effect on rarefied gas flow with respect to the relation of grain size d to average free molecular path λ . It is usually supposed that boundary condition are averaged on the local surface size l_0 if $d \ll l_0 \ll \lambda$. Validity of this averaging had never been discussed before. But there are two circumstances which need an explanation.

First, the fine structure of distribution function following from grained boundary conditions disappear on the distance about λ from the surface, not about l_0 , because it results from the molecular collisions. As a result the Boltzmann equation solution with grained boundary conditions has fine structure (with period about d) in the region with size about λ . But the Boltzmann equation solution with averaged boundary condition is smooth at the same distance. So, we don't know whether the averaging (and type of this averaging) of the solution for fine structure exists that leads to the solution of Boltzmann equation with smooth boundary condition. Second, the algorithm of obtaining not only zero order term (limiting term with $d/\lambda \rightarrow 0$) but also the first order one is desired. In this report the attempts to answer the first question and outline the path to solution of the second problem are made.

2 Model and method

The simple problem of one component gas condensation on grained plane is examined. The simplest model of grained surface is the chess plane with $d \times d$ square (with the x axis as a normal). One value of condensation coefficient on "white" square is specified as well as other one on "black" square (periodic boundary condition).

The problem is solved by the method of matched asymptotic coordinate expansions with the small value of the reciprocal Knudsen number d/λ . The structure of grained solution of Boltzmann equation is analyzed. It's established that the distribution function in velocity space at $x \sim \lambda$ becomes not the usual function with $d/\lambda \rightarrow 0$, but discontinued one at all points in the velocity space, or the distribution (generalized function). So the averaging of distribution function in velocity space Δ^3 is introduced: $F(x) = \langle f(x) \rangle$. The volume in velocity space is small $\Delta^3 \ll c^3$ (c - specified velocity value). Moreover it's suggested that $(d/\lambda)(c/\Delta) \ll 1$. If $d/\lambda \rightarrow 0$ the averaged distribution function F coincide with f at $x \sim d$. At $x \sim \lambda$ the function F is not the grained distribution function f , but a usual smooth function (more rigorously the zero order term $F^{(0)}$ in d/λ expansion is a usual function). It's shown that it is the distribution function F where the method of matched asymptotic expansion may be applied in the usual sense. The zero order term $F^{(0)}$ of asymptotic expansion is the solution of averaged (in Δ^3 volume) Boltzmann equation at $x \sim d$ as well as usual Boltzmann equation and only averaged Boltzmann equation at $x \sim \lambda$. The boundary condition for $F^{(0)}$ is such as for f . The zero order condition of matching of outer $F_{out}^{(0)}$ and inner $F_{in}^{(0)}$ solution lead to averaging in the "chess plane" boundary condition for $F_{out}^{(0)}$.

To demonstrate the validity of this approach the more difficult problem of flow through capillary sieve [1] was solved by DSMC method at $d/\lambda=0$ and $d/\lambda=0.1$. For first case the averaged boundary condition was used and for the second case the "fine-grained" one. The results of this solutions correlate satisfactorily. The possibility to generalize of this approach to rarefied gas flow past porous/rough complex surfaces is discussed. Also potential possibility of calculation of the first order term of matched asymptotic expansion is discussed.

*Abstract 2068 submitted to the 21st International Symposium on Rarefied Gas Dynamics, Marseille, France, July 26-31, 1998

Acknowledgement

The work is carried out at support of Russian Foundation for Basic Research (grant 96-01-01805), State Program for Leading Research Groups (grant 96-15-96063) and International Science and Technology Center (Project 200)

References

- [1] Erofeev A.I., Friedlander O.G., Kogan M.N., *Rarefied gas flow through porous layer*. Abstract 4941 submitted to the 21st International Symposium on Rarefied Gas Dynamics

GAS - SURFACE INTERACTION - GS 1

ROOM PÉRÈS

MONDAY, JULY 27, 1998

9:45

Identification of Energy Accommodation Coefficients on a Blunted Cone in Hypersonic Free Jet Flow *

A. Danckert, H. Legge

Institute for Fluid Mechanics, German Aerospace Center, Göttingen, Germany

1 Introduction

In rarefied flow, gas-surface interaction plays a major role for the forces and heat transfer acting on a body. A phenomenological description of this interaction is based on accommodation coefficients, which appear as parameters in many mathematical models of gas-surface interaction used for numerical simulation of rarefied gas flows with the Direct Simulation Monte Carlo (DSMC) method [1, 2]. Therefore, the knowledge of the accommodation coefficients is essential for the numerical prediction of forces and heat transfer of a given configuration. The aim of the present paper is to identify the energy accommodation coefficients of a blunted cone model in hypersonic free jet flow by comparing measurements of the heat transfer and drag with corresponding free molecular and DSMC calculations, where the Cercignani-Lampis model [1] of gas-surface interaction is used.

2 Experimental set-up and conditions

The 70° blunted cone model was made of massive copper and has a base diameter of $d_b = 2r_b = 5$ mm. The flow is produced by a N₂ orifice free jet expansion. The model wall temperature T_w was adjusted by two radiators placed laterally above it. The heat transfer coefficient C_H was determined by using the model itself as a calorimeter. The drag D was directly measured by balances. More details about the experimental set-up and the conditions can be found in [3].

Two stagnation temperatures $T_0 \approx 300$ K and $T_0 \approx 500$ K were chosen, with corresponding wall temperature ranges were 290 – 450 K and 400 – 750 K, respectively. The nominal free stream val-

ues listed in Table 1 were used for experimental data reduction and for the calculations.

3 Results and discussion

In this abstract, we concentrate on the the heat transfer coefficient C_H for the cases 1–3. First, we assumed complete accommodation of all degrees of freedom in the calculations, which is the standard assumption for technical surfaces. The results are shown in Fig 1. Large discrepancies between measurements and calculations are observed at higher wall temperatures for the most rarefied cases 1 and 2. Therefore, the model of complete accommodation is not suitable for the present configuration, at least for wall temperatures above 500 K.

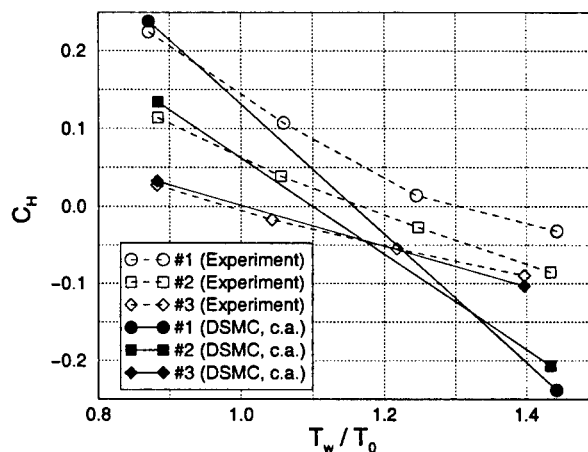


Figure 1: Comparison between measured and calculated heat transfer coefficients for complete accommodation

The full presentation shows that the discrepancies may be mainly attributed to an incomplete accommodation of rotational energy. To determine suitable values of the corresponding accommodation coefficient, parameter studies were performed with a variant of the Cercignani-Lampis model in free

*Abstract 1640 submitted to the 21st International Symposium on Rarefied Gas Dynamics, Marseille, France, July 26-31, 1998

GAS - SURFACE INTERACTION - GS 1

#	T_0 [K]	n_∞ [m ⁻³]	u_∞ [m/s]	T_∞ [K]	Kn_∞
1	495	0.06376e21	983	28.6	3.2
2	495	0.4776e21	983	28.6	0.43
3	495	4.771e21	983	28.6	0.043
4	295	0.1077e21	755	17.1	1.3
5	295	0.8004e21	758	17.1	0.18

Table 1: Nominal free stream values

molecular and DSMC calculations. This model's parameters α_t and α_r can be interpreted as accommodation coefficients for the translational and rotational energy, respectively. The best parameter values found by physical reasoning (e.g. assuming only wall temperature dependence) and some fitting are $\alpha_t \approx 0.9$, and α_r drawn from Fig 2. Now, good agreement between measured and calculated heat transfer coefficients is achieved for the whole wall temperature range (see Fig. 3). A complete description of the identification procedure and further results may be found in [4].

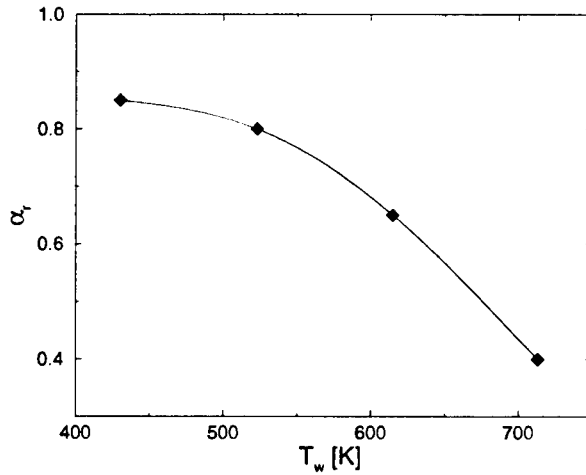


Figure 2: Temperature dependence of α_r

4 Concluding remarks

The present results show that assuming the rotational energy accommodation coefficient to be a decreasing function of the wall temperature enables a reasonable prediction of the heat transfer coefficient for wall temperatures up to 750 K. This behaviour of the accommodation coefficient has been observed also on several single crystal surfaces, and is known in the literature as rotational cooling effect in scattering through adsorption/desorption [5].

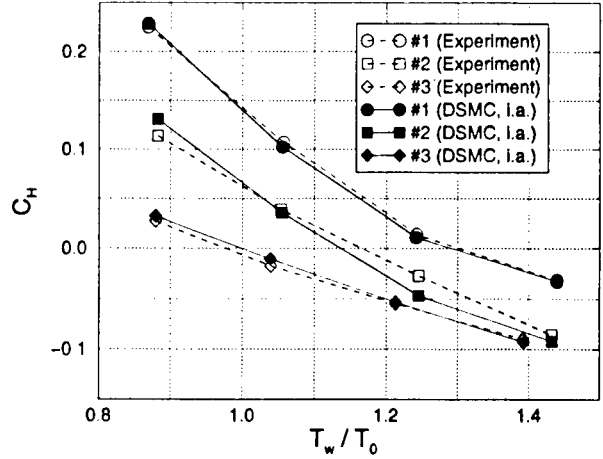


Figure 3: Comparison between measured and calculated heat transfer coefficients for incomplete accommodation (Cercignani-Lampis model)

References

- [1] Cercignani, C., *The Boltzmann Equation and Its Applications*, Springer Press, New York, 1987
- [2] Bird G.A., *Molecular Gas Dynamics and the Direct Simulation of Gas Flows*, Clarendon Press, Oxford, 1994
- [3] Legge H., *Heat Transfer and Forces on a Blunted 70 Deg Half Angle Cone Measured in Hypersonic Free Jet Flow*, DLR-IB 222-93 A 33, DLR Göttingen, 1993
- [4] Danckert A., *Entwicklung und Anpassung von Streukernmodellen der Molekül-Oberflächenwechselwirkung und ihre Anwendung in der numerischen Simulation verdünnter Hyperschallströmungen*, Dissertation, DLR-FB 96-29, DLR Köln, 1997
- [5] Asscher M., Guthrie W.L., Lin T.-H., *Energy redistribution among internal states of nitric oxide molecules upon scattering from Pt(111) crystal surface*, J. Chem. Physics 78 (11), 1983

Gas-surface Interaction Experiments at High Kinetic Energies *

C. Dankert¹, G. Gundlach¹, A. Mohamed²,
S. Novopashin³, T. Pot²

¹ German Aerospace Center (DLR), Institute for Fluid Mechanics, Göttingen, Germany

² ONERA, Palaiseau, France

³ Institute of Thermophysics, Siberian Branch of Russian Acad. of Sci., Novosibirsk, Russia

The interaction of N_2 and NO-molecules of high kinetic energy colliding with a solid wall is investigated by two spectroscopic methods: electron beam fluorescence (EBF) and laser induced fluorescence (LIF). Both methods allow to measure the population of rotational levels of the molecules, which is necessary to define the rotational temperatures of the incoming (undisturbed) and the reflected (coming back from the wall) ones. Fig. 1 shows the flow field situation in a vacuum system using supersonic free jet expansion of the diatomic gases N and NO or several mixtures ($NO + N_2$, $NO + He$, $N_2 + He$) blowing against the solid test walls made of Cu, Pt, SiC, steel, gold, tungsten at temperatures up to 1200 K. Spectroscopically measured are the rotational temperatures of the incoming N_2 - or NO-molecules with relatively low rotation but high kinetic energies and the reflected ones of high rotation and low speeds.

All experiments show a strong influence of the kinetic energy of the incoming flow (for N_2 and NO), nearly no influence of the wall temperature for N_2 and a small but measurable one for PNO, a minor influence of most of the wall materials except the combination NO on Pt, and an influence of the Knudsen number except for free molecular conditions. Fig. ?? shows the results for gas-surface interaction in low density for the N_2 -molecules. Plotted are the measured rotational temperatures after collision as function of the energy before colliding with the wall, and the correlation of rotational temperature with kinetic energy is much better than with wall temperature [1] or surface material.

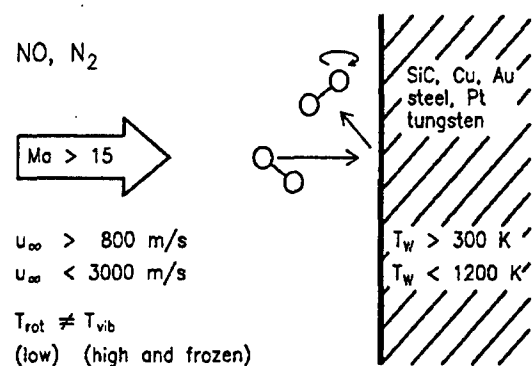


Figure 1: Gas-surface interaction at high kinetic energies

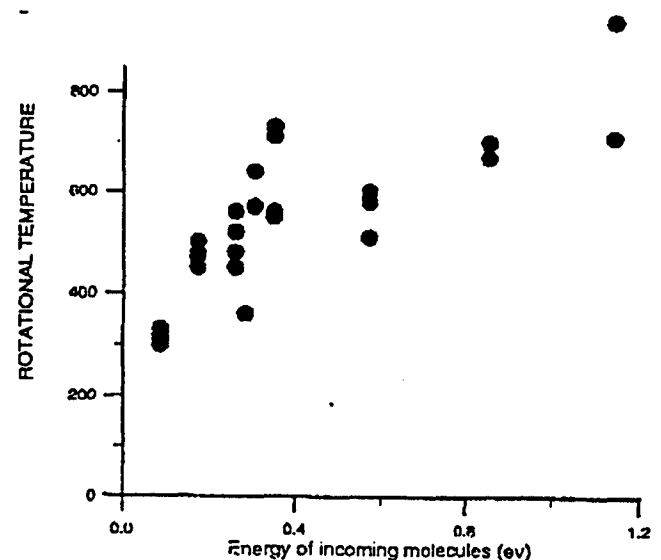


Figure 1: Influence of kinetic energy on rotation of reflected N_2 -molecules

* Abstract 1656 submitted to the 21st International Symposium on Rarefied Gas Dynamics, Marseille, France, July 26-31, 1998

References

- [1] S. Novopashin, C. Dankert, K. Lehmköster, A. Mohamed, T. Pot, *Rotational Temperature Measurements of N₂-Molecular Reflected from a wall*, 20th RGD, Peking University Press, Beijing/China, 1997.

Experimental Investigations of Gas-Surface Interaction Models *

S.R. Cook, M.A. Hoffbauer
Los Alamos National Laboratory, New Mexico, USA

Introduction

Modeling aerodynamic behavior in rarefied flows is difficult for many applications because the velocity distribution functions of the molecules scattered from the surfaces are unknown. Since these distribution functions are unknown, it is commonly assumed that some fraction of the incident molecules scatters diffusely from the surface with complete thermal accommodation while the remaining fraction scatters specularly. However, for many applications the behavior of the scattered molecules cannot be accurately described using this assumption.

In an attempt to overcome this problem, empirical models have been developed to more accurately describe the velocity distribution functions of the scattered molecules [1, 2, 3]. The Nocilla model adjustable parameters can be determined from the momentum and energy accommodation coefficients [4]. In the original Cercignani-Lampis model, the adjustable parameters are the tangential momentum and normal energy accommodation coefficients [2]. The recently proposed model by Cercignani, Lampis, and Lentati has three adjustable parameters that can be determined from a knowledge of three independent physical quantities, such as drag, lift, and heat transfer coefficients. It should also be possible to determine these three parameters from a knowledge of the average energy of the scattered molecules and the magnitude and direction of the average velocity of the scattered molecules.

Singularity problems associated with the momentum accommodation coefficients render them unusable for many applications. To overcome these problems a formalism has been developed based upon two parameters called the reduced force coefficients [5, 6]. The reduced force coefficients once known for a particular gas-surface intersection can be used to calculate the magnitude and direction of the flux-weighted average (hereafter referred to as average) velocity of the scattered molecules. Also, the reduced force coefficients can be used to accu-

ately approximate the average translational energy of the scattered molecules. Thus, the reduced force coefficient formalism could be used to determine the adjustable parameters in the recently proposed model by Cercignani, Lampis, and Lentati. It has also been shown that the reduced force coefficient formalism can be used to determine the adjustable parameters in the Nocilla model [6, 7].

In this paper it is shown how the adjustable parameters in the original Cercignani-Lampis model and the new model proposed by Cercignani, Lampis, and Lentati can be determined from a knowledge of the reduced force coefficients for a particular gas-surface interaction. The reduced force coefficients are then measured for H₂ and N₂ incident upon the solar array material to be used on the international space station. The Nocilla, Cercignani-Lampis, and Cercignani, Lampis, and Lentati parameters are then calculated for these gas-surface interactions. Measurements are then made of the actual velocity distribution functions of the scattered molecules and then compared to the predictions made by the three models. These experimental results will provide much needed information that indicates the accuracy of the existing empirical models, and will aid in the formulation and modification of future models constructed to describe gas-surface interactions.

The Reduced Force Coefficients

The tangential f_t and normal f_n reduced force coefficients can be expressed in terms of the force exerted on a surface by a molecular beam as

$$f_t = \frac{F_t}{N_i \bar{p}_i}, \quad (1)$$

$$f_n = \frac{F_n}{N_i \bar{p}_i}, \quad (2)$$

where F is the magnitude of the force exerted on the surface by the molecular beam, N_i represents the number of molecules incident upon the surface per unit time, \bar{p}_i is the magnitude of the average

*Abstract 2471 submitted to the 21st International Symposium on Rarefied Gas Dynamics, Marseille, France, July 26-31, 1998

momentum of the incident molecules, and the subscripts t and n represent the tangential and normal components, respectively. The force components are measured using a torsion balance with samples of the surfaces mounted on the end of the lever arm. Measurements are made with the angle between the surface normal and the molecular beam at 0° , 20° , 40° , 60° , 80° . A beam-stop designed to eliminate the force due to the exiting molecules is mounted on the other lever arm of the torsion balance [8]. For molecular beams composed of one element, the quantity the torsion balance measures with the beam-stop in the beam is precisely $N_i \bar{p}_i$. Since the same torsion balance is used to measure both the force components and $N_i \bar{p}_i$, error due to uncertainties in the torsion constant of the suspension wire are eliminated. Standard time-of-flight methods are used to measure the velocity distribution functions of the molecular beams [8].

Distribution Function Measurements of Scattered Products

A differentially pumped time-of-flight system is mounted to the chamber that houses the torsion balance. The time-of-flight system is oriented perpendicular to the molecular beam axis. With this system the velocity distribution functions of molecules scattered from surfaces can be measured. Because the orientation is fixed, measurements can only be made where the sum of angle of incidence and the scattering detection angle is 90° . The angle of incidence is defined to be the angle between the surface normal and the molecular beam. The scattering detection angle is the angle between the surface normal and the time-of-flight system axis.

A small fraction of the scattered molecules pass through an aperture into the first differential pumping stage of the time-of-flight system. There the gas is modulated into spatially narrow pulses with a rotating disk chopper [8]. The pulses then pass through a second aperture into the second differential pumping stage where they are detected using a mass spectrometer. A multi-channel scalar is used to measure the flight-time distribution function signal from the mass spectrometer. The flight-time distribution function is then used to calculate the velocity distribution function of the scattered molecules.

Conclusion

The results of this investigation will provide much needed information on the accuracy of the existing

empirical models, and also information that can be used to improve the existing models.

References

- [1] Nocilla S., *The Surface Re-Emission Law in Free Molecule Flow, Rarefied Gas Dynamics*, edited by J. A. Laurmann, Academic Press, New York, pp. 327-346, 1964.
- [2] Cercignani C. and Lampis M., *Kinetic Models for Gas-Surface Interactions*, Transport Theory and Statistical Physics, Vol. 1, No. 2, pp. 101-114, 1971.
- [3] Cercignani C. and Lampis M., *New Scattering Kernel for Gas-Surface Interaction*, AIAA Journal, Vol. 35, No. 6, pp. 1000-1011, 1997.
- [4] Hurlbut F. C. *Two Contrasting Modes or the Description of Wall-Gas Interactions, Rarefied Gas Dynamics: Experimental Techniques and Physical Systems*, edited by B. D. Shizgal and P. D. Weaver, Progress in Astronautics and Aeronautics, AIAA, Washington DC, Vol. 158, pp. 494-506, 1994.
- [5] Cook S. R. and Hoffbauer M. A. *Analyzing Gas-Surface Interactions Using the Reduced Force Coefficients*, Phys. Rev. E, Vol. 55, No. 4, pp. R3828-3831, 1997.
- [6] Cook S. R. and Hoffbauer M. A. *Absolute Momentum Accommodation in Gas-Surface Scattering, Rarefied Gas Dynamics 20*, edited by C. Chen, Peking University Press, Beijing, pp. 467-472, 1997.
- [7] Cook S. R. and Hoffbauer M. A. *Nocilla Model Parameters Obtained from Forces Exerted on Surfaces by Molecular Beams*, J. of Spacecraft and Rockets, Vol. 34, No. 3, pp. 379-383, 1997.
- [8] Cook S. R. Hoffbauer M. A. Cross J. B. Wellenstein H. and Fink M. *A Specialized Torsion Balance Designed to Measure the Absolute Flux Density of Hyperthermal Molecular Beams Containing Reactive Species*, Rev. of Sci. Instrum. Vol. 67, No. 5, pp. 1781-1789, 1996.

GAS - SURFACE INTERACTION - GS 2

ROOM PÉRÈS

MONDAY, JULY 27, 1998

11:00

Atom Recombination and Vibrational Distribution in O₂ Molecules Formed on Silica Surface *

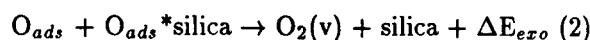
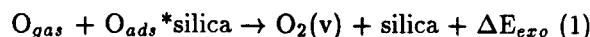
M. Rutigliano¹, G.D. Billing², M. Cacciatore¹

¹ CNR-Centro per lo Studio della Chimica dei Plasmi-Dip. Chimica
Universita' di Bari - Via Orabona, 4 - 70126 Bari - Italy

² Department of chemistry, H.C. Oersted Institute,
University of Copenhagen, DK2100, Copenhagen- Denmark

1 Introduction

In this study the dynamics of oxygen atom recombination reaction on silica surface is considered. The Eley-Rideal (E-R) (1) and the Langmuir-Hinshelwood (L-H) (2) mechanisms are considered in the dynamical simulation:



The energy released in the reaction, ΔE_{exo} , can be shared among the translational and the internal degrees of freedom of the formed O₂ molecule and the solid substrate. Depending on the catalytic properties of the wall, reactions (1) and (2) can be a very effective source of vibrationally excited molecules, as well as among the main responsible for the heat flux toward the surface. In this respect the oxygen atom recombination on silica-based compounds can play a role in a variety of plasmochemical processes, including the thermal protection problem in the reentry missions [1]. Despite a great deal of experimental and theoretical work [1, 2] the exact understanding of the catalytic activity of silica is not completely achieved. On the other hand, to gain an insight in the heat transfer problem at the surface, collisional dynamic calculations can be of great relevance as demonstrated in previous works on atom recombination and dissociation at wall [3]. The aim of this contribution is to present part of our results recently obtained on the dynamics and the energetic of the oxygen recombination reactions on silica surfaces.

2 Collisional Model and Results

The semiclassical collisional approach to heterogeneous catalysis has been used to describe the dynamics of reactions (1) and (2) [3]. According to this model the time evolution of the translational and internal motions of the atom/molecule in the gas-phase is described classically, whereas the phonon excitation processes in the substrate are treated quantum mechanically in the harmonic approximation. The coupling between the gas atom and the surface atom dynamics is obtained defining the effective hamiltonian $H_{eff} = \langle \Psi(t) | V_{int} | \Psi(t) \rangle$, where $\Psi(t)$ is the total wave function of the phonon state and V_{int} is the molecule-surface interaction potential. Thus we get:

$$H_{eff} = V_I^0 + \sum_k \omega_k^{-1} \epsilon_k(t)$$

$$\epsilon_k(t) = V_k^1(R(t)) \int dt' V_k^1(R(t')) \sin[\theta_k(t) - \theta_k(t')]$$

where ω_k is the phonon frequency of the k-th normal mode, and $\epsilon_k(t)$ are the 'phonon excitation strength' calculated from the Fourier transform of the external perturbation force, $V_k^1(R(t))$. The Hamilton's equation of motion of the atoms are then determined by adding to the usual hamiltonian for the free particles the time-dependent H_{eff} given above. In the calculations, the surface consist of a 3D sample of β -cristobalite, the silica phase which is stable at the two surface temperatures considered in our simulation, i.e. $T_s = 1000K$ and $T_s = 600K$. Since the interaction potential for the O₂/silica system is not known, we have assumed a semiempirical potential energy surface constructed by us from the known O-O and Si-O interactions in the gas-phase and in solid, respectively. Several dynamical effects

*Abstract 1771 submitted to the 21st International Symposium on Rarefied Gas Dynamics, Marseille, France, July 26-31, 1998

have been explored concerning, among the others, the effect on the wall catalicity of the adsorption surface site for O_{ads} , the surface top-layer structure and surface temperature. A full presentation and discussion of the large body of results obtained from the calculations will be given at the conference. From the calculations we get the recombination coefficient $\gamma=0.024$ for the E-R mechanism at $T_s=1000K$, in very good agreement with the experimental results [4]. We did not observe any surface temperature dependence of the γ coefficient calculated for the E-R mechanism. Instead, the γ coefficient calculated by us for the L-H recombination reaction at $T_s=600K$ matches the observed γ value at this temperature [4]. This result would support the switching of the mechanism for oxygen recombination reaction from E-R to L-H in the same manner as the surface temperature decreases. A valuable quantity that can be obtained in molecular dynamics calculations are the state-to-state recombination coefficients, that is the recombination coefficient for O_2 formation in a specific vibrational level v . These probabilities have been obtained and inserted in the modelling of the dissociation-recombination kinetics in the boundary layer [5]. In Fig.1 we have reported the energy flow pathways for reaction (1): E_{vib} , E_{rot} and E_{tr} are, respectively, the energy fraction transferred to the vibrational, rotational and traslational motion of O_2 , E_{ph} is the energy transferred to the surface. From the reported results it is evident that the largest fraction of the total available energy goes into molecular vibrations while the energy loss to the surface is rather small (contrary to what is generally assumed).

3 Acknowledgments

This research was supported by the Italian Space Agency (ASI).

References

- [1] C.D. Scott, AIAA-90-0054, 1990.
- [2] W.A. Seward and E.J. Jumper, Jour. of Thermophy. and Heat Transfer Vol.8 p.460, 1994;
F. Nasuti, M. Barbato, C. Bruno, Jour. of Thermophy. and Heat Transfer Vol.10 p.131, 1996.
- [3] M. Cacciatore and G.D. Billing, Surface Science 232 p.35, 1990;
- [4] J.C. Greaves and J.W. Linnett, Trans. Faraday Soc., 55 p.1355, 1955;
V.D. Berkut, V.M. Doroshenk, S.A. Zhdanok, V.V. Kovtun, N.N. Kudrjavidzev, S.S. Noikov and A.I. Sharovarov, A.V. Luykov Heat and Mass Transfer Institute, Belarus Academy of Sciences Report, 1989
- [5] I. Armenise, M. Cacciatore, M. Capitelli, E.V. Kustova, E.A. Nagnibeda, M. Rutigliano, *The influence of nonequilibrium vibrational and dissociation-recombination kinetics on the heat transfer and diffusion in the boundary layer under reentry conditions*, Abstract 1946 submitted to this Symposium.

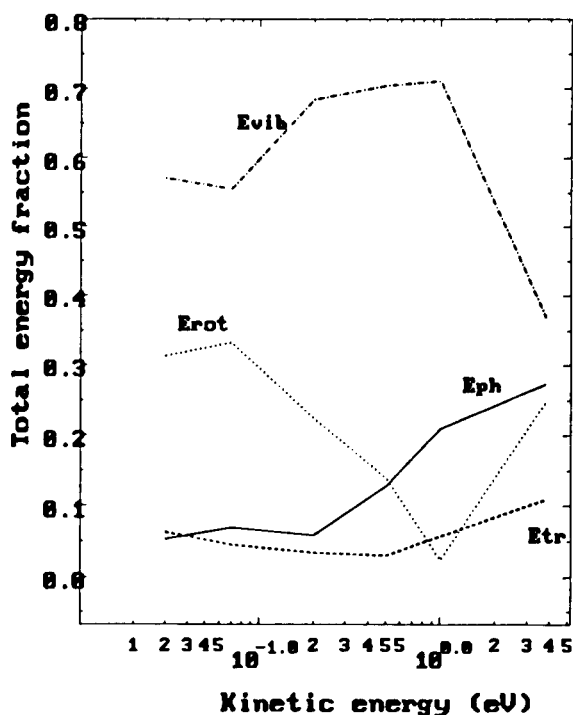


Figure 1: Total energy partitioning in the E-R reaction (1)

Electron Gas Density Functional Calculations of Intermolecular Potentials Between Noble Gas Atoms and Noble Metal Surfaces *

Carl Nyeland¹ and J. Peter Toennies²

¹ Institute of Chemistry, University of Copenhagen, Denmark

² Max - Plank - Institute für Strömungsforschung, Blumenstraße 10,
D 37073 Göttingen, Germany

Abstract

An electron gas-density functional approach recently applied to the two body interaction of inert gas atoms has been applied to the calculation of the interactions of rare gas atoms with surfaces of noble metals. Results obtained for helium atoms interacting with copper and silver surfaces considered as an atomic structure and as the surface of jellium are presented and compared with the corresponding published ab initio results. Some remarks on calculations on other systems and about the use of potentials obtained for estimating adsorption and tracer diffusion are also given.

In the electron gas-density functional (EGDF) method [1] one assumes the short range potential V_T to be given by the following sum of density functionals

$$V_T[\rho] = V_{Kin}[\rho] + V_{Coul}[\rho] + h_{Exch} V_{Exch}[\rho] + h_{Corr} V_{Corr}[\rho] \quad (1)$$

where V_{Kin} is the contribution to the intermolecular potential from the Thomas-Fermi kinetic energy, V_{Coul} the classical electrostatic energy, V_{Exch} the Dirac exchange contribution and V_{Corr} the contribution from the local spin density (LSD) correlation energy. The correction factors h_{Exch} and h_{Corr} are introduced to take self-exchange, self-correlation and eventually gradient corrections into account. The charge distributions are obtained from Hartree-Fock calculations. As these results appear to be very well exponential the calculations of the 'short range' potentials turn out to be rather simple to do. On fig. 2 some results for the 'short range' potential for He-Cu are given. The definitions of the coordinates can be seen on fig. 1. The 'long range' dispersion potentials can easily be added to V_T of eq. (1) as

$$-f(b(z-z_{vdW})) \frac{C_{vdW}}{(z-z_{vdW})^3} \quad (2)$$

where $f(x)$ is a damping function, [5], b is the exponential parameter from the 'short range' potential, and C_{vdW} and z_{vdW} are the well-known dispersion potential constants, [6]. Only the location of the 'jellium edge' z_B on fig. 1, has to be estimated for obtaining the final, non-corrugative potential given on the usual form, $V(R)$, as a function of the distance to the solid surface. From comparisons of the two types of results presented in fig. 2, the jellium-atom potentials as a function of z and the atom-atom potentials as a function of R' , results for the 'jellium-edge' can be obtained. The full potential is then given by

$$V(R) = V_T(R) - f(b(R-z_B-z_{vdW})) \frac{C_{vdW}}{(R-z_B-z_{vdW})^3} \quad (3)$$

where R is the distance between the inert gas atom and the top-layer of the solid. The numerical results for helium on copper and silver will be shown at the symposium and compared with the few Hartree-Fock results available (7).

References

- [1] C. Nyeland and J.P. Toennies, Chem. Phys., **188**, 205 (1994) and manuscript (1997).
- [2] I.P. Batra, P.S. Bagus and J.A. Barker, Phys. Rev. B **31**, 1737 (1985).
- [3] A. Chizmeshya and E. Zaremba, Surface Sci. **268**, 432 (1992), Surface Sci. **220**, 443 (1989).
- [4] P. Nordlander and J. Harris, J. Phys. C **17**, 1141 (1984).
- [5] K.T. Tang and J.P. Toennies, J. Chem. Phys. **80**, 3726 (1984), Surface Sci. **279**, L 203 (1992).
- [6] E. Zaremba and W. Kohn, Phys. Rev. B **13**, 2270 (1976), Phys. Rev. B **15**, 1769 (1977). See also ref. 3.
- [7] K. Lenarčič-Poljanec, M. Hodošek, D. Lovrić and B. Gumhalter, Surface Sci. **251/251**, 706 (1991).

* Abstract 2916 submitted to the 21st International Symposium on Rarefied Gas Dynamics, Marseille, France, July 26-31, 1998

GAS - SURFACE INTERACTION - GS 2

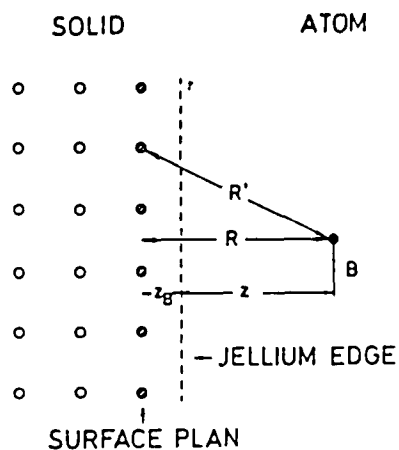


Fig. 1

The solid surface-atom interaction model. \bullet the "free" atom, \odot the surface atoms and \circ the other atoms of the solid. R is the distance between the atom B and the surface. R' the distance between the atom B and a surface atom. z_B is the distance between the surface plan and the jellium edge from the jellium-atom interaction model. Obviously one has $R = z_B + z$.

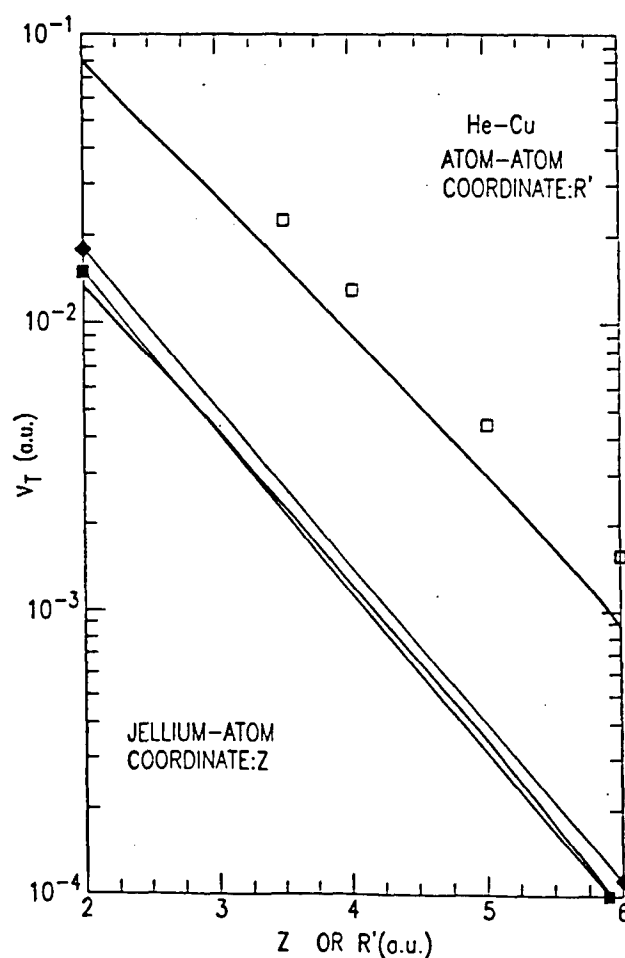


Fig. 2.

Total short range potentials for He-Cu. $V_T(z)$ for the jellium model and $V_T(R')$ for the atom-atom model. — present calculations. Atom-atom data: (\square) Ref. [2]. Jellium-atom data: (\blacksquare) Ref. [3], (\blacklozenge) Ref. [4].

Kinetic Model for Gas-Wall Interaction in Hypersonic Flow *

L. Aufrère, J.G. Méolans
IUSTI/MHEQ, Marseille, France

In this work we look at dissociating diatoms interacting with a cold wall at high temperature. We disregarded the macroscopic velocity of the gas considered as suddenly contacting a wall. Such a situation occurs, for example, behind a reflected shock wave on the end of a shock tube : Two main phenomena take place, generally defined as "accommodation" and "catalycity" that is to say the tendency of the gas components (atoms and molecules) to exchange energy with the wall (accommodation) and the possibility of internal gas exchange (catalycity). Numerous attempts have been developed in order to determine the wall temperature jump [1][2][3], usually under the assumption that the heat flux is maintained through the Knudsen layer ; and no previous works take into account a vibrational and chemical nonequilibrium. In the present work we first consider only the vibrational nonequilibrium of a pure gas disregarding dissociation. The particle collisions are classified according to their vibrational relaxing time. The Translation-Rotation, Translation-Translation and resonant Vibration- Vibration collisions are called type (1) collisions ; the Vibration-Vibration and Vibration- Translation collisions are type (2) collisions. The Boltzmann equation is split considering type (1) to be preponderant compared to type (2). Let us call θ the characteristic flow time, τ_1 and τ_2 respectively the intercollisional time of types (1) and (2), we have :

$$\tau_1/\theta \ll 1 \sim \tau_2/\theta$$

The first order collisional term of type (1) collisions is developed on a polynomial orthogonal function set according to a Gross-Jackson method. We disregard the usual assumption of heat flux conservation in the Knudsen layer (recently found as highly erroneous [4]). Linearizing the zero order distribution function at the wall and using the Maxwell reflexion law we obtained the wall jump temperature. It appears the Translational-Rotational temperature

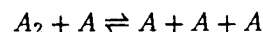
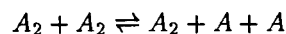
jump ΔT is linearly dependent on the temperature gradient ; we have :

$$\Delta T = A + B \frac{\partial T}{\partial x} \quad (1)$$

where T is the Translation-Rotation temperature, x the normal coordinate and where A et B depend on the accommodation coefficients, internal energies (vibrational and rotational) and on a parameter characterizing the perturbation. Furthermore the vibrational temperature jump ΔT_v also depends on the T_v vibrational temperature gradient :

$$\Delta T_v = A' + B' \frac{\partial T}{\partial x} + C' \frac{\partial T_v}{\partial x} \quad (2)$$

The results are compared to the one obtained with the DSMC method. Moreover in the same way, now taking into account the dissociation and recombination phenomena corresponding to reaction :



we find more-complex temperature jump expressions in addition to the previous terms we also obtain parameters corresponding to the reactive collisional term.

References

- [1] P. Welander. Arkiv För fysik 7, 507(1954).
- [2] R. Brun, M. Larini. Modèles cinétiques de l'interaction gaz polyatomique-paroi. Acta Astronautica, vol.1, pp1041-1050, July 1974.
- [3] R. Brun, P.C. Philippi. Kinetic models and relaxation effects in the Knudsen layer of gas mixtures. Paper 124 at the Twelfth International Symposium on Rarefied Gas Dynamics, Charlottesville, Va, July 7.11.1980.
- [4] R. Goniak and G. Duffa. Corrective term in wall slip equations for knudsen layer. J. Thermophysics, vol.9 N 2, pp383-384, 1995.

* Abstract 3291 submitted to the 21st International Symposium on Rarefied Gas Dynamics, Marseille, France, July 26-31, 1998

Free Molecular Flow past a Body of Clean Surface *

Kyoji Yamamoto

Dept. of Mechanical Eng., Fac. of Eng., Okayama Univ., Okayama, Japan

1 Introduction

The free molecular flow past a convex body is easily calculated if the interaction between impinging particles and the body surface is specified. The diffuse reflection or specular reflection of the incident molecule is usually assumed at the surface. The drag and lift acting on a convex body like a sphere are calculated under these boundary conditions [1]. However, it is said that the simple boundary condition like the diffuse reflection can not describe the gas-wall interaction well when the solid surface is exposed to high temperature or a high speed flow or in ultra vacuum [2]. Therefore, it is interesting to investigate the gas-wall interaction to understand the flow fields accurately even in a simple case of the free molecular flow.

Recently, the author studied the gas-wall interaction by the molecular dynamics method and analysed the Couette flow [3]. The result obtained shows that the tangential momentum accommodation depends on the Mach number and the Knudsen number. This seems to indicate that the normal momentum accommodation is also dependent on the Knudsen number and the Mach number. Since the flow velocity relative to the wall surface is different at different position of the surface if it is curved, the accommodation may depend on the position of the body.

In the present study, we consider the free molecular flow past a convex body with clean surface. We apply the molecular dynamics method for the gas-wall interaction and calculate the drag or energy flux. We shall compare the results with those of the diffuse reflection.

2 Method of Analysis

Let take the Maxwellian distribution function with the number density n_∞ , the temperature T_∞ and the uniform flow V_∞ , which makes an angle θ with

the tangent plane of the wall surface. A molecule having this Maxwellian distribution hits on the wall and is reflected from it. We shall apply the molecular dynamics method to obtain the velocity of the reflected molecule after interacting with the wall surface. For this analysis, we construct the wall with molecular structure. We take platinum as the wall. The structure of the wall molecule and the method of analysis are the same as in the previous calculations [3]. The Xe molecule is taken as the gas molecule to interact with Pt wall. We take temperatures of the uniform flow and of the wall to be the same 300K. The molecular velocity is chosen at random according to the Maxwellian distribution with the uniform flow, and one molecule having this velocity is injected to the solid wall. We emitted 1000 molecules for one case. We calculated five cases of speed ratio S , which is defined by $S = \frac{V_\infty}{C_m}$, where $C_m = \sqrt{2RT_\infty}$ is the most probable speed and R is the gas constant. The angle θ is taken at every ten degree from -90° to 90° .

3 Results

We here briefly describe some of the results obtained. First, we discuss on the accommodation coefficient. The tangential and normal momentum accommodation coefficients α_X and α_N , which are defined by the conventional way, are shown in Figs. 1 and 2. Here and in the following figures, the numbers 1, 2, 3, 5 and 7 besides marks mean the speed ratios of the uniform flow. Figure 1 shows the variation of the tangential momentum accommodation coefficient α_X with θ . It will be seen that α_X depends on not only the speed ratio but also θ . The decrease of α_X with increasing speed ratio is seen to be remarkable for small θ . It is as small as 0.3 when $S=7$ and $\theta=0$. The normal momentum accommodation coefficient α_N is plotted in Fig. 2. This shows that there is not so much variation of α_N with respect to θ even when $S=7$. The value is about 0.94 at $S=1$ when $\theta \geq 30^\circ$. There are some numerical error for small θ because the normal component of the molecular velocity is rather small for these values of

*Abstract 4701 submitted to the 21st International Symposium on Rarefied Gas Dynamics, Marseille, France, July 26-31, 1998

θ . Figure 3 shows the variation of the thermal accommodation coefficient α_T , which is also defined in the conventional form, with θ . This figure also shows that the thermal accommodation coefficient is dependent on θ as well as S for small θ . However, it takes about 0.9 when θ is larger than 40° for all speed ratios.

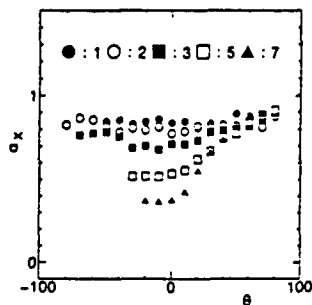


Figure 1: Tangential momentum accommodation coefficient.

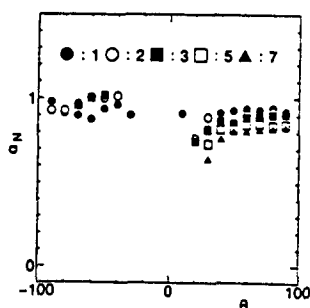


Figure 2: Normal momentum accommodation coefficient.

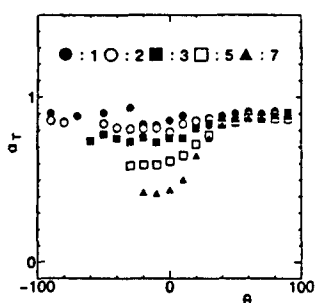


Figure 3: Thermal accommodation coefficient.

We now take a two-dimensional free molecular flow past a flat plate of length L with an angle of attack θ . We shall calculate the drag and lift when the plate temperature is kept constant at 300K. The results shown are in the non-dimensional form in the conventional form. Figure 4 shows the drag coefficient C_D versus the angle of attack θ . The curves are drawn from the expressions when the reflected molecules are of the diffuse reflection. This figure shows that the drag for θ smaller than about 50 degree is lower than that of the diffuse reflection. This

is due to the slip of the tangential flow velocity at the wall. The drag for θ larger than 50 degree shows higher value than that of the diffuse reflection, especially at large speed ratio. This is due to the fact that the reflected molecule is not completely accommodated. In this case, the reflected molecule gives more momentum to the wall and hence produces a large drag on the plate. Figure 5 shows the lift coefficient C_L versus θ . It is quite interesting to see in this figure that the lift in the present wall case is not so much different from that of the diffuse reflection wall.

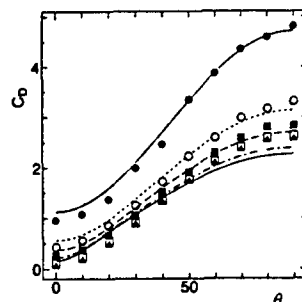


Figure 4: Drag coefficient.

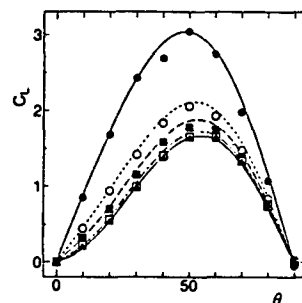


Figure 5: Lift coefficient.

It is not difficult to calculate the drag and lift acting on a convex body like a cylinder by integrating the stress distributions on the body surface obtained in the present calculation. We shall show them in the full paper.

References

- [1] Schaaf, S. A. and Chambre, P. L., *Flow of Rarefied Gases*, Princeton University Press, 1961.
- [2] Goodman, F. O. and Wachman, H. Y., *Dynamics of Gas-surface Scattering*, Academic Press, 1976.
- [3] Yamamoto, K. and Yamashita, K., *Analysis of the Couette Flow Based on the Molecular Dynamics study for Gas-wall Interaction*, in *Rarefied Gas Dynamics*, (ed. Shen Shing) pp.375-380, 1997.

GAS - SURFACE INTERACTION - GS 3

ROOM PÉRÈS

MONDAY, JULY 27, 1998

14:40

Rarefied Gas Flow over a Rough Platinum Wall Surface *

Kyoji Yamamoto and Tsuyoshi Shiota

Dept. of Mechanical Eng., Fac. of Eng., Okayama Univ., Okayama, Japan

1 Introduction

The diffuse reflection of gas molecule at the solid surface has been widely used as a boundary condition for the analysis of various kinds of flow of rarefied gas. It is, however, said that the diffuse reflection cannot describe well the gas wall interaction when the solid surface is exposed to high gas temperature or a high speed flow or when the gas is in an ultra vacuum [1]. Therefore, the gas-wall interaction has been one of important and interesting subjects in the rarefied gas dynamics.

Recently, the author studied the rarefied gas flow between two parallel walls by the molecular dynamics method to investigate the gas-wall interaction [2],[3]. The solid wall consists of the platinum molecule and its surface is flat. We call it a smooth surface. The solid surface, however, may be more or less rough in molecular scale even if it seems to be smooth macroscopically. In the present study, we shall take the platinum wall whose surface has roughness in molecular scale, and investigate the characteristics of the gas-wall interaction and of the flow quantities between two walls. We apply the molecular dynamics method for the gas interaction with the rough wall.

2 Method of Analysis

We consider the rarefied gas flow between two infinite parallel walls whose distance is L . Let the temperature of both walls be 300K. The upper wall has the velocity $-U/2$, whereas the lower wall moves with velocity $U/2$. We assume that the wall consists of platinum. The molecular arrangement of the wall surface is taken as follows: The wall surface is set on $(1,1,1)$ plane, and on this plane we take 6 and 6 Pt molecules in the direction of motion of the wall and normal to it, respectively. Four molecular layers are taken normal to the surface. We further make a protuberance on the surface. We

put six Pt molecules next to the surface and another Pt molecule is placed above these 6 molecules. This protuberance consisting of seven molecules is a model of the surface roughness (see Fig.1). The periodic condition is applied to the parallel direction to the surface as is usually assumed in the molecular dynamics.

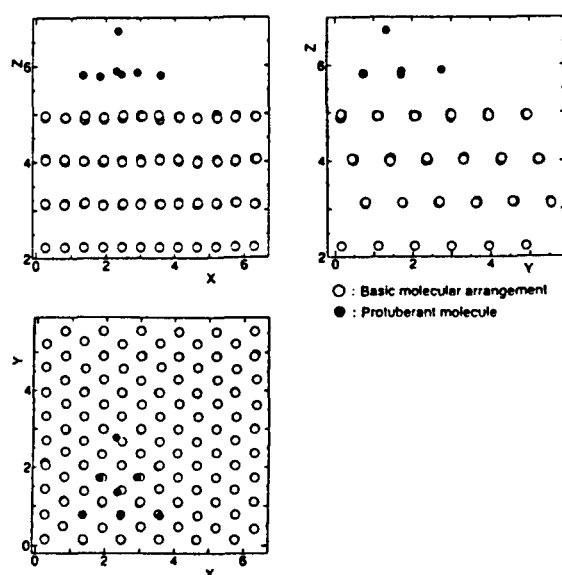


Figure 1: Molecular structure of the wall.

The Xe molecule is taken as the gas molecule for the analysis of the interaction with the wall molecule. The potentials between molecules and the method of analysis are the same as in the previous study [2],[3]. That is, we apply the Monte-Carlo method for the analysis of the gas flow between two walls. The molecular dynamics method is applied for the interaction between gas and solid molecules.

3 Results

Two cases of wall speed have been calculated, that is, $S_L = 0.5$ and 2.5 , where $S_L = U/C_m$, $C_m = \sqrt{2RT_w}$ is the most probable speed, R the gas constant, and T_w the wall temperature. We have calcu-

*Abstract 4702 submitted to the 21st International Symposium on Rarefied Gas Dynamics, Marseille, France, July 26-31, 1998

lated five cases of the Knudsen number. We here show only a few result obtained.

Figure 2 shows the flow velocity distributions between two walls when $S_L = 0.5$. Only half of the distribution is shown because of symmetry.

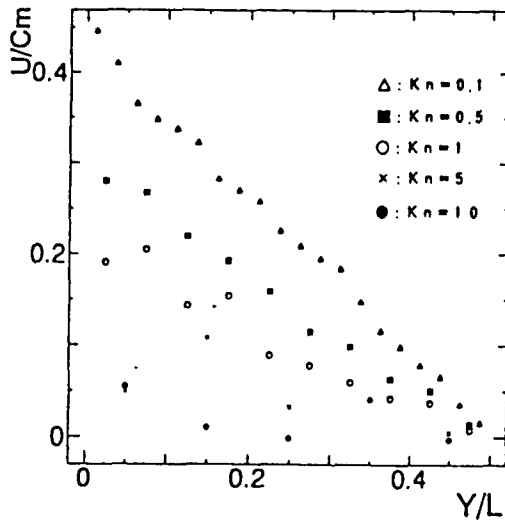


Figure 2: Velocity distribution when $S_L = 0.5$ (rough wall).

The velocity distribution of the smooth wall surface [2] is shown in Fig. 3 for comparison. It will be seen that the velocity slip at the wall surface is smaller in the present study than in the smooth wall. The difference between the rough wall and the smooth wall may be found clearly in the temperature distribution when $S_L = 2.5$. This is , however, not shown here for shortness.

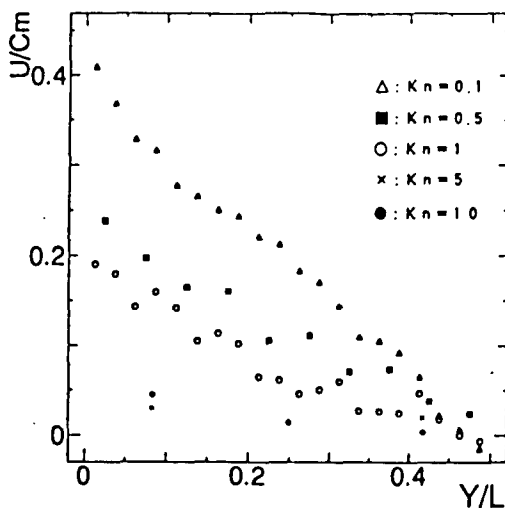


Figure 3: Velocity distribution when $S_L = 0.5$ (smooth wall).

Figure 4 shows the tangential momentum accommodation coefficient, which is defined by the conventional way. It will be seen that the accommodation coefficient is close to unity when $S_L = 0.5$ for the rough wall irrespective of the Knudsen number, whereas it is about 0.8 for the smooth wall. The momentum accommodation coefficient for $S_L = 2.5$ is smaller than unity and depends of the Knudsen number. It may be said that the surface roughness affects the accommodation greatly even if the roughness is as small as molecular scale. The value of the accommodation coefficient greater than one is due to lack of the numerical accuracy.

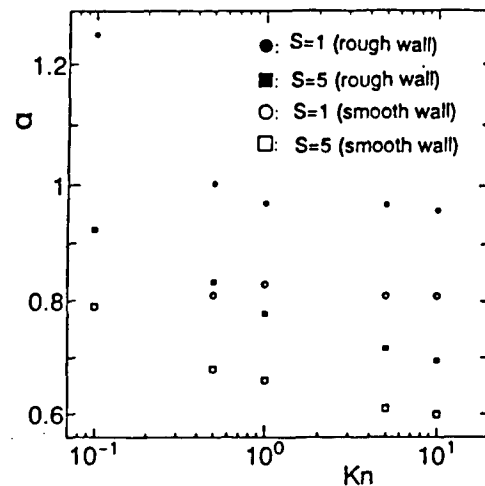


Figure 4: Tangential momentum accommodation coefficient.

References

- [1] Goodman, F. O. and Wachman, H. Y., *Dynamics of Gas-surface Scattering*, Academic Press, 1976.
- [2] Yamamoto, K. and Yamashita, K., *Analysis of the Couette Flow Based on the Molecular Dynamics study for Gas-wall Interaction*, in *Rarefied Gas Dynamics*, (ed. Shen Shing) pp.375-380, 1997.
- [3] Yamamoto, K., *Rarefied Gas Flow over a Solid Surface with Adsorbates*, *Proc. Int. Conf. on Fluid Engineering (JASME)*, Vol.3, pp.1247-1252, 1997.

Energy Transfer in the Process of Diatomic-Surface Collision *

T.N. Zolotoukhina¹, S. Kotake²¹ Nanotechnology Division, Mech. Eng. Laboratory, Tsukuba, Ibaraki, Japan² Faculty of Engineering, Toyo University, Kawagoe, Saitama, Japan

Energy transfer at gas-solid interface is one of the most important problems for the development of new applications and technology and demands fundamental understanding of individual interactions between atoms and molecules of the interface. These interactions should be viewed not exclusively in the framework of classical, molecular dynamics description, but also in the domain of the quantum mechanical description. In the latter, individual vibrational and rotational states of interacting particles are to be accounted for in the process of energy transfer.

With time-dependent quantum dynamics methods, the number is limited of vibrational and rotational degrees of freedom pertinent that suits to describe gas molecules at the interface. Essentially large numbers of vibrational degrees of freedom of the surface can be taken into account currently only by means of the molecular dynamics (MD) methods. Only a way to treat sufficient degrees of freedom is the mixed method of quantum and classical description of the interacting system by introducing the mean field approximation for the quantum part in order to connect it with the classical part of the system. The interaction at the interface can be considered as a time-dependent external field for each of interacting parts. However, it will be associated with a number of difficulties to incorporate such an external field into the quantum solution since the external field is of the order of interaction in each internal part or exceeding those interactions.

We studied the dynamics of a diatomic molecule collision with a thermally active surface, using the quantum dynamics close-coupling wave-packet method (CCWP) with the molecular dynamics method. The kinetic features of the process were discussed with the system parameters changed such as the initial vibrational level, coupling potential of atomic configuration and initial incident energy, being referred to the real physical parameters of the H₂

molecule and the low-temperature N atom surface.

In order to understand the mechanism of energy transfer in the process of the molecule-surface collision, the parameters of a reference case have been selected to be 0.036 eV for the incident energy, with the momentum normal to the surface, and 0.1815 eV for the energy of the stationary second vibrational level ($\nu = 2$) relative to the Morse potential of the incident molecule ($r_e = 1.4$ a.u., $D_m = 1.148$ eV = $0.25 D$ (experimental), $\alpha = 7.61$). The range of the opened vibrational channels was taken as [0-3]. The rotational motion was excluded by introduction of the rotational level $j = 0$. The surface of N atoms can be formed only at the temperatures below the melting point of this solid, which is around 80 K, but artificially has been selected as ϵ_s of the Lennard-Jones (LJ) potential equal 248.9 K. That was approximately 2.5 times higher than an experimental value, however it let us to describe the inelastic collision with the high energy incident molecule in the molecular dynamics framework as compared with the experimental value of potential. The interaction potential between the H₂ molecule and the surface atoms was set as $\epsilon_m = 0.5 \epsilon_s$. The reference case was taken as a set of the above parameters of the system. The duration of H₂ propagation was 472 fsec. We represented the N solid substrate by a two-dimensional cluster of 9 layers of N atoms in the fcc projection with either 10 or 9 atoms in each layer.

At the molecule and surface interface, the interaction as the time-dependent external introduces the necessity to insure that the solution methods can incorporate variations in the external field correctly. For the quantum dynamics part of the solution, it means to extend the grid space in the direction of the molecule propagation up to 128 a.u. because fluctuations in the interaction energy are high in the vicinity of the turning point of the colliding molecule. For the molecular dynamics part, the periodic boundary conditions for the substrate cluster are relaxed in order to prevent the build up of an artificial amplification of the cluster energy due to

* Abstract 4392 submitted to the 21st International Symposium on Rarefied Gas Dynamics, Marseille, France, July 26-31, 1998

the action of the high magnitude external field and possible fast oscillations at the turning point of the collision.

The wave packets representing the translational part of wave function is propagated for each internal rovibrational state until the molecule moves out of the interaction region and the norms of the packets are examined to define the change in the energy of each internal state. Though the number of vibrational channels [0-3] opened is relatively small, the selected depth of the Morse potential incorporates only 5 non-zero stationary vibrational levels. With the difference of energy level larger than the magnitude of interaction with the surface, the transfers between levels are unlikely during collision. Consequently, the changes in the energy of the initial vibrational levels can show the result of interaction in the process of collision.

The effect of the initial vibrational level of the incident diatomic molecule was considered in the range of vibrational levels $\nu = 0$, $\nu = 1$, and $\nu = 2$. The norm of the initial wave packet for each of these states was equal 1.0 at the start of propagation. At the end of propagation, the final norm of each initial state was 1.1726 ($\nu = 0$), 1.1919 ($\nu = 1$), and 1.4236 ($\nu = 2$), respectively. It shows that all states have gained energy as the result of interaction with the thermal substrate. The energy transfer to the initially unpopulated vibrational channels is relatively negligible: two or more orders less than the transfer into the initially populated channel. Even such a small energy gain in the side channels should be at least partly attributed to the effect of interaction with the substrate. Such behavior of the wave packet solution originates primarily due to the interaction with the dynamically changing surface, since the solution obtained on the static surface typically defines transfers between internal vibrator states of the colliding molecule.

Having found that the time-dependent external field changes the energy transfer mechanism essentially, we varied the main parameter of the field, namely, $\epsilon_m = 0.5\epsilon_s$, increasing it two- and threefold ($\epsilon_m = 1.0$ and $1.5\epsilon_s$) relative to the reference case ($\nu = 2$). The response of the norm of the final wave packet was remarkable: 1.9856 for the $\epsilon_m = 1.0\epsilon_s$, and 2.3368 for the $\epsilon_m = 1.5\epsilon_s$, relative to the 1.4236 for the $\epsilon_m = 0.5\epsilon_s$. In Fig.1, time histories of the kinetic and potential energies of the initial wave packet are shown during propagation for the three cases of the interaction potential, 0.5, 1.0 and $1.5\epsilon_s$. We only propagated the translational wave packets corresponding to the appropriate stationary vibrational state. Therefore, the only mechanism at-

tributable to the energy transfer described above is the increase in the energy of the translational wave packet. Since a more realistic distribution of energy changes between translational and vibrational degrees of freedom as a consequence of the external interaction is required, the time-dependent incorporation of vibration into the solution of our interacting system should be implemented.

In the present study, we outlined the interaction mechanism in the molecule-surface system in the process of collision. The time-dependent coupling between these two parts of the system provides quantum channel for the energy transfer between the colliding molecule and the thermal surface. These energy transfer is strongly affected by the characteristics of the interaction and by the internal rovibrational state of the colliding molecule.

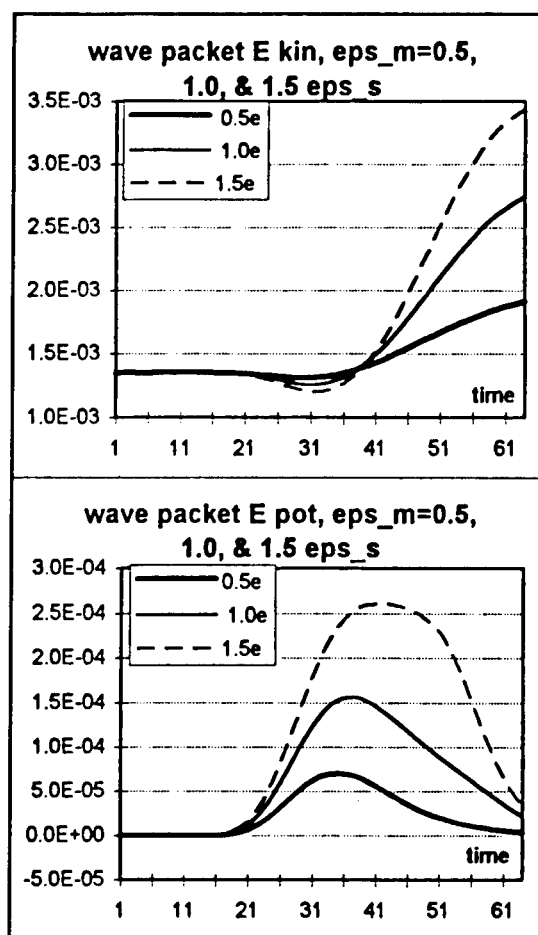


Figure 1: Time history of the kinetic and potential energy of the wave packet of the colliding molecule during propagation

A New Approach to Model and Simulate Numerically Heterogeneous Catalysis in Rarefied Flows *

I. Choquet

ITWM, Kaiserslautern, Germany

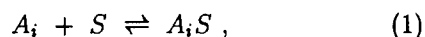
ONERA, Châtillon, France

1 Introduction

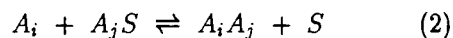
Heterogeneous catalysis affects the gas composition as well as the surfacic heat fluxes of gas flows in chemical nonequilibrium in the vicinity of surfaces. Within the particular framework of rarefied flows, previous studies describe the gas and the surface at the same scale, macroscopic in Ref. [1] or microscopic in Ref. [2] for instance. A new approach, combining both descriptions, is proposed to satisfy all together the following points: *i*) describe the gas at the microscopic scale, as required in rarefied flows, *ii*) describe the surface at the macroscopic scale, to consider not only crystalline but also amorphous surfaces, *iii*) reproduce on average macroscopic laws correlated with experimental results and *iv*) derive analytic models in a systematic and exact way.

2 Statement and resolution of the problem

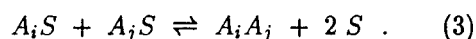
The problem lies in the definition of the microscopic probabilities of adsorption and desorption of a gas atom A_i by a surfacic site S



of Eley-Rideal (ER) recombination and dissociation



and of Langmuir-Hinshelwood (LH) recombination and dissociation



It consists in linking the required microscopic probabilities to macroscopic probabilities correlated

with experimental results, applying this average procedure to the gas phase contribution. It is stated within the general framework of a non static flow, assuming that the surface is not porous. To that purpose, one can notice that the adsorption, the ER recombination and the ER and LH dissociations are all initiated by a collision between a gas particle and an empty or occupied surfacic site. The LH recombination can also be interpreted in this way remembering that it is coupled with adsorption. The macroscopic probability associated with one of these elementary processes is thus the flux of gas particles impinging on the surface that undergo the process under consideration, with the microscopic probability p , divided by the total flux of particles colliding with the surface

$$\langle p \rangle = \frac{\int \int \int_{\vec{v} \cdot \vec{n} \geq 0} p \vec{v} \cdot \vec{n} f d\vec{v}}{\int \int \int_{\vec{v} \cdot \vec{n} \geq 0} \vec{v} \cdot \vec{n} f d\vec{v}} \quad (4)$$

where \vec{v} is the gas particle velocity and \vec{n} the normalized surfacic vector. The thermal velocity distribution function of the gas particles, f , is given by a Maxwellian since the macroscopic laws to be reproduced are defined in the literature assuming equilibrium

$$f = \left(\frac{m}{2\pi kT} \right)^{3/2} \exp \left[- \frac{m(\vec{v} - \vec{v}_o)^2}{2kT} \right] \quad (5)$$

where \vec{v}_o is the mean molecular velocity, m the mass of the gas particle, T the gas temperature and k Boltzmann's constant.

The unknown p should then be derived from this integral equation assuming that the macroscopic probability $\langle p \rangle$ is given. To obtain a systematic and exact derivation one can show that the resolution method based on the Laplace Transform, introduced previously in Ref. [3] to model thermal nonequilibria in the gas phase, can be extended to the present problem, cf. Ref [4].

*Abstract 1406 submitted to the 21st International Symposium on Rarefied Gas Dynamics, Marseille, France, July 26-31, 1998

3 Applications

The first proposed models are associated with a coverage at equilibrium (Langmuir's isotherm). The individual probability for a gas particle to recombine following an ER and a LH mechanism are then derived from Eq. (4) using the inverse Laplace transform (cf. Ref. [4]). A numerical test is proposed to check that these models allow to reproduce, at equilibrium, macroscopic laws correlated with experimental results. The numerical results associated with the LH recombination are plotted Figure 1.

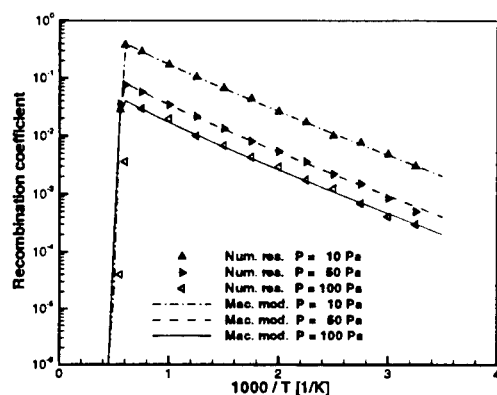


Figure 1: LH recombination of oxygen on RCG surfaces. Macroscopic model (Mac. mod.) and numerical results (Num. res.) associated with various atomic pressures P .

Next, the assumption concerning the coverage locally at equilibrium is reduced. The main difficulty lies then in the modelling and the numerical simulation of the desorption process, which is initiated by the thermal motion of wall atoms. It can seem natural to define directly the number of desorbed particles per unit time and surface. However, the numerical results obtained in this way are not satisfying due to the strong and quick change in residence time of adsorbed particles when the wall temperature reaches the characteristic temperature of desorption.

To define correctly the coverage, we propose to switch from a macroscopic probability of desorption per unit time and surface to a probability per unit collision with the surface. The problem stated Eq. (4) is then recovered but its meaning is now different: desorption is updated at each gas-wall collision but it is not initiated by the collision. The individual probability of desorption is derived using the inverse Laplace transform, cf. Ref. [4]. The numer-

ical results obtained at equilibrium, plotted Figure 2, allow to check that this model reproduces with accuracy Langmuir's isotherm (as well as the ER and LH recombination coefficients, cf. Ref. [4]).

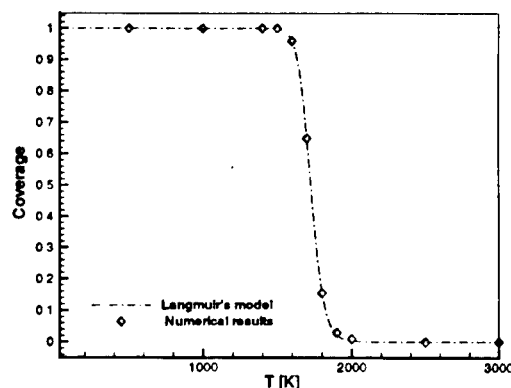


Figure 2: Oxygen coverage on RCG surfaces associated with an atomic pressure of 100 Pa.

4 Concluding remarks

This new approach associates a microscopic description of the gas with a macroscopic description of the surface. The problem formulated Eq. (4) applies to each process described Eqs. (1-3), including desorption. The resolution method allows to reproduce macroscopic models correlated with experimental results and none new parameter is required.

The applications can be extended to the general case of several atomic species, cf. Ref. [4], and to a non constant energy of activation for adsorption for instance.

References

- [1] Bergemann F., *A Detailed Surface Chemistry Model for the DMC Method*, 19th RGD Symp.
- [2] Simmons R. S. and Lord G., *DSMC Simulation of Hypersonic Metal Catalysis in a Rarefied Hypersonic Nitrogen/Oxygen Flow*, 20th RGD Symp.
- [3] Choquet I., *Physics of Fluids*, Vol. 6, No. 12, Dec. 1994, pp. 4042-4053.
- [4] Choquet I., *Heterogeneous Catalysis Modelling and Numerical Simulation in Rarefied Gas Flows*, preprint.

Surface Reactions Under the Thermal Fluctuations in the Framework of Random Quantum Oscillator Model *

A.V. Bogdanov, A.S. Gevorkyan, A.G. Grigoryan

Institute for High-Performance Computing and Data Bases, St-Petersburg, Russia

1 Introduction

The thermal fluctuations effect of the molecule-surface scattering is usually described in terms of Debay-Waller factor and surface form-factor. Several techniques were suggested for evaluation of both of them, but in most of this attempts scatterings of only structureless or at least non-reactive (with rotational-vibrational excitation only) particles were considered. Reactive scattering itself is a rather complicated problem. A lot of mechanisms and channels of its realization rises many difficulties for construction of the correspondent formalism as well as for its lucid description. Therefore we restrict ourselves by consideration of diatomic dissociative adsorption process via Eley-Redeal mechanism. The problem of dissociative adsorption on the surface at finite temperature $(AB)_n + M_T \rightarrow A + (BM_T)_m$ (where A and B are atoms, M_T is the surface at finite temperature T) is formulated as a problem of random motion of quantum harmonic oscillator (QHO) [1]

$$id\Psi_{stc} = \frac{1}{2} [-\partial_x^2 + \Omega^2(t; \{W\}) x^2] \Psi_{stc}, \quad (1)$$

$$-\infty < t, x < +\infty,$$

with the frequency $\Omega(t; \{W\})$ and the wave state $\Psi_{stc}(x, t; \{W\})$ being the functionals of Markovian process $W(t) = \{W\}$. It's assumed also that the frequency can be expressed in the following form

$$\Omega^2(t; \{W\}) = \Omega_0^2(t) + F(t; \{W\}), \quad (2)$$

where the $\Omega_0(t)$ is a regular part of the frequency and has the following asymptotic value

$$\lim_{t \rightarrow \mp\infty} \Omega_0(t) = \Omega_{in(out)}. \quad (3)$$

And as to the stochastic force $F(t; \{W\})$ it's represented in the following form

$$F(t; \{W\}) \rightarrow \begin{cases} 0, & \text{if } t \rightarrow -\infty \\ F(t), & \text{if } t < t_c \\ F_+(t), & \text{if } t_c \leq t = t_+ < +\infty \end{cases}, \quad (4)$$

where t_c is the time at which the $\Omega_0(t)$ turns to the asymptotic frequency Ω_{out} and after which the nature of stochastic force changes.

Using the stochastic model equation method [1] the correspondent variables are separated and as a result the explicit representation for the wave function is derived. This circumstance provide exact mathematical basis of the constructed mixed functional-wave representation of average complete function $\Psi_{br}^+(n; x, t)$ of random quantum harmonic oscillator (where n is the vibration quantum number). Further the $\Psi_{br}^+(n; x, t)$ wave function is projected to the similarly constructed wave function of (out) asymptotic space (taking into account the crossover of stochastic force $F(t; \{W\})$). In result the generalized transition matrix is obtained, that with the temperature T going to absolute zero turns to usual S -matrix of nonstationary quantum harmonic oscillator (QHO) problem.

Below the expressions for transition probability between the ground states of asymptotic channels are given with account, that the $F(t)$ and $F_+(t)$ being the gaussian stochastic functions

$$\Delta_{0 \rightarrow 0}^{br}(\lambda, \lambda_+; \rho) = \sqrt{1 - \rho} \times \times \{I_1^2(\lambda, \lambda_+; \rho) + I_2^2(\lambda, \lambda_+; \rho)\}, \quad (5)$$

where

$$I_1(\lambda, \lambda_+; \rho) = \int_{-\infty}^{+\infty} dx \int_{-\infty}^{+\infty} dy Q(\lambda, \gamma; x) \times \times Q(\lambda_+, \gamma; y) \left(\frac{a+1}{2a^2}\right)^{\frac{1}{2}}, \quad (6)$$

$$I_2(\lambda, \lambda_+; \rho) = \int_{-\infty}^{+\infty} dx \int_{-\infty}^{+\infty} dy Q(\lambda, \gamma; x) \times \times Q(\lambda_+, \gamma; y) \left(\frac{a-1}{2a^2}\right)^{\frac{1}{2}}, \quad (7)$$

*Abstract 5235 submitted to the 21st International Symposium on Rarefied Gas Dynamics, Marseille, France, July 26-31, 1998

$$Q(\lambda, \gamma; x) = J_0 \exp\left(-\frac{x^3}{3} - \lambda\gamma x\right) \times \int_{-\infty}^{+\infty} dz \exp\left(\frac{z^3}{3} + \lambda\gamma z\right), \quad (8)$$

$$J_0 = \int_0^{+\infty} dz z^{-1/2} \exp\left(-\frac{z^3}{12} - \lambda\gamma z\right), \quad (9)$$

$$a = \left[1 + \frac{1}{\lambda\gamma} \left(x - \sqrt{\frac{\lambda}{\lambda_+}} y\right)^2\right]^{-\frac{1}{2}}.$$

Let us remember, that in formulae (5)-(9) the λ and λ_+ are fluctuation parameters before and after crossover and connected with the medium temperature via the Debay-Waller factor, $\gamma = \left(\frac{\Omega_{out}}{\Omega_{in}}\right)^2$ and depend on energy of collision of molecule with surface, ρ is the coefficient of refraction from barrier in the one-dimensional problem of quantum mechanics with momentum $k(x) = \Omega_0(x)$, where t is substituted by x [2].

The results of computations of "ground state-ground state" transition probability for the case when $\lambda_+ \rightarrow +\infty$, i.e. for the pure (out) asymptotic state, are given of Fig. 1.

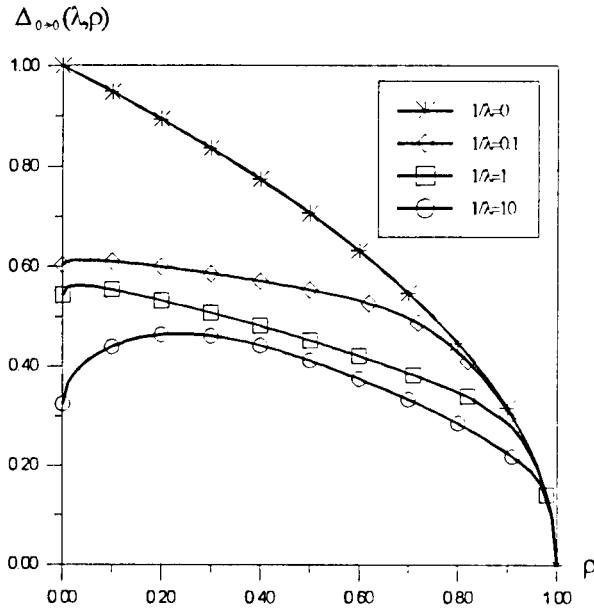


Figure 1: The "ground state-ground state" transition probability for the case when $\lambda_+ \rightarrow +\infty$

References

- [1] Bogdanov A.V. and Gevorkyan A.S., *Three Body Multichannel Scattering as a Model of*

Irreversible Quantum Mechanics, Los Alamos National Laboratory e-Print archive, quant-ph/9712022.

- [2] Bogdanov A.V., Gevorkyan A.S. et. al., *Quasi-Classical Analytical Approximation of the S-matrix for the Three-Particle Collinear Rearrangement Reaction*, Theoretical and Mathematical Physics, Vol.107, No.2, pp.609-619, 1996.

GAS - SURFACE INTERACTION - GS 4

ROOM PÉRÈS

MONDAY, JULY 27, 1998

16:20

Carbon Monoxide and Atomic Oxygen Recombination At High Temperatures and Low Pressures Thermal Flux and Recombination coefficient γ^*

M. Balat¹, J.M. Badie¹, E. Mariage², A. Smith³

¹ IMP-CNRS, Inst. science et génie des Matériaux et Procédés, Odeillo, France

² SEP Division de SNECMA, Le Haillan, St Médard-en-Jalles, France

³ Fluid Gravity Eng. Ltd., Liphook, Hampshire, United Kingdom

1. Introduction

During an atmospheric entry, a space vehicle is submitted to extreme conditions. Entry speeds of 7 to 9 km/s have been proposed for a manned mission to Mars to keep travelling time to an acceptable level of 5 to 8 months. Due to the shock wave, produced by the entering vehicle, gas species can be electronically excited, dissociated and ionised. The chemical composition of Mars' atmosphere has been determined to consist of 95.7% CO₂, 2.7% N₂ and 1.6% Ar.

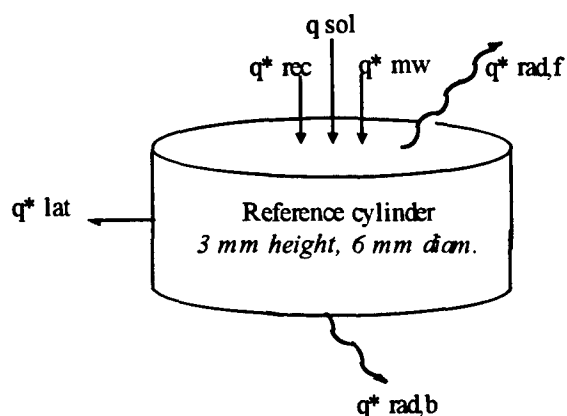


Figure 1 : Representation of the thermal fluxes on the reference cylinder under gas plasma conditions

Catalytic recombination is the formation of a molecule, on a solid surface, by a gaseous dissociated species (heterogeneous recombination). The surface acts as a catalyst, augmenting the reaction rate relative to that of recombination in the rarefied gas

flow (homogeneous recombination). Part or all of the reaction enthalpy will be transferred to the surface. This process doesn't change the chemical state of the surface, but can cause a considerable increase in the surface temperature and therefore an increase in the heat flux towards the inner structure of the vessel. Catalytic recombination will occur mostly during the initial stages of atmospheric entry, where the mean free path of the gas species is sufficiently large for the dissociated species to cross the boundary layer to the surface of the TPS (Thermal Protection System), without recombination in the gas phase.

2. Recombination flux evaluation (experiment and modeling)

In this paper, we present some results about the recombination of carbon monoxide and atomic oxygen at the surface of sintered silicon carbide and C/SiC composite with a CVD-SiC coating, at high temperature (1000 - 1800 K) and in a pressure range of 200 - 2000 Pa CO₂.

Recombination thermal flux q_{rec} is obtained using a method that we have previously developed in our laboratory (IMP) for terrestrial entry (air) using an experimental set-up which associates a solar radiation concentrator (high temperatures) to a microwave generator (dissociated species).

We have developed a thermal approach for molecular and/or atomic species recombination using a heat balance on a reference cylinder volume in the sample. The surface of this cylinder (6 mm diameter, 3mm height) in the sample (25 mm diameter, 3mm height), considered for the thermal balance (Fig. 1),

* Abstract 1141 submitted to the 21st International Symposium on Rarefied Gas Dynamics, Marseille, France, July 26-31, 1998

represents the measurement area by pyrometry. Convective phenomena are neglected (rarefied gas flows) compared to the radiative fluxes to establish the equations for steady state heat transfer under different environments.

The thermal balance is established under each atmosphere : standard gas, gas plasma, standard argon and argon plasma, the determination of the recombination flux being done by difference between the experiments under air or CO₂ plasma (reactive) and argon plasma (inert).

The comparison is made between the two atmospheres: air (Earth entry) and CO₂ (Mars entry) on the basis of recombination flux, the recombination of CO and O leading to higher thermal flux than atomic oxygen recombination (Fig. 2).

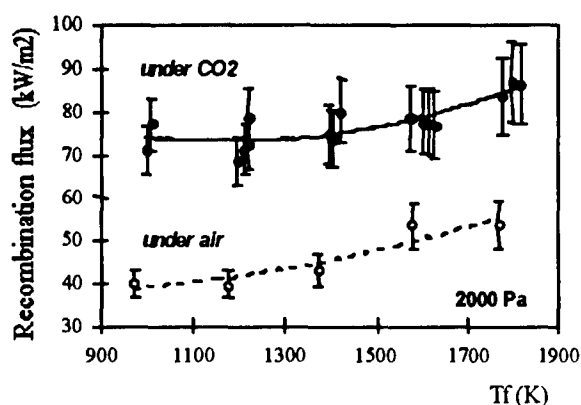


Figure 2 : Recombination flux for the composite C/SiC under dissociated CO₂ or air, at 2000 Pa.

A bidimensional model has been developed in order to estimate the radial thermal losses by conduction (at the limit of the reference cylinder) which have been neglected in the first part (experimental) and to calculate by parameter identification the recombination flux.

This model is based on the simulation of axial and radial heat transfers in the material at high temperature. The bidirectional heat equation with an added source term due to the interaction between microwaves and material is solved with a finite difference scheme which is applied to a cylindrical shape.

The code is written with Matlab™ to finally obtain a mapping of the front face temperatures of the sample (where recombination occurs) which is compared to infra-red images obtained with a camera.

3. Experimental determination of the recombination coefficient γ

We have also developed a chemical approach using VIS-spectroscopy for the determination of the catalytic recombination coefficient. The atomic emission spectroscopy allows to determine the relative concentration (species/ actinometer) to obtain the concentration profile above the sample. This method is limited to low pressure and can be applied with several constraints.

The atomic oxygen concentration evolution is described by diffusion equation (radial gradient is neglected). The resolution of this equation using boundary conditions leads to the catalytic recombination coefficient γ determination :

$$\gamma = \left(\frac{R_0}{R_L} - 1 \right) \frac{4 \cdot D_{O, air}}{V^* \cdot L}$$

R_0 and R_L represent the ratios of the intensities I_0/I_{Ar} (respectively initial and at the sample surface), $D_{O, air}$ the binary diffusion coefficient, V^* the atomic oxygen velocity and L the thickness of the boundary layer.

Some results on ceramic materials are presented.

4. Conclusion

- The recombination flux obtained under dissociated CO₂ is higher than that obtained under air, and this is true for all the pressure range. We find also that the composite C/SiC is more catalytic than sintered SiC, like in the case of air environment.
- Using the 2 D model, we can evaluate the thermal losses at the limit of the reference cylinder in the sample, and validate the experimental approach (like 1D). The difference between the losses under CO₂ or air and argon plasma is very small, and always comprised in the accuracy of the experimental results.
- The chemical approach using actinometry by spectroscopic measurements have given good first results at around 1000 K, for the three materials tested and confirms the experimental thermal results. This chemical evaluation is actually transferred at high temperature simultaneously with the thermal method to both obtain the recombination flux and the recombination coefficient γ in the same range of temperature (1000 - 1800 K) but only at 200 Pa due to the validity of actinometry measurements.

Details of Modeling of Heat Transfer with Catalytic Surfaces in the Re-enter Atmosphere Problem *

V.L. Kovalev¹, A.A. Krupnov²

¹ Dept. of Mechanics and Mathematics of Moscow State University, Moscow, Russia

² Institute of Mechanics of Moscow State University, Moscow, Russia

1 Introduction

In hypersonic flow, surface catalysis is a primary mechanism for transferring energy to surface of entry vehicle. For Earth atmospheric entry heat transfer to a chemically neutral surface can be less than that to an ideal catalytic surface by factor of 2.5.

In [1,2] the phenomenological model, based on the Langmuir layer theory, has been constructed to describe the catalytical properties of the heat shield coatings of reusable hypersonic vehicles. It can predict and explain some experimental effects, particularly, the nonmonotonic temperature and pressure dependences of the heterogeneous recombination coefficients. It is important that this model gives a good agreement with the laboratory and full-scale experimental data.

In [3] the possibilities of using some phenomenological models [4-6] for Earth's atmospheric entry have been analyzed.

In this paper effects of heterogeneous catalytical reactions involving nitrogen monoxide and ionized components on heat transfer in hypersonic atmospheric flight are studied and some phenomenological models are analyzed.

2 Boundary condition on catalytic surfaces in ionized air

In studying ionized air flow ($O_2, N_2, NO, NO^+, O_2^+, N_2^+, O, N, E$) past a blunt body, in the gas phase we took the dissociation-recombination, associative recombination and exchange reactions into account.

The set of heterogeneous catalytical reaction involved Eley-Rideal and Langmuir-Hilshelwood recombination mechanisms, reactions with ionized compo-

nents and reactions with nitrogen monoxide (31 elementary stages were taken into account).

If we will assume that the heterogeneous catalytical reactions involving ionized components are fast, then on the catalytic surface for ionized components we can obtain the relations

$$v_{NO^+} = K_{p_4}^{-1} x_O x_N - x_{NO^+} x_E = 0,$$

$$v_{O_2^+} = K_{p_5}^{-1} x_O^2 - x_{O_2^+} x_E = 0,$$

$$v_{N_2^+} = K_{p_6}^{-1} x_N^2 - x_{N_2^+} x_E = 0$$

Here x_i are molar concentration of components, K_{p_i} - equilibrium constant of corresponding gas-phase ionization reactions.

If the surface temperature $T_w \leq 3000^\circ K$ then $K_{p_i} \gg 1$ for $i = 4, 5, 6$ and for charged particles on the surface we have typical boundary condition

$$x_{NO^+} = x_{O_2^+} = x_{N_2^+} = 0$$

In case of fast heterogeneous catalytic reactions involving nitrogen monoxide we obtain

$$v_{NO} = x_{NO}^2 - p K_{NO} x_{N_2} x_O^2 = 0,$$

$$K_{NO} = K_{p_2} K_{p_3}^{-2}$$

The deviations from equilibrium $v_{NO}, v_{NO^+}, v_{O_2^+}, v_{N_2^+}$ can be eliminated from boundary conditions for the atoms. Then, the boundary conditions for oxygen and nitrogen atoms will be

$$J_O = -m_O \left[\frac{J_{NO}}{m_{NO}} + \frac{J_{NO^+}}{m_{NO^+}} + 2 \frac{J_{O_2^+}}{m_{O_2^+}} + \frac{\rho}{m} \cdot \frac{k_w O p K_3}{1 + p K_3 (x_O + x_N)} \cdot \left(x_O^2 - \frac{K_{pO}}{p} x_{O_2} \right) \right],$$

* Abstract 4966 submitted to the 21st International Symposium on Rarefied Gas Dynamics, Marseille, France, July 26-31, 1998

4 Conclusion

$$J_N = -m_N \left[\frac{J_{NO^+}}{m_{NO^+}} + 2 \frac{J_{N_2^+}}{m_{N_2^+}} + \frac{\rho}{m} \cdot \frac{k_{wNP} K_4}{1 + p K_4 (x_O + x_N)} \cdot \left(x_N^2 - \frac{K_{pN}}{p} x_{N_2} \right) \right];$$

$$k_{wi} = \sqrt{\frac{RT}{2\pi m_i}} \gamma_i, \quad \gamma_i = a_i \exp \left(-\frac{E_i}{RT} \right), \quad i = O, N;$$

$$a_O = 16, \quad a_N = 0.0734,$$

$$\frac{E_O}{R} = 10271^\circ K, \quad \frac{E_N}{R} = 2219^\circ K;$$

$$K_3 = K_4 = 0.2236T \exp \left(46 \left(\frac{492}{T} - 0.311 \right) \right).$$

Here we used the published facts that on variation of the surface temperature and pressure of practical interest ($300^\circ K \leq T_w \leq 2000^\circ K$) predominate oxygen and nitrogen atom recombinations in accordance with Eley-Redeal mechanisms. In order to determine the rate constants in elementary stages Eley-Redeal mechanisms we used the results of laboratory experiments on reaction-cured glass. For slowly heterogeneous catalytic reaction involving oxygen monoxide we obtain $J_{NO} = 0$. Similarly, for slowly heterogeneous catalytic reaction involving charge particles we obtain $J_i = 0$; $i = NO^+, O_2^+, N_2^+$. These relationships must be used in previous boundary conditions as well as.

3 Numerical modeling

In this paper the heat and mass transfer between a blunt body and hypersonic flow is investigated within the framework of the system of equations and boundary conditions for a chemically-reacting multicomponent full viscous shock layer. An efficient method of global iteration for solving these problems was created by authors before.

The numerical modeling demonstrates that the dependence of effective catalytic coefficients on diffusion fluxes is significant to the heat transfer.

For example, the heat flux in the neighborhood of the stagnation point of a sphere obtained in presence of fast heterogeneous catalytic reactions involving nitrogen monoxide maybe twice as many heat fluxes to surface calculated in presence of slow heterogeneous catalytic reactions involving nitrogen monoxide (the flight height $H = 65 \text{ km}$, the flight velocity $V_\infty = 8 \text{ km/c}$).

- From the boundary condition obtained it follows that in presence of fast some heterogeneous catalytic reactions the catalytic activity coefficients are functions not only of the temperature, pressure and chemical composition but also the diffusion fluxes of components.
- Dependences of catalytic activity coefficients on diffusion fluxes maybe significant to the heat transfer in Earth atmospheric entry problem.

References

- [1] Kovalev V.L., Suslov O.N., *Model of the interaction between partially-ionized air and a catalytic surface*, Investigation of Hypersonic Aerodynamics and Heat Transfer with Allowance for Nonequilibrium Chemical Reactions [in Russian], Izd. MGU, Moscow (1987).
- [2] Kovalev V.L., Suslov O.N., *A Simulation of the Interaction between Partially - Ionized Air and Catalytic Surface on High-Temperature Reusable Thermal Insulation.*, Fluid Dynamics, v.31, No 5, p.775-784, 1996.
- [3] Kovalev V.L., Krupnov A.A. *Catalytical Activity Models of Thermal Protection Reusable Surface Insulation.*, 15th IMACS World Congress. August 24-29, 1997, Berlin. V.3: Computational Physics, Chemistry and Biology. Edited by Achim Sydow. p. 627-632.
- [4] Jumper E. J., and Seward W. A., *Model for oxygen recombination on reaction-cured glass* J. Thermophys. and Heat Transfer, 8, 291 (1994)
- [5] Willey R. J., *Comparison of kinetic models for atom recombination on high-temperature reusable surface insulation*, J. Thermophys. and Heat Transfer, 7, 55 (1993)
- [6] Deutschmann O, Riedel U. and J. Warnatz J., *Modeling of nitrogen and oxygen recombination on partial catalytic surfaces*, Preprint No. 23, June 1994, Institut für Technische Verbrennung, University of Stuttgart (1994).

Asymptotic Formulas for the Heat and Diffusion Fluxes to a Catalytic Surface in a Chemically Nonequilibrium Multicomponent Boundary Layer *

V.L. Kovalev¹, O.N. Suslov²

¹ Department of Mechanics and Mathematics of Moscow State University, Moscow, Russia

² Institute of Mechanics of Moscow State University, Moscow, Russia

1 Introduction

Fay-Riddell and Goulard approximate formulas [1,2] are widely used in analyzing heat exchange with catalytic surfaces. However, the use of these formulas is limited by the the Fay-Riddell formula was obtained for an ideally catalytic surface and the Goulard formula for a frozen flow in the boundary layer. In the present paper, on the basis of asymptotic solution of the boundary layer equations for large Schmidt numbers, formulas are obtained for the heat flux and diffusion fluxes of reaction products and chemical elements on the surface with arbitrary catalytic activity and any degree of nonequilibrium in the boundary layer. A comparison of results with analytic and numerical solutions reveals the high accuracy of the formulas proposed.

Early, the authors used this approach for parametric investigation of the diffusion separation of chemical elements on catalytic surface as a function the Damkoehler numbers of homogeneous and heterogeneous reactions [3].

2 Equations and boundary conditions

We will consider the case of supersonic gas flow over a blunt body when in the neighborhood of its catalytic surface a multicomponent partially-ionized, chemically-nonequilibrium boundary layer is formed.

The system of equations and boundary conditions describing the flow in the neighborhood of the stagnation point have the form

$$\frac{\partial Y}{\partial \eta} = -\frac{Sc}{l} f \Pi Y + W, \quad \frac{\partial Z}{\partial \eta} = -\frac{Sc}{l} f Y$$

* Abstract 4967 submitted to the 21st International Symposium on Rarefied Gas Dynamics, Marseille, France, July 26-31, 1998

$$\eta = 0: \quad Y = R^s, \quad \eta \rightarrow \infty: \quad Z = Z_e$$

$$Z = (c_1, \dots, c_{n-n_e}, h)^t,$$

$$Y = \beta^0 J, \quad W = \beta^1 w, \quad R^s = \beta^0 r,$$

$$J = (J_1, \dots, J_{n-n_e}, J_{n-n_e+1}^*, \dots, J_n^*, J_q)^t$$

$$w = (w_1, \dots, w_{n-n_e}, 0, \dots, 0)^t$$

$$r = (w_1, \dots, w_{n-n_e}, 0, \dots, r_q)^t$$

$$\beta^0 = (\beta \mu_w \rho_w (\nu + 1))^{-1/2},$$

$$\beta^1 = \beta \rho (\nu + 1), \quad l = \mu \rho / (\mu \rho)_w$$

Here $c_i, c_i^*, J_i, J_i^*, J_q, h, \rho$, and μ are the mass concentrations of reaction products and chemical elements, the components of diffusion fluxes and heat flux along the normal to the surface, enthalpy, density, and viscosity of the mixture, respectively; f, Sc, η , and β are the reduced stream function, the characteristic Schmidt number, the Dorodnitsyn variable in Lees form, and longitudinal velocity component gradient on the outer edge of the boundary layer; n_e and n are the numbers of elements and components, the subscript w relates to conditions on the surface and subscript e to the conditions at the outer edge of boundary layer, while the subscript t denotes the transposition operation; $\nu = 0$ for plane and $\nu = 1$ for axisymmetric flow.

The elements of the matrix Π depend on the unknown functions and the total transport coefficients. The rates of formation of the components in homogenous and heterogeneous catalytic reactions W and R are expressed in terms of the quantities V , which represent the deviations from equilibrium of independent homogeneous chemical reactions only [3]:

$$W = W_g \varepsilon_g^{-1} V, \quad R = W_s \varepsilon_s^{-1} V$$

3 Asymptotic formulas

If we restrict our attention to zeroth term of the series expansion in $(l/Sm)^{1/3}$ and the first term of the series calculating the integrals of Laplace type, then the asymptotic expansion of the solution [4] of the problem, constructed on assumption $l/Sm \rightarrow 0$, $W = O((l/Sc)^{1/3})$, makes it possible to obtain formulas for the concentration drops of the reaction products and chemical elements and for the enthalpy in the form

$$Z_w - Z_e = \beta^0 (l/Sc)^{-1/3} M J_w + N$$

Substituting the fluxes from the boundary condition on the body in this relation, we obtain a system of algebraic equations for determining the concentration of reaction products, the diffusional separation on chemical elements, and the enthalpy on the surface:

$$Z_w - Z_e = BL^{1/3} B^{-1} (A_d W_s \zeta_s + BL^{-1/3} B^{-1} A_b \zeta_g W_g) V$$

$$\zeta_g = \varepsilon^{-1/3} \varepsilon_g^{-1}, \quad \zeta_s = \varepsilon^{-2/3} \varepsilon_s^{-1}, \quad \varepsilon = l/Sc$$

where the columns of the matrix B are eigenvectors of the matrix Π , and the elements of diagonal matrix L are eigenvalues of the matrix Π . The matrix A_d and A_b are functions of B , L , and $f'(0)$ [4].

For a known composition and enthalpy on the surface, all the fluxes can be found from the formula

$$J_w = K(Z_w - Z_e), \quad K = \frac{1}{\beta^0} C B L^{-1/3} B^{-1}$$

$$C = (A_d + BL^{-1/3} B^{-1} A_b (W_g \zeta_g) (W_s \zeta_s)^{-1})^{-1}$$

We note that K is the heat transfer coefficient matrix a multicomponent partially-ionized nonequilibrium boundary layer on a surface with arbitrary catalytic activity.

4 Comparison of the results with numerical and analytical solutions

A comparison with the results of papers [5-7] of the diffusion separation of dissociated air showed that concentration of oxygen element obtained in the present paper differ by no more than 2-3 %. The difference of the order of 3-10 % from the results of numerical calculations [8,9] of heat fluxes can be attributed to use of different data for rate constants of homogeneous reactions and transport coefficients.

5 Conclusion

- The use of the asymptotic formulas proposed makes it possible to investigate the heat and transfer between a chemically nonequilibrium multicomponent boundary layer and catalytic surface over a wide range of key parameters of problem.
- For various models describing catalytic properties of the surface the heat transfer reduction isolines were obtained in the (flight velocity, flight height) plane.

References

- [1] Fay J.A., and Riddell F.F., *Theory of stagnation point transfer in dissociated air*, J. Aeronaut. Sci., 25, No. 2, 73 (1958).
- [2] Goulard R., *On catalytic recombination rates in hypersonic stagnation heat transfer*, Jet Propulsion, 28, 737 (1958).
- [3] Kovalev V.L., Suslov O.N., *Diffusional separation of chemical elements on catalytic surface*, Izv. Akad. Nauk SSSR, Mekh. Zhidk. Gasa, No. 4, 115 (1988).
- [4] Suslov O.N., *Asymptotic integration of the equations of a multicomponent, chemically nonequilibrium boundary layer*, in: Aerodynamics of Hypersonic Flows with Blowing [in Russian], Izd. MGU, Moscow (1976), p.6.
- [5] Anfinov N.A., *Some effects associated with multicomponent nature of gas mixtures*, Izv. Akad. Nauk SSSR, Mekh. Zhidk. Gasa, No. 5, 117 (1963).
- [6] Tirsikii G.A., *Determination of effective diffusion coefficients in a laminar multicomponent, boundary layer*, Dokl. Akad. Nauk SSSR, 155, 1278 (1964).
- [7] Gromov V.G., *Chemically nonequilibrium laminar boundary layer in dissociated air*, Izv. Akad. Nauk SSSR, Mekh. Zhidk. Gasa, No. 2, 3 (1966).
- [8] Voroncin V.G., and Geraskina L.K., *Nonequilibrium laminar dissociating-air boundary layer on axisymmetric bodies*, Izv. Akad. Nauk SSSR, Mekh. Zhidk. Gasa, No. 3, 144 (1969).
- [9] Scott C.D., *Space Shuttle laminar heating with finite rate catalytic recombination*, AIAA Paper, No. 757 (1974).

Adsorption and Catalysis in CO-Oxidation on a Hot Platinum Surface *

V. Sankovitch

Dept. Fisica Fundamental, UNED, Madrid, Spain

The surface-catalyzed reaction is one of the most interesting and complex gas-solid interaction phenomena. Although CO-oxidation reaction is considered the simplest one and the best studied, there remain quite a number of unclear and questionable issues that require solution. The fact that the reaction occurs only in case one or both reagents are adsorbed on the surface does not raise any doubts: adsorption is a necessary condition for the heterogeneous reaction to take place. But we do not have a clear notion about the reagents adsorption-desorption mechanisms, about the state of the adsorbed molecules on the metal surface, about why their reactivity increases in this state, about the role of metal in this process, as well as about a number of other components of this very important reaction. In these conditions, it is reasonable to enlarge the experimental research field of this phenomenon in order to confirm more convincingly one hypothesis and reject erroneous ones.

The actual concept of the reaction mechanism is briefly analyzed and some basic hypothesis, in particular, the oxygen dissociative chemisorption one, are called in question. Experimental results for CO adsorption and oxidation on a polycrystalline platinum foil are presented. They were carried out in vacuum conditions with a continuous flow of reagents on a surface in a large platinum temperature range, up to its boiling-point. The experimental data indicate the existence of two CO adsorption states for the temperature interval 500-1000 K and, as for oxygen, exhibit a tendency to the repeatability of CO adsorption-desorption processes on a platinum temperature scale. Such repeatability is discovered for the oxidation reaction up to the platinum boiling-point too. The reaction in the intermediate temperature interval 1200-1800 K is provoked by the connection of a dry battery negative terminal to the platinum foil during its heating. This last experiment indicates two very distinct ox-

idation reactions and a strong dependence of their rates on the battery voltage. In conclusion, a new reaction mechanism is proposed. It is based on a notion that takes into account the wave structure of atom and allows, to the author's mind, to understand many of the surface reaction steps.

*Abstract 5367 submitted to the 21st International Symposium on Rarefied Gas Dynamics, Marseille, France, July 26-31, 1998

Nonthermal Chemical Reactions near the Spacecraft Surface *

A.A. Pyarnpuu¹, A.V. Rymarchuk², V.I. Shematovich³

¹Moscow State Aviation Institute (Technical University), Moscow, Russia

²Moscow Institute of Physics and Technology, Dolgoprudnij, Russia

³Institute of Astronomy of the Russian Academy of Sciences, Moscow, Russia

1 Introduction

The problem of a atmospheric gas flow near the spacecraft surface is very complicated due to the own surface outgassing. Therefore, it is necessary to take into account the real properties of atmospheric gas particles, to consider the mixtures of outgassing and ambient atmospheric species, and the chemical reactions both on a spacecraft surface and in the near-surface layer.

It is known, that the flyby of the spacecraft with actively outgassing surface results in the formation of the slowly vanishing pollution spot. This spot contains many radiatively and chemically active admixture species, some of them are ecologically dangerous and strongly emitting in the infrared wavelength range.

2 Results

In the report the input of chemical processes into the formation of chemically and radiatively active pollution species caused by interaction of the own external spacecraft atmosphere with the ambient atmospheric gas is numerically investigated using the direct statistical modeling (DSMC) [1,2].

In the numerical experiments it was found that the transition region in which the interaction between the outgassing products and ambient atmospheric gas takes place is formed. In particular, this transition region is characterized by the following features: (i) the effect of surface shielding is increased for the stronger outgassing; (ii) the influence of chemical reactions mainly leads to the formation of new species in the spacecraft exhaust, some of them would being ecologically dangerous both for the Earth's atmosphere and the spacecraft surface. Also the production rates of some IR-radiatively emitting admixture species in the near-

surface region were estimated. The abundances of the strongly IR-emitting H₂O(nu) and OH(nu) molecules formed in the near-surface region were calculated. These numerical estimates were compared with experimental measurements [3] of IR-emissions in the Shuttle spot.

References

- [1] Pyarnpuu, A.A., Tsvetkov G.A., and Shematovich, V.I. *Kinetic simulation of chemical reactions in the rarefied multicomponent gas near the solid surface*, in *Rarefield Gas Dynamics* (ed. by A.Beylich), VCH, New York, pp. 1385-1390, 1991.
- [2] Pyarnpuu, A.A., Shematovich V.I., and Svirschevsky S.B. *Kinetic investigations of the near-surface phenomena in the gas and dust envelopes of small celestial bodies*, in *Rarefied Gas Dynamics-19* (ed. by J.Harvey and G.Lord), University Press, Oxford, v.II, pp. 1079-1085, 1995.
- [3] Bernstein, L.S., Elgin J.B. and oth. *Sources of infrared radiation generated by the interaction of fast O(¹D) with H₂O in space* J. of Geophysical Research, vol. 101, A1, pp. 383-393, 1996.

*Abstract 5111 submitted to the 21st International Symposium on Rarefied Gas Dynamics, Marseille, France, July 26-31, 1998

MONTÉ CARLO METHODOLOGY - MCM 1

ROOM LAVOISIER

MONDAY, JULY 27, 1998

9:45

Shock Wave Structure in a Gas with Transverse Gradients

G.A. Bird

GAB Consulting Pty. Ltd.

The paper is concerned the flow that is produced by the instantaneous blocking of a moving gas flow that has either a temperature or a flow velocity gradient in the direction normal to the direction of motion.

First consider the case of a temperature gradient in a gas with a uniform velocity u . Figure 1 shows the results from one-dimensional theory for the shock Mach number M_s and the speed V_s of the reflected shock wave in the frame of reference in which the blocking surface is stationary. This shows that weak and moderate strength shock waves move more rapidly, relative to the blocking surface, into the gas at the higher temperature and consequently lower Mach number. The reflected shock speed becomes independent of the upstream temperature for very strong shock waves.

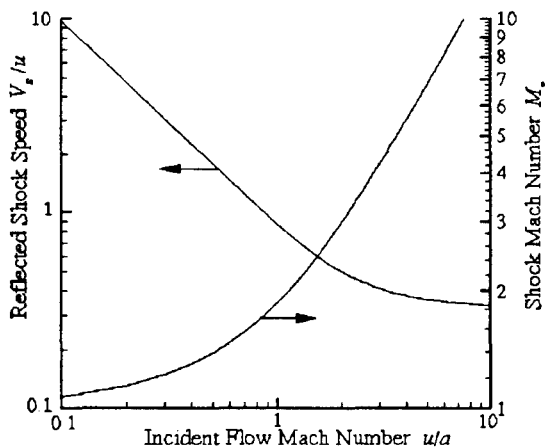


Fig. 1. Predictions of one-dimensional theory for a constant velocity u and a variable speed of sound a .

Next consider a velocity gradient in a gas at a uniform temperature. The situation is reversed in that a similar one-dimensional analysis predicts that the reflected shock speed is independent of the upstream velocity and Mach number for weak and moderate strength shocks, while very strong shocks move more rapidly into the gas at the higher Mach number.

*Abstract 1006 submitted to the 21st International Symposium on Rarefied Gas Dynamics, Marseille, France, July 26-31, 1998.

It is difficult to predict even the qualitative nature of these flows. The direct simulation Monte Carlo (or DSMC) method [1] has therefore been used to make a numerical study. The calculations must be made on a scale that is very large in comparison with a typical shock wave thickness and two-dimensional DSMC calculations have been made for flowfields with linear dimensions up to a thousand mean free paths.

The first test case involved a gas with a 5:1 linear temperature gradient between specularly reflecting boundaries and a uniform flow velocity such that the Mach number ranged from 0.87 to 1.94. The distance between the boundaries was one hundred mean free paths at the mean temperature, although the mean free path varied by a factor of five between the cold gas at the lower boundary and the hot gas at the upper boundary. The one-dimensional theory of Fig. 1 predicts a reflected shock speeds at the higher temperature boundary 1.98 times that at the lower boundary. The shock develops a curved shape that reflects this difference, but the speed of this wave is intermediate between the one-dimensional values and a vortex develops between the wave and the stationary blocking surface. Figure 2 shows contours of non-dimensional scalar pressure ($p = nkT$) at the non-dimensional time 1.0. The pressure is normalized by the pressure in the undisturbed gas, and the time by the time that is required for the undisturbed gas to move a distance equal to the distance between the boundaries.

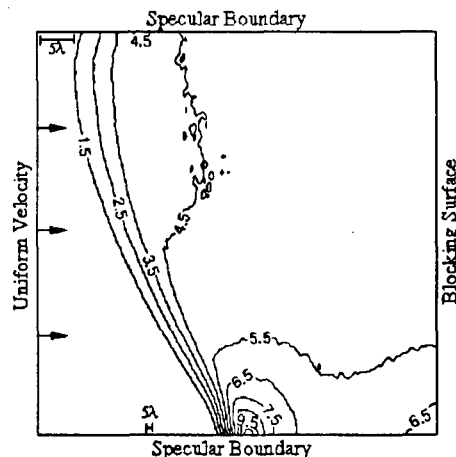


Fig. 2. Contours of scalar pressure at time 1.0.

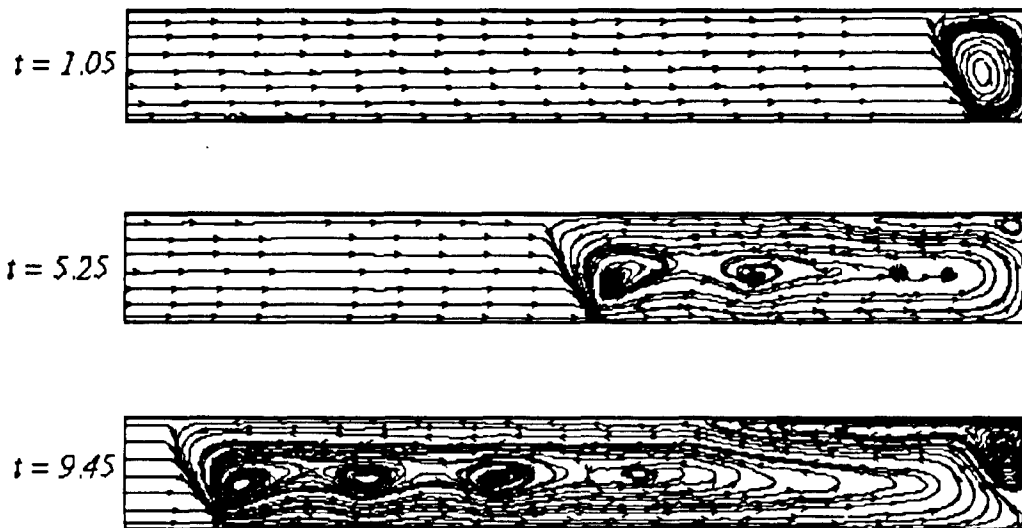


Fig. 3. Flow direction lines at various times.

The flow direction lines in Fig. 3 are from a similar calculation employing a flowfield of 120×1000 mean free paths at the average temperature in the undisturbed gas. The shock develops a steady shape at a non-dimensional time of about four. The large flow deflection occurs at a non-dimensional scalar pressure of about four.

If the wave conformed to the one-dimensional Rankine-Hugoniot conditions at the boundaries, the flow velocity behind the wave at the hot boundary would be in the same direction as the original flow, while that at the cold surface would be in the opposite direction. The direction of the primary vortex is, however, in the opposite direction and two-dimensional effects are clearly important within the wave. At large times, a secondary contra-rotating vortex appears at the intersection of the blocking plane and the boundary adjacent to the initially hot stream. This secondary vortex grows to fill the space between the boundaries and develops a maximum speed that actually exceeds the maximum speed in the primary vortex. At the same time, the central region of the primary vortex splits into discrete smaller vortices and the flow becomes strongly modulated along the boundary adjacent to the initially cold gas.

Despite their complexity, the secondary flows do not appear to be instabilities. This observation is based on the fact that, unlike Taylor-Couette and similar flows, the flow history remains unchanged when separate runs are made with different random number sequences. Advantage will be taken of this to employ ensemble averaging in additional calculations with larger flowfields.

The effect of a transverse velocity gradient has been investigated through a case with a similar ratio of reflected shock speeds at the boundaries. As noted earlier, this necessarily involved higher velocities and stronger shock waves. The initial stage of the flow again conformed to the one-dimensional theory with the shock moving faster into, in this case, the gas at the higher velocity and Mach number. However, the higher energy of this flow soon became the dominant factor, the direction of the primary vortex was reversed and the shock wave at the lower velocity surface advanced more rapidly than that at the higher velocity boundary. Unlike the temperature gradient case, a strong secondary shock wave developed in the front.

The calculations demonstrate that the DSMC method is capable of determining the nature of complex two-dimensional unsteady flows of a class that has barely been touched by continuum CFD methods.

Reference

- [1] Bird G.A., *Molecular Gas Dynamics and the Direct Simulation of Gas Flows*, Oxford University Press, 1994.

Direct Simulation Monte Carlo Method Coupled with Classical Trajectory Calculations for Rigid Diatomic Molecules *

K. Koura

National Aerospace Laboratory, Chofu, Tokyo, Japan

For an accurate simulation of the rotational relaxation of diatomic molecules, the direct simulation Monte Carlo (DSMC) method coupled with the classical trajectory calculations (CTC) for rigid diatomic molecules is developed. The present CTC formulation is made in Cartesian coordinates using the canonical equations of motion with a rigid rotor constraint and the Euler equations of motion in quaternions. These equations are free from singularity difficulties and numerically integrated using a variable-step eighth-order Runge-Kutta method and a modified leapfrog method. Although the Runge-Kutta method solves more efficiently the constrained equations than the quaternion equations and the leapfrog method solves more efficiently the quaternion equations than the constrained equations, a choice between the Runge-Kutta (constrained equations) and leapfrog (quaternion equations) methods may depend on the conditions of simulations. The null-collision technique introduced into the DSMC method for the accurate and efficient evaluation of the molecular collision frequency is used in the CTC-DSMC method.

The CTC-DSMC method is applied to the simulation of the rotational relaxation of nitrogen through a normal shock wave. The intermolecular potential is taken as the extended Morse and Lennard-Jones potentials and the Parker potential. The CTC-DSMC results are compared with the experimental results of Robben and Talbot, Smith, and Alsmeyer and agree well with the measured data except Smith's data in the rearward portion of the shock wave, where several experimental difficulties were indicated. This fact may enhance the reliability of both the empirical potentials and experimental results. Although the computation time required for the CTC-DSMC calculation of a nitrogen shock wave is about 100 times or more as large as that for the ordinary DSMC calculation with a phenomenological rotational model, the CTC-DSMC

results with more information than the experimental results should serve as the standard data for the assessment of phenomenological rotational models. Work on further computational efficiency and applications of the CTC-DSMC method is in progress.

* Abstract 4396 submitted to the 21st International Symposium on Rarefied Gas Dynamics, Marseille, France, July 26-31, 1998

Study of Time Counter Effects in the Direct Simulation Monte Carlo Method for Rarefied Gases *

S. Rjasanow¹, W. Wagner²

¹ University of Saarland, Department of Mathematics
Postfach 15 11 50, 66041 Saarbrücken, Germany

² Weierstrass Institute for Applied Analysis and Stochastics
Mohrenstraße 39, 10117 Berlin, Germany

1 Introduction

A commonly used tool for the numerical treatment of rarefied gas flows in real world applications (like the reentry of a space shuttle into the atmosphere) is the DSMC (direct simulation Monte Carlo) method (see, e.g., [2], [5]).

An important part of the DSMC method is the mechanism that determines the number of collisions among the simulation particles during a given time interval. The original procedure, called "time counter", assigned an appropriate individual amount of time to each of the collisions. Later this procedure was replaced by a tool that was called "no time counter" method (to be clearly distinguished from the previous one). Here the number of collisions on the given time interval was calculated in advance, which is numerically more convenient. We refer to [4], [1] and the detailed discussion of this development in [2, § 11.1].

From a mathematical point of view, the time evolution of rarefied gas flows is described by the Boltzmann equation (see, e.g., [3]). The relationship between the DSMC method and the Boltzmann equation was established in [6], where both the "time counter" and the "no time counter" versions of the method were treated.

Generally speaking, the behaviour of the stochastic particle system is determined by three main components - the time step between subsequent interactions (collisions), the random mechanism for the choice of the collision partners, and the (again random) mechanism for calculating the result of the collision.

The purpose of this paper is to illustrate the interplay between these various components and to propose some new modifications of the DSMC

method. We derive different time counting procedures and show how they influence the other (random) parts of the corresponding algorithms. We compare the various modifications of the DSMC method with respect to different criteria such as efficiency, systematic error, and statistical fluctuations.

2 Time counting procedures

Consider the collision simulation in a given spatial cell D_l . In the standard DSMC method the time step between subsequent collisions has the form

$$\tau = \frac{2n|D_l|}{c_B n_l(n_l - 1)U_{max}}, \quad (1)$$

where n is the number of simulation particles, $|D_l|$ is the volume of the cell, n_l is the number of simulation particles in cell D_l , and c_B is some physical constant. The indices i, j of collision partners are generated uniformly. The probability of a fictitious collision is

$$1 - \frac{\|v_i - v_j\|}{U_{max}}. \quad (2)$$

The function U_{max} denotes the maximal norm of the relative velocities and is accumulated during the simulation process. At the beginning of the collision simulation step, there will be a certain additional error in this procedure. This error will vanish when U_{max} increases and adapts to the system. On the other hand, U_{max} remembers all events from the past. Therefore it will be too large later on and create redundant fictitious collisions. These effects will be illustrated by numerical examples.

We propose a procedure using localized upper bounds for the relative velocity norm.

* Abstract 3971 submitted to the 21st International Symposium on Rarefied Gas Dynamics, Marseille, France, July 26-31, 1998

In the cell D_l we consider the mean velocity

$$V = \frac{1}{n_l} \sum_{i: x_i \in D_l} v_i$$

and the temperature

$$T = \frac{1}{3} \left[\frac{1}{n_l} \sum_{i: x_i \in D_l} \|v_i\|^2 - \|V\|^2 \right].$$

Note that these local quantities are preserved during the collision simulation step. We introduce some values $0 =: b_0 < b_1 < \dots < b_K$, $K \geq 1$, where

$$\frac{\|v_i - V\|}{\sqrt{T}} \leq b_K, \quad \forall i: x_i \in D_l. \quad (3)$$

The normalized velocities are divided into groups according to their individual majorants. The **time step** is

$$\tau = \frac{2n|D_l|}{c_B(n_l - 1)2\sqrt{T} \sum_{k=1}^K b_k \gamma_k}, \quad (4)$$

where γ_k denotes the number of particles with normalized velocities between b_{k-1} and b_k . The procedure for generating the indices of the collision partners takes the form

- choose the index of a group k on $\{1, \dots, K\}$ according to the distribution

$$\frac{b_1 \gamma_1}{\sum_{\mu=1}^K b_\mu \gamma_\mu}, \dots, \frac{b_K \gamma_K}{\sum_{\mu=1}^K b_\mu \gamma_\mu}; \quad (5)$$

- choose the index i of the first collision partner uniformly among the indices in the group I_k ;
- choose the index j of the second collision partner uniformly on $\{j \neq i: x_j \in D_l\}$.

The probability of a **fictitious collision** is

$$1 - \frac{\|v_i - v_j\|}{\sqrt{T} [\hat{b}(v_i) + \hat{b}(v_j)]}, \quad (6)$$

where $\hat{b}(v)$ denotes the local bound for velocity v .

3 Numerical tests

We consider the problem of relaxation (spatially homogeneous case). The initial distribution in our test example is a weighted mixture of two Maxwellians, namely

$$f_0(v) = \alpha \frac{1}{(2\pi T_1)^{3/2}} \exp\left(-\frac{\|v - V_1\|^2}{2T_1}\right) + (1 - \alpha) \frac{1}{(2\pi T_2)^{3/2}} \exp\left(-\frac{\|v - V_2\|^2}{2T_2}\right),$$

method	real	fict. (%)	coll	CPU
DSMC	330123	96.8	1.00	1.00
K=4	334633	93.3	0.48	0.82
K=16	332348	74.7	0.13	0.52
K=64	338708	46.7	0.06	0.48
K=256	336520	28.9	0.05	1.31

Table 1: Numbers of collisions

with $\alpha = 0.001$ and

$$V_1 = (-999, 0, 0), \quad V_2 = (1, 0, 0), \quad T_1 = T_2 = 1.$$

The number of particles is $n = 100000$.

Some results concerning the number of collisions for different methods are shown in Table 1. The second column shows the absolute numbers of real collisions. The third column shows the relative amounts of fictitious collisions. The fourth column shows the number of collision attempts in relation to the standard DSMC method. The last column shows the corresponding relative values for the CPU time. The method using localized upper bounds with $K = 64$ gives a gain factor of about 16 as far as the number of collisions is concerned. Most of this advantage is lost due to the effort needed for sorting the particles with respect to the local bounds. However, a gain factor of 2 remains. This factor depends on the length of the time interval.

References

- [1] Bird G.A., *Perception of numerical methods in rarefied gas dynamics*, Progr. Astronaut. Aeronaut., Vol.118, pp.211-226, 1989.
- [2] Bird G.A., *Molecular Gas Dynamics and the Direct Simulation of Gas Flows*, Clarendon Press, Oxford, 1994.
- [3] Cercignani C., Illner R., Pulvirenti M., *The Mathematical Theory of Dilute Gases*, Springer, New York, 1994.
- [4] Koura K., *Null-collision technique in the direct-simulation Monte Carlo method*, Phys. Fluids, Vol.29, No.11, pp.3509-3511, 1986.
- [5] Harvey J., Lord G. (eds.), *Rarefied Gas Dynamics*, Oxford University Press, Oxford, 1995.
- [6] Wagner W., *A convergence proof for Bird's direct simulation Monte Carlo method for the Boltzmann equation*, J. Statist. Phys., Vol.66, No.3/4, pp.1011-1044, 1992.

MONTÉ CARLO METHODOLOGY - MCM 2

ROOM LAVOISIER

MONDAY, JULY 27, 1998

11:00

Electron Energy Distributions in an Inductively Coupled Plasma Reactor *

S. Yonemura¹, K. Nanbu¹, T. Morimoto², K. Sakai¹

¹ Institute of Fluid Science, Tohoku University, Aoba-ku, Sendai, Japan

² Central Research Laboratory, Tokyo Electron, Ltd., Nirasaki, Japan

1 Introduction

Plasma discharges in rarefied gases have been playing a key role in materials processing such as etching, sputtering, and chemical vapor deposition. Many physical and chemical parameters govern the structure of plasma discharges. One of the most important quantities is the electron energy distribution function (EEDF) because all rate constants are determined from the EEDF. Let $f(\varepsilon)$ be the EEDF. The rate constant of ionization is given by

$$K_{iz} = \langle \sigma_{iz}(\varepsilon)v \rangle = \sqrt{\frac{2}{m}} \int_0^\infty \sqrt{\varepsilon} \sigma_{iz}(\varepsilon) f(\varepsilon) d\varepsilon$$

where v is the speed and $\varepsilon (= mv^2/2)$ is the kinetic energy of electron, and $\sigma_{iz}(\varepsilon)$ is the ionization cross section, m being the mass of electron. Similarly, if we replace σ_{iz} by electronic or vibrational excitation cross section, we have the corresponding rate of excitation. A rough approximation is to use the Maxwellian distribution

$$f_0(\varepsilon) = \frac{2}{(kT)^{3/2}} \left(\frac{\varepsilon}{\pi} \right)^{1/2} e^{-\varepsilon/kT}$$

instead of $f(\varepsilon)$, T being the electron temperature. However this is far from true for plasma discharges. The real distribution $f(\varepsilon)$ is much higher than $f_0(\varepsilon)$ in a high energy tail, and this very tail governs the rate K_{iz} because the threshold energy of ionization is located in the tail.

We consider the discharge in argon gas. The electron energy ε depends on all microscopic processes in the discharge such as elastic collisions, ionizing collisions, exciting collisions, acceleration in sheath, and absorption on electrodes. All these processes have been taken into consideration in the previous works on the analysis of plasma discharges.

These works hold good for conventional parallel-plate radio-frequency plasma etcher, where plasma density is of order $10^{10}/\text{cm}^3$ and gas pressure is 0.1 – 1 Torr. However, the realization of electronic devices with quarter micrometer patterns of high aspect ratio requires the change in plasma sources. A recent trend in plasma-assisted materials processing is towards “low gas density and high plasma density” as seen in inductively coupled, electron cyclotron resonance, and helicon sources. A typical plasma density is $10^{11} - 10^{12}/\text{cm}^3$. This means that the Coulomb collisions are important in such high density plasma and that only the particle approach makes sense in such low gas density less than 10 mTorr. The fluid model is not applicable. The objective of the present work is to clarify the effect of the Coulomb collisions on the electron energy distribution function.

2 Problem Setup

We consider the discharge of argon gas at rest in an inductively coupled plasma reactor with radius of 10 cm. The coil is wound on the cylindrical wall of the reactor. Electrons and ions move in the electric and magnetic fields induced by the radio-frequency current in the coil. As for electron-atom collision, we employ the most detailed set of collision cross sections; not only elastic and ionizing collisions but also 25 exciting collisions are taken into consideration. The drift velocity obtained by use of these cross sections agrees very well with the measured data. As for ion-atom collision, we use our own model [1], the use of which was shown to give a good agreement with experimental data. The Coulomb collisions are treated based on the theory of Nanbu [2]. The motions of sample electrons and ions and the electric and magnetic field are calculated by use of the particle-in-cell method [3]. The EEDF can be obtained from a set of kinetic energies of sample electrons.

*Abstract 4476 submitted to the 21st International Symposium on Rarefied Gas Dynamics, Marseille, France, July 26-31, 1998

3 Results

Calculation conditions are as follows. The gas pressure is 5mTorr and gas temperature is 298K. The number of coil turns per meter is 15/m. The coil current is 7A. The frequency f of the coil current is 13.56MHz. The plasma density averaged over the discharge space is $10^{11}/\text{cm}^3$.

Figure 1 shows the preliminary EEDF without Coulomb collisions. It is obtained by the time averaging. The EEDF has a peak at a lower energy than the peak position of the Maxwellian distribution, and the EEDF is higher than the Maxwellian distribution in a high energy tail. Figure 2 shows the variation of the electron energy in a rf period, ϵ_{av} representing the average energy of the whole electrons. The electron energy is time-modulated. It's frequency is twice as large as the driving frequency.

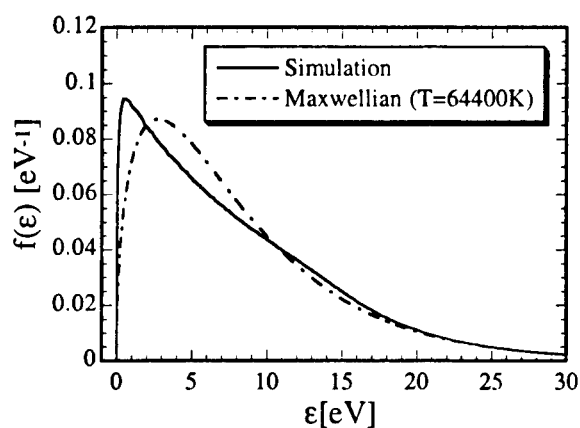


Figure 1: the EEDF and the Maxwellian distribution

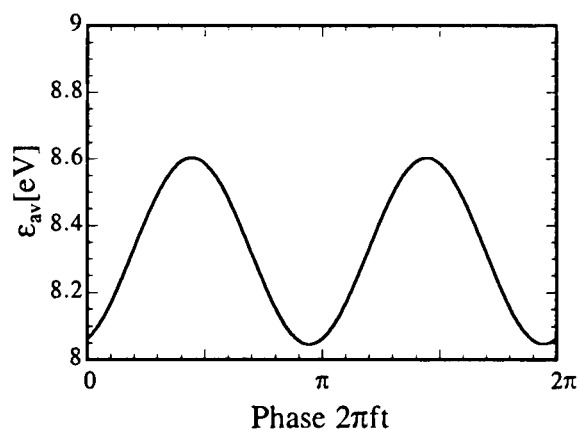


Figure 2: Variation of electron energy in a rf period

References

- [1] Nanbu, K. and Kitatani Y., *An ion-neutral species collision model for particle simulation of glow discharge*, J. Phys. D: Appl. Phys., Vol.28, pp.324-330, 1995.
- [2] Nanbu, K., *Theory of cumulative small-angle collisions in plasmas*, Phys. Rev. E, Vol.55, No.4, pp.4642-4652, 1997.
- [3] Birdsall, C. K. and Langdon, A. B., *Plasma Physics via Computer Simulation*, McGraw-Hill, 1985.

Implementation of a Self-Consistent Test Particle Monte Carlo Method to Solve the Nonlinear Boltzmann Equation *

S. Longo¹, I.D. Boyd²

¹ Chemistry Department, University of Bari, Italy

² Sibley School of Mechanical & Aerospace Engineering, Cornell Univ., Ithaca, U. S. A.

We illustrate the application of a self-consistent Test Particle Monte Carlo technique to the solution of the nonlinear Boltzmann equation in rarefied flows, a task traditionally undertaken by using the direct simulation Monte Carlo method developed by Bird [1].

Basically, as an alternative to *direct* simulation Monte Carlo (DSMC) the self-consistent relaxation technique is based on the iteration of Test Particle Monte Carlo simulations where the background field of scattering partners is a representation of the flow field resulting from the previous iteration.

After a random collision partner for the test particle is selected, the probability for a scattering event is calculated according to the linearized collision term of the Boltzmann equation: the whole process is equivalent to evaluating a Monte Carlo contribution to the linearized Boltzmann collision integral. The process is repeated up to the steady state.

Test particles are produced according to the source term and tracked up to the outlet(s). Since the equation solved at any step is linear there is no need for an absolute particle weight during the simulation: the sampled distribution function is subsequently normalized in order to match the macroscopic flow at the inlet.

The idea of self-relaxing iteratively the solution of a linearized Boltzmann equation is straightforward, and it has been applied to the calculation of the electron energy distribution function in uniform weakly ionized plasmas taking into account electron-electron collisions [2].

The application of the principle to rarefied gas dynamics is not so direct for two reasons:

(1) In the application to weakly ionized plasmas the electron-electron collision term is only a small perturbation of the linear collision term describing the interaction of electrons with gas atoms. Convergence is simply attained in this case, but not

necessarily in the application to gas dynamics where the nonlinear collision term is predominant.

(2) Different from the case of weakly ionized gases, the velocity distribution function in rarefied fluid dynamic problems can be strongly anisotropic. This circumstance, together with the necessity to extend the approach to non uniform systems, raises a strong problem of storage, connected with an accurate but affordable representation of the velocity distribution function in different positions. This accurate representation is necessary in order to calculate the linearized collision term at any iteration.

The solution we propose is to represent the local velocity distribution function by the product of a "radial" part which is only a function of position and speed $|v|$ and an angular part which is a function of (position and of) the two angles θ and ϕ defined by $v_x = v \cos \theta$, $v_y = v \sin \theta \cos \phi$, $v_z = v \sin \theta \sin \phi$, i.e.

$$f(r, v) = R(r, |v|) \chi(r, \theta, \phi) \quad (1)$$

In any cell of the space mesh, the radial part $R(r, |v|)$ is stored by velocity bins, while the angular part $\chi(r, |v|)$ is developed into a limited set of spherical harmonics:

$$\chi(r, \theta, \phi) \simeq \sum_{l=0}^{l_{max}} \sum_{|m| \leq l} a_{lm}(r, |v|) Y_l^m(\theta, \phi) \quad (2)$$

The calculation of the coefficient of a given harmonic contributing to $\chi(r, |v|)$ for a definite position and speed $|v|$ is based on the statistical sampling of appropriate expressions connected to the orthogonality properties of the spherical harmonics (the most direct solution of local interpolation would again raise the problem of storage). For example, only the combination of harmonics: $Y_1^1 + Y_1^{-1}$ can contribute to the quantity $\langle v_x/|v| \rangle$, i.e. the average of the quantity $v_x/|v|$ evaluated in the velocity bin and mesh element with representative speed and position $|v|$ and r respectively.

We will present results of a numerical code based on this strategy of calculation, for different flow fields

*Abstract 2367 submitted to the 21st International Symposium on Rarefied Gas Dynamics, Marseille, France, July 26-31, 1998

of practical interest. In particular the code will be applied to the problem of rarefied flow in micron-sized channels.

References

- [1] G.A. Bird, Molecular Gas Dynamics and the Direct Simulation of Gas Flows, Clarendon Press, Oxford (1994).
- [2] M. Yousfi, A. Himoudi, A. Gaouar, Physical Review A 46, 7889-7901 (1992).

Continuous Time Monte Carlo Methods for Nonlinear Spatially Inhomogeneous Boltzmann Equation *

A.I. Khisamutdinov

Sobolev Institute of Mathematics, Russian Academy of Sciences, Novosibirsk, Russia

This paper is concerned with two problems:

1) on properties of "continuous time" Monte Carlo (CTMC) methods based on certain Markov processes,

2) on relation between these processes and Boltzmann equation.

The CTMC methods were introduced and studied in [1]–[6]. Here we represent some new results.

Let $\mathcal{P}_0 = \{N_t, \mathcal{X}_t\}_t^T$ be the Markov process with states in $\{0 + \bigcup_{N=1}^{N_\infty} [N \times (G)^N]\}$, which

describes an evolution of rarefied gas in some bounded volume (\bar{V}) , $(G) = (\bar{V}) \times R^3$; here N_t is the random number of particles in (\bar{V}) at the time t , $0 \leq t \leq T < \infty$, $\mathcal{X} = (x^1, \dots, x^N)$, $x = (r, v) \in (G)$, $(r \in \bar{V}, v \in R^3)$, $N_\infty \leq \infty$. We consider that $(\bar{V}) = (V) \cup (S)$, $(V) \cap (S) = \emptyset$, where (S) is the boundary surface of (V) with exterior normal $n_S(r_S)$ almost everywhere, $r_S \in (S)$. It is assumed that the particles may intersect the surface from both sides of some parts (S_1) of the (S) , leaving (\bar{V}) or coming into (V) ; and may be reflected into (V) according to a given boundary transform $\Gamma(v \rightarrow v'|r_S)$ on some other parts (S_2) of the (S) ; $(S_1) \cup (S_2) = (S)$. The entries of particles into (V) across (S_1) happen according to a given law. Let $\mathcal{M}(\cdot)$ and $\tilde{\omega}$ be the symbols of mean value and random trajectory, respectively, at the (\mathcal{P}_0) ; let $f(t, x)$ and $f^{(2)}(t, x, y)$ be the densities of the average numbers of particles and pairs, respectively, involved in the (\mathcal{P}_0) ; and let $\mathcal{E}(t, x)$ and $\mathcal{E}_S(t, r, v, v')$ be given functions on $(0, T) \times (V) \times R^3$ and $(0, T) \times (S) \times R^6$, respectively. Also we denote $\tilde{\mathcal{E}}(t, N_t, \mathcal{X}_t) = \sum_{i=1}^{N_t} \mathcal{E}(t, x_i^i)$,

$\bar{N}_0 = \mathcal{M}(N_0) = \int f(0, x) dx$; here and further the domain of integration is not marked, if it coincides with all set of integration. We consider the CTMC methods for a computing linear functionals of stan-

dart types $\mathcal{I} = \int dt \int_{(V)} dr \int dv f(t, x) \mathcal{E}(t, x)$, $\mathcal{I}_S =$

$\int dt \int_{(S)} dS \int dv \int dv' |(n_S(r_S), v)| f(t, r_S, v, v') \times$

$\mathcal{E}_S(t, r_S, v, v')$, and use three "simulation" estimators: η_1 , ξ_1 and η_S ; $\eta_1(\tilde{\omega}) = \int dt \tilde{\mathcal{E}}(t, N_t, \mathcal{X}_t)$,

$\eta_S(\tilde{\omega}) = \sum_{j=1}^{\infty} \mathcal{E}_S(t_j^i, r_S^{ij}, v_S^{ij}, v_S^{ij})$,

where aggregate $(t_j^i, r_S^{ij}, v_S^{ij}, v_S^{ij})$ describes j -th intersection of the (S) , i_j is the number of particle intersecting (S) ; and ξ_1 is well known estimator "over the collisions (in (V))"

$(\xi_1(\tilde{\omega}) = \sum_{j=1}^{\infty} \tilde{\mathcal{E}}(t_j, N_{t_j}, \mathcal{X}_{t_j-0}))$.

There exists a connection between the CTMC methods and well known Direct Simulation Monte Carlo (DSMC) methods [7],[8] (and others). The DSMC methods can be deduced from one of CTMC methods by discretizing the time variable t (using a time step Δt) and splitting an operator of master equations of the (\mathcal{P}_0) . Because the DSMC methods are close to the CTMC ones at rather small Δt , the properties of CTMC methods are characteristic for all DSMC ones.

If we take into account their structure, the CTMC methods should be associated with Monte Carlo methods for "iteration of linear operators" (ILO). First, a topic on connection between these methods is developed in the paper. An integral form of direct and inverse master equations of the (\mathcal{P}_0) is constructed and studied. Thus the calculation of physical characteristics of rarefied gases is reduced to classical problem of computational mathematics (to the ILO), and to attract main principles and constructions of that large division of Monte Carlo methods is possible on clear base. As for the estimators η_1 , ξ_1 and η_S , their variances' expressions written by means of solutions of master equations are deduced, and their formal unbiasedness is demonstrated, i.e. that $\mathcal{M}(\eta_1) = \mathcal{M}(\xi_1) = \mathcal{I}$, $\mathcal{M}(\eta_S) = \mathcal{I}_S$.

The density $f(\cdot, \cdot)$ satisfies the Boltzmann equation under well known condition of "chaos". We believe that the "chaos" is an asymptotic property

*Abstract 4916 submitted to the 21st International Symposium on Rarefied Gas Dynamics, Marseille, France, July 26-31, 1998

at $\bar{N}_0 \rightarrow \infty$. Second, in the paper some asymptotic properties of difference $[f^{(2)}(\cdot, x, y) - f(\cdot, x) \cdot f(\cdot, y)]$, density $f(\cdot, \cdot)$ and variance of η_1 are considered. This work is supported with grant 97-01-00776 of Russian Foundation of Basic Research.

References

- [1] Khisamutdinov A.I. , *On a simulation Monte Carlo method for modeling of dynamics of rarefied gases* ,Preprint No 599, Vychisl. Tsentr Sibirsk. Otdel. Akad. Nauk SSSR, Novosibirsk, 1985. (in Russian)
- [2] Khisamutdinov A.I. , *Simulation statistical modeling of the kinetic equation of rarefied gases*,Dokl. Akad. Nauk SSSR, Vol. 302, No. 1, pp. 75-79, 1988, (in Russian); Engl. transl. in Soviet Phys. Dokl., Vol. 33, (1988).
- [3] Khisamutdinov A.I. , *The null collisions algorithms of the continued time Monte Carlo methods for the Boltzmann equation* , Ross. Akad. Nauk Dokl., Vol. 328, No. 6, pp. 662-665, 1993, (in Russian); Engl. transl. in Russian Acad. Sci. Dokl. Math., Vol. 47, (1993).
- [4] Khisamutdinov A.I., Sidorenko L.L., *The algorithms of the continuous time Monte Carlo methods for kinetic equation of rarefied gases*,Mat. Modelirovanie, Vol. 6, No 2, pp. 47-60, 1994. (in Russian)
- [5] Khisamutdinov A.I., Sidorenko L.L., *The continuous time Monte Carlo methods and algorithms for the Boltzmann equation of rarefied gases*,Book of Abstracts.19th Int. Symp. Raref. Gas Dynam. Oxford, p. 78, 1994.
- [6] Khisamutdinov A.I., Sidorenko L.L., *Monte Carlo fictitious collision algorithms for nonlinear Boltzmann equation* ,Monte Carlo Methods and Applications, VSP, Utrecht, The Netherlands, Tokyo, Japan, Vol. 1, No 3, pp. 221-240, 1995.
- [7] Bird G.A. *Molecular gas dynamics*, London, Oxford Univ., Press, 1976.
- [8] Belotserkovskii O.M., Yanitskii V.E., *Statistical particle-in-cell method for solving rarefied gas dynamics problems*, Part 1. Zh. vychisl. Matem. matem. Fiz., Vol. 15, No. 5, pp. 1195-1208 ; Part 2. Vol. 15, No. 6, pp. 1553-1557, 1975. (in Russian)

Density Pulsations in a Shock Wave Flow *

O.A. Azarova, V.E. Yanitskii

Computing Center of Russian Academy of Sciences, Moscow, Russia

Presented are the results of numerical investigation of density pulsation fields in rarefied and turbulent compressed gas flows and of the shock wave influence on these pulsations. This research is important not only from the physical point of view, but also for developing efficient Monte Carlo methods to simulate rarefied gas flows. In a rarefied gas density fluctuations are due to a changing number of molecules in a volume unit. They vanish to zero when the number of molecules grows. In a continuous medium fluctuations of flow parameters are usually connected with turbulence and depend on its intensity.

The method of direct statistical simulation (DSMC) was applied to a rarefied gas [1]. It turned out that in a free flow in front and behind the shock wave the mean value of squared pulsations of the particle number in a cell to a high degree of accuracy is equal to the value of the average number of particles in this cell. The theoretical analysis showed that this dependence exists if fluctuations of the number of particles in cells obey the Poisson law. This assumes absence of space correlations. Hence corresponding correlational functions were also obtained.

The discovered connection of density pulsations with its mean value allows to find a law of increase of these pulsations in a rarefied gas flow with a shock wave. The increase coefficient equal to the relation of mean squared density pulsations behind and in front of the shock exactly corresponds to the square root out of the relation of densities behind and in front of the shock. This value depends only on the wave Mach number.

There is a known analogy between a mole transition in a turbulent flow and a molecular transition in a rarefied flow. In this connection of interest is the law of increasing of macroscopic density pulsations when the shock wave moves in a turbulent flow. Numerical simulation of interaction between a flat shock wave and turbulentlike disturbances was carried out on the basis of the Euler equation. The

problem was solved in a statement similar to [2]. The turbulent field in the flow in front of the shock was simulated by a group of sign-changing rectangular impulses with random amplitude. That disturbance resulted in the development of a corresponding succession of density, temperature and pressure pulsations. The shock wave ran onto this field of disturbance and interacted with it. The increase coefficient of density pulsations and correlational and spectral functions before and after the shock were investigated. Different nature of fluctuations in a rarefied gas and turbulent flow gives different correlational functions in these two cases. Though the discovered law for a rarefied gas about the increase coefficient being equal to square root out of mean density jump in the shock is valid for a turbulent flow as well (with the error of 3-5%). Thus, the law worked out for the coefficient of density pulsation increase in the shock wave turned out to be universal and independent of the nature of fluctuations in a gas flow.

Acknowledgements

The research was carried out under support of the Russian Fund of fundamental research, project No 97-01-00298

References

- [1] Yanitskiy V.E. *Operator Approach to Direct Monte Carlo Simulation Theory in Rarefied Gas Dynamics* In: Beylich E. Ed., *Rarefied Gas Dynamics*. 770-777. Weinheim, New York, Basel, Cambridge: VCH, 1991
- [2] Azarova O.A., Samsonov A.V., Yanitskii V.E. *Shock Wave Propagation in Gases with Random Non-Uniformities* In: Ching Shen Ed., *Rarefied Gas Dynamics*. 200-204. Beijing, China: Peking University Press; 1997

*Abstract 5276 submitted to the 21st International Symposium on Rarefied Gas Dynamics, Marseille, France, July 26-31, 1998

MONTÉ CARLO METHODOLOGY - MCM 3

ROOM LAVOISIER

MONDAY, JULY 27, 1998

14:40

Homogeneous relaxation and shock wave structure for a polyatomic gas. *

C. Cercignani¹, M. Lampis¹, J. Struckmeier²

¹ Dipartimento di Matematica, Politecnico di Milano, Milano, Italy

² Department of Mathematics, University of Kaiserslautern, Kaiserslautern, Germany

1 Introduction

In the last few years several scattering models of polyatomic gases have been proposed by researchers working on direct simulation Monte Carlo methods (DSMC) to solve the Boltzmann equation. In the present paper the homogeneous relaxation and the structure of a shock wave for a polyatomic gas is studied, making use of a new model for the differential cross section appearing in the Boltzmann equation for gases of classical rigid molecules [1], [2]. This kind of model applies to a polyatomic gas in the interval of temperature where only the rotational degrees of freedom are excited and has been extensively studied in the last few years. The model has already been applied to the calculation of transport coefficients for linear molecules [3], [4].

2 Equations and References

We follow the same approach and notations used by Kušcer [1], [2]. We use the distribution function $f(c, \mathcal{E}, r, t)$, where \mathcal{E} is the rotational energy; the phase space element is $dc \mathcal{E}^\mu d\mathcal{E} dr$, where $\mu = 0$ for linear molecules and $\mu = 1/2$ for the non-linear ones.

The total energy in the center of mass system ($E = mc_r^2/4 + \mathcal{E} + \mathcal{E}_1$, where $c_r = |c - c_1|$ is the relative speed of the couple of molecules), is a collisional invariant. $\sigma(E; e' \cdot e; \mathcal{E}', \mathcal{E}_1 \rightarrow \mathcal{E}, \mathcal{E}_1)$ is the differential cross section. A further step is the assumption that $\sigma(\dots)$ can be written as a product of the integral cross section $\sigma_{tot}(E)$ times a transition probability density $\theta(\epsilon', \epsilon'_1, \epsilon, \epsilon_1)$, depending only upon the energies ratios of the pair of molecules, before and after the collision, $\epsilon', \epsilon'_1, \epsilon, \epsilon_1$, ($\epsilon = \mathcal{E}/E$), etc. :

$$\sigma(E; e' \cdot e; \mathcal{E}', \mathcal{E}_1 \rightarrow \mathcal{E}, \mathcal{E}_1) =$$

* Abstract 4112 submitted to the 21st International Symposium on Rarefied Gas Dynamics, Marseille, France, July 26-31, 1998

$$\frac{\sigma_{tot}(E)}{4\pi E^{2\mu+2}} \theta(\epsilon', \epsilon'_1, \epsilon, \epsilon_1). \quad (1)$$

The basic properties that this transition probability density must satisfy are positiveness, normalization and reciprocity [1][2].

In the case of elastic and maximally inelastic collisions the expressions of $\theta(\epsilon', \epsilon'_1, \epsilon, \epsilon_1)$ are well known:

$$\theta_{el}(\epsilon', \epsilon'_1, \epsilon, \epsilon_1) = \epsilon^{-\mu} \epsilon_1^{-\mu} \delta(\epsilon - \epsilon') \delta(\epsilon_1 - \epsilon'_1), \quad (2)$$

$$\theta_{in}(\epsilon', \epsilon'_1, \epsilon, \epsilon_1) = \frac{(2\mu+3)!}{(\mu!)^2} (1 - \epsilon - \epsilon_1), \quad (3)$$

The one-parameter Borgnakke-Larsen model is also well known [5]

$$\theta_{BL}(\dots) = e^{-\tau} \theta_{el}(\dots) + (1 - e^{-\tau}) \theta_{in}(\dots). \quad (4)$$

We allow σ_{tot} to depend upon energy according to [2]:

$$\sigma_{tot}(\hat{E}kT) = \sigma_\infty \left(1 + 5T_s/(\hat{E}T)\right) \quad (5)$$

where $E = \hat{E}kT$, σ_∞ and T_s are two parameters: with this choice the Sutherland model for viscosity is reproduced

The BL model considers all the collisions as a mixture of the elastic or completely inelastic collisions, disregarding the possibility of a partially inelastic one. In order to construct a more general model we start from a sensible approximate kernel $\theta_0(\epsilon', \epsilon'_1, \epsilon, \epsilon_1)$, chosen on the basis of intuition, which, however, does not satisfy the basic properties. At this point we add to it some other terms, which ensure that the three fundamental properties are satisfied. Let us define:

$$H(\epsilon', \epsilon'_1) = \int_0^1 \int_0^{1-\epsilon} \theta_0(\epsilon', \epsilon'_1, \epsilon, \epsilon_1) \epsilon^\mu \epsilon_1^\mu d\epsilon d\epsilon_1, \quad (6)$$

$$I = 1 - \frac{(2\mu+3)!}{(\mu!)^2} \int_0^1 \int_0^{1-\epsilon} (1 - \epsilon - \epsilon_1) \times H(\epsilon, \epsilon_1) \epsilon^\mu \epsilon_1^\mu d\epsilon d\epsilon_1. \quad (7)$$

We write

$$\begin{aligned}\theta(\dots) &= H(\epsilon', \epsilon'_1) \theta_1(\dots) + (1 - H(\epsilon', \epsilon'_1)) \theta_2(\dots) \\ \theta_1(\dots) &= \theta_0(\dots) / H(\epsilon', \epsilon'_1) \\ \theta_2(\dots) &= \frac{(2\mu+3)!}{(\mu')^2} (1 - \epsilon - \epsilon_1) (1 - H(\epsilon, \epsilon_1)) / I.\end{aligned}\quad (8)$$

This approach is similar to that already introduced many years ago in the theory of scattering kernel for gas-surface interaction [6] and applied in some papers of our research group [7]. As in the above-mentioned case, Eq.(8) may be interpreted as the linear combination of two normalized kernels $\theta_1(\dots)$ and $\theta_2(\dots)$, while $H(\epsilon', \epsilon'_1)$ is a sort of accommodation coefficient depending on the energies of the impinging molecules ($H(\epsilon', \epsilon'_1)$ must lay in the interval $[0,1]$). The expression of $\theta_2(\dots)$ is suggested by the requirement that $(1 - H(\epsilon', \epsilon'_1)) \theta_2(\dots)$ must satisfy reciprocity; the definition of I is chosen in order to get the normalization of $\theta_2(\dots)$.

In a paper presented at the last RGD Symposium [3], we proposed a kernel that requires the introduction of a cut-off in order to avoid a singularity. A correction of the model, that does not presents singularities, was recently introduced [4]. In conclusion we proposed the following kernel:

$$\begin{aligned}\theta_0(\epsilon', \epsilon'_1, \epsilon, \epsilon_1; a, b) &= \frac{2ba}{\pi} \epsilon^{-\frac{\mu}{2}} \epsilon_1^{-\frac{\mu}{2}} \epsilon'^{-\frac{\mu}{2}} \epsilon'_1^{-\frac{\mu}{2}} \times \\ &\times \frac{(1-\epsilon-\epsilon_1)}{(1-\epsilon-\epsilon_1)+(1-\epsilon'-\epsilon'_1)} \times \\ &\times \exp \left[-a(\epsilon - \epsilon')^2 - a(\epsilon_1 - \epsilon'_1)^2 \right].\end{aligned}\quad (9)$$

According to this kernel the collisions are inelastic, but not in general maximally inelastic; for $a \rightarrow \infty$, $\theta_0(\dots) \rightarrow \theta_{el}$ and the B-L model is recovered. In the present paper we apply the model to some test problems, for instance to the study of homogeneous relaxation or shock wave structure in polyatomic gases. The results are compared with those previously obtained by other authors by means of the B-L model: many numerical examples have been obtained.

In order to take into account the elastic collisions as well, we propose another possible kernel as follows:

$$\begin{aligned}\theta(\epsilon', \epsilon'_1, \epsilon, \epsilon_1; a, b) &= \theta_0(\epsilon', \epsilon'_1, \epsilon, \epsilon_1; a, b) + \\ &+ (1 - H(\epsilon', \epsilon'_1)) \delta(\epsilon - \epsilon') \delta(\epsilon_1 - \epsilon'_1).\end{aligned}\quad (10)$$

Due to the second term, this kernel describes also elastic collisions. The application of this last model is under way and comparisons of the results of the different models will be presented at the RGD Symposium.

References

- [1] Kušćer I., *A model for rotational energy exchange in polyatomic gases.*, Phisica A, Vol.1, No.158, pp.784-800, 1989.
- [2] Kušćer I., *Models for Energy Exchange in Polyatomic Gases*, Operator Theory: Advances and Applications, Vol.51, pp.180-188, 1991.
- [3] Cercignani C., Lampis M., *A new model for the differential cross section of a polyatomic gas*, Rarefied Gas Dynamics, pp.731-736, Peking University Press, Beijing 1997.
- [4] Cercignani C., Lampis M., Struckmeier J., *New models for the differential cross section of a polyatomic gas in the frame of the scattering kernel theory*, submitted to Mechanics Research Communications, 1997.
- [5] Borgnakke C. and Larsen P. S., *Statistical Collision Model for Monte Carlo Simulation of Polyatomic Gas Mixture*, J. Comp. Phys., Vol.18, pp.405-420, 1975.
- [6] Cercignani C., *Theory and Application of the Boltzmann Equation*, Scottish Academic Press, Edinburgh 1975.
- [7] Cercignani C., Lampis M., Lentati A., *A new scattering kernel in kinetic theory of gases*, Transport Theory and Statistical Physics, Vol.24, pp.1319-1336, 1995.

Development of Computing Hardware Specialized for DSMC *

T. Abe, K. Funabiki

Institute of Space and Astronautical Science, Sagami-hara, Japan

1 Introduction

The direct simulation Monte Carlo method is one of the most successful numerical simulation method for rarefied gas flows. The method has been applied to various problems, most of which require significant computational resource.

The method is based on the dynamical simulation of pseudo-particle which obeys the Boltzmann equation statistically. One of the main part of the dynamical simulation is the integration of the particle motion and another is the collision calculation. Since the heaviest part of the dynamical simulation is the collision calculation, there is a possibility to significantly improve the computational efficiency by accelerating the collision calculation. There are two possibilities for this; one is the improvement of the algorithm, another is the improvement of the computational hardware. In the present work, we consider the hardware improvement and have developed the computer hardware specialized to the existing collision calculation algorithm.

2 Outline of the computing hardware

Let us consider a set of particles having various velocities. The algorithm of the collision calculation for the set can be broken down into the following procedure;

- (1) to select a pair of particles,
- (2) to calculate the relative velocity,
- (3) to statistically decide whether the pair performs the collision,
- (4) to calculate the velocities after the collision,
- (5) to renew the velocities,

*Abstract 1816 submitted to the 21st International Symposium on Rarefied Gas Dynamics, Marseille, France, July 26-31, 1998

This procedure is iterated by a specified number defined in relation to a time step.

In the standard calculation, the processes in the procedure are executed sequentially. Hence, to speed up the calculation, it is inevitable to execute the processes in parallel. To make this possible, each process must be manipulated by individual hardware. That is, individual operations in each process must be realized by individual hardware. To realize the operator easily, we break down each operation into 2-inputs- 1-output operator. This operator can be realized easily, for example, by using a standard read-only-memory (ROM), in which case the 2-inputs correspond to a half of address bits respectively and the data stored in the address corresponds to the output (see Fig. 1).

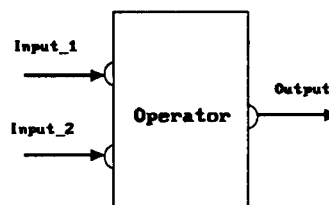


Figure 1: Schematic diagram for the operator with 2-inputs and 1-output

In the present concept, we assume a host computer which can carry out the calculation except the part included in the present computer specialized to DSMC. That is, the host computer sends the necessary data to the present computer, retrieves the processed data from it and executes the necessary calculation. These processes are iterated. We have developed the hardware for the computer to demonstrate the present concept.

For the moment, the process (1) is not included in the hardware, but is calculated by a host com-

puter and the tabulated data for collision pair is transferred from the host computer to the present hardware and is stored in a random access memory (RAM), RAM1 in it. The velocity set is also transferred from the host computer to the second RAM, RAM2. The velocity of the selected pair of particles are obtained by using the RAM1 and RAM2. For the process (2), the 2-inputs-1-output operator can carry out necessary operations. For the process (3), when we employ the acceptance rejection method, the random value with specific maximum value is necessary to be compared with the relative velocity. For this purpose, the series of random value is stored in a ROM which can be retrieved sequentially. To compare both the values, the 2-inputs-1-output operator can be employed, in which case the output is 1 bit (1 for collision event and 0 for no collision event). For the process (4), the random number is also necessary to realize the random direction after collision. For this, the ROM storing the values for the random velocity can be employed. The calculations after that, which is necessary to calculate the velocities after collision, are also realized by the 2-inputs-1-output operator. The velocities after the collisions are stored into the third RAM's, RAM3. The calculations are iterated by a specified number. After the iteration, the velocity after collision are transferred to the host computer and the velocities is renewed. This is the one cycle of the collision calculation corresponding to a specified time step.

The schematic diagram of the present hardware architecture is shown in Fig. 2. In the figure, the symbols with labels A and A' correspond to RAM1 and the output from these RAM's are used for addressing the RAM's (designated by the symbols with the labels X, Y, Z, X', Y', and Z') which include the sets of velocity (v_x, v_y, v_z) and (v'_x, v'_y, v'_z). Those RAM's correspond to RAM2 while the RAM's designated by the symbols with labels $\underline{X}, \underline{Y}, \underline{Z}, \underline{X'}, \underline{Y'}, \underline{Z'}$ correspond to RAM3 which store the velocities after collision. The ROM's designated by the symbols with the labels X'', Y'' and Z'' store the values corresponding the unit vector with random direction. The ROM designated by the symbol with a label Ra stores the random number ranging from 0 to the maximum relative velocity. The other symbols are the ROM's corresponding to each operation. The operation proceeds from Step 1 to Step 8 in a so-called pipe-line method. Therefore, in each clock count, each operation is accomplished simultaneously. In the present demonstrator, the 8 bits ROM's and RAM's with 16 bits addressing are employed for simplicity. Hence the numerical quantity used in the calculation is realized as an integer rang-

ing from -125 to 126.

In the present hardware, the approximately 20 floating point operations are carried out in 10 M-Hz clock. This means the present hardware has an computational capability of 200 M-Flops. The limit for the clock frequency comes from the connection technology between IC's. The proper connection technology enable us to use about 100 M-Hz clock even when the discrete IC's are employed like present hardware. This means that 2 G-Flops operation can be easily realized. If we consider to make a specialized IC including the entity of the present hardware, the 1 order faster operation can be possible. It should be noted that this calculation speed is attainable by only a single machine. However the present hardware is suitable to parallel use. In this case, we can speed up the calculation as much as we want by using a necessary numbers of the hardware.

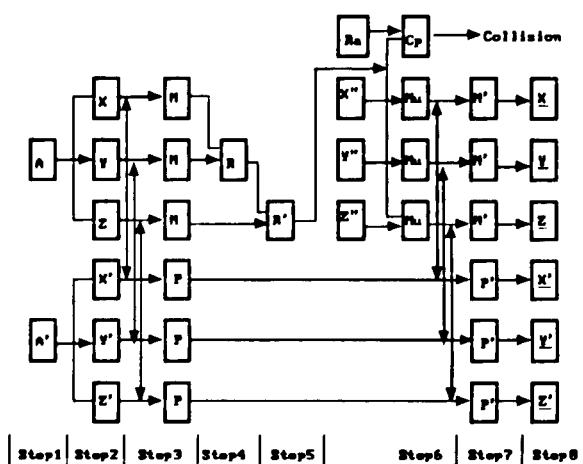


Figure 2: Schematic diagram of the computing hardware architecture specialized for DSMC

3 Conclusions

It was demonstrated that the specialized computer for the DSMC is possible, which enables us to carry out the calculation in significant speed. It is expected that the many problems requiring a significant computer resource will be tackled for the future.

Breaking with the Past: An Object-Reuse-Oriented Re-design of DSMC Software *

T.L. Parsons, M. A. Gallis, J. K. Harvey

Dept. of Aeronautics, Imperial College of Science Technology and Medicine
London, England

1 Introduction

DSMC has a long history dating back to the early days of computing, but as a consequence there is a tendency to use inefficient software design and management techniques, something which threatens its viability. In this paper, we describe how the current best practices of Software Engineering - "Object-Oriented Design", "Software Reusability" and "Open-Systems" computing - were combined and applied to create a new software platform for supporting DSMC-based research into RGD phenomena. This novel strategy was pursued to improve the overall performance of DSMC research by making it easier and safer to make modifications.

The new platform - dubbed DST, Direct Simulation Toolsuite - was used to explore a range of groundbreaking new ideas for solving computational challenges in DSMC. Extensive verification and validation work was conducted to ensure that new codes based on DST faithfully represent the DSMC method, and a long-term evaluation process ensured that they reflect the ideas of Imperial College's DSMC group. Significant enhancements to research capabilities were realised, including greatly expanded 2-D and 3-D geometric modelling capabilities, large reductions in testcase turnaround-times, a more efficient way to implement and test new ideas, and finally faster executing codes.

2 The Trouble with DSMC Software Research

DSMC was originally designed using an early design methodology known as Functional Decomposition, and implemented using an equally early example of the FORTRAN language, FORTRAN 66.

* Abstract 5712 submitted to the 21st International Symposium on Rarefied Gas Dynamics, Marseille, France, July 26-31, 1998

This combination was extremely good at organising the main actions the DSMC algorithm and allowed codes to easily be hand-optimised to make best use of the limited computing resources then available. This approach does not address the problems of Software Maintenance however, which later research has shown typically consumes upwards of 67 % of Total-Lifecycle Costs (Schach [1]). By focusing on actions and neglecting the organisation of the code's data, representation of the current state of execution of the simulation must instead be delegated to variables and arrays which can be accessed by all the different parts of the program. This leads to the problem of interdependencies being created between subroutines in the program: any change to these globally accessible variables and arrays in one subroutine will have an impact on subsequent subroutines which use those variables and arrays, and because of the rather manual Functional Decomposition + FORTRAN paradigm, the responsibility for checking the consistency of this chain of dependency falls to the human programmer during coding and testing, rather than to the language compiler during compilation.

3 New Approach to DSMC-Software-Based Research

To address this problem, a new set of requirements for DSMC was drawn up re-emphasising the longer-term needs of the DSMC researcher. These identified execution speed as still highly important, but that emphasising it had little effect on research cost and efficiency. Enabling modifications to be performed more easily however, was identified as key multiplier of efficiency and cost-reduction measures especially given that DSMC software-based research can itself in fact be seen as a continuous, never-ending process of modification.

To directly address this new priority, an extensive review was conducted of the latest and best de-

sign methodologies, languages, and maintenance-support strategies. "Object-Oriented Design" was identified as the leading design and development methodology in use today. It takes a much more data-oriented approach by modelling real-world problems as groups of interacting objects each defined by data "hidden" within the object (ie. Inaccessible to other objects), and a number of "visible" methods (ie. functions) which act on that data. Such objects allow highly abstract models of reality to be constructed which convey a great deal more meaning than can be expressed in Fortran, meaning which simultaneously is checked by the language compiler to ensure correctness. The fact that data is "hidden" and methods are "visible" ensures that interdependencies between sub-routines are minimised or even eliminated, making for much simpler and less error-prone modification. When coupled with a deliberate strategy of "Software Reuse" however, Object-Oriented Design gains flexibility without losing its strict control of the meaning of code. By constructing what are essentially Software ICs for key algorithmic and data steps in DSMC, one can switch easily from one methodology to another, and in fact build up an archive of examples of different methods of say, scattering, or searching, or collision thereby capturing and storing the vital knowledge of the group for future use. These can then be tested honestly against one another with no other changes being required of the host code.

4 The Final Product Validation-Verification

A system which could run 1-D, 2-D, Axisymmetric, and 3-D testcases with the change of only 5% of the DSMC code was implemented and tested, thereby leveraging validation in Axisymmetric, for example, for 2-D and 3-D testcases. The validation was conducted with comparisons of the results of DST with experimental and numerical results of other codes. One of these cases was the second case of experiments conducted by Allegre and Bisch. In this test case the density around a 70 deg cone flowfield was measured. The flow was pure nitrogen and the free stream Mach number 20. The numerical results in comparison with the experimental ones appear in Fig. 1. We note that the numerical results are in good agreement with the experimental ones. We note that the numerical results are in good agreement with the experimental ones.

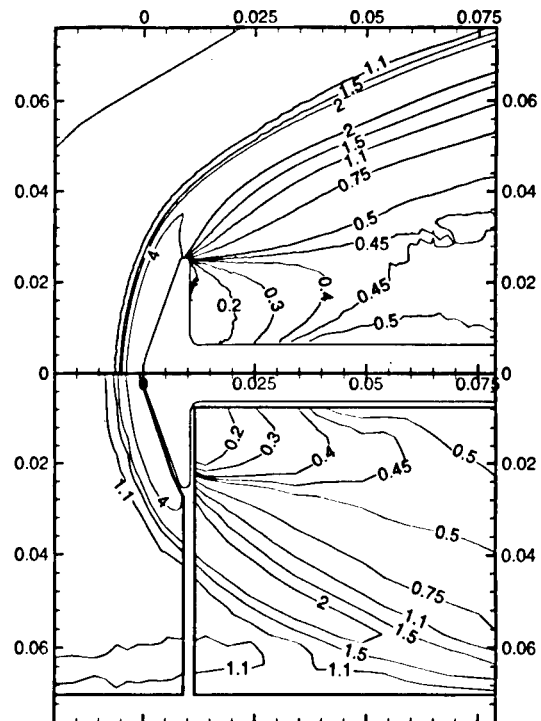


Figure 1: Comparison between measured and calculated results

5 Conclusions

This 'final' baseline design (DST) represents much more than just a DSMC simulation code, rather a platform and an architecture to support the entire process of DSMC software research. DST has been used to implement multiple search, geometry, boundary-condition, energy-exchange, species, reaction, and scattering methods on unstructured mesh systems in 1-D, 2-D, Axisymmetric, and 3-D flows. As an open system, it can be integrated with external mesh-generation and data-reduction packages and will run on virtually any computer. Finally, as an important vindication of the development approach adopted, DST-based DSMC codes execute faster than any previous FORTRAN-based derivatives.

References

- [1] Scach, S.R. *The economic impact of Software Reuse on Maintenance*, Software Maintenance: Research and Practice, Vol 6, pp185-196, 1994.

Deterministic Method for the Boltzmann Equation with Parallel Computing *

V.V. Aristov¹, S.A. Zabelok¹, A.V. Lukshin²

¹ Computing Center of the Russian Academy of Sciences, Moscow, Russia

² Moscow State University, Moscow, Russia

Recently the discrete velocity approaches with constant coefficients in the quadratic form approximating the right-hand side of the Boltzmann equation have been used. Such numerical schemes are attractive due to the simple structure of terms that evaluate the collision integrals, good perspectives for parallelizing, a clear way to estimate the numerical errors etc. The deterministic (regular) method of solving the Boltzmann equation with analytical integration over impact parameters has been proposed in [1-2]. The other methods have been considered in [3,4]. In the present paper our approach is developed with the use of parallel machines both to obtain accurate test solutions for simple problems and for computations of complex problems. The accuracy of the method is estimated and comparison with the analogous approaches is made as well.

In the most of such schemes the special system of velocity nodes (closed in the sense of collisions) are used to ensure the conservation laws for the collision integrals. The questions concerning the convergence of the discrete velocity schemes has been considered in [4]. In our method the velocity step is constant. In fact the system of cells in the velocity space is applied and the conservation laws are satisfied by the correction in the framework of the conservative splitting method (CSM) [5]. The estimations of approximation of the collision integrals contain only the value of the velocity step (the value of the radius of the bounded velocity domain also appears).

The use of parallel algorithms for the Boltzmann equation is the important direction to speed-up calculations and increase the amount of data. The last item is important for the given approach where the large matrix of the coefficients is used. The first experiences [6] of parallelizing have demonstrated a good speed-up. In the present paper the computations on two parallel machines PARSYTEC are

* Abstract 1931 submitted to the 21st International Symposium on Rarefied Gas Dynamics, Marseille, France, July 26-31, 1998

p	s	e
2	2.10	1.05
4	4.18	1.046
8	8.24	1.03
16	16.2	1.012
32	30.73	0.96
64	46	0.72

Table 1: Computations by the first machine

p	s	e
2	1.92	0.961
4	3.99	0.998
8	8.04	1.005

Table 2: Computations by the second machine

studied with the distribution of the matrix over parallel processors (the part of this matrix is located to each processor). The first computer has 64 processors and the peak performance is 100Mfl. The second one has 8 processors but the peak performance is 2Gfl. The total storage is 256 Mbt in both cases. The typical examples for speed-up s and efficiency e are presented in Tabl.1 and in Tabl.2 (p is the number of processors). If the number of nodes in the velocity space increases then the efficiency at the same number of processes p would increase because the quantity of arithmetical operations on the processor depends quadratically on the number of nodes and the quantity of information exchanging between processors only linearly: if the number of nodes is twice as much in comparison with the table value (Tabl.1), then $e = 0.97$ at $p = 32$ and $e = 0.9$ at $p = 64$.

It is found that the efficiency of parallel computations with the large matrix of the coefficients can be more than 1 in well-parallelized problems. This appears to be explained by transputer memory organization. The Inmos transputer has on-chip memory which is little in amount but very fast in data

exchange. As the number of processors increases adding processors add such fast memory which reduced overhead and elapsed time for exchanging between processors.

The first problem under consideration is the classical relaxation problem. The test solutions are obtained with the accuracy higher than 0.1% for the distribution function at any velocity point (in the bounded domain). The problems of a shock wave structure and of a heat transfer are also considered and comparisons with known results are made. The three-dimensional problem on a free jet at different Knudsen numbers is solved as well.

References

- [1] Aristov V.V., *On solving the Boltzmann equation with the discrete velocity technique*, Dokl. Acad. Nauk. SSSR, Vol. 283, No.4, pp.831-834, 1985.
- [2] Aristov V.V., *Regular method of the integration of the Boltzmann equation and nonuniform relaxation problems*, Proc. 17th Intern. Symp. on Rarefied Gas Dynamics. VCH, Weinheim: A.Beylich ed., pp.879-885, 1991.
- [3] Martin Y.-L., Rogier F., Schneider J., *Une méthode déterministe pour la résolution de l'équation de Boltzman inhomogene*, C.R.Acad.Sci., t.314, Serie 1, pp.483-487, 1992.
- [4] Bobylev A.V., Palczewskii A., Schneider J. *Discretization of the Boltzmann equation and Discrete Velocity Models*, Proc. 19th Intern. Symp. on Raref. Gas Dynam. Oxford Univ. Press, : J.Harvey, G.Lord eds., Vol.2. pp. 857-863, 1995.
- [5] Aristov V.V., Tcheremissine F.G., *Conservative splitting method for solving the Boltzmann equation*, USSR Journ. Comp. Math. Math. Phys., Vol.20, No.1, pp.208-225, 1980.
- [6] Aristov V.V., Mamedova I.G., *Parallel algorithms for solving the Boltzmann kinetic equation*, Comp. Maths Math. Phys., Vol.36, No.2, pp.247-253, 1996.

MONTE CARLO METHODOLOGY - MCM 4

ROOM LAVOISIER

MONDAY, JULY 27, 1998

16:20

Stochastic Smoluchowski Equation and Coagulation of Particles in a Turbulent Collision Regime. *

K.K. Sabelfeld

Institute of Comp. Mathem. and Mathem. Geophysics
Siberian Branch of Russian Acad. Sci., Novosibirsk, Russia

The coagulation processes of aerosol particles or clusters in a spatially homogeneous flow are governed by the Smoluchowski equation (e.g., see, [7]; the existence and uniqueness of solutions are treated, e.g., in [1]):

$$\frac{\partial n_l}{\partial t} = \frac{1}{2} \sum_{i+j=l} K_{ij} n_i n_j - n_l \sum_{i=1}^{\infty} K_{li} n_i + F_l(t) \quad (1)$$

with the initial conditions $n_l(0) = 0$, $l = 1, 2, \dots$. We will consider two main cases of the particle's source, namely, (a): instantaneous monomer source $F_l(t) = n\delta(t)\delta_{1,l}$, and (b): stationary (constant) source of monomers: $F_l(t) = F\delta_{1,l}$, where n and F are constants. The structure of K_{ij} for different collision regimes is presented, e.g., in [7]. In the case of isotropic turbulent mixing of the host gas, which is the situation we are interested in, the coefficients K_{ij} were suggested in [6]: $K_{ij} = \left(\frac{\pi^2 \epsilon}{120\nu}\right)^{1/2} (i^{1/3} + j^{1/3})^3$, where ϵ is the mean rate of dissipation of kinetic energy per unit mass, and ν is the kinematic viscosity of the fluid. This seems to describe satisfactorily the evolution of the size spectrum of particles mixed by a fully developed turbulence without taking into account the intermittency. In the intermittent turbulence, ϵ is considered as a random process with lognormal distribution [2]. Thus mathematically, we have the Smoluchowski equation whose coefficients are random processes. Generally, even linear PDE's with stochastic coefficients are very difficult to be solved by conventional numerical methods. To evaluate statistical characteristics of solutions of this kind of random equations by Monte Carlo methods, the double randomization method is an efficient technique (e.g., see [5]). In nonlinear case the situation is more complicated. However it is also possible to develop the double randomization technique. In

[3], [4], the authors gave the convergence proof of the Nanbu type algorithm for solving the spatially homogeneous equation (1).

A rigorous approach to estimate the influence of the intermittency on the aerosol formation rate needs to solve the inhomogeneous Smoluchowski equation

$$\frac{\partial n_l(r)}{\partial t} + \mathbf{v} \cdot \nabla n_l(r) = D_l \Delta n_l(r) + \frac{1}{2} \sum_{i+j=l} K_{ij} n_i n_j - n_l \sum_{i=1}^{\infty} K_{li} n_i + F_l(t), \quad (2)$$

where n_l is the concentration of particles of size l , $l = 1, 2, \dots$ at a point r at time t ; \mathbf{v} is the host gas velocity which can be constructed using the model [5], K_{ij} is the free molecular coagulation coefficient. The quantity D_i is the Brownian diffusion coefficient of a particle of size i , $F_l(t)$ is the intensity of l -cluster generation source. It is assumed that between collisions, the particles follow the host gas flow and undergo the Brownian diffusion. In this presentation we discuss the results of numerical simulation of the coagulation process in the turbulent regime by solving the coagulation equation and applying the double randomization technique for evaluation of the mean solution to this equation. We compare the results with another approach we used in [4] where the coagulation process in the isotropic turbulence is considered as described above, with the coagulation coefficient given by Saffman and Turner [6]. To investigate the influence of the intermittency effect on the rate of formation of aerosol particles, we compare the solution of the Smoluchowski equation with deterministic coagulation coefficient against the mean solution of the same equation whose coefficients are lognormal random processes with the means equal to the above deterministic coagulation coefficients. It turns out that during the first time interval, the intermittency leads to a decrease of the rate of aerosol formation, whilst after that, the growth of particles is accelerated, and again decreases in the part of

*Abstract 2511 submitted to the 21st International Symposium on Rarefied Gas Dynamics, Marseille, France, July 26-31, 1998

large particle sizes.

We have applied the double randomization technique also to the following variants of coefficients: $K_{ij} = \varepsilon$ and $K_{ij} = \varepsilon(i+j)$ where ε is a random variable.

It is interesting to compare the true mean solution $\langle n_i(t) \rangle$ with the solutions to the "averaged equation". A series of calculations show that the difference between these two functions can be very large depending on the parameters of the fluctuating part.

Let us take the Smuluchowski equation (2) in the form ($D_t \equiv 0$):

$$\frac{\partial n^E(t, x)}{\partial t} + v(t, x) \cdot \nabla_x n^E(t, x) = K(n^E(t, x)) + F(x, t) \quad (3)$$

with the initial conditions $n^E(0, x) = 0$; $x \in R^3$, $t \in [0, T]$. Here $n^E(t, x) = \{n_i^E(t, x)\}_{i=1}^{\infty}$; and

$$K(n^E(t, x)) = \frac{1}{2} \sum_{i+j} K_{ij} n_i^E(t, x) n_j^E(t, x) - n_i^E(t, x) \sum_{i=1}^{\infty} K_{ii} n_i^E(t, x).$$

Let us introduce the Lagrangian trajectories through

$$\frac{\partial X(t, x_0)}{\partial t} = v(t, X(t, x_0)), \quad t \in [0, T]; \quad (4)$$

$$X(0, x_0) = x_0.$$

We assume, that the random velocity field is incompressible; this leads to the properties: (i) for each x_0 and $t \in [0, T]$ there exists a unique solution $X(t, x_0)$ to (4); (ii) $\frac{DX(t, x_0)}{Dx_0} = 1$ for each x_0 and $t \in [0, T]$. Let us denote the solution to (2) in the Lagrangian coordinates by $n^L(t, x_0) = \{n_i^L(t, x_0)\}_{i=1}^{\infty}$:

$$\frac{\partial n^L(t, x_0)}{\partial t} = K(n^L(t, x_0)) + F(X(t, x_0), t);$$

$$n^L(0, x_0) = 0; \quad x \in R^3; \quad t \in [0, T].$$

Here $X(t, x_0)$ is defined in (4). Note that for each x and $t \in [0, T]$ there exists unique x_0 , such that $X(t, x_0) = x$ and $n^E(t, x) = n^L(t, x_0)$. We denote by $n(t, F) = \{n_i(t, F)\}_{i=1}^{\infty}$ the solution to

$$\frac{\partial n(t, F)}{\partial t} = K(n(t, F)), \quad n(0, F) = F$$

and assume, that there exists a unique solution for each F . It is shown that using the Lagrangian coordinates, it is possible to express the solution of

inhomogeneous Smuluchowski equation (3) through the latter equation in the case of a point source at x_* , i.e., when $F(x, t) = \delta(x - x_*)S(t)$. This leads to an explicit representation of the average solution to (3) through the Lagrangian transition density $p_L(t, x|x_0) = \langle \delta(X(t, x_0) - x) \rangle$ in the form of integral

$$\langle n^E(t, x) \rangle = \int_{G_0} n(t, S(x_0)) p_L(t, x|x_0) dx_0.$$

References

- [1] J.M. Ball, J. Carr. The discrete coagulation-fragmentation equations: existence, uniqueness and density concentration. *J. Stat. Phys.* (1990), **61**, 203-234.
- [2] Frisch U. *Turbulence*. Cambridge University Press, 1996.
- [3] Kolodko A.A. and Wagner W. Convergence of a Nanbu type method for Smuluchowski equation. *Monte Carlo Methods and Appl.* (1997), **3**, 4, 255-273.
- [4] Sabelfeld, K.K. and Kolodko, A.A. Monte Carlo simulation of the coagulation processes governed by Smuluchowski equation with random coefficients *Monte Carlo Methods and Appl.* (1997), **3**, 4, 275-311.
- [5] Sabelfeld K.K. *Monte Carlo Methods in Boundary Value Problems*. Springer Verlag. Heidelberg, New York, Berlin, 1991.
- [6] Saffman P. and Turner J.S. On the collision of drops in turbulent clouds. *J. Fluid Mech.* (1956), **1**, 16-30.
- [7] Williams M.M.R. and Loyalka S.K. *Aerosol Science. Theory and Practice*. Pergamon, New York, 1991.

Transient Simulations of a Plasma Expansion Using DSMC *

Timothy Bartel, and Mary Hudson
Plasma and Aerosol Sciences Dept.

Sandia National Laboratories, Albuquerque, NM 87185

Abstract

A neutron generator is a very small ion accelerator where the basic purpose is to generate sufficient energy ions which undergo a surface interaction to create neutrons. The device operates in a transient mode with a very short time constant and is initially at a near vacuum condition. The initial source density is in the tens of torr. The transient flow is near continuum at the source and becomes free molecular at the edge of the expansion. Since the goal is to accelerate ions, there is a grid to extract electrons from the flow before a large potential is applied to accelerate the ions to the target. The plasma is approximately 50% ionized so neutral species are important. Based on the length and time scales, the Direct Simulation Monte Carlo (DSMC) technique [1], a kinetic simulation of the Boltzmann equation, is ideally suited for this system since it has the capability of correctly modelling the high density inlet, the collisional processes between ions and neutrals, and the multi-species transport in the system. However, the system response is time dependent based on the system size (< 0.1 m) and time duration (< 0.01 s). Although the DSMC algorithm is based on the time dependent Boltzmann equation, the method has typically been applied in a steady state mode. Sampling statistics become a key area of concern since the ergodic nature of the method cannot be as easily exploited for a transient simulation as it can be for a steady-state one.

The focus of this paper will be on presenting a self-consistent kinetic model for a low pressure chemically reacting transient plasma and comparing with data. We use a 2D DSMC code which has been optimized for the massively parallel computing environment [2] to transport the neutrals and ions. Currently, we treat the plasma as locally charge neutral since external fields dominate the ion motion; however, we are exploring including kinetic electrons. We allow collisions and subsequent chemistry between neutrals, ions, and surfaces in the reactor. The Variable Hard Sphere model is used to determine neutral-neutral and neutral-ion collision frequencies. A Coulomb interaction model is used for ion-ion collisions. Gas phase chemistry can be modeled with either a kinetic approach (steric factors)

or a continuum-like treatment (reaction rates). Surface chemistry is modelled with either a simple reaction probability (sticking factor) or a site coverage dependent model.

We use a bulk plasma approximation for modelling the plasma: we assume local charge neutrality in the bulk and a sheath model to compute the potential jump from the surface to the bulk. The sheath thickness is still very small at these pressures and the Debye length is much smaller than a physical dimension. Therefore, we do not transport electrons; the local electron density is determined from summing the local ion densities. The space charge field is computed assuming the electrons are in a Boltzmann equilibrium:

$$E = \nabla(kT_e n_e) / (q n_e),$$

where k , T_e , n_e , and q are the Boltzmann constant, electron temperature, electron density, and charge, respectively. The total electric field is determined assuming a superposition of the space charge and the applied, fixed external fields. For the current work, we are using a fixed electron temperature. This is a reasonable assumption since the external fields are much higher than the local space charge fields.

We will present simulations of this model and compare with experimental data as available.

Figure 1 is a diagram of the general system. The ion accelerator is basically axisymmetric around a line from the source to the target. The regions designated as 1, 2, and 3 are of interest to the DSMC simulations. After the screen (3), the mean free path is very large, with respect to the system, so the optic region is collisionless. The ion trajectory is determined by the large external field applied from the screen to the target and adjusted by local space charge effects. The neutral trajectory is free molecular. The system dimensions are less than 0.1 m.

Figure 2 shows pressure contours for neutral species for three times into the transient. This preliminary simulation for neutral species was used only to determine the computational requirements and degree of non-continuum. Note that the \log_{10} of pressure is shown; there are very large pressure variations in this system. Approximately 15 million DSMC particles were used in the simulation; the grid contained approximately 35,000 cells for this 2D problem. Reasonable statistics

* Abstract 2337 submitted to the 21st International Symposium on Rarefied Gas Dynamics, Marseille, France, July 26-31, 1998

appear to have been achieved based on the smoothness of the results. This simulation was run on an old 1024 node nCUBE-2 parallel supercomputer. We plan to run the full plasma case on our 4,000 node parallel machine based on Pentium-Pro processors. We anticipate simulating from 1 to 10 billion particles.

Finally, Figure 3 shows the local Knudsen number for this case based on a local number density gradient for a near steady-state. Generally, this number is only less than 0.1, indicative of continuum flow behavior, near the source. The rapidly expanding flow results in very large gradients which drive the local Knudsen to the non-continuum regime. The 'wavy' behavior near the screen region is simply do to pressure oscillations which have not damped out; the simulation was not quite in steady-state. One would expect a much smaller region of validity for continuum during the transient since the gradient would be higher near the source.

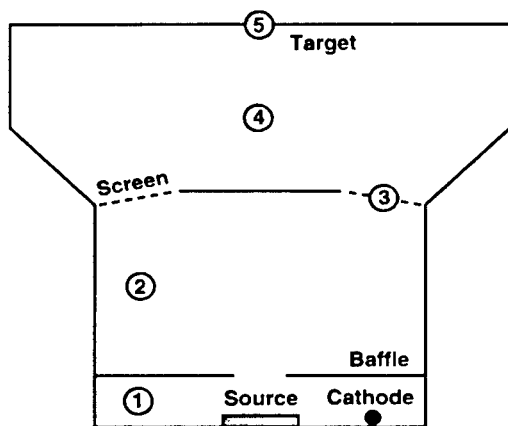


Figure 1 - General Geometry

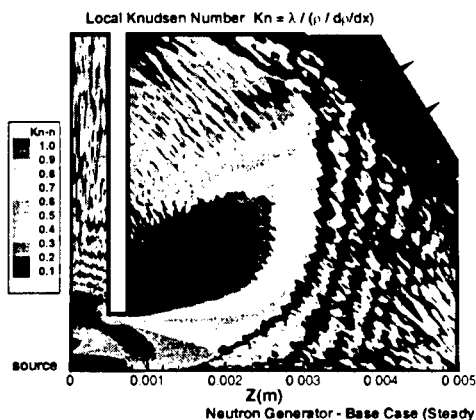


Figure 3. Local Knudsen Number at Steady-State

REFERENCES

- 1- Bird, G. A., Molecular Gas Dynamics and the Direct Simulation of Gas Flows, Oxford University Press, 1994.
- 2- Bartel, T., Plimpton, S., Johannes, J., Payne, J., "Icarus: A 2D Direct Simulation Monte Carlo (DSMC) Code for Parallel Computers User's Manual - V3.0," Sandia Report 96-0591, October 1996.

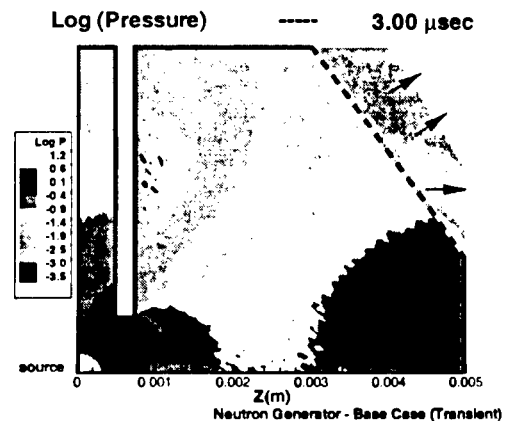
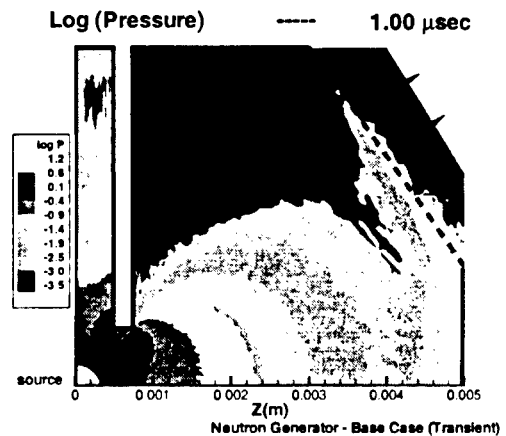
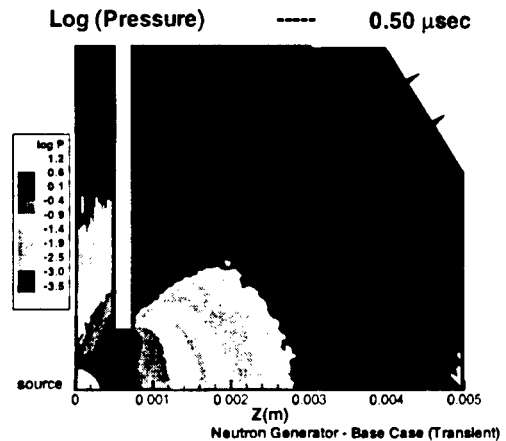


Figure 2. Pressure Contours for Neutral Flow Case

On Stochastic Conservation Law Related to A Burgers Model and The Monte Carlo Simulation. *

Shigeyoshi Ogawa

Dept. Computer and Electrical Engineering, Faculty of Technology
Kanazawa University, Kanazawa, Japan

1 Burgers like equations

The Monte Carlo simulation of the motion of non-linear dynamical systems with infinitely many particles, such as fluids or gas, has been of one of the principal subjects in stochastic numerics. Among these the case of viscous and incompressible fluids attracts special interests of the probabilists who like to apply the well established theory of stochastic calculus about the Brownian motion. In fact, in the last decade, a steady development has been made in the research of the random particle methods combined with the numerical simulation of stochastic differential equations (e.g., the recent works of french group around D.Talay and M.Bossy [4] and those of the author [2], [3]). The present article is of this category, where we aim to introduce a new stochastic model for such phenomena that are governed by a class of nonlinear equations including the Burgers equation as special case.

$$\begin{aligned} \frac{\partial}{\partial t} u^i(t, x) + \nu_i \sum_j a_j(t, x, u) \frac{\partial}{\partial x_j} u^i &= \mu_i^2 \Delta u^i, \\ (t, x) &\in (0, T] \times \mathbb{R}^d \\ u^i(0, x) &= u_0^i(x). \quad (1 \leq i \leq d). \end{aligned}$$

Though the Burgers equation is merely a caricature of the real phenomenon of fluids, we believe that we have much to do for the contribution to the analysis through our approach.

2 Aims of the article

We notice that such phenomenon can be seen as a transport process due to the motion of thermodynamically agitated particles and thus can be expressed by a stochastic PDE of the hyperbolic type

like

$$\begin{aligned} \left\{ \frac{\partial}{\partial t} u^i(t, x, \omega) + \sum_j \left\{ \frac{d}{dt} W^j + a_j(t, x, \bar{u}) \right\} \frac{\partial}{\partial x_j} u^i \right\} &= 0 \\ u^i(0, x) &= u_0^i(x), \quad (1 \leq i \leq d) \\ \text{where } \bar{u}^i(t, x) &= \langle u^i(t, x, \omega) \rangle \\ \text{and } W(t) &\text{ is the } d\text{-dim Brownian motion} \end{aligned}$$

This idea, which was first introduced by S.Ogawa[1] in early seventies for the linear equation case, may enable us to treat the problem in the framework of the PDE of hyperbolic type. The first aim of the article is to show that the idea works in getting a stochastic model of the motion of viscous and incompressible fluids. But differently from the case of linear equations, we will see that, in 1-dim case, we have two possibilities for such stochastic model, both are hyperbolic PDEs of divergence form and one of which is a conservation law.

We will also note that such formulation can also apply to the analysis of the reaction-diffusion phenomena. Based on that formulation, we are going to study the possibility of a new Monte Carlo method for the simulation of relevant nonlinear phenomena, which is our second aim in this article.

References

- [1] Ogawa S., *A PDE including the white noise as a coefficient*, Z.W. verw.Geb., 1973, Springer-Verlag
- [2] Ogawa, S., *Monte Carlo simulation of nonlinear diffusion processes, I*, Japan J.Indust.Appl.Math., vol.9, No.1, pp.25-33, 1992, Kinokuniya
- [3] Ogawa S., *On the numerical of nonlinear SDEs and Burgers like processes*, Proc.of The Workshop on Turbulent Diffusion and Related Problems in Stochastic Numerics, pp.159-174, ISM Reports on Statistical Computing, vol.99, 1997, ISM Tokyo
- [4] Bossy, S. and Talay, D., *A stochastic particle Method for the McKean-Vlasov and Burgers equations*, Math.Comp., 88, pp.157-192, 1997

*Abstract 6961 submitted to the 21st International Symposium on Rarefied Gas Dynamics, Marseille, France, July 26-31, 1998

Applications of Enskog Theory to the Study of Rough Hard Sphere Gas and Granular Fluids *

A. Frezzotti

Dipartimento di Matematica del Politecnico di Milano, Italy

1 Introduction

The following kinetic equation:

$$\frac{\partial f}{\partial t} + \vec{\xi} \circ \nabla_{\vec{x}} f + \frac{\vec{F}}{m} \circ \nabla_{\vec{\xi}} f = J_E(f, f) \quad (1)$$

$$\begin{aligned} J_E(f, f) = & a^2 \int \{Y(n^+) f(\vec{x}^+, \vec{\xi}_1^+, t) f(\vec{x}, \vec{\xi}^-, t) \\ & - Y(n^-) f(\vec{x}^-, \vec{\xi}_1^-, t) f(\vec{x}, \vec{\xi}^-, t)\} \\ & \times H(\vec{\xi}_r \circ \vec{k})(\vec{\xi}_r \circ \vec{k}) d\vec{\xi}_1 d^2 \vec{k} \end{aligned} \quad (2)$$

$$\begin{aligned} \vec{x}^+ &= \vec{x} + a\vec{k}, & \vec{x}^- &= \vec{x} - a\vec{k} \\ n^+ &= n(\vec{x} + \frac{a}{2}\vec{k}), & n^- &= n(\vec{x} - \frac{a}{2}\vec{k}) \end{aligned}$$

was proposed by Enskog[1] as a generalization of the Boltzmann equation[2] to moderately dense hard sphere fluids. In Eqs.(1,2) $f(\vec{x}, \vec{\xi}, t)$ is the one-particle distribution function of the molecular velocities $\vec{\xi}$, $\vec{\xi}_r = \vec{\xi}_1 - \vec{\xi}$ is the relative velocity of two colliding molecules, whereas \vec{k} is a unit vector which specifies their relative position at the time of impact. H is the Heaviside step function, whereas \vec{F} is an external force field. In the simplest formulation of Enskog equation, the so called SET[3], the factor $Y(n)$ is a given function of the density, which plays the role of a velocity independent pair correlation function[4] which is set equal to the value of the uniform equilibrium pair correlation function at contact position[4]. It is clear that the Enskog equation should be regarded as a phenomenological equation, nevertheless recent investigations[5] have shown that numerical solutions of Eq.(1) exhibit very good agreement with molecular dynamics (MD) simulations, even at relatively high densities. Although interesting from the theoretical point of view, this result is not relevant for the study of real dense gases since the hard sphere model gives generally a poor approximation of intermolecular forces.

* Abstract 4081 submitted to the 21st International Symposium on Rarefied Gas Dynamics, Marseille, France, July 26-31, 1998

A better chance of testing Eq.(1) on real fluids is offered by granular materials whose mathematical description might be based on Enskog-like kinetic equations[6].

2 A mathematical model for granular fluids

Following Ref.[6], we consider a fluid composed of spheres having a mass m and a diameter a . The physical state of a sphere is characterized by the position \vec{x} and velocity $\vec{\xi}$ of its center, and by the angular velocity $\vec{\omega}$. The fluid motion is assumed to be governed by Eq.(1) in which the collision integral is modified as follows:

$$\begin{aligned} J_E(f, f) = & a^2 \int \{Y(n^+) f(\vec{x}^+, \vec{\gamma}_1^+, t) f(\vec{x}, \vec{\gamma}^-, t) \Lambda \\ & - Y(n^-) f(\vec{x}^-, \vec{\gamma}_1^-, t) f(\vec{x}, \vec{\gamma}^-, t)\} \\ & \times H(\vec{\xi}_r \circ \vec{k})(\vec{\xi}_r \circ \vec{k}) d\vec{\gamma}_1 d^2 \vec{k} \end{aligned} \quad (3)$$

$$\vec{\gamma} = (\vec{\xi}, \vec{\omega})$$

In Eq.(3) $\vec{\gamma}^*$ and $\vec{\gamma}_1^*$ are the velocities (linear and angular) of two spheres which, after a collision, will change their velocities to $\vec{\gamma}$ and $\vec{\gamma}_1$, respectively. Λ is the Jacobian of the transformation relating $\vec{\gamma}^*$ and $\vec{\gamma}_1^*$ to $\vec{\gamma}$ and γ_1 :

$$\begin{aligned} \vec{\xi}^* &= \vec{\xi} + \frac{\eta_1}{e} (\vec{W} \circ \vec{k}) \vec{k} + \frac{\eta_2}{\beta} \vec{W}_t \\ \vec{\omega}^* &= \vec{\omega} - \frac{a}{2I} \frac{\eta_2}{\beta} (\vec{k} \wedge \vec{W}) \\ \vec{\xi}_1^* &= \vec{\xi}_1 - \frac{\eta_1}{e} (\vec{W} \circ \vec{k}) \vec{k} - \frac{\eta_2}{\beta} \vec{W}_t \\ \vec{\omega}_1^* &= \vec{\omega}_1 - \frac{a}{2I} \frac{\eta_2}{\beta} (\vec{k} \wedge \vec{W}) \end{aligned}$$

In the above equations \vec{W} is the relative velocity of the colliding sphere at the contact point, I is the moment of inertia, e and β are two coefficients which determine the collision dynamics through the relationship:

$$\vec{W}' = -e(\vec{W} \circ \vec{k}) \vec{k} + \beta \vec{W}_t, \quad 0 \leq e \leq 1, -1 \leq \beta \leq 1$$

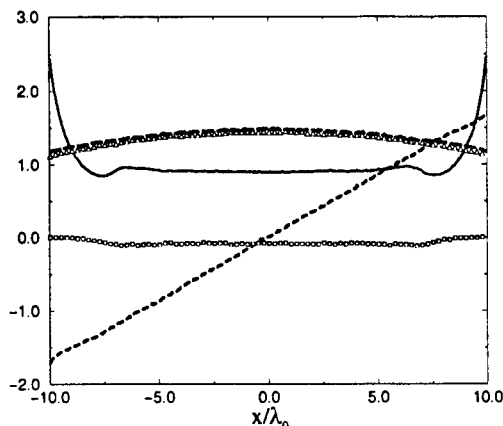


Figure 1: Couette flow in a dense rough hard sphere gas. Continuous line: density n/n_0 . Dashed line: velocity $U_z/\sqrt{RT_w}$. Long dashed line: translational temperature T_{tr}/T_w . Squares: angular velocity ω_y . Triangles: rotational temperature T_{rot}/T_w .

\vec{W}' is the relative velocity after the collision and \vec{W}_t the component of \vec{W} in the plane normal to \vec{k} . The coefficients η_1 and η_2 are defined as $\eta_1 = (1 + e)/2$, $\eta_2 = \frac{\kappa(1+\beta)}{2(1+\kappa)}$, being $\kappa = 4I/ma^2$. It can be easily shown that kinetic energy is conserved in a collision only in the following two cases:

1. $e=1$, $\beta = -1$, $\vec{W}' = -\vec{W}$, perfectly rough spheres
2. $e=1$, $\beta = 1$, $\vec{W}' = \vec{W}_t$, elastic collision in which angular velocities do not change

It is interesting to note that Eq.(1) for rough spheres has been used to derive hydrodynamic equations by a suitable Chapman-Enskog expansion[6], but it has not yet been directly solved. The aim of the present work is to obtain and discuss numerical solutions for simple 1 and 2D flow geometries. The numerical method is based on a straightforward extension of a DSMC-like particle scheme proposed by the Author to solve Eq.(1) for perfectly elastic hard spheres [7]. Comparisons with molecular dynamics simulations will also be presented. An example of computed profiles is shown in Fig. (1) for the Couette flow of a dense gas of perfectly rough spheres ($e = 1$, $\beta = -1$). Diffuse reemission is assumed at the walls whose velocity is $U_w = 2\sqrt{RT_w}$. The reference value of the reduced density (or volume fraction), based on the average density n_0 , is $\eta_0 = \pi a^3 n_0 / 6 = 0.2$; the separation of the walls is 20 mean free paths. As a first step, the Carnahan-

Starling equation of state[8] has been used to approximate $Y(n)$.

References

- [1] S. Chapman, and T. G. Cowling, *The Mathematical Theory of Non Uniform Gases*, Cambridge University Press, Cambridge, 1960.
- [2] C. Cercignani, *Mathematical methods in kinetic theory* (Plenum Press, New York, 1990).
- [3] H. van Beijeren, and M. H. Ernst, *The Modified Enskog Equation*, Physica, Vol.68, pp.437-456, 1973.
- [4] P. Resibois, and M. DeLeener, *Classical kinetic theory of fluids* J. Wiley & Sons, New York, 1977.
- [5] A. Frezzotti, *Molecular dynamics and Enskog theory calculation of one dimensional problems in the dynamics of dense gases*, Physica A, Vol.240, pp.202-211, 1997.
- [6] A. Goldshtein and M. Shapiro, *Mechanics of Collisional Motion of Granular Materials. Part I*, J. Fluid Mech., Vol.282, pp.75-114, 1995.
- [7] A. Frezzotti, *A particle scheme for the numerical solution of the Enskog equation*, Physics of Fluids, Vol.9, pp.1329-1335, 1997).
- [8] N. F. Carnahan, and K. E. Starling, *Equation of state for nonattracting rigid spheres*, J. Chem. Phys., Vol. 51, pp. 635-636, 1969.

Multilevel Monte Carlo Methods for Linear Transport Problems *

S. Heinrich

Fachbereich Mathematik, Universität Kaiserslautern, Germany

We discuss the application of multilevel strategies for variance reduction in Monte Carlo Methods for the solution of linear integral equations. New methods are proposed and analysed. In particular, wavelet decompositions are considered.

*Abstract 7111 submitted to the 21st International Symposium on Rarefied Gas Dynamics, Marseille, France, July 26-31, 1998

INDUSTRIAL PROCESSES - IP 1

ROOM PÉRÈS

TUESDAY, JULY 28, 1998

9:15

A 2-D Self-Consistent DSMC Model for Chemically Reacting Low Pressure Plasma Reactor *

Tim Bartel, Justine Johannes, Mary Hudson
Dept. of Plasma and Aerosol Sciences
Sandia National Laboratories, Albuquerque, NM 87185

Demetre Economou
Dept. of Chemical Engr., University of Houston
Houston, TX 77204-4792

Abstract

The microelectronics industry is pursuing low pressure etch and deposition reactor systems to achieve the uniformity which is required to meet the demands of gigascale integrated circuits. These reactors operate at pressures < 50 mtorr and the high density plasma etch reactors have plasma densities $\sim 10^{17} - 10^{18} \text{ #/m}^3$ in an effort to achieve a high etch rate and anisotropic etching. High plasma density provides high ion fluxes to surfaces, which assures processing rates that match or exceed those of conventional high pressure (20-100 mtorr) reactive-ion etch (RIE) systems. Low gas pressures are necessary to ensure collisionless ion transport through plasma sheaths, which provides anisotropy in the ion flux directed toward the surface. This enables etching of high aspect-ratio features. Etching uniformity over large area (> 200 mm diameter) wafers is of particular importance in these systems as the trend is towards large area, single-wafer processes.

The collisional mean-free-path at 1 mtorr is 100 mm and the diameter of the wafer is 200 mm; therefore, a continuum treatment of the neutral and ion transport is suspect. The Direct Simulation Monte Carlo (DSMC) technique [1], a kinetic simulation of the Boltzmann equation, is ideally suited for these processes since it has the capability of correctly modelling the high density inlet, the complex gas phase chemistry, and the multi-species transport in the system. However, these reactor systems are composed of three distinct time constants for the transport of neutrals, ions, and electrons and as such have not been modelled in a self-consistent manner for these low pressures. Typically, a hybrid approach such as modelling the neutral and ion transport with a kinetic method and the electrons and ions with a continuum method has been applied [2]. This approach is inconsistent due to the inherently different transport physics in a continuum and kinetic code; while this approach is suitable for an electro-positive gas, this strategy will not converge for an electro-negative gas.

The focus of this paper will be on presenting a self-consistent kinetic code for a low pressure chemically reacting plasma and comparing with data. We use a 2D DSMC code which has been optimized for the massively parallel computing environment [3] to transport the neutrals and ions. We allow collisions and subsequent chemistry between neutrals, ions, and surfaces in the reactor. The Variable Hard Sphere model is used to determine neutral-neutral and neutral-ion collision frequencies. A Coulomb interaction model is used for ion-ion collisions. Gas phase chemistry can be modeled with either a kinetic approach (steric factors) or a continuum-like treatment (reaction rates). Surface chemistry is modelled with either a simple reaction probability (sticking factor) or a site coverage dependent model.

We use a bulk plasma approximation for modelling the plasma: we assume local charge neutrality in the bulk and a sheath model to compute the potential jump from the surface to the bulk. The sheath thickness is still very small at these pressures and the Debye length is much smaller than a reactor dimension. Therefore, we do not transport electrons; the local electron density is determined from summing the local ion densities. The Inductively Coupled Power (ICP) deposition is computed using the ORMAX code[4]: a simple control volume method is used to determine the local Maxwellian electron temperature. The space charge field is computed assuming the electrons are in a Boltzmann equilibrium[4]:

$$E = \nabla(kT_e n_e) / (q n_e),$$

where k , T_e , n_e , and q are the Boltzmann constant, electron temperature, electron density, and charge, respectively. The sheath was described with the semi-analytical model developed by Riley [5].

In the paper, we will also discuss our special treatment of trace species chemistry. That is, infrequently occurring chemistry which results in a trace species product. In this application, the trace species are the ions which physically drive the entire system. So modelling their generation/destruction is very

*Abstract 2336 submitted to the 21st International Symposium on Rarefied Gas Dynamics, Marseille, France, July 26-31, 1998

important.

We will compare this model to a bulk plasma/sheath continuum model[6] for two reactor systems: the GEC reference cell for a pure chlorine discharge (no wafer) at 20 mtorr and a High Density Plasma commercial etch tool with C_2F_6 chemistry at 5-10 mtorr. Both systems are electro-negative; the GEC cell has a simple and relatively understood chemistry, the HDP system is a real and complex commercial system. An additional advantage to kinetic modelling approaches was determined during the C_2F_6 modelling comparison: kinetic models are extremely useful for debugging new and complex chemistries since kinetic methods are inherently robust and do not have any convergence constraints--they always work!

Figure 1a and 1b show DSMC comparisons to Cl_2 data from the GEC test cell. Both figures compare radial distributions of 2 ions: Cl^+ and Cl^- ; the DSMC results are shown by the lines and the data by the discrete points. Since the data for Cl^+ only is qualitative and not quantitative, we set the DSMC value to the centerline data value. The data shows a much sharper drop-off than the simulations, both in radial and axial directions. Figure 1b shows a poor comparisons for the Cl^- ion. We are still working on various physics models which may explain this.

Figure 2 shows the comparison for etch rates for a commercial C_2F_6 plasma processing reactor. The comparisons are quite good. The difference at the edge of the wafer ($r = 0.1m$) is attributed to a surface chemistry effect from the focus ring.

Finally, although the focus of the present work was 2D; this methodology is easily extendable to 3D.

REFERENCES

- 1- Bird, G. A., Molecular Gas Dynamics and the Direct Simulation of Gas Flows, Oxford University Press, 1994.
- 2- Johannes, J., Bartel, T., Sears, D., Payne, J., "Gemini: A Hybrid Plasma Modelling Capability for Low Pressure Systems, User's Manual - V1.7," Sandia Report 96-0590, October 1996.
- 3- Bartel, T., Plimpton, S., Johannes, J., Payne, J., "Icarus: A 2D Direct Simulation Monte Carlo (DSMC) Code for Parallel Computers User's Manual - V3.0," Sandia Report 96-0591, October 1996.
- 4- Jeager, E. F. and Berry, L., Phys. Plasmas 2, 6, 2597 (1995).
- 5- Riley, M., Sandia Report SAND95-0775, May 1995.
- 6- Wise, R, Lymberopoulos, D. and Economou, D., "Rapid two-dimensional self-consistent simulation of inductively coupled plasma and comparison with experimental data", Appl. Phys. Lett. 68 (18), 29 April 1996.

Cl^+

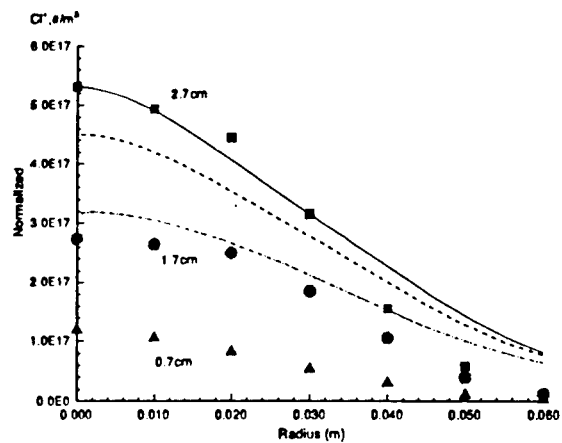


Figure 1a: Radial comparisons of Cl^+ ion for GEC

Cl^-

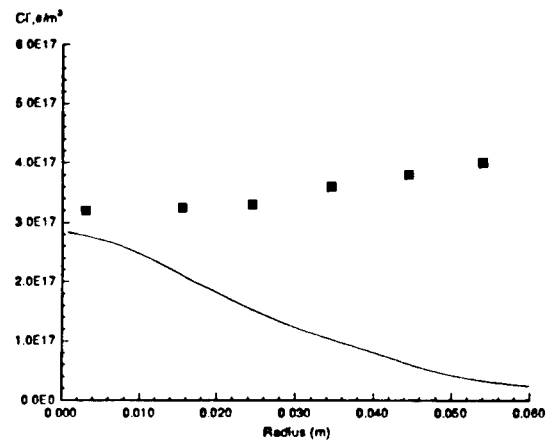
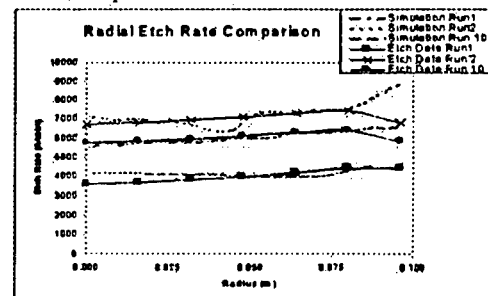


Figure 1b: Radial comparisons of Cl^- for GEC Cell

2D C_2F_6 AMAT HDP Plasma Simulations Comparison to Blanket Oxide Etch Data



AMAT HDP Etch Conditions

	Run 1	Run 2	Run 10
Source Power (W)	3000	2600	2400
Bias (W)	1250	1550	1400
Flow Rate (sccm)	30	50	40
Room Temp (C)	245	245	260
Pressure (mtorr)	5.0	8.0	6.7

Figure 2: Etch profile comparisons for C_2F_6 plasma.

High-density Plasma Reactors: Simulations for Design *

D. B. Hash¹, M. Meyyappan²

¹ Thermosciences Institute, NASA Ames Research Center, Moffett Field, CA USA

² NASA Ames Research Center, Moffett Field, CA USA

The development of improved and more efficient plasma reactors is a costly process for the semiconductor industry. Until five years ago, the industry made most of its advancements through a trial and error approach. More recently, the role of computational modeling in the design process has increased. Both conventional computational fluid dynamics (CFD) techniques like Navier-Stokes solvers as well as particle simulation methods are used to model plasma reactor flowfields. However, since high-density plasma reactors generally operate at low gas pressures on the order of 1 to 10 mTorr, a particle simulation may be necessary because of the failure of CFD techniques to model rarefaction effects. The direct simulation Monte Carlo method [1] is the most widely accepted and employed particle simulation tool and has previously been used to investigate plasma reactor flowfields [2, 3, 4].

A plasma DSMC code is currently under development at NASA Ames Research Center with its foundation as the object-oriented parallel Cornell DSMC code, MONACO [5]. The present investigation is a followup of a neutral flow investigation [6] of the effects of process parameters as well as reactor design on etch rate and etch rate uniformity. The previous work concentrated on silicon etch of a chlorine flow in a configuration typical of electron cyclotron resonance (ECR) or helical resonator type reactors. The effects of the plasma on the dissociation chemistry were modeled by making assumptions about the electron temperature and number density. The electrons or ions themselves were not simulated. The present work extends these results by simulating the charged species. The electromagnetic fields are calculated such that power deposition is modeled self-consistently. Electron impact reactions are modeled along with mechanisms for charge exchange. An ambipolar diffusion assumption is made whereby electrons remain tied to the ions [7]. However, the velocities

of the electrons are allowed to be modified during collisions and are not confined to a Maxwellian distribution. The interaction between the neutral flow and plasma is examined, and results for etch rate uniformity from the previous research and the present plasma simulations are compared.

References

- [1] Bird G. A., *Molecular Gas Dynamics and the Direct Simulation of Gas Flows*, Clarendon Press, Oxford, 1994.
- [2] Nanbu K. and Warabioka I., "Monte Carlo Simulation of an Argon Magnetron Discharge and Target Erosion", *Rarefied Gas Dynamics*, eds. Bernie Shizgal and David Weaver, Progress in Astronautics and Aeronautics, Vol. 158-159, AIAA, Washington, DC, 1994.
- [3] Economou D. J., Bartel T. J., Wise R. S., and Lymberopoulos, D. P., *Two-Dimensional Direct Simulation Monte Carlo (DSMC) of Reactive Neutral and Ion Flow in a High Density Plasma Reactor*, IEEE Transactions on Plasma Science, Vol.23, No.4, pp.581-590, 1995.
- [4] Font G. I. and Boyd I. D., *Numerical Study of the Effects of Reactor Geometry on a Chlorine Plasma Helicon Etch Reactor*, J. Vac. Sci. Technol. A, Vol.15, No.2, pp.313-319, 1997.
- [5] Dietrich S. and Boyd I. D., *Scalar and Parallel Optimized Implementation of the Direct Simulation Monte Carlo Method*, J. Comp. Phys., Vol.126, pp.328-342, 1996.
- [6] Hash D. B. and Meyyappan M., *A Direct Simulation Monte Carlo Study of Flow Considerations in Plasma Reactor Development for 300 mm Processing*, J. Electrochem. Soc., Vol.144, No.11, pp.3999-4004, 1997.
- [7] Bird G. A., *Nonequilibrium Radiation During Re-entry at 10 km/sec*, AIAA Paper 87-1543, 1987.

*Abstract 5921 submitted to the 21st International Symposium on Rarefied Gas Dynamics, Marseille, France, July 26-31, 1998

DSMC Simulation of Flow through Microchannels and Micropumps*

Mary L. Hudson and Timothy J. Bartel
Sandia National Laboratories
Albuquerque, NM 87185
mlhudso@sandia.gov, tjbate@sandia.gov

Advances in micromachining technology have enabled fabrication of Micro-Electro-Mechanical Systems (MEMS): valves, pumps, heat exchangers, and gas turbines. Flow through these micro-devices can range from rarefied to transitional due to the comparable size of the MEMS features and the mean free path of the gas. Thus, the Direct Simulation Monte Carlo¹ (DSMC) technique is an appropriate simulation tool for MEMS devices as it is accurate for both the rarefied and continuum flow regimes.

Our DSMC code can run on parallel computer systems which enable conceptual design simulations to be run in a timely fashion. However, before the code can be used with confidence for design, benchmark MEMS experiments were compared to assess appropriate gas-surface interaction models. We have simulated the gaseous flow through three devices and compared with pressure and flow rate data. The three devices are a microchannel, a capillary tube for gas chromatography, and an accommodation pump. These three cases span a range of Knudsen numbers which the DSMC code accurately modeled. DSMC simulations can now be used to identify critical parameters for optimized performance of MEMS devices and to develop and evaluate analytical models for transitional flows.

The first test case is the flow of nitrogen through a microchannel which is 3000 μm long and 1.2 μm high as shown in Figure 1. The 2-D DSMC results were compared with Navier-Stokes predictions with slip boundary conditions² and with experimental data^{3,4}. The data show that there exists nonlinear behavior of the pressure distribution along the microchannel for two different inlet pressures. This behavior is well matched by the DSMC simulations as shown in Figure 2. As the degree of rarefaction increases (decreasing inlet pressure), a trend of increasing pressure curve linearity is observed which is not predicted with a continuum formulation. Piekos and Breuer⁵ also confirmed this observation with their DSMC results. Their simulation was somewhat simplified by a smaller L/H of 60 as compared to our 2500 which represents a more realistic length. A smaller L/H allows less cpu time to gather good statistics which is difficult in this case since the ratio of the mean to

thermal velocity in the channel is 1/400, i.e., a small signal to noise ratio.

The next test case is flow through a separation column for gas chromatography. This is a critical component for gas-phase detection in Sandia's $\mu\text{ChemLab}$ program. The design and evaluation of the separation column includes both a simulation and experimental effort. Initially, experimental data on uncoated and coated capillary tubes will be used in conjunction with DSMC simulations to develop gas-surface interaction models which can then be used in a continuum simulation. The gas-surface interaction model must describe the diffuse or specular nature of the column surfaces as well as define sticking coefficients for various coatings. These columns are typically 10 to 100 cm in length and 50 μm or less in diameter and the carrier gas is hydrogen or helium. The inlet pressure is 130 to 170 kPa while the outlet is atmospheric. The final column design on the $\mu\text{ChemLab}$ will probably employ a serpentine or spiral channel deeply etched to maximize surface area in order to conserve chip real estate. Parametric studies can be performed using the developed gas-surface interaction models to assess optimum channel configurations with various carrier gases to obtain good separations.

The third test case in our DSMC validation effort for MEMS is an accommodation pump. Tracy⁶ obtained limited data on various configurations to illustrate the accommodation or thermomolecular pump concept. Briefly, direct thermal pumping of gases under molecular flow conditions occurs due to directed molecular scattering from certain heated "active" surfaces. As in the above separation column, the operation of the thermomolecular pump is governed by the gas-surface interaction. Since the active surface is difficult to reproduce experimentally, DSMC simulations are useful to characterize these surfaces and optimize the geometry and operating conditions. Tracy obtained data in a chamber filled with helium at 0.1 mTorr with an active surface of carbonized nickel at 873 K. All other chamber surfaces were 303 K. Flow was directed from the 5 mm wide active surface through a 5 mm wide, 2 mm high aperture 3 mm below the active surface. For this configuration, Tracy measured a pressure ratio of 1.06. Contours of number density from an initial 2-D DSMC simulation of this configuration are shown in Figure 3. The ratio of the computed number densities, which is equivalent to pressure ratio for constant temperature, is about 1.03.

* Abstract 5966 submitted to the 21st International Symposium on Rarefied Gas Dynamics, Marseille, France, July 26-31, 1998.

All surfaces had a thermal accommodation of 1.0 and were diffuse. As the director becomes more specular, a higher pressure ratio is expected. Tracy obtained higher pressure ratios on other configurations, including a multi-stage device, and measured the effect of the active surface temperature. DSMC results will be compared with data and results will be presented on the effects of gas-surface interaction, geometry, Knudsen number, and temperature on the performance of the accommodation pump.

References

- ¹ Bird, G. A., *Molecular Gas Dynamics and the Direct Simulation of Gas Flows*, Clarendon Press, Oxford, 1994.
- ² Arkilic, E. B., Breuer, K. S., and Schmidt, M. A., "Gaseous Flow in Microchannels," FED-Vol. 197, Application of Microfabrication to Fluid Mechanics, ASME 1994, pp. 57-66.
- ³ Liu, J. and Tai, Y-C., "MEMS for Pressure Distribution Studies of Gaseous Flows in Microchannels," IEEE Proceedings, Micro Electro Mechanical Systems, Amsterdam, the Netherlands, 1995, IEEE Catalog Number 95CH35754.
- ⁴ Pong, K-C., Ho, C-M., Liu, J., and Tai, Y-C., "Non-Linear Pressure Distribution in Uniform Microchannels," FED-Vol. 197, Application of Microfabrication to Fluid Mechanics, ASME 1994, pp. 51-56.
- ⁵ Piekos, E. S. and Breuer, K. S., "DSMC Modeling of Micromechanical Devices," AIAA 95-2089.
- ⁶ Tracy, D. H., "Thermomolecular Pumping Effect," Journal of Physics E: Scientific Instruments, 1974, Volume 7, pp. 533-536.

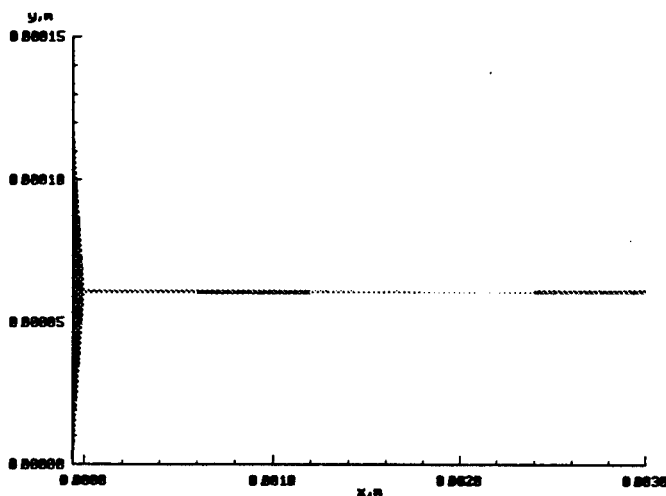


Figure 1. Microchannel Geometry

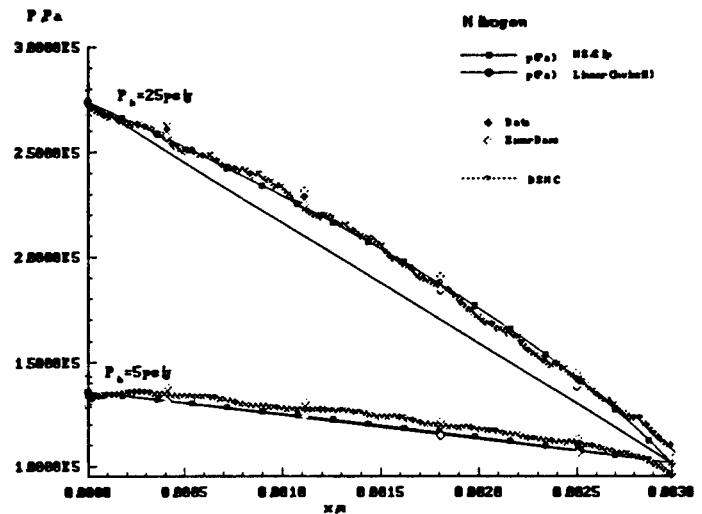


Figure 2. DSMC Pressure Distribution vs. Data in Microchannel

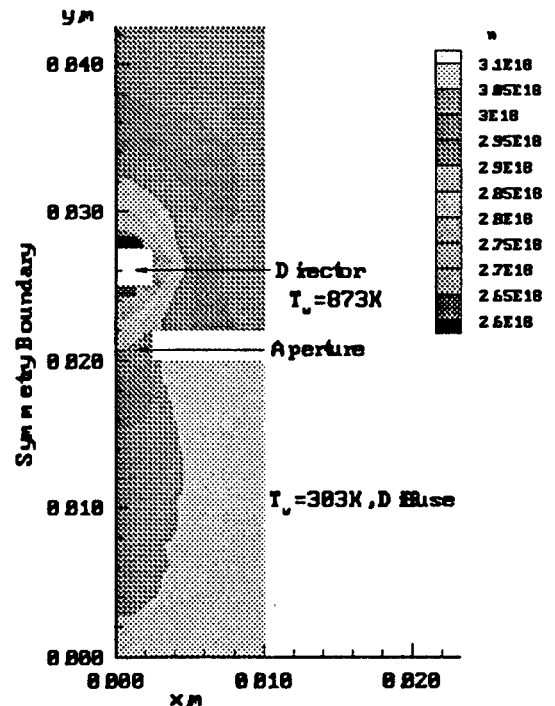


Figure 3. Number Density Distribution in Accommodation Pump

Comparison of Experiment and Prediction for Transitional Flow in a Single-Stage Micromechanical Knudsen Compressor *

S.E. Vargo, E.P. Muntz

University of Southern California, Dept. of Aerospace Eng., Los Angeles, CA USA

Introduction

A MEMS based thermal transpiration Knudsen Compressor was first described by Pham-Van-Diep et al [1] and is a modern version of the original transpiration compressor described by Knudsen [2, 3]. A series of stages comprise a Knudsen Compressor. Each stage has a capillary section where the temperature increases causing a pressure increase due to the rarefied gas dynamic phenomenon of thermal transpiration. The capillaries are followed by a connector section where the pressure is approximately constant while temperature drops to its original value entering the stage.

At USC, we have recently completed an experimental study of a laboratory model of a Knudsen Compressor and verified that single and multiple stage Knudsen Compressors not only work but that their performance can be adequately predicted using the analysis of Pham-Van-Diep [4]. This analysis was accomplished assuming the ideal situation of free-molecule or collisionless flow in the capillary section of a compressor stage and continuum flow in the connector section of the stage. While these conditions can be closely matched in experimental compressors it is expected in practice that both the capillary and connector sections of the compressor frequently will operate in the transitional flow regime. An extension of the previous Knudsen Compressor stage analysis to the transitional flow regime has recently been developed [5]. This analysis removes the two critical assumptions of free-molecule and continuum flow. The modeling is accomplished using the results for transitional flows reported by Sone and his colleagues and is detailed in [5]. The expanded stage analysis can be incorporated in a cascade analysis similar to that developed earlier [1], resulting in a more realistic estimate of Knudsen Compressor performance for a wide range of operating conditions.

For a single-stage Knudsen Compressor in transitional flow, the mass flow rate is developed in [5] and is stated in Eq.1.

$$\dot{M} = (1 - \kappa) p_{AVG} (2(k/m)T_{AVG})^{-1/2} A \left| \frac{\Delta T}{T_{AVG}} \right| \times \left[\frac{Q_T}{Q_P} - \frac{Q_{T,C}}{Q_{P,C}} \right] \left[\frac{(L_r/L_r)}{FQ_P} + \frac{(L_X/L_R)_C}{Q_{P,C}} \right]^{-1} \quad (1)$$

The parameter κ describes the upflow in the stage and ranges between 0 (maximum upflow, no pressure increase) and 1 (zero upflow, maximum pressure increase). T_{AVG} and p_{AVG} are the average values for temperature and pressure in the stage, respectively. L_r is the capillary length and L_r is the radius of the capillary. L_X is the connector length and L_R is the radius of the connector. The variables Q_T and Q_P are functions of the Knudsen number, Kn . They are numerically obtained coefficients that describe the various transitional flows studied by Sone and his collaborators as reported in [5]. The capillary section values are designated Q_T and Q_P and the connector section values are designated as $Q_{T,C}$ and $Q_{P,C}$. The maximum pressure change over the stage, $\sum \Delta p_I$, resulting from $\dot{M} = 0$, can be found from Eq.2.

$$\frac{\sum \Delta p_I}{p_{AVG}} = \left| \frac{\Delta T}{T_{AVG}} \right| \left[\frac{Q_T}{Q_P} - \frac{Q_{T,C}}{Q_{P,C}} \right] \quad (2)$$

Results

Previous single-stage Knudsen Compressor maximum pressure differences (no flow) and throughput results have been published in [4]. Fig.1 outlines the results for single-stage maximum pressure differences obtained using helium and nitrogen. For these laboratory Knudsen Compressors the Kn of the flows is larger than 10 for operating pressures less than about 100 Torr, thus a good portion of the operational pressure range (up to 1 Atm.) can be considered to be in the transitional regime.

*Abstract 6032 submitted to the 21st International Symposium on Rarefied Gas Dynamics, Marseille, France, July 26-31, 1998

As the operating pressure is increased above 100 Torr the resulting decrease in Kn causes the maximum pressure difference values to depart from free-molecule assumed linear predictions. Since these departures from predicted values occur in the transitional regime it seems appropriate at this time to reevaluate the laboratory Compressor's performance utilizing the transitional flow analysis of [5] and summarized in Eqs.1 and 2.

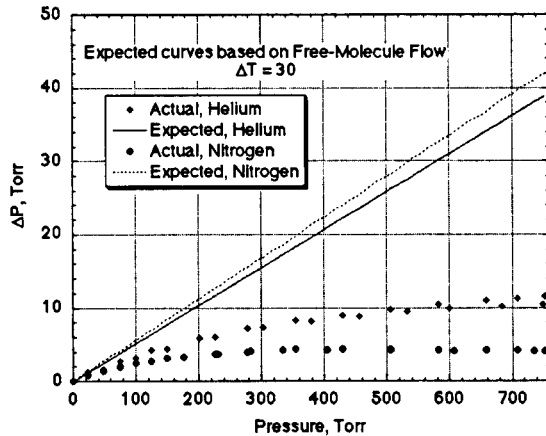


Figure 1: Single-stage Knudsen Compressor results

Conclusion

A comparison of the expected and experimental single-stage maximum pressure difference and throughput results can be made in the transitional flow regime using Eqs.1 and 2. Setting $\kappa = 1$ in Eq.1 results in zero upflow ($\dot{M} = 0$) for the Compressor. Using Eq.2 with the experimental temperature and appropriate transition flow coefficients (Q values) a comparison of the maximum pressure difference results can be made. Previously obtained experimental throughput values at transitional pressures can be numerically integrated in order to find their corresponding mass flow rates. This allows a comparison to be made with the expected values obtained using Eq.1. In the final manuscript a performance and experimental study of a single-stage Knudsen Compressor that operates in the transitional regime will be presented and compared to transitional flow analysis.

References

- [1] Pham-Van-Diep, G., Keeley, P., Muntz, E.P., Weaver, D.P., *A Micromechanical Knudsen*

Compressor, in *Rarefied Gas Dynamics*, J. Harvey and G. Lord eds., Oxford University Press, pp.715- 721, 1995.

- [2] Knudsen M., *Eine Revision der Gleichgewichtsbedingung der Gase. Thermische Molekularströmung*, Ann. Physik, Vol.31, pp.205-229, 1910.
- [3] Knudsen M., *Thermischer Molekulardruck der Gase in Röhren*, Ann. Physik, Vol.33, pp.1435-1448, 1910.
- [4] Vargo, S.E. and Muntz, E.P., *An Evaluation of a Multiple-Stage Micromechanical Knudsen Compressor and Vacuum Pump*, in *Rarefied Gas Dynamics*, Ching Shen ed., Peking University Press, Beijing, 1997.
- [5] Muntz, E.P., Sone, Y., Aoki, K. and Vargo, S.E., *Performance Analysis of a Knudsen Compressor in Transitional Flow*, in preparation, 1997.

INDUSTRIAL PROCESSES - IP 2

ROOM PÉRÈS

TUESDAY, JULY 28, 1998

10:50

Simulation of Evaporized Titanium in Electron Beam Physical Vapor Deposition Process *

M.C. Çelenligil¹, Ö. Yiğiter¹, G. Trapaga², A. Powell²

¹ Aeronautical Eng. Dept., Middle East Technical University, Ankara, Türkiye

² Dept. of Materials Science and Eng., MIT, Cambridge, Massachusetts, U.S.A.

The durability of many engine parts subjected to very high temperatures can be substantially improved by coating them with thin films of metals and ceramics. Thermal barrier coatings of aircraft engine turbine blades are an example for such applications, and proper manufacturing of these coatings is a major interest for the aerospace industry today.

The research work of this paper is a part of the simulation efforts for the thermal barrier coatings on engine parts during electron beam physical vapor deposition process. The present study models the vapor phase portion of this process and focuses on identifying the problems related with the simulation, estimating the unknown input parameters, and code validation. This problem was first studied by P. Minson [1] at Massachusetts Institute of Technology as an undergraduate thesis. The rarefied flow of the vapor inside the deposition chamber is simulated by writing a computer program for two chemical gas species with a hard sphere collision model and using the Direct Simulation Monte Carlo method of G.A. Bird [2]. The present investigation is aimed to study the same problem using the G3 computer code developed by G.A. Bird. The G3 code has been successfully applied to various aerothermodynamics problems [3, 4, 5] over the past ten years and considerable confidence has been built on it. This is the first time that it is used for the simulation of a physical vapor deposition process.

In the G3 code, the three-dimensional domain is gridded using a body-fitted mesh which is divided into a network of deformed hexahedral (six-faced) cells. The four corners of a cell face may not be coplanar and this makes the generation of body-fitted grids possible on doubly curved surfaces. Each cell is further subdivided into six tetrahedral

subcells (which have four well-defined triangular faces) to enable tracking the molecules moving from one cell to another. Also, because it is desirable to choose the collision partners from the nearest candidates, these partners are selected probabilistically from the same subcells. For the flow problems considered, the adjacent cells and subcells are exactly matched in the whole domain.

In the present study, a generic shape is used for the deposition chamber geometry. A 2 m × 2 m × 1 m rectangular chamber with a 3-cm-radius circular ingot at the bottom face is used in the simulations. However, due to the existence of symmetry planes, only one quarter of this domain is needed.

In the early part of this study, efforts are first concentrated on checking the applicability of various boundary conditions to the physical vapor deposition problem. Then, the computer code is modified for the gas model used in the simulations. In many recent thermal barrier coating applications yttria-stabilized zirconia is being used. But, unfortunately, the non-proprietary data on the thermo-physical properties of these materials are extremely limited and this is a big handicap for the simulations. Consequently, in the present study electron beam evaporation of titanium is studied and a two-species gas model (Ti, Ar) is developed. For this gas model, several properties of the gas species (such as the viscosity of the vaporized titanium) could not be found from the literature and these properties are assumed.

As for the boundary conditions, several assumptions are made. At the ingot melt pool surface, the titanium atoms are assumed to move randomly at a temperature of 2100 K after evaporation. The part (on which titanium is deposited) is assumed to be a thin rectangular plate with dimensions of 50 cm × 10 cm located 0.5 m away from the ingot. Argon gas (at a temperature of 100° C and a Mach number of 1) is supplied from small inlet pipes to

*Abstract 2171 submitted to the 21st International Symposium on Rarefied Gas Dynamics, Marseille, France, July 26-31, 1998

affect the shape of the titanium plume. The surface temperatures of the part and the chamber walls are assumed to be 1300 K and 1000 K, respectively. All surfaces are assumed to be completely adsorbing the striking titanium atoms. On the other hand, the argon atoms are assumed to be bouncing back from the walls. There are openings on the walls to prevent continuous argon build-up, and stationary states are eventually reached in the simulations.

In order to build confidence, the code is applied to a collisionless flow problem for which solution is already known. In this case, the molecules are allowed to move freely in the computational domain without any intermolecular collisions. The mass deposition results on the part are compared with those of the theoretical line-of-sight method.

In the present study, sensitivity of the results on the computational grids are also checked. For example, the early calculations were first performed on a coarse grid with constant cell sizes in the direction normal to the ingot surface. Later, the calculations are repeated using a refined grid with small cells near the ingot and large cells away from it so that the basic Direct Simulation Monte Carlo requirements are satisfied (i.e. the cell sizes are smaller than the local mean-free-paths; the local time steps are smaller than the local mean-free-times, etc.). It is observed that the total mass deposition rate results show considerable differences.

References

- [1] Minson, P., "Evaluating the Suitability of the Direct Simulation Monte Carlo Method Technique to Modeling PVD at Very Low Background Pressure", Bachelor of Science Thesis, Department of Materials Science and Engineering, Massachusetts Institute of Technology, January 1996.
- [2] Bird, G.A., *Molecular Gas Dynamics and the Direct Simulation of Gas Flows*, Clarendon Press, Oxford, U.K., 1994.
- [3] Çelenligil, M.C. and Moss, J.N., "Hypersonic Rarefied Flow About a Delta Wing - Direct Simulation and Comparison with Experiment", *AIAA Journal*, Vol. 30, No. 8, pp. 2017-2023, August 1992.
- [4] Çelenligil, M.C., Moss, J.N., and Blanchard, R.C., "Three-Dimensional Rarefied Flow Simulations for the Aeroassist Flight Experiment Vehicle", *AIAA Journal*, Vol. 29, No. 1, pp. 52-57, January 1991.
- [5] Çelenligil, M.C., "Rarefied Wake Flow Simulation for a 70-deg Blunted Cone at Incidence", *Rarefied Gas Dynamics*, edited by C. Shen, Peking University Press, Beijing, China, pp. 239-244, 1997.

Titanium Vapor Deposition Modelling using the Direct Simulation Monte Carlo Method. *

J. Balakrishnan † I. D. Boyd ‡

Sibley School of Mechanical and Aerospace Engineering
Cornell University, Ithaca, U. S. A.

Introduction

Vapor phase deposition of titanium is an important process used in various manufacturing industries. A novel scheme for titanium deposition is being studied at the Lawrence Livermore National Laboratory (LLNL). Titanium and other metallic atoms are vaporized from a liquid pool of a titanium alloy, usually Ti6Al4V, using the energy from an electron beam. The vapor plume expands through a chamber and impinges on a substrate, causing deposition. The computational modelling of the deposition process is carried out using the direct simulation Monte Carlo (DSMC) technique [1]. The modelling of the physics is thus carried out at the particle level.

Traditional DSMC algorithms consider three basic modes of energy for a particle — the translational, rotational and vibrational energies. In most practical applications, the consideration of these three modes of energy is sufficient to accurately account for the net energy content of the flow. Due to the high temperature of the molten pool, a large proportion of the titanium atoms are electronically excited. Hence, a significant part of the energy is in the electronic mode and it would not be possible to account for the total energy content of the flow without taking the electronic energy of the titanium atoms into consideration. The energy transferred between the electronic and the translational modes can significantly affect the velocity of the flow, and hence the flux. This becomes especially important at the substrate where deposition takes place.

This study includes the modelling of electronic energy of atoms in the flow domain. The electronic energy is considered as a particle property that can

be changed by collisions. The degeneracy of the electronic levels are also taken into account in the modelling. The energy levels considered for a particle are selected by an analysis of the population distribution and the energy content of the energy levels under equilibrium conditions. The electronic temperature is defined based on the relative populations of the energy levels of particles in the simulation, extrapolated to an equilibrium distribution. This provides a means of measurement of the excitation of particles in the flow domain, and for comparison between the translational and electronic modes of energy.

Preliminary Results

The numerical simulations detailed in this work are carried out using Monaco [2], a code that employs the direct simulation Monte Carlo method. The simulations were carried out on an unstructured grid of the flow domain. The inflow was modelled using a profile of the molten pool.

Fig. 1 shows contour plots of the number density and the absolute velocity of titanium atoms in the flow domain. The contours show a rapid fall-off in the number density of titanium atoms near the top of the flow domain. This is accompanied by an increase in the velocity of the atoms in the plume, as they expand through the chamber to hypersonic speeds.

Fig. 2 shows the contours of the electronic and translational temperature, which are the only two modes of energy that the titanium atoms possess. The contours show that the temperatures of the two modes fall as the plume expands. There is also energy transfer between the two modes, due to collisions between particles in the plume. The electronic temperature near the melt surface indicates that a large proportion of the atoms that evaporate from the melt surface are in the excited state. As the

* Abstract 2369 submitted to the 21st International Symposium on Rarefied Gas Dynamics, Marseilles, France, July 26-31, 1998

† Graduate Student

‡ Associate Professor

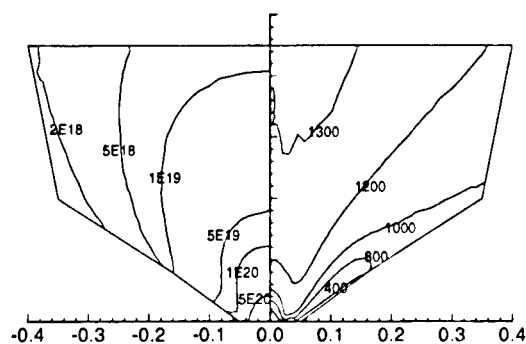


Figure 1: Number density (left) and absolute velocity (right) contours of titanium in the flow domain

plume expands, the proportion of atoms that are excited drops, causing the electronic temperature to fall correspondingly. The energy released due to the de-excitation of atoms is converted to translational energy and plays a significant part in the rapid increase in the velocity of the vapor.

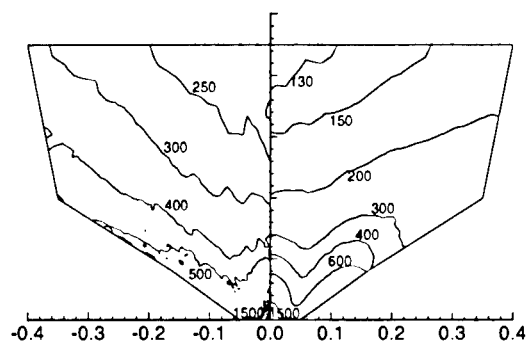


Figure 2: Electronic temperature (left) and translational temperature (right) contours of titanium in the flow domain

Measurements of the absolute velocity and the translational temperature of the vapor plume are available from the Electron Test Facility (ETF) at LLNL. These measurements are used for diagnostic purposes and are taken using laser spectroscopy. The vapor is allowed to pass through 2 slits that are equidistant from the axis, at a distance of 0.16 m. The values obtained at these locations are then av-

eraged to provide an idea of the behavior of the flow with changes in various melt conditions. In an experiment related to the simulation carried out, the velocity measured ranged between 1400 and 1450 m/s, which is in good agreement to the value predicted in the simulation. The translational temperature measured was in the range of 140 - 150 K, which agrees very well with the simulation too. The results from the simulation for the properties along the substrate are presented in Fig. 3.

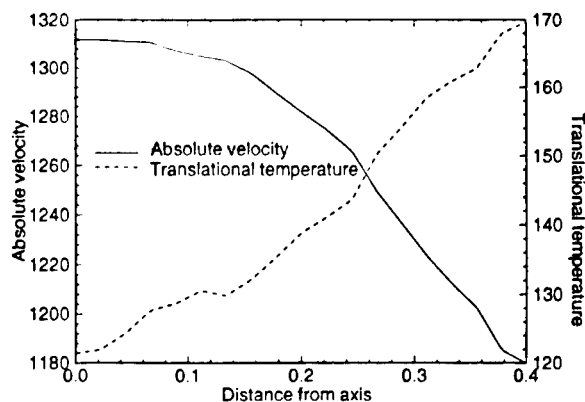


Figure 3: Absolute velocity and translational temperature along the substrate

The DSMC simulations will be refined with a general probability of electronic exchange affecting the collisions in the flow domain. The comparison with the experimental data, from the ETF at LLNL, will also be presented for various flow conditions tested in the experimental facility.

References

- [1] Bird, G. A., *Molecular Gas Dynamics*, Clarendon Press, Oxford, 1994.
- [2] Dietrich, S., and Boyd, I. D., *Scalar and Parallel Optimized Implementation of the Direct Simulation Monte Carlo Method*, Journal of Computational Physics, Vol. 126, 1996, pp. 328-342.

An Experimental Investigation of Titanium Nitriding Using an Arc-Plasma Jet*

A. Vizcaino, W. Röck, V. Lago, M. Dudeck
Laboratoire d'Aérothermique du CNRS, Meudon, France

An experimental study of arc-jet plasma-surface interaction has been carried out in the 'Laboratoire d'Aérothermique'. This subject involves the knowledge of the characteristics of the plasma flow and the physical properties of the substrate (Gauthering 1983). Plasma source is successfully used for treating surfaces of different materials, offering a wide range of industrial applications. The performed experiments are based on nitriding titanium substrates under vacuum, using an Arc Plasma source and high purity N_2 .

Titanium nitrides have been considered high technology materials in the fields of microelectronics, aerospace and biomaterials for a long time. They exhibit exceptional properties: their electrical and thermal conductivity are near that of pure metals; due to their chemical stability they can be used as diffusion barriers in integrated circuit fabrication; and finally, their low friction coefficient and high hardness make them suitable for the wear resistance coating on tools (Sang-Hyeob Lee, et al. 1994). This explains the large amount of investigation still dedicated to these materials (Gerlach, et al. 1996; Meng and Curtis 1997).

The aim of this research is to study the synthesis of the compound TiN, in order to explain the physical processes involved in the nitriding method by plasma. The influence of temperature, plasma generator-to-substrate distance, electric plasma power, plasma stability and total mass flow rate on the film characteristics, are discussed in this paper.

The experimental work was carried out using the plasma wind tunnel SR5, with a length of 4.5m and 1m diameter. A DC arc-jet generator (described by Lasgorceix, et al. 1993) with an anode exit of 48mm of diameter, was set up to produce the plasma flows. The arc is generated between a cathode made out of copper with a small zirconium insert at the tip (insert diameter 1.6 mm) and the nozzle throat of a water-

cooled copper anode. The generator is set up on a support with a displacement system which enables to select the (x,y) position of the generator in reference to the target sample.

The experimental conditions, typically used in this study are shown in Table 1. The resulting arc-plasma jets exhibit dimensions of up to 1m length and 0.5 m diameter.

Arc voltage	40-60 V
Arc current	100 A
N_2 mass flow	20-30 slm
Generator chamber pressure	170-240 Torr
Tank pressure	10^{-1} Torr.
Treatment period	up to 3 hours

Table 1. Experimental conditions

Titanium nitride layers are synthesized at the titanium substrate. In order to understand the titanium nitride layer formation it is necessary to characterise the plasma as well as the surfaces treated by plasma. Since the arc-jets are luminous some of their physical parameters can be determined by optical emission spectroscopy. This diagnostic tool offers the advantage that does not influence the plasma (Lago, et al. 1995). Using this technique it is possible to identify the different plasma components, the rotational and vibration temperature of the N_2^+ and the excitation temperature of the N. The measurements are undertaken along the plasma, from the area close to the nozzle exit of the plasma source to the area next to the substrate. These analyses

* Abstract 3166 submitted to the 21st International Symposium on Rarefied Gas Dynamics, Marseille, France, July 26-31, 1998

provide information about the species that are transported to the substrate.

The chemical and physical properties of the synthesized layers are investigated with different complementary techniques. Rutherford backscattering spectroscopy (RBS) allow us to determine the in-depth concentration of nitrogen in the titanium matrix. Atom Force microscopy (AF) is used to measure the thickness of the layers obtained. X-ray photoelectron spectroscopy (XPS) enables to analyse the titanium chemical bonds with the elements present in the layer such as oxygen, carbon, or nitrogen. X-ray diffraction provides microstructural information of the surface layers. The morphology of the surface is characterised by Scanning electron microscopy (SEM).

The 'Laboratoire d'Aérothermique', aims to continue the research on substrate-plasma interaction, especially focusing to treat metallic substrates using Plasma Immersion Ion Implantation (PIII). PIII is an emerging technology which offers interesting industrial applications, not only for modifying the near-surface region of bulk materials, but also for thin films (Brown, et al. 1994; Mantese, et al. 1996.).

References

- [1] Brown, I.G., Anders, A., Anders, S., Dickinson, M.R., MacGill, R.A. (1994). Metal ion implantation: Conventional versus immersion. *American Vacuum Society B* **12**(2), 823-827.
- [2] Gerlach, W., Wengenmair, H., Hartmann, J., Assmann, W., Rauschenbach, B. (1996). Ion-beam-assisted deposition induced composition changes in titanium nitride. *Physica status solidi A-Applied research*, **155**(1), 181-188.
- [3] Gautherin, G. (1983). Interaction Plasma-Surface. In *Réactivité dans les plasmas. Applications aux lasers et au traitement de surfaces*. Pointu, A. M. and A. Ricard, Eds. Les éditions de physique. Aussois (Savoie).
- [4] Lago, V., Schoenemann, A., Buuron, A., Lasgorceix, P., Dudeck, M. (1995). Supersonic Plasma Jets Device for Testing Space Crafts Materials. Proceedings of the Second European Symposium on Aerothermodynamics for Space Vehicles, 349-356. ESTEC, Noordwijk, The Netherlands.
- [5] Lasgorceix, P., Lago, V., Asselin, P., Dudeck, M. (1993). Générateurs de plasmas. *Rapport de Laboratoire*, R 93-8. Paris, Laboratoire d'Aérothermique.
- [6] Mantese, V.J., Brown, U.G., Cheung, N.W., Collings, G.A. (1996). Plasma-Immersion Ion Implantation. *MRS Bulletin*, 52-56.
- [7] Meng, W.J., Curtis, T.J. (1997). Inductively coupled plasma assisted physical vapor deposition of titanium nitride coatings. *Journal of electronic materials*, **26**(11), 1297-1302.
- [8] Sang-Hyeob Lee, Ho-Joon Ryoo, Jung-Joong Lee (1994). (Ti_{1-x}Al_x)N coatings by plasma-enhanced chemical vapour deposition. *J. Vac. Sci. Technol. A*, **12**(4), 1602-1607.

DSMC Modelling of Gas Flows in Low Pressure Chemical Vapour Deposition Reactors *

C. D. Robinson, J.K. Harvey

Department of Aeronautics, Imperial College, London, SW7 2BY, U.K.

1 Introduction

This paper will describe the gas dynamic portion of a collaborative project to develop an accurate model of the entire chemical vapour deposition (CVD) process of silicon. The project aims to tie together *macro-scale* gas flow simulations using DSMC, to *meso-scale* kinetic Monte-Carlo (KMC) surface growth simulations which will in turn make use of quantum mechanical *nano-scale* calculations. The coupled model will be validated by an experimental programme underway at DERA Malvern in the U.K. There have been several recent applications of the direct simulation Monte Carlo (DSMC) method to the modelling of the gas inside chemical vapour deposition (CVD) reactor chambers [1], [2] [3]. In general each of these studies has neglected certain aspects of the simulation of the gas flow inside the reactor, a fact which this work aims to redress.

Modelling of gas flows inside CVD reactors has presented a number of new challenges to the DSMC community. CVD reactor chambers are characterised by complex geometrical configurations, unlike many of the conventional DSMC-modelled flows which tend to be around simple geometries. As a result a very flexible geometric representation capability is required. The modelling of the common molecular species found in air, such as N_2 and O_2 , is fairly well established for DSMC simulations, and the relevant physical parameters for these molecules are readily available. However the species inside the reactor tend to be less well understood reactant gases such as SiH_4 , GeH_4 , or even more "exotic" chemical combinations. The relevant physical parameters required for a successful DSMC calculation of such gases are not readily found in the literature. A key to the successful modelling of the flow, and in turn the prediction of

silicon CVD growth rates is the boundary condition applied at the growth surface-gas interface. Whilst some of these challenges have been addressed individually it is the aim of this work to bring together solutions to these problems in a single framework.

2 CVD Reactor Geometry

The aim of the project is initially to simulate the flow inside the Defence Evaluation Research Agency (DERA) Malvern, CVD reactor.

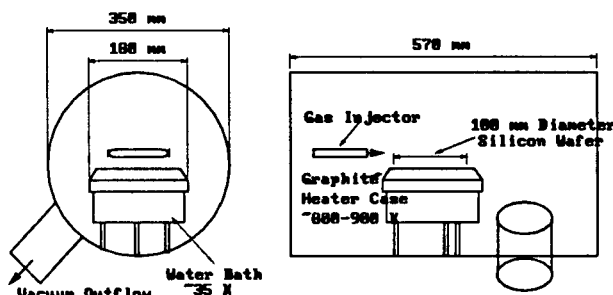


Figure 1: Schematic of DERA Malvern CVD Reactor.

A schematic of the reactor geometry is shown in Figure 1. The reactor is cylindrical and is made largely from stainless steel. The gases are introduced via the injector as indicated and these gases flow over the silicon wafer which is mounted on a heater assembly. The gas is injected at near atmospheric conditions, but vacuum pumping means the working pressures are of the order of a few Pascals. The carrier gas is usually H_2 and the trace species are usually SiH_4 , and/or GeH_4 . The CVD growth on the silicon wafer takes place by dissociation of the silicon/germanium from the silane/germane molecules on the wafer surface. Therefore it is clear that a multi-species code capable dealing with complex geometries is required.

*Abstract 5713 submitted to the 21st International Symposium on Rarefied Gas Dynamics, Marseille, France, July 26-31, 1998

3 Gas Flow Modelling and Work to be Presented

The gas is modelled using the DSMC+ flow solver [4] developed at Imperial College. This multi-species solver uses unstructured triangular and tetrahedral grids to enable complex geometry modelling. The dimensions of the CVD reactor and the working pressures generate the need for powerful computing resources in order to model the gas flows properly. DSMC+ has been specifically designed for use on powerful multi-processor computers and makes use of dynamic load balancing techniques in order to utilise the computational resources effectively.

The required physical parameters for the silane and germane molecules, such as their collision cross sections are being derived from quantum chemistry calculations, due to a lack of experimental data in the literature. A particularly novel approach that is currently under development is the treatment of the boundary condition at the gas - silicon wafer interface. It is proposed that the DSMC solution of the gas flow impacting on the wafer is closely coupled to KMC model of the surface. The KMC model is under development by researchers at DERA Malvern with initial data provided by calculations performed with DSMC+ using a simple boundary condition for the silicon gas interface.

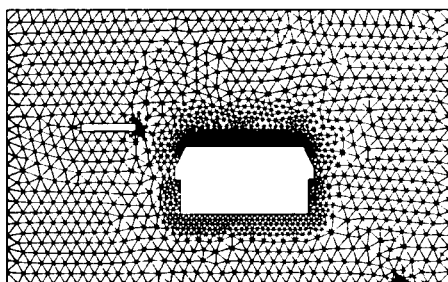


Figure 2: Unstructured mesh discretisation of reactor chamber.

A sample of a two dimensional calculation of the central "slice" the reactor chamber is shown in Figures 2 and 3. Figure 2 shows a typical

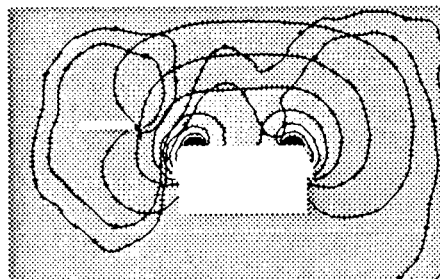


Figure 3: Temperature contours and sample streamlines.

unstructured mesh on which the DSMC calculation is performed. Figure 3 shows a sample of nominal value temperature contours along with some gas flow streamlines in a $H_2 - SiH_4$ gas mixture.

The paper will present details of three dimensional calculations of the reactor chamber. Details of the techniques used to derive relevant gas phase collision parameters from quantum mechanical calculations will also be provided. Comments on the progress of the DSMC-KMC gas surface model will also be provided.

References

- [1] L.A. Gochberg and D.F.G. Rault *DSMC Modelling of High Density Plasma Enhanced CVD for Simultaneous Etch and Deposition*, Rarefied Gas Dynamics, 775-780, Peking University Press 1997.
- [2] G. Chen and I.D. Boyd *Monte Carlo Simulation of Silicon Thin Film Deposition using Supersonic Molecular Beams*, Rarefied Gas Dynamics, 573-578, Peking University Press 1997.
- [3] M.A. Gallis and J.K. Harvey *Direct Simulation of the Chemical Deposition of Silicon*, AIAA96-1816.
- [4] C.D. Robinson *Particle Simulations on Parallel Computers with Dynamic Load Balancing*, PhD Thesis, Imperial College, 1998.

Numerical Study of Pulsed Laser Sputtering into Diluted Background Gas *

T. E. Itina¹, A.A. Katasonov¹, A.N. Rouminsky¹,
W. Marine², M. Autric³

¹ Central Scientific Research Institute of Machine Building (TSNIIMASH),
Moscow Region, Russia

² Laboratoire Interdisciplinaire Ablation Laser et Applications, CNRS, France

³ IRPHE- LP3, UMR, CNRS, Marseilles, France

Pulsed laser deposition (PLD) is known to be a promising technique for growth thin films. The development of PLD technology requires investigation of pulsed laser sputtering process both in vacuum and into rarefied ambient gas. Due to the absence of thermal equilibrium at the evaporation stage and during the transport of energetic ablated particles through background gas toward the substrate, kinetic study is necessary in order to consider these phenomena.

In this paper, we present the results of a three-dimensional simulation of pulsed laser sputtering, where Monte Carlo methods are used allowing to study both the formation of a cloud of interacting particles and its free-expansion into diluted Maxwell-distributed gas. The attention is focused on the influence of both collisions of ablated particles and that of the ambient gas on the characteristics of the deposited particles under various initial and experimental conditions.

In particular, we compare the results of calculations where the ablation from a finite area (with different dimensions) and initial collision stage followed by the transport of non-interactive particles in diluted ambient gas were simulated with the results obtained for a point source without simulation of the self-collisions stage and setting different initial velocity distributions (i.e., half-Maxwell, Maxwell-Boltzmann with flow velocity, elliptical Maxwell-Boltzmann). The simulation results show, that at sufficient background pressure initial conditions are concealed due to thermalization of the ablated particles and their random scattering in collisions with the ambient gas.

In addition, we investigate the role of a diluted background gas in formation of film thickness profiles for several experimental conditions like plume tilting, ambient gas flow, deposition on a substrate placed parallel to the surface normal, etc. The deposition profiles and energy distributions are found to be considerably affected by the increase of the ambient gas pressure.

The study presents particular interest not only for PLD, but also for other deposition techniques, as heavy-ion sputtering, magnetron discharge, etc., where diluted ambient gases are used. In these techniques, the influence of the background gas is important since it defines the shape of the deposition profiles, the deposition rate and the kinetic energy of particles affecting the structure and quality of thin films.

*Abstract 6811 submitted to the 21st International Symposium on Rarefied Gas Dynamics, Marseille, France, July 26-31, 1998

IONIZATION AND RADIATION - IR 1

ROOM MARION

TUESDAY, JULY 28, 1998

14:35

Nonequilibrium Radiation Spectra Behind Strong Shock Waves in Low-Density Air *

T. Morioka, N. Sakurai, K. Maeno, H. Honma

Graduate School of Science and Technology, Chiba University, Chiba, Japan

1 Introduction

Thermal protection of a reentry vehicle under hypervelocity conditions is one of the most important problems. In the MUSES-C mission [1], which is in development at the Institute of Space and Astronautical Science (ISAS) of Japan, the reentry capsule enters directly the earth's atmosphere from hyperbolic trajectory. The reentry velocity is expected 12.5 km/s at altitude 100 km. Under the extreme condition, radiative heating to the capsule isn't negligible. Furthermore, due to the lack of data at hypervelocity more than 10 km/s, it is necessary to study experimentally.

In Chiba University, several experimental studies on the radiation behind strong shock waves in air have been done [2], [3]. Some interesting features have been observed for the total radiation and the spectral radiation.

In the present paper, in order to elucidate the contribution of spectral radiation to total radiation, simultaneous measurements are conducted for the time-frozen total radiation and the time-resolved spectral radiation behind strong shock waves in low-density air, whose velocities range from 9 km/s to 12.1 km/s at the initial pressure 13.3 Pa.

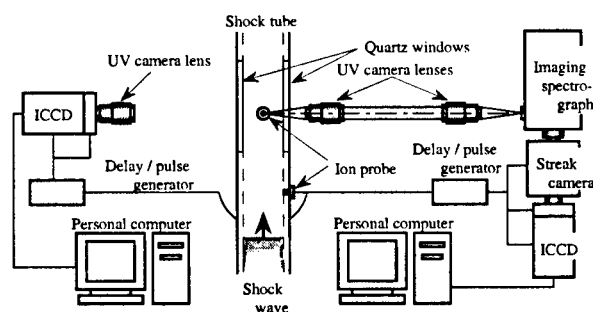


Figure 1: Layout of the diagnostic system for radiation behind strong shock waves

*Abstract 5581 submitted to the 21st International Symposium on Rarefied Gas Dynamics, Marseille, France, July 26-31, 1998

2 Diagnostic systems

A free-piston, double-diaphragm shock tube is used to generate strong shock waves in low-density air. The shock speeds of 9 km/s to 12.1 km/s are obtained for the initial pressure of 13.3 Pa. Figure 1 shows the layout of the diagnostic system, which consists of the observation systems for time-frozen total radiation on the left side of the shock tube and for time-resolved spectral radiation on the right side.

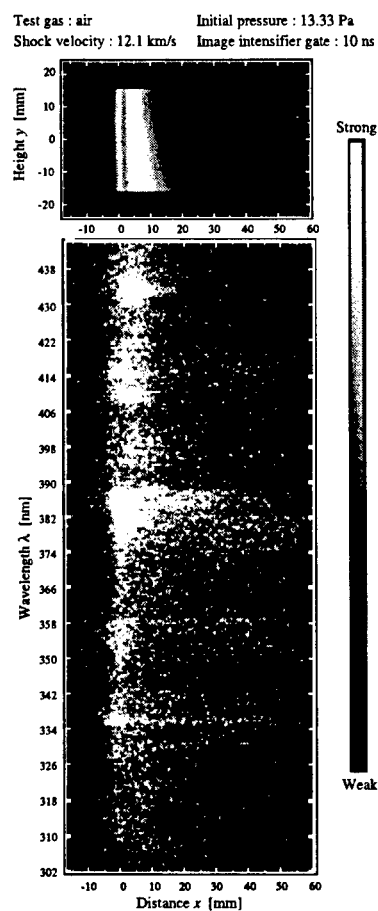


Figure 2: Total and the broadband spectral radiation

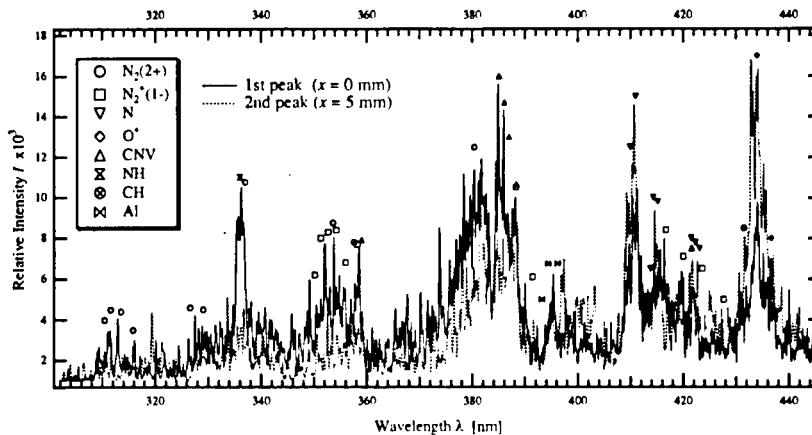


Figure 3: Radiation spectra integrated for 200 ns centered at the 1st peak and at the 2nd peak of the total radiation in case of Fig.2

3 Results and discussion

Figure 2 shows a time-frozen, two-dimensional total radiation image (upper) and a broadband streak image (lower) obtained by using the diagnostic systems as shown in Fig.1, for the shock velocity 12.1 km/s in the initial pressure 13.3 Pa. The wavelength range indicated at the streak image is from 302 nm to 444 nm. This streak image are constructed by seven streak image which are obtained in different wavelength range. In the seven run, the shock velocities are reproducible within 0.6 %. Also, the total radiation image is selected one of them. The ordinate is corresponding to distance in mm as the origin at which the total radiation profile indicates a peak just behind the shock front (so-called first-peak). As seen from the total radiation image, the radiation profile has two peaks along the center line ($y = 0$ mm). From comparison among these images, the spectral radiation in the wavelength range begins to emit simultaneously with the total radiation.

Figure 3 shows the radiation spectra in the wavelength range from 302 nm to 444 nm obtained from Fig.2. The solid and dotted lines are the radiation spectra centered at the first peak ($x = 0$ mm) and the second peak ($x = 5$ mm) of the total radiation profile, respectively, integrated for 200 ns time interval. As seen in this figure, the $N_2^+(1-)$ and the CN violet band system are distinctive around first peak. On the other hand, around second peak, spectral lines due to N and O^+ , which are observed in the wavelength range from 410 nm to 440 nm, become relatively strong. In this wavelength range, it is expected that the Balmer series in H ($H_\delta: \lambda =$

410 nm and $H_\gamma: \lambda = 434$ nm) are also overlapped.

4 Conclusion

The observation of nonequilibrium radiation behind strong shock waves in low-density air is carried out. The conclusion is following as:

- The contribution of spectral radiation to total radiation is found by using the diagnostic systems which can observe simultaneously time-frozen total radiation and time-resolved spectral radiation.
- The radiation spectra due to N, O^+ and H are distinctive around the second peak, while the band spectra due to $N_2^+(1-)$ and CNV around the first peak of the total radiation profile, for which the shock velocity is more than 11.3 km/s.

References

- [1] The Institute of Space and Astronautical Science, *A Program of Exploring an Asteroid(MUSES-C), The Proposal*, 1995.
- [2] Honma H. et al., *Observation of Radiation Behind Strong Shock Waves in Air*, Theoretical and Applied Mech., Vol.45, Yagawa G., Ohtsubo H. Editors, pp.231-239, 1996.
- [3] Morioka T. et al., *Imaging Spectroscopy of Radiation Behind Strong Shock Waves in Air*, Theoretical and Applied Mech., Vol.46, Yagawa G., Miki C. Editors, pp.307-315, 1997.

Emission Spectroscopy of Nonequilibrium Radiation from behind Shock Waves at Super-orbital Reentry Velocity *

K. Fujita¹, S. Sato¹, Y. Ebinuma², T. Abe¹

¹ The Institute of Space and Astronautical Science, Kanagawa, Japan

² Aoyama Gakuin Univ., Graduate School

1 Introduction

An asteroid sample return mission (MUSES-C) has been planned by The Institute of Space and Astronautical Science for launch at the beginning of 2002. The reentry vehicle is currently designed to reenter the earth atmosphere directly from the interplanetary orbit in order to reduce the system mass, which in turn increases the aerodynamic heating rate of the vehicle. Investigation of nonequilibrium thermochemical phenomena behind a strong shock wave is of great importance for designing the thermal protection system.

Several thermochemical models proposed for this field of problems so far are known to show plausible agreement with the experiment at the moderate shock speed below 8 km/s. However, if we apply these models to the shock speed above 10 km/s in the rarefied atmosphere, the calculated results show significant differences in some cases. Especially the radiative heating, whose contribution to the total heating of the vehicle increases in this flight regime, varies by an order of magnitude according to the thermochemical models [1]. It seems that the nonequilibrium thermochemical phenomena behind a strong shock wave have not yet well-understood for the shock speed range above 10 km/s in the rarefied atmospheric region.

2 Imaging Spectroscopy

Experimental investigations are conducted using a free-piston double-diaphragms shock tube which can generate a strong shock wave at a velocity of 14 km/s propagating into the background air at 0.3 torr. Density discontinuity of the shock wave, which has a spread width of several millimeters due to the low background pressure, is detected by the laser

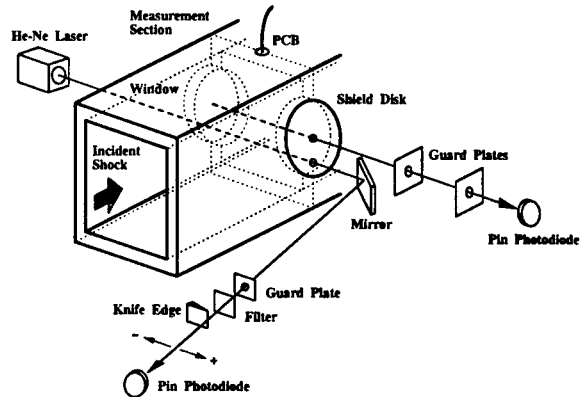


Figure 1: Experimental setup of laser schlieren system.

schlieren system shown in Fig.1.

Thermochemical information behind the shock wave has been obtained by one-dimensional imaging spectroscopy. A one-dimensional radiation image along the center axis of the measurement section is focused by a quartz lens on an objective slit of a spectrometer. This linear radiation image is then separated into its spectral components by the imaging optics, which generate a two-dimensional spectral \times spatial image on a photosensitive surface of a CCD camera attached to the spectrometer. Spatial resolution of this system is 0.7 mm at the objective slit, while spectral resolution is 2.5 nm in the present experiment. A typical example of the CCD image is shown in Fig. 2 for $P_0 = 0.3$ torr and $V = 12.0$ km/s. Using laser schlieren system simultaneously, we obtain the spatial variation of spectra with respect to the shock wave.

The shock tube is driven using the simulated air composed of 78.7-% nitrogen and 21.3-% oxygen in mole fraction. Figure 3 shows spectral distributions at 1, 2, 3, and 4 mm behind the density front. The incident shock speed and the background pressure are 12.0 km/s and 0.3 torr, respectively. Emission

*Abstract 1817 submitted to the 21st International Symposium on Rarefied Gas Dynamics, Marseille, France, July 26-31, 1998

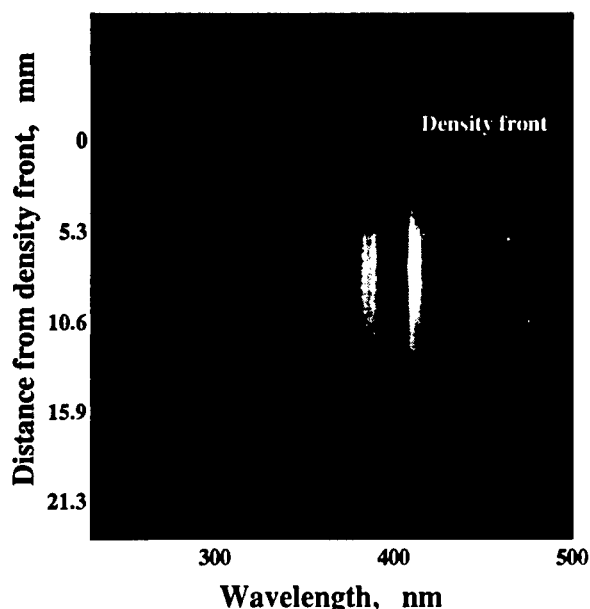


Figure 2: Spectral \times spatial image on CCD ($P_0 = 0.3$ torr and $V = 12.0$ km/s).

from 1 mm behind the density front is relatively weak, mainly composed of the Schumann-Runge system of O_2 and the second positive system of N_2 . With increasing the distance from the density front, emission of the first negative system of N_2^+ begins to dominate. These facts suggest strong chemical nonequilibrium just behind the shock wave. In contrast, in the region far behind the density front, atomic line spectra contribute to the major part of emission in this spectral range, as shown in Fig. 4.

3 Numerical Method

A radiation computation program called SPRADIAN is developed to quantitatively determine physical properties such as level population and temperatures from the experimental spectra[2]. The numerical procedure is currently at the final phase of development, and we have already obtained several results of the electric temperature and molecular vibrational population, though they are not shown here. We are also trying to develop a computer program in which rarefied gasdynamics and nonequilibrium chemistry are taken into consideration. Detailed description of these procedure and results will be shown at the following paper and presentation.

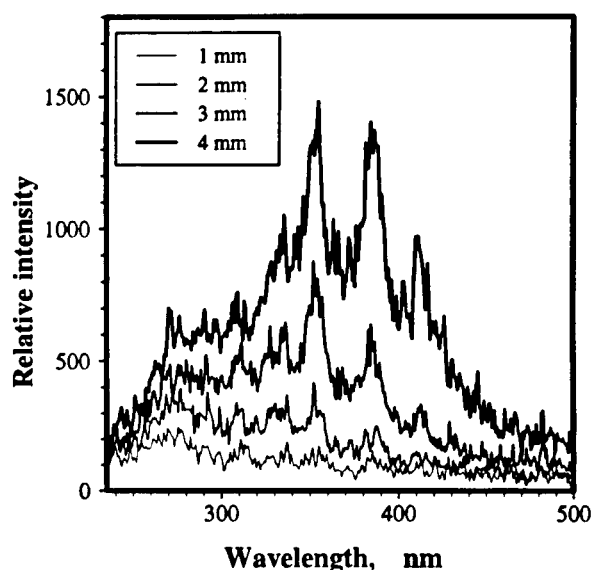


Figure 3: Spectra just behind the density front ($P_0 = 0.3$ torr and $V = 12.0$ km/s).

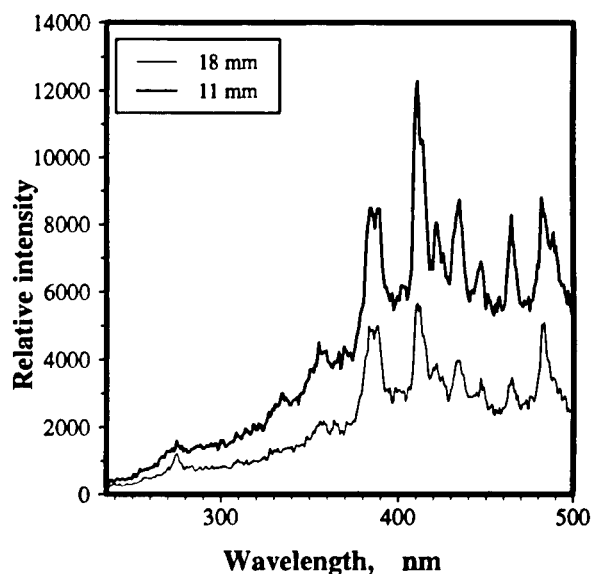


Figure 4: Spectra far behind the density front ($P_0 = 0.3$ torr and $V = 12.0$ km/s).

References

- [1] Fujita, K., Abe, T., and Suzuki, K., "Air Radiation Analysis of a Superorbital Reentry Vehicle," AIAA Paper 97-2561, 1997.
- [2] Fujita, K. and Takashi, A., "SPRADIAN, Structured Package for Radiation Analysis: Theory and Application," The Institute of Space and Astronautical Science Report No.669, September, 1997.

Infra-red and Visible Optical Emission Spectroscopy in a CO₂ Plasma Flow *

W. Röck¹, V. Lago¹, S. Pellerin², J. Koulidiati³, M. Dudeck^{1,4}

¹ Laboratoire d'Aérodynamique du CNRS, Meudon, France

² Groupe de Recherche sur l'Energétique des Milieux Ionisés, Univ. d'Orléans, France

³ Université de Ougadougou, Département de Physique, Ougadougou, Burkina-Faso

⁴ Université Pierre et Marie Curie (Paris 6), Paris, France

Low pressure and high temperature carbon dioxide gas flows are studied in ground test facilities to simulate the plasma conditions appearing around a spacecraft entering the atmosphere of Mars at high altitudes and high velocities. The knowledge of the plasma conditions is necessary for the analysis of the radio transmission perturbations, of the gas composition near the probe and the plasma-wall interactions.

In the laboratory of Aérodynamique at the CNRS a vacuum chamber is equipped with a plasma generator. The injected gas is heated by an electric arc and accelerated through a nozzle. It is partly dissociated and ionised. With pure CO₂ or with a CO₂-N₂ gas mixture corresponding to the composition of the Martian atmosphere a plasma flow at stationary conditions is produced. Previous mass spectrometry measurements in [1] showed that in such a plasma the main mole fractions of neutral particles are due to CO₂, CO, O₂ and N₂, NO⁺, O₂⁺ and CO₂⁺ were the most abundant ionized particles which could be detected. Only small fractions of CN, C₂, C⁺ and N⁺ were found.

Two different spectrographs are available to investigate the emitting particles in a wide spectral range. In the ultraviolet and visible range from 200 - 750 nm a monochromator with a focal length of 1.5 m and equipped with an OMA is used. Emission of CN, C₂, N, O and C should occur in this range in some amount [2]. These are well-known species and rotational and vibrational temperatures can be calculated from the spectra of the molecules and the electronic excitation temperature can be deduced from the atomic lines. For the spectral measurements in the infrared range between 1000 nm and 5000 nm a monochromator with a focal length of

110 mm and a PbSe or an InSb detector is available. In this range excited CO and CO₂ molecule emit radiation. Most of the spectroscopic constants for these two molecules were obtained with measurements at atmospheric conditions and low temperatures. At higher temperatures more vibrational and rotational transitions will appear which may not be included in existing data bases such as HITRAN [3]. By comparison between experimental and calculated CO and CO₂ spectra the rotational and vibrational temperatures of these species can be evaluated. These results will be compared to the temperatures received with the high resolved spectra in the ultraviolet and visible range.

The purpose of the proposed paper is to characterise the plasma jet simulating the conditions around a vehicle entering the Martian atmosphere by spectroscopic means over a wide wavelength range.

References

- [1] Schönemann A. T., Lago V., Dudeck M., *Investigation of CO₂ and CH₄ Containing Arcjet Plasma with Mass Spectrometry and Optical Emission Spectroscopy*, AIAA 95-1959, 26th Plasmadynamics and Laser Conference, San Diego, June 1995.
- [2] Park C., Howe J. T., Laffe R. L., Candler G. V., *Review of Chemical-Kinetic Problems of Future NASA Missions, II: Mars Entries*, Journal of Thermophysics and Heat Transfer, Vol. 8, No. 1, January-March 1994, pp.9-23.
- [3] Rothman L. S., Hawkins R. L., Wattson R. B., Gamache R. R., *Energy Levels, Intensities, and Linewidths of Atmospheric Carbon Dioxide Bands*, J. Quant. Spectrosc. Radiat. Transfer, Vol. 48, No. 5/6, 1992, pp. 537-566.

* Abstract 3167 submitted to the 21st International Symposium on Rarefied Gas Dynamics, Marseille, France, July 26-31, 1998

Investigation of a Low Pressure Supersonic Turbulent Argon Plasma Jet with Electrostatic Probes *

L. Leborgne, B. Van Ootegem, P. Vervisch
UMR 6614 CORIA, Université de Rouen, France

1 Introduction

In the trailing wake of supersonic missile afterbody, electron density fluctuations are strong enough to be responsible of a significant electromagnetic signature. For a better understanding of this electron density behaviour, we study a high speed turbulent plasma jet. This behaviour is determined by several interaction processes. Especially, coupling between kinetics and turbulence seems to be of great importance. In order to focus on this interaction, the argon gas has been chosen for its well-known simple chemistry.

The electronic density measurements were performed in the laboratory H. F. wind tunnel (fig 1).

The plasma is produced at 300 mbar by a 1.70 MHz frequency inductive torch. The argon gas is injected in a water cooled double-wall quartz chamber. The injected power is 45 kW for a flow rate of 0.9 g.s^{-1} . After a water-cooled copper cylindrical convergent nozzle, the plasma jet is expanded in a vacuum test chamber at a pressure of 50 mbar. The supersonic jet has a spatial periodic structure (four nodes). After this structure, the jet becomes wider and turbulent.

The electron density and temperature are measured by a fast sweeping Langmuir probes method that we developed. It consists in doubling the measuring circuit by a balanced circuit wich supplies a dummy probe. This probe is outside the test-chamber and its signal is analogically differentiated to the measuring probe signal. This method reduces significantly the noise that is induced by the RC characteristics of coaxial cables when the sweeping frequency increases [1]. This technique allows to obtain I-V characteristic curves for a 100 kHz scanning frequency. In order to avoid the hysteresis effects, the sweeping frequency is 10 % lower to the ion plasma frequency (2 MHz) [2]. Then it is possible

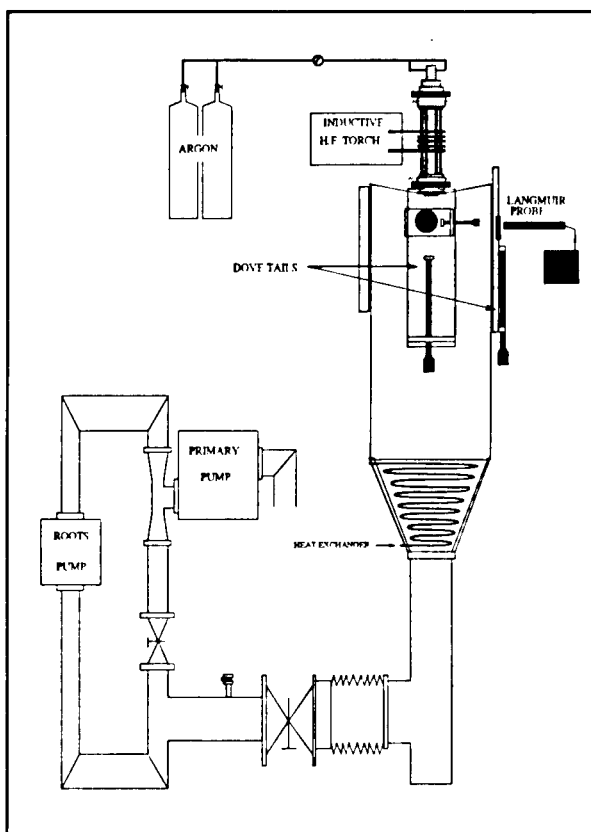


Figure 1: Experimental facility

to measure the instantaneous (N_e, T_e) couple.

To determine electron density fluctuations on a long time scale, a continuous voltage close to the plasma potential was applied to the electrostatic probes. Measurement signals were acquired at a time of 2 ms with a 0.5 MHz sampling frequency. These data were statistically treated (mean electron density, standard deviation ...).

For both applications, the probe is a 0.2 mm diameter, 1.5 mm long tungsten round tip, insulated by an alumina tube. The axial exploration is carried out using a dove tail, as shown in figure 1. The radial exploration is carried out by the setting of

*Abstract 6723 submitted to the 21st International Symposium on Rarefied Gas Dynamics, Marseille, France, July 26-31, 1998

the probe with a piston the stroke of which is adjustable.

2 Results and discussion

The electron temperature is on the average equal to 10000 K in all the jet. This value is significant compared to the mean kinetic temperature which is on the average equal to 1000 K. Therefore, the thermal nonequilibrium is important. This phenomenon is specific to argon and has been observed in different inductive torches [3]. This is due to the well known Ramsauer effect in $Ar - e$ collisions.

The measurements of the electron density allow to visualize on the jet edge the formation of a turbulent mixing layer. The latter opens out owing to the turbulence and invades through the jet progressively.

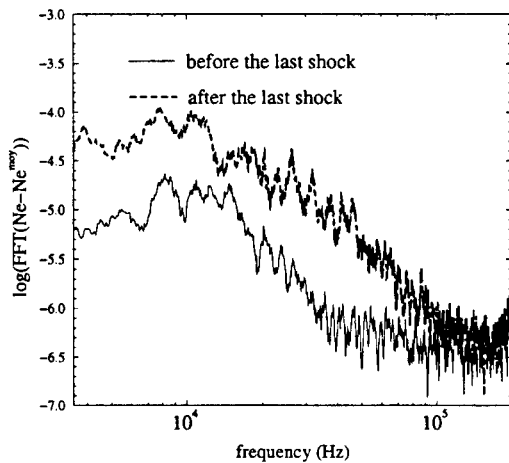


Figure 2: Fourier spectrum of the electron density fluctuations

The passage of the shock increases the turbulence, as illustrated in figure 2. For the Fourier spectrum obtained after the shock, the 15 kHz-80 kHz frequency range contribution is more important than for the Fourier spectrum obtained before the shock. This is accompanied by a turbulence intensity increase which is put forward by the electronic density fluctuation absolute value.

Figure 3 shows the axial evolution of the electron density after the last shock, which is located at 53 mm from the nozzle exit. The electron density standard deviation σ_{N_e} increases rapidly and for $x \geq 120$ mm is equal to the electron density. Then the fluctuation rate σ_{N_e}/N_e^{moy} becomes

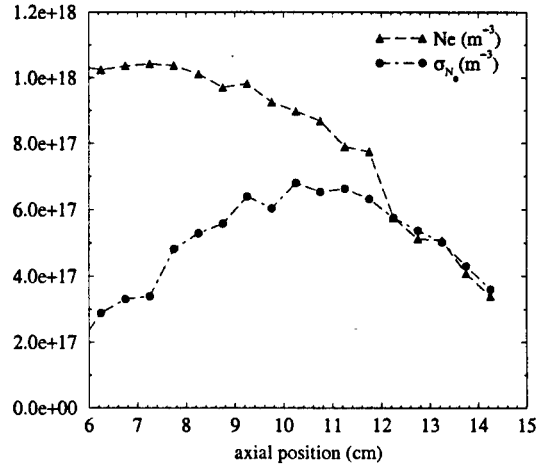


Figure 3: Axial profile of electron density and its standard deviation

rapidly strong. It grows up from 20 % to 80 % between $x = 6$ mm and $x = 10$ mm. At the end of the jet, the fluctuation rate is equal to 100 %.

Currently, similar measurements by Rayleigh Scattering are underway to obtain the total density fluctuations in the plasma jet.

In conclusion, this work shows the influence of the shock on the turbulence. The electron density behaviour in a high velocity turbulent argon plasma jet was measured. The electron density fluctuations are very strong (up to 100 %).

This work was sponsored by the Commissariat à l'Energie Atomique (C.E.A. C.E.S.T.A.).

References

- [1] L. Leborgne, J.C. Goulet, B. Van Ootegem, P. Vervisch *A 30 kHz - 1 MHz fast sweeping method for Langmuir probes applied to turbulent plasmas*, ICPIG XXIII July 1997.
- [2] R. Deutsch, E. Räuchle, *Hysteresis effects in the plasma-electrode boundary sheath for frequencies of the order of the ion plasma frequency*, *Plam. Chem. Plasm. Proc.*, Vol.11, No.4, pp.501-512, 1991.
- [3] M. Dresvin, *Analysis of deviation from thermal and ionization equilibrium in an argon plasma flow*, *Compte rendu de réunion du club "Chimie des hautes températures (plasma)"*, EDF, 1997.

Kinetic Model for Electrons and Heavy-particles in Low-pressure O₂-N₂ Microwave Discharges *

V. Guerra and J. Loureiro

Centro de Física de Plasmas e Departamento de Física
Instituto Superior Técnico, 1096 Lisboa Codex, Portugal

Great interest has been devoted in the last few years to the study of low pressure microwave discharges in O₂ and O₂-N₂, since these discharges can produce active species with interest for etching and material treatments, namely O(³P) and N(⁴S) atoms, O₂(a ¹Δ_g) metastables, and NO, NO₂ and N₂O nitric oxides. In particular, in the case of fabrication of SiO₂ films, it has been found that the silicon oxidation rate can be largely increased by the microwave excitation of O₂ gas and to be further enhanced by the addition of N₂ to O₂ in the discharge [1].

In this paper we report the results from a self-consistent kinetic model for a low-pressure O₂-N₂ microwave discharge in a quartz tube, at 433 and 2450 MHz, and a comparison with previous published data is carried out [2,3]. The model is based on the coupled solutions to the homogeneous electron Boltzmann equation, under the effective field approximation [4], and a system of kinetic master equations for the populations of the various neutral and ionic species created in a O₂-N₂ discharge (e.g., vibrational excited molecules O₂(X ³Σ_g⁻, v) and N₂(X ¹Σ_g⁺, v'); metastables species O₂(a ¹Δ_g), N₂(A ³Σ_u⁺, N₂(a' ¹Σ_u⁻), etc; radiative states N₂(B ³Π_g), etc; O(³P) and N(⁴S) atoms; positive and negative ions O₂⁺, O⁺, NO⁺, N₂⁺, N₄⁺ and O⁻; and NO and O₃ species).

Both volume and surface processes are considered in the model. In what concerns the latter, the wall recombination of O(³P) and N(⁴S) atoms and the deactivation of O₂(b ¹Σ_g⁺) and N₂(X ¹Σ_g⁺, v') molecules have been included. In the case of recombination of O(³P) atoms on the quartz surface, a Monte Carlo simulation of a sequence of elementary processes has been used to describe the wall mechanisms, including steps for atomic and dissociative adsorption, desorption and diffusion of physisorbed atoms on the adsorption layer, and both recombina-

tion between a physisorbed and a chemisorbed atom and between a gas phase and a chemisorbed atom [5]. On the other hand, the reduced electric field for the discharge maintenance is derived from the solutions to the continuity and transport equations for the charged particles in the framework of a theory valid for electronegative gases due to the presence of ions O⁻ [6].

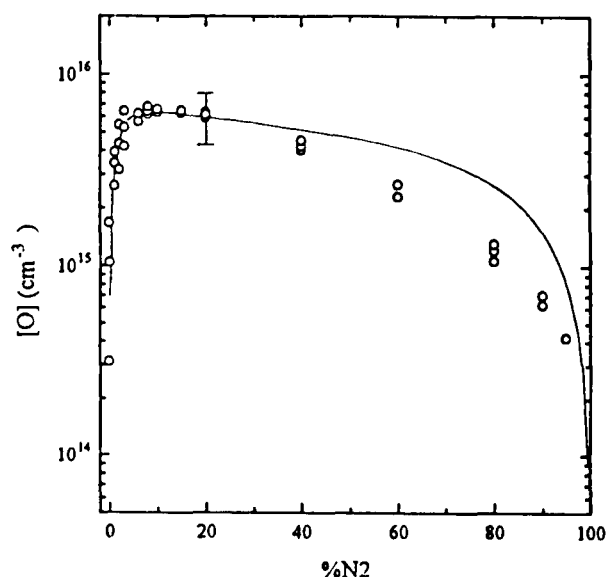


Figure 1: Concentration of O(³P) atoms against the relative concentration of nitrogen in a O₂-N₂ mixture.

Fig.1 shows the concentration of O(³P) atoms calculated in this work and measured in [2,3], for a O₂-N₂ microwave discharge at 2.45 GHz and p=1 Torr, in a 0.8 cm inner radius quartz tube. The kinetics of O atoms is extremely simple when compared with the kinetics of other active species. The atoms are mainly created by electron impact on O₂(X ³Σ_g⁻) and O₂(a ¹Δ_g) molecules and lost by recombination on the tube walls, so that the in-

*Abstract 4781 submitted to the 21st International Symposium on Rarefied Gas Dynamics, Marseille, France, July 26-31, 1998

crease observed in $[O]$ when low concentrations of N_2 as small as 2% are added to O_2 , results from a decrease of the wall recombination probability of O atoms, *i.e.* from surface processes, rather than from an enhancement of the dissociation rate. We note that our calculations show that the modifications on the electron dissociation rate are always vanishingly small for relative N_2 concentrations in the range 0–20%.

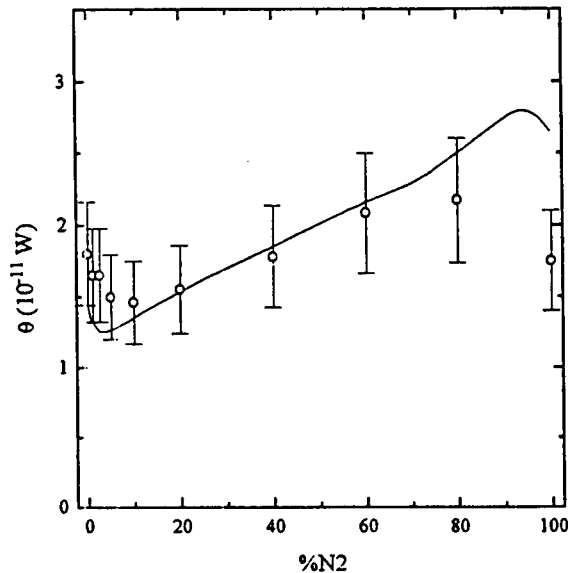


Figure 2: Mean absorbed power per electron against the relative concentration of nitrogen in a O_2 - N_2 mixture.

Fig.2 shows the mean input power absorbed by the electrons from the field per electron, θ , for the same conditions as in Fig.1, along with measurements taken from [3]. The decrease in θ with the addition of very small N_2 percentages results from the increasing contribution of $O(^3P)$ ionization to the total ionization rate, since the electron ionization cross section is larger in O than in $O_2(X)$ and due to the fact of the medium rapidly transforms into a O_2 - O plasma (see Fig.1). On the other hand, the increase in θ for N_2 percentages larger than $\approx 3\%$ is a consequence of a smaller ionization efficiency in N_2 owing to the higher electron-energy losses spent in N_2 excitation (*e.g.* in excitation of the manifold of vibrational levels $N_2(X^1\Sigma_g^+, v')$).

References

- [1] Y. Yasuda *et al* 1990 J.Appl.Phys. **67**(5) 2603.
- [2] A. Granier *et al* 1994 J.Appl.Phys. **75**(1) 104

- [3] R. Safari 1992 PhD Thesis *Université de Paris-Sud XI* (France).
- [4] P.A. Sá *et al* 1992 J.Phys.D: Appl.Phys. **25** 960.
- [5] V. Zvoníček *et al* 1997 Proc. 23th Int. Conf. on Phenom. in Ionized Gases, Toulouse (France), vol.4: p.160.
- [6] C.M. Ferreira *et al* 1988 J.Phys.D: Appl. Phys. **21** 1403.

Acknowledgment

This work has been carried out under the support of a PRAXIS XXI Research Grant (Portuguese Ministry of Science and Technology).

IONIZATION AND RADIATION - IR 2

ROOM MARION

WEDNESDAY, JULY 29, 1998

9:10

On the Numerical Resolution of an Ion / Electron Collision Operator of the Type Fokker-Planck Coupled with an Electronic Equation.*

C. Buet, St. Dellacherie, R. Sentis
Commissariat à l'Energie Atomique
Centre d'Etude de Bruyères le Châtel, France

1 Introduction : the model and its main properties

We consider a one species hot homogeneous plasma and study only the electron / ion interactions. The time scale is then the ion / electron collision time. The model consists of

- a Fokker-Planck equation for the ions,
- a macroscopic equation for the electronic temperature,
- the quasi-neutrality relations.

We then write the model in the following way (see [1])

$$\left\{ \begin{array}{l} \partial_t f(t, v) = S(f), \\ \frac{3}{2} \frac{d}{dt} (N_e k T_e) = -3 \Omega N k (T_e - T), \\ N_e = ZN, \quad \vec{U}_e = \langle \vec{v} f \rangle / \langle f \rangle \\ \text{with } N = \langle f \rangle \quad \text{and} \quad kT = \langle m v^2 f \rangle / \langle f \rangle \end{array} \right.$$

where $\langle g \rangle \equiv \int g(v) dv$ in the continuous case and $\langle g \rangle \equiv \sum_j g(v_j) \Delta v$ in the discrete case. $f(t, v)$ is the ionic distribution, $\Omega(T_e) = C^{ste} / T_e^{3/2}$ is the collision frequencies and T_e is the electronic temperature; m , Z and k are respectively the atomic mass, the atomic number and the Boltzmann's constant. $S(f)$ describes the collisions between ions and electrons and is defined by

$$S(f) \equiv \Omega \nabla_v \cdot \left[(\vec{v} - \vec{U}_e) \cdot f(t, v) + \frac{k T_e}{m} \nabla_v f(t, v) \right]$$

in the *convection-diffusion form*. Denoting

$$\mathcal{M}_f(t, v) = \frac{N}{(2\pi k T_e / m)^{3/2}} \exp \left[-\frac{m(\vec{v} - \vec{U}_e)^2}{2k T_e} \right],$$

*Abstract 1466 submitted to the 21st International Symposium on Rarefied Gas Dynamics, Marseille, France, July 26-31, 1998

$S(f)$ can be written in the *Landau form*

$$S(f) \equiv \frac{\Omega k T_e}{m} \nabla_v \cdot \left[f(t, v) \nabla_v \log \left(\frac{f(t, v)}{\mathcal{M}_f(t, v)} \right) \right]$$

whose discretization naturally leads to a numerical version of the H theorem i.e.

$$\langle \log \left(\frac{f(t, v)}{\mathcal{M}_f(t, v)} \right) \cdot S(f) \rangle \leq 0$$

and

$$S(f) = 0 \iff f(t, v) = \mathcal{M}_f(t, v).$$

In this article, we present a new scheme solving the ion / electron collision operator expressed in the *convection-diffusion form*. It allows an easy implicit treatment of the diffusion part of $S(f)$. This numerical scheme has good properties similar to those found from a discretization of the Landau form (see for example [2], [3] and [4]).

2 Explicit resolution of the linear Fokker-Planck equation

In the second part, we propose a new numerical method to solve the linear Fokker-Planck equation (linear version of the ion / electron collision operator $S(f)$ in which \vec{U}_e , T_e and Ω are constants) in a cartesian geometry established from the *convection-diffusion form* (see above) and not from the *Landau form*.

To do so, we introduce the definition of the *entropic average* defined with

$$\begin{aligned} \tilde{f}_{x,y} &= \frac{f(x) - f(y)}{\log f(x) - \log f(y)} \text{ if } f(x) \neq f(y), \\ &= f(x) \text{ if not} \end{aligned}$$

which makes equivalent *from a numerical view point* the convection-diffusion form and the Landau form.

We prove that the explicit scheme proposed here converges toward thermodynamical equilibrium and that the numerical entropy decreases under a CFL criterium.

3 Explicit and semi-implicit resolution of the ion / electron collision operator

In the third part, after having proved that the semi-discretized scheme (i.e. continuous in time) converges toward the thermodynamical equilibrium, we show that the explicit scheme proposed to solve the linear Fokker-Planck equation has good properties in the case of the ion / electron collision operator too.

Indeed, this scheme preserves the mass, the impulsion, the energy of the plasma and the thermodynamical equilibrium. More over, we prove that, under a CFL criterium, this scheme preserves the positivity of the density f and of the temperature T_e and that the entropy decreases.

Because of all these good properties, we think that this new scheme can be at least compared to the schemes which use the Chang and Cooper method in the case of ion / electron collisions (see [5] and [6]).

After that, we describe the semi-implicit version of this scheme which preserves the mass, the impulsion, the energy and the thermodynamical equilibrium too.

4 Extension to the cylindrical geometry

In the fourth part, we show that the above results can be extended to the case of the cylindrical geometry. This extension is important because, in the field of Inertial Confinement Fusion, we solve the collision operators in this geometry.

5 Numerical results and conclusion

In the last part, we present numerical results which prove that the semi-implicit scheme in the case of the cartesian geometry is good.

References

- [1] M. Casanova, O. Larroche and J.P. Matte, *Kinetic Simulation of a Collisional Shock Wave in a Plasma*, Physical Review Letter, Volume 67, Number 16, October 1991.
- [2] Yu. A. Berezin, V. N. Khudick and M. S. Pekker, *Conservative Finite-Difference Schemes for the Fokker-Planck Equation Not Violating the Law of an Increasing Entropy*, Journal of Computational Physics, Volume 69, Number 1, March 1987. C. Buet and St.
- [3] C. Buet and St. Cordier, *Numerical Analysis of Conservative and Entropy Schemes for the Fokker-Planck-Landau Equation*, private communication, submitted to SIAM, Journal of Numerical Analysis, 1997.
- [4] C. Buet and St. Cordier, *Conservative and Entropy Numerical Scheme for the Isotropic Fokker-Planck-Landau Equation*, private communication, submitted to SIAM, Journal of Numerical Analysis, 1997.
- [5] J.S. Chang and G. Cooper, *A Practical Difference Scheme for Fokker-Planck Equations*, Journal of Computational Physics 6, 1, 1970
- [6] V.A. Mousseau and D.A. Knoll, *Fully Implicit Kinetic Solution of Collisional Plasmas*, Journal of Computational Physics 136, 308-323, 1997.

A discrete velocity model describing the cooling of an atomic beam by means of laser light *

C. Reitshammer¹, A. Rossani², F. Schürer¹

¹ Institut für Theoretische Physik, Technische Universität Graz, Austria

² Dipartimento di Matematica, Politecnico di Torino, Italy

1 Introduction

Slowing and trapping of neutral atoms by means of resonant laser light has become an important field over the last few years. Different methods, like the Stark effect cooling or the Zeeman effect cooling have been used to control the velocity and position of atoms and ions.

Up to now the problem of laser cooling has been treated mainly with quantum mechanical tools. Our aim, however, is to tackle the problem from a statistical point of view. Such a consideration has the advantage to get new, direct insights into the space-dependent velocity distribution of the slowed atoms.

The physical system consists of ground level atoms A , excited atoms A^* and photons p . Atoms and photons interact within an infinite slab $x \in [0, L]$. At a position $x = 0$ and for $y \in [-h_1, h_1]$, particles A are continuously injected with a direction normal to the slab. These atoms follow a given distribution. At a position $x = L$ and for $y \in [-h_2, h_2]$, where $h_2 > h_1$, photons at a fixed frequency ν_L are continuously injected within a direction normal to the slab counter-propagating to the atoms. Within the slab, only the following interaction events are considered:

1. Absorption: $A + p \rightarrow A^*$
2. Spontaneous emission: $A^* \rightarrow A + p'$
3. Stimulated emission: $A^* + p \rightarrow A + 2p$

Due to the Doppler effect, a shifted frequency

$$\nu'_L = \nu_L \left(1 + \frac{v_x}{c} \right) \quad (1)$$

is seen by moving atoms, where $v_x = \mathbf{v} \cdot \mathbf{i}$, and c is the speed of light. Hence, only a few atoms within

a velocity interval $v_{res} \pm \Delta v$ are able to interact with photons. We, however, want to slow down almost all atoms within the slab and for this reason, for $x \in [0, L]$ an electric field $\mathbf{E}(x) = \mathbf{j}E(x)$ is introduced to compensate the Doppler effect. Here \mathbf{i} and \mathbf{j} are unit vectors in x - and y -direction, respectively. Due to the Stark effect the internal energy jump E_{12} depends on x through $E(x)$ so that the transition frequency ν_0 becomes a function of x : $\nu_0(x) = E_{12}(x)/h$, where h is Planck's constant. We assume that $E_{12}(x)$ is a given, monotonically decreasing function of x , for example,

$$E_{12}(x) = c_1(1 - c_2 x), \quad (2)$$

with positive constants c_1 and c_2 .

By folding the laser and the atomic profile, we obtain the cross section like function

$$b(x, v_x) = \nu_2 \frac{B_{12} c}{4\pi^2 \nu_L} \times \left\{ \left[v_x - v_{max} \left(1 - \frac{x}{L} \right) \right]^2 + v_2^2 \right\}^{-1}, \quad (3)$$

which regulates the interaction between atoms and photons within the slab.

2 Discrete velocity model

Instead of applying the full Boltzmann model [1], we discretize the velocity space [2] according to momentum transfer due to atom-photon interaction: $\mathbf{v}_{k,\ell} = (k\mathbf{i} + \ell\mathbf{j}) \Delta v$, where $k, \ell \in Z$, and $\Delta v = h\nu_L/mc$. This discretization leads to the following notation. The number density of particles A and A^* with velocity $\mathbf{v}_{k,\ell}$ are $N_{k,\ell}(x, y, t)$ and $N_{k,\ell}^*(x, y, t)$, respectively. The intensity $I(x, y, t)$, is the number of photons p per unit volume $\times ch\nu_L$ counter-propagating to the atoms. Furthermore, we are only interested in stationary solutions of the problem. Therefore, the kinetic equations for particles A and

* Abstract 2602 submitted to the 21st International Symposium on Rarefied Gas Dynamics, Marseille, France, July 26-31, 1998

A^* read:

$$\mathbf{v}_{k,\ell} \cdot \nabla N_{k,\ell} = \mathcal{J}_{k,\ell}^a(b_k) + \mathcal{J}_{k,\ell}^{sp} + \mathcal{J}_{k,\ell}^{st}(b_{k-1}), \quad (4)$$

$$\mathbf{v}_{k,\ell} \cdot \nabla N_{k,\ell}^* = \mathcal{J}_{k,\ell}^{a,*}(b_{k+1}) + \mathcal{J}_{k,\ell}^{sp,*} + \mathcal{J}_{k,\ell}^{st,*}(b_k), \quad (5)$$

where the $\mathcal{J}_{k,\ell}^e$ and $\mathcal{J}_{k,\ell}^{e,*}$, ($e = a, sp, st$), are the collision rates corresponding to the events (1), (2) and (3), and $b_k(x) = b(k\Delta v, x)$.

3 One-dimensional case

In a one-dimensional case atoms enter the deceleration path in direction x counter-propagating to the laser beam. We assume that spontaneous emission only occurs in direction x or $-x$ and that the laser intensity I is constant within the slab. Under these restrictions we can formulate the balance equations for atoms in the ground state:

$$k \Delta v \frac{d}{dx} N_k(x, y) = \frac{A_{12}}{2} (N_{k+1}^* + N_{k-1}^*) + b_{k-1}(x) I N_{k-1}^* - b_k(x) I N_k, \quad (6)$$

and the excited state:

$$k \Delta v \frac{d}{dx} N_k^*(x, y) = b_{k+1}(x) I N_{k+1} - A_{12} N_k^* - b_k(x) I N_k^*. \quad (7)$$

In order to obtain a system of coupled differential equations with constant coefficients, we divide the deceleration path into $k_0 = v_{\max}/\Delta v$ layers with a thickness of $\Delta x = L/k_0$. In each layer of the deceleration path, only atoms within the resonance range are able to interact with photons. The probability of an interaction is given by $b_k(x)$. All other atoms are not affected, i.e. the corresponding number densities do not change. This fact reduces the number of differential equations dramatically. The reduced system corresponding to the j -th layer can be written as

$$\frac{d}{dx} \hat{\mathbf{N}}^{(j)} = M^{(j)} \cdot \hat{\mathbf{N}}^{(j)}, \quad (8)$$

where $\hat{\mathbf{N}}^{(j)}$ is a vector including only the number densities of affected atoms in the ground state and in the excited state. The sparse coefficient matrix $M^{(j)}$ results from the coupled systems (Eq. (6) and Eq. (7)) of differential equations, however, in its reduced form. Calculating the eigenvalues $z_n^{(j)}$ and the eigenvectors $\mathbf{V}_n^{(j)}$ of the matrix $M^{(j)}$, we obtain the following solution vector

$$\hat{\mathbf{N}}^{(j)}(x') = \sum_{n=1}^S c_n^{(j)} \mathbf{V}_n^{(j)} \exp(z_n^{(j)} x'), \quad (9)$$

where S is the size of the matrix depending on the chosen discretization.

This formalism gives not only a straightforward intuitive interpretation of resonant radiation pressure, allowing us to visualize the random walk and internal dynamics of an atom in a propagating external light wave, but also shows us how to implement this picture in a numerical simulation of the distribution function. We also investigate the effect of the laser intensity on the distribution function.

4 Results

In saturation, i.e. when intensity is sufficiently high, all atoms are slowed and caught in a so-called cooling peak. We obtain a corresponding temperature of $T = 1010 \mu K$, which is in good agreement with quantum mechanical calculations.

For lower intensities not all atoms within the resonance range interact with photons. Figure 1 shows the change of the given Maxwell distribution during the cooling process.

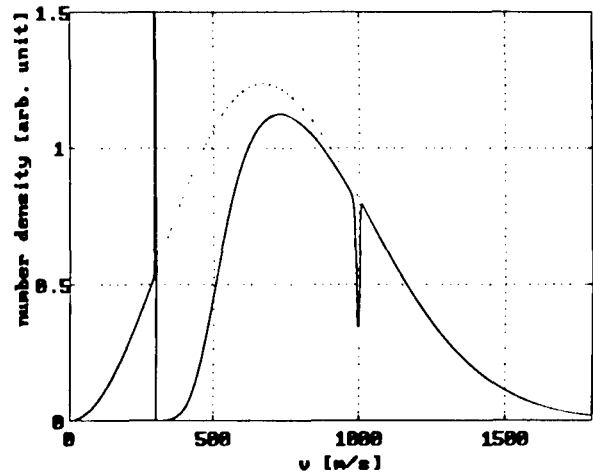


Figure 1: Velocity distribution of ground level atoms (solid curve) at the end of the cooling path for $I = 18 W/m^2$. The dotted curve is the original Maxwell distribution.

References

- [1] A. Rossani, G. Spiga, and R. Monaco, *Mech. Research Comm.* **24**, 237 (1997).
- [2] R. Monaco and L. Preziosi, *Fluid Dynamic Applications of the Discrete Boltzmann Equation*, (World Scientific, London, Singapore, 1991).

Monte Carlo Direct Simulation of RF Discharge for Plasma Processing *

S.F. Gimelshein, V.A. Schweigert, M.S. Ivanov
Computational Aerodynamics Lab., ITAM SB RAS, Novosibirsk, Russia

1 Introduction

Several important areas of semiconductor manufacturing can be extracted where numerical modeling play a significant role [1]. First is an equipment design. As new equipment is often created using time-consuming and expensive trial-and-error procedure, modeling can be useful in order to reduce time and cost of this stage. Second is process optimization where modeling can be used in multi-parametric study of many process variables and input parameters. Finally, a validated model seems to be helpful for real-time process control aimed at the increasing of a process yield and a final chip yield.

Development, optimization and validation of numerical models are therefore indispensable in the way of further enhancements of plasma processing. The main goals of plasma process modeling can be summarized as follows: obtaining of credible information on growth/etch rate, film composition, uniformity, etch selectivity, anisotropy (for etching) and surface quality. These quantities are simply derived from the following data which have to be obtained from plasma process simulations: gas velocity, gas temperature, density of each neutral species, and electron and ion characteristics. The last mean electron and ion density, mean energy, directed velocity, and distribution functions. Finally, potential of electric field must be also computed.

2 Process equations

Many of modern plasma reactors operate at low gas pressures (millitorr range for etching and torr range for deposition reactors). For these pressures, the mean free path of neutrals, ions, and even electrons, becomes comparable with or exceeding other reference lengths, primarily the thickness of near-electrode layer. Kinetic approach therefore

should be used for numerical modeling of physics and chemistry in such reactors. The kinetic approach implies a self-consistent solution of a system of Boltzmann kinetic equations for distribution functions of neutrals $f_n(t, \vec{r}, \vec{v})$, ions $f_i(t, \vec{r}, \vec{v})$, and electrons $f_e(t, \vec{r}, \vec{v})$

$$\frac{\partial f_n}{\partial t} + \vec{v} \frac{\partial f_n}{\partial \vec{r}} = \sum_s J_{n,s}$$

$$\frac{\partial f_i}{\partial t} + \vec{v} \frac{\partial f_i}{\partial \vec{r}} + \frac{e Z_i \vec{E}}{m_i} \frac{\partial f_i}{\partial \vec{v}} = \sum_s J_{i,s},$$

$$\frac{\partial f_e}{\partial t} + \vec{v} \frac{\partial f_e}{\partial \vec{r}} - \frac{e \vec{E}}{m_e} \frac{\partial f_e}{\partial \vec{v}} = \sum_s J_{e,s},$$

along with the Poisson equation for electric field potential

$$\Delta \phi = 4\pi e (n_e - \sum_i Z_i n_i), \quad \vec{E} = -\frac{\partial \phi}{\partial \vec{r}}.$$

Here e , m_e are the charge and mass of electrons, $e Z_i$, m_i are the charge and mass of ions of i th species, and J_s are the collisional integrals for corresponding species.

3 Particle modeling

Particle modeling is a principal means to obtain kinetic information (distribution function, rates, etc.) in a self-consistent manner and to study the particle motion across the reactor volume in response to applied field. The most widely used technique for particle simulation is presently particle-in-cell/Monte Carlo collision (PIC/MCC) method. In this method, a set of test particles that substitute real ions and electrons is followed simultaneously. The test particles move in the background gas and experience collisions (elastic and inelastic) with gas particles. The common approximation for the background gas is the homogeneous equilibrium gas at rest [2] (in rare cases the neutral flow is computed in order to be used then in PIC/MCC computations).

*Abstract 4832 submitted to the 21st International Symposium on Rarefied Gas Dynamics, Marseille, France, July 26-31, 1998

One of assumptions of PIC/MCC method is the absence of the feedback from the test particles to the background gas. The role of this feedback has not been studied yet, though in some cases it may be significant due to both momentum and energy exchange (note here charge-exchange reactions as a source for background gas heating). The approach that enables one to consider the interconnection between charged and neutral particles is the Direct Simulation Monte Carlo (DSMC) method which seems to be the most general approach for particle modeling of plasma processes.

The DSMC method, which was first constructed phenomenologically by Bird [3], is conventionally regarded as a technique for the computer modeling of real gas by several thousands or millions of simulation molecules. Conversely, this method may be constructed directly from the Leontovich master kinetic equation for the N-particle distribution function [4]. Since the Boltzmann equation can be derived from the Leontovich equation for an N-particle system under the conditions of molecular chaos, the DSMC method may be regarded as a numerical method for solving the Boltzmann equation. A number of numerical schemes for the DSMC method based on the majorant frequency principle have been obtained in [4] directly from the master kinetic equation.

4 Subject and objectives

The main objective of the paper is the numerical comparison of PIC/MCC and DSMC methods for modeling the RF discharge in plasma reactors in one-dimensional and axysimmetric statements. The majorant scheme of the DSMC method is used in simulations which was extended for the case of charged particles (self-consistent modeling of the Boltzmann kinetic equation and the Poisson equation). The principal attention will be paid to the computation of gas density and composition throughout all the reactor, and the determination of distributions of gas dissociation rates and ion velocity distribution functions over the wafer processed, that is the data used for calculating growth/etch rate and anisotropy (in etching).

The application of particle methods to plasma simulation meets a number of problems. The main ones are

1. a considerable difference between the characteristic time required for the discharge stabilization, t_d , and characteristic times determining heavy particle and electron transport t_h , t_e ($t_d \gg t_h \gg t_e$);
2. large number of model particles required;

3. a large difference of concentrations of different species.

It is common knowledge that PIC/MCC schemes, as they stand today, are computationally very intensive. The DSMC approach is generally even more time-consuming, but the difference between two approaches is very small as compared with conventional fluid (moment equations) models.

An approach is therefore proposed to speed up discharge simulations. General plasma relaxation is split into fast relaxation of the electron distribution function and slow relaxation of the electron and ion density distributions. For each period of the RF discharge, the electron distribution function is determined for a fixed ion density distribution (only the electron transport is considered). Then, a much larger time step is used in order to compute the ion distribution function in average electric field at a fixed profile of gas ionization rate. To avoid the emergence of artificial charge at this stage, the average electron density is adjusted to keep the total charge constant. This approach allows one to reduce the simulation time by factor $10^1 \div 10^2$ depending on the gas pressure.

The RF discharge was computed for typical reactor conditions: generator frequency is 13.67 MHz, discharge voltage is 50 V with a sinusoidal voltage waveform. Gas consisted of Ar with pressure of about 1 Torr, ions Ar^+ and electrons e^- . A one-dimensional configuration is a good basis for comparative analysis, and the solution for this case is obtained by DSMC, PIC/MCC and fluid approaches. Note a considerable difference in electron density and mean energy for kinetic and continuum approaches. For axisymmetrical configuration, two kinetic approaches have been applied.

References

- [1] *Computational modeling in semiconductor processing*, edited by M. Meyyappan, Artech House, Boston-London, 1995, 363p.
- [2] Serikov V.V., Nanbu K. *3D Monte Carlo simulation of dc glow discharge for plasma-assisted material processing*, Proc. of 20th Symp. on RGD, Beijing, 1997, 829-834.
- [3] Bird G.A. *Molecular Gas Dynamics*, Clarendon Press, Oxford, 1976.
- [4] Ivanov M.S., Rogasinsky S.V. *Theoretical analysis of traditional and modern schemes of the DSMC method*, Proc. of 17th Symp. on RGD, Aachen, 1991, 629-642.

Ionised Gas Modelling with DSMC *

M. A. Gallis, J. K. Harvey

Dept. of Aeronautics, Imperial College of Science Technology and Medicine
London, England

1 Introduction

In this paper a new scheme to simulate plasma flows within the context of the Direct Simulation Monte Carlo (DSMC) method is developed. Particles are used for a conventional representation of atoms, ions and electrons. To calculate the electric field, the charge of flow is distributed to the nodes of the computational grid using a Cloud-in-Cell (CIC) technique. The electric field is then calculated by the solution of the Poisson equation over the computational domain. The new method is compared with theoretical predictions for simple flows and with experimental measurements for complicated flows.

2 Modelling of Ionised Flows

Free electrons move with speeds that are typically 3-4 orders of magnitude greater than the average speed of the particles. Such high speeds require a greatly reduced computational time step to deal specifically with electrons (which account for up to 10 % of the total number of particles in the flow) and this would impose a large overhead in the computation.

The approach adopted in this study is to model both ions and electrons as particles and move the electrons with their own time step and let them collide within the ion time step as many times needed to match the ion time step (Serikov and Nambu [?]). Since the mass of the electrons is smaller than the ion mass, two particle time steps are introduced in the code for each species. During the move phase of the code the electric and the magnetic fields are calculated to update the charged particle velocities before they enter the collision phase. In this case we introduce therefore a new phase into the DSMC code; the plasma phase.

3 The Plasma Phase

In particle simulations of ionised gases it is important to distribute the charges correctly on the computational mesh to avoid any numerical inconsistencies that may appear due to the fact that our space time is discretised. In this approach we have used a Cloud-in-Cell (CIC) technique in which we spread the charge to more than one mesh points. The scheme employed in this modeling is a TSC (triangular shaped cloud) which has a piecewise quadratic assignment interpolation function. This way of assigning the charge belongs to the area weighting cloud in cell schemes. A second scheme is also used, the results of which will be in the final paper, where the charge distribution is assumed to be constant within a cell. If the number of particles in our computation is N_p then in order to find the charge density at mesh point p due to charges at position x_i we have to do the sum:

$$\rho_o = \frac{q}{H} \sum_{i=1}^{N_p} W(x_i - x_p) \quad (1)$$

where x_p is the position of mesh point p , W is the charge assignment function and H is the shaping of the mesh points. Selection of an appropriate assignment function guarantees not only a correction to the discretisation of space time but a very important smoothness in the calculation of forces as a charge moves along the mesh.

After the charge has been assigned on the mesh the next step in the computational code is the calculation of the forces on each particle. A Poisson solver must be employed in order to calculate the electric field due to the external potentials and charge separations inside the plasma.

Once the potential is calculated the electric field can be calculated using a second order accurate scheme. This gives the electric field at each grid point. The final step is to calculate the electric field at the position of each particle. To do so accurately i.e., the self force on a particle has to be zero and to have the correct solution to the Green function problem,

*Abstract 5711 submitted to the 21st International Symposium on Rarefied Gas Dynamics, Marseille, France, July 26-31, 1998

the function that we will interpolate the force at the position of each particle must be the same as the assignment function W . After the electric field has been calculated we perform the stepping of the particles. This procedure is repeated in each electron time step. After a sufficient number of time steps and when the electron time has matched the ion time, the ions are advanced.

4 Numerical Results

Before applying this scheme to a multi-dimensional flow around realistic spacecraft a simple case was selected where the code could be verified. The first test case studied was for a hydrogen gas in a box of temperature 250K in contact with two walls at 300K temperature. It was assumed that the reflection of the wall is diffuse so that the gas would soon acquire the temperature of the wall. For a first approximation the collision routine of the numerical code was turned off and a configuration where two electron beams are drifting against each other with a velocity of ten times the thermal velocity of the background plasma was set up. Plasma instabilities are very small and they do not appear anywhere in the following diagrams due to the smallness of these effects. Periodic boundary conditions are assumed in this calculation and we have also included a 10% of neutral particles in the plasma along with a thermal background.

For the case of two electron beams of equal density drifting through each other with relative speed V_0 it is usually assumed that the ions are stationary and are part of a uniform neutralizing background, and hence this means that it is assumed that the ions are infinitely heavy. In this case it can be found that the oscillation frequency is given by:

$$\omega^2 = \frac{\omega_{pe}^2}{2} + \frac{k^2 V_0^2}{4} + \sqrt{\frac{\omega_{pe}^2}{2} + \frac{k^2 V_0^2}{4} + \frac{k^2 V_0^2}{4} (\omega_{pe}^2 + \frac{k^2 V_0^2}{4})} \quad (2)$$

and the maximum growth rate is:

$$\omega = \frac{\omega_{pe}}{\sqrt{8}} \quad (3)$$

where ω_{pe} is the oscillation frequency under an effectively infinite wavelength. Figure 1 presents the growth rate (normalised) as a function of the particle density and it is in good agreement with what was expected from the theoretical calculation that was performed. The discrepancies for small densities are there because the maximum growth rate

appears only when all energy of the instability is given to the fields and not in the beams. It is expected that the usual growth rate will be slightly smaller as is seen. The two curves cross and the observed growth is faster than the theoretically calculated, because for larger densities the instabilities grow so fast that nonlinear phenomena begin to act in such way as to speed them up at these stages of the instability.

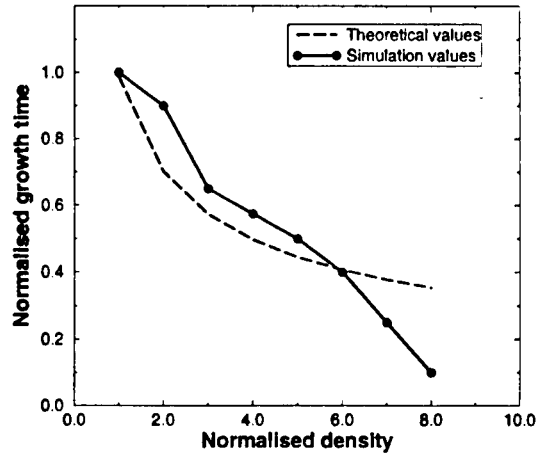


Figure 1: Comparison between measured and calculated results

5 Conclusions

In this study a particle code has been developed based on principles of the Direct Simulation Monte Carlo method employing a Poisson solver to deal with the calculation of electrostatic potential and the electric field. Results of the numerical scheme are in good agreement with theoretical solutions of simple problems. The full paper will contain a complete description of the method employed as well as results for realistic cases in comparison with experimental results.

References

- [1] Serikov VV, Nambu K, *3D Monte Carlo Simulation of DC glow discharge for plasma-assisted materials processing*, Rarefied Gas Dynamics 20, Peking University Press, China, pp.829-834

Hybrid (Fluid/PIC/DSMC) Simulation of Partially Ionized Jets *

N. A. Gatsonis and Xuemin Yin
 Computational Gas & Plasma Dynamics Laboratory
 Mechanical Engineering Department, Worcester

Partially ionized plasma jets appear in a wide range of science and engineering disciplines: space plasma physics, spacecraft-induced environment interactions, space power and propulsion, and plasma-aided materials processing. As often is the case the study of plasma jets has been pursued by these scientific communities in parallel with not much communication between them. Over the years, analyses and modeling efforts developed and/or utilized a variety of computational methods -fluid, particle and hybrid- but emphasized different physical aspects of plasma jets.

Plasma jets in space plasma physics may be natural or artificial. In the case of active release or ionospheric modification experiments, neutrals are injected which after a series of chemical interactions with the background environment create a plasma jet. The study of the motion of an artificial plasma jet (or plasma cloud) can reveal information about the ambient electric fields and currents, map the distant magnetic field and measure the ambient neutral winds. Plasma jets (or plumes) can also be the product of the release of neutrals and/or ions from spacecraft power and propulsion systems. These plasma jets play a crucial role in spacecraft interactions. They affect spacecraft charging, the contamination of sensitive spacecraft surfaces due to backflow, they contribute to radiation emission, enhance and modify the electromagnetic noise in the vicinity of a spacecraft, and finally they perturb the ambient environment. With the utilization of advanced electric propulsion technologies on spacecraft the issue of plasma plumes and their effects become very important. The projected expansion in the use of such technologies, fueled by the growth in space telecommunication services, emphasizes the study of plasma jets even more. Plasma jets find also important applications in plasma-aided materials processing. Many of the plasma sources used in materials processing are identical to those used in propulsion systems. It is, therefore, important to investigate plasma jets and develop a predictive ability that could be applied to a wide range of engineering applications.

In the past three decades theories, experiments and computations have explored various aspects of plasma (fully ionized) and neutral jets. In space plasma physics, for example, studies have been mainly concentrated on the electrodynamic behavior and instabilities of plasma jets, and led to the development of 2- and 3-d, single- and multi-fluid models. In gasdynamics, emphasis has been placed in the interactions of expanding neutral jets, both in the continuum and rarefied regimes. As a result, advanced three-dimensional Navier-Stokes and Direct Simulation Monte Carlo (DSMC) codes have been developed. With the advent of Particle-in-Cell (PIC) and PIC-Monte Carlo methods kinetic phenomena related to plasma jets have been investigated as well. Computational advances in the past decade led to fluid, particle and hybrid models that explored significant neutral and fully ionized jet interactions. However, in the case of partially ionized jets

* Abstract 6602 submitted to the 21st International Symposium on Rarefied Gas Dynamics, Marseille, France, July 26-31, 1998

many of the neutral/charged particle interactions are not well understood and have not been treated comprehensively due to theoretical and numerical limitations.

Simulation of neutral jets is a very mature field with Navier-Stokes solvers covering the continuum regime, and Direct Simulation Monte Carlo (DSMC) solvers covering the transitional to rarefied regimes. The DSMC method developed by *Bird* treats non-equilibrium effects, backflow, chemical reactions, and surface interactions very effectively. Computational studies of fully ionized collisionless plasma plumes have used primarily the Particle-in-Cell method. To alleviate difficulties associated with electron time-steps, various formulations of PIC/Fluid (hybrid) methodologies have been developed and used in a variety of problems. Recently, such hybrid methodologies have been used successfully in the simulation of ion thruster plumes. A simulation methodology applicable to partially ionized plasmas is the PIC-Monte Carlo (PIC-MCC). The method is strictly applicable to low plasma densities due to Debye length limitations and to problems where neutral densities dominate the flow. In addition, the method is limited due to the lack of a kinetic description of the neutrals. The DSMC method has also been used to model flows with ionization. In most of these cases simple models for the plasma flow have been used. Problems with the DSMC relate to the treatment of electrons, as well as the modeling of charged particle collisions. In addition to the Monte Carlo extensions to PIC, many variations of hybrid (particle/fluid) approaches have been proposed for the intermediate regime between the collisionless and Coulomb dominated plasmas. Finally, purely fluid approaches have been used to address large-scale plasma jets. Of course, as with any fluid description, the major shortcoming comes from the loss of the kinetic description of the flow.

In this study we present the first comprehensive physical and computational model of a partially ionized jet. Our numerical model is based on a hybrid approach that results in a novel combination of DSMC, PIC and fluid computational techniques. A hybrid physical jet model is derived based on a particle description of neutrals and ions and a fluid description of electrons. In order for the model to be applicable to plasma flows where the magnitudes of Debye lengths restrict practical computations a quasineutral approach is adopted. Therefore, electric fields are obtained from a current balance equation under the assumption of quasineutrality. An axisymmetric, hybrid numerical code is developed based on a combination of DSMC, PIC and fluid computational techniques. The code incorporates a dual-grid structure, sub-cycling for the time integration, and time-varying particle injection. The No-Time-Counter methodology is used for neutral-neutral, elastic ion-neutral, and charge exchange collisions. Ion-electron collisions are modeled with the use of a collision force field. A typical simulation of a plasma jet is presented. The results demonstrate the expansion of the neutral and ion components of the plume and the generation of a low energy ion population due to charge exchange reactions.

MOLECULAR PROPERTIES AND TRANSPORT

ROOM PÉRÈS

TUESDAY, JULY 28, 1998

14:35

On the Influence of Gravity on the Thermal Conductivity *

M. Tij¹, V. Garzó², A. Santos²

¹ Département de Physique, Université Moulay Ismaïl, Meknès, Morocco

² Departamento de Física, Universidad de Extremadura, E-06071 Badajoz, Spain

1 Introduction

The simplest heat flow problem consists of a gas enclosed between two infinite, parallel plates kept at different temperatures. In the continuum limit, the Fourier law establishes a linear relation between the heat flux and the thermal gradient, i.e., $\mathbf{q} = -\kappa \nabla T$, where κ is the thermal conductivity coefficient. The continuum description applies when $\lambda/L \ll 1$ and $\lambda/\ell \ll 1$, where λ is the mean free path, L is the separation between the plates, and $\ell \sim T|\nabla T|^{-1}$ is the characteristic length over which the temperature changes. Nevertheless, exact results from the Boltzmann equation for Maxwell molecules and from the BGK model for general interactions [1] show that the Fourier law still holds for large gradients ($\lambda \sim \ell$), provided that the Knudsen number $\text{Kn} = \lambda/L$ is small.

In this paper we are interested in studying the influence on the heat flux of an external field g (e.g., gravity) normal to the plates. The presence of gravity introduces a fourth characteristic length, namely $h \sim k_B T/mg$, which represents the vertical distance over which the field produces a significant effect. In ordinary laboratory conditions, h is several orders of magnitude larger than λ and ℓ , so that the constitutive equations are not affected by the action of gravity. However, discrepancies with respect to the Navier-Stokes predictions can be expected if h is not extremely large. According to a recent perturbative solution of the Boltzmann equation through second order in g [2], one can estimate that the heat flux deviates from the Fourier law as much as 10% if $\lambda \sim \ell \sim 0.01h$. The aim of this paper is to go beyond the second order in g by using the BGK model of the Boltzmann equation.

2 Description of the problem

Let us consider a dilute gas enclosed in a slab between two plates at different temperatures. We are interested in a stationary state with spatial variation along the normal direction (z) only and a *constant* external field $\mathbf{F} = -mg\hat{z}$ along that direction. The constant g can be interpreted as the gravitational acceleration. In addition, we assume that there is no convection, i.e., $\mathbf{u} = 0$. We choose an *arbitrary* point in the bulk as the origin and take the quantities at that point (denoted by a subscript 0) as reference units, i.e., $T_0 = p_0 = \lambda_0 = k_B = m = 1$. In these units, $g = \lambda_0/h_0$ and the stationary BGK equation reads

$$\left(1 + v_z \frac{\partial}{\partial s} - g \frac{T}{p} \frac{\partial}{\partial v_z}\right) f = f_L, \quad (1)$$

where f_L is the local equilibrium distribution function and $ds = \nu(z)dz$, $\nu = \sqrt{T}/\lambda$ being the collision frequency. Furthermore, for the sake of concreteness, we have restricted ourselves to the case of Maxwell molecules (i.e., $\nu \propto p/T$). In the geometry of the problem, the relevant velocity moments are defined as $M_{\alpha\beta} = \int d\mathbf{v} v^{2\alpha} v_z^\beta f$.

In the absence of gravitation ($g = 0$), Eq. (1) has an *exact* solution [1] characterized by a constant pressure, $p^{(0)} = 1$, and a "linear" temperature profile, $T^{(0)} = 1 + \epsilon s$ (where the superscript (0) refers to quantities with $g = 0$), that applies to arbitrary values of the reduced thermal gradient $\epsilon = \lambda_0/\ell_0$. The velocity moments are *polynomials* in both s and ϵ [1]. In particular, $M_{11}^{(0)} = -5\epsilon$, which means that the Fourier law holds even for large thermal gradients. The motivation of this paper is to analyze the influence of gravitation on the profiles and transport properties of the above steady Fourier flow by carrying out a perturbation expansion in powers of g :

$$f = f^{(0)} + f^{(1)}g + f^{(2)}g^2 + \dots \quad (2)$$

Analogously, the moments $M_{\alpha\beta}$ and the hydrodynamic quantities p and T are expanded in powers of g . By definition, $p^{(k)}(0) = T^{(k)}(0) =$

* Abstract 5376 submitted to the 21st International Symposium on Rarefied Gas Dynamics, Marseille, France, July 26-31, 1998

$\partial T^{(k)}/\partial s|_{s=0} = 0$ for $k \geq 1$. It must be emphasized that the terms of order g^k are *nonlinear* functions of ϵ and no restriction as to the order on ϵ exists.

3 Results

Insertion of Eq. (2) into Eq. (1) yields

$$f^{(k)} = \sum_{j=0}^{\infty} \left(-v_z \frac{\partial}{\partial s} \right)^j \left[f_L^{(k)} + \frac{\partial}{\partial v_z} \sum_{i=0}^{k-1} \left(\frac{T}{p} \right)^{(i)} f^{(k-i-1)} \right]. \quad (3)$$

This is a *formal* solution, since $f_L^{(k)}$ is a functional of $f^{(k)}$ through its dependence on the pressure and temperature. In order to convert Eq. (3) into an explicit equation that can be solved recursively, we need to know the spatial dependence of $p^{(k)}$ and $T^{(k)}$. As in the pure Fourier flow, we will follow a heuristic method and assume simple profiles, to be confirmed later. More specifically, we assume that $p^{(k)}$ is a polynomial of degree k in s , while $T^{(k)}$ is a polynomial of degree $k+1$:

$$p^{(k)}(s) = \sum_{l=1}^k p_l^{(k)} s^l, \quad T^{(k)}(s) = \sum_{l=2}^{k+1} T_l^{(k)} s^l. \quad (4)$$

Thus, at a given order k the number of unknowns is $2k$. These coefficients are determined by inserting Eq. (4) into Eq. (3) and taking moments in both sides. After tedious but straightforward calculations, one can get the successive approximations. Here we give the explicit results through order $k=4$:

$$p = 1 - sg - \frac{276}{5} \epsilon^2 s g^3 - \frac{1}{5} s \left[\frac{12}{5} \epsilon (112 973 \epsilon^2 + 30) + 588 \epsilon^2 s \right] g^4 + \mathcal{O}(g^5), \quad (5)$$

$$T = 1 + \epsilon s + \frac{1}{2} \epsilon s^2 g - \epsilon s^2 \left(\frac{66}{5} \epsilon - \frac{1}{3} s \right) g^2 - \epsilon s^2 \left[\frac{16}{25} (6624 \epsilon^2 + 5) + \frac{346}{15} \epsilon s - \frac{1}{4} s^2 \right] g^3 - \frac{1}{5} \epsilon s^2 \left[\frac{12}{25} \epsilon (50 765 962 \epsilon^2 + 31 445) + \frac{2}{15} (399 621 \epsilon^2 + 200) s + \frac{971}{6} \epsilon s^2 - s^3 \right] g^4 + \mathcal{O}(g^5). \quad (6)$$

Once the hydrodynamic profiles are known, Eq. (3) can be used to obtain all the velocity moments at

a given order. The most relevant moments are M_{02} and M_{11} , which are related to the pressure tensor and the heat flux, respectively. Their expressions are

$$M_{02} = 1 - sg + \frac{84}{5} \epsilon^2 g^2 + \frac{12}{25} \epsilon (19 693 \epsilon^2 + 10) g^3 + \frac{12}{125} \epsilon^2 (131 658 163 \epsilon^2 + 81 780) g^4 + \mathcal{O}(g^5), \quad (7)$$

$$M_{11} = -5\epsilon - 58\epsilon^2 g - \frac{16}{5} \epsilon (2998 \epsilon^2 + 5) g^2 - \frac{4}{25} \epsilon^2 (42 855 388 \epsilon^2 + 45 985) g^3 - \frac{4}{125} \epsilon (370 692 375 508 \epsilon^4 + 300 269 715 \epsilon^2 + 31 150) g^4 + \mathcal{O}(g^5). \quad (8)$$

As expected from the balance equations, the heat flux is spatially uniform and $\partial P_{zz}/\partial s = -g$. The numerical coefficients appearing in Eqs. (5)–(8) clearly suggest that the expansion in powers of g is only asymptotic. Consequently, its usefulness is restricted to very small values of g , which is the situation of practical interest.

The main conclusions are that the external field induces (i) anisotropy in the pressure tensor, $(P_{zz} - p)/p \simeq \frac{84}{5} \epsilon^2 g^2$, and (ii) deviations from the Fourier law, $q_z/(-\kappa \partial T/\partial z) - 1 \simeq \frac{58}{5} \epsilon g$. While the first effect is of second order, the correction to the heat flux is of first order, so that it depends on the sign of the thermal gradient. As a consequence, the heat transport is inhibited when the gas is heated from below ($\epsilon < 0$), while the opposite happens when the gas is heated from above ($\epsilon > 0$).

References

- [1] Santos A. and Garzó V., *Exact non-linear transport from the Boltzmann equation*, in *Rarefied Gas Dynamics 19*, Oxford University Press, Vol.1, pp.13–22, 1995.
- [2] Tij M., Garzó V. and Santos A., *Nonlinear heat transport in a dilute gas in the presence of gravitation*, Phys. Rev. E, Vol.56, No.6, pp.6729–6734, 1997.

Non-Newtonian Shear Viscosity in a Dense System of Hard Disks *

J.M. Montanero¹, A. Santos²¹ Dpto. de Electrónica e Ingen. Electromec., Universidad de Extremadura,
E-06071 Badajoz, Spain² Dpto. de Física, Universidad de Extremadura, E-06071 Badajoz, Spain

1 Introduction

It is well known that many interesting physical phenomena associated with finite-density effects lie beyond the validity of the Boltzmann equation. On the other hand, the revised Enskog theory provides a remarkably broad description of the system of hard spheres, with no *a priori* limitations on the density, space scales, or phase of the states considered. However, its complexity has precluded applications outside the domain of linear response, and even in this latter case linear kinetic models have been required.

Recently, two methods have been proposed to deal with the technical problem of solving the Enskog equation, in the same spirit as parallel methods successfully applied in the past to the Boltzmann equation. On the one hand, a kinetic model has been obtained [1] by replacing the known collision operator with a simpler form that preserves the most important physical properties; it reduces in the low density limit to the simplest kinetic model for the Boltzmann equation, the Bhatnagar-Gross-Krook (BGK) model. On the other hand, the Monte Carlo simulation techniques have been extended [2] to apply to the Enskog equation; this Enskog simulation Monte Carlo (ESMC) method reduces to the well-known DSMC method in the low density limit. The aim of this paper is to use these two methods to calculate the rheological properties (viscosity, viscometric functions, shear dilatancy) of a dense fluid of hard disks under shear far from equilibrium. As happens in the three-dimensional case [3], the agreement between both approaches is excellent.

2 The ESMC method

Let us consider a system of hard disks of diameter σ in a shear state characterized by a linear flow

velocity profile, $\mathbf{u}(\mathbf{r}) = \mathbf{a} \cdot \mathbf{r}$, where $\mathbf{a} = a\hat{\mathbf{x}}\hat{\mathbf{y}}$ (a being a constant shear rate), and uniform density and temperature. To compensate for the viscous heating, a thermostat force $\mathbf{F} = -m\alpha(a)\mathbf{V}$ ($\mathbf{V} = \mathbf{v} - \mathbf{u}$ being the peculiar velocity) is applied. Under these conditions, the Enskog equation becomes

$$-\left(aV_y\frac{\partial}{\partial V_x} + \alpha\frac{\partial}{\partial \mathbf{V}} \cdot \mathbf{V}\right)f = \sigma\chi \int d\mathbf{V}_1 \int d\hat{\sigma} \Theta(\hat{\sigma} \cdot \mathbf{g}) \times (\hat{\sigma} \cdot \mathbf{g}) [f(\mathbf{V}')f(\mathbf{V}'_1) - f(\mathbf{V})f(\mathbf{V}_1)], \quad (1)$$

where $\mathbf{g} = \mathbf{V} - \mathbf{V}_1 - \sigma\mathbf{a} \cdot \hat{\sigma}$, $\mathbf{V}' = \mathbf{V} - (\hat{\sigma} \cdot \mathbf{g})\hat{\sigma}$, and $\mathbf{V}'_1 = \mathbf{V}_1 + 2\sigma\mathbf{a} \cdot \hat{\sigma} + (\hat{\sigma} \cdot \mathbf{g})\hat{\sigma}$. In Eq. (1) χ is the pair correlation function at contact. The objective is to obtain the pressure tensor \mathbf{P} as a function of both the density n and the shear rate a . In particular, the non-Newtonian shear viscosity is defined as $\eta(n, a) = -P_{xy}(n, a)/a$. In the limit of vanishing shear rate one recovers the Navier-Stokes viscosity $\eta(n, 0) = \eta_0(1 + \frac{\pi}{4}n\sigma^2\chi)^2/\chi + \frac{1}{4}n^2\sigma^3\chi(\pi mk_B T)^{1/2}$, where $\eta_0 = 1.022(mk_B T/\pi)^{1/2}/2\sigma$ is the Boltzmann viscosity.

The ESMC method, as applied to this simple shear flow, proceeds as follows. The one-particle distribution function $f(\mathbf{V})$ is represented by the peculiar velocities $\{\mathbf{V}_i\}$ of a sample of N "simulated" particles. These velocities are updated at integer times $t = \Delta t, 2\Delta t, 3\Delta t, \dots$, where the time-step Δt is much smaller than the mean free time and the inverse shear rate. This is done in two stages: free streaming and collisions. The free-streaming stage consists of making $\mathbf{V}_i \rightarrow e^{-\alpha\Delta t}(\mathbf{V}_i - \mathbf{a} \cdot \mathbf{V}_i\Delta t)$, where the thermostat parameter α is adjusted to assure that the temperature $T = (m/2Nk_B) \sum_i V_i^2$ remains constant. In the collision stage, a sample of $\frac{1}{2}N\tilde{w}$ pairs are chosen at random with equiprobability, where \tilde{w} is an upper bound estimate of the probability that a particle collides in the time interval between t and $t + \Delta t$. For each pair ij belonging to this sample, the following steps are taken: (1) a given direction $\hat{\sigma}_{ij}$ is chosen at random with equiprobability; (2) the collision between

*Abstract 5377 submitted to the 21st International Symposium on Rarefied Gas Dynamics, Marseille, France, July 26-31, 1998

particles i and j is accepted with a probability equal to $\Theta(\hat{\sigma}_{ij} \cdot \mathbf{g}_{ij})w_{ij}/\tilde{w}$, where $w_{ij} = 2\pi\sigma\chi n\hat{\sigma}_{ij} \cdot \mathbf{g}_{ij}\Delta t$ and $\mathbf{g}_{ij} = \mathbf{V}_i - \mathbf{V}_j - \sigma\mathbf{a} \cdot \hat{\sigma}_{ij}$; and (3) if the collision is accepted, post-collision velocities are assigned to both particles: $\mathbf{V}_i \rightarrow \mathbf{V}_i - \hat{\sigma}_{ij}(\hat{\sigma}_{ij} \cdot \mathbf{g}_{ij})$, $\mathbf{V}_j \rightarrow \mathbf{V}_j + \hat{\sigma}_{ij}(\hat{\sigma}_{ij} \cdot \mathbf{g}_{ij})$. In the case that in one of the collisions $w_{ij} > \tilde{w}$, the estimate of \tilde{w} is updated as $\tilde{w} = w_{ij}$. In the course of the simulations, the kinetic and collisional transfer contributions to the pressure tensor are evaluated. They are given as

$$\mathbf{P}^k = \frac{mn}{N} \sum_{i=1}^N \mathbf{V}_i \mathbf{V}_i, \quad (2)$$

$$\mathbf{P}^c = \frac{mn}{N} \frac{\sigma}{\Delta t} \sum_{ij}^{\dagger} (\hat{\sigma}_{ij} \cdot \mathbf{g}_{ij}) \hat{\sigma}_{ij} \hat{\sigma}_{ij}, \quad (3)$$

where the dagger means that the summation is restricted to the accepted collisions.

3 The kinetic model

For a detailed account of the kinetic model of the Enskog equation, see Ref. [3]. In the special case of the shear flow problem considered in this work, the kinetic model replaces Eq. (1) by

$$-\left(aV_y \frac{\partial}{\partial V_x} + \alpha \frac{\partial}{\partial \mathbf{V}} \cdot \mathbf{V}\right) f = -\nu(f - f_L) - \frac{P_{xy}^c}{nk_B T} a \left(\frac{mV^2}{2k_B T} - 1\right) f_L + 2A_{xy} \frac{mV_x V_y}{k_B T} f_L, \quad (4)$$

where ν is an effective collision frequency, f_L is the local equilibrium distribution function, P_{xy}^c is the collisional part of the shear stress (which is a nonlinear functional of f), and $A_{xy} = -\frac{\pi}{4}(k_B T/m)^{1/2} n \sigma \chi \bar{a}(1 + \frac{3}{8}\bar{a}^2)$, with $\bar{a} \equiv \frac{1}{2} a \sigma (m/k_B T)^{1/2}$.

Taking moments in both sides of Eq. (4) one can easily get the kinetic part of the pressure tensor. In particular,

$$P_{xy}^k = nk_B T \frac{\nu + 2\alpha}{(\nu + 2\alpha)^2 + a^2} (2A_{xy} - a), \quad (5)$$

where we have taken into account that $aP_{xy} = -2nk_B T\alpha$, as follows from energy conservation. In order to have a closed equation for α , we need to express P_{xy}^c in terms of α . In principle, this implies to use the formal solution to Eq. (4). Instead, we obtain a reasonable estimate for P_{xy}^c by using the first Sonine approximation $f \rightarrow f_L[1 + m(V_x^2 - V_y^2)(P_{xx}^k - P_{yy}^k)/4nk_B^2 T^2 + mV_x V_y P_{xy}^k/nk_B^2 T^2]$.

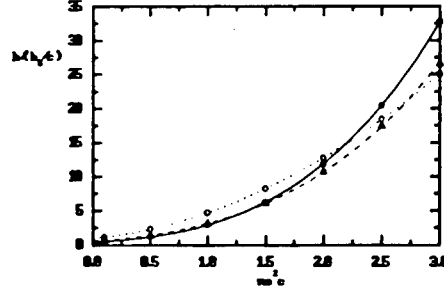


Figure 1: Density dependence of the shear viscosity for three values of the shear rate. Symbols are simulation data and lines are results from the kinetic model

4 Results

Comparison between the elements of the pressure tensor as obtained from simulations of the Enskog equation and from the numerical solution of the model shows an excellent agreement for a wide range of densities and shear rates. As an illustration, Fig. 1 shows the (normalized) shear viscosity as a function of the density parameter $n\sigma^2\chi$ for $a = 0$ (dotted line, open circles), $a = 0.7\nu$ (dashed line, triangles), and $a = \nu$ (solid line, filled circles). In general, non-Newtonian effects are more important at finite densities than at zero density. In addition, a transition from shear thinning (viscosity smaller than the Navier-Stokes value) to shear thickening (viscosity larger than the Navier-Stokes value) takes place at large density and/or shear rate.

References

- [1] Dufty J.W., Brey J.J., Santos, A., *Kinetic models for hard sphere dynamics*, Physica A, Vol.240, Nos.1-2, pp. 212-220, 1997.
- [2] Montanero J.M., Santos A., *Monte Carlo simulation method for the Enskog equation*, Phys. Rev. E, Vol.54, No.1, 438-444, 1996; *Simulation of the Enskog equation à la Bird*, Phys. Fluids, Vol.9, No.7, 2057-2060, 1997.
- [3] Santos A., Montanero J.M., Dufty J.W., Brey J.J., *Kinetic model for the hard-sphere fluid and solid*, Phys. Rev. E, Vol.57, No.2, 1998.

State-to-State Approach in the Transport Kinetic Theory *

E. Kustova, E. Nagnibeda

Math. and Mech. Dept., St.Petersburg University, 198904, St.Petersburg, Russia

This paper deals with the transport properties of a multi-component reacting gas mixture in the case of strong vibrational and chemical nonequilibrium. Considered are the conditions when the quasi-stationary distributions of the molecules over vibrational levels do not exist and the state-to-state kinetic approach is developed for the simulation of transport and relaxation processes in a gas flow.

The experimental data concerning the relaxation times of different processes in reacting mixtures [1] show that in many cases of practical interest the following relation between the relaxation times is valid:

$$\tau_{el} < \tau_r \ll \tau_{vibr} < \tau_{react} \sim \theta, \quad (1)$$

where τ_{el} , τ_r , τ_{vibr} , τ_{react} are the mean times between the collisions with the translational, rotational and vibrational energy transfer and those with chemical reactions, θ is the macroscopic time. The translational energy distribution is known to equilibrate fast and the rotational relaxation time is of the same order as the translational one and much smaller in comparison to the vibrational and chemical relaxation time. The simultaneous process of the vibrational and chemical relaxation can be described by the state-to-state approach in nonequilibrium gas dynamics. In this case the macroscopic conservation equations for the mass, momentum and total energy should be considered together with the equations for level populations of different chemical species. This model is important for the study of vibrational-chemical coupling in the boundary layer [2], in the short relaxation zone behind a shock wave where the steady-state vibrational distributions do not establish [3], in the expanding flows [4]. The state-to-state approach can give the limits of the validity of the models based on the quasi-stationary distributions of molecules over vibrational levels.

In the present study the transport kinetic theory of multi-component reacting mixtures is developed under the condition (1) and the effect of vibrational-

chemical coupling on the transport properties is investigated. The heat flux, diffusion velocities of molecules of different chemical species at the various vibrational levels are shown to depend on the gradients not only the gas temperature and number density of chemical species but also nonequilibrium level populations. The system of the diffusion coefficients in the condition under consideration contains the thermal diffusion coefficients for different chemical species D_{T_c} , the multi-component diffusion coefficients of the molecules of c and d chemical species D_{cd} , the diffusion coefficients of the molecules of the same chemical species c at different vibrational levels D_{cc} , and the self-diffusion coefficients for the molecule of c species at the i th vibrational level D_{cici} . The practical algorithm for the calculation of the heat conductivity, viscosity and diffusion coefficients is given. All transport coefficients are expressed in terms of the nonequilibrium level populations, gas temperature and elastic collision integrals.

The obtained formulas are used for the investigation of the heat transfer and diffusion behind a plane shock wave. The nonequilibrium level populations are found from the equations of nonequilibrium chemical-vibrational kinetics and conservation equations of the momentum and total energy. The mixtures (O_2 , O) and (N_2 , N) are considered and the nonequilibrium distributions and the gas temperature are found as a function of the distance from the shock front. On the basis of these distributions the heat flux, thermal conductivity and diffusion and thermal diffusion coefficients behind a shock wave are calculated and the influence of vibrational and chemical nonequilibrium on the transport of total energy is estimated. The results obtained in the dissociating (N_2 , N) mixture are compared with the ones computed using the two-temperature and one-temperature approaches based on the steady-state Boltzmann distributions over vibrational energy. The one-temperature approach corresponds to thermal equilibrium in a dissociating gas, in this case there exists the equilibrium Boltzmann distribution over internal energy with the gas temperature. The two-temperature ap-

*Abstract 4996 submitted to the 21st International Symposium on Rarefied Gas Dynamics, Marseille, France, July 26-31, 1998

proach is based on the assumption that the nonequilibrium Boltzmann distribution with the vibrational temperature T_v is established. The distribution of the molecules over vibrational levels in the free stream is assumed to be Boltzmann, 20 excited vibrational levels in N_2 are taken into account. The molecular spectra are simulated as anharmonic oscillators. The transition probabilities are calculated using the *SSH*-theory generalized for anharmonic oscillators [5]. The Treanor-Marrone model [6] is applied for the computation of the probability of dissociation from each vibrational level. The following conditions in the free stream are considered: $T_0 = 293$ K, $p_0 = 100$ Pa, $M_0 = 15$, $n_{N_2}^{(0)}/n^{(0)} = 1$. The total heat flux behind a shock wave calculated in the state-to-state, multi-temperature and one-temperature approaches is presented in Fig.1 as a function of the distance from the shock front x . One can conclude that the total heat flux decreases approaching the equilibrium. At $x > 1$ cm all three approaches give the close values of the heat flux. On the contrary, in the beginning of the relaxation zone there exists an essential discrepancy between the heat fluxes calculated using different models. The one-temperature approach provides a very strong peak of the heat flux just behind the shock front. This effect can be explained by the fact that the one-temperature approach does not describe the process of the vibrational excitation of the molecules just after the shock. It leads to a more sharp decrease of the gas temperature in the very beginning of the relaxation zone compared to the two other approaches and therefore to the very high values of the temperature gradient. The two-temperature approach yields a more smooth behaviour of the macroscopic parameter gradients and the heat flux but there remains a noticeable distinction between the heat flux calculated using the state-to-state and two-temperature approach. Thus in the zone of vibrational excitation where the steady-state vibrational distributions do not exist the more rigorous state-to-state approach should be used for the evaluation of heat transfer in a reacting gas mixture.

References

- [1] Ye.V. Stupochenko, S.A. Losev, and A.I. Osipov. *Relaxation in Shock Waves*. Springer-Verlag, Berlin, Heidelberg, New York, 1967.
- [2] I. Armenise, M. Capitelli, G. Colonna, and C. Gorse. Nonequilibrium vibrational kinetics in the boundary layer of re-entering bodies.

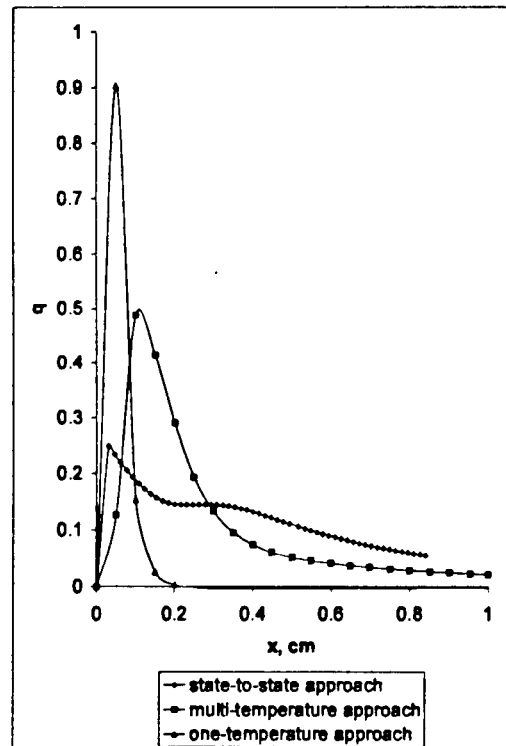


Figure 1: Total heat flux q , $10^6 \cdot W/m^2$, behind a shock wave calculated in different approaches

Journ. of Thermophysics and Heat Transfer, 10(3):397-405, 1996.

- [3] E.V. Kustova and E.A. Nagnibeda. The effect of level nonequilibrium kinetics on transport properties of dissociating gas flow behind a shock wave. In *Proc. of the 21st International Symposium on Shock Waves*, Great Keppel Island, Australia, 1997 (in press).
- [4] D. Shizgal and F. Lordet. Vibrational nonequilibrium in a supersonic expansion with reactions: Application to $O_2 - O$. *Journ. of Chem. Phys.*, 104(10):3579-3597, 1996.
- [5] B.F. Gordietz and S.A. Zhdanok. Analytical theory of vibrational kinetics of anharmonic oscillators. In M. Capitelli, editor, *Nonequilibrium Vibrational Kinetics*. Springer-Verlag, Berlin, Heidelberg, New York, Tokyo, 1986.
- [6] P.V. Marrone and C.E. Treanor. Chemical relaxation with preferential dissociation from excited vibrational levels. *Phys. of Fluids*, 6(9):1215, 1963.

Observation of Spin-Symmetry-Violating Collisions *

L.J.F. Hermans¹, B. Nagels¹, P. Bakker¹ and P.L. Chapovsky²¹ Huygens Laboratory, Leiden University, The Netherlands² Institute of Automation and Electrometry, Novosibirsk, Russia

Collisional state-to-state transitions in molecules play an important role in various applications of gas kinetics. Most often, such transitions have to obey selection rules, which can result in extremely small cross sections for certain processes. The most strict selection rule known to date requires that the symmetry of the nuclear spin state be conserved in a collision. The classic example is ortho and para H_2 , for which the conversion time is known to be extremely long: on the order of years for pure H_2 gas at ambient conditions. For this case it is known that the dominant conversion mechanism relies upon the magnetic field gradients produced by an external collision partner.

It has been well established recently that, for molecules with a less simple structure, the dominant conversion mechanism is based on mixing of states by *intramolecular* interactions (see refs. [1, 2, 3] and references therein). Depending on the details of the energy level structure, this mechanism can lead to relatively short conversion times. An example is $^{13}CH_3F$, where the conversion time is around 1 minute at 1 Torr.

The question is now whether such spin-symmetry-violating collisions in molecules like CH_3F can also be caused directly by the collision partner's magnetic field gradients.

In order to answer this question we have experimentally studied the ortho-para conversion rate of both gaseous $^{12}CH_3F$ and $^{13}CH_3F$ interacting with N_2 and O_2 as collision partners. Since the (dominant) mixing-of-states mechanism heavily depends on the details of the rotational level structure, this mechanism is found to be much less important for $^{12}CH_3F$ than for $^{13}CH_3F$. On the other hand, the importance of the magnetic moment μ of the collision partner can be varied by measuring the conversion of CH_3F in mixtures with O_2 ($\mu \approx 2$ Bohr magnetons in its ground state) and with N_2 ($\mu \approx 2$ nuclear

magnetons). For separating the ortho and para species we use Light-Induced Drift, and for measuring the conversion rate we use optical absorption. The transitions employed are rovibrational excitations of the ν_3 fundamental (C-F stretch), which are coincident with CO_2 laser lines ($10\ \mu m$). For details the reader is referred to refs. [1, 2, 3].

The results show that direct conversion by the magnetic moment of the collision partner does indeed occur. The corresponding cross section is found to be on the order of $10^{-30}\ m^2$. This compares fairly well with a theoretical estimate for this mechanism (see ref. [4]). To the author's knowledge, this is the first observation of nuclear-spin-symmetry-violating collisions in polyatomic molecules.

References

- [1] B. Nagels, N. Calas, D.A. Roozmond, L.J.F. Hermans and P.L. Chapovsky, *Level-Crossing Resonance in Nuclear Spin Conversion of Molecules*, Phys. Rev. Lett. Vol. 77, pp.4732-4735, 1996.
- [2] B. Nagels, L.J.F. Hermans and P.L. Chapovsky, *Quantum Zeno Effect Induced by Collisions*, Phys. Rev. Lett., Vol. 79, pp.3097-3100, 1997.
- [3] B. Nagels, P. Bakker, L.J.F. Hermans and P.L. Chapovsky, *Nuclear spin conversion in CH_3F at elevated temperatures*, Phys. Rev. A, 1998 (accepted for publication).
- [4] P.L. Chapovsky, *Nuclear spin conversion in CH_3F induced by magnetic particles*, Chem. Phys. Lett., Vol. 254, pp.1-5, 1996.

* Abstract 5456 submitted to the 21st International Symposium on Rarefied Gas Dynamics, Marseille, France, July 26-31, 1998

Semiclassical Analysis of the Tietz-Hua and Morse Model Potentials for Describing Properties of Diatomic Molecules *

F.J. Gordillo-Vázquez, J.A. Kunc

Departments of Aerospace Engineering and Physics,
University of Southern California, Los Angeles, California 90089-1191, USA

1 Introduction

The Hamilton-Jacoby theory and the Bohr-Sommerfeld quantization rule[1] allow one to derive and compare the rotational-vibrational energy levels, radial probabilities and diameters of diatomic molecules (both homo- and heteronuclear) represented by the rotating Tietz-Hua and Morse oscillators. Accurate analytical expressions for the rovibrational levels would greatly simplify the evaluation of the probabilities of large number of atom-molecule and molecule-molecule interactions with the molecules being in highly excited levels. Such interactions are common, for example, in material and plasma processing and high energy flows. The radial probability $P(R)dR$ that the atoms in a diatomic molecule are separated by a distance between R and $R+dR$ plays a key part in modelling of molecular dynamics, especially in trajectory calculations of the atom-molecule and molecule-molecule collisions, where the distance between the atoms in the molecule is one of the variables specifying the initial state of the collision system.

Studies of kinetic properties of low-temperature gases are often based on the assumption that the gas particles have finite 'size'. The molecular 'size' is characterized by the so-called 'molecular diameter', and the sum of the molecular diameters of two colliding particles, the 'collision diameter', is frequently used in studies of transfer of energy and linear momentum between the particles in the gas. The finite-size model of atom-molecule and molecule-molecule collisions would be of great advantage in studies of transport phenomena (Boltzmann integrals, viscosity, etc) in *high-temperature* gases if accurate molecular diameters in such gases were easily available.

2 Internuclear potentials

We assume that diatomic molecules can be treated as rotating anharmonic oscillators stretched by the molecular centrifugal force. The internuclear potential of the rotationally unexcited molecules is then assumed to be either the Morse potential[1],

$$U_M(R) = D \left[1 - e^{-\beta(R-R_e)} \right]^2, \quad (1)$$

or the Tietz-Hua potential[2]-[3],

$$U_{TH}(R) = D \left[\frac{1 - e^{-b_h(R-R_e)}}{1 - c_h e^{-b_h(R-R_e)}} \right]^2, \quad (2)$$

where

$$b_h = \beta(1 - c_h), \quad (3)$$

D is the well-depth of the potential, R_e is the molecular bond length, R is the internuclear distance, β is the Morse constant and c_h is an optimization parameter obtained from *ab initio* or RKR (Rydberg-Klein-Rees) potentials[2].

The rotational (centrifugal) part of the molecular internuclear potential is taken as

$$U_J(R) = \frac{L^2}{2\mu R^2}, \quad (4)$$

where μ is the reduced mass, and L is the angular momentum of the rotating molecule.

The effective internuclear potential of the molecules under consideration is taken as

$$V_{eJ}(R) = U_J(R) + U_V(R), \quad (5)$$

where $U_V(R)$ is given, depending on the assumed oscillator model, by either $U_M(R)$ or $U_{TH}(R)$.

3 Energy expressions

We compare the simplified energy expression for the Morse rotating oscillator,

$$E_1 = \omega_e x_1 - \omega_e x_e x_1^2 + B_e x_1' - D_e x_1'^2, \quad (6)$$

*Abstract 6651 submitted to the 21st International Symposium on Rarefied Gas Dynamics, Marseille, France, July 26-31, 1998

($x_1 = v + 1/2$ and $x_1' = J(J + 1)$), with energies obtained from the Bohr-Sommerfeld quantization of the rotating Morse (E_2)[4] and rotating Tietz-Hua (E_3)[2] oscillators, and with the energy (E_4) obtained from numerical solution[5] of the Schrödinger equation for the Tietz-Hua oscillator;

$$E_2 = D + L^2 A_M - \left[\frac{\beta \hbar x_1}{(2\mu)^{1/2}} - f(L^2) \right]^2, \quad (7)$$

and

$$E_3 = D + L^2 B_J B_J'' - \left(F_0 x_1 - F_{v,J}(L^2) \right)^2, \quad (8)$$

where the functions A_M , $f(L^2)$, B_J , B_J'' , F_0 and $F_{v,J}(L^2)$ are defined in Refs. [2] and [4].

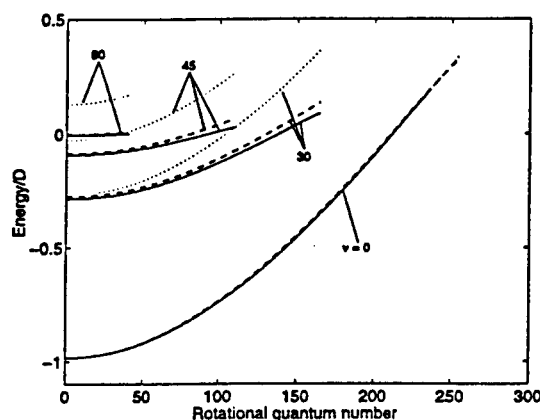


Figure 1: Rovibrational energies E_1 (dotted line), E_3 (dashed line) and E_4 (solid line) for $N_2(X^1 \Sigma_g^+)$. The zero energy corresponds to the dissociation continuum of the rotationless molecule.

4 Diameters and probabilities

Our approach allows one to derive analytical expressions for the molecular diameters and radial probability distributions of atoms in rotationally-vibrationally excited diatomic molecules. The rovibrational energy of the molecules increases with gas temperature and so are the molecular diameters. Since the molecular scattering cross sections are (roughly) proportional to square of the collisional diameters, the rovibrational excitation of molecules can have a significant effect on the kinetic properties of high-temperature gases. The relative increase of the mean internuclear distance $\langle R_{v,J} \rangle_{th,m}$ caused by molecular rovibrational excitation can be given as

$$\rho_{th,m} = \frac{\langle R_{v,J} \rangle_{th,m} - R_e}{R_e}. \quad (9)$$

where $\langle R_{v,J} \rangle_{th,m}$ is defined in Ref. [6].

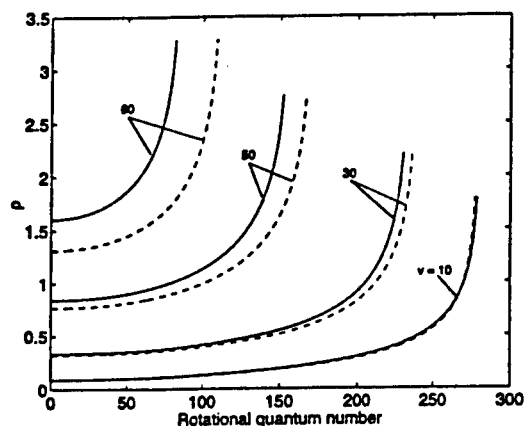


Figure 2: Dependence of the ratios ρ_{th} (solid line) and ρ_m (dashed line) on quantum numbers v and J of the $NO(X^2 \Pi_r)$ molecule.

The present approach also allows to derive the following analytical expression for radial distribution of atoms (as a function of the internuclear distance R) in diatomic molecules represented by the rotating Tietz-Hua oscillator:

$$P'_{th}(R) = \frac{2\mu \sqrt{-\varphi_3'}}{\pi |p_R^h|} \left[\frac{b_h}{\sqrt{2\mu}} - g(v, J) \right], \quad (10)$$

where the functions φ_3' , $|p_R^h|$ and $g(v, J)$ are defined in Ref. [7].

References

- [1] Porter R. N., Raff L.M. and Miller W.H., J. Chem. Phys, Vol 63, p. 2214, 1975.
- [2] Kunc J. A. and Gordillo-Vázquez F.J., J. Phys. Chem. A, Vol 101, No. 8, p. 1595, 1997.
- [3] Hua W., Phys. Rev. A, Vol. 42, p. 2524, 1990.
- [4] Gordillo-Vázquez F.J. and Kunc J. A., J. Thermophysics and Heat Transfer (in press).
- [5] Le Roy R.J., *LEVEL 5.1*; University of Waterloo Chemical Physics Research Report CP-330R-1992.
- [6] Gorbachev Y.E., Gordillo-Vázquez F.J. and Kunc J. A., Physica A (in press).
- [7] Gordillo-Vázquez F.J. and Kunc J. A., J. Mol. Structure (Theochem), (in press).

NUMERICAL SIMULATION - NS 1

ROOM PÉRÈS

WEDNESDAY, JULY 29, 1998

9:10

Numerical Analysis of the Taylor-Couette Problem for a Rarefied Gas by the Direct Simulation Monte Carlo Method *

K. Aoki, Y. Sone, M. Yoshimoto, T. Honda

Department of Aeronautics and Astronautics, Graduate School of Engineering,
Kyoto University, Kyoto 606-8501, Japan

1 Introduction

The Taylor-Couette flow between two coaxial rotating cylinders is one of the most important stability problems in classical fluid dynamics and has been investigated by many scientists and engineers (e.g., [1]). In contrast, the study of the problem for a rarefied gas was commenced rather recently, and some results of numerical analysis using the direct simulation Monte Carlo (DSMC) method have been reported so far (e.g., [2]). In the present study, we also tackle this problem by means of the DSMC method, aiming at clarifying the parameter range for which the steady Taylor vortex flow exists and the detailed structure of the flow. In particular, the effect of the temperature difference of the two cylinders on the existence range and on the flow pattern is investigated in detail.

2 Problem

Consider a rarefied gas in an annular domain $r_1 \leq r \leq r_2$, $0 \leq \theta < 2\pi$, $0 \leq z \leq d$, where (r, θ, z) is the cylindrical coordinate system, bounded by two coaxial circular cylinders and by top and bottom boundaries. The inner cylinder (radius r_1 , temperature T_1) is rotating at angular speed Ω , whereas the outer cylinder (radius r_2 , temperature T_2) is at rest. Investigate the (steady) flow of the gas on the basis of kinetic theory under the following assumptions: (i) the gas molecules are hard (or rigid) spheres; (ii) the gas molecules are reflected diffusely on the inner and outer cylinders and specularly on the top and bottom boundaries ($z = 0, d$); and (iii) the flow field is axisymmetric.

In what follows, we use the following additional notations: ρ is the density of the gas; T is the temperature; v_r , v_θ , and v_z are the r , θ , and z components

of the flow velocity, respectively; ρ_0 is the average density over the annular domain; ℓ is the mean free path of the gas molecules in the equilibrium state at rest with temperature T_1 and density ρ_0 ; $\text{Kn} = \ell/r_1$ is the Knudsen number; and R is the gas constant per unit mass.

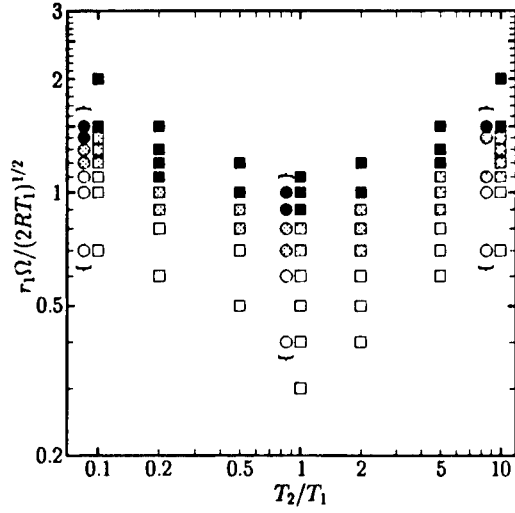
3 Analysis and results

The problem is characterized by the following nondimensional parameters: r_2/r_1 , d/r_1 , $r_1\Omega/(2RT_1)^{1/2}$, T_2/T_1 , and Kn . Taking the equilibrium state at rest with temperature T_1 and density ρ_0 as the initial state, we analyze the problem numerically by the standard DSMC method ([3]) for various values of these parameters. As an example of the result, the existence range of the steady Taylor vortex flow in the $(T_2/T_1, r_1\Omega/(2RT_1)^{1/2})$ plane is shown in Fig. 1 for $r_2/r_1 = 2$, $d/r_1 = 1$, and $\text{Kn} = 0.02$. In the computation, the cross section of the annular domain $r_1 \leq r \leq r_2$, $0 \leq z \leq d$ is divided into 80×80 cells, and basically 50 particles per cell on the average are used. But for $T_2/T_1 = 0.1$, 1, and 10, the results of computation using 100 particles per cell on the average are also shown in the braces (the positions are shifted leftward). Figure 1 shows that the Couette flow is more stabilized as T_2/T_1 decreases from 1 or increases from 2. This fact is contrary to what is inferred from the Bénard problem. Between the region of the Taylor vortex flow and that of the Couette flow, there is a band in which no clear steady state is obtained. At present, it is not clear whether this phenomenon is physical or computational. The typical patterns of the Taylor vortex flow are shown in Figs. 2 and 3.

References

- [1] G. I. Taylor, *Philos. Trans. Roy. Soc. London Ser. A* **223**, 289 (1923); P. Chossat and G.

*Abstract 4361 submitted to the 21st International Symposium on Rarefied Gas Dynamics, Marseille, France, July 26-31, 1998



Symbols	Number of cells ($N \times N$)	Average number of particles per cell
■, □, ○	80 × 80	50
●, ●, ○	80 × 80	100

■ ● : Steady vortical flow (Taylor vortex flow) occurs.
 ■ ● : No steady state is obtained.
 □ ○ : Couette flow occurs.

Figure 1: Existence range of the steady Taylor vortex flow in the $(T_2/T_1, r_1\Omega/(2RT_1)^{1/2})$ plane for $r_2/r_1 = 2$, $d/r_1 = 1$, and $Kn = 0.02$.

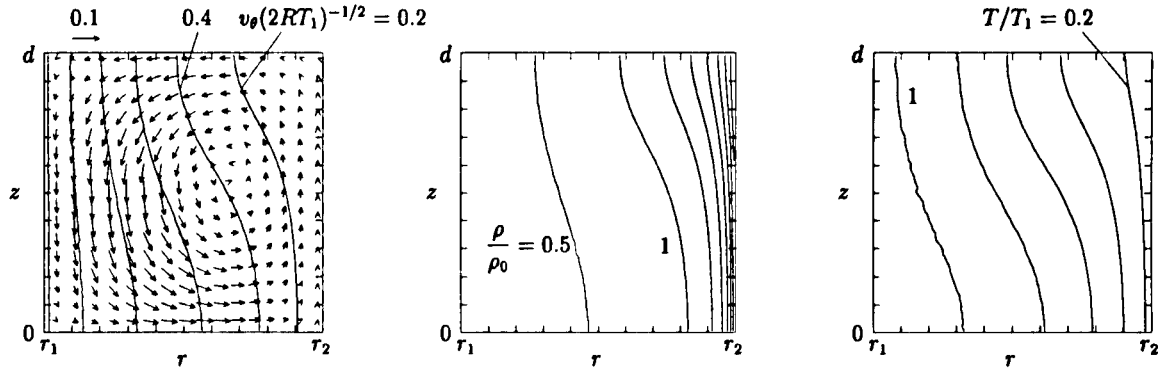


Figure 2: Taylor vortex flow for $T_2/T_1 = 0.1$ and $r_1\Omega/(2RT_1)^{1/2} = 1.5$ ($r_2/r_1 = 2$, $d/r_1 = 1$, $Kn = 0.02$). The isolines $v_\theta/(2RT_1)^{1/2} = 0.2n$, $\rho/\rho_0 = 0.5m$, and $T/T_1 = 0.2k$ are shown in the figures. With respect to v_θ , the inner cylinder is assumed to be rotating in the direction of increasing θ . The arrow indicates the flow velocity (v_r, v_z) in the rz plane, and the scale of $(v_r^2 + v_z^2)^{1/2}/(2RT_1)^{1/2} = 0.1$ is shown in the figure.

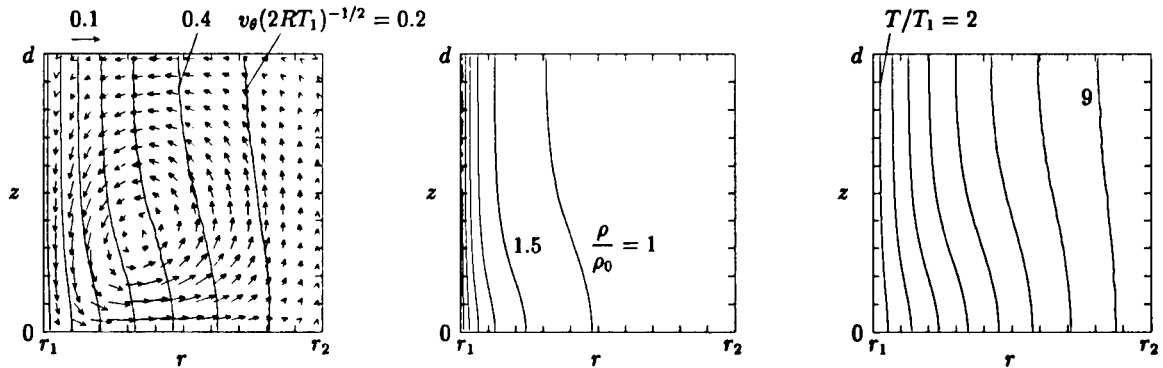


Figure 3: Taylor vortex flow for $T_2/T_1 = 10$ and $r_1\Omega/(2RT_1)^{1/2} = 1.5$ ($r_2/r_1 = 2$, $d/r_1 = 1$, $Kn = 0.02$). The isolines $v_\theta/(2RT_1)^{1/2} = 0.2n$, $\rho/\rho_0 = 0.5m$, and $T/T_1 = k + 1$ are shown in the figures. See the caption of Fig. 2.

Iooss, *The Couette-Taylor Problem* (Springer, New York, 1994).

[2] Stefanov and C. Cercignani, J. Fluid Mech. 256, 199 (1993); D. Riechmann and K.

Nambu, Phys. Fluids A 5, 2585 (1993).

[3] G. A. Bird, *Molecular Gas Dynamics and the Direct Simulation of Gas Flows* (Oxford Univ. Press, Oxford, 1994).

Efficient Modeling of Rarefied Aerothermodynamic Problems with DSMC Method *

M.S. Ivanov, G.N. Markelov, S.F. Gimelshein
Computational Aerodynamics Lab., ITAM SB RAS, Novosibirsk, Russia

1 Introduction

The study of physical phenomena in rarefied nonequilibrium flows is a challenging problem directly related to the development of new aerospace and microelectronic technologies. Rarefied gas dynamics (RGD), that deals with these phenomena, is the synthesis of a great number of fundamental problems such as molecular collision dynamics and energy transfer phenomena in collisions, gas-surface interactions, condensation and evaporation, plume and expansion flows, and many others. All these problems are in close connection with applied, practical issues that can be conventionally divided into two groups. The first group covers the questions related to hypersonic flight of vehicles at high altitudes (mainly external flows), the second direction being mainly represented by the problems that involve material processing, micromechanical devices and microelectronics (mainly internal flows).

Substantial difficulties arising in the study of such flows are caused by both the problems related to rarefaction and physical and chemical effects. It is commonly known that experimental simulation of nonequilibrium low-density flows is rather problematic and expensive. The difficulties of experimental modeling have stimulated an intense development of various approaches for numerical simulation of these flows. Presently there are numerous numerical approaches for solving the problems of RGD, and the choice of this or that approach depends usually on the flow rarefaction, the problem dimension and the presence of real gas effects.

The Direct Simulation Monte Carlo (DSMC) method has become de facto the main technique for the study of complex multidimensional rarefied flows. This is primarily conditioned by a number of its obvious merits: a possibility of using various models of gas particle interaction, including the models of internal degrees of freedom and chemi-

cal reactions, without substantial complication of the computational algorithm; comparative simplicity of extension from one-dimensional problems to two- and three-dimensional ones; a possibility of effective application of the method on up-to-date parallel computers.

The main objective of the paper is to discuss important issues related to the physical and numerical aspects of the DSMC method and aimed at enhancing the efficiency of computer implementation of the method.

2 Efficient DSMC strategy

It is well-known that two different approaches exist to construction and substantiation of the DSMC method. The first approach, developed by G. Bird, can be defined as the physical one, since it is based on physical concepts of rarefied gas and on physical assumptions which form the basis for the phenomenological derivation of the Boltzmann equation.

The second approach is connected with the derivation of a numerical scheme directly from kinetic equations. In [1] the DSMC method was constructed directly from the spatially non-uniform Leontovich master kinetic equation for the N-particle distribution function. The direct use of the N-particle master equation seems to be natural since in numerical calculations by the DSMC method a finite system of simulation molecules is always employed. As the Boltzmann equation may be derived from the master kinetic equation for an N-particle system under the conditions of molecular chaos, the DSMC method is in a certain sense a numerical method for solving the Boltzmann equation. A number of numerical schemes for the DSMC method based on the majorant frequency principle have been obtained in [1] from the Leontovich master kinetic equation. These schemes are derived both in cell and free cell treatments of molecular collisions.

*Abstract 4890 submitted to the 21st International Symposium on Rarefied Gas Dynamics, Marseille, France, July 26-31, 1998

In this paper, SMILE software system for direct statistical simulation using the majorant frequency schemes is presented. Several illustrative examples of application of SMILE to different problems of RGD are shown.

SMILE consists of three subsystems: pre-processing, processing and post-processing. The first one is used for defining the geometrical model, physical properties of its surfaces (wall temperature, etc.), gas-surface interaction laws, computational domain, and the inflow and outflow conditions. Then the DSMC method is used at the processing stage. The analysis of results obtained is performed by means of a postprocessing system that provides for the visualization of flowfields and distributed surface characteristics.

Many principal features are inherent to SMILE, most important of which are the following.

1. Complex 2D, axisymmetrical and 3D flows may be computed with SMILE. Both internal and external flows may be considered. Plume option enables one to obtain a credible solution for plume interactions and plume impingement problems.
 2. Collision procedure is based on the efficient majorant frequency scheme [1] of DSMC method and provides for an accurate capturing collision rate, even for a small number of particles in a cell. One- and multi-species options are available. The discrete Larsen-Borgnakke model is used for RT energy exchange.
 3. Physically correct model [2] for molecular vibrations is used. It is based on a quasiclassical approximation of the scattering theory and includes VT and VV level-by-level transitions. The model [2] for chemical reactions is employed that takes into account vibration-dissociation coupling.
 4. Computational grid is rectangular and adaptive to local flow gradients [3]. The combined use of cell (background cells) and free cell (virtual cells which are smaller than background cells) makes it possible to achieve an adequate spatial resolution in the entire flow field.
 5. Zone decomposition [4] is available in SMILE, which implies the division of the whole computational domain into subdomains with consequent DSMC computations separately in each subdomain. This multi-zone capability is very effective for plume flows.
 6. Parallel implementation [5] may be utilized with either static or dynamic load balancing which yields efficient and scalable parallelization.
- Some additional features, such as a particle cloning and fast particle tracing, are aimed at the reduction of computational costs. A more detailed description

of all these features will be given in the full-length paper.

3 Numerical applications

- 1). *Chemically reacting flow about a wedge.* There is a lack of experimental data on chemically reacting rarefied flows. We therefore used for validation of SMILE's chemical model and numerical scheme the experimental data on the shock stand-off distance, obtained for a wedge in the continuum regime ($Kn = 3.5 \cdot 10^{-4}$).
- 2). *The flow about a ramp and a hollow cylinder.* The computations were performed for experimental conditions ($Re = 30,000$, $M = 10$, $T_0 = 1050$ K).
- 3) *3D flow about a planetary probe model and the Soyuz reentry capsule.* The computations of reacting 3D flows at altitudes 85–90 km were conducted on parallel computers with 256 processors.
- 4). *Plume flows.* The multi-zone capability has been used to compute these flows. The flow inside the nozzle of a 400 N thruster and near plume flowfield was examined and compared with Navier-Stokes results.

References

- [1] Ivanov M.S., Rogasinsky S.V. 1991. *Theoretical analysis of traditional and modern schemes of the DSMC method*, Proc. of 17th Symp. on RGD, Aachen, 629-642.
- [2] Gimelshein S., Gorbachev Yu., Ivanov M., Markelov G. *Statistical Simulation of Nonequilibrium Rarefied Flows with Quasiclassical VVT Transition Models*, Atlanta, 1997, AIAA Paper 97-2585.
- [3] Ivanov M.S., Markelov G.N., Gimelshein S.F., Mishina L.V., Krylov A.N., Grechko N.V. *High-Altitude Capsule Aerodynamics with Real Gas Effects. Journal of Spacecraft and Rockets*, January-February 1998, Vol. 35, No.1.
- [4] Ivanov M., Markelov G., Kashkovsky A., and Giordano D. *Numerical analysis of thruster plume interaction problems*, Second European Spacecraft Propulsion Conference, ESA SP-398, August 1997, 603-610.
- [5] Ivanov M., Markelov G., Taylor S., Watts J. *Parallel DSMC strategies for 3D computations*, Proc. Parallel CFD'96, P.Schiano et al. eds., North Holland, Amsterdam, 1997, 485-492.

Nature of Gasdynamical Measurements and the DSMC Method: some Corrections *

V.P. Memnonov
SPbSU, St Petersburg, Russia

In direct simulation Monte Carlo (DSMC) method simulation of molecular collisions is based on the assumption that molecules are located equally probable inside their cells. This is related to the nature of the gasdynamical measurements where density inside of small space extensions with linear size say R_1 could not be determined during the measurements. So that for any state of the gas system such kind of an assumption is understood as well but it does not contradict long-term experience. It should be also underlined that the time of the gasdynamical measurements is limited from below. And characteristic times of all the processes must be much larger then some time interval Δt_1 , commonly $\Delta t_1 \approx R_1/c$, where c is a characteristic speed. It is true, for instance, for local optical Doppler's shift measurements of the molecular velocity in a cell. Usually all parameter's changes during this time step Δt_1 are so small that the system could be considered quasi-stationary within the latter. Thus when our DSMC decoupling time step Δt is of order of this value Δt_1 we can take advantage of some results of Khinchin for stationary random processes.

Indeed derived with the help of this equal probability assumption configurational distributions for each pair of molecules at the beginning of the collision time interval Δt could be converted into probabilities of some their encounter in the time between t and $t + dt$ building up this way random collision fluxes. Superposition of all such fluxes in a cell forms a stochastic process. Through asymptotical estimates it was established that constituent random fluxes mutually independent, stationary, ordinary and with limited after-effect. So that applicability conditions for the Khinchin limit theorem [1] are verified. The superposition of these random fluxes proves to be then the Poisson process, the number of collisions in a cell K_c being the Poisson variate.

Unlike Kac model results of Yanitskiy [2] the men-

tioned above properties of collision fluxes have direct implications to some refinement of practical implementation of the DSMC method. Ordinarity of the collision fluxes which follows from the neglect of small probabilities for repeated collisions of the same particle within Δt assumes that selection of colliding pairs in the Bird's algorithm should be performed without replacement. Though our results of the up to now simulated problems using this modification have not showed noticeable variations one can expect that for statistical dependence studies like those of Ivanov et al. [3]-[4] it will completely change their findings.

On the other side stationarity of the fluxes allows to approximate in the mean any real trajectory of colliding particles. In fact owing to the decoupling of the molecular convective motion and mutual molecular collisions a collided particle in the Bird's algorithm moves straight from the very beginning of the subsequent "convective" time interval Δt with its newly obtained velocity c' instead of running at least over two asymptotes of a real trajectory first with an old velocity c and then with the new one c' after an apex at the collision time point t somewhere inside Δt . The probability of the apex location does not depend approximately upon time hence the probability of an encounter between t and $t + dt$ within Δt is equal to $dt/\Delta t$, so that the average displacement $Ec(s)$ of the collided particle with velocities c before and c' after an encounter, with

$$s = ct + c'(\Delta t - t)$$

proves to be

$$Ec(s) = c\Delta t/2 + c'\Delta t/2$$

It is quite easy to implement this refinement in the DSMC algorithm by introducing the space corrections for each of the collided pair particles already within the collision time step Δt so that together with the usual line segment $c'\Delta t$ of the subsequent convective motion step they form real two-asymptot trajectory.

*Abstract 5057 submitted to the 21st International Symposium on Rarefied Gas Dynamics, Marseille, France, July 26-31, 1998

In order to estimate the practical significance of this trajectory correction a two-dimensional non-stationary flow in the cavity with one moving and diffusively reflecting wall was simulated by DSMC method both with and without it. If one observes for instance velocity circulation over rectangular contours divided by their lengths, $q(y)$, at the different distances y from the moving wall then in all cases one finds that uncorrected version shows higher $q(y)$ values, the relative error being increased with the distance y up to 10%. Inasmuch as the momentum transport is carried out by the molecules which have been experienced even more collisions in their routes from the moving wall to the closest part of the contour and the error accumulates with every additional encounter. Changes in values of the other parameters for developing rotational motion in the cavity due to this trajectory correction, for instance, vorticity near different cells which shows sensitivity to the correction, are also listed in the paper.

In general the trajectory correction recovers in the mean the joint development inside Δt of the decoupled in DSMC processes by mapping the collision events onto subsequent convective time step. The uncorrected version, on the contrary, accelerates the whole evolution locating all collisions at one time point at the beginning of the convective step instead of distributing them somehow within it.

In real problems cells frequently contain only few particles. Then collisions between particles from neighbouring cells should be accounted for too. In this case the equal probability distributions for each molecule in their cells result in nonstationary collision fluxes nevertheless all necessary formulas are obtained and implemented in the Bird's algorithm with only small modifications. For example mathematical expectation of the 'intercell' collision number $K_{1,2}$ for two neighbouring cells with the molecule numbers N_1 and N_2 during Δt is equal to

$$K_{1,2} = \pi d^2 N_1 N_2 \frac{(v_{m12} \Delta t)^2}{2R^4}$$

where R is linear size of a rectangular cell, d molecular hard sphere diameter and v_{m12} maximum molecular 'intercell' relative velocity. An important condition for this approximate formula to be true is

$$\frac{(v_{m12} \Delta t)^2}{R^2} \ll 1$$

To this order of approximation the number of collisions for molecules from one and the same cell, K_1 ,

should be used with a correction as well

$$K_1 = \frac{\pi d^2 N_1 (N_1 - 1) v_m \Delta t}{2R^3} (1 - 3v_m \Delta t / 2R)$$

Collision probability for a particular pair of molecules w_{ij} is also changed to

$$w_{ij} = \frac{v_{ij}(1 - 0.5\Delta t \sum v_{ijk}/R)}{v_m(1 - 1.5v_m \Delta t / R)}$$

where v_{ijk} is projection of the relative velocity v_{ij} onto the k face normal of the cell and sum goes from 1 to 3. The dependence between relative velocity of the molecules and the cell normals is also present in a similar expression for intercell collisions both promising an opportunity for a description of some weak vorticity in the close vicinity of a single cell. But up to now it was used only in the two-dimensional cavity problem resulting in increase of the mean number of collisions experienced by a molecule up to 12%. Alterations of some system parameters due to intercell collisions are presented in the paper. The influence of the rough surface condition implementation for the moving wall was examined as well.

References

- [1] Yanitskiy V.E., *Operator Approach to Direct Monte Carlo Simulation Theory in Rarefied Gas Dynamics*, Proc. of the 17th Int. Symp. on RGD, ed. A.E.Beylich, Aachen, Germany, pp.770-777, 1991.
- [2] Khinchin A.Y., *Mathematical Methods of Queuing*, Proc. Math. Inst. after Steclov, Vol.49, pp.3-122, 1955 (In Russian).
- [3] Gimelshein S.F., Ivanov M.S., Rogasinsky S.V. *Investigation of Shock Wave Structures by Majorant Cell and Free Cell Schemes of DSMC*, Proc. of the 17th Int. Symp. on RGD, edited by A.E.Beylich, Aachen, Germany, pp.717-726, 1991.
- [4] Ivanov M.S., Rudyak V.Y., *Master kinetic equation and direct statistical simulation* Matem. Model. Vol.1, No 7, pp.93-99, 1989 (In Russian).

Mesh and Algorithm Refinement Using Direct Simulation Monte Carlo *

A.L. Garcia^{1,2}, J.B. Bell¹, Wm.Y. Crutchfield¹, B.J. Alder³

¹ CCSE/LBNL, Berkeley, USA

² Dept. Physics, SJSU, San Jose, USA

³ LLNL, Livermore, USA

When a large range of scales must be spanned, computational fluid dynamics (CFD) calculations employ local mesh refinement so that a fine grid scale is used only in those regions that require high resolution. This paper describes Mesh and Algorithm Refinement (MAR), in which a continuum algorithm, such as a Navier-Stokes solver, is replaced by a particle algorithm, namely Direct Simulation Monte Carlo [1], at the finest grid scale.

The application we consider is the flow of a gas past a microscopic object. When the fluid is not rarefied, this flow is well described by the Navier-Stokes equations except within a few mean free paths of the object's surface. Slip effects are significant within this Knudsen layer and a kinetic formulation is required. DSMC is accurate in both the kinetic and continuum regimes but is computationally intensive in the latter. CFD methods such as finite difference are more efficient than DSMC but are not accurate at mean free path scales. Mesh and Algorithm Refinement is useful since often the kinetic region is a small fraction of the entire computational domain.

In conventional mesh refinement, coarse and fine grids are advanced at different rates yet the steps are taken such that a fine level synchronizes with the overlying coarse grid after a fixed number of time steps. When a fine grid is embedded within a coarse grid, the latter provides boundary conditions on an extended patch surrounding the fine grid. Grid cells at each level of refinement are updated using fluxes computed on their own grid. When coarse grid cells are adjacent to a fine grid, coarse and fine grid fluxes are available on the shared faces. To preserve strict conservation and accuracy, the coarse grid is updated using the fine grid fluxes; these fluxes are accumulated over several fine grid steps since the coarse grid takes larger time steps.

This correction of fluxes at the coarse scales using the fine scales is known as "refluxing." Also, at the end of a coarse time step, the cells of the coarse grid that have a fine grid below them are reset according to the averages over the fine cells that they cover.

In Mesh and Algorithm Refinement, the finest grid level is evaluated by a DSMC calculation. First, the fluxes at each coarse cell face are computed using an explicit Godunov algorithm for the convective fluxes and conventional finite difference methods for the diffusive fluxes [2]. These fluxes are used to advance the conserved densities (mass, momentum and energy) by one coarse grid time step. To maintain accuracy, the DSMC calculation advances by smaller time steps, typically a fraction of the mean collision time. The DSMC region is surrounded by buffer cells (see Fig. 1). At the beginning of each DSMC time step, the buffer cells are filled with particles using the Chapman-Enskog distribution [3] according to the hydrodynamic values (density, fluid velocity, temperature) and their gradients on the overlaying coarse grid. Since the coarse grid advances first, these values are time interpolated between coarse time steps. Next, particles in both the central and buffer regions move a single DSMC time step. If a particle crosses the interface between these regions, a "flux register" accumulates its contribution to the fluxes of the conserved densities for the buffer cell face that the particle passes. After moving the particles, any outside the central DSMC region are discarded and collisions among the remaining particles are evaluated. A cell/subcell structure, which is independent of the continuum mesh, is used in selecting and evaluating DSMC collisions.

When the DSMC region has advanced for an entire coarse grid time step, refluxing corrects the conserved densities for the continuum cells that lie within the buffer region. The cells of the coarse grid that overlay the central DSMC region are reset

* Abstract 5821 submitted to the 21st International Symposium on Rarefied Gas Dynamics, Marseille, France, July 26-31, 1998

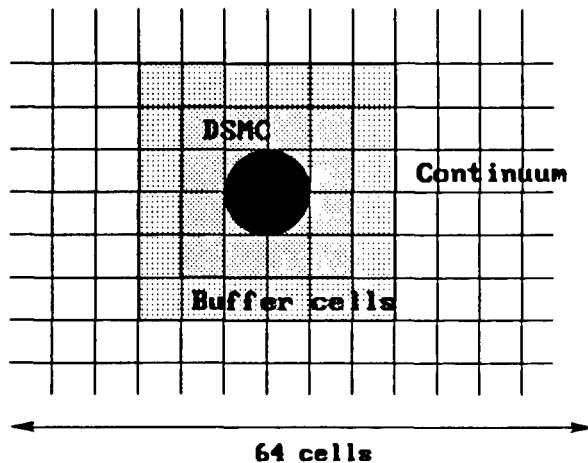


Figure 1: Schematic showing a DSMC region, which contains a microscopic sphere, embedded within a continuum CFD calculation.

according to the conserved densities in the DSMC region. These two steps guarantee that, in the absence of external sources, total mass, momentum and energy are conserved (to within round-off error) in the computational domain. DSMC patches can be adaptively expanded or reduced during a computation by specifying the criterion (e.g., gradient local Knudsen number [4], Chapman-Enskog breakdown parameter [3]) when a kinetic description is necessary.

Results from an MAR calculation are shown in Fig. 2. The coarse grid is $64 \times 64 \times 64$ with a $4 \times 4 \times 4$ DSMC region containing a sphere at its center. The DSMC region has 2.8×10^5 particles and is located midway between the center and left side of the figure. The width of the computational domain is 8×10^{-4} cm, the sphere's diameter is 2.5×10^{-5} cm, and in the free stream $\lambda = 2.74 \times 10^{-6}$ cm. The paper will present further examples of MAR calculations, describe the details of its implementation, and compare it with other continuum/DSMC hybrids [5]–[8].

References

- [1] Bird G.A., *Molecular Gas Dynamics and the Direct Simulation of Gas Flows*, Clarendon, Oxford, 1994.
- [2] Saltzman M.J., *An Unsplit 3D Upwind Method for Hyperbolic Conservation Laws*, J. Comp. Phys., Vol. 115, pp. 153–168, 1994; Steinthorsson E., Modiano D., Crutchfield Wm.Y., Bell J.B., and Colella P., *An Adap-*

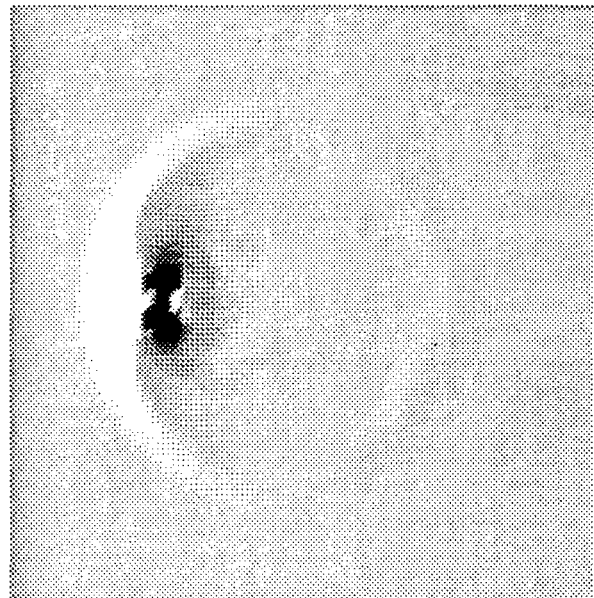


Figure 2: Pressure distribution near an impulsively started sphere moving at Mach 2.

tive Semi-implicit Scheme for Simulations of Unsteady Viscous Compressible Flows, AIAA Paper 95-1727, 1995.

- [3] Garcia A.L., and Alder B.J., *Generation of the Chapman-Enskog Distribution*, to appear in J. Comp. Phys., 1998.
- [4] Boyd I.D., Chen G., and Candler G.V., *Predicting Failure of the Continuum Fluid Equations in Transitional Hypersonic Flows*, Phys. Fluids, Vol. 7, pp. 210–219, 1995.
- [5] Wadsworth D.C., and Erwin D.A., *Two-Dimensional Hybrid Continuum/Particle Simulation Approach for Rarefied Hypersonic Flows*, AIAA Paper 92-2975, 1992.
- [6] Eggers J., and Beylich A., *New Algorithms for Application in the Direct Simulation Monte Carlo Method*, Prog. Astro. Aero., Vol. 159, pp. 166–173, 1994.
- [7] Hash D.B., and Hassan H.A., *A Hybrid DSMC/Navier-Stokes Solver*, AIAA Paper 95-0410, 1995.
- [8] Le Tallec P., and Mallinger F., *Coupling Boltzmann and Navier-Stokes Equations by Half Fluxes*, J. Comp. Phys., Vol. 136, pp. 51–67, 1997.

A Hybrid Euler/DSMC Approach to Unsteady Flows *

R. Roveda, D.B. Goldstein, P.L Varghese
University of Texas at Austin, Austin, USA

1 Introduction

Renewed interest in vehicles that operate in the transitional regime has spurred the development of hybrid codes incorporating methods that model both rarefied and continuum regions simultaneously. Recent effort to create hybrid continuum-rarefied methods include those of Hash and Hassan, Erwin and Wadsworth, Bourgat *et al* and Dutweiler *et al*. Hybrid methods generally interface an Euler or Navier-Stokes equation solver (continuum) with a Lagrangian method (DSMC).

2 Adaptive, hybrid solver

Roveda *et al*. [1] proposed a hybrid solver that combines Nadiga's Euler Adaptive Discrete Velocity (ADV) [2] approach with Bird's DSMC [3]. Patches of DSMC automatically resolve rarefied regions where the Knudsen number exceeds a pre-set threshold, whereas ADV simulates the remaining regions in translational equilibrium. Exchange of information occurs at every time step through an overlapping, multi-cell interface that uses sampled macroscopic DSMC properties as boundary conditions for ADV and, conversely, macroscopic ADV properties to initialize and inject particles into the DSMC region. The hybrid method has also been successfully applied to unsteady, single species, 2-dimensional pressure driven slit flow.

The purpose of the present work is three-fold; first to upgrade the hybrid, adaptive ADV/DSMC to handle multiple species; second, to implement the exchange of rotational energy between ADV (fully excited rotation) and DSMC (classical Larsen-Borgnakke model); and third to adopt adaptive sampling "free cells" that vary in relation to the unsteady flow gradients.

*Abstract 6326 submitted to the 21st International Symposium on Rarefied Gas Dynamics, Marseille, France, July 26-31, 1998

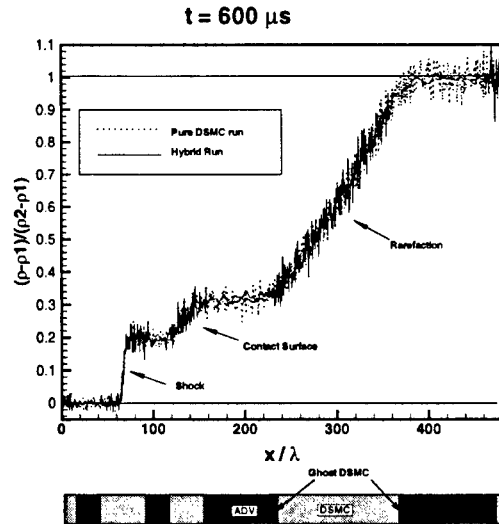


Figure 1: Adaptive, hybrid simulation of shock tube. Comparison of hybrid density profile to full DSMC calculation.

3 Multi-species ADV solver

Extension of the current DSMC code to multiple species is straightforward and requires the specification of distinct molecular masses and collision cross sections. On the other hand, ADV requires the solution of the multi-component Euler equations as presented in [4] for a n-component mixture:

$$\frac{\partial(\rho_m Y_n)}{\partial t} + \frac{\partial(\rho_m u_m Y_n)}{\partial x} = 0 \quad (1)$$

$$\frac{\partial(\rho_m u_m)}{\partial t} + \frac{\partial(\rho_m u_m^2 + P_m)}{\partial x} = 0 \quad (2)$$

$$\frac{\partial E_{tm}}{\partial t} + \frac{\partial(u_m E_{tm} + u_m P_m)}{\partial x} = 0 \quad (3)$$

where Y_n represent the mass fractions for the n^{th} mixture species and the subscript m refers to mixture quantities. The Euler equations (1-3) are integrated with the original ADV finite volume technique that sums the half fluxes of the mass fractions and of the mixture energy and momentum.

The mixture half fluxes result from superposition of the single-species energy and momentum half fluxes that arise from the kinetic splitting of each species distribution function.

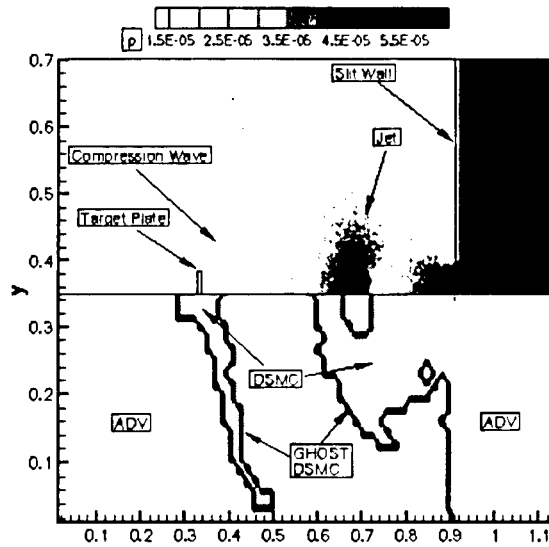


Figure 2: Adaptive, hybrid simulation of slit flow showing density contours (top half) and regions of application of DSMC and ADV (Euler) solvers (bottom half).

4 Rotational energy

In DSMC the classical Larsen-Borgnakke model governs the exchange between translational and rotational energies of colliding DSMC molecules. Because the interface exists in a region of translational and rotational equilibrium, the macroscopic temperature sampled from the DSMC particles is sufficient to calculate the internal energy ($e = e_T + e_R = \frac{5}{2}RT$ for diatomic molecules) of the ADV buffer cells (DSMC cells which provide boundary conditions for the ADV finite volume integration).

5 DSMC collision algorithm

The "free cell" technique of reference [5] incorporates variable sized "collision" sub-cells. The collision partner selection region at equilibrium coincides with background (property sampling) DSMC cells whereas the particle interaction distance (size of the "collision" cell) in nonequilibrium regions varies adaptively with the property gradients. The "free cell" technique is incorporated in the ADV/DSMC code to provide an adaptive resolution capability *within* DSMC. The approach of

adaptively modifying the "collision" sub-cells size in *unsteady* DSMC calculations appears unique.

6 Conclusion

The following improvements to the hybrid, adaptive Euler/DSMC approach will be presented:

- the upgrade of the ADV solver and the ADV/DSMC interface to simulate multi-species gas flows,
- the hybrid capability to simulate rotationally active diatomic gases,
- the adaptation of the free cell idea to an *unsteady* DSMC simulation. The improvements in the discrete velocity solver and the creation of a stable and consistent Euler/DSMC interface for multi-component, rotationally active gases represent a novel effort. The improved hybrid, adaptive method will simulate a 1-D shock-tube for a gas composed of two diatomic species with dissimilar masses. Further 2-D results will be presented if available.

References

- [1] Roveda, R., Goldstein, D. B., and Varghese, P. L., "A Hybrid Euler/Particle Approach for Continuum/Rarefied Flows," To be published in the *Journal of Spacecraft and Rockets*.
- [2] Nadiga, B. T., "An Euler Solver Based on Locally Adaptive Discrete Velocities," *J. Stat. Physics*, Vol. 81, No. 1-2, 1995, pp. 129-146.
- [3] Bird, G. A., *Molecular Gas Dynamics and the Direct Simulation of Gas Flows*, Clarendon Press, Oxford, 1994.
- [4] Larrouturou, B., and Fezoui, L., "On the Equations of Multi-Component Perfect or Real Gas Inviscid Flow," in *Nonlinear Hyperbolic Problems*, edited by Carasso Charrier Hanouzet Joly (Lectures Notes in Mathematics, Vol. 1402, Springer-Verlag, Heidelberg, 1989).
- [5] S. F. Gimelshein and M. S. Ivanov, "Investigation of Shock Wave Structures by Majorant Cell and Free Cell Schemes of DSMC," paper in proc. of 17th International Symposium on Rarefied Gas Dynamics., Aachen, Germany, July, 1990, pp. 718-726.

NUMERICAL SIMULATION - NS 2

ROOM PÉRÈS

THURSDAY, JULY 30, 1998

9:10

Characteristic Methods for Fokker-Planck and Fermi Pencil Beam Equations *

M. Asadzadeh

Department of Mathematics, Chalmers University of Technology and
the University of Göteborg, S-412 96 Göteborg, Sweden

Introduction

A pencil beam is a particle beam that enters a medium through a single point on the boundary, with all incident particles moving in the same direction. The earliest pencil beam formula was proposed by Fermi [5]. Starting from a microscopic model of monoenergetic particle transport, under the small-angle approximations, ($\sin \theta \approx \theta$ and $\cos \theta \approx 1$), Fermi derived a formula resembling the Fokker-Planck equation. Energy dependence was subsequently added to the formula by Eyges [4]. Recently, a more accurate pencil beam formula is obtained by Jette [6], where the small arguments are extended to one term beyond the leading behavior. Pencil beam algorithms, also referred as *Fermi-Eyges multiple-scattering theory*, are now in widespread use in electron dose calculations in radiative cancer therapy. These algorithms are fast and efficient, however, they are derived, mostly, in perfectly heuristic manner leaving unresolved, critical treatment, regions. The, extremely popular, Monte Carlo codes, based on mathematical formalism, resolve criticalities, however, are too slow.

For the Fermi equation, closed-form solution is available for the boundary value problem describing a pencil beam normally incident on a homogeneous, scattering, nonabsorbing media filling a half-space. (No such closed-form solution is known for the Fokker-Planck equation itself, neither for the general case of energy dependent Fermi equation in a nonhomogeneous, scattering/material, media).

The Fermi equation can be viewed as the leading term in a certain asymptotic expansion of the Fokker-Planck equation [3]. The Fokker-Planck equation in turn can be viewed as the leading term in an asymptotic expansion of the linear Boltzmann equation [7].

In the present paper, we study approximate solutions for certain boundary value problems for Fokker-Planck and Fermi pencil beam equations modeling an energy dependent, unisotropically scattering particle transport through an object, with layer inhomogeneities, occupying a two dimensional polygonal domain.

Model Problems and Results

The general Fokker-Planck equation is a degenerate type, convection dominated, convection-diffusion equation given by

$$\omega \cdot \nabla_r J(r, \omega) = \frac{\sigma_{tr}}{2} \mathcal{A}J, \quad (1)$$

where $\omega = (\omega_1, \sqrt{1 - \omega_1^2} \cos \theta, \sqrt{1 - \omega_1^2} \sin \theta)$ and

$$\mathcal{A} = \frac{\partial}{\partial \omega_1} (1 - \omega_1)^2 \frac{\partial}{\partial \omega_1} + \frac{1}{(1 - \omega_1)^2} \frac{\partial^2}{\partial \theta^2}, \quad (2)$$

is the Laplace operator on the unit sphere. The two dimensional correspondence to Eq. 1 models both Fokker-Planck and Fermi equations, where $r = (x, y)$, $\omega = (1, z)$, $z = \tan \theta$, and

$$\mathcal{A} = \frac{\partial}{\partial z} \left(a(z) \frac{\partial}{\partial z} b(z) \right), \quad (3)$$

with $a(z) = 1 + z^2$ and $b(z) = (1 + z^2)^{3/2}$, corresponds to Fokker-Planck equation, while

$$\mathcal{A} = \frac{\partial^2}{\partial z^2}, \quad (4)$$

associated with a certain, *forward peakedness*, assumption, $\theta \in (-\pi/2, \pi/2)$, see [1], gives the simplest form of the Fermi equation.

For these model problems, we study the stability of *Characteristic streamline diffusion*, (CSD), method. CSD is a modified Characteristic Galerkin method for hyperbolic type problems based on discretizations with piecewise polynomials. For a reliable and

*Abstract 2100 submitted to the 21st International Symposium on Rarefied Gas Dynamics, Marseille, France, July 26-31, 1998

efficient, phase-space discretization, algorithms we have employed the *a posteriori* error procedure.

Optimal *a priori* estimates for approximate solutions of PDEs', in some weighted L_2 -norms, can be written as, (see [1] and [2]),

$$\|e\| \leq Ch^{r+s} \|u\|_{H^{r+1}}, \quad (5)$$

where $e = u - u_h$, with u and u_h being the continuous and discrete solutions, respectively, C is a constant, $r \in \mathcal{R}$, $s = 1$, for the elliptic and parabolic type problems, and $s = 1/2$, for the equations of hyperbolic character. The draw back in (5) lies in the presence of the constant C , which might be large or grow by reducing mesh parameter function h , and also the norm of the, *unknown*, solution u on the right hand side. In the CSD method:

(i). A *streamline diffusion* modification of the test function, along the characteristic, is added in the variational formulation in order to get a weighted least square control of the residual $R(u_h)$ of the approximate solution u_h and

(ii). In numerical algorithms for solving Eq. 1, (a degenerate type, convection dominated, since σ_{tr} is very small, convection-diffusion equation), both non-smooth data and layer inhomogeneities introduce, propagated, discontinuities to the system advancing in the direction of the characteristics. To prevent oscillations at the discontinuities an artificial viscosity term with a coefficient $\varepsilon(h) \rightarrow 0$, as the *mesh size* $h \rightarrow 0$, is added to the diffusion term. This corresponds to adding more dissipation, to the system, enough to control oscillations when $\varepsilon \approx \varepsilon(Ch^\alpha R(u_h))$, $\alpha \approx 2$.

In a *a posteriori* estimates combining (i) and (ii) we may replace C by $C^s C^i$ and u by $R(u_h)$ in the right hand side of (5). Here, C^s is a stability constant, C^i is an interpolation constant and the residual term $R(u_h)$, which depends on the known approximate solution, measures how well the discrete solution satisfies the given differential equation locally. Hence

$$\|e\| \leq C^s C^i h^{r+s} \|R(u_h)\|_{H^{r+1}}. \quad (6)$$

Observe that ε , depending on u_h , suggests to discretize linear problems having oscillatory behavior with nonlinear algorithms. The structure of the proof of the *a posteriori* error estimate (6) is as follows:

a) Representation of the error e in terms of the residual $R(u_h)$ and the solution φ of a linearized dual problem with e as right hand side.

b) Use of the Galerkin orthogonality to replace φ by $\varphi - \Phi$, where Φ is a finite element interpolant of φ .

c) Interpolation error estimates for $\varphi - \Phi$ in terms of certain derivatives $D\varphi$ of φ and the mesh function h .

d) Strong stability estimate for the dual solution φ estimating $D\varphi$ in terms of the data e of the dual problem.

Our analysis, associated with appropriate adaptive algorithms, provide a reliable, (the error is controlled by known bounded parameters decreasing with the mesh size $h \rightarrow 0$), and efficient, (in the sense that approximately minimum number of nodes are involved in a, not overly refined, discrete mesh), mathematical approach to approximate solution of pencil beam equations with physically relevant boundary data. The adaptive FEM tool boxes are getting fast and concise. With these properties, adaptive *a posteriori* studies may serve as a realistic alternative to the, existing, Monte Carlo based approaches.

References

- [1] Asadzadeh, M., *Streamline Diffusion Methods for Fermi and Fokker-Planck Equations*, TTSP, 26, 319-340(1997).
- [2] Asadzadeh, M., *On Convergence of FEM for the Fokker-Planck Equation*, Proc. 20RGD, ed. by Ching Shen, Peking University press, 309-314(1997).
- [3] Börgers, C. and Larsen, E. W., *Asymptotic derivation of the Fermi pencil beam approximation*, Nucl. Sci. Eng. 123, 343-357(1996).
- [4] Eyges, L., *Multiple scattering with energy loss*, Phys. Rev. 74, 1534(1948).
- [5] Fermi, E., quoted in Rossi B. and Greisen K., *Cosmic ray theory*, Rev. Mod. Phys. 13, 240(1941).
- [6] Jette, D., *Electron dose calculation using multiple-scattering theory. A. Gaussian multiple-scattering theory*, Med. Phys. 15, 123-137(1988).
- [7] Pomraning, G. C., *The Fokker-Planck operator as an asymptotic limit*, Math. Mod. Meth. Appl. Sci. 2, 21-36(1992).

Statistical Simulation of Low-Speed Unidirectional Flows in Transition Regime *

J. Fan, C. Shen
Institute of Mechanics, CAS, Beijing 100080, China

Low-speed flows in transition regime, due to their importance in micro-electro-mechanical systems (MEMS), become more interesting. To understand the features and mechanisms of this kind of flows, a lot of experimental work has been carried out, especially about microchannel flows (cf. e.g. study by Ho's group^[1]). Typical channel dimensions are $1.2\text{ }\mu\text{m}$ high by $3000\text{ }\mu\text{m}$ long, the undisturbed gas pressure and temperature being 1 atm and 298K, respectively, and the typical inflow velocity less than 1m/s. Slip flow is observed, and the measured mass flow rate is higher than that based on the Navier-Stokes equation with the non-slip boundary condition. Though the mass flow rate calculated from the Navier-Stokes equation with a slip boundary condition is in agreement with the experimental data, the predicted rate is sensitive to the accommodation coefficient which is introduced to represent the tangential momentum transfer between the impinging molecules and the wall. Some investigators attempted to use the DSMC method to analyze low-speed transitional flows^[2,3,4], but the speed range investigated was not typical for MEMS. The unavoidable statistical scatter, and the fact that it declines only as the square root of the sample size, has been a major problem for the DSMC method^[5], and becomes unsurmountable when the flow velocity is very small. In the simulation of a stationary homogeneous gas, the statistical fluctuation would give rise to an unrealistic macroscopic velocity at different sample sizes. When the gas temperature is 273K, the x component of which in the unit of m/s is listed in table 1. It shows that a useful small value macroscopic information would be completely lost in the background noise for even rather large sample sizes.

To overcome this difficulty a modification in the DSMC method is attempted which suggests to preserve some macroscopic information a molecule had originally and to use it to obtain the macroscopic

Table.1 x component of unrealistic macroscopic velocity in a stationary homogeneous gas at different sample sizes

No. of rus	x component at different sample sizes in m/s				
	2×10^4	2×10^5	2×10^6	2×10^7	2×10^8
1	2.31955	-.22111	-.12976	.09033	.01571
2	-.48467	-.08253	.10709	-.10442	-.00225
3	-2.52984	-.17185	-.17960	-.03966	.02669
4	2.00947	.77852	-.13855	.01377	.00223
5	.81402	.34463	.12286	.11974	.00135
.
.
.
96	1.23108	.17202	-.11175	-.00985	-.01312
97	-.95669	-.26057	.09389	.03015	.02429
98	-1.22438	-.17159	.02310	-.07220	-.00433
99	1.59241	-.46803	-.06548	-.02074	.01210
100	-5.00094	.74079	.00648	-.06647	.02256
maximum in 100 runs	-6.24661	1.83010	.53007	.15443	.03654

quantities. In the context of slow unidirectional flow problems with attention focused on the momentum issue it is suggested to record the velocity of a molecule as composed of a thermal part and an information preserving part: the thermal part in the whole obeys the normal distribution law and changes its values during molecular collision, the information preserving part in this case is the macroscopic velocity and is uniform for all molecules originated from the same free stream or the same wall and remain unchanged during molecular collisions but gains new values when reflected from a wall. The molecular trajectory is determined by c_i and u_i . Macroscopic quantities such as the flow velocity and shear stresses are determined solely by the statistical sums of u_i .

This method, called the Original Information Preservation(OIP) method, has been used to simulate low-speed unidirectional flows in transition regime, namely the Couette flow and Rayleigh problem. The calculations are accomplished with a PC computer in several minutes. For the Couette flow at temperature of 273K, one of the plates is at $y=h/2$ moving in x direction with speed of 20cm/s,

*Abstract 2847 submitted to the 21st International Symposium on Rarefied Gas Dynamics, Marseille, France, July 26-31, 1998

and the other at $-h/2$ moving with -20cm/s . The Knudsen number is defined as λ/h , where h is the channel height. The simulated velocity distribution in y direction and shear stress on the wall in the whole transitional regime are in excellent agreement with the numerical solution of the linearized Boltzmann equation provided by Sone, et al.^[6] (see Fig.1). For the Rayleigh problem (for gas temperature 273K and the wall speed 1m/s), the simulated velocity distribution in the normal direction agrees well with exact solution in the case of free molecular flow and analytical solution of the Navier-Stokes equation with the a slip-flow boundary condition in the two extremes of the Kn number. In transition regime, to obtain a benchmark, the direct simulation Monte Carlo method was used. In order to reduce the statistical scatter small enough, the sample size reached 2×10^8 which took about 180 CPU hours on a DEC Alpha Server 1000A. Excellent agreement in trend of the OIP and DSMC simulated results is obtained (see Fig.2 where t denotes time non-dimensionalized with the collision time).

References

- [1] C.M.Ho & Y.C.Tai, *Micor-electro-mechanical systems(MEMS) and fluid flows*, Ann. Rev. Fluid Mech., vol.30, pp.579-612 (1998).
- [2] K.S.Breuer, E.S.Piekos and D.A.Gonzales, *DSMC simulations of continuum flows*, AIAA Paper 95-2088(1995).
- [3] E.S.Piekos and K.S.Breuer, *DSMC modelling of micromechanical devices*, AIAA Paper 95-2089(1995).
- [4] C.K.Oh, E.S.Oran and B.Z.Cybyk, *Microchannel flow computed with the DSMC-MLG*, AIAA-Paper 95-2090.
- [5] G.A.Bird, *Molecular Gas Dynamics and the Direct Simulation of Gas Flows*, Clarendon Press, Oxford (1994).
- [6] Y.Sone, S.Takata and T.Ohwada, *Numerical analysis of the plane Couette flow of a rarefied gas on the basis of the linearized Boltzmann equation for hard-sphere molecules*, Eur. J. Mech., B/Fluids, vol.9(3), pp.273-288 (1990).
- [7] E.P. Gross and S.Ziering, *Kinetic theory of linear shear flow*, Phys.Fluids, vol.1(3), pp.215-224(1958).

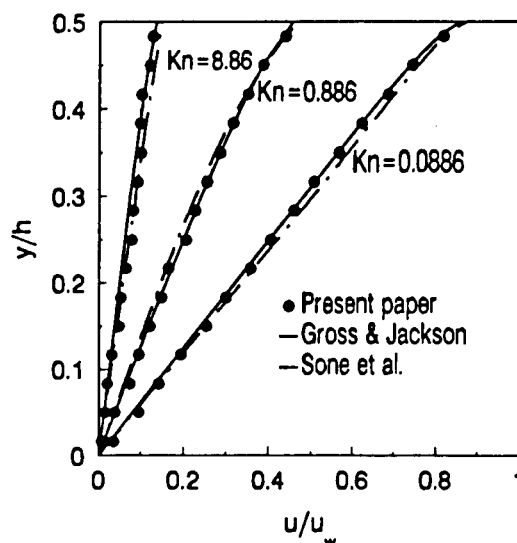


Figure 1: Comparison of velocity distribution in the Couette flow

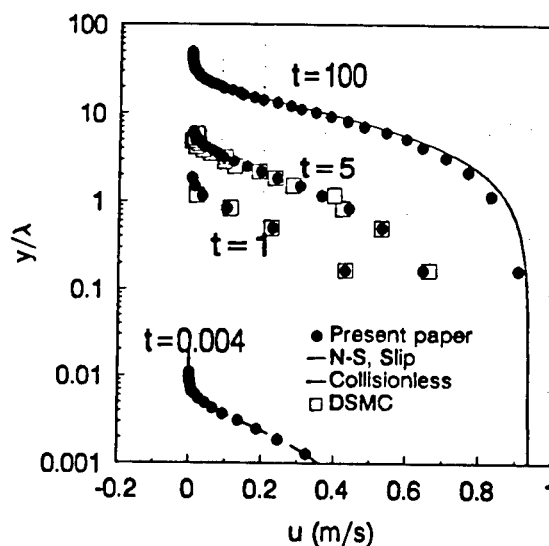


Figure 2: Comparison of velocity distribution in the Rayleigh problem

Self-Consistent Particle Simulation of Physical Processes with Disparate Time Scales in Low Pressure Gas Discharges *

V.V. Serikov¹, S. Kawamoto¹, K. Nanbu²

¹ Advanced Simulation Crew, NSG Co., Ltd., Japan

² IFS, Tohoku University, Japan

1 Introduction

Nowadays simulation has become indispensable in the design of the increasingly sophisticated equipment for plasma assisted materials processing [1]. However, the basic capabilities of the simulation models and techniques are still not enough for a great number of engineering problems. One of the reasons is the variety and complexity of the physical processes to be taken into account in a model [2, 3]. These processes are typically characterized by disparate time and length scales, what makes their coupling in a single model quite a challenge.

To be more specific, we shall consider a low pressure (42 mTorr) glow discharge in argon between two parallel electrodes separated by 40 mm. The electrodes are kept at a constant temperature $T_w = 323$ K. The discharge voltage may range from several hundreds to a thousand volts. For the above-mentioned conditions, the typical time scales are $\tau_e \sim 10^{-9}$ s for electrons (period of electron plasma oscillations), $\tau_i \sim 10^{-7}$ s for ions (period of ion oscillations and mean free time for charge-exchange collisions), $\tau_n \sim 10^{-6}$ s for energetic charge-exchange or sputtered neutrals (relaxation time for thermalization), $\tau_a \sim 10^{-3}$ s for pressure equalization, and $\tau_d \sim 10^{-2}$ s for diffusion processes (e.g., heat conduction) in the background gas.

One way to handle such a problem is to subdivide it into a number of blocks according to the time scales and to create a simulation module for each of these blocks. Then, an iterative procedure has to be designed wherein the output of one module is used as input for another, thus providing the coupling among the blocks. The simulation is repeated until convergence is achieved. This seems to be a simple though computationally extensive approach.

Following are two examples showing how to self-

consistently treat the disparate time scale processes in the glow discharge within the framework of a single particle simulation model.

2 Plasma Simulation

When simulating the evolution of the ion-electron particle system from the initial state of uniform plasma prevailing in the gap between the electrodes, a major part of the computational time is spent for attaining the steady state of the discharge. The evolution rate is limited primarily by the ion loss to the walls during the sheath formation, which is a quite slow process on the electron time scale.

For the direct current discharge, there is a possibility to accelerate this evolution by handling the ion and electron systems somewhat independently, e.g., by advancing the ions through the time interval τ_i (comprised of several Δt_i), while the electrons are advanced through a shorter time interval τ_e (generally, also consisting of a number of Δt_e), as shown schematically in Fig.1. Note, if $\tau_i = \tau_e = \Delta t_i$, we have a conventional subcycling scheme [4].

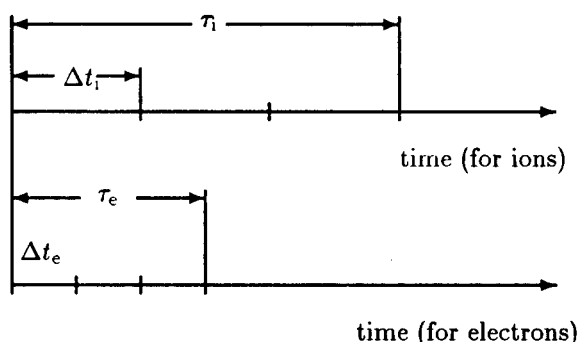


Figure 1: Time scales for ions and electrons

However, the ion and electron systems are coupled through the ion impact secondary electron emission

*Abstract 4576 submitted to the 21st International Symposium on Rarefied Gas Dynamics, Marseille, France, July 26-31, 1998

from the surfaces and through electron-atom ionization collisions. The flux of ions, increased by a factor of τ_i/τ_e as compared to that in the conventional algorithm, should be properly balanced by the ion creation resulting from ionization. To achieve this, every secondary electron emitted due to ion impact is considered as a real electron - with the probability τ_e/τ_i , and as a fake electron - with the additional probability $1 - \tau_e/\tau_i$. The real and fake electrons are followed further in the course of simulation, being always distinguished. If they produce ionization, the new born electrons are of the same kind as the parent ones. The fake electrons are not counted when the charge assignment is carried on to calculate the self-consistent electric field. They are necessary only for ion creation in ionization collisions, thus making up the local balance of ions whose flux is increased. The fake electrons are eliminated from the simulation in the bulk region, when their energy falls to a certain level which is below the ionization potential. The speedup factor, roughly estimated as τ_i/τ_e , can be in the range of 10 - 100, as our test calculations show. The described scheme has been successfully employed for the 3D glow discharge simulation [5].

3 Plasma and Gas Simulation

The background gas in glow discharge does not necessarily have uniform and constant density and temperature as is usually assumed in simulations. It can be substantially affected by the discharge plasma and/or sputtered material atoms in the vicinity of the cathode (e.g., the so-called "sputtering wind" phenomenon [6]). A pronounced background gas heating effect has been recently predicted by the particle-in-cell/Monte Carlo (PIC-MC) simulation in which the heat conduction equation was solved based on the sampled thermal energy input into the gas [7]. Here we outline a PIC/DSMC model wherein all species and processes are treated by the particle method.

The simulation algorithm incorporates two basic modules: a plasma module and a neutral-species module. In the former, the glow discharge is simulated by the PIC-MC method with a self-consistent treatment of the electric field. In the latter, the motions and collisions of both background gas atoms and sputtered atoms are simulated by the DSMC method. Simulation starts with a steady-state discharge for a uniform distribution of the gas number density n_0 and temperature $T = T_0$ equal to the temperature T_w of the electrodes, the gas be-

ing considered in equilibrium all over the discharge space. The main cycle consists of one step Δt_i of discharge plasma simulation and N_{cycl} steps Δt_n of neutral species simulation which are followed by sampling of the molecular microparameters. This cycle is repeated N_{update} times, whereupon the the gas temperature and density are calculated from the sampled data. The simulation is continued until the steady state is achieved and enough statistics is gathered to calculate the macroparameters of interest. Note that the time step in the plasma module is $\tau_i = \Delta t_i = 10^{-9}$ s (the electrons are advanced with the time step $\tau_e = \Delta t_e = 0.5 \times 10^{-10}$ s, as described in the previous section), while it is equal to $\Delta t_n = 0.5 \times 10^{-7}$ s in the neutral-species module. The difference of the time steps is accounted for by the statistical weights of the produced sputtered atoms W_s , i.e.,

$$W_s = W_i \frac{\Delta t_n N_{cycl}}{\Delta t_i},$$

where W_s , and W_i stand for the weights of sputtered atoms and ions, respectively. It is also taken into account while simulating collisions among ions (viewed as if they have statistical weights equal to $W_i \Delta t_n N_{cycl} / \Delta t_i$) and background gas atoms (with weights W_n). In other words, we presume that the discharge is in a steady state over a longer time period $\Delta t_n N_{cycl}$ and hence the production rates of the energetic neutral particles are constant in $\Delta t_n N_{cycl}$.

References

- [1] Kushner M., Solid State Technology, pp.135-144, June 1996.
- [2] Nanbu K. and Uchida S., Proc. 19th Int. Symp. Rarefied Gas Dynamics, Vol.1, pp.602-610, Oxford University Press, 1995.
- [3] Serikov V.V. and Nanbu K., J. Vac. Sci. Technol. A, Vol.14, No.6, pp.3108-3123, 1996.
- [4] Birdsall C.K. and Langdon A.B., *Plasma Physics via Computer Simulation*, McGraw-Hill, New York, 1985.
- [5] Serikov V.V. and Nanbu K., Proc. 20th Int. Symp. Rarefied Gas Dynamics, pp.829-834, Peking University Press, 1997.
- [6] Hoffman D.W., *A Sputtering Wind*, J. Vac. Sci. Technol. A, Vol.3, No.3, pp.561-566, 1985.
- [7] Serikov V.V. and Nanbu K., J. Appl. Phys., Vol.82, No.12, pp.5948-5957, 1997.

Conservative Method of Evaluation of Boltzmann Collision Integrals for Cylindrical Symmetry *

A.A. Raines

St.-Petersburg University, Dept. Math.- Mech., St.Petersburg, Russia

Accurate numerical solution of the complete kinetic Boltzmann equation still presents a difficult problem. Approximating the left-hand side of Boltzmann equation by a conservative finite-difference scheme, we have developed a technique for conservative evaluation of collision integrals for a gas mixture in cylindrical coordinates, generalizing [1]. The system of Boltzmann equations in the momentum space for two gas components consisting of hard sphere molecules has the form

$$\frac{\partial f_i}{\partial t} + \frac{\vec{p}_i}{m_i} \frac{\partial f_i}{\partial \vec{x}} = I_i = -L_i + G_i, \quad i = 1, 2. \quad (1)$$

The collision integral has the following form:

$$I_i = \sum_{j=1}^2 \left(\frac{d_i + d_j}{2} \right)^2 \int_{-\infty}^{+\infty} \int_0^{2\pi} \int_0^1 (f'_i f'_j - f_i f_j) \cdot q_{ji} db d\varphi d\vec{p}_j, \quad q_{ji} = |(\vec{g}_{ji} \cdot \vec{n})|. \quad (2)$$

In kinetic momentum space we have the equalities

$$\begin{aligned} \vec{p}'_\alpha &= \vec{p}_\alpha + \delta \vec{p}_{\beta\alpha}, \quad \vec{p}'_\beta = \vec{p}_\beta - \delta \vec{p}_{\beta\alpha}, \\ \delta \vec{p}_{\beta\alpha} &= 2(m_1 m_2)(m_1 + m_2)^{-1} (\vec{g}_{\beta\alpha} \cdot \vec{n}) \vec{n}, \quad (3) \\ \vec{g}_{\beta\alpha} &= \frac{\vec{p}_\beta}{m_2} - \frac{\vec{p}_\alpha}{m_1}, \end{aligned}$$

where \vec{n} is a unique vector directed along the interaction line of molecules.

Consider the integral operator:

$$Q_i(\phi) = \int_{-\infty}^{+\infty} \sum_{j=1}^2 \left(\frac{d_i + d_j}{2} \right)^2 \cdot \int_{-\infty}^{+\infty} \int_0^{2\pi} \int_0^1 \phi f_i f_j q_{ji} db d\varphi d\vec{p}_j d\vec{p}_i.$$

Taking for ϕ a three-dimensional δ -function and making use of (3), we can write:

$$L_i(\vec{p}^*) = \frac{1}{2} Q_i \left(\frac{\delta(\vec{p}^* - \vec{p}_i)}{\rho_i} + \frac{\delta(\vec{p}^* - \vec{p}_j)}{\rho_j} \right), \quad (4)$$

$$G_i(\vec{p}^*) = \frac{1}{2} Q_i \left(\frac{\delta(\vec{p}^* - \vec{p}'_i)}{\rho'_i} + \frac{\delta(\vec{p}^* - \vec{p}'_j)}{\rho'_j} \right). \quad (5)$$

Let us take two cylindrical systems for each component in a momentum space: $\vec{p}_i(p_i, \rho_i, \theta)$ and $\vec{p}_j(p_j, \rho_j, \theta_1)$. Introduce in a bounded domain of the physical space a fixed grid for \vec{x} . Impose limits on momentum variables by introducing domain Ω with the volume V and construct in Ω a discrete momentum net of N_0 equidistant nodes $(p_{i\beta}, \rho_{i\beta})$ and $(p_{j\beta}, \rho_{j\beta})$ separated by a step h_1 and h_2 ($h_1 = h_2$ or $h_1 \neq h_2$). Then introduce a uniform integration net

$$p_{i\alpha_\nu}, \rho_{i\alpha_\nu}, p_{j\beta_\nu}, \rho_{j\beta_\nu}, \theta_\nu, \theta_{1\nu}, b_\nu, \varphi_\nu$$

with N_ν nodes in such a way that $p_{i\alpha_\nu}, \rho_{i\alpha_\nu}$ and $p_{j\beta_\nu}, \rho_{j\beta_\nu}$ belong to the momentum net and the angles are arbitrary. One obtains:

$$\begin{aligned} \tilde{L}_i(\vec{p}^*) &= A \sum_{j=1}^2 \sum_{\nu=1}^{N_\nu} J_\nu^{ij} \cdot \\ &\cdot \left(\frac{\delta(\vec{p}^* - \vec{p}_{i\alpha_\nu})}{\rho_{i\alpha_\nu}} + \frac{\delta(\vec{p}^* - \vec{p}_{j\beta_\nu})}{\rho_{j\beta_\nu}} \right), \end{aligned} \quad (6)$$

$$\begin{aligned} \tilde{G}_i(\vec{p}^*) &= A \sum_{j=1}^2 \sum_{\nu=1}^{N_\nu} J_\nu^{ij} \cdot \\ &\cdot \left(\frac{\delta(\vec{p}^* - \vec{p}'_{i\alpha_\nu})}{\rho'_{i\alpha_\nu}} + \frac{\delta(\vec{p}^* - \vec{p}'_{j\beta_\nu})}{\rho'_{j\beta_\nu}} \right), \end{aligned} \quad (7)$$

$$A = \frac{\pi V^2}{N_\nu}, \quad J_\nu^{ij} = f_{i\alpha_\nu} f_{j\beta_\nu} \left(\frac{d_{i\alpha_\nu} + d_{j\beta_\nu}}{2} \right)^2 \cdot q_{i\alpha_\nu j\beta_\nu} \chi_{i\alpha_\nu j\beta_\nu} \rho_{i\alpha_\nu} \rho_{j\beta_\nu}$$

*Abstract 5116 submitted to the 21st International Symposium on Rarefied Gas Dynamics, Marseille, France, July 26-31, 1998

When $\vec{p}_i^* = \vec{p}_{i\beta}$ one directly obtains from (6) the values of $\tilde{L}_i(\vec{p}_\beta) = \tilde{L}_{i\beta}$:

$$\tilde{L}_{i\beta} = B \sum_{j=1}^2 \left(\sum_{\nu=1}^{N_\nu} J_{\nu}^{'ij} + J_{\nu}^{''ij} \right), \quad B = \pi V / (N_\nu / N_0) \quad (8)$$

with the primes ' or '' marking contributions with $\alpha_\nu = \beta$ or $\beta_\nu = \beta$. The way of evaluation of $\tilde{G}_{i\beta}$ values is the decomposition of each term in parentheses in (7) on δ -functions which have singularities in discrete ordinate nodes:

$$\frac{\delta(\vec{p}^* - \vec{p}_{i\alpha_\nu}')}{\rho_{i\alpha_\nu}'} + \frac{\delta(\vec{p}^* - \vec{p}_{j\beta_\nu}')}{\rho_{j\beta_\nu}'} = \sum_{s, \tilde{s}} r_{s, \tilde{s}} \cdot \left(\frac{\delta(\vec{p}^* - \vec{p}_{i, \lambda_\nu + s})}{\rho_{i, \lambda_\nu + s}} + \frac{\delta(\vec{p}^* - \vec{p}_{j, \mu_\nu + \tilde{s}})}{\rho_{j, \mu_\nu + \tilde{s}}} \right), \quad (9)$$

where $\vec{p}_{i\lambda_\nu}, \vec{p}_{j\mu_\nu}$ are the nodes nearest to $\vec{p}_{i\alpha_\nu}'$ and $\vec{p}_{j\beta_\nu}'$ respectively and vectors $\vec{s}, \vec{\tilde{s}}$ are displacements along the grid. The coefficients can be determined from the conditions of conservation of density, kinetic momentum and energy in the decomposition (9) for a pair of cells specified earlier including their vertices.

So, we have $r_{s, \tilde{s}} \geq 0$, $\sum_{s, \tilde{s}} r_{s, \tilde{s}} = 1$ and the energy equation. For economy of computations it is preferable to have a decomposition with minimum number of terms. Such a solution contains only two nonzero coefficients: the first one $(1 - r_\nu)$ corresponding to $s = \tilde{s} = 0$ and the second r_ν corresponding to $s = s^* \neq 0$, $\tilde{s} = \tilde{s}^* \neq 0$ depending on a combination of parameters in the energy equation. One obtains

$$\tilde{G}_{i\beta} = B \sum_{j=1}^2 \sum_{\nu=1}^{N_\nu} \left[\left(J_{\nu}^{'ij} + J_{\nu}^{''ij} \right) (1 - r_\nu) + \left(J_{\nu}^{'ij} + J_{\nu}^{''ij} r_\nu \right) \right], \quad (10)$$

where indices ', or '', or *, or ** mark the contributions J_{ν}^{ij} having the indices $\lambda_\nu = \beta$, or $\mu_\nu = \beta$, or $\lambda_\nu + s^* = \beta$, or $\mu_\nu + \tilde{s}^* = \beta$ correspondingly. The expressions (8) and (10) define the conservative discrete ordinate method, when the coefficients r_ν are found. Let us consider now their determination.

On a grid in momentum space for $h_1 = h_2 = h$ we have

$$\begin{aligned} \vec{p}_{i\lambda_\nu} &= \vec{k}_{i\lambda_\nu} \cdot h, & \vec{p}_{j\mu_\nu} &= \vec{k}_{j\mu_\nu} \cdot h, \\ \vec{p}_{i\alpha_\nu} &= \vec{p}_{i\lambda_\nu} + \vec{\Delta}_{i\lambda_\nu}, & \vec{p}_{j\beta_\nu} &= \vec{p}_{j\mu_\nu} + \vec{\Delta}_{j\mu_\nu}, \\ \vec{k}_{i\lambda_\nu} &= (k_1, l_1), & \vec{k}_{j\mu_\nu} &= (k_2, l_2), \\ \vec{\Delta} &= \frac{\vec{\Delta}_{i\lambda_\nu}}{h} = (\Delta_1, \Delta_2), & -\frac{1}{2} &\leq \Delta_i \leq \frac{1}{2}, \end{aligned}$$

$$\vec{\tilde{\Delta}} = \frac{\vec{\tilde{\Delta}}_{j\mu_\nu}}{h} = (\tilde{\Delta}_1, \tilde{\Delta}_2), \quad -\frac{1}{2} \leq \tilde{\Delta}_j \leq \frac{1}{2},$$

$$\begin{aligned} \vec{s} &= (\delta_1, \delta_2), & \vec{\tilde{s}} &= (\tilde{\delta}_1, \tilde{\delta}_2), & \text{where} \\ \delta_i &= 0, \tilde{\delta}_j = 0 & \text{or} & \delta_i = \text{sign} \Delta_i, \tilde{\delta}_j = \text{sign} \tilde{\Delta}_j; \\ \tilde{\Delta}_1 &= -\Delta_1, & \tilde{\delta}_1 &= -\delta_1. \end{aligned}$$

The condition of energy conservation leads to equation:

$$\sum_{s, \tilde{s}} r_{s, \tilde{s}} a_{s, \tilde{s}} = R. \quad (11)$$

The sum contains all values of s, \tilde{s} with the exception of $\delta_1 = \delta_2 = \tilde{\delta}_1 = \tilde{\delta}_2 = 0$. The values of R and of $a_{s, \tilde{s}}$:

$$\begin{aligned} R &= (2k_1 \Delta_1 + \Delta_1^2 + 2l_1 \Delta_2 + \Delta_2^2) m_2 + \\ &+ (-2k_2 \Delta_1 + \Delta_1^2 + 2l_2 \tilde{\Delta}_2 + \tilde{\Delta}_2^2) m_1, \\ a_{01} &= m_1 + m_2 + 2(l_1 \delta_2 m_2 + l_2 \tilde{\delta}_2 m_1), \\ a_{10} &= m_1 + m_2 + 2(k_1 \delta_1 m_2 - k_2 \delta_1 m_1), \\ a_{11} &= 2(m_1 + m_2) + 2(k_1 \delta_1 m_2 - k_2 \delta_1 m_1) + \\ &+ 2(l_1 \delta_2 m_2 + l_2 \tilde{\delta}_2 m_1). \end{aligned} \quad (12)$$

The described method of evaluation of collision integrals of the Boltzmann equation with numerical technique for approximation of the differential part of the Boltzmann equation (mentioned previously) and the splitting procedure for its solution was tested on the problem of a shock wave in a mixture (argon-helium). The results were compared with the results of other authors and with physical experiments [2, 3].

References

- [1] Tcheremissine F.G., *Conservative Evaluation of Boltzmann Collision Integral in Discrete-Ordinates Approximation*, Doklady of RAN, Vol. 357, No. 1, pp. 1-4, 1997.
- [2] Mausbach P. and Beylich A.R., *Numerical Solution of the Boltzmann Equation for One-dimensional Problems in Binary Mixtures*, Proc. of XIII Internat. Symp. on RGD, Vol. 1, pp. 285-292, Plenum Press, N.-Y., 1985.
- [3] Harnett L.N. and Muntz E.P., *Experimental Investigation of Normal Shock Wave Velocity Distribution Functions in Mixtures of Argon and Helium*, Phys. Fluids, Vol. 15, No. 4, pp. 565-572, 1972.

Heat Conduction and Couette Flow in a Hard-Sphere Gas Using Multicell Molecular Dynamics Computational Method *

M. Woo¹, I. Greber², I. Kandemir²

¹ Osborn Engineering Company, U.S.A.

² Case Western Reserve University, U.S.A.

1 Introduction

This paper presents results of molecular dynamics computations of one- dimensional heat conduction and parallel plate Couette flow in a hard sphere gas. Temperature and velocity profiles were determined, along with heat transfer rates, wall shearing stresses, and temperature and velocity slip, for Knudsen numbers ranging from 0.046 to 1.0. The very low Knudsen number computations were made possible by the development of a multicell method that makes the number of computations proportional to the number of molecules, rather than to the square of the number of molecules as in previous molecular dynamics computations.

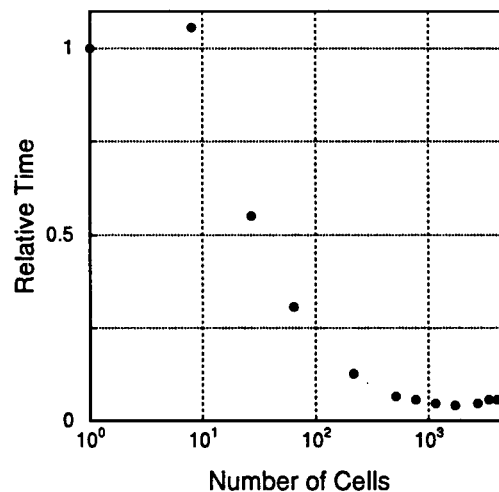
2 Computational Model

The molecules were considered as hard spheres with elastic intermolecular collisions. The computational domain was cubical. In the one- dimensional heat transfer computations two opposite walls were held at different temperatures. Reemission from these walls was diffuse. Reemission from the four lateral walls was specular, modeling an unbounded lateral region. In the Couette flow computations two opposite walls moved with equal speeds in opposite directions parallel to these walls. Reemission from the moving walls was diffuse. For the streamwise boundaries, a molecule reaching one boundary was replaced by an identical molecule at the opposite boundary. Reemission from the sidewalls was specular.

The computations involve determining the times of potential collisions, from which the shortest time identifies the collision that actually occurs. If potential collision times are found for all molecules in the global computational region then the number of

computations is approximately proportional to the square of the number of molecules. Consequently computations involving large numbers of molecules, which are needed for low Knudsen number computations, become lengthy. Therefore a multicell method and associated search strategy was developed, using the idea that a molecule must leave its local region of occupancy in order to have the possibility of colliding with a distant particle. The new method significantly decreases computational time and required computer memory. The number of collisional computations becomes approximately proportional to the number of molecules rather than to its square, as has been usual in previous molecular dynamics computations. No real collisions are lost, only potential ones, and hence the results of the multicell method and the single cell method are identical.

Fig.1 - Computer Time Comparison



Tests of the computer time saving using the new methods were made, using as a measure the time for computing a given number of real collisions. for

*Abstract 5861 submitted to the 21st International Symposium on Rarefied Gas Dynamics, Marseille, France, July 26-31, 1998

a fixed number of molecules colliding specularly. The computations were made using a fixed occupied volume of about 1.2 per cent. The number of molecules therefore varied with the Knudsen number, to a maximum of 216,000 molecules at a Knudsen number of 0.046. The results are shown in Figure 1. The computer time decreases dramatically; in this test the minimum time is only 4 per cent of the single cell value! The decrease in required memory is equally dramatic, and will be discussed in the full paper.

3 Sample Results

Figure 2 presents sample temperature profiles for several Knudsen numbers, with a fixed wall temperature difference. The temperature distributions are not linear, and at the higher Knudsen numbers the profiles are not symmetric. The temperature non-symmetry is related to density non-symmetry, with lower gas density near the hot wall. The non-linearity, but not the non-symmetry, is also shown in numerical solutions of the linearized Boltzmann equation (Ohwada, Aoki and Sone in "Rarefied Gas Dynamics", Muntz, Weaver and Weaver eds, 1989). Figure 3 presents the variation of heat transfer rate with Knudsen number, as obtained from energy exchange at the boundaries. The results are very close to those of the linearized Boltzmann equation computations, and extrapolate closely to the simple kinetic theory value as the Knudsen number goes to zero. Also shown is the temperature slip, which is greater at the hot than at the cold wall. The slip results obtained from the linearized Boltzmann equation fall within the hot and cold wall values of the current computations. Finally the figure shows the overall mean free path obtained from the molecular excursions. The computed mean free path is slightly less than the Maxwell mean free path, primarily because of the boundedness of the computational region. The Couette flow results for the transport properties are qualitatively similar to the related properties in the one dimensional heat transfer, except that the velocity profiles are nearly symmetric. Although the temperatures of the two walls are the same, the flow field is not isothermal, because the moving walls impart energy to the gas. The non-isothermal behavior will be presented in the full paper.

The full paper will present details of the multicell method and associated search strategy, as well as the complete set of heat transfer and Couette flow computational results.

4 Acknowledgements

This work was supported by a grant from NASA Lewis Research Center, monitored by Dale C. Ferguson. Some of the computations were performed under a grant of the NAS program of NASA. The authors thank Professor Harold Y. Wachman of M.I.T for insightful discussions.

Fig.2 - Temperature Profiles

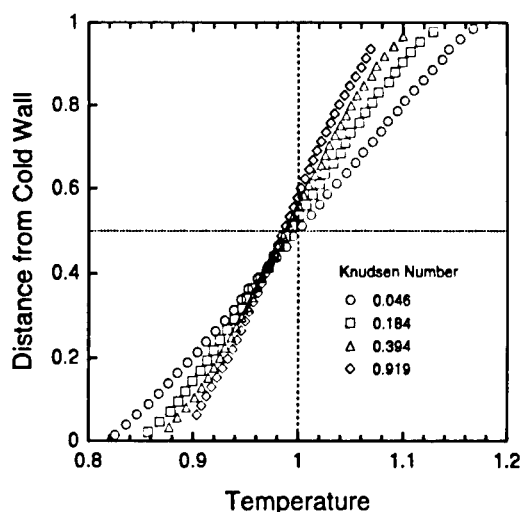
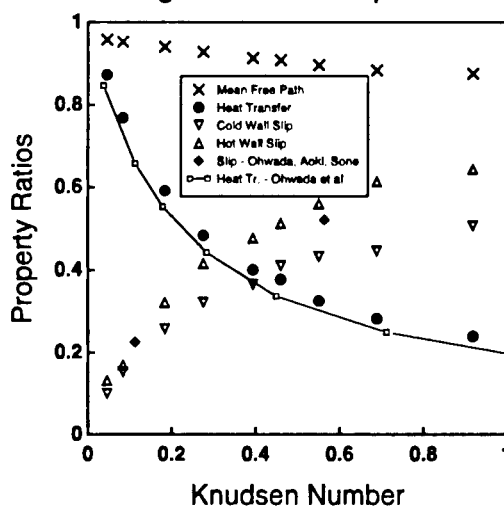


Fig.3 - Overall Properties



TWO-PHASE FLOWS - TP 1

ROOM MARION

WEDNESDAY, JULY 29, 1998

11:10

Bifurcation in Cylindrical Couette Flow with Evaporation and Condensation: Effect of Initial Condition *

T. Ohwada, Y. Sone, Y. Makihara

Department of Aeronautics and Astronautics, Graduate School of Engineering
Kyoto University, Japan

1 Introduction

Recently a new type of bifurcation of a flow was found in a cylindrical Couette flow of a gas between two concentric circular cylinders consisting of the condensed phase of the gas, where condensation or evaporation takes place.^[1] According to the numerical results in Ref. [1] based on the BKW (or BGK) equation for the case where the outer cylinder is at rest and the inner cylinder is rotating, the bifurcation of flow can occur even in the simple case where the state of the gas is axially and circumferentially uniform. Since the problem is considered as a steady problem in Ref. [1], in the present paper we will consider the problem as an initial value problem and clarify the evolution of solution from different initial conditions. Further we consider a hard-sphere molecular gas instead of the BKW model. The computation is carried out by the direct simulation Monte-Carlo (DSMC) method^[2].

2 Problem

Consider a rarefied gas between two concentric cylinders which consist of the condensed phase of the gas. Each cylinder is kept at a uniform temperature and is rotating around its axis with a constant circumferential velocity. We investigate the steady behavior of the gas as the limit of a transient problem under the axially and circumferentially uniform condition on the basis of the Boltzmann equation for hard-sphere molecules and the complete condensation condition on the condensed phase.

The steady problem is characterized by six nondimensional parameters: L_2/L_1 , T_2/T_1 , p_{s2}/p_{s1} , $V_{\theta 1}/\sqrt{2RT_1}$, $V_{\theta 2}/\sqrt{2RT_1}$, and Kn , where L_i , T_i , and $V_{\theta i}$ are, respectively, the radius, temperature, and circumferential velocity of the inner ($i = 1$) or outer

($i = 2$) cylinder, p_{si} is the saturation gas pressure at temperature T_i , R is the specific gas constant, and Kn (the Knudsen number) is defined by $\text{Kn} = l_1/L_1$, where l_1 is the mean free path of the gas molecules at the equilibrium state at rest with temperature T_1 and pressure p_{s1} .

3 Results of simulation

We consider the case where $V_{\theta 2} = 0$, $p_{s2}/p_{s1} = 1.2$, $T_2/T_1 = 1$ and $L_2/L_1 = 2$ and carry out the simulation for various values of Kn and $V_{\theta 1}/\sqrt{2RT_1}$ under the axially and circumferentially uniform condition. The mass flow M from the inner to the outer cylinder per unit time and unit axial length versus the circumferential speed $|V_{\theta 1}|$ of the inner cylinder is shown for various Knudsen numbers in Fig. 1. For $\text{Kn} \geq 0.02$, the solution is unique, and M increases monotonically with $|V_{\theta 1}|$. For $\text{Kn} = 0.005$ and 0.01 , there are two families of solutions; one with $M < 0$ and the other with $M > 0$. Two solutions exist for some values of $V_{\theta 1}$, e.g., $|V_{\theta 1}|/\sqrt{2RT_1} = 0.7, 0.8, 0.9$ at $\text{Kn} = 0.005$ and $|V_{\theta 1}|/\sqrt{2RT_1} = 0.7$ at $\text{Kn} = 0.01$. In this range of $V_{\theta 1}$, the solution with $M > 0$ results from the initial state of rigid rotation with angular velocity $V_{\theta 1}/L_1$, uniform temperature T_1 , and average density p_{s1}/RT_1 , and the other with $M < 0$ results from the stationary state at temperature T_1 and pressure p_{s1} . As an example of the nonuniqueness of solution, the profiles of pressure p , temperature T , and radial and circumferential components v_r and v_θ of flow velocity for $\text{Kn} = 0.005$ and $V_{\theta 1}/\sqrt{2RT_1} = 0.8$ are shown in Fig. 2.

References

- [1] Sone Y. and Sugimoto H., *Abstracts of XIXth International Congress of Theoretical and Applied Mechanics*, p. 139, 1996.
- [2] Bird G.A., *Molecular Gas Dynamics*, (Clarendon Press, Oxford, 1976).

*Abstract 4531 submitted to the 21st International Symposium on Rarefied Gas Dynamics, Marseille, France, July 26-31, 1998

TWO-PHASE FLOWS - TP 1

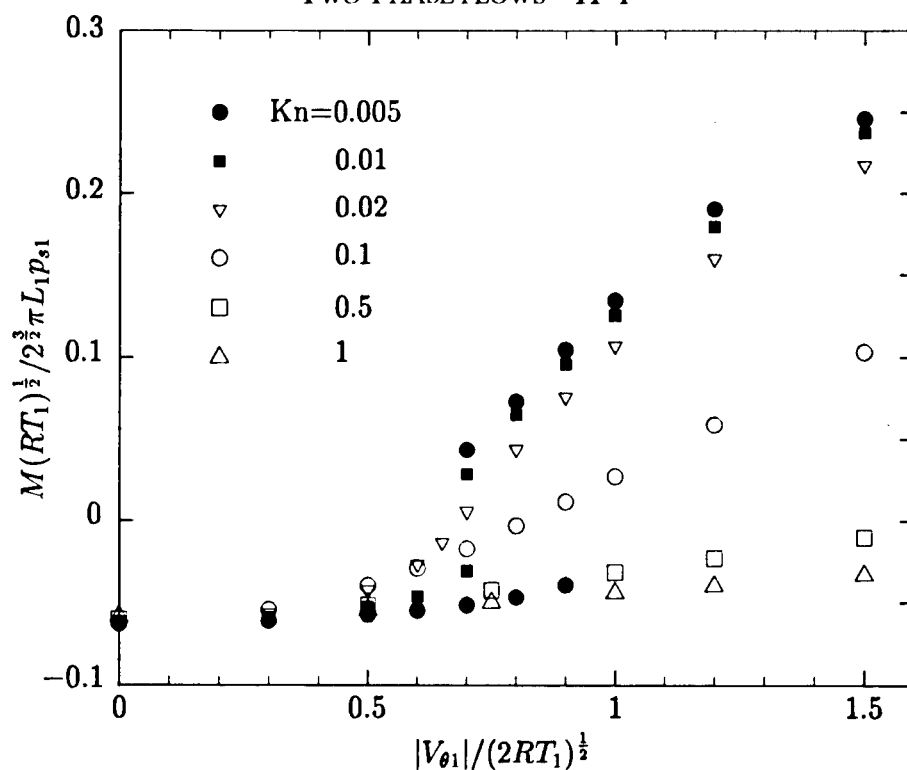


Figure 1: The mass-flow rate M from the inner to the outer cylinder versus the circumferential speed $|V_{\theta 1}|$ of the inner cylinder for various Knudsen numbers ($p_{s2}/p_{s1} = 1.2$, $T_2/T_1 = 1$, $L_2/L_1 = 2$).

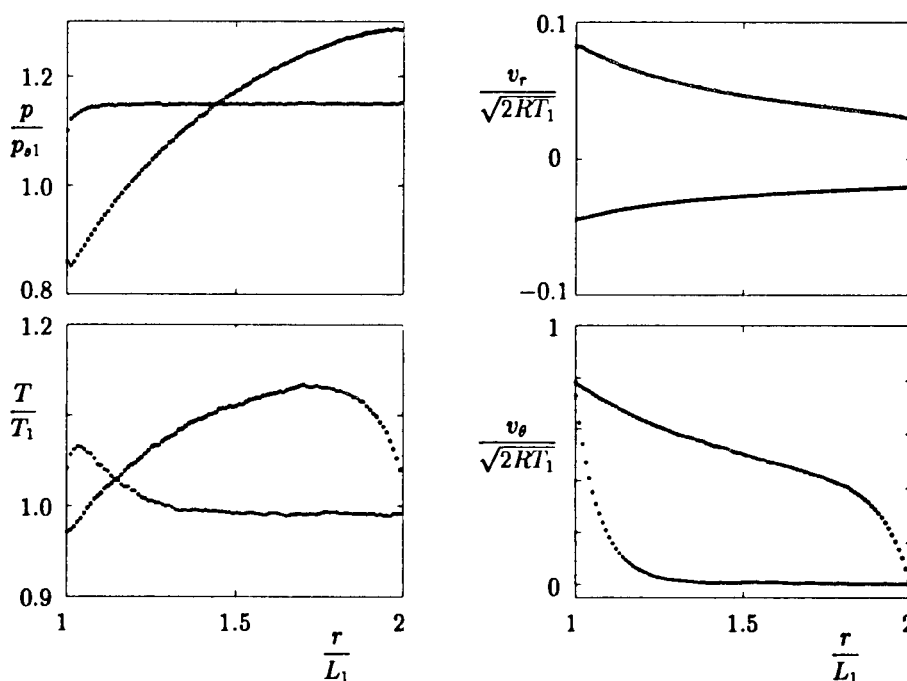


Figure 2: Two different solutions, the profiles of pressure p , temperature T , and radial and circumferential components v_r and v_{θ} of flow velocity, for a given set of parameters ($Kn = 0.005$ and $V_{\theta 1}/\sqrt{2RT_1} = 0.8$, $V_{\theta 2} = 0$, $p_{s2}/p_{s1} = 1.2$, $T_2/T_1 = 1$, and $L_2/L_1 = 2$). The radial coordinate is denoted by r . The two solutions are distinguished by \bullet and \circ .

Behavior of a Vapor-Gas Mixture between Two Parallel Plane Condensed Phases in the Continuum Limit *

S. Takata, K. Aoki

Department of Aeronautics and Astronautics, Kyoto University, Japan

1 Introduction

Recently, serious defects in classical gasdynamics in describing the behavior of a gas in the continuum limit were pointed out on the basis of kinetic theory [1],[2]. For example, the temperature distribution in a stationary gas cannot, in general, be described correctly by the commonly believed heat-conduction equation [1]. This is due to the fact that the gas flow which is caused by the effect of gas rarefaction and vanishes in the continuum limit may give a finite effect on the behavior in this limit (*ghost effect* [2]). In the present study, by asymptotic and numerical analyses of the Boltzmann equation, we will show that the ghost effect appears even in the simple one-dimensional heat and mass transfer problem between two parallel walls when the gas is a binary mixture and the walls are made of the condensed phase of one of the gas components.

2 Problem

In the region $0 \leq X_1 \leq D$ (X_i : rectangular space coordinates) between two stationary plane walls made of a condensed phase, a binary mixture of its vapor (A-component) and an incondensable gas (B-component) is contained (thus, the vapor may either evaporate or condense on the walls). Let the temperature of the wall at $X_1 = 0$ be T_0 and that at $X_1 = D$ be T_1 . Investigate the steady behavior of the vapor and incondensable gas, with special interest in the continuum limit, on the basis of kinetic theory under the assumptions: (i) the molecules of both components are hard spheres; (ii) the velocity distribution of the vapor molecules and that of the incondensable-gas molecules leaving the walls are, respectively, described by the conventional condition for evaporation and condensation and the diffuse reflection condition (the results in Sec. 3 are valid for more general conditions); (iii) the amount

of the vapor and that of the incondensable gas are comparable.

We use the following notations: p_0^A (p_1^A) is the saturation pressure of the vapor at temperature T_0 (T_1); m^α and d_m^α ($\alpha = A, B$) the mass and the diameter of a molecule of α -component; κ the Boltzmann constant; $n_0^A = p_0^A/\kappa T_0$; $\ell_0 = [\sqrt{2}\pi(d_m^A)^2 n_0^A]^{-1}$ the mean free path of the vapor molecules at the reference state; $\text{Kn} = \ell_0/D$ the Knudsen number; $n^\alpha (= n_0^A \hat{n}^\alpha)$ the molecular number density of α -component; $p^\alpha (= p_0^A \hat{p}^\alpha)$ the partial pressure of α -component; $p (= p_0^A \hat{p})$ and $T (= T_0 \hat{T})$ the pressure and temperature of the total mixture; $v_1^A [= (2\kappa T_0/m^A)^{1/2}(\hat{v}_1^A, 0, 0)]$ the vapor flow velocity; $n_{av}^B = D^{-1} \int_0^D n^B dX_1$ the average number density of the incondensable gas; and $x_1 = X_1/D$.

The problem is characterized by the following nondimensional parameters: T_1/T_0 , p_1^A/p_0^A , Kn , m^B/m^A , d_m^B/d_m^A , and n_{av}^B/n_0^A .

3 Asymptotic analysis

We first carry out asymptotic analysis of the present problem for small Kn . Then, we find that (i) \hat{v}_1^A is of $O(\text{Kn})$, and therefore the vapor flow vanishes in the continuum limit ($\text{Kn} \rightarrow 0$); (ii) $\hat{n}^{A,B}$, $\hat{p}^{A,B}$, \hat{p} , and \hat{T} in the *continuum limit*, together with an unknown function δ , are determined by the following fluid-dynamic type equations and boundary conditions.

$$\left. \begin{aligned} \frac{d\hat{p}}{dx_1} &= 0, \quad \frac{d}{dx_1}(\hat{n}^A \delta) = 0, \\ \frac{d}{dx_1}(\hat{\lambda} \hat{T}^{1/2} \frac{d\hat{T}}{dx_1}) - \frac{d}{dx_1}[(\frac{\hat{D}_T}{\hat{D}_{AB}} \hat{p} + \frac{5}{2} \hat{p}^A) \delta] &= 0, \\ \delta &= -\frac{\hat{p}^2 \hat{T}^{1/2}}{\hat{p}^A \hat{p}^B} (\hat{D}_{AB} \frac{1}{\hat{p}} \frac{d\hat{p}^A}{dx_1} + \hat{D}_T \frac{d}{dx_1} \ln \hat{T}), \\ \hat{p} &= \hat{p}^A + \hat{p}^B, \quad \hat{p}^A = \hat{n}^A \hat{T}, \quad \hat{p}^B = \hat{n}^B \hat{T}, \\ \text{b.c.} \quad \hat{p}^A &= 1, \quad \hat{T} = 1 \quad \text{at } x_1 = 0, \\ \hat{p}^A &= p_1^A/p_0^A, \quad \hat{T} = T_1/T_0 \quad \text{at } x_1 = 1, \end{aligned} \right\} (1)$$

where $\hat{\lambda}$, \hat{D}_{AB} , and \hat{D}_T are functions of \hat{n}^A , \hat{n}^B , m^B/m^A , and d_m^B/d_m^A and are related to transport coefficients $[(2\kappa T/m^A)^{1/2} \ell_0 (n_0^A \kappa \hat{\lambda}, \hat{D}_{AB}, \hat{D}_T)]$

*Abstract 4621 submitted to the 21st International Symposium on Rarefied Gas Dynamics, Marseille, France, July 26-31, 1998

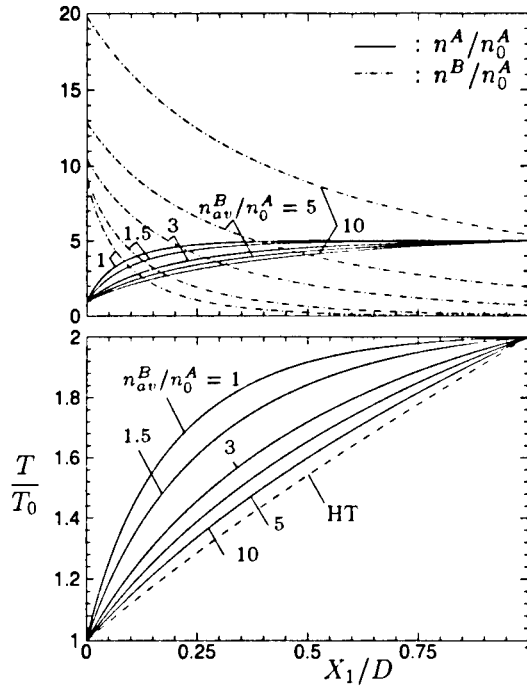


Figure 1: n^A , n^B , and T in the continuum limit for various n_{av}^B/n_0^A in the case $T_1/T_0 = 2$, $p_1^A/p_0^A = 10$, $m^B/m^A = 1$, and $d_m^B/d_m^A = 1$.

are the coefficients of thermal conductivity, diffusion, and thermal diffusion]. An example of n^A , n^B , and T obtained by Eq. (1) is shown in Fig. 1, where the dashed line (HT) indicates the corresponding temperature distribution when A-component is also incondensable (i.e., the conventional heat-transfer problem between solid walls; in this case, T does not depend on the concentration of each component when $m^B/m^A = d_m^B/d_m^A = 1$).

In the continuum limit ($\text{Kn} \rightarrow 0$), evaporation and condensation stop, and the state becomes stationary. Therefore, the problem appears to be identical with the conventional heat-transfer problem. Nevertheless, as shown in Fig. 1, the temperature distribution deviates significantly from that of the latter problem. This is due to the fact that δ occurs in Eq. (1). [Note that the solution of the conventional heat-transfer problem is given by Eq. (1) with $\delta = 0$ (heat-conduction equation in the absence of diffusion) and without the conditions $\hat{p}^A = 1$ ($x_1 = 0$) and $\hat{p}^A = p_0^A/p_1^A$ ($x_1 = 1$) (n_0^A and p_0^A should be interpreted as appropriate reference values, n_1^A and p_1^A being discarded)]. Here, we note that δ is identified as $\delta = \hat{v}_1^A/\text{Kn}$ [$= O(1)$] in the asymptotic analysis. Therefore, in the continuum limit, although \hat{v}_1^A itself vanishes, its effect remains finite in the form of δ (ghost effect [2]). Owing to this effect, the classical gasdynamics treatment cannot

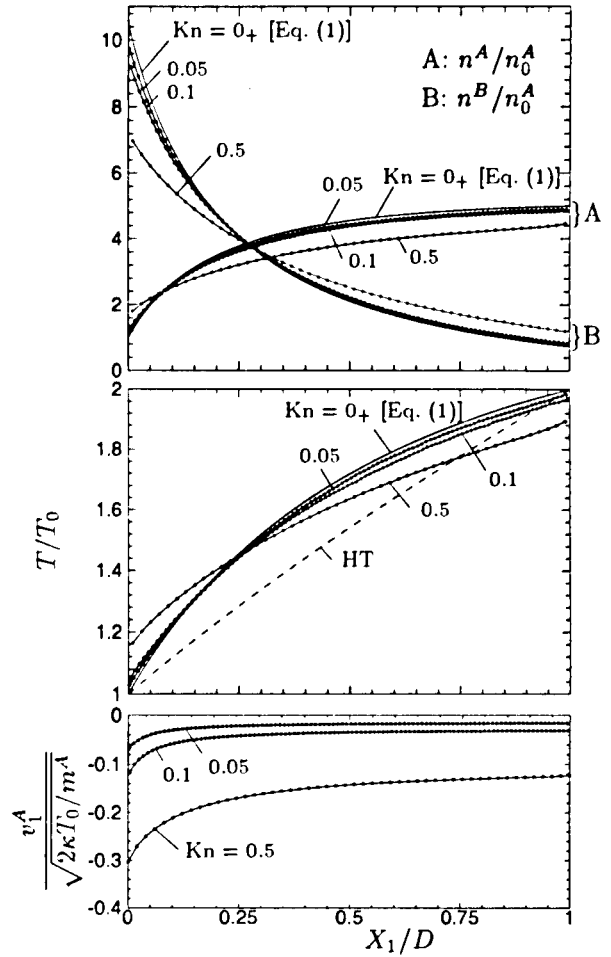


Figure 2: n^A , n^B , T , and v_1^A in the case $n_{av}^B/n_0^A = 3$, $T_1/T_0 = 2$, $p_1^A/p_0^A = 10$, $m^B/m^A = 1$, and $d_m^B/d_m^A = 1$ (DSMC).

describe the temperature field correctly even in the continuum limit. (The ghost effect also appears in the density field, the discussion on which is omitted in this abstract.)

4 Numerical analysis

Next, in order to confirm the result in Sec. 3, we carry out numerical analysis of the original problem by Bird's DSMC method. Figure 2 shows an example of the distributions of n^A , n^B , T , and v_1^A . As $\text{Kn} \rightarrow 0$, the vapor flow tends to vanish, and the density and temperature profiles approach the results obtained by Eq. (1).

References

- [1] Sone Y. et al., Phys. Fluids **8**(2), pp. 628–638, 1996; Phys. Fluids **8**(12), pp. 3403–3413, 1996.
- [2] Sone Y., in *Rarefied Gas Dynamics*, ed. Shen C., Peking University Press, 1997, pp. 3–24.

The Inverted Temperature Gradient in Condensation-Revisited *

Tor Ytrehus

Division of Applied Mechanics, Norwegian University of Science and Technology
Trondheim, Norway

Among the many results on vapor fluid- and thermodynamics that have been derived from kinetic theory of gases over the last, say 30 years, the prediction of a temperature increase in a hot vapor approaching a colder interphase surface in condensation is a more remarkable one. This effect, which to the best of our knowledge has still not been confirmed experimentally, is commonly referred to as the paradox of inverted temperature profile, and is mostly associated with the two-surface problem of evaporation and condensation between parallel plates. However, the effect is also predicted in half-space condensation, as indicated in figure 1, which is a part of the two-surface situation in the high Reynolds number case.

For given dense-phase temperature T_L and corresponding vapor saturation density $\rho_s(T_L)$, along with the temperature T_∞ and density ρ_∞ in the external stream, the temperature jump across the Knutsen layer $\Delta T_K = T_K - T_L$ can be computed if gas kinetic boundary conditions are prescribed at the interphase surface. It so happens that the jump ΔT_K may be less than or larger than the total temperature difference in the problem, $\Delta T = T_\infty - T_L$, according to choices of physical parameters for the condensing substance. In the latter case (B in the figure) there is a region of inverted temperature gradient $dT/dx < 0$ outside of the Knutsen layer, in a Navier - Stokes flow regime of extent λ/M , where λ is the mean free path and M is the small Mach number in the flow. This effect was apparently first predicted by Pao[1][2], and it has been further elaborated upon by several authors, for instance in Refs. 3 -9, all in cases of weak transfer rates and linear flow conditions[10][11]. In particular, Aoki and Cercignani[6] pointed out the significance of the temperature jump ΔT_K as computed from the inner Knutsen layer solution in determining the gradients in the external macroscopic flow. The effect has also been predicted to occur under non-linear

flow conditions[10][11]. The main classical finding is that the sign of the temperature gradient depends upon the normalized latent heat, L/RT_L , such that for $L/RT_L > \beta_c$ where β_c is a criticality parameter of the order 4.5 - 4.8, we have $dT/dx < 0$ and the inverted-gradient case. This result pertains to the simpler gas kinetic boundary conditions with unity evaporation/condensation coefficient, σ . In the present study we consider non-unity values of this coefficient, assuming a distribution function at the interphase surface of the type

$$f_w^+ = \sigma f_e + (1 - \sigma) f_r, \xi_x > 0 \quad (1)$$

where f_e is a standard evaporative Maxwellian and f_r denotes molecules that are reflected at the surface. For perfect thermal accommodation and diffuse reflection in this latter mode, we obtain the result

$$\Delta T_K = \frac{\sigma L/RT_L}{\sigma \beta_c + 8(1 - \sigma)} \Delta T \quad (2)$$

from a linearized moment solution of the same type as applied in Ref. 8. For $\sigma = 1$, the previous main finding as referred to above is readily recovered. In general, however, Eq.(2) implies an inverted temperature gradient if $\Delta T_K > \Delta T$, which requires the inequality

$$\frac{L}{RT_L} > \beta_c + 8\left(\frac{1 - \sigma}{\sigma}\right) \equiv \bar{\beta}_c \quad (3)$$

For low values of σ , such as are being inferred from recent molecular dynamics simulations [12], this inequality is only satisfied for larger latent heat values: Example ($\sigma = 0.5$, $\bar{\beta}_c = 12.8$), ($\sigma = 0.1$, $\bar{\beta}_c = 76.8$), ($\sigma = 0.01$, $\bar{\beta}_c = 796.8$). The first of these $\bar{\beta}_c$ values corresponds closely to physical data for water vapor, whereas the latter two values are outside of the range of latent heat for common substances. However, the first value of σ is considerably higher than typical MDS findings[12] ($\sigma \sim 10^{-2}$), such that the latter two cases may be the more typical ones. From these results it appears that the evaporation/condensation coefficient is even more critical to the temperature gradient than is the value of the

* Abstract 4731 submitted to the 21st International Symposium on Rarefied Gas Dynamics, Marseille, France, July 26-31, 1998

latent heat. It is suggested that accurate values of evaporation/condensation coefficient and latent heat of evaporation should be compiled for a variety of substances, to check if the inequality (3) is ever satisfied in actual physical systems. It may indeed never be, since L/RT_L and σ are not independent quantities, but rather derive from the same molecular bindings in the substance. On this background, previous critical remarks made in Ref.5 as to the very existence of the inverted temperature gradient may be more justified.

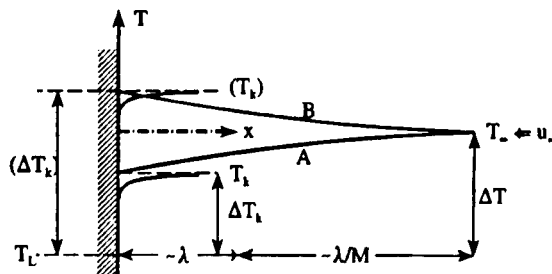


Figure 1: Temperature profile in front of dense phase surface in condensation(inner and outer solutions).A, normal case $dT/dx > 0$. B, inverted gradient-case $dT/dx < 0$

References

- [1] Y.P.Pao, *Phys. Fluids* 14, 306(1971)
- [2] Y.P.Pao, *Phys. Fluids* 14, 1340(1971)
- [3] J. W. Cipolla, Jr., H. Lang, and S. K. Loyalka, *J. Chem. Phys.* 61, 69 (1974)
- [4] Y. Sone and Y. Onishi, *J. Phys. Soc. Jpn.* 35, 1773 (1973)
- [5] L. D. Koffman, M. S. Plesset, and L. Lees, *Phys. Fluids* 27, 876 (1984)
- [6] K. Aoki and C. Cercignani, *Phys. Fluids* 26, 1163 (1983)
- [7] C. Cercignani, W. Fiszdon, and A. Frezzotti, *Phys. Fluids* 28, 3237 (1985)
- [8] T. Ytrehus and T. Aukrust, in *Rarefied Gas Dynamics*, edited by V. Boffi and C. Cercignani (Teubner, Stuttgart) Vol II, 271 (1986)
- [9] R. E. Caflish, *J. Transp. Th. Stat. Phys.* 16, 701 (1987)
- [10] P. Gajewski, A. Kulicki, A. Wisniewski, and M. Zgorelski, *Phys. Fluids* 17, 321 (1974)
- [11] T. Ytrehus and J. A. Alvestad, in *Rarefied Gas Dynamics*, edited by G. Fisher (AIAA, New York) Part I, 330 (1981)
- [12] M. Matsumoto, K. Yasuoka, and Y. Kataoka, *Therm. Sci. Eng.* 64, (1994)

The Condensation on a Black Sphere. Knudsen Layer Structure. *

A.K. Rebrov, M.Yu. Plotnikov
Institute of Thermophysics, Novosibirsk, Russia

The classical problem of the condensation of vapor on the spherical surface was a subject of a large number of investigations used kinetic approach. Almost all solutions of the Boltzman equation are given for small variation temperature and pressure at the surface of condensation from ones at infinity and relatively weak nonequilibrium in the Knudsen layer. The main practical interest in studies of the condensation on a sphere was the determination of the specific vapor flow rate to the surface due to condensation. In the late completed researches, such as [1], the dependence of mass flux was determined in the form

$$J = J_0 \left[\alpha(Kn) \frac{\Delta P}{P_\infty} + \beta(Kn) \frac{\Delta T}{T_\infty} \right],$$

where J_0 is the flow rate for free molecular regime, $\alpha(Kn)$, $\beta(Kn)$ are functions of Knudsen number, defined by mean free path of molecules in a background and radius of a sphere, $\Delta T = T_\infty - T_s$, $\Delta P = P_\infty - P_s$; ∞ and s mark the parameters in infinity and saturation ones correspondingly. Using the direct simulation Monte-Carlo method (DSMC) [2] allows to consider the processes of condensation for any nonequilibrium situations including the condensation on the absolutely black sphere.

The aim of this work is the study of kinetics of steady and nonsteady condensation in the region of Kn from ∞ to 0.01 for the case of absolutely black sphere ($T_s = 0$) and for the case of black sphere at low difference of saturation and background parameters. Special attention was paid to the formation of the Knudsen layer and its structure.

The process of condensation on the sphere with radius R was considered for temperature and density in infinity T_∞ and n_∞ . Condensation on a black sphere means that all molecules colliding with the sphere are condensed. At this formulation of the problem all processes are defined by Knudsen number and stagnation parameters. For the case $T_s > 0$ this value becomes determining parameter as well. The external spherical boundary of computa-

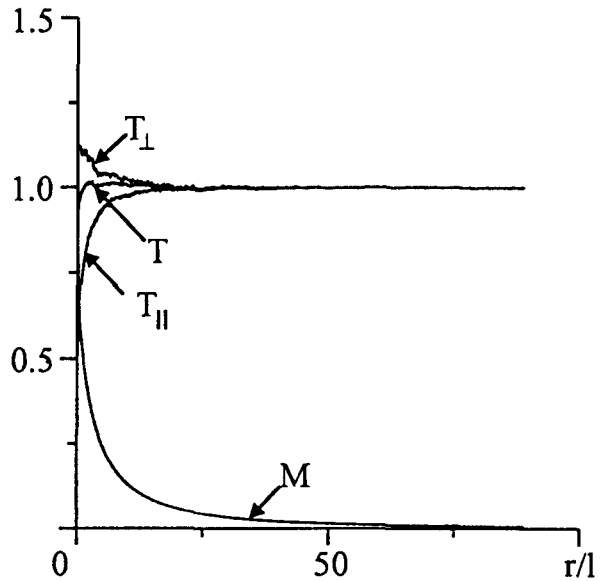


Figure 1: Dependence of density, Mach number, temperatures $T_{||}$ and T_{\perp} and T on radius for $Kn = 0.1$.

tional region was chosen at the distance where Mach number $M < 0.01$. The typical data for Knudsen layer structure are given in the Fig.1 and Fig.2 for $Kn = 0.1$ and 0.01 as dependence of density, Mach number M , temperatures $T_{||}$ and T_{\perp} (along and perpendicular to the radius) and $T = (2T_{\perp} + T_{||})/3$ on radius. In the case of $Kn = 0.1$ the temperature anisotropy as illustration of the translational nonequilibrium is clearly pronounced. The velocity is subsonic in all region up to the surface. When $Kn = 0.01$ (Fig.2) Knudsen layer is much thinner and temperature anisotropy is weaker. It turns ones attention that in this case the flow near the surface becomes supersonic and the point with $M = 1$ is located out of Knudsen layer.

The computations of nonstationary processes discover the forced temperature anisotropy close to the surface at all Knudsen numbers, initiated probably shock character of sudden beginning of condensation. For example at some regimes T_{\perp} exceeds the stagnation temperature.

* Abstract 5121 submitted to the 21st International Symposium on Rarefied Gas Dynamics, Marseille, France, July 26-31, 1998

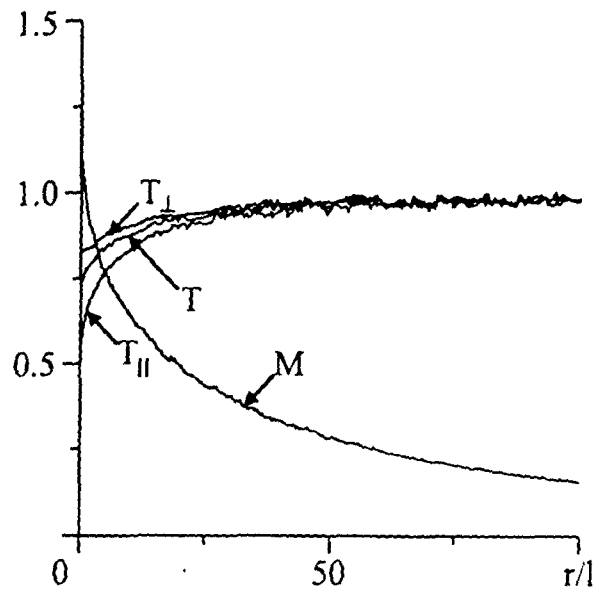


Figure 2: Dependence of density, Mach number, temperatures T_{\parallel} and T_{\perp} and T on radius for $Kn = 0.01$.

The results of this study have exposed qualitative dependence of the mechanism of condensation on Knudsen number.

References

- [1] Hubmer G.F. and Titulaer U.M., *Droplet growth in the transition regime.* // Proc. of the 17th Int. Symposium on Rarefied Gas Dynamics, ed. by E. Beilich, 1990, pp. 1266-1273.
- [2] Bird G.A., *Molecular gas dynamics and the direct simulation of gas flows*, Oxford, Clarendon Press, 1994.

TWO-PHASE FLOWS - TP 2

ROOM MARION

THURSDAY, JULY 30, 1998

11:10

Evaporation-Condensation Processes on the Interface Surface of Superfluid Helium *

A.P.Kryukov, I.N.Shishkova

Department of Low Temperatures, Moscow Power Engineering Institute,
Krasnokazarmennaya Street 14, Moscow 111250, Russia

New great interest to research in superfluid helium (He II) was appeared after successful american Lambda Point Experiment (LPE) aboard the Space Shuttle in October 1992. Authors of present paper believe that this interest concerning the film boiling of HeII is actual for RGD owing to reasons: i) in this process the strong nonequilibrium is realized: heater can have temperature of order 100K but interphase: liquid(HeII) - vapour temperature is order of 1K; ii) in difference of usual liquid thermal resistance in conjugate transfer problem takes place mainly on the interphase.

In this work one- and two-dimensional problems are studied on the base of the Boltzmann equation. This equation is solved by two methods. The main of them is the method of direct numerical solving [1] and second one for the steady stage is the moment method. Solutions results obtained by these two methods are compared and the validity domains for each of them are determined.

At the beginning different statements of problem are discussed. In one of them (main) vapour is considered to occupy the space between heater surface and interphase of superfluid helium (Fig.1). At the initial time moment the temperatures of these surfaces are accepted equal to some known values.

For two-dimensional problem vapour helium is in a volume limited by the surfaces AB, BC and AD having temperatures $T_1 = 2T_s$, $T_2 = T_s$, where T_s is the temperature of the interface surface of superfluid helium, $T_s = 2K$, and the corresponding density of saturated vapour are chosen as basic parameters. Further all densities and temperatures are given in relation to basic parameters, and values of x and y coordinates are given in mean free paths of vapor molecules λ_s . The distance $AB = CD = 40\lambda_s$, $AD = BC = 10\lambda_s$. In one-dimensional problems the distance $AB = CD$ is

much more than $AD = BC$.

One-dimensional evaporation-heat transfer problems were solved for different vapour film thicknesses d from $d = 10\lambda_s$ to $d = 100\lambda_s$. Solution results as time evolution are illustrated by Fig.2. The solution example for the steady stage of two-dimensional problem is presented in Fig.3.

Besides the evaporation - heat transfer problem presented above with one non-penetrable and one penetrable for the mass flux interface surfaces the problem of heat transfer through the vapour layer limited by surfaces unpenetrable for the mass flux was studied.

In concluding part as a test for this type of problem the solution of two surfaces evaporation-condensation (reevaporation) task for $d = 500\lambda_s$ was obtained. Corresponding figures and illustrations will be presented in RGD 21 Symposium.

The authors wish to thank the Microgravity Science and Applications Division of NASA for its support of project TM-16 with contract NAS 15-10110 between NASA and Russian Space Agency.

References

- [1] Aristov V.V., Tcheremissine F.G., *The direct numerical solving of the kinetic Boltzmann equation*, Moscow: Computing Center of the Russian Academy of Science. 1992.

*Abstract 4981 submitted to the 21st International Symposium on Rarefied Gas Dynamics, Marseille, France, July 26-31, 1998

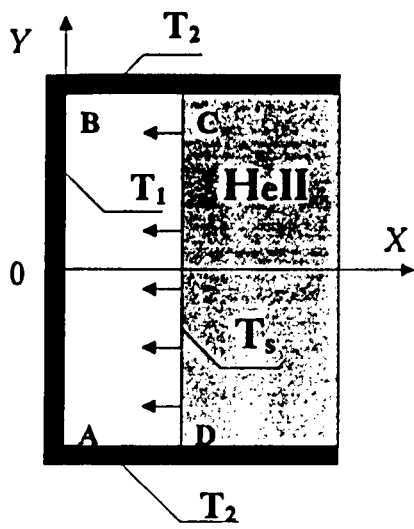


Fig.1

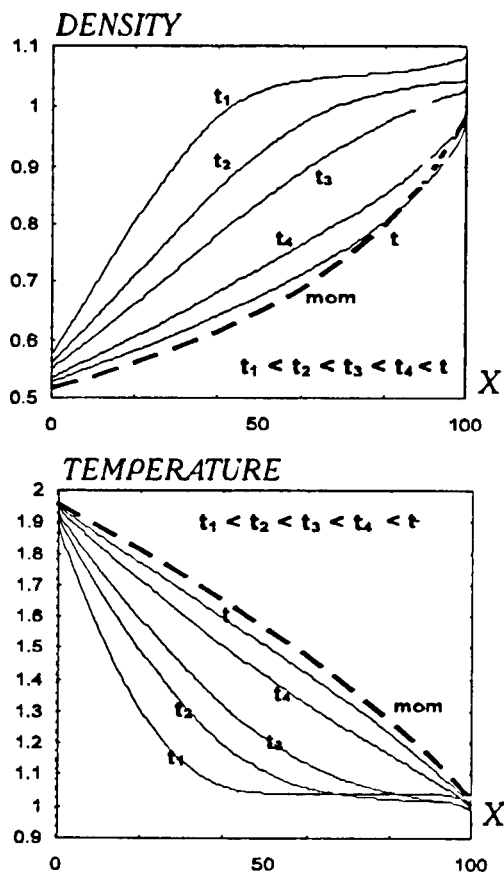


Fig.2

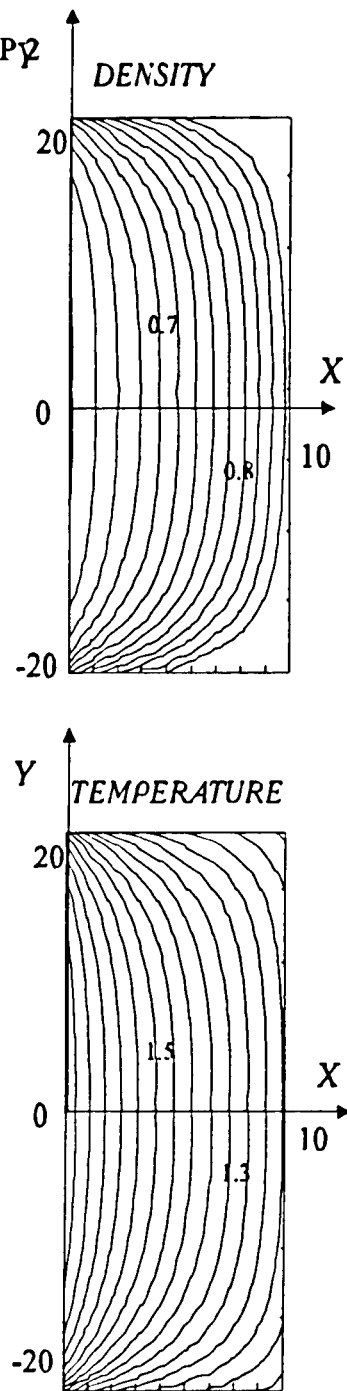


Fig.3

Molecular Dynamics Simulation of Submicron Droplet Vaporization Under Quiescent and Convective Conditions *

T. L. Kaltz, L. N. Long, M. M. Micci
The Pennsylvania State University, USA

1 Introduction

When rarefied gases are simulated using a discrete particle model, the powerful technique of DSMC [1] is usually the method of choice. But if the system to be studied contains regions of high density and is time dependent, such as a vaporizing droplet, then alternate approaches should be considered.

The method used in this research is molecular dynamics [2], in which the classical equations of motion are solved for a system of molecules interacting through a soft sphere potential. Molecular dynamics (MD) can capture the rich physics of the interfacial region between the liquid and gas regardless of the particular flow regime.

This abstract describes three-dimensional MD simulations of submicron oxygen droplets in systems with Knudsen numbers greater than 0.1 (see Fig. 1). The computational domain is a cube containing either hydrogen or helium as the ambient gas. The Lennard-Jones 12-6 potential is used for all intermolecular interactions. The oxygen is treated as completely rigid, and the bond length is maintained using the methods of constraint dynamics. Hydrogen and helium are both modeled as a single Lennard-Jones site. For a complete description of the molecular model and finite difference algorithm, see Kaltz, *et al.*, [3].

Due to the computationally intense nature of MD, all simulations are performed on parallel computers using the Message Passing Interface subroutine library for parallel communication. The method of parallelization, called 'atom decomposition', distributes the molecules evenly across the processors regardless of location. This allows almost perfect load-balancing to be achieved. The current results were obtained using 8 to 32 nodes of IBM's Scalable Powerparallel 2 (SP-2).

*Abstract 6146 submitted to the 21st International Symposium on Rarefied Gas Dynamics, Marseille, France, July 26-31, 1998

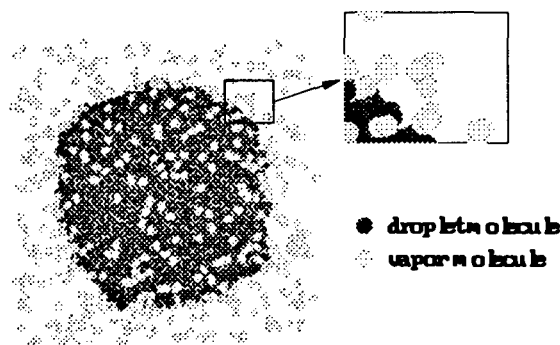


Figure 1: Saturated oxygen droplet at 100 K containing roughly 9300 molecules.

2 Vaporization Results

Droplet vaporization in a quiescent gas was performed for the cases listed in Table 1. All boundaries were periodic and maintained at a constant temperature by scaling the velocities of the molecules in this region. Thermodynamic properties, including the droplet surface tension, were obtained for all cases, as well as estimates of vaporization rates.

At low to moderate ambient pressures, the droplet retains a spherical shape and a sharp interface between the liquid and gas. In addition, surface tension is present throughout the entire vaporization. At high pressure, however, the interface between the liquid and gas becomes less distinct and the droplet geometry becomes non-symmetric (see Fig. 2). This is accompanied by a complete dissipation of surface tension.

Previous research [3] found that this transition in vaporization behavior corresponded with the pressure exceeding the species' critical pressure when the system was comprised of a single chemical component. The results with two components, however, did not exhibit a transition vaporization behavior until the environment pressure was two to

Case	Environment		Number of Droplet (O ₂) Molecules	Total Number of Molecules	Knudsen Number
	Species	Temperature Pressure			
1	H ₂	300 K 4 MPa	9328	44,656	0.31
2	H ₂	200 K 7.5 MPa	9216	42,928	0.11
3	H ₂	300 K 20 MPa	9216	43,216	0.067
4	He	300 K 2 MPa	4944	26,040	1.2
5	He	300 K 4 MPa	4944	22,408	0.59
6	He	300 K 10 MPa	5040	21,392	0.24
7	He	300 K 20 MPa	4944	28,320	0.13

Table 1: Summary of quiescent vaporization simulations. The initial droplet diameter ranged from 7.8 to 9.8 nanometers.

three times the critical pressure of oxygen. This suggests a very high mixture critical pressure.

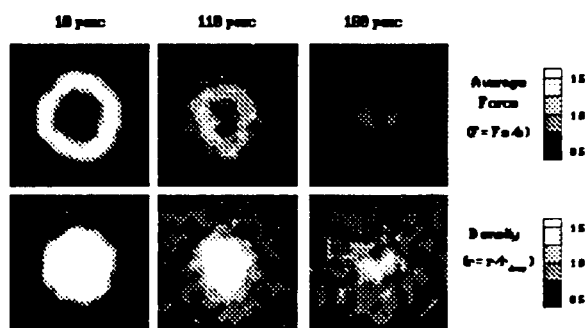


Figure 2: Contour plots of average force and density of an oxygen droplet vaporizing into hydrogen at 300 K and 20 MPa. Elapsed times are 10, 110 and 180 picoseconds. The average force indicates surface tension, and the density is normalized so the droplet surface density is equal to one.

3 Convection Studies

The natural extension of this research is to determine the effects of convection on vaporization behavior. This involves imparting the droplets with an initial velocity corresponding to Weber numbers around 20. The only modification of the simulation is to remove temperature control from the boundaries perpendicular to the flow direction.

Under these conditions the environment quickly becomes entrained along with the droplet. Hence the presence of bulk flow has little effect on the vaporization rates. The relaxation times are of the expected order of magnitude from a simple analysis of particle motion in a flow. Fig. 3 shows a velocity plot of an oxygen droplet in hydrogen at 20 MPa and 200 K.

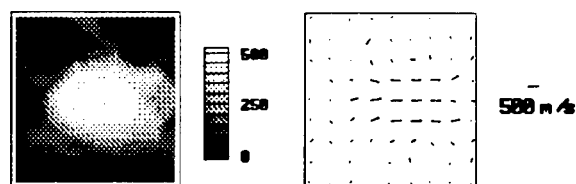


Figure 3: Velocity of an oxygen droplet in hydrogen at 20 MPa and 200 K in units of m/s.

In order to ever approach macroscopic dimensions, however, the number of molecules required by MD would be too large to ever be simulated over the desired time interval. Hence replacing the large number of actual molecules by a much smaller number of particles that still interact through an interparticle potential is currently being pursued [4].

References

- [1] Bird, G. A. *Molecular Gas Dynamics and the Direct Simulation of Gas Flows*, Oxford University Press, 1994.
- [2] Allen, M. P., and Tildesley, D. J., *Computer Simulation of Liquids*, Oxford University Press, 1987.
- [3] Kaltz, T. L., Long, L. N., and Micci, M. M. *Molecular Dynamic Modeling of Supercritical LOX Evaporation*. Presented at the 33rd AIAA/ASME/SAE/ASEE Joint Propulsion Conference & Exhibit, July 6-9, 1997, Seattle, WA, USA.
- [4] Greenspan, D. *Quasimolecular Simulation of Large Liquid Drops*. J. Phys. D: Appl. Phys., Vol. 22, pp. 1415-1417, 1989.

Dynamic Phase Transitions by Model Kinetic Equations: The Conley Index Approach *

K. Piechor, B. Kazmierczak

Institute of Fundamental Technological Research, Centre of Mechanics
Polish Academy of Sciences, Warszawa, Poland

1 Introduction

There are two general different concepts to liquid-vapour systems. The first one, going back to Laplace, assumes that the liquid and its vapour are separated by a sharp interface endowed with energy and entropy. This concept bifurcates into two further approaches. One version uses the continuum-based fluid dynamics equations to both phases with suitably chosen equations of state and transport coefficients, whereas the other approach uses methods of kinetic theory to describe the motion of the vapour. The reason of this is that the continual hydrodynamics cannot describe correctly the process of evaporation and condensation occurring at the interface. In the kinetic approach, however, one usually proceeds as follows: the Boltzmann equation (or equations if mixtures are investigated) or some models of it, including the discrete velocity ones, is applied to the gaseous domain and the liquid bulk is treated as a source (evaporation) or sink (condensation) of particles.

In this paper we propose a more radical approach consisting in the use of one kinetic equation both to the liquid and gaseous phases. Thus, up to a degree, we attempt to follow the lines of the van der Waals philosophy of fluids, which constitutes the second general concept to liquid-vapour systems. Roughly speaking, the van der Waals idea consists in the use of one equation of state suited to both liquid and its vapour, without introducing any sharp surface separating them. It has to be added that the Navier-Stokes equations with the van der Waals formula for the pressure fail to describe the dynamic phase changes including the structure of the thin transitional layer between the 'liquid' and the 'vapour'. To overcome this difficulty so called Korteweg theory of capillarity, known also as the second gradient theory, is used. Roughly speaking, this theory

incorporates higher, greater than two, order space gradients of the density into the equations of conservation of momentum and energy.

The essential difference between this approach, still based on the phenomenological thermodynamics, and that of ours consists in that we want to replace the hydrodynamic description of the system with a kinetic one and next to compare the results.

2 The model

In the paper the simplest, but far from being trivial, example of a kinetic approach to the problem of phase changes will be presented. Our idea consists in the use of one kinetic equation both to the liquid and the gaseous phases. However, if one proceeds to realise such a project then one faces a very fundamental question: simply, there is no universal and fully satisfactory kinetic equation suited to liquid dynamics and phase transition. Therefore, it is necessary to decide upon one out of not very many models. We have chosen so called Enskog-Vlasov equation proposed by Grmela [1] because: i) it is relatively simple: ii) the transport coefficients evaluated with the use of this equation exhibit a pretty good agreement with the experimental data in a wide range of pressures and for fluids with quite chemical structure [2]; iii) the above-mentioned capillarity equations used in the phenomenological approach can be derived, at the formal level, from it [3].

In this model the intermolecular potential is split into a repulsive hard-core and an attractive tail. The hard-core is treated as in the Enskog equation, whereas the tail enters the equation only linearly, in a mean-field term. Unfortunately, this equation is too complicated to be used for determination of any nontrivial flow. That is why we constructed a four-velocity model of it. In connection with that a proposal of solution of two problems

*Abstract 4756 submitted to the 21st International Symposium on Rarefied Gas Dynamics, Marseille, France, July 26-31, 1998

will be given: i) four-velocity model of the Enskog collision operator; ii) four-velocity model of kinetic equations with self-consistent force. The model equations form a system of four highly non-linear integro-differential equations. To simplify them we are forced to take additional assumptions. First, we define the Knudsen number for hard-core collisions and expand those parts of the equations which represent such collisions in a power series keeping the first two non-vanishing terms. Secondly, we assume that the range of the attractive tail is small compared to the macroscopic length-scale and expand the term representing the attractive forces in a power series as well. As the result we obtain a system of purely differential equations.

- [2] Karkheck J., Stell G., *Kinetic mean-field theories*, J. Chem. Phys., 75, pp.1475-1486, 1981.
- [3] Piechor K., *Kinetic theory and thermocapillarity equations*, Arch. Mech., 46, 6, pp.937-951, 1994.

3 The dynamic phase changes

We limit our considerations to one-dimensional unsteady flows. Then some symmetry properties allow us to reduce the system to three non-linear partial differential equations. Next, we focus our attention on travelling wave solutions to this system and confine ourselves to the most interesting case of phase boundaries. These are defined as such travelling waves which connect two different states of rest, in a suitable phase space, which are both saddles, so both of them are unstable. This can be interpreted as the fact that the waves of this type are subsonic with respect to the sound speed before and after it. The existence of such solutions is a difficult problem of ordinary differential equations. To solve it we make use of the Conley connection index. This index is invariant under continuations. Using this property we construct a family of isolating neighbourhoods which are related to each other by continuation. Their Conley indices are unchanged. This allows us to replace our problem by a simpler one for which the connection index can be effectively computed. The method has topological character, and was applied to some other sets of equations behaving in a similar way. The theorem we prove says that, given one state of rest subject to some conditions, there is a unique wave speed, unknown in advance, uniquely determined the other state of rest for which the solution to the considered limit value problem exists and is unique.

References

- [1] Grmela M., *Kinetic approach to phase transitions*, J. Statist. Phys., 3, 3, pp.347-364, 1971.

RAREFIED FLOWS - RF 1

ROOM PÉRÈS

WEDNESDAY, JULY 29, 1998

11:20

Influence of Rarefaction on Oscillations in Underexpanded Jet Impinging on a Flat Plate : Numerical Simulation *

E.I. Sokolov, A.V. Savin

Institute for High Performance Computing and Data Bases, Saint - Petersburg, Russia

Self-excited oscillations originated inside supersonic underexpanded jet impinging upon orthogonal flat plate is a subject of keen interest because of possible various applications [1]. As it was shown in [2] rarefaction may strongly affect on this phenomenon. Physical experiments, however, cannot provide scientist with detailed information about inner complex space - time structure of flow pattern originated during developed process studied here. This paper presents some results obtained by numerical simulation of the flow.

Full Navier - Stokes equations were used for numerical simulation; domain calculated represented main peculiarities of physical experiments [2, 3]. No - slip conditions were put along both inner and outer walls of receiver, nozzle and flat plate. The grid contained about 50.000 cells; knots distribution was more dense near walls and inside subsonic region in front of the plate. New finite - difference scheme and computer code [4] was realised on Pentium - type and PARSYTEC CC/16 computers.

Qualitative analysis of the flow was done by means of two types of computer films. First type contains two films consists of frames with instantaneous isolines of entropy and static pressure. These films allow to observe a moving of shock waves and contact discontinuities inside the flow. Second type of film consists of frames in color RGB pallet; each basic color corresponds to one of main flow quantities. Besides, instantaneous streamlines of subsonic region originated in front of flat plate were placed on these frames.

Results of numerical investigation is presented here with respect of detailed description of two different regimes. First one (Argon, $T_o = 300K$, $M_e = 1$, $n = 52.9$, $h/d_e = 12.5$, $Re_* = 4250$, $Re_L = 410$) was studied experimentally in [3]. Some range of frames allow to conclude that both kinds of feedback loops described in [1] exist here: the loop connecting by means of acoustic waves in ambient me-

dia and loop connecting with propagation of strong shock wave inside subsonic region. One also may see the generation of non - stationary supersonic fan get propagates towards central stagnation point from ring peripheral stagnation region attached to the plate. Colliding at near - axis region it generates supersonic counterflow from plate towards central shock at some time periods (Fig.1).

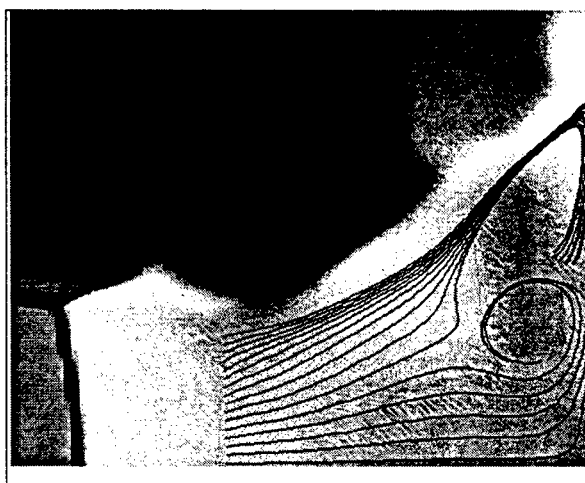


Figure 1:

Numerical simulation of more rarefied regime investigated earlier in [2] (Nitrogen, $T_o = 300K$, $M_e = 2$, $n = 11.13$, $h/d_e = 5.44$, $Re_* = 1300$, $Re_L = 300$) allowed to establish the existence of never described and observed before flow pattern. It consists of the "floating" peripheral circulation zone, periodically appears and disappears just after central shock of the jet. Before its appearance streamlines become S-shaped, and two inner stagnation points originate inside the flow above the plate. Then circulation zone restricted by those points begin grow with generation of collapsing vortex (Fig.2).

The data related to another rarefaction values are obtained and discussed, too, as well as detailed distributions of main flow quantities. Conditions of the existence of instantaneous critical points inside

* Abstract 5231 submitted to the 21st International Symposium on Rarefied Gas Dynamics, Marseille, France, July 26-31, 1998

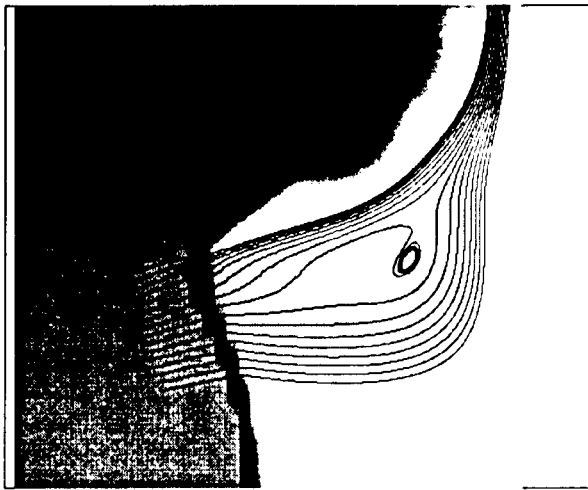


Figure 2:

the flow under study are discussed.

References

- [1] Powell A., *The Sound - Producting Oscillations of Round Underexpanded Jets Impinging on Normal Plates*, Journal of Acoustic Soc. of America. V.83, pp. 515-533.
- [2] Favorsky V.S., Savin A.V., Shatalov I.V., Sokolov E.I. *Rarefaction Effect on the Non - Stationary Underexpanded Supersonic Jet/Infinite Flat Plate Interaction*. Proceedings of the 17-th Int. Symposium on Rarefied Gas Dynamics. Aachen, pp. 979-986, 1990.
- [3] Lukyanov G.A., Sokolov E.I., Shatalov I.V. *Impinging of a Supersonic Underexpanded Rarefied Jet upon a Surface*, Proceedings of the 13-th Int. Symposium on Rarefied Gas Dynamics. Novosibirsk, V.2, pp. 993-1000, 1982.
- [4] Varentsov V.L., Ignatiev A.A., Sokolov E.I., *Computer Simulation of the Internal Molecular-Beam Targets Generation*, STOR 96: 3rd Int Conf. on Nuclear Physics at Storage Rings. Bernkastel-Kues, Germany. Book of Abstracts, p. P32, 1996.

Complete Flowfield Survey of a Continuum Jet Interacting with a Rarefied Freestream Using Planar Laser- Induced Iodine Fluorescence *

J. C. McDaniel

Department of Mechanical & Aerospace Engineering University of Virginia, USA

Problem: Calculation of the flowfield consisting of a continuum sonic jet interacting with rarefied flow about a sharp leading edge flat plate at zero incidence (ref. 1) using a combination of direct simulation Monte Carlo (DSMC) and CFD. CFD and DSMC results agree well everywhere, except in the interaction region between the continuum and rarefied regions of the flowfield. An experimental database is needed for full validation of the computational results and matching of the two calculations in the interaction region.

Objective: Complete surface and in-stream database generation for validation of computational methodology for RCS calculations.

Approach: Use of planar laser-induced iodine fluorescence for nonintrusive, quantitative in-stream measurement of all gasdynamic parameters (pressure, temperature - both rotational and vibrational are possible -, density, jet injectant concentration fraction and all velocity components. Surface

*Abstract 6686 submitted to the 21st International Symposium on Rarefied Gas Dynamics, Marseille, France, July 26-31, 1998

measurements to be via thermographic phosphors for temperature distribution and wall pressure taps.

Facility: A hypersonic freejet facility at the University of Virginia will provide a range of freestream conditions, with typical conditions of 0.2 mm mean free path, altitude of 60 km, and Knudsen number of 0.05, based on free stream mean free path and the jet orifice diameter. The nominal free stream Mach number is 9.8. The facility maintains a flow rate of about 0.2 kg/sec, with a throat area of 300 square mm.

Experimental methodology: Iodine is seeded into the freestream and/or the transverse jet, mounted on a flat plate held in the freejet flowfield which is maintained in a large vessel with optical access windows. By using a planar laser sheet, the RCS iodine-seeded flowfield is induced to fluoresce and the resulting emission collected via a digital camera. The laser is tuned in frequency and a portion of the iodine absorption spectrum is mapped out at every point on the planar laser sheet. In the continuum jet region of the flowfield, the pressure and temperature are measured by determining a pressure and a temperature parameter from the collisionally-broadened spectrum (ref 2). In the rarefied portion of the flowfield, the signal from an isolated transition provides the density and the ratio of two lines determines the rotational and/or vibrational temperature. In both cases, the velocity is determined via the Doppler shift of the iodine lineshape relative to a static cell. The thermographic phosphor on the model surface is excited via a UV lamp and a second digital camera is used to image the phosphorescent emission, which is proportional to surface temperature via suitable calibration.

References:

1. "Numerical Study of a Continuum Sonic Jet Interacting with a Rarefied Flow," Christopher E. Glass and Gerald J. LeBeau, AIAA 97-2536.
2. "Computer-Controlled, Multi-parameter Mapping of 3D Compressible Flowfields using Planar Laser-Induced Iodine Fluorescence," Donohue, J.M., Victor, K.G. and McDaniel, J.C., AIAA 93-0048.

A Parametric Study of Jet Interactions with Rarefied Flow *

Christopher E. Glass
NASA Langley Research Center, Hampton, VA, USA

1 Introduction

A critical concern for vehicles that traverse the transitional flow regime of an atmosphere is vehicle aerodynamic control. For active vehicle control, a reaction control system (RCS), consisting of thrusters strategically placed about the vehicle is used. However, it has been shown that when jet plumes from the RCS interact with the local flow field, unanticipated aerodynamic forces may result. For example, during the initial bank maneuvers of the first shuttle Orbiter flights, the rolling moment that occurred when the yaw thrusters were fired was less than expected, causing greater RCS fuel usage. The cause of the discrepancy was later attributed to improper scaling of wind tunnel derived RCS interaction correlations to the flight condition [1].

Recently, direct simulation Monte Carlo (DSMC) studies have been performed for the Mars Global Surveyor (MGS) [2] that show during the MGS aerobraking maneuver in the transitional regime, the attitude control system (ACS) jets interact with the free stream and cause thrust reversal. That is, a net torque is produced in the direction opposite from that induced by the ACS thruster; the ACS jet plume shadows a downstream portion of the spacecraft from the transitional free stream flow, which causes lower local surface pressure than without the shadowing. Therefore, it is important to understand the interaction of a RCS jet plume with the surrounding rarefied flow field to accurately incorporate the effects of the interaction in the vehicle design and aerodynamic control laws.

The purpose of the paper is to report results of a numerical study of a jet interaction with a rarefied flow. The free stream number density, n , is varied to produce changes in the interaction strength to provide insight to the underlying fluid mechanics of these interactions. A recently reported numerical technique [3] is used in this study. The technique uncouples computational fluid dynamics (CFD) and DSMC solutions at an appropriate breakdown sur-

face [4] to produce a flow solution for the entire flow field.

2 Scope of Present Research

The present numerical study models, as a baseline case, a jet interaction experiment performed by Warburton at the Defence Evaluation and Research Agency (DERA) low density wind tunnel. The experimental test condition provides a rarefied free stream flow for the baseline 3-D jet interaction numerical study. Numerical results for the baseline case were reported earlier [3]. (Comparisons of prediction to measurement will be included in the final paper contingent on the availability of the experimental data.) In addition to the baseline case (case 1), two other 3-D cases will be presented in the present study. To establish parametric variation, the baseline free stream density is lowered by one and two orders of magnitude, which are cases 2 and 3, respectively, holding all other free stream conditions constant.

The jet nozzle and plume flow is predicted using the GASP code [5], a commercially available finite volume Navier-Stokes flow solver from AeroSoft, Inc.; and DSMC is applied using the DSMC analysis code (DAC) of LeBeau at NASA Johnson [3] and [6]. The boundary between the continuum (CFD) and rarefied (DSMC) flow analysis is defined at a value of the Bird breakdown surface that assures the CFD portion of the flow solution is not influenced by the interaction region. This allows the rarefied and interacting portions of the flow to be calculated using the DSMC technique.

3 Results and Discussion

Shown as Figs. 1, 2, and 3 are number density contours at the plane of symmetry for the three cases described above. Number density is normalized by Loschmidt's number, n_0 , the number density at standard conditions. As the free stream number density decreases, the extent of the jet interaction

* Abstract 6741 submitted to the 21st International Symposium on Rarefied Gas Dynamics, Marseille, France, July 26-31, 1998

bow shock increases, which is shown by comparing Figs. 1, 2, and 3. Also, comparing Figs. 1 and 2, the forward separation vortices become larger for decreasing free stream number density, and as shown in Fig. 3, when the free stream number density is decreased by two orders of magnitude, the separation vortices have disappeared. This is significant because the forward separation vortices allow free stream flow and jet plume flow to stagnate along the forward separation vortex reattachment line. Without the separation region present, the jet gas is directed outward away from the nozzle with no surface stagnation. The boundary where the free stream number density just supports the formation of the forward separation will be sought for the final paper. Also included will be a thorough discussion of the fluid mechanics of these rarefied jet interactions and comparisons between the cases studied.

References

- [1] Scallion, W. I., Compton, H. R., Suit, W. T., Powell, R. W., Blackstock, T. A., and Bates, B. L., "Space Shuttle Third Flight (STS-3) Entry RCS Analysis," AIAA 83-0116, AIAA 21st Aerospace Sciences Meeting, Reno, NV, January 10-13, 1983.
- [2] Shane, Russell W., Rault, Didier F. G., and Tolson, Robert H., "Mars Global Surveyor Aerodynamics for Maneuvers in Martian Atmosphere," AIAA 97-2509, AIAA 32nd Thermophysics Conference, Atlanta, GA, June 23-25, 1997.
- [3] Glass, Christopher E. and LeBeau, Gerald J., "Numerical Study of a Continuum Sonic Jet Interacting with a Rarefied Flow," AIAA 97-2536, AIAA 32nd Thermophysics Conference, Atlanta, GA, June 23-25, 1997.
- [4] Bird, G. A., *Molecular Gas Dynamics and the Direct Simulation of Gas Flows*, Clarendon Press, Oxford, 1994.
- [5] AeroSoft, *GASP Version 3, The General Aerodynamic Simulation Program, Computational Flow Analysis Software for the Scientist and Engineer, Users Manual*, AeroSoft, Inc., Blacksburg, Virginia, May 23, 1996.
- [6] Wilmoth, Richard G., Le Beau, Gerald J., and Carlson, Ann B., "DSMC Grid Methodologies For Computing Low-Density, Hypersonic Flows About Reusable Launch Vehicles," AIAA 96-1812, 31st AIAA Thermo-

physics Conference, New Orleans, LA, June 17-20, 1996.

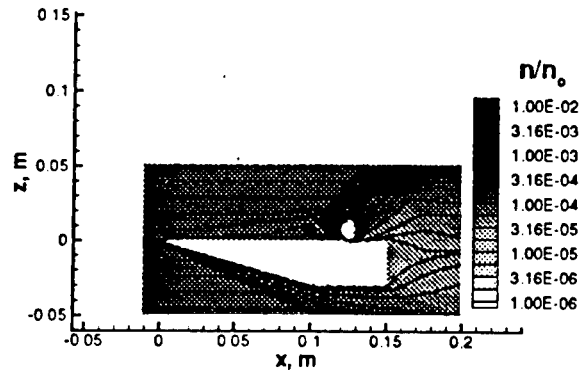


Figure 1: Number density contours for baseline (case 1).

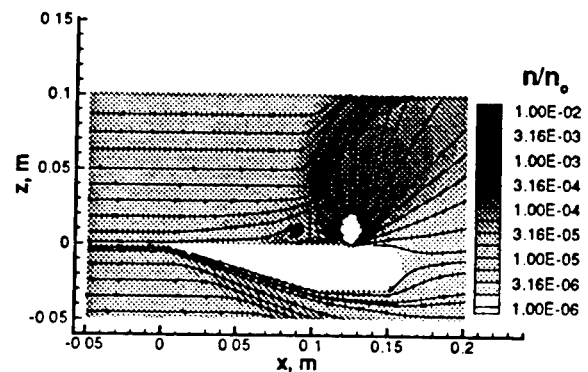


Figure 2: Number density contours for case 2.

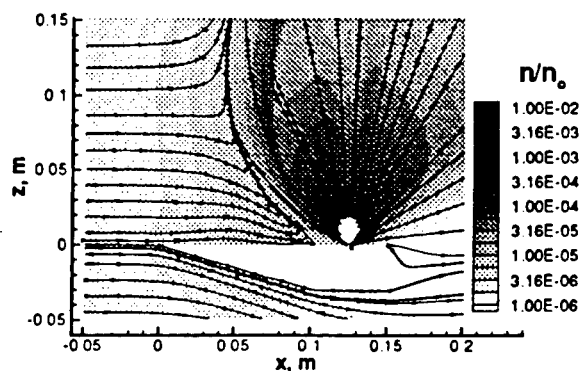


Figure 3: Number density contours for case 3.

RAREFIED FLOWS - RF 2

ROOM PÉRÈS

THURSDAY, JULY 30, 1998

11:10

Comparison of Decoupled Hybrid Navier-Stokes – DSMC Calculations with Experiments in Nozzle Backflows *

M. Rosenhauer, K. Plähn

Institute for Fluid Mechanics, German Aerospace Center
Bunsenstraße 10, D-37073 Göttingen, Germany

1 Introduction

Hybrid computation methods coupling Navier-Stokes solvers for continuum and DSMC methods for rarefied flow have gained much interest to treat flow conditions where strong nonequilibrium situations and large expansion ratios occur in hypersonic flow, e.g. in shocks, blunt body wakes and around nozzle lips. The present paper concerns, as a first step from the effort to build and validate such a program, decoupled NS-DSMC calculations of a nozzle flow from throat far into the backflow region. This case gains interest from the opportunity of comparing it to now available corresponding experiments from the new DLR High Vacuum Facility STG. By powerful cryopumps, STG allows reliable measurements in nozzle backflow regions formerly not accessible due to background pressure disturbances, such delivering data urgently needed to check computational models over the whole range of flow conditions. Especially hybrid methods with their sensitive parameters controlling switching and DSMC details rely on such possibility for validation.

2 The decoupled hybrid approach

The process of coupling a continuum method to DSMC can be divided into two main tasks. At first the domains, to which the continuum approach and DSMC, resp. will be applied, have to be found. In general the assumptions which lead the the Navier Stokes equations allow only small deviations from the Maxwellian distribution f_0 . Therefore, a suitable criterion could be based on the distance of the distribution function f to the Maxwellian,

$$\|f_0 - f\|.$$

*Abstract 1657 submitted to the 21st International Symposium on Rarefied Gas Dynamics, Marseille, France, July 26-31, 1998

Unfortunately this criterion is only useful in the DSMC domain. A criterion which can be used on both domains has to be based on the macroscopic flow properties provided by the Navier Stokes equations. There are several parameters which describe the breakdown of the continuum assumptions [1]. One is the local Knudsen number

$$Kn_l = \frac{\lambda}{Q} \left| \frac{dQ}{dl} \right|,$$

where λ is the local mean free path, Q is a flow property (density or temperature), and l is some distance between two points in the flow field. Another one is the 'breakdown parameter' proposed by Bird [2]:

$$P = \frac{U}{\rho\nu} \left| \frac{d\rho}{ds} \right| = M \sqrt{\frac{\pi\kappa}{8}} \frac{\lambda}{\rho} \left| \frac{d\rho}{ds} \right|,$$

where U is the local velocity, ρ is the density, ν is the collision frequency, M is the local Mach number, κ is the ratio of specific heats, and s is the distance along a streamline. Each parameter has its own strengths and weaknesses. Therefore, the right parameter has to be found individually for a given problem.

The second task is to determine the properties at the interface between Navier-Stokes and DSMC domains. In this special case we will use a decoupled approach which means that no information is passed upstream from the DSMC to the Navier-Stokes domain. Therefore, the properties at the interface are only determined by the Navier-Stokes solution. With the coupled properties at the interface, a distribution has to be generated from which the new DSMC molecules are taken.

Testgas	p_0 [bar]	Re_E	Θ range
N ₂	0.5	800	0° - 105°
N ₂	2	3200	0° - 150°
H ₂	0.5	800	0° - 120°

Testgas	p_0 [bar]	Re_E	Θ	r range [mm]
N ₂	0.5	800	0°	250 - 3000
N ₂	0.5	800	90°	50 - 400
N ₂	2	3200	0°	250 - 5000

Table 1: Test conditions. Θ -profiles at $r = 1$ m. Stagnation temperature $T_0 \approx 300$ K. Reynolds number variation via p_0 .

3 Nozzle flow calculations compared to experiments in STG

In experiments on simulated plumes emanating from a conical 0.5 N - thruster nozzle (see Fig. 1), N₂ and H₂ as test gases have been investigated in the DLR STG facility [3]. Table 1. shows the test conditions and ranges of the measured profiles.

The very high vacuum ($< 10^{-5}$ mbar) provided by the STG facility during thruster operation enables measurements with a free molecule pressure probe with negligible background disturbances in the backflow region ($\Theta > 90^\circ$). These experiments provide an excellent opportunity to test hybrid numerical codes. The high expansion ratio around the nozzle lip which leads to strong gradients in nearly all flow properties, has a high impact on the flow conditions in the backflow region.

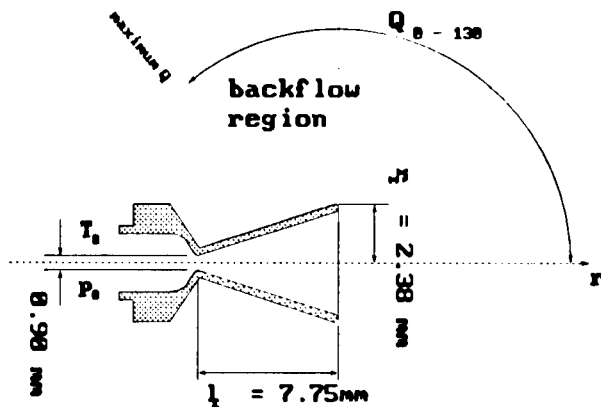


Figure 1: Thruster nozzle geometry

In the presented hybrid Navier-Stokes - DSMC approach, method switching criteria will be compared on the basis of experimental backflow results. Critical regions are the expansion around the nozzle

lip and the boundary layer, which has a thickness δ_E of up to $\delta_E \approx \frac{1}{2}r_E$ for a Reynolds Number of $Re_E = 800$. The thick boundary layer is the reason why a Navier-Stokes solver has to be used for the continuum region. Although a proper continuum breakdown parameter switches to DSMC near the nozzle wall, most of the boundary layer is left to the continuum solver which has to allow for viscous effects.

Secondly, as experiments with H₂ show, the influence of a varying rate of specific heats κ at low temperatures resp. high expansion on the flowfield is not negligible. Therefore, an adapted modelling of a variable κ for H₂ will be attempted.

References

- [1] I. D. Boyd, G. Chen, and G. V. Candler. Predicting failure of the continuum fluid equations in transitional hypersonic flows. *Phys. Fluids*, 7(1):210-219, January 1995
- [2] G. A. Bird. *Molecular Gas Dynamics and the Direct Simulation of Gas Flows*. Oxford University Press, 1994.
- [3] G. Dettleff and K. Plähn. Initial Experimental Results from the new DLR-High Vacuum Plume Test Facility STG. *AIAA 97-3297*

Structure of Converging, Cylindrical Shocks *

Z.A. Walenta

Institute of Fundamental Technological Research, Polish Academy of Sciences

Curved shocks are often encountered in laboratory experiments and in numerous applications of shock waves. When the radius of curvature of the shock is large compared to its thickness, the shock may be treated as plane and its behaviour can be predicted with good accuracy with the Rankine-Hugoniot relations. In the narrow region where the radius of curvature of the shock is of the same order of magnitude as its thickness the standard Rankine-Hugoniot relations can no longer be applied. Such shocks are called the "non Rankine-Hugoniot shocks" [1]. The "non R-H shocks" may behave in a different way than ordinary plane shocks. This concerns, in particular, the dependencies of the thicknesses and jumps of thermodynamic parameters on the shock speed.

In the present study we investigate the behaviour of cylindrical, converging shocks close to the axis of symmetry, as measured in mean free paths of the gas particles. Both, experimental and numerical methods are employed.

In the experiment, conducted in a classical, large-diameter shock tube, plane shocks are transformed into cylindrical ones using the Perry-Kantrowitz device [2]. To make it possible to distinguish the details of the shock structure, the initial gas density is so low, that the mean free path of the particles is of the order of one millimeter. The gas density measurements are performed with the suitably modified Laser Differential Interferometer [3].

Numerical calculations are performed with the standard Direct Simulation Monte-Carlo procedure, with the hard-sphere model of the gas particles and the ballot-box scheme for selection of the particles for collisions [4].

The obtained results indicate, that the Rankine-Hugoniot relations are applicable surprisingly close to the axis of symmetry (for the radii of curvature of the shocks not less than about six shock thicknesses). Closer to the axis more serious discrepan-

cies between the curved and plane shock structures appear, however the shock maintains its character even for the radii of curvature nearly equal to their thicknesses. For even smaller radii the "focus" is produced, where the gas parameters jump to very high values. The diameter of this region is equal to about two shock thicknesses.

References

- [1] Sichel M., *Structure of weak non-Hugoniot shocks*, Phys. Fluids, Vol.6, No.5, pp.653-662, 1963.
- [2] Perry R.W., Kantrowitz A., *The production and stability of converging shock waves*, J. Appl. Phys. Vol.22, pp.878-886, 1951.
- [3] Smeets G., George A., *Gasdynamische Untersuchungen im Stossrohr mit einem hochempfindlichen Laserinterferometer*, ISL-R 14/71, 1971.
- [4] Yanitskiy V.E., Belotserkovskiy O.M., *The statistical method of particles in cells for the solution of problems of the dynamics of a rarefied gas*. Part I, Zh. Vychisl. Mat. Mat. Fiz., Vol.15, pp.1195-1208; Part II, Zh. Vychisl. Mat. Mat. Fiz., Vol.15, pp.1553-1567, 1975.

* Abstract 4771 submitted to the 21st International Symposium on Rarefied Gas Dynamics, Marseille, France, July 26-31, 1998

Rarefied Gas Flow through Porous Layer *

A.I. Erofeev, O.G. Friedlander, M.N. Kogan
Central Aerohydrodynamics Institute (TsAGI)
1, Zhukovsky str., 140160 Zhukovsky, Russia

Porous media are often encountered in nature as well as in technical applications. Creation of capillary catalyzers and filters, porous particles motion and coagulation analysis etc. require in general case detailed investigation of rarefied gas flow through porous media. There are two types of porous body channels interactions. One is the interaction of channels inside the body, where they can intersect, combine or merge. But even when the channel are isolated inside the body each of them interacts with other in the outer region, thus, changing the channel inflow and outflow conditions. The latter effect will be considered in the present research. The simplest tubular model of porous layer consisting of parallel channels will be investigated. Particularly the channels with plane walls will be considered most carefully.

Not so many investigations have been devoted to this problem up to now and most of them are experimental. Sometimes crude so-called dusty gas model is used for inner flow description. To estimate the flow rate through tubular porous layer the flow through a single channel is often used. In the last case three possible solutions exist: for infinite tube, for a tube connecting two infinite vessels and for the simplified problem when the boundary conditions prescribed at infinity in the vessels are removed to the ends of the channel. All three solutions differ sufficiently. The boundary conditions at the ends of the channel for each of these solutions are different and differ also from the case when the interaction of channels is taken into account. The main aim of the present work is to analyse the role of the outer interaction between channels and to develop the method of corresponding calculations.

The simplest porous layer consisting of flat zero thickness plates of length L and with distance d between it is considered first of all. Stationary rarefied gas flows inside channels and in adjacent layers are described by non-linear Boltzmann equation.

The diffuse law with surface temperature T_w is assumed for reflected molecules. Far from the ends of the porous layer the flow becomes uniform with maxwellian distribution function. The oncoming stream is in some sense similar to the flow near condensing plate and the flow passed the porous layer is similar to that of evaporating plate. In accordance with this analogy number density $n_{-\infty} = n(x \rightarrow -\infty)$ and temperature $T_{-\infty} = T(x \rightarrow -\infty)$ must be prescribed in oncoming flow and only number density $n_{\infty} = n(x \rightarrow +\infty)$ in the flow after porous layer may be stated [1-2]. The velocities $u_{-\infty}$ and u_{∞} are found by the problem solution.

This boundary problem was solved by DSMC method. VHS molecular model was used corresponding to parameter $\omega=0.7$ in the viscous/temperature relation $\mu \propto T^{\omega}$. Fitting procedure and algorithm taken from work [3] were utilized. The flow for small number density differences $(n_{-\infty} - n_{\infty})/n_{-\infty} = 0.12$ and 0.2 were calculated. The temperature of the channel walls T_w was assumed equal to $T_{-\infty}$. Computational transition regions in front of and behind porous layer were 10-200 free molecular path length $\lambda_{-\infty}$. The error in molecular flow rate was less than 3% for Knudsen number $Kn > 0.5$ and less than 5% at $0.1 < Kn < 0.5$. The calculations were performed for Knudsen number $Kn = 0.1 \div 10$ and $L/d = 5, 10, 20$. The comparison of this results taking into account transition regions adjoined to the porous layer with molecular flow rate for single channel show possible difference up to 50%.

Application of the above mentioned analogy between transition layers and Knudsen layers near condensing and evaporating surfaces allowed us to develop the approximate molecule flux calculation method for small pressure differences. The proposed method is applicable for tubular porous layer model with channels of arbitrary form of cross sections, arbitrary their distribution and porosity. Comparison of the results of approximate method with data obtained by DSMC method demonstrates satisfactory accuracy.

*Abstract 4941 submitted to the 21st International Symposium on Rarefied Gas Dynamics, Marseille, France, July 26-31, 1998

Acknowledgement

The work is carried out at support of International Science and Technology Center (Project 200) and State Program for Leading Research Groups Support (grant 96-15-96063)

References

- [1] Abramov A.A., Kogan M.N., *Possible regimes of supersonic gas condensation* Dokl. Acad. Nauk SSSR, 1984, 278(9), p.1078 (in Russian). See also: Sov. Phys. Dokl., 29, p.763.
- [2] Kogan M.N. , *Evaporation/condensation kinetics*, Rarefied Gas Dynamics. Proc.19th Intern. Symp./ Ed. J.Harvey and G. Lord. Oxford. 1995.
- [3] Frezzotti A., *Kinetic theory description of the evaporation of multi-component substances*. Rarefied Gas Dynamics. Proc. 20th Intern. Symp./Ed. Shen Ch. Beijing: Peking Univ. Press. 1997. P.837-846.

Joint Solution of Boltzmann and Boundary Layer Equations *

S.P.Popov, F.G.Tcheremissine
Computing Center of RAS, Moscow, Russia

Gas flows at small Knudsen numbers usually are accompanied by the formation of narrow highly nonequilibrium zones like shock wave fronts and Knudsen layers in which flow parameters sharply change at a scale of a molecular mean free path, while outside these regions a hydrodynamic regime take place. For such flows the application of kinetic numerical methods in a whole computational domain is not efficient, and hybrid algorithms in which only highly nonequilibrium zones are computed on the base of Boltzmann kinetic equation, and hydrodynamic regime is studied by solving Euler or Navier-Stokes equations should be preferred.

In presented paper a hybrid numerical scheme that combine the solution of Boltzmann equation with that of Boundary Layer equations (which are the simplified version of Navier-Stokes equations) is described. The scheme is studied on a problem of subsonic rarefied gas flow over a flat plate of finite length and zero thickness posed in parallel to the flow direction. The flow is considered in (x, y) plane for $y \geq 0$ and the plate is located along the x axis. Boltzmann equation is solved near the plate in a rectangular $x_{min} \leq x \leq x_{max}$, $0 \leq y \leq y_s$, and Boundary Layer equations are solved for $x_{min} \leq x \leq x_{max}$, $y_s \leq y \leq y_{max}$. The mesh of computational grid in kinetic region is taken less then a molecular mean free path, while in the hydrodynamic region it much exceeds this value. At the line $y = y_s$, both solution sticks together.

The problem is solved by an iterative method. An iteration corresponds to the advancement on a time step of the unsteady stabilization method of solving Boltzmann equation [1] in the kinetic region. At each iteration a new distribution function $f_s = f_B + f_M$ at the line $y = y_s$ is composed. The function f_B presents the solution of Boltzmann equation for positive molecular velocity vectors in the y direction, and f_M is a part of the maxwellian distribution function for negative molecular velocities in the same direction. The function f_M is defined by

hydrodynamic parameters which are found from the solution of the Boundary Layer equations at $y = y_s$.

The function f_s gives the upper boundary condition for solving Boltzmann equation at the next time step and macroscopic fluxes $nv = \int \xi_y f_s d\xi$, $nuv = \int \xi_x \xi_y f_s d\xi$, $\mu \partial u / \partial x = -p_{xy} = -\int (\xi_x - u)(\xi_y - v) f_s d\xi$, that provides boundary conditions in the hydrodynamic region. In these formulae u and v are macroscopic gas velocities in x and y directions, ξ_x and ξ_y are corresponding molecular velocities, ξ is molecular velocity vector, n is density, p is pressure, μ is the coefficient of viscosity.

The iterative process continue until the stabilization of solutions in both kinetic and hydrodynamic regions is reached.

The problem is solved for different gas-surface interaction conditions and for different Knudsen and Mach numbers. The influence of the matching line distance y_s on computed flow field and on aerodynamic reactions at the plate is studied.

References

- [1] Tcheremissine F.G., *Conservative Discrete Ordinates Method for solving of Boltzmann kinetic equation*, Proceedings of 20-th Internat.Symp.on RGD, Ching Shen ed., Peking Univ.Press, Beijing, China, pp.297-302, 1997.

* Abstract 5246 submitted to the 21st International Symposium on Rarefied Gas Dynamics, Marseille, France, July 26-31, 1998

RAREFIED FLOWS - RF 3

ROOM PÉRÈS

THURSDAY, JULY 30, 1998

14:00

Rayleigh-Bénard Chaotic Convection in a Rarefied Gas *

S.Stefanov¹, V. Roussinov¹, C. Cercignani²

¹ Institute of Mechanics, Bulgarian Academy of Sciences, Sofia, Bulgaria

² Dipartimento di Matematica, Politecnico di Milano, Milan, Italy

1 Introduction

The recent studies on the Rayleigh-Bénard instability of rarefied gas flow [1][2][3][4] report about a stable vortex formation for Knudsen numbers $Kn(= \ell/L) = 0.01 - 0.045$ and various magnitudes of temperature ratio and Froude number $Fr(= V_{th}^2/gL)$ (g is a "gravity" acceleration, V_{th} is the most probability velocity). We will present a comparative analysis of DSMC simulations and Navier-Stokes finite difference computations of the problem for considerable less $Kn = 0.001$ and temperature ratio $T_{cold}/T_{hot} = 0.1$. Within a given interval of values of the "gravity" force both methods exhibit a secondary instability with a final flow state of permanently chaotic vortex formation (the so-called "strange attractor"). A similar result has been obtained by Bird [5] for the Taylor-Couette cylindrical flow.

2 Numerical simulations

The numerical calculations employ "hard sphere" molecular model. The gas flow is considered in a rectangular computational domain $2L \times L$ i.e. with an aspect ratio equal to 2. The domain is confined in the vertical direction by two diffusively reflecting walls (lower wall temperature is greater than the upper one $T_{hot} > T_{cold}$) and a periodic boundary condition is implemented in horizontal direction at two planes with a distance $2L$ between them. A constant gravity acceleration acts on the gas in each point of the computational domain. As it was mentioned above for certain sets of the governing parameters the final state of the flow is a strange attractor and consequently should be calculated by using an unsteady-state numerical approach. We have used two completely different computational methods to investigate the problem. The first one is based on the use of the contin-

uum Navier-Stokes equations of compressible viscous gas with "repaired" transport coefficients according to the first approximation of the Chapman-Enskog theory. The corresponding slip boundary conditions are added for the computation of flow conditions close to the diffusively reflecting walls. An implicit finite difference scheme is used with internal iteration process within each time step and the computational grid has 200×100 nodes. The second approach is the Bird's DSMC method, which is a suitable numerical technique giving reasonable results for a wide range of Knudsen numbers. The simulation employs about 3×10^6 particles and two computational grids: a high resolution (microscopic or kinetic) grid (800×400 cells) required for correct calculation of the basic steps of the method and a coarser (macroscopic) grid (100×50 cells) used for calculation of the macroscopic properties. It is worth noting that for low Knudsen number flows both space scales microscopic and macroscopic are separated clearly and this leads naturally to the use of two computational grids. The same reason is valid for the time scales. Thus, it allows an additional time averaging over interval which is short with regard to macroscopic time scale but might be relatively very large concerning the kinetic scale. The motives for performing such parallel calculations of both continuum and molecular solutions are connected with our belief that the answer of many fundamental questions of the flow instability onset and the transition to turbulence can be sought for on the edge between molecular and continuum description of the gas flow[6]

3 Results

The low Knudsen number calculations are very complicated and time consuming. This do not allow us to investigate the whole space of values of the governing parameters. Here we will illustrate the Navier-Stokes calculations for the case $Fr = 1.0$, where the final flow state has been found to be a strange attractor. The velocity vector field at

* Abstract 2697 submitted to the 21st International Symposium on Rarefied Gas Dynamics, Marseille, France, July 26-31, 1998

$t = 1413.0$ is shown in Fig. 1.

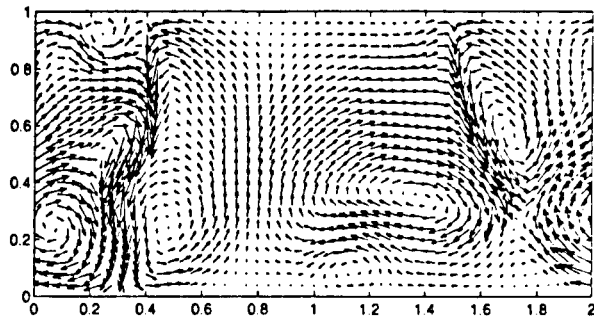


Figure 1: The velocity vector field at $t=1413.0$

The evolution of the vortex structure is very complicated and is not repeatable. The influence of the chaotic vortex formation on the non-dimensional heat flux (the Nusselt number) at the hot wall is shown in Fig. 2

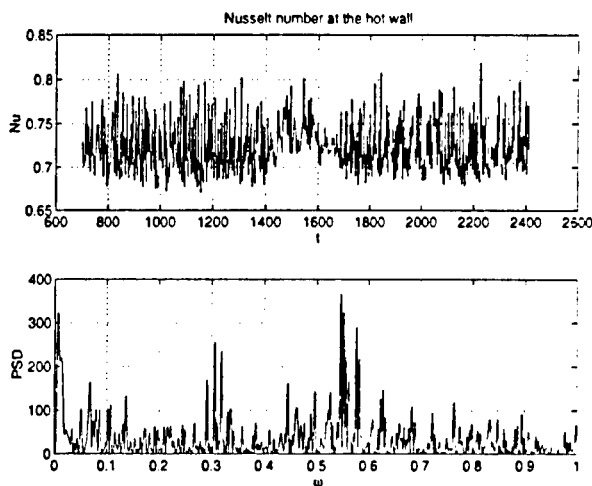


Figure 2: Nusselt number oscillations and power spectral density over a long time interval

References

- [1] Stefanov S., Cercignani C., *Monte Carlo Simulation of Bènard's Instability in a Rarefied Gas*, Euro. J. of Mechanics B/Fluids, Vol. 11, No 5, pp543-552, 1992.
- [2] Sugimoto H., Sone Y. Aoki K., Motohashi H. *The Bènard Problem of Rarefied Gas Dynamics*, In 19th Rarefied Gas Dynamics Symposium Proceedings, Oxford University Press, 1995.
- [3] Watanabe T., Kaburaki H., Yokokawa M., *Simulation of a Two-dimensional Rayleigh-Bènard*

System using the Direct Simulation Monte Carlo Method, Phys. Rev. E, Vol. 49, No.5, pp.4060-4064, 1994.

- [4] Robinson C., Harvey J., *Two Dimensional DSMC Calculations of the Rayleigh-Bènard Instability*, In 20th Rarefied Gas Dynamics Symposium Proceedings, Peking University Press, 1997.
- [5] Bird G., *The Initiation of Centrifugal Instabilities in an Axially Symmetric Flow*, In 20th Rarefied Gas Dynamics Symposium Proceedings, Peking University Press, pp.624-629, 1997.
- [6] Stefanov S., Gospodinov P., Cercignani C., *Monte Carlo Simulation and Navier-Stokes Finite Difference Calculation of Unsteady-State Rarefied Gas Flows*, Phys. Fluids, Vol. 9, No. 12, 1997.

Stability of Bénard Multi-Rolls in a Rarefied Gas *

Y. Sone, K. Aoki, H. Sugimoto

Dept. Aeronautics and Astronautics, Kyoto University, Kyoto, Japan

1 Introduction

Recently, the study of the Bénard instability problem for a rarefied gas became active, and various features of the convection flow have been clarified (e.g., [1]-[3]). In our previous papers ([2], [3]), where the problem was investigated numerically by an accurate finite-difference analysis of the Boltzmann-Krook-Welander (BKW or BGK) equation, the parameter range for which a steady convection flow exists, steady flow patterns, transition processes to steady convection rolls, etc. have been studied in detail. In particular, in [3], we started the study of stability of multi-roll solutions and obtained the stable range of double-roll solutions. In the present study, we extend this work and investigate the stability of three to five-roll solutions.

2 Problem

Let us consider a rarefied gas in a two-dimensional rectangular domain $0 \leq X_1 \leq L$, $0 \leq X_2 \leq D$ (X_i : the Cartesian coordinate system) and subject to a uniform gravity in the negative X_2 direction. The lower boundary at $X_2 = 0$ is heated to a uniform temperature T_h , whereas the upper one at $X_2 = D$ is cooled to a uniform temperature T_c . Restricting ourselves to the two-dimensional flow, we investigate the stability of multi-roll solutions under the assumptions: (i) the behavior of the gas is described by the BKW equation; (ii) the gas molecules are reflected diffusely on the upper and lower boundaries; (iii) the gas molecules are reflected specularly on the side boundaries at $X_1 = 0$ and L .

The following additional notations are used: t is the time, f is the velocity distribution function, v_i is the gas flow velocity, g is the acceleration of gravity, R is the gas constant per unit mass, ρ_0 is the average density in the rectangular domain, ℓ_0 is the mean free path of the gas molecules in the equilibrium state at rest with temperature T_h and density ρ_0 ,

$Fr = 2RT_h/Dg$ is the Froude number, and $Kn = \ell_0/D$ is the Knudsen number.

3 Analysis

The problem is characterized by the four nondimensional parameters: L/D , T_c/T_h , Fr , and Kn . If there is a *stable* steady single-roll solution for $L/D = a$ (say f_a^1), then, by arranging it and its mirror image alternately, one can generate a steady N -roll solution (say f_a^N or $\overline{f_a^N}$) for the domain with $L/D = Na$ (for the same values of T_c/T_h , Fr , and Kn). Here, we denote by f_a^N the solution with the *clockwise* leftmost roll and by $\overline{f_a^N}$ that with the *counterclockwise* leftmost roll. The multi-roll solution thus obtained is not necessarily stable even if the original single-roll solution is stable. (Obviously, for odd N , there is no difference between f_a^N and $\overline{f_a^N}$ with respect to stability.) We investigate the stability of the multi-roll solution numerically by an accurate finite-difference analysis using a slightly perturbed multi-roll solution as the initial velocity distribution f_0 . To be more specific, for even rolls,

$$f_0 = [1 - \epsilon \sin(2N\pi X_1/L)] f_{L/2ND}^{2N}, \quad \text{or (1)}$$

$$f_0 = [1 - \epsilon \sin(2N\pi X_1/L)] \overline{f_{L/2ND}^{2N}}, \quad (2)$$

and for odd rolls,

$$f_0 = [1 + \delta - \epsilon \sin((2N+1)\pi X_1/L)] f_{L/(2N+1)D}^{2N+1}, \quad (3)$$

where ϵ is a parameter characterizing the size of perturbation, and δ is a constant introduced to make the mass of the gas in the domain for f_0 equal to that for $f_{L/(2N+1)D}^{2N+1}$.

4 Results

The numerical computation of the stability analysis is carried out for the three to five-roll solutions to find the stable range with respect to the aspect ratio L/D of the domain with the other parameters fixed at $Fr = 3$, $T_c/T_h = 0.4$, and $Kn = 0.02$. Since

* Abstract 4586 submitted to the 21st International Symposium on Rarefied Gas Dynamics, Marseille, France, July 26-31, 1998

	L/D				
f_0	1.8	2.4	3.0	3.6	4.0
Eq. (3)	D	T	T	T	$\overline{\mathbf{Q}}$

Table 1: Stability of the three-roll solution $f_{L/3D}^3$. The type (**D**, **T**, or $\overline{\mathbf{Q}}$) of the limiting solutions as $t \rightarrow \infty$ from the initial distribution (3) ($N = 3$) is shown for various L/D .

	L/D				
f_0	2.4	3.2	4.0	4.8	5.4
Eq. (1)	T	$\overline{\mathbf{Q}}$	$\overline{\mathbf{Q}}$	$\overline{\mathbf{Q}}$	$\overline{\mathbf{V}}$
Eq. (2)	T	$\overline{\mathbf{Q}}$	$\overline{\mathbf{Q}}$	$\overline{\mathbf{Q}}$	$\overline{\mathbf{VI}}$

Table 2: Stability of the four-roll solutions $f_{L/4D}^4$ and $\overline{f}_{L/4D}^4$. The type (**T**, **Q**, $\overline{\mathbf{Q}}$, $\overline{\mathbf{V}}$, or $\overline{\mathbf{VI}}$) of the limiting solutions as $t \rightarrow \infty$ from the initial distributions (1) and (2) ($N = 4$) is shown for various L/D .

	L/D				
f_0	3.0	4.0	5.0	6.0	6.75
Eq. (3)	T	V	V	V	$\overline{\mathbf{VI}}$

Table 3: Stability of the five-roll solution $f_{L/5D}^5$. The type (**T**, **V**, or $\overline{\mathbf{VI}}$) of the limiting solutions as $t \rightarrow \infty$ from the initial distribution (3) ($N = 5$) is shown for various L/D .

a stable single-roll solution is found in the range $0.525 \leq L/D \leq 1.36$ for these values of Fr , T_c/T_h , and Kn in [3], we can generate N -roll solution for $0.525N \leq L/D \leq 1.36N$. The result of computation [with $\epsilon = 0.01$ in Eqs. (1) - (3)] about the type of flow established finally is shown in Tables 1-3, where the symbols **D**, **T**, **Q**, **V**, and **VI** denote the solution $f_{L/ND}^N$ with $N = 2, 3, 4, 5$, and 6, respectively, and bar over the letter is used for $\overline{f}_{L/ND}^N$. An example of the transition process (perturbed $\mathbf{Q} \rightarrow \overline{\mathbf{V}}$) is shown in Fig. 1.

References

- [1] Stefanov S. and Cercignani C., Eur. J. Mech., B/Fluids, Vol.11, No.5, pp.543-553, 1992.
- [2] Sone Y., Aoki K., Sugimoto H., and Motohashi H., in *Rarefied Gas Dynamics*, edited by J. Harvey and G. Lord (Oxford Univ. Press, Oxford, 1995), pp.135-141.

- [3] Sone Y., Aoki K., and Sugimoto H., Phys. Fluids, Vol.9, No.12, pp.3898-3914, 1997.

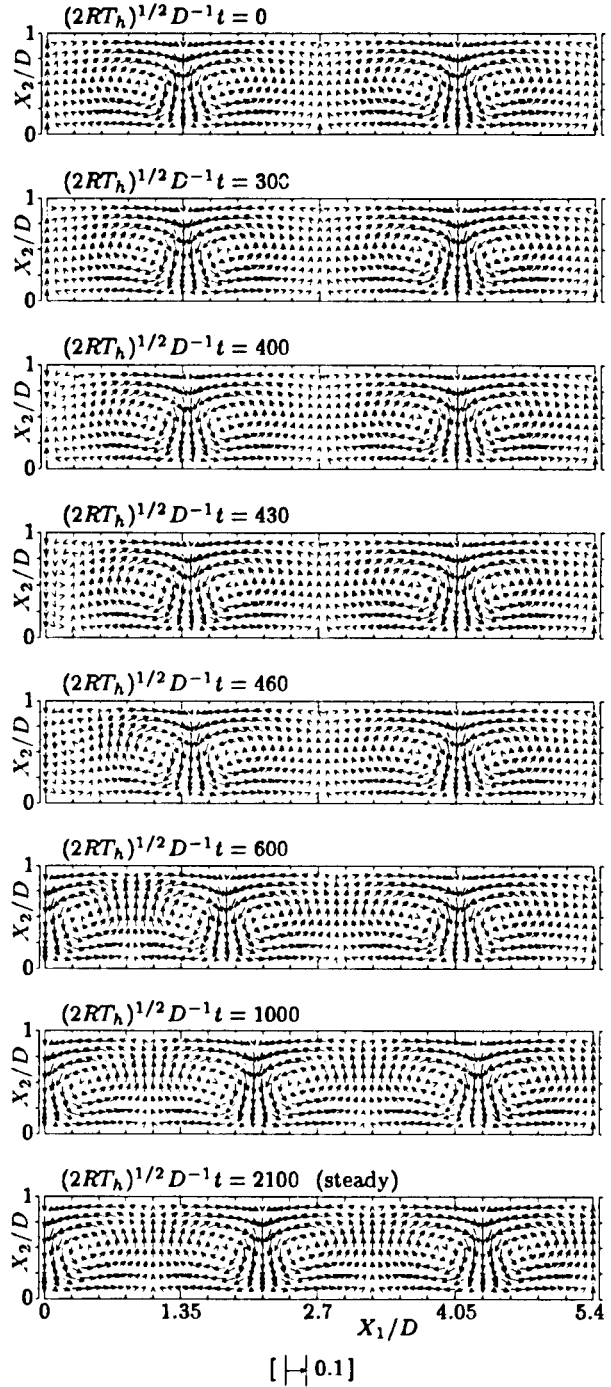


Figure 1: Transition process from the perturbed four-roll solution (1) ($N = 4$) to the five-roll solution $f_{L/5D}^5$ for $L/D = 5.4$. The arrow indicates the flow velocity vector (v_1, v_2) at its starting point, and the scale $(v_1^2 + v_2^2)^{1/2} (2RT_h)^{-1/2} = 0.1$ is shown in the figure.

Numerical Modeling of Near-Continuum Hypersonic Flow About a Hollow Cylinder Flare *

M.S. Ivanov, G.N. Markelov, A.N. Kudryavtsev, S.F. Gimelshein
Computational Aerodynamics Lab., ITAM SB RAS, Novosibirsk, Russia

1 Introduction

One of the most important problems of high-altitude aerodynamics is the shock wave/boundary layer interaction in the near-continuum regime. In this regime, the flow rarefaction manifest itself near the surface and can be taken into account through the boundary conditions (slip velocity and temperature jump) for Navier-Stokes equations. The flow physics is considerably complicated in case when the flow separation is formed, and simulation of such flows by the continuum approach is still an open question. The use of two different approaches, kinetic and continuum, is therefore beneficial since it allows one to increase the validity of numerical results on the shock wave/boundary layer interaction for moderate Reynolds numbers (20,000–30,000).

Such studies was started by the authors in [1] where the computations of viscous interactions for the 2D ramp with various angles of flap deflection were performed by kinetic and continuum approaches. The majorant frequency scheme [2] of the DSMC method was used for kinetic computations. The Navier-Stokes computation were performed by a time-accurate explicit upwind TVD scheme using HLLEM solver for calculation of inviscid fluxes and 2nd order central differences for viscous terms. The results for two approaches are in very good agreement for the entire flowfield. The comparison of numerical and experimental [3] data manifests some difference downstream of the reattachment point which is likely caused by three-dimensional effects in experiment.

It is difficult to maintain the flow two-dimensionality at experimental conditions for a model with small spanwise size used in [3]. This motivated the conduction of similar experiments [4] for an axisymmetric hollow cylinder flare configuration. The advantage of this configuration is twofold since it enables one a) to put baseflow far enough

downstream of the interaction region, in order to avoid the influence of the baseflow on the interaction region; b) to eliminate three-dimensional effects.

The main objectives of this work are to study an axisymmetrical shock wave / boundary layer interaction for a moderate Reynolds number ($Re = 18900$) by kinetic and continuum approaches and analyze the influence of slip conditions for Navier-Stokes equations on the bow shock position.

2 Results and discussions

The kinetic and the continuum approaches are the same as they described in [1]. A comparison numerical results with experimental data shows that numerical results obtained by solving Navier-Stokes equations with no-slip conditions overpredict the size of separation zone and DSMC results slightly underpredict this size.

Kinetic results are in excellent agreement with experimental data on the position of the bow shock whereas the continuum approach gives a shift of the bow shock further from the body (the distance from the surface increases on 10-15 percent). Note that such a shift was also observed for a ramp configuration in [1].

The shift of the bow shock is probably connected with the fact that Navier-Stokes equations, even with account of slip velocity and temperature jump, fail near the leading edge, and the introduced unphysical perturbations affect far downstream of the leading edge. The kinetic approach is valid in the entire flow field. DSMC results obtained for $Kn = 0.001$, or $Re = 18,900$, show a noticeable flow nonequilibrium, especially near the leading edge. The flowfield of T_y/T is shown in Fig.1 which illustrates the nonequilibrium of the translational temperature in different directions. The 20-percent deviation of the temperature in Y-direction from the average value T is observed near the leading edge,

*Abstract 5041 submitted to the 21st International Symposium on Rarefied Gas Dynamics, Marseille, France, July 26-31, 1998

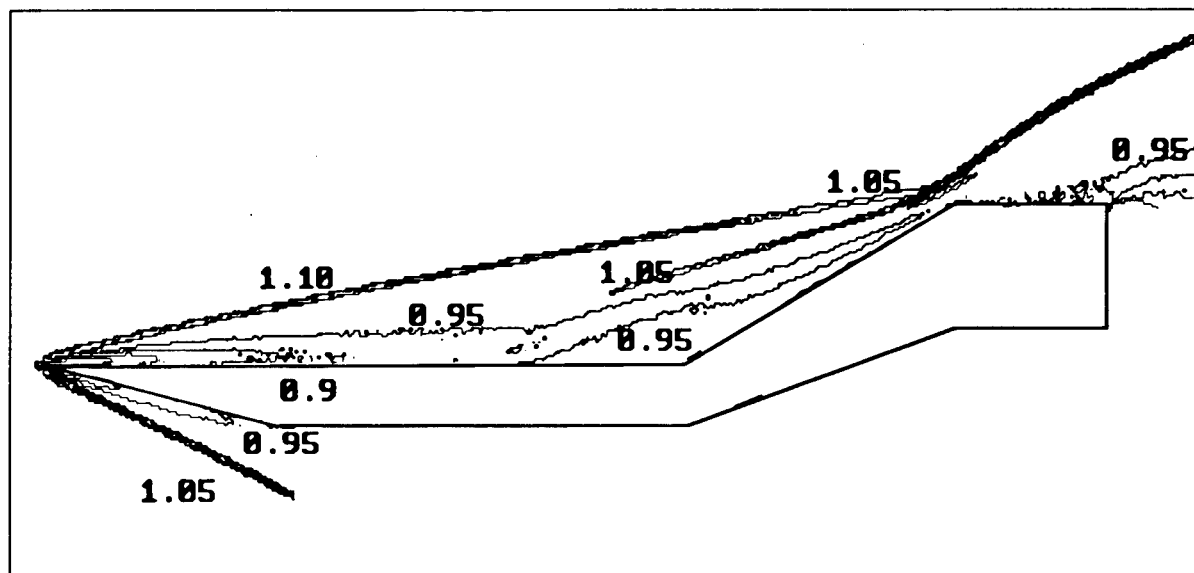


Figure 1: T_y/T flowfield (DSMC method)

and the 10-percent difference maintains till 1/3 hollow cylinder length.

Moreover, Navier-Stokes computations are planned to be conducted where the DSMC data in the vicinity of the leading edge (20-30 molecular mean free paths) will be used as inflow conditions.

laminar flow, TR RT 42/4362 AN, ONERA, Febraury 1995.

References

- [1] Ivanov M.S., Markelov G. N., Kudryavtsev A.N., Gimelshein S.F., *Numerical Investigation of Shock Wave Boundary Layer Interaction in the Near-Continuum Hypersonic Flow over Concave Bodies.*, In: ed. J.-A.Desideri et al. Computational Fluid Dynamics 96, Proc. III European Comp. Fluid Dynamics Conf., Paris, France, Wiley, 1996, pp 656-661.
- [2] Ivanov M.S, Rogasinsky S.V., *Theoretical analysis of traditional and modern schemes of the DSMC method*, Proc. XVII Int. Symp. on Rarefied Gas Dynamics, edited by A.E. Beylich, VCH, 1991, pp. 629-642.
- [3] Chanetz B., Coet M.-C., Nicout D., Pot T., *Shock wave - boundary layer interaction in hypersonic two dimensional laminar flow*, Colloque sur les Ecoulements Hypersoniques Garchy (France), 5-7 octobre 1992, ONERA, No. 1992-182.
- [4] Chanetz B., *Study of axisymmetric shock wave/boundary layer interaction in hypersonic*

Experimental Investigation and Direct Simulation of Flow in Gasdynamic Window *

V.M. Karsten, R.G. Sharafutdinov, P.A. Skovorodko, A.V. Skrynnikov
Institute of Thermophysics SB RAS, Novosibirsk, Russia

1 Introduction

By the term "gasdynamic window" we denote the gas jet technical device for obtaining the axisymmetric flow with low pressure in its near axis region. Such kind of device may be used, for example, for electron beam extraction into the region with high pressure when it is necessary to protect the electron gun from the action of this pressure.

The flow in gasdynamic window does not attract much attention in literature and present investigation may clarify some features of such kind of flow.

2 Experiment

The experiments were performed on gasdynamic low density wind tunnel of the Institute of Thermophysics SB RAS. The scheme of nozzle block is shown in Fig.1 together with the table, containing all the principal dimensions of the device (in *mm*). From 7 investigated ring-shaped nozzles the results for 3 of them will be illustrated below - for sonic nozzle 1 and for two supersonic nozzles 4, 7, differing by the expansion degree.

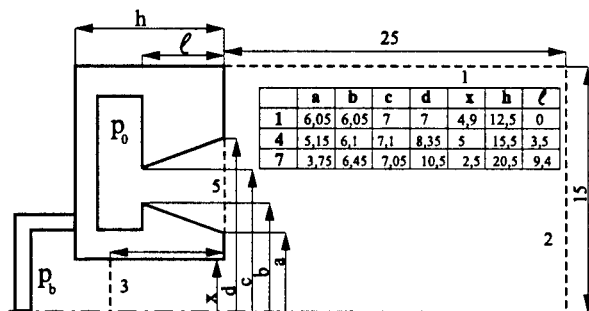


Figure 1: The scheme of nozzle block and the domain of simulation

*Abstract 5216 submitted to the 21st International Symposium on Rarefied Gas Dynamics, Marseille, France, July 26-31, 1998

In the experiments the dependence of base pressure p_b from the stagnation pressure p_0 was measured. Argon was used as working gas in all the experiments with room stagnation temperature. The pressures p_0 and p_b were measured by membrane gauges. The pressure in vacuum chamber p_h was checked by thermocouple vacuum-gauges. In all the experiments this pressure was lower than $1Pa$ and it does not affect the base pressure p_b .

3 Simulation

The flow behind the nozzle was simulated by DSMC method [1] on uniform grid without weighting factors. The domain of simulation consists of two regions of cylindrical shape. The first one is bound by the nozzle exit section and the surfaces 1 and 2, where the full absorption of incident molecules was assumed (see Fig.1) The second region is bound by solid surfaces 3 and 4.

The flow in the exit section 5 for nozzle 1 was assumed to be sonic and uniform. The distribution of parameters in this section for supersonic nozzles 4 and 7 was obtained by calculation of nozzle flowfield in the frames of reduced Navier-Stokes equations by marching procedure [2].

The computations were made for VSS molecular model for Maxwell molecules [1]. The value of $\langle \sigma v \rangle = 3.685 \cdot 10^{-10} \text{ cm}^3 \text{ c}^{-1}$ derived from the viscosity of argon at temperature $300K$ was used.

The injection of molecules into the region of computation from the surface 5 was made by assuming maxwellian distribution of molecular velocities on this surface. The solid surfaces are assumed to be diffusively reflecting.

The number of simulated molecules N in the domain on the steady stage was in the range $2.5 \cdot 10^4 - 10^5$, depending on the type of nozzle and the Knudsen number. The latter being defined by the ratio of the mean free path in the stagnation chamber to the height of nozzle exit section was in the range of $1.7 \cdot 10^{-4} - 3.5 \cdot 10^{-3}$ for $4000 > p_0 (Pa) > 1333$.

The computed values of p_b were obtained as the force per unit area of surfaces 3 and 4, the latter being estimated based on momentum that molecule brings to these surfaces at each collision. The averaging of the results of simulation was made based on $3 \cdot 10^4$ time steps at steady stage. The accuracy of data for p_b is estimated to be about 1% for nozzle 1, 5% for nozzle 4 and 10% for nozzle 7.

4 Results and Discussion

Fig.2 illustrates the streamline picture in the flow-field for nozzle 1 and $p_0 = 1815 \text{ Pa}$. The picture reveals the important features of the flow – the shock wave, formed due to the reflection of the flow from the axis, and the vortex in the entrance part of diagnostic cylinder. Similar picture takes place for supersonic nozzles 4 and 7. The structure of flow in gasdynamic window is similar, therefore, to that in the wake region of based body moving in the gas.

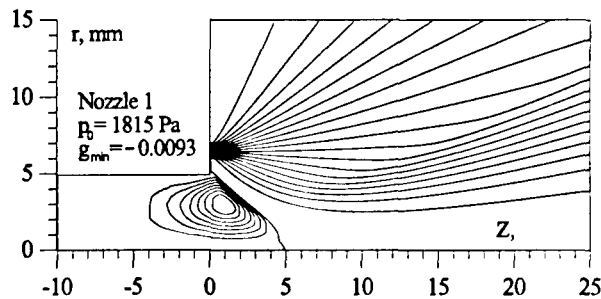


Figure 2: Streamline picture of flow in gasdynamic window

The comparison between simulated and measured results is made on Fig.3, where the dependencies of relative base pressure p_b / p_0 from p_0 are presented. The experimental results are shown by solid circles joined by solid lines. Simulated results obtained by the above described procedure are shown by open circles. The experiments reveal the important feature of this dependence – for each of tested nozzles the value of p_b / p_0 remains constant at sufficiently large p_0 . The level of this constant depends on the nozzle type – the more expansion degree of the nozzle the less the ratio p_b / p_0 . In spite of satisfactory agreement between simulated and measured results, in contrast with experiment the tendency of ratio p_b / p_0 decreasing with p_0 increasing for supersonic nozzles 4 and 7 is observed.

To clarify the reasons of the above tendency the direct simulation of flow inside the nozzle was made for nozzle 4. These computations allow one to obtain the distributions of parameters on the nozzle

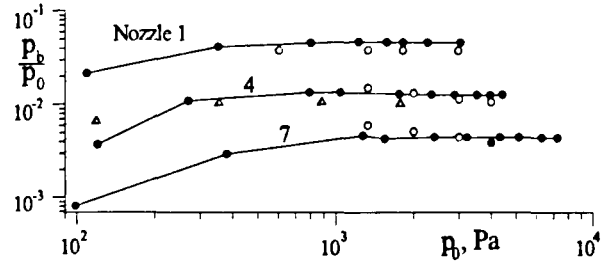


Figure 3: The dependence of base pressure from p_0 .

exit section for flow expanding into vacuum, that were used as boundary conditions for jet flow instead of distributions, obtained by Navier-Stokes equations. The corresponding results for p_b / p_0 are shown on Fig.3 by open triangles. Obviously, these results are in good qualitative and quantitative agreement with the experiment.

The main feature of nozzle exit distributions of parameters obtained by DSMC method is the absence of subsonic zones. The sonic line passes through the nozzle lip [3]. This effect can not be obtained by marching procedure since its nature is connected with upstream spreading of disturbances.

5 Conclusion

The flow in gasdynamic window may be efficiently computed by DSMC method with appropriately specified distributions of parameters on the nozzle exit section. The rearrangement of the flow near exit section results in the absence of subsonic zones for sufficiently low external pressure that leads to some similarity of jet flow to the Knudsen number.

References

- [1] Bird G.A., *Molecular Gas Dynamics and Direct Simulation of Gas Flows*, Oxford, Clarendon, 1994.
- [2] Skovorodko P.A., *Nonequilibrium Flow of Gas Mixture in Supersonic Nozzle and in Free Jet behind It*, Rarefied Gas Dynamics, Proc. 20th Intern. Symp., Ching Chen Ed., Peking University Press, Beijing, China, 1997, pp. 579-584.
- [3] Bird G.A., *The Nozzle Lip Problem*, Rarefied Gas Dynamics, Proc. 9th Intern. Symp., M. Becker, M. Fiebig, Eds., DFVLR - Press, Göttingen, Germany, 1974, Vol. 1, pp. A22-1 - A22-8.

Simulation Models for Rarefied Flow Past a Sphere in a Pipe *

F. Liu¹, N. Gatsonis², A. Beskok³, G.E. Karniadakis¹¹ Brown University, ² WPI, ³ MIT

The investigation of rarefied gases by measuring the gaseous drag of rotating devices is dated back to Maxwell about 120 years ago. The spinning rotor gauge (SRG) is one such instrument which is free of mechanical friction since its rotor is suspended magnetically. In recent years, great progress has been made in employing SRG in laboratory and industrial work and extensive research work has been done by Fremery [1], and more recently by S. Tison and his group at the National Institute for Standards (NIST).

In the current work, we perform numerical simulations for an idealized case of a stationary sphere in a pipe. The Reynolds number is very low and we cover the entire Knudsen number regime from continuum to free-molecular flux. In particular, we start with the continuum regime (Knudsen number below 10^{-3}) and consider as model problem the Stokes flow in a pipe. The objective here is to determine the influence of the walls, i.e. the blockage effect, for different aspect ratios, H/D , where H, D are the diameters of pipe and sphere, respectively. To this end, we employed our spectral element code **NEKTAR** and computed systematically the drag coefficient. It was found that there exists a strong influence of the aspect ratio, especially for values of H/D lower than 5, where the drag coefficient becomes at least three times larger than the corresponding drag coefficient in an unbounded domain. For flows at Reynolds number greater than 1 this effect is much less important.

In the slip flow regime we have developed the compressible code μ **Flow** with partial slip at the walls based on a high-order boundary condition we have developed [2]. We have performed several simulations for Knudsen number in the range $10^{-3} \leq Kn \leq 0.5$. Finally, in the transitional and free-molecular regime we employed the DSMC code **F3** of Bird, which is capable of handling arbitrary complex geometry.

The overall objective of this study is to investigate

the different flow patterns and the corresponding effect blockage, and to provide a set of reference data of drag coefficients C_d in a broad Knudsen number range for further SRG applications.

The main conclusions of this study are:

- C_d of the sphere is inversely proportional to Kn, Re and H/D in the sphere-pipe case.
- In the rarefied gas flow, for the sphere-only case, the drag is proportional to Speed ratio (S) and C_d is proportional to $1/S$.
- In the rarefied gas flow, for the sphere-pipe case with fixed Kn and H/D , the drag is proportional to Speed ratio.
- In the high Knudsen number regime (beyond transition) the blockage effect is negligible even for small values of H/D .

In the paper, we will describe in some detail the three different simulation approaches and we will compare results in overlapping regions. For example, by comparing **NEKTAR** and μ **Flow** we identify the role of incompressibility versus rarefaction in the slip flow regime, and by comparing μ **Flow** with **F3** we can validate the new slip boundary condition we have developed for the slip flow regime.

References

- [1] Fremery J.K., *The spinning rotor gauge*, J. Vac. Sci. Technol. A, Vol. 3(3), p. 1715, 1985.
- [2] Beskok A., Karniadakis G.E, Trimmer W., *Rarefaction and compressibility effects in gas micro-flows*, J. Fluids Engin., Vol. 118, p. 448, 1996.

* Abstract 6021 submitted to the 21st International Symposium on Rarefied Gas Dynamics, Marseille, France, July 26-31, 1998

On the Use of Combined Similarity Parameters for Transitional Rarefied Flow Analyzes *

E.R. Abramovsky¹, M.G. Abramovskaja², V.P. Bass²

¹ Dniepropetrovsk State University, Dniepropetrovsk, Ukraine

² Institute of Technical Mechanics of Ukrainian National Academy of Science,
Dniepropetrovsk, Ukraine

The new, combined similarity parameters, reflecting both the transitional flow conditions and overall body shape influence are suggested in this paper. It was shown, that with the aid of these parameters an improvement in generality and accuracy may be gained.

The approximate, engineering technique based on laboratory experiments and (or) flight tests data, still remain one of the most widely used means of transitional flow analyses. Such semiempirical solutions may be divided in three major groups. The first group is based on so-called "local interaction" principle. In this case local pressure P_n and shear stress P_τ on the body surface are usually expressed in the form of polynoms with respect to local angle of attack. The coefficients of these polynoms, being written in conventional form, do not depend on body shape and are the functions of flow parameters only. They are determined on the basis of experimental data.

In the second group of solutions overall body aerodynamic characteristics, like normalized drag coefficient $\overline{C_D} = (C_D - C_D^C)/(C_D^M - C_D^C)$, are presented as functions of rarefaction parameters. The so-called bridging relations of this type have to fit the correlated experimental data and match the computed extreme points, corresponding to free - molecular value C_D^M and continuum value C_D^C .

The third group is actually the combination of the previous two ones. The sense of it is to determine local quantities P_n and P_τ by using the relations for overall body coefficients, obtained from experimental data.

The various similarity parameters, which determine the degree of rarefaction and other flow conditions, are usually used in these solutions: Knud-

sen Number $Kn = \lambda/L \sim M/Re$, Reynolds Number $Re = \rho UL/\mu$, viscous interaction parameter $V = M/\sqrt{Re}$, Mach Number M and others. Here λ is mean free path, L - reference length, ρ - density, U - flow velocity, μ - dynamic viscosity coefficient.

The great number of semiempirical correlational expressions, which were suggested up to now contain one of those parameters. Unfortunately, each of them is actually valid only for limited types of body configurations.

It was shown later, that the use of combined similarity parameters, which reflect several different factors, like flow condition, overall body shape, flow - surface interaction and so on, might substantially widen the variety of considered bodies. One of such parameters was introduced by P. Gorenbuch [1]: $\Delta = Re_0 \sin \alpha_m$, where $Re_0 = \rho_\infty U_\infty L/\mu_0$. Subscripts " ∞ " and " 0 " denote free stream and stagnation conditions respectively. The reference length L is the mean integral dimension of body cross-section, α_m is the mean integral value of local angle of attack. The use of this parameter in correlational expression for $\overline{C_D}$ as a function of Δ , demonstrates reasonable accuracy for various bodies. It should be noted, however, that determination of L and α_m for complex configurations involves the complicated procedure.

The new combined rarefaction parameters, suggested in this paper, may help to avoid such inconveniences on one hand and to take into account some additional factors on other hand. First of all the new overall body shape parameters are introduced in the form

$$\epsilon = C_D^C/C_{pS}; \nu = C_{Dp}^M/(C_{Dp}^M + C_{DF}^M), \quad (1)$$

where C_{pS} is pressure coefficient behind the normal shock. Aerodynamic characteristics C_{Dp}^M and C_{DF}^M are pressure and friction components of free - molecular drag coefficient C_D^M . The reference area

*Abstract 2282 submitted to the 21st International Symposium on Rarefied Gas Dynamics, Marseille, France, July 26-31, 1998

for C_{DF}^M and C_{DP}^M in (1) should be the same. In transitional flow analysis the extreme values of aerodynamic coefficients C_D^C and C_D^M , are usually known in advance. From this point of view the shape parameters ε and ν may be easily obtained and quite simply interpreted. Considering, for example, the sharp cone with semiangle ϑ we will have (in the framework of Newtonian impact theory)

$$C_D^C = C_{pS} \sin^2 \vartheta; \varepsilon = \sin^2 \vartheta \quad (2)$$

In the hypersonic free-molecular flow with diffuse reflection from cold wall ($T_w/T_0 \rightarrow 0$) we obtain

$$C_{DP}^M = 2 \sin^2 \vartheta; C_{DF}^M = 2 \cos^2 \vartheta; \nu = \sin^2 \vartheta \quad (3)$$

Geometrical interpretations of ε and ν are obvious. In general case parameter ν contains more information and should be used, when this information is important.

On the basis of relations (2) and (3) equivalent body method [2] has been developed and used for transitional flow analysis.

The new combined similarity parameters are suggested in the form

$$\overline{Re} = Re_0 \varepsilon; Re' = Re_0 \nu \quad (4)$$

$$\overline{K} = (Re_{1\infty}/M_\infty) \nu + (\sqrt{Re_{2\infty}/M_\infty})(1 - \nu) \quad (5)$$

The first term of (5) reflects the similarity of bluff bodies with small finess ratio ($\nu \rightarrow 1$) and second one - the similarity of long slender bodies ($\nu \rightarrow 0$). The rational selection of reference length L plays also very important role in presentation of similarity parameters. In expressions (4) L is the length of equivalent body contour. For the axisymmetrical and semi-axisymmetrical bodies the equivalent body will be sharp cone with semiangle ϑ , obtained from (2) or (3).

The reference length in Re_1 is chosen to be either D_B or $\sqrt{S_+}$, where D_B is body base diameter and S_+ is the area of body frontal projection. For Re_2 it will be the body length L_B . When free stream parameters Kn_∞ and Re_∞ are used the combined formula for reference length L_C may be recommended

$$L_C = D_B \nu + L_B (1 - \nu) \quad (6)$$

Several correlational expressions were obtained with the use of combined similarity parameters. One of them has a form [2]

$$\overline{C_D} = -Au^2 + 2(A+1)u^{1.5} - (A+1)u^{1.25} \quad (7)$$

where $u = [1 + \exp(\lg \overline{Re})]^{-1}$ and $A = 10$. Reference area in calculation of C_D is chosen to be S_+ .

The validity of such expression was proven by means of comparison with experimental data for the wide variety of bodies like sharp cones with 5, 10, 15, 90 (flat disc), sphere, circular cylinder and other configurations.

The local characteristics of the flow P_n and P_t might be obtained from the expression for overall body coefficients with the use of special technique. In this case P_n and P_t become the function of combined parameters. The known local values of P_n and P_t makes it possible to obtain other aerodynamic characteristics like lift and pitching moment coefficients.

The calculational results analyzes show that application of combined parameters may provide the higher level of accuracy.

References

- [1] Gorenbuch P.I., *Correlational Expression for the Bodies Drag Coefficients in Hupersonic Rarefied Flow*, Uchenije Zapisky TSAGI, 1986, v. N 2 (In Russian)
- [2] Abramovsky E.R., *On the Application of Equivalent Cone and Wedge Method to Rarefied Flow Aerodynamics*, Hydroaeromechanika i Teorija Uprugosti, Dniepropetrovsk University Press, Dniepropetrovsk, Ukraine, 1989. (In Russian).
- [3] Abramovskaja M.G., Bass V.P., *Aerodynamic Characteristics of Axisymmetric Cones in Transitional Gas*, Uchenije Zapiski TSAGI, 1980 v, XI, N 1 (In Russian).

RAREFIED FLOWS - RF 4

ROOM MARION

FRIDAY, JULY 31, 1998

9:15

Experimental Investigation of Fully Expanding Free Jets and Plumes *

G. Dettleff, K. Plähn

Deutsches Zentrum für Luft- und Raumfahrt (DLR), Göttingen, Germany

At the DLR-research centre in Göttingen the new vacuum facility STG has been installed which allows the undisturbed expansion of plumes into the rarefied flow regime. Its main feature is a liquid helium (*LHe*-) driven cryopump (temperature 4.3 K) with an area of about 30 m^2 which encloses completely the cylindrical expansion room with a length of about 5 m and a diameter of about 1.6 m.

The effect of cryopumping is that the gas after the expansion directly impinges on the cold surface and freezes immediately in the solid state. In conventional vacuum chambers with mechanical pumps the gas after the expansion remains in the chamber for a certain time before it is pumped and thus forms the residual background gas with a pressure typically $> 10^{-2}\text{ mbar}$. Due to this residual gas the undisturbed expansion of the plume terminates usually within the continuum regime, indicated by a compression shock system (barrel shock). Such a shock system does not exist in the new DLR-high vacuum test facility STG (in German: Simulationsanlage für Treibstrahlen Göttingen). The plume gas expands undisturbed into the rarefied regime.

The investigation of plumes emanating from supersonic nozzles is of interest because of the plume impingement problem encountered in space technology. In addition during the acceptance tests of the facility free jets emanating from sonic orifices have been investigated.

To compare these two kinds of expansions equal sonic conditions ($d^* = 0.6\text{ mm}$) and equal stagnation conditions (N_2 : $p_0 = 0.5/2.0\text{ bar}$, H_2 : $p_0 = 0.95\text{ bar}$, both gases $T_0 = 300\text{ K}$) were used.

The main goals of these first investigations were to produce a fully expanding flow in STG, to compare free jet and plume expansion, to compare the influence of different gases (N_2 and H_2 , but both

$\kappa = 1.4$) and to check the validity of analytic expressions to describe such a flowfield ([1],[2]).

In the first experiments priority was given to the determination of the molecular number flux

$$\dot{n}_1 = n u$$

$$\begin{aligned} \text{with } n &: \text{ number density } \left[\frac{1}{\text{m}^3} \right] \\ u &: \text{ flow velocity } \left[\frac{\text{m}}{\text{s}} \right] \end{aligned}$$

since this flow quantity (or the corresponding mass flux) and its distribution in the plume is most important for the determination of impingement effects.

The measurements were performed with a free molecular pressure probe (fig. 1) in the far field region where the Knudsen number is

$$Kn = \frac{\lambda}{l_{ref}} > 10$$

$$\begin{aligned} \text{with } \lambda &: \text{ mean free path of the gas molecules } [\text{m}] \\ l_{ref} &: \text{ reference length } [\text{m}]. \end{aligned}$$

As reference length l_{ref} we have chosen the diameter of the probe tube. Inside the cylindrical converter an ionization gauge is installed. The gas enters the tube, mounted below the converter, through a slot. After a few seconds a constant pressure p_c is obtained so that the number flux \dot{n}_1 could be calculated from the transmission probabilities at the slot and the measured data p_c , T_c and T_s .

With this probe number flux profiles have been measured along the free jet axis, some other interesting streamlines (fig. 2, radial profiles $\dot{n} = \dot{n}_1(r)$) and transverse to the flow, keeping the distance r to the orifice or nozzle fixed (fig. 3, angular profiles $\dot{n} = \dot{n}_1(\theta)$). The radial profiles in fig. 2 show on the one hand that we have reached rarefied flow conditions and on the other hand that the source flow assumption $\rho \sim \frac{1}{r^2}$ used in many model calculations holds.

* Abstract 1666 submitted to the 21st International Symposium on Rarefied Gas Dynamics, Marseille, France, July 26-31, 1998

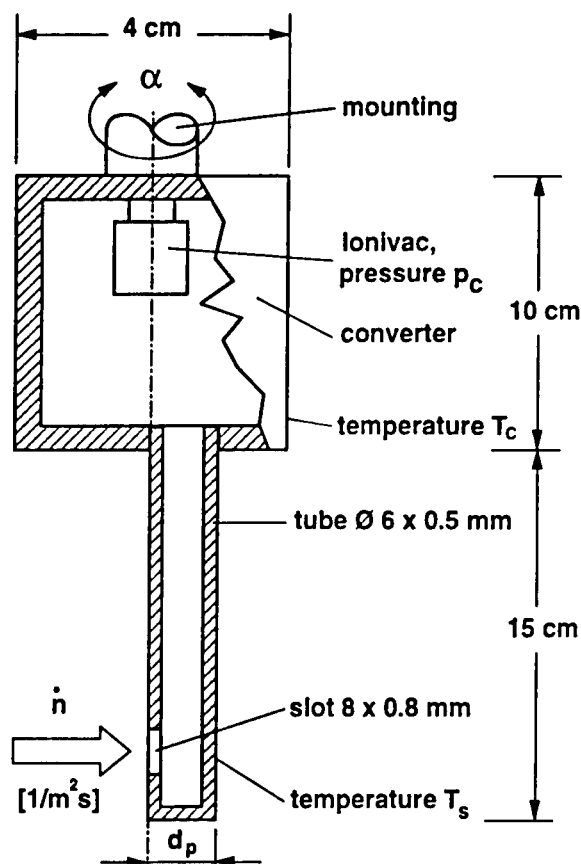


Figure 1: Free molecule pressure probe

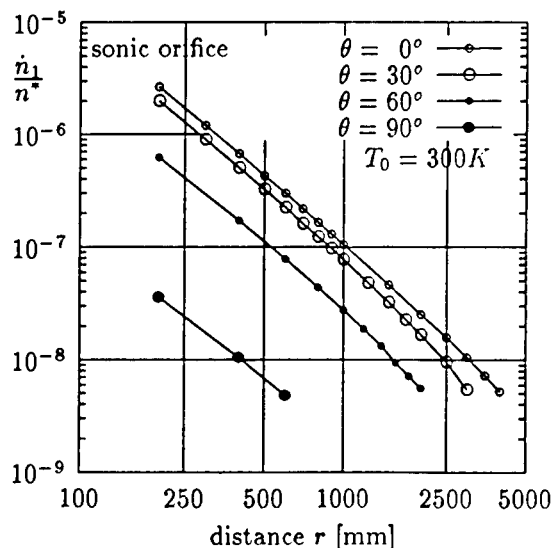


Figure 2: Radial profiles of a free jet with N_2

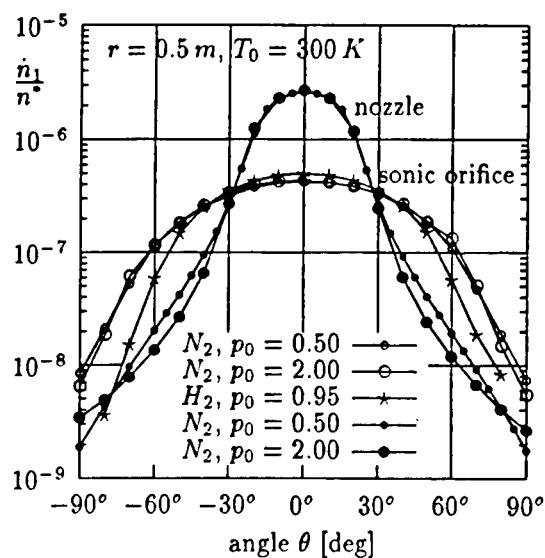


Figure 3: Angular profiles of a free jet and a plume emanating from conical nozzle (15° half angle)

The comparison of the free jet profiles in fig. 3 shows the independence of the stagnation pressure p_0 and the dependence on the gas species. The comparison of the plumes in this figure shows a dependence on the increase of the nozzle exit Reynolds number adjusted by the stagnation pressure p_0 , due to the decrease of the boundary layer thickness.

References

- [1] Simons, G.A.: *Effect of the nozzle boundary layers on rocket exhaust plumes*
AIAA J., 10 (11), 1534-1535, 1972
- [2] Legge, H.; Boettcher, R.D.: *Modelling control thruster plume flow and impingement*
Proceedings of the 13th International Symposium on Rarefied Gas Dynamics, Novosibirsk 1982, Vol. 2, p. 983-992; Plenum Press, New York, 1985

Rayleigh and Raman Scattering used for Compressible Flow Diagnostics *

R.A.L. Tolboom, N.M. Sijtsma, N.J. Dam, and J.J. ter Meulen
Applied Physics, University of Nijmegen, the Netherlands

Quantitative information on the local density, velocity, temperature, and pressure distributions in a flow field can be obtained in many ways. Laser based techniques such as Laser Induced Fluorescence (LIF), Raman scattering, and Rayleigh scattering [1, 2] use the intrinsic property of energy quantisation in molecules. Therefore, it is the molecules that make up the flow that serve as a probe rather than added (macroscopic) seeding particles. Furthermore, it is possible to get a good spatial as well as temporal resolution (snapshots on nanosecond time-scale) and obtain molecule-specific information (LIF & Raman scattering).

In our experiments, we employed both Rayleigh and Raman scattering to obtain 2D-images of the density distributions of compressible flows. Part of the flow was illuminated with a collimated laser sheet ($25 \times 0.1 \text{ mm}^2$) that was produced by a pulsed ArF excimer laser (rep. rate = 10 Hz; $E = 100 \text{ mJ/pulse}$; $\lambda = 193 \text{ nm}$). Subsequently, images were recorded by detecting the scattered light with an intensified CCD-camera (figure 1). As each pixel value in the image is proportional to the intensity of the locally scattered light, this value is a measure for the *local* density.

Thus, we studied underexpanded free jet flows emanating from two different nozzles. First, we investigated the density distribution of a continuous, dry air, supersonic nozzle flow into ambient air. The nozzle used consists of an inlet followed by a settling chamber ($\varnothing 35 \text{ mm}$) smoothly contracting to a cylindrical exit tube ($\varnothing 5.0 \times 60 \text{ mm}^2$). Figure 2(a) shows typical results of the Rayleigh scattering measurements [2] for flows produced at various stagnation pressures (p_s ; measured in the settling chamber by a Pitot tube). In these measurements, the back pressure (p_b) was 1 bar. The results presented are 25 laser shot averages. In addition, we performed single shot measurements, in

which instationary behaviour of the flow was revealed (computer screen in figure 1). At low stagnation pressures (i.e. $p_s < 2.5 \text{ bar}$), the flow was subsonic. However, for increasing p_s , the jet became supersonic, and the occurrence of both expansion waves and shock waves resulted in a so-called 'diamond pattern' with sharply separated alternating density minima and maxima. For $p_s \gtrsim 4 \text{ bar}$, a Mach disk started to grow. The Rayleigh results will be compared (both qualitatively and quantitatively) to Schlieren measurements, Euler calculations as well as interferometric tomography measurements [3].

Raman scattering measurements in flows under similar conditions show comparable density distributions for the various species present (e.g. O_2 , N_2). Additionally, we will use this technique to analyse the large lobes, occurring at high p_s , to check the hypothesis that these lobes are caused by Mie scattering on condensed water vapour.

Figure 2(b) presents some data on our second application: a propane jet that was produced by a pulsed valve (rep. rate = 10 Hz). The valve outlet consisted of a cylindrical tube ($\varnothing 0.50 \times 9.0 \text{ mm}^2$), and the whole assembly was situated in a vacuum chamber. With varying back pressures in this chamber, different flow profiles resulted. For $p_b \lesssim 10 \text{ Torr}$, the flow became supersonic, and a Mach disk appeared. Additionally, a maximum started to grow upstream from this Mach disk. The density in this maximum decays as z^{-2} (where z is the distance from the nozzle exit), which is typical for molecular beams.

As this valve is pulsed, we followed the evolution of the flow with time-resolved measurements by increasing the delay between the laser pulse and the gas pulse in intervals of $1 \mu\text{s}$. We observed that the growth of the flow takes approximately $10 \mu\text{s}$, depending not only on p_b , but also on parameters like p_s and the electric current needed to open the valve. Also the duration of the gas pulse largely depended upon these parameters. Besides these qualitative data, we quantitatively checked both the scaling law for the position of the Mach disk as a function of

*Abstract 2156 submitted to the 21st International Symposium on Rarefied Gas Dynamics, Marseille, France, July 26-31, 1998

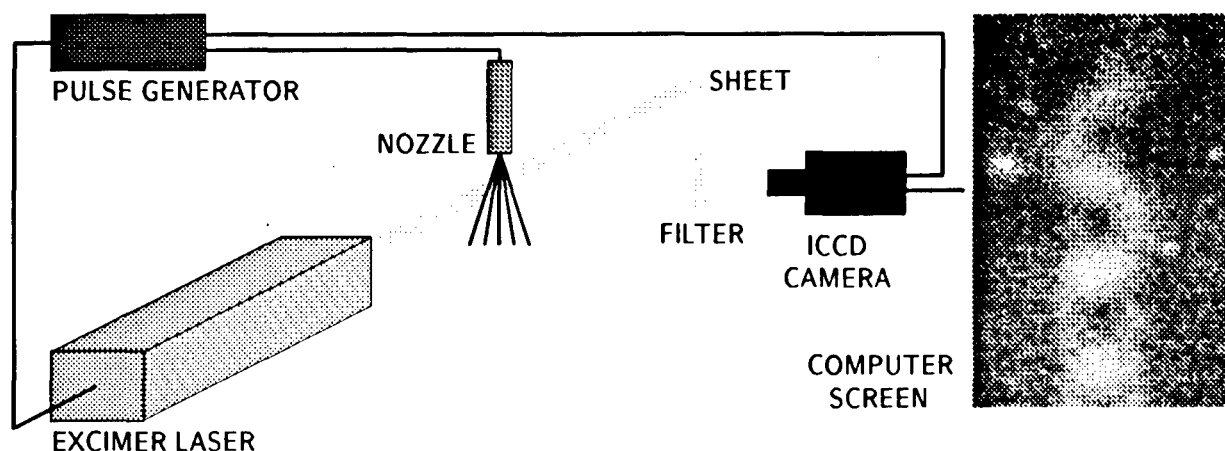


Figure 1: Experimental setup. The filter indicated in the figure is needed only for the Raman scattering measurements. The computer screen shows an example of a single shot Rayleigh image of the same flow as can be found in figure 2(a) at $p_s = 3.0$ bar.

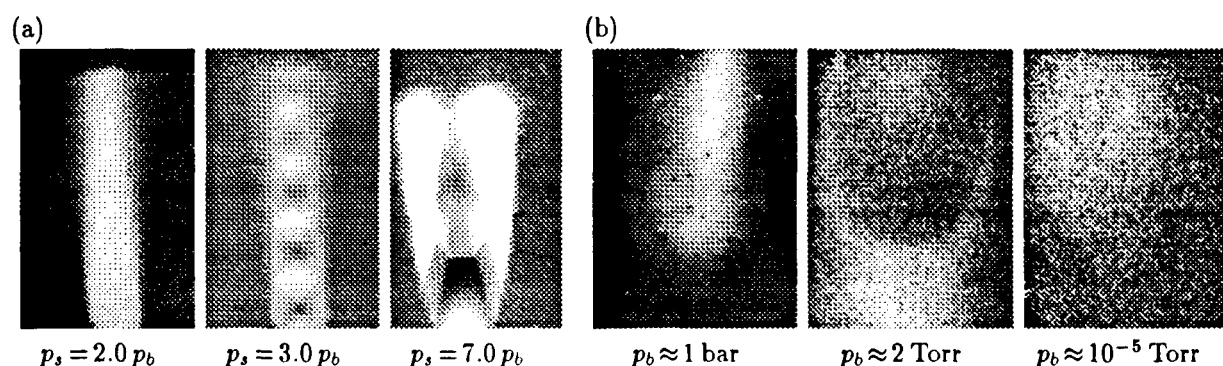


Figure 2: Rayleigh images of the density distributions of (a) a continuous dry air flow for different stagnation pressures (flow directed upward; $p_b = 1$ bar; image size $\approx 25 \times 15 \text{ mm}^2$); and (b) a pulsed propane flow for different back pressures (flow directed downward; $p_s = 5$ bar; image size $\approx 4.5 \times 3.0 \text{ mm}^2$).

p_s and p_b and the scaling law for the density on the axis of the flow mentioned above. Furthermore, we have planned to visualise the phase-separation of the species in a mixed gas molecular beam using Raman scattering measurements.

In conclusion, these applications demonstrate that laser sheet methods are very useful for the quantitative visualisation of continuous as well as pulsed compressible flows, with high spatial and temporal resolution.

References

- [1] Eckbreth A.C., *Laser Diagnostics for Combustion Temperature and Species*, volume 7 of *Energy and Engineering Science Series*, Abacus Press, Mass (USA), 1988. A.K. Gupta and D.G. Lilley (eds).
- [2] Dam N., Rodenburg M., Tolboom R.A.L., Stoffels G.G.M., Huisman-Kleinherenbrink P.M., and ter Meulen J.J., *Imaging of an Underexpanded Nozzle Flow by UV Laser Rayleigh Scattering*, Exp. in Fluids, accepted, 1997.
- [3] Timmerman B.H., *Holographic Interferometric Tomography for Unsteady Compressible Flows*. PhD thesis, Delft University of Technology, Delft (NL), 1997.

Macroscopic Fluctuations in Low Knudsen Number Hypersonic Flow Around a Cylinder *

S. K. Stefanov¹, C.-P. Cai², I. D. Boyd²

¹ Institute of Mechanics, Bulgarian Academy of Sciences, Sofia, Bulgaria

² Sibley School of Mechanical and Aerospace Engineering, Cornell University, Ithaca, New York, USA

1 Introduction

The hypersonic flow around a circular cylinder is a classic gas dynamic problem studied widely by many authors. From kinetic theory view-point it has also been investigated extensively for relatively moderate Knudsen and Mach numbers ($0.01 < Kn < 0.1, 1 < Ma < 20$) by using different numerical techniques. In our report we will present DSMC results for considerably lower Knudsen number $Kn = 0.002$ and higher Mach number $Ma = 26.0$. The choice of these parameters is connected with the attempt to calculate directly the macroscopic velocity fluctuations using the mean macroscopic characteristic fields. In this case, the magnitude of the macroscopic velocity fluctuations may be considered as an important indicator of the eventual existence of a turbulent regime in a fully developed, steady-state, low Knudsen number flow. Let us advance an argument: from the estimation [1] of the ratio between the mean free path ℓ and the Kolmogorov dissipative scale of turbulence ℓ_D

$$\ell/\ell_D \sim (Ma)^{3/4}(Kn)^{1/4} = 2.4349 \quad (1)$$

one can see that ℓ and ℓ_D are of the same order and it seems the instabilities and the arising turbulent eddies in the flow should not be suppressed. Consequently, the macroscopic fluctuations should accumulate the turbulent oscillations and are expected to be larger than the numerical fluctuations arising due to the finite number of particles used in the DSMC calculations (the correct reproduction of physical macroscopic fluctuations in particle simulation has been pointed out for the first time in the work of Mansour et al.[2]). In the present work a simple estimation of the numerical fluctuations proposed by Stefanov and Cercignani [3] is used in order

to separate these from the physical macroscopic fluctuations.

2 Flow Simulation

The two-dimensional hypersonic steady-state flow of a hard sphere simple gas is calculated using the DSMC program system MONACO[4]. A finite element adaptive grid with a total number of more than 200000 cells covers the rectangular computational domain. The grid is adapted to the computed local mean free paths. The gas flow is argon with conditions at infinity: $n_\infty = 1 \times 10^{20} m^{-3}$, $T_\infty = 295 K$, $U_\infty = 8500 m/s$. The case of a cold cylinder ($T_c = T_\infty$) with full energy accommodation is assumed. After some numerical experiments a computational domain $(20 \times 8)m$ and a cylinder radius $R_c = 2.5m$ have been chosen so that $Kn \approx 0.002$. The simulation reaches the steady state after 50,000 – 70,000 variable time steps with a final $\Delta t \sim 1 \times 10^{-8} s$. The simulation of a steady-state flow containing about 1×10^7 particles is running another 20,000 steps in batch mode on 24 SP-2 processors to obtain smooth macroscopic results.

3 Macroscopic Velocity Fluctuations

The DSMC method is naturally suited for investigation of macroscopic fluctuations. Here we restrict ourselves by the study of a steady-state flow because the unsteady-state analysis is extremely complicated even for DSMC and we are still not ready to carry it out. If $\mathbf{v} = \{u, v\}$ and $\mathbf{V} = \{U, V\}$ are the instant and average velocity vectors in a given cell of the 2D-computational grid then the time averaged components of macroscopic velocity fluctuations can be defined as follows

$$\overline{u^2} = \overline{u'u'} = \langle (u - U)(u - U) \rangle_t$$

*Abstract 2368 submitted to the 21st International Symposium on Rarefied Gas Dynamics, Marseille, France, July 26-31, 1998

$$\begin{aligned}\overline{v^2} &= \overline{v'v'} = \langle (v - V)(v - V) \rangle_t \\ \overline{u'v'} &= \langle (u - U)(v - V) \rangle_t\end{aligned}$$

Multiplied by density ρ equations 2 give the well-known Reynolds stresses. The instant velocity in given cell is computed simply as the mean velocity of all particles in that cell within the given step. Computed in this way, fluctuations contain not only the physical macroscopic fluctuations. The particle finite number contribution is also included and should be found explicitly. If one supposes that the velocity distribution is close to a Maxwellian function then the numerical fluctuation contribution can be estimated as follows [2]:

$$\sigma^2 = \frac{RT}{\bar{N}}, \quad (3)$$

where T is the average temperature in given cell, R is specific gas-constant, \bar{N} is average number of particles in the same cell. Dividing Eq. 2 by σ^2 one can obtain useful and very informative non-dimensional estimators of macroscopic velocity fluctuations

$$\sqrt{u^2/\sigma^2}, \sqrt{v^2/\sigma^2}, \sqrt{u'v'/\sigma^2}. \quad (4)$$

4 Results

In figures 1 and 2 are shown number density field and macroscopic fluctuations $\overline{v^2}$ respectively. The figures illustrate some preliminary results, obtained by running the simulation with a total number of 3,000,000 particles on six SP-2 processors for the pointed out flow-conditions. Let us concentrate on the following two details of the wake flow (Fig. 1) one can clearly see the separation point which indicates the existence of reversed flow in a single vortex form; and the secondary shock wave in the wake flow under these conditions.

Figure 2 shows span wise macroscopic velocity fluctuations $\overline{u^2}$. The largest fluctuations are contained within the shock wave front and the wake flow. We plan to improve these results and show more details in the final report.

References

- [1] Cercignani C. and Stefanov S., *Vortices and Turbulence in Hypersonic Rarefied Flows* J. Harvey and G. Lord eds., Oxford Science Publications, Oxford, UK, Vol. 2, pp. 1147-1153, 1995.
- [2] Malek Mansour M., Garcia A., Lie G. and Clementi E., *Fluctuating Hydrodynamics in a*

Dilute Gas, Phys. Rev. Lett., Vol. 58, No. 9, pp. 874-877, 1987.

- [3] Stefanov S. and Cercignani C., *Monte Carlo Simulation of the Propagation of a Disturbance in the Channel Flow of a Rarefied Gas*, Special issue "Simulation methods in Kinetic Theory" J. Computers and Mathematics with Applications, 1997 (in print).
- [4] Dietrich S. and Boyd I., *Scalar and Parallel Optimized Implementation of the Direct Simulation Monte Carlo Method*, J. Comp. Phys., Vol. 126, pp. 328-342, 1996.

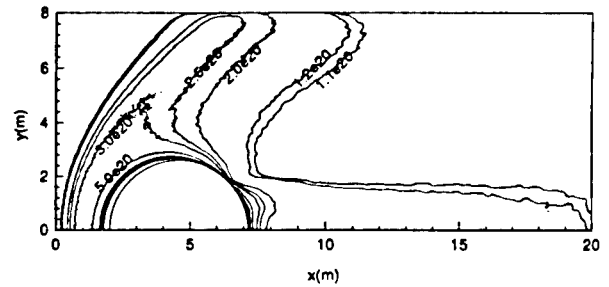


Figure 1: Contours of number density.

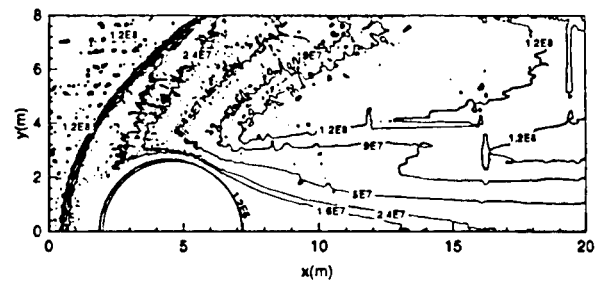


Figure 2: Contours of fluctuations in x-velocity.

Vorticity and Shock Wave in a Compressible Turbulent Flow of Molecular Kinetic Gas Model *

A. Sakurai¹, F. Takayama²

¹ Tokyo Denki University, Hatoyama, Saitama 350 Japan

² Iwaki Meisei University, Iwaki, Fukushima 970 Japan

1 Introduction

We are concerned here with the kinetic molecular model approach to the problem of turbulence oriented computation of compressible flow in particular attention to the phenomenon of production and dissipation of vorticity and shock wave in the flow field. We consider for this the Taylor-Green type initial value problem [1] with use of the Boltzmann equation in its integral form [2] which is reduced for small time step Δt as

$$f(\mathbf{c}, \mathbf{x} + \mathbf{c}\Delta t, t + \Delta t) - f(\mathbf{c}, \mathbf{x}, t) = \Delta t \frac{\partial_e f}{\partial t},$$

where $f = f(\mathbf{c}, \mathbf{x}, t)$ is the molecular velocity distribution function with the molecular velocity \mathbf{c} and the spacial coordinate \mathbf{x} and $\frac{\partial_e f}{\partial t}$ denotes the rate of change in molecular particle number owing to their encounters. In practice, we utilize BGK and DBE (Discrete Boltzmann Equation) model [3] for the term $\partial_e f / \partial t$.

2 Taylor-Green type problem

Consider here Taylor-Green type initial value problem which is periodic to a square region for 2-D case and a cube region for 3-D case started from initial conditions at the time $t = 0$ postulated as local Maxwellians with their flow velocity \mathbf{u} , density ρ and temperature T given for $\mathbf{x} = (x, y, z)$, respectively as;

$$\begin{aligned} \mathbf{u} &= (A \sin 2\pi x \cos 2\pi y, B \cos 2\pi x \sin 2\pi y), \\ \rho &= 1 + C \sin 2\pi x \cos 2\pi y, \\ T &= 1 + D \cos 2\pi x \sin 2\pi y, \end{aligned} \quad (1)$$

for 2-D case, and

$$\mathbf{u} = (E \cos 2\pi x \sin 2\pi y \sin 2\pi z,$$

$$F \sin 2\pi x \cos 2\pi y \sin 2\pi z,$$

$$G \sin 2\pi x \sin 2\pi y \cos 2\pi z),$$

$$\rho = 1 + H \sin 2\pi x \sin 2\pi y \sin 2\pi z,$$

$$T = 1 + I \cos 2\pi x \cos 2\pi y \cos 2\pi z \quad (2)$$

for 3-D case. Here all quantities are dimensionless based on the length of the square or the cube, the initial uniform density and temperature.

3 Results

Some of the results of numerical computation are shown in figures: Fig.1 shows the pressure contours at a certain time t , where (a) is for the 2-D case of (1) with $A=0.5$, $B=-0.4$, $C=D=0.1$, the initial Knudsen number $K_n=0.01$, and (b) is for the 3-D case of (2) at $z=0.5$ with $E=0.5$, $F=G=-0.2$, $H=I=0.01$, $K_n=0.1$. Figs.2 (a),(b) show the energy spectra $E(k)$ to the wave number k for the corresponding cases above, where we show for comparison the lines with slope -3 and -5/3 respectively for 2-D(a) and 3-D(b) cases.

References

- [1] Taylor, G. I. and Green A. E., Proc. of Royal Soc. London A, 158, (1937), p.499.
- [2] Chapman, S and Cowling, T. G., The Mathematical theory of Non-Uniform Gases, Cambridge Univ. Press, (1970), p.46.
- [3] Oguchi, H., Morinishi K., and Satofuka N., Proc. RGD-13, 1, (1985), p.293.
- [4] Sakurai, A. and Takayama F., Proc. RGD-20(Bijing), (1997), p.291; Fluid Dynamic Research (Elsevier), 21, (1997), p.211.

* Abstract 4561 submitted to the 21st International Symposium on Rarefied Gas Dynamics, Marseille, France, July 26-31, 1998

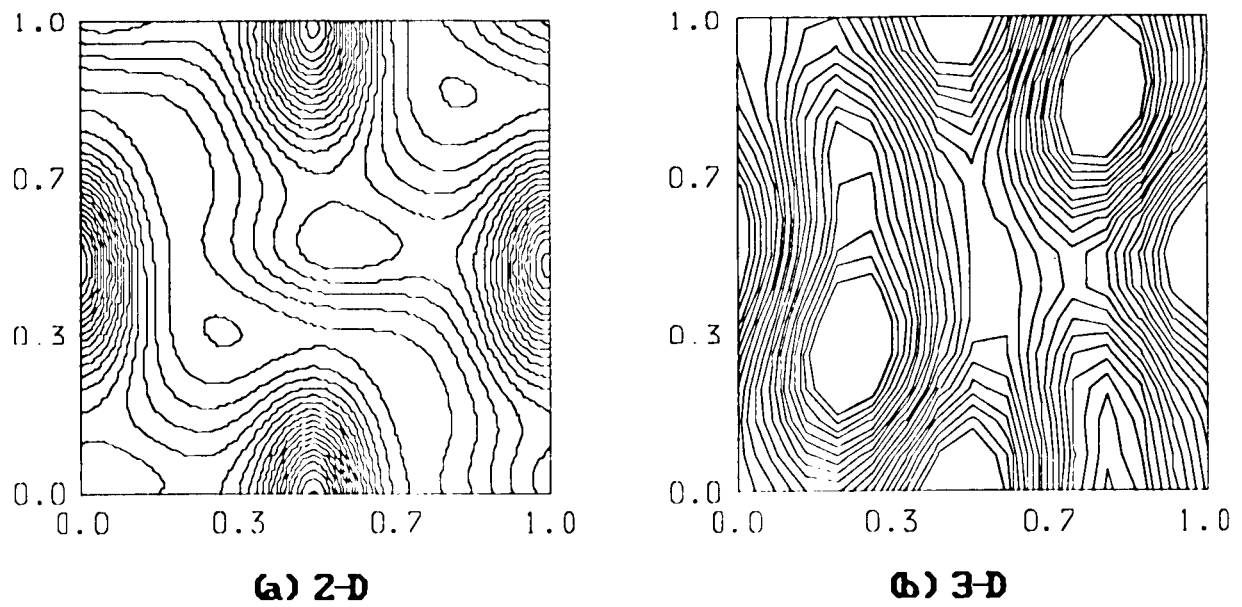


Figure 1: Pressure contours (a) 2-D, (b) 3-D at $z = 0.5$

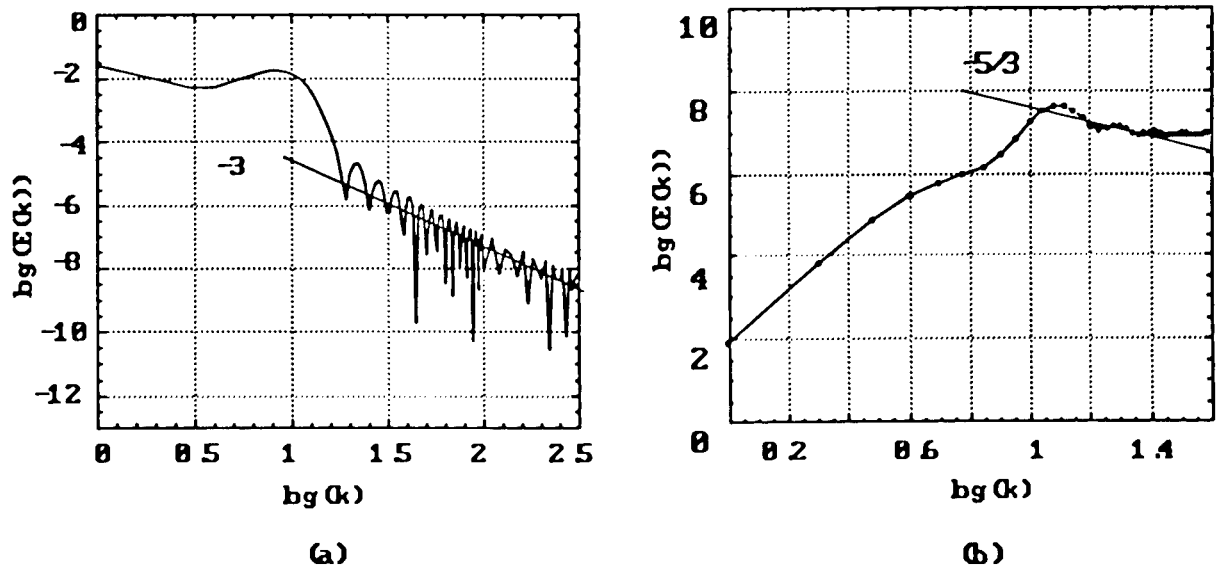


Figure 2: Energy spectra: (a)2-D, (b)3-D

Interactions between two Particles Translating through a Rarefied gas at Large Knudsen number and small Mach Number. *

A. Gopinath, D. L. Koch

School of Chemical Engineering, Cornell University, Ithaca, NY 14853, USA.

To obtain quantitatively accurate predictions of the rates of coagulation of aerosol particles, one must calculate the forces of particle interaction that arise when pairs of particles are separated by distances comparable with their radii a . In addition to van der Waals and electrostatic forces, these include modifications of the hydrodynamic drag acting on each particle due to the velocity disturbance created by its neighbour. These hydrodynamic interactions are well characterized in the limit of continuum flow $\text{Kn} \equiv \lambda/a \ll 1$, where Kn is the Knudsen number and λ is the mean-free path of the gas. However, little is known about the interactions between particles in rarefied gas flows. As a first step toward addressing this problem, we have developed a method to determine the flow-induced interactions between particles in the free-molecular limit $\text{Kn} \gg 1$.

When the gas flow satisfies linear equations of motion, the forces and torques \mathbf{F} acting on the two interacting particles can be related to the velocities and rotation rates \mathbf{U} by $\mathbf{F} = \mathbf{R} \cdot \mathbf{U}$, where \mathbf{R} is the resistivity matrix whose components are functions of radial separation but are independent of \mathbf{U} . By determining \mathbf{R} for all radial positions, one has all the information necessary to simulate the dynamics of two-particle collisions. For continuum flows, this formulation applies at low Reynolds numbers where the inertia of the gas is negligible. The resistivity formulation may also be applied to non-continuum flows provided the Mach number $\text{Ma} \equiv U/\bar{c}$ is small, where \bar{c} is the speed of sound in the gas and U is a characteristic particle speed.

Previous calculations of the effects of particle interactions on drag in free-molecular flow have used molecular simulations to determine the molecular flux and momentum transfer to the particles (Chan and Dahneke [1]; Peters [2]). These authors provided values of the force at a small number of relative positions for common motion of two spheres

along and perpendicular to their line-of-centers. A disadvantage of molecular simulation is that the statistical noise associated with the thermal motion of the molecules grows relative to the drag force as $\text{Ma} \rightarrow 0$ and yet it is precisely this limit which is most important for aerosol applications.

Instead, we have used the collisionless Boltzmann equation to derive a set of integral equations for the molecular flux impinging on a pair of interacting particles with diffuse reflection boundary conditions. These equations may be linearized in the limit $\text{Ma} \ll 1$ and solved by numerical quadrature. Balance equations for the molecular flux to the particle surfaces are obtained by equating the incident flux to the reflected flux. Consider two interacting bodies with surfaces S_i ($i = 1, 2$) moving in a gas that is at rest far from the particles. Let point \mathbf{x}_i on surface S_i move with velocity $\mathbf{U}(\mathbf{x}_i)$. The linearized balance equation for the scaled excess molecular flux per unit area, ν_1 , to point \mathbf{x}_1 can then be written as:

$$\begin{aligned} \nu_1(\mathbf{x}_1) = & A \int_{\hat{\mathbf{c}}_1 \cdot \mathbf{e}_1 < 0} |\hat{\mathbf{c}}_1 \cdot \mathbf{e}_1| (-\mathbf{U}(\mathbf{x}_1) \cdot \hat{\mathbf{c}}_1) d\Omega \\ & + A \int_{\Omega_{21}} |\hat{\mathbf{c}}_1 \cdot \mathbf{e}_1| (\mathbf{U}(\mathbf{x}_2) \cdot \hat{\mathbf{c}}_1) d\Omega \\ & + \frac{1}{\pi} \int_{\Delta S_2(\mathbf{x}_1)} \frac{|(\mathbf{x}_{21} \cdot \mathbf{e}_1)(\mathbf{x}_{21} \cdot \mathbf{e}_2)| \nu_2(\mathbf{x}_2) dS_2}{x_{21}^4}. \end{aligned}$$

The first term on the right hand side is the excess flux due to the motion of \mathbf{x}_1 relative to the bulk gas and represents the flux in the absence of body 2. The second term on the right hand side arises due to the mean velocity of the molecules reflected from particle 2. The number densities at points on S_2 differ from the bulk number density, n_0 , and this difference results in an additional flux given by the third term on the right hand side. \mathbf{e}_i is the unit normal to surface S_i at point \mathbf{x}_i and $\mathbf{x}_{21} = \mathbf{x}_2 - \mathbf{x}_1$ is the relative position vector. Ω_{21} is the solid angle subtended at \mathbf{x}_1 by $\Delta S_2(\mathbf{x}_1)$ which denotes the part of S_2 visible from \mathbf{x}_1 . The constant $A = (9m_g/8\pi k_b T_g)^{1/2}$ where m_g is the mass

*Abstract 6056 submitted to the 21st International Symposium on Rarefied Gas Dynamics, Marseille, France, July 26-31, 1998

of a gas molecule, T_g is the temperature of the gas and k_b is the Boltzmann constant. The vector \mathbf{c} is the molecular velocity as seen from a frame in which \mathbf{x}_1 is at rest. After solving for the molecular flux, one can perform a momentum balance to determine the force per unit area on the solid surfaces and integrate to find the total force and torque on each particle.

As a first application of this method, we determined all eight components of the resistivity tensor necessary to compute the forces and torques for the two-dimensional problem of two interacting aligned cylinders (Gopinath and Koch [3]). The interactions between cylinders translating perpendicular to the line-of-centers or rotating were weak; the forces and torques deviated by no more than 8% from their values in the absence of interactions. However, the effects of interactions on the common and relative motion along the line-of-centers was quite substantial. In fact, the force resisting the normal relative motion of two cylinders diverges as the separation between the two particles approaches zero, although this divergence is weaker than that obtained for the corresponding continuum problem.

We have recently extended the method to the three-dimensional problem of determining the free-molecular flow driven by the translation of two spherical particles. This extension is straightforward in principle, although the geometrical considerations necessary to determine the portion of one particle's surface that is accessible to molecules reflected from the other particle is involved.

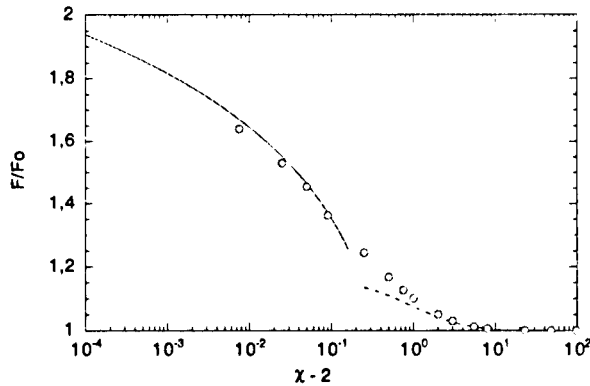


Figure 1: The scaled force for relative motion acting on each sphere as a function of center-to-center distance χ .

In figure 1, we show the results for the force acting on each of a pair of equal-sized spheres of radius a moving relative to each other along their line-of-centers with equal and opposite speeds U . The

force acting on each sphere, F , non-dimensionalized by the force

$$F_0 = a^2 n_o U \left(\frac{m_g k_b T_g}{2\pi} \right)^{1/2} \frac{2\pi(8 + \pi)}{3}$$

acting on a particle in the absence of interactions, is plotted as a function of $\chi - 2$ where $a\chi$ is the center-to-center separation. The circles are the computed force and the dashed and solid lines are analytical asymptotic formulas:

$$F/F_0 \sim 1 + \frac{0.684}{\chi^2}$$

$$F/F_0 \sim 1 + \frac{3\pi}{16 + 2\pi} \ln \ln \frac{1}{\chi - 2}$$

valid in the limit of large and small particle separations, respectively. It is interesting to note that the interaction force diverges weakly as the separation approaches zero. However, the total work done by drag forces (the integral of F with respect to χ) is finite. This contrasts with the case of continuum motion where the energy required to bring two particles into contact is infinite.

References

- [1] Chan, P. and Dahneke, B.J., *Monte-Carlo calculations of the free-molecular drag on chains of uniform spheres*, in *Rarefied gas Dynamics: Progress in Astronautics and Aeronautics*, Ed. Fischer, S.S., Vol. 74, Part 2, pp. 1031-1039, 1980.
- [2] Peters, M.H., *Non-equilibrium molecular dynamics simulation of free-molecular gas flows in complex geometries with application to Brownian motion of aggregate aerosols*, *Phys. Rev. E*, Vol. 50, No. 6, pp. 4609 - 4617, 1994.
- [3] Gopinath, A. and Koch, D.L., *A method for calculating hydrodynamic interactions between two bodies in low Mach number free-molecular flows with application to the resistivity functions for two aligned cylinders*, *Phys. Fluids*, Vol. 9, No. 11, pp. 3550 - 3565, 1997.

NON-EQUILIBRIUM FLOW - NE 1

ROOM MARION

THURSDAY, JULY 30, 1998

9:10

Influence on Dissociation Rates of the State-to-State Vibrational Kinetics of Nitrogen in Nozzle Expansions *

G. Colonna¹, M. Tuttafesta¹, M. Capitelli¹, D. Giordano²

¹ Chemistry Department, University of Bari,

and Centro di Studio per la Chimica dei Plasmi del CNR, Bari 70126, Italy

² ESA/ESTEC, Aerothermodynamics Section, 2200 AG, Noordwijk, The Netherlands.

High-enthalpy wind tunnel flows are very important to reproduce environments for experimental testing under hypersonic conditions. Many theoretical and experimental studies have been performed to determine both physical (pressure and temperature profiles) and chemical parameters (vibrational population distributions and chemical composition). In this regard, the work performed by Sharma et alii [1] probably appears as one of the most typical studies on the subject. These authors determined experimentally the concentrations of the first eight vibrational levels of nitrogen expanding ($T_0 = 5600$ K, $P_0 = 100$ atm) through a nozzle ($l = 0.10$ m) and, from this information, derived the profile of vibrational temperature along the nozzle axis. Consistently, they also tried to reproduce the experimental results by one- and two-dimensional flow calculations. However, the physical models they used, as well as all other models essentially based on Boltzmann distributions, hide the non-equilibrium character of the tail of the vibrational distributions; the latter is important because it determines the reactivity of the molecules. This aspect has been recently discussed by our group [2] for hypersonic boundary layer flows. In Ref. [2] it was shown that non-Arrhenius dissociation constants can arise along the coordinate normal to the body wall as a consequence of the selective pumping of the near-continuum levels. The model used in Ref. [2] is the ladder-climbing model which describes the kinetics of all the vibrational levels of molecular nitrogen. A pseudo-level located in the continuum of the vibrational ladder is included to simulate the presence of atomic nitrogen and to account for the dissociation-recombination processes. In this work, the ladder-climbing model has been applied to calculate the nozzle flow expansion studied in Ref. [1]. For this purpose, the model has been implemented in a one-

dimensional nozzle code. The major findings of the study are illustrated in Figs. 1-3.

Figure 1 shows the vibrational distributions of nitrogen at different stations along the nozzle axis. The main feature revealed in this figure is that, in the initial stations, the bulk of vibrational levels reproduces essentially a Boltzmann trend while, from a given distance onward ($x/l = 0.24$) a plateau develops as a result of the recombination process. In the same figure a comparison is also reported with the experimental data (symbols) from Ref. [1] for the first eight vibrational levels. The theoretical results underestimate the experimental data, probably due to the selection of V-V and V-T rates accounted for in the ladder-climbing model. This aspect is also evident in the profiles (see Fig. 2) of the vibrational (T_v/T_0) temperature: the comparison between experimental data and theoretical results shows a satisfactory agreement up to $x/l = 0.25$ while some discrepancy settles in after that axial station. At any rate, both theoretical and experimental profiles show a qualitative agreement. The same figure shows also the axial profile of the calculated translational temperature. It is important to emphasize that the concept of vibrational temperature based on the population of the first vibrational levels misrepresents the non-equilibrium vibrational character of the distributions. This point is well evidenced in the non-Arrhenius behaviour of the second-order dissociation constant (see Ref. [2] for the definition) illustrated in Fig. 3. The non-Arrhenius character of the dissociation constant is the result of the non-equilibrium vibrational distributions shown in Fig. 1.

In conclusion, even if the populations of the lower levels (eight in the case of Ref. [1]) follow a Boltzmann trend, it is not guaranteed that the chemical kinetics will evolve accordingly because the major influence on the chemical reactivity derives from the tails of the population distributions. The chemical kinetics models based on the idea of a Boltzmann

*Abstract 1801 submitted to the 21st International Symposium on Rarefied Gas Dynamics, Marseille, France, July 26-31, 1998

distribution, and this is the case for the vast majority of the flow solvers being used in engineering applications, misrepresent the physics of the flow and inevitably lead to a non-negligible inaccuracy in the prediction of the mixture composition, which, in turn, will be carried forward to the evaluation of performance parameters such as, just to cite a few, heat fluxes and thrust.

References

- [1] S. Sharma, S. Ruffin, W. Gillespie and S. Meyer. Vibrational relaxation measurements in expanding flow using spontaneous Raman scattering. *J. Thermophysics and Heat Transfer* 7(4):697-703, 1993
- [2] I. Armenise, M. Capitelli, C. Gorse. Non-equilibrium vibrational distributions and non-Arrhenius dissociation constants of N_2 in hypersonic boundary layers. To appear in *J. Thermophysics and Heat Transfer*, Vol. 12, 1998.

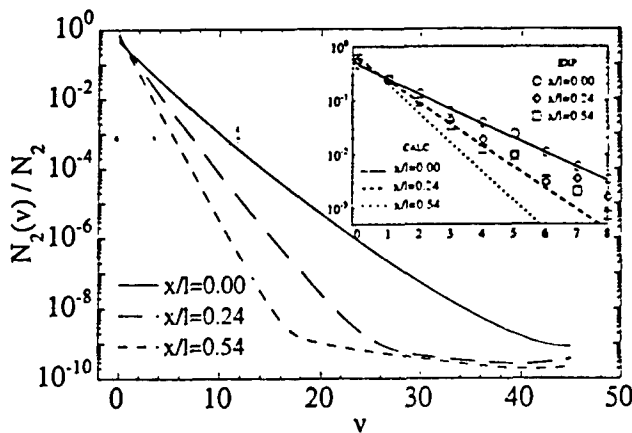


Figure 1: N_2 vibrational population distributions at different stations along the nozzle axis.

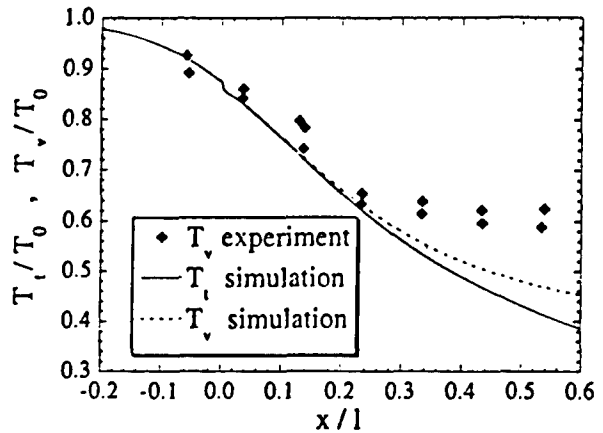


Figure 2: Comparison between experimental (symbols) and theoretical (dashed line) axial profiles of vibrational temperature (theoretical translational temperature profile included for reference).

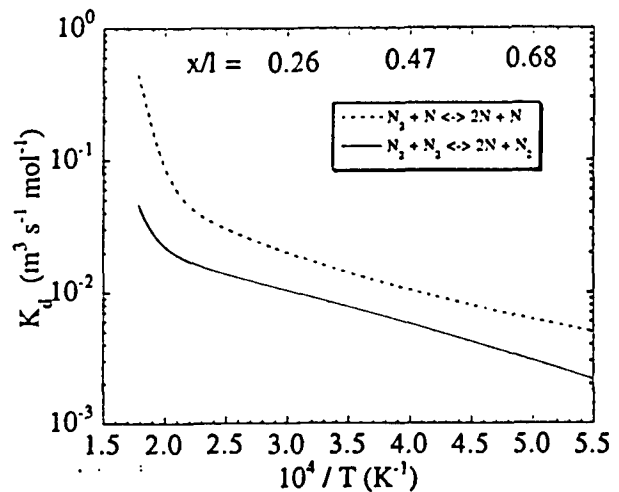


Figure 3: Axial profile of the second-order dissociation rate constants.

The influence of Nonequilibrium Vibrational and Dissociation-Recombination Kinetics on the Heat Transfer and Diffusion in the Boundary Layer under Reentry Conditions *

I. Armenise¹, M. Cacciatore¹, M. Capitelli¹,
E. Kustova², E. Nagnibeda², M. Rutigliano¹

¹ Chemistry Department, University of Bari,

and Centro di Studio per la Chimica dei Plasmi del CNR, Bari 70126, Italy

² Math. and Mech. Dept., St.Petersburg University, 198904, St.Petersburg, Russia

In this paper the heat transfer and diffusion in the boundary layer near re-entering bodies are studied on the basis of the kinetic theory taking into account strong vibrational nonequilibrium, dissociation and recombination.

Commonly used transport kinetic models are based on the quasi-stationary Boltzmann or Treanor distributions over vibrational levels. But if the characteristic times of vibrational relaxation and chemical reactions are comparable with the mean macroscopic time, the quasi-stationary distributions are not valid and the state-to-state approach should be used for modelling of transport and relaxation processes.

Recently the state-to-state approach was applied for the investigation of the vibrational and chemical kinetics in the boundary layer surrounding a space vehicle reentering the air atmosphere at hypersonic speed [1], [2], [3], and new nonequilibrium effects were found. In this case vibrationally excited molecules and atoms generated in the high temperature free stream diffuse towards the cool surface of the vehicle, in the result the vibrational temperature occurs much higher comparable to the gas temperature. The interplay of VV and VT exchanges, dissociation and recombination defines changing of nonequilibrium level populations. The influence of these nonequilibrium conditions on the transport properties near the surface of the space apparatus is studied in the present paper.

Transport kinetic theory in the level approximation is developed in [4], [5] where the heat transfer and diffusion are shown to depend on the gradients not only of the gas temperature and densities of chemical species but also on the gradients of the vibra-

tional level populations. The transport coefficients also depend on the nonequilibrium level populations which should be found from the equations of the detailed chemical-vibrational kinetics coupled with the macroscopic conservation equations.

In the present paper the nonequilibrium kinetics was studied using the model given in [1], [2], [3] and inserted in the kinetic theory code developed in [4], [5]. The binary mixture (O_2, O) of dissociating molecules and atoms is considered and the heat transfer and diffusion in the flow of this mixture in the nonequilibrium boundary layer surrounding a space vehicle are studied. The calculation of the total heat flux, diffusion and heat conductivity coefficients is performed using the formulas derived in [4], [5] and the nonequilibrium level populations, atomic density and the gas temperature obtained in the frame of the model [2], [3]. Different conditions in the free stream and at the surface were examined. The effects of recombination, dissociation, vibrational nonequilibrium and catalycity of the surface on the heat transfer and diffusion in the flow are estimated. In the case of the catalytic wall the probabilities of oxygen atoms recombination on β -cristobalite to selected vibrational states of O_2 obtained in [6] are used.

The flux of the total energy, thermal conductivity coefficients as well as thermal diffusion and binary diffusion coefficients of chemical species and new self-diffusion coefficients for different vibrational levels are calculated at different distances from the surface. For the same conditions presented are the nonequilibrium level populations, number densities of atoms, gas temperature and its gradient. The gradient of the gas temperature plays the most important role in the process of the heat transfer in the conditions under consideration. The role of vibrational nonequilibrium increases with de-

*Abstract 1946 submitted to the 21st International Symposium on Rarefied Gas Dynamics, Marseille, France, July 26-31, 1998

of the gas temperature in the free stream. It is due to the fact that when the temperature in the free stream is much higher than the characteristic vibrational temperature of the molecular species, the total number of molecules in the flow becomes low because of dissociation, and the effect of the nonequilibrium distributions over vibrational levels on the total heat flux is not important in this case. The increasing of the molecular number density leads to an increase of the influence of the nonequilibrium vibrational distributions on the diffusion and heat transfer. The comparison of the heat fluxes q in the flow of (O_2, O) mixture near the catalytic and non-catalytic wall is presented in Fig.1 in dependence of the dimensionless distance from the wall η ($\eta = 0$ at the wall). The following free stream conditions are studied: $p_e = 1000$ Pa, $T_e = 5000$ K, $T_w = 300$ K, where p_e and T_e are the pressure and the temperature in the free stream, T_w is the wall temperature. The results show the important influence of catalyticity of the wall on the transport of the total energy. In the case of recombination at the catalytic wall the gas temperature and its gradient near the surface occur higher compared to the case of noncatalytic wall. The difference in the heat flux values in these cases reaches 30-35%. It leads to an increase of the heat flux just near the surface.

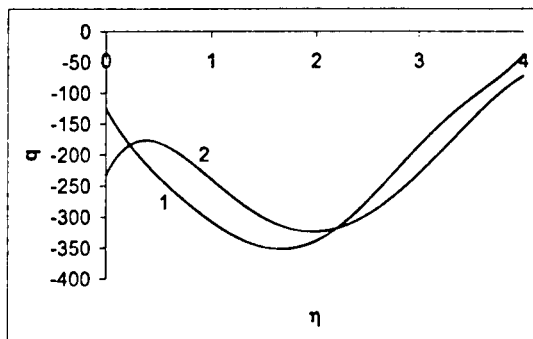


Figure 1: Total heat flux q , W/m^2 , as a function of the distance from the surface. 1 - noncatalytic wall, 2 - catalytic wall.

Acknowledgement.

This work has been partially supported by Agenzia Spaziale Italiana. One of us (E.Nagnibeda) thanks CNR for the grant.

References

- [1] M. Capitelli, I. Armenise and C. Gorse. State-to-state approach in the kinetics of air components under re-entry conditions. *Journ. of Thermophysics and Heat Transfer*, 11(4):570-578, 1997.
- [2] I. Armenise, M. Capitelli, and C. Gorse. On the coupling of non-equilibrium vibrational kinetics and dissociation-recombination processes in the boundary layer surrounding an hypersonic reentry vehicle. In J.J. Hunt, editor, *Aerothermodynamics for Space Vehicles*, ESTEC, Noordwijk, The Netherlands, 1995. ESA Publication Division.
- [3] I. Armenise, M. Capitelli, R. Celiberto, G. Colonna, C. Gorse, and A. Lagana. The effect $N - N_2$ collisions on the nonequilibrium vibrational distribution of nitrogen under reentry conditions. *Chem. Physics Letters*, 227:157-163, 1994.
- [4] E.V. Kustova and E.A. Nagnibeda. The effect of level nonequilibrium kinetics on transport properties of dissociating gas flow behind a shock wave. In *Proc. of the 21st International Symposium on Shock Waves*, Great Keppel Island, Australia, 1997 (in press).
- [5] E.V. Kustova and E.A. Nagnibeda. Transport properties of a reacting gas mixture with strong vibrational and chemical nonequilibrium. *Submitted to Chemical Physics*, 1997.
- [6] M. Cacciatore, M. Rutigliano, G.D. Billing. Energy flows, recombination coefficients and dynamics for oxygen recombination on silica surfaces. *Submitted to 7-th AIAA Joint Thermophysics and Heat Transfer Conference, Albuquerque (USA)*, 1998.

A Comparative Analysis of the Chemical Nonequilibrium Flow Calculations in the Framework of the VSL Equations, the NS Equations and the Chemical Partial Equilibrium Model *

V.I. Sakharov, E.I. Fateeva, V.G. Gromov
Institute of Mechanics, Moscow State University, Russia

1 Abstract

The dissociated and partially ionized gas flows past the blunt-nosed bodies are considered with the nonequilibrium nature of the gas-phase chemical reactions taken into account. Implicit numerical methods for such flow problems has been developed for solving the viscous shock layer (VSL) equations and the Navier-Stokes (NS) equations. The solution may be achieved using the full diffusion problem (full model) or the chemical partial equilibrium model (simplified model). The model of chemical partial equilibrium has been worked out for flow problems with gas-phase chemical reactions whose rates essentially differ. Examples of such flows are given. The comparisons between the results obtained in the framework of the VSL equations and the NS equations, using the full model and the simplified model are analyzed. Applicability range and efficiency of simplified model are estimated. It is demonstrated that the chemical partial equilibrium model is applicable for simulation of the hypersonic flow fields over blunt bodies with a nose radius of more than several centimeters on "Space Shuttle" reentry trajectory in the Earth's atmosphere.

2 Introduction

The multicomponent gas flows past blunt-nosed bodies entering planetary (Earth's and Martian) atmospheres at hypersonic velocities are accompanied by reactions whose rates differ widely, i.e. chemical partial equilibrium sets in. For instance, as a reentry vehicle with 1 m characteristic radius enters the Earth's atmosphere at 5-8 km/s velocities and 50-75 km altitudes, the gas-phase exchange reactions proceed quite fast in the disturbed region,

while the dissociation rates are finite. The motion of a reentry vehicle with a small blunted nose along a gliding trajectory in the Martian atmosphere is another example. At altitudes exceeding 35 km the ionized mixture flow past a landing module cannot be considered as chemical equilibrium. So the associative ionization reactions are close to equilibrium, while the O_2 , N_2 and C_2 molecules dissociate either slowly or with finite rate.

The model of chemical partial equilibrium has been developed for the above-mentioned flows. In this model the part of differential diffusion equations is degenerated into algebraic relations of detailed chemical equilibrium. The number of such equations is equal to the number of high-rate independent chemical reactions. The component formation sources on the right-hand sides of the remaining diffusion equations of new unknown functions ("slow" linear combinations of mass fractions) do not contain fast stages. It permits to overcome the stiffness problem.

3 Numerical Methods

The finite-volume implicit numerical method is developed to solve the two-dimensional time-dependent Navier-Stokes equations in the conservation form. It is assumed that the flux vector can be split into "viscous" and "inviscid" parts. The solution of the Riemann problem of heat-conducting gas with frozen chemical composition has been obtained for the computation of "inviscid" fluxes. The spatial derivatives in the "viscous" terms are approximated with second-order accuracy. Piecewise-parabolic distribution of the physical variables over the network cells and "minmod" limiters lead to TVD-scheme of second-order accuracy. Finite-difference equation set is resolved by the sweep method along the lines normal to the surface and the Gauss-Seidel iteration procedure. Coordinate-oriented differ-

* Abstract 5156 submitted to the 21st International Symposium on Rarefied Gas Dynamics, Marseille, France, July 26-31, 1998

ences are introduced in the implicit part of the finite-difference operator in accordance with signs of eigenvalues of Jacobi matrices in convective terms.

The new finite-difference scheme for the solution the VSL equations with multicomponent diffusion and nonequilibrium chemical reactions in gas and on the body surface is developed due the finite-volume approach. The flux-difference splitting method based on the linearized solution of Riemann problem in isoenergetic approximation is applied for the calculations the inviscid fluxes through the interfaces of cells. Introducing into the expression for the fluxes limited anti-diffusion corrections provide the TVD conditions realization and the second order of accuracy on smooth solution. The viscous fluxes are calculated with the space centered scheme. The boundary conditions on the body surface and on the shock wave are approximated in the context of general conception the finite-volume method with second order of accuracy on equations solution. The steady solution of the difference equations is found by iterative procedure based on the solving with implicit scheme pseudotime-dependent VSL equations. The flowfield calculation on every time step is performed due Gauss-Seidel line relaxation numerical technique.

4 Results and Discussion

The model of chemical partial equilibrium was used for the numerical simulation of hypersonic viscous multicomponent gas flows past a blunt bodies in the framework of the boundary layer equations on stagnation streamline in [1]. The flow conditions corresponded to proceeding along the part of the reentry trajectory of the "Space Shuttle" (5th flight, $H = 50 - 70$ km). 11-species air model with 49 chemical reactions was considered. The preliminary analysis of the Damköhler numbers and the comparison between the obtained numerical solutions of the full diffusion problem and simplified model demonstrated that it was enough to enter only one "slow" combination of mass fractions (and diffusion fluxes accordingly) in the considered case:

$$u_1^s = \frac{c_O}{m_O} + \frac{c_N}{m_N} + 2 \left(\frac{c_{NO+}}{m_{NO+}} + \frac{c_{O_2^+}}{m_{O_2^+}} + \frac{c_{N_2^+}}{m_{N_2^+}} \right) + 3 \left(\frac{c_{O+}}{m_{O+}} + \frac{c_{N+}}{m_{N+}} \right)$$

In the present paper applicability of the chemical partial equilibrium model is analyzed under

the similar conditions in the framework of the full Navier-Stokes equations. Note, that the numerical simulation of a hypersonic flow in the framework of the full Navier-Stokes assumes deriving the solution in a whole disturbed region over the body including the shock wave structure. An analysis of the Damköhler numbers for such conditions does not permit to limit by one "slow" combination. It is connected with the strong chemical nonequilibrium in the relaxation zone near the smeared bow shock wave. In this case the whole group of chemical reactions being high-rate in the boundary layer passes into category "slow" ones, and the maximal number of independent high-rate reactions decreases by unit. Because of this, the second "slow" combination linearly independent with the first one is introduced:

$$u_2^s = \frac{c_N}{m_N} + \frac{c_{NO}}{m_{NO}} + \frac{c_{NO+}}{m_{NO+}} + \frac{c_{N+}}{m_{N+}} + 2 \left(\frac{c_{O+}}{m_{O+}} + \frac{c_{N_2^+}}{m_{N_2^+}} \right)$$

It means that instead of 8 stiff diffusion equations of reaction product mass fractions one can use only two nonstiff diffusion equations for above-proposed "slow" combinations during a numerical simulation. So in the following we will use "the simplified model" along with "the chemical partial equilibrium model".

For a comparison between the results obtained in the framework of the VSL equations, the NS equations using the full diffusion model, and the NS equations using the simplified models the calculations of flowfield over a 90-deg spherical segment for conditions corresponding to several points of a space vehicle "Space Shuttle" reentry trajectory ($H=85\text{km}-54\text{km}$, $V_\infty=7.5\text{km/s}-4.6\text{km/s}$) are carried out.

Close agreement is obtained between solutions computed using the VSL and the NS equations for the corresponding freestream conditions and the values of sphere radius $R=50\text{cm}$ and more (i.e. Re number is large). The agreement is observed over all gas-dynamic parameters, the distributions of air component mass fractions in the disturbed flow region, as well as the distributions of heat flux and skin friction coefficients along the surface. The chemical partial equilibrium model using two "slow" combinations gives identical results. The chemical partial equilibrium model with one "slow" combination can produce the distributions of dissociated air components differing from "exact" solution, but the heat exchange parameters and skin friction coefficients are obtained with reasonable accuracy. Distinction

in the numerical solutions of the VSL and the NS equations is observed for small values of sphere radius ($R \sim 5\text{cm}$, several centimeters), since the Re number becomes small. The chemical partial equilibrium model with two "slow" combinations in this case provides the solution agreeing with the NS solution using the full diffusion model.

References

- [1] V. I. Sakharov, O. N. Suslov, E. I. Fateeva, Fluid Dynamics, Vol.32, No.2, 1997.

Vibration-Dissociation Kinetics of Tri-atomic Molecules at High Temperatures *

A.V.Eremin, V.V.Shumova

Lab. of Nonequilibrium Processes, HEDR Center, Moscow, Russia

1 Introduction

At temperatures about 5000 – 10000K energy-exchange processes and chemical reactions of polyatomic molecules proceed in conditions of essential vibrational nonequilibrium which affects strongly on the rates of transformations. The most complicated problem for numerical simulation of these processes is the description of dissociation in conditions of considerable depletion of vibrational degrees of freedom down to low-lying levels and simulation of the activation mechanism at high temperatures. The well-known theoretical models of vibration-dissociation coupling of two-atomic molecules, based on level approximations [1], [2], are hardly applicable for more complicative molecular systems such as tri-atomics.

This study is aimed to elucidate the correlation mechanism between the rate of dissociation and the distribution of vibrational energy of tri-atomic molecules in wide temperature range, and in particular to determine the role of supercollisions at high temperature decomposition of these molecules. The CO₂ molecule was considered as an example of complicative and widely used species. The theoretical approach to the solution of master equation (ME) for dissociation of polyatomic molecules is based on "step-ladder" approximation ([3], [4]) for vibrational states populations, including relaxation under weak and strong collisions, along with V-E-exchange, chemical reactions and dissociation consideration.

2 Kinetical Model

According to the "step-ladder" approximation, the solution of ME for the population A_i of any micro-

scopic state of polyatomic molecule is given by:

$$\frac{dA_i}{dt} = W_+ + W_- + W_f(i) + W_{bm}(i) + W_{ev}(i). \quad (1)$$

Thus, the kinetical mechanism includes the vibrational relaxation within both ground and electronically excited states with rates W_+ and W_- ; energy exchange between these states with rates W_{ev} ; spontaneous decay of overbarrier states with rate W_f and bimolecular reactions with rates W_{bm} . Here $W_+ = k_a(i)M A_{i-1} + k_d(i+1)M A_{i+1}$, $W_- = k_d(i)M A_i - k_a(i+1)M A_i$, where k_a and k_d – activation and deactivation rate constants, M is full concentration of bath gas.

The particular attention at the present study is devoted to the consideration of two mechanisms of vibrational relaxation – weak and supercollisions mechanisms. The deactivation rate constant k_d is written as a sum:

$$k_d(i) = a_1(T) \cdot k_{d,w}(i) + a_2(T) \cdot k_{d,s}(i), \quad (2)$$

where: $k_{d,w}$ is weak collisions rate constant, describing transitions between levels with energies $E(i) \rightarrow E(i) - \Delta E_1$, $\Delta E_1 = \Theta_2(\text{CO}_2) \approx 2000\text{K}$; $k_{d,s}$ is rate constant of supercollisions for transitions between levels with energies $E(i) \rightarrow E(i) - \Delta E_2$, $\Delta E_2 = kT$; $a_1(T)$, $a_2(T)$ are temperature depending weight factors of both mechanisms. The activation and deactivation rate constants are linked by detailed balance.

Weak collisions term of Eq.2 is shown to correspond to normal one-quantum vibrational relaxation and ΔE_1 being determined by the individual structure of molecule. Supercollisions are supposed to reflect the possibility of transition of large portions of energy with ΔE_2 depending on the energy of collision and $k_{a,s}$ depending on the bath gas property.

3 Results and Discussion

The supposed model has been tested on the data of vibrational relaxation and dissociation rate constant k_{di} [5].

*Abstract 6623 submitted to the 21st International Symposium on Rarefied Gas Dynamics, Marseille, France, July 26-31, 1998

It appeared that at the temperatures 2000-4000K the rate of CO_2 dissociation is determined by the population of highly excited vibrational states (HES) and the mean portion of energy transferred is close to ΔE_1 . Based on this $a_1(T)$, $a_2(T)$ were determined.

The population of low-lying levels is shown to depend mainly on the weak collisions efficiencies, while population of HES depends also on the efficiency of supercollisions, which are enhanced by the intensive interaction between HES of different vibrational modes. In Fig.1 the formation of quasistationary distribution function of ground state of CO_2 at $T=2500\text{K}$ is given. One can see the depletion of HES near to dissociation barrier.

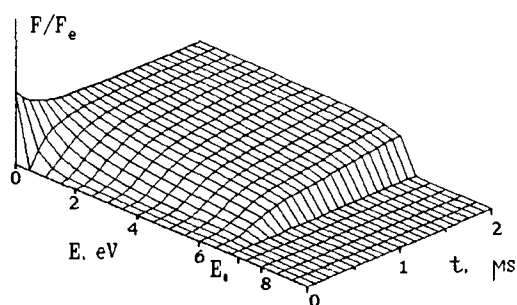


Figure 1: Vibrational relaxation within $\text{CO}_2(X^1\Sigma)$ state at $T=2500\text{K}$, $P=1\text{ atm}$. F/F_e - normalized to equilibrium distribution function (DF). E_0 is the threshold of spin-allowed dissociation channel.

At the temperatures above 4000K the CO_2 dissociation proceeds in essentially nonequilibrium conditions, and the rate of dissociation is limited by the vibrational relaxation of low levels. In Fig.2 the cross sections of the surface similar to one represented in Fig.1, obtained at $T=6000\text{K}$, $t=1\text{ μs}$ (which correspond to the quasistationary stage of dissociation) are shown. Line 1 represents the DF for weak collisions assumption, while line 2 is obtained for complete mechanism. The combined mechanism reflects: 1) noticeable depletion of DF already at low energies, and 2) increase of populations of HES and of overbarrier states due to supercollisions influence.

Thus, the proposed model is able to describe the vibration-dissociation coupling of tri-atomic molecules in a wide temperature range (2000 - 10000 K). It is shown that the weak and supercollisions relaxation mechanisms complete each other and the role of supercollisions increases at $T>4000\text{ K}$. One more important result of this study is that the suggested model gave the possibility to

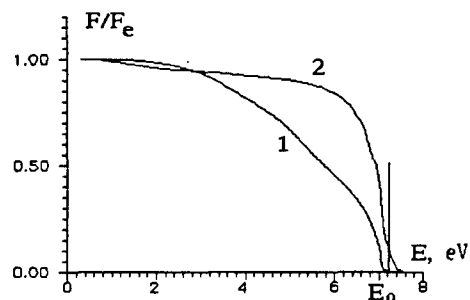


Figure 2: Quasistationary DF of the ground state of CO_2 . $T=6000\text{K}$, $P=1\text{ atm}$, $t=1\text{ μs}$. Line 1 is given in weak collisions mechanism assumption. Line 2 represents the combined weak and supercollision mechanisms.

describe high temperature deviation of k_{dis} of CO_2 [5], from RRKM-theory predictions.

Acknowledgement. The financial support of Russian Fundamental Research Foundation (Grant N 96-02-19694) is gratefully acknowledged.

References

- [1] Lordet F., Meolans J.G., Chauvin A., Brun R. *Nonequilibrium vibration-dissociation phenomena behind a propagating shock wave: vibration population calculation*. Shock Waves, 1995, 4, pp. 299 - 312.
- [2] Chikhaoui A., Dudon J.P., Kustova E.V., Nagnibeda E.A. *Kinetic modelling of transport properties in reacting gas mixtures at high temperatures*. Proc. of Rarefied Gas Dynamics 20. Beijing, China, 1996.
- [3] Zaslonko I.S., Eremin A.V., Shumova V.V. (1995) *Spectroscopic Detection of HES Transformations Behind Shock Waves and Master Equation Implementation* Proc. of the ISSW-20, Pasadena, V. 2, p. 917, 1995.
- [4] Eremin A.V., Shumova V.V., Ziborov V.S., Roth P. *Kinetics of CO_2 dissociation behind shock waves under multi-mode vibrational nonequilibrium conditions*. Proc. of the ISSW-21, Great Keppel, 1997, Paper N 2180.
- [5] Ibragimova L.B. *Dissociation and recombination of CO_2 molecules*. Chem.Phys.Reports, 1990, V. 6, N 9.

Study of a supersonic air nozzle flow in thermo-chemical nonequilibrium *

A. Bourdon, A. Leroux, P. Domingo, P. Vervisch
UMR 6614 CORIA, Université de Rouen, France

1 Introduction

In order to simulate in ground facilities, the real environment of spatial vehicles, supersonic flows are generated by expanding high-enthalpy gas through convergent-divergent nozzles. At the outlet, the flow is generally in strong thermo-chemical nonequilibrium (vibrationally excited, dissociated and even ionized). Then, temperatures and densities behind the shock formed around a test model located downstream the nozzle exit are affected by the energy contained in these real-gas modes. Thus, to obtain the upstream conditions of the test model, an accurate prediction of the nozzle flowfield is necessary. In this work, we propose to study the flow in the nozzle of the TT1 facility located at Tsniimach (Moscow). TT1 is a 10MW arc-jet facility built for material testing. Its nozzle is axisymmetric and contoured. A thorough experimental investigation has been carried out in this facility: *NO* number density, velocity and temperature have been measured over different test samples and on the flow axis at the nozzle exit [1]. The objective of this work is to study the influence on the outflow conditions of all the physical models used in the computation of this flow, and in particular of the models for the air kinetic scheme, Vibration-Vibration (V-V), Vibration-Translation (V-T) and Chemistry-Vibration (C-V) energy exchange terms. The equations that describe a flow in nonequilibrium are solved using a finite volume approach. For non viscous fluxes, the second order Harten-Yee TVD scheme is used. Five species are taken into account: N_2 , O_2 , NO , N and O . Two sets of reaction rate coefficients have been considered: the one proposed by Park [2] which is used as a reference for this work, and the one (denoted hereafter Losev's model) based on [3]. The V-T energy exchange term is modeled using the Landau-Teller relaxation equation. Two sets of relaxation times have been

tested: as a reference, the one proposed by Millikan and White, and a set (denoted Doroshenko's model) of more recent relaxation times based on different studies but mainly on [4]. For the V-V energy exchange term, as a reference, the expression proposed by Candler [5] (denoted model 1) has been used in which all collision probabilities are assumed to be equal to 10^{-2} . This model is not correct theoretically since at thermal equilibrium, the V-V term is not equal to zero. To avoid this drawback, Knab *et al.* [6] propose to use a slightly modified expression (model 2). Other authors [7] have derived from kinetic theory a very different expression for the V-V term (model 3). For collision probabilities, we have used the best possible data of the literature. For our conditions, all the probabilities are much less than 10^{-2} . For the C-V energy exchange, the Coupled Vibration-Chemistry-Vibration (CVCV) model proposed by Knab *et al.* [6] has been used.

2 Results and discussion

We have noted that thermochemical models have only a small influence on the velocity and pressure in the nozzle and the calculated velocity at the exit of the nozzle (3030 ms^{-1}) is close to the measured one (3300 ms^{-1}). Whatever kinetic scheme is used, species concentrations are rapidly frozen in the divergent. Despite the significant discrepancies between the reaction rates in Park's model and in Losev's one, both models strongly overestimate the *NO* concentration at the nozzle exit. In fact, the experimental value turns out to be close to the equilibrium concentration. With Millikan and White's model for V-T and model 1 for V-V exchanges, Fig. 1 shows that the temperatures are rapidly frozen in the divergent ($x > 0$): all vibrational temperatures are close to each other and the flow is in strong thermal nonequilibrium. Figures 2 and 3 show that models 2 and 3 for the V-V term correct efficiently model 1 in the convergent

*Abstract 6721 submitted to the 21st International Symposium on Rarefied Gas Dynamics, Marseille, France, July 26-31, 1998

($x < 0$) where the flow is in thermal equilibrium. With model 2 for V-V and Doroshenko's model for V-T relaxation times, Fig. 2 shows that the flow is nearly in thermal equilibrium in the divergent. This results first, from the very high efficiency of the V-V coupling which enforces the vibrational temperatures to be close to each other. Second, the V-T relaxation times for $NO-O$ and O_2-O proposed by Doroshenko are much smaller than those estimated by Millikan and White, and as the O concentration is not negligible in the flow, V-T exchanges for O_2 and NO are very efficient. On Fig. 3, model 3 for V-V exchanges is used with more accurate data on collision probabilities. In this case, in the divergent, $T_{v,NO} \simeq T_{v,O_2} \simeq T$ whereas T_{v,N_2} remains higher. Then, in our flow conditions, V-T exchange is more efficient than V-V one. As the temperatures are relatively low and the thermal nonequilibrium remains small, the implementation of the CVCV model turns out to have a negligible influence on the calculated temperatures and NO density. Finally, whatever thermochemical model is used, the calculated translational temperature remains smaller than the measured one (1200K). The latter is much closer to the equilibrium value.

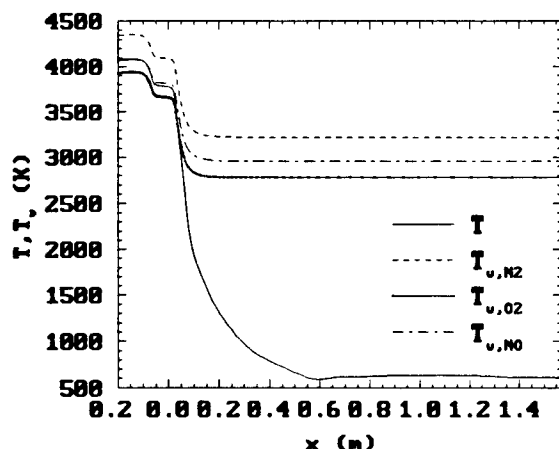


Figure 1: Axial temperatures with Millikan and White for V-T and model 1 for V-V exchanges

References

- [1] Robin L. and Vervisch P. submitted to J. Thermophysics and Heat transfer.
- [2] Park C., AIAA Paper 89-1740, 1989.
- [3] Krivososova O.E., Losev S.A., Nalivaiko V.P., Mukoseev Yu.K. and Shatalov O.P., Reviews of Plasma Chemistry, Vol.1, pp.1-29, 1991.

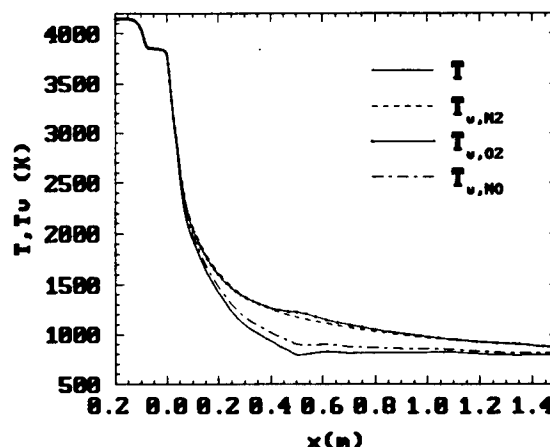


Figure 2: Axial temperatures with Doroshenko's model for V-T and model 2 for V-V exchanges

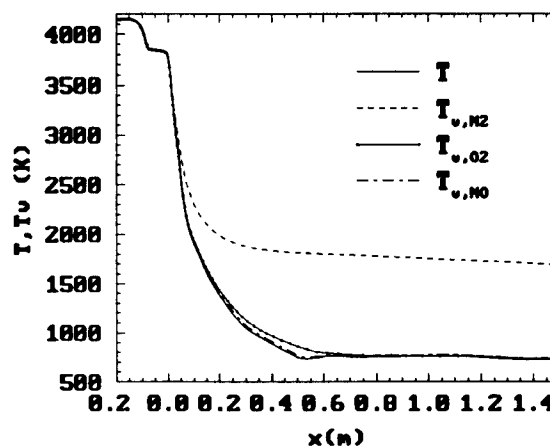


Figure 3: Axial temperatures with Doroshenko's model for V-T and model 3 for V-V exchanges

- [4] Doroshenko V.M., Kudryavtsev N.N. and Smetanin V.V., *Equilibrium of internal degrees of freedom of molecules and atoms in hypersonic flight in the upper atmosphere* translated from *Teplofizika Vysokikh Temperatur*, Vol.29, No.5, pp.1013-1027, 1991.
- [5] Candler G.V., PhD. thesis, Stanford University, 1988.
- [6] Knab O., Frühauf H.-H., and Messerschmidt E.W., J. Thermophysics and Heat Transfer, Vol.9, No.2, pp.219-226, 1995.
- [7] Thivet F., Perrin M.Y., and Candel S., Phys. Fluids, Vol.3, No.11, pp.2799-2812, 1991.

NON-EQUILIBRIUM FLOWS - NE 2

ROOM MARION

THURSDAY, JULY 30, 1998

14:00

Moment Description of Dissociating Gas Mixture *

V.M. Zhdanov

Moscow Engineering Physics Institute

The description of transport and relaxation phenomena in the dissociating gas on the basis of moment equation obtained from the kinetic equation with collision integral in Ludwig and Heil form is presented/ The moment method is extended to the dissociating gas mixture in the case of strong vibrational nonequilibrium.

The distribution function is expanded in a series in the Hermite irreducible tensor polynomials of the molecular velocities and Waldmann-Trubnacher polynomials of the nondimensional internal energies of molecules. The weight function ("zeroth approximation" function) has the form

$$f_{\alpha ij}^{(0)} = n_{\alpha} \left(\frac{m_{\alpha}}{2\pi k T^{tr}} \right)^{3/2} \times \quad (1)$$

$$\exp\left(-\frac{m_{\alpha} c_{\alpha}^2}{2k T^{tr}} - \frac{E_{\alpha j}}{k T^{rot}}\right) N_{\alpha i}^{(0)} \quad (2)$$

where T^{tr} and T^{rot} are the translational and the rotational temperatures respectively, $E_{\alpha j}$ is the internal energy of the j -th rotational state and $N_{\alpha i}^{(0)}$ is the "zeroth approximation" distribution function for the vibrational nonequilibrium/ It is convenient to determine the vibrational temperatures as

$$k T_{\alpha}^{vib} = (E_{\alpha 1}^{vib} - E_{\alpha 0}^{vib}) / \ln(N_{\alpha 0}^{(0)} / N_{\alpha 1}^{(0)}) \quad (3)$$

that ensures its correspondence to parameters using in the vibrational relaxation theory, when $N_{\alpha i}^{(0)}$ has the form of the Boltzmann or Treanor distributions.

The equation for the determination of $N_{\alpha i}^{(0)}$ can be obtained by the integration of the kinetic equation over the velocities and summation over j . Using the inequalities for the effective relaxation times

$$\tau_{TT} < \tau_{RR} < \tau_{RT} < \tau_{VV} \ll \tau_{VT} < \tau_D \quad (4)$$

we can simplify this equation and obtain the quasistationary distribution in the form $N_{\alpha i}^{(0)} = F(i, T^{tr}, T^{rot}, E_{\alpha}^{k(0)})$.

Multiplying the kinetic equation by the appropriate polynomials, integrating over the velocities and summing over i and j we are led to an infinite set of the differential equations for the moments/ Limiting ourselves to a finite number of terms in the series we obtain the close set of the moment equations for the quantities which have a clear physical meaning. The dissociating gas mixture state is determined in this case by 21 parameters for the molecular components and 13 parameters for the atomic components.

The formal expressions for the "moments with respect to the collision integral" are presented. In the case of slowly changing flows the linear transport relations and the general expressions for the kinetic coefficients (shear and volume viscosities, thermal conductivity, diffusion etc.) are obtained.

* Abstract 5296 submitted to the 21st International Symposium on Rarefied Gas Dynamics, Marseille, France, July 26-31, 1998

Three-dimensional Nonperturbative Analytic Model of Vibrational Energy Transfer*

I.V. Adamovich, J. W. Rich

Dept. of Mechanical Engineering, The Ohio State University, Columbus, OH 43220-1107

Analytic model of vibrational energy transfer in collisions between a rotating diatomic molecule and an atom or between two rotating diatomic molecules has been developed. The model is based on the analysis of classical trajectories of a free-rotating (FR) molecule acted upon by a superposition of repulsive exponential atom-to-atom potentials. The energy transfer cross-sections have been evaluated using the nonperturbative Forced Harmonic Oscillator (FHO) model [1]. The model predicts the cross-sections for vibrational energy transfer as functions of orientation of a molecule, its translational and rotational energies, and impact parameter. The model predictions have been compared with the results of the three-dimensional close-coupled semiclassical trajectory calculations using the same potential energy surface [2]. The comparison demonstrated not only very good agreement between the analytic and numerical rate constants across a wide temperature range, but also showed that the analytic FHO-FR model correctly reproduces the cross-section dependence on all collision parameters such as orientation angle, impact parameter, rotational and translational energies. The model equally well predicts the cross-sections of single-quantum and multi-quantum transitions and is applicable up to very high temperatures. It is important to note that the resultant analytic expressions for the cross-sections do not contain any arbitrary adjustable parameters such as "steric factors". The model provides new insight into kinetics of vibrational energy transfer and yields accurate and simple expressions for the energy transfer rates that can be used in kinetic modeling calculations.

References

- [1] I.V. Adamovich, S.O. Macheret, J.W. Rich, and C.E. Treanor, *AIAA Journal*, vol.33, No. 6, 1995, p.1064
- [2] G.D. Billing, *Computer Physics Communications*, vol. 32, 1984, p. 45

* Abstract 2286 submitted to the 21st International Symposium on Rarefied Gas Dynamics, Marseille, France, July 26-31, 1998

Phenomenological Modeling of Vibrational - Translational Energy Exchange in the Direct Simulation Monte Carlo Method. *

P. Vijayakumar † I.D. Boyd ‡

Sibley School of Mechanical and Aerospace Engineering
Cornell University, Ithaca, U. S. A.

1 Introduction

In computing rarefied flows, the Larsen-Borgnakke phenomenological model [1] is widely used to distribute the total energy between the translational and internal energy modes. The relaxation rate is governed by the probability of energy exchange. The focus of this study is to review different models used to calculate this probability. A constant probability of energy exchange can be used to reduce computational load. However, this approach is inadequate because it does not capture the temperature dependence of the rate of energy exchange. A comparatively better approach would be to find the translational temperature in every cell in the flow domain and to use continuum expressions to evaluate the probability. For particle simulations like DSMC, no temperature values are associated with the particle. This study uses a relative velocity dependent probability expression given by Boyd [2] which is derived from the temperature dependent continuum expression. Park's [3] modification to the continuum expression is also implemented, after converting it to a velocity dependent form.

A straightforward extension from continuum expressions to an instantaneous probability of energy exchange for a given relative velocity may fail due to several reasons. It is important to verify that this instantaneous probability model satisfies the principle of detailed balance. This study uses Abe's [4] modification to the Larsen-Borgnakke model for this purpose. Also, a correction factor proposed by Lumpkin, Haas and Boyd [5] is employed to resolve the differences between the definitions of internal energy exchange probability for continuum

and particle simulations.

2 Preliminary Results

The velocity dependent probability expression and the modified Larsen-Borgnakke model is tested on two geometries. The first is a 2D simulation of nitrogen molecules in a square box. The walls of the box are considered to be specularly reflecting. The vibrational energy is initially set to zero and translational temperature is maintained at a constant value. The relaxation profile computed by the new model is compared with the theoretical result obtained with the continuum expression for the vibrational relaxation time in Fig. 1.

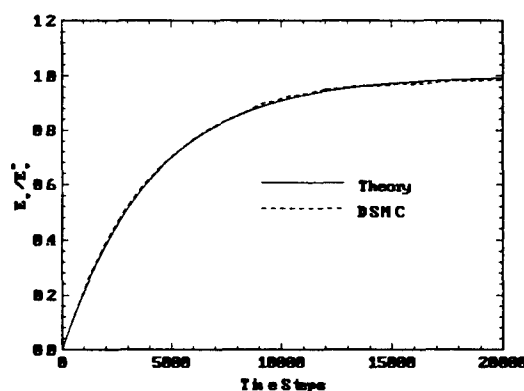


Figure 1: Isothermal relaxation rates, N_2 : translational temperature = 10,000 K.

It is seen that the new model relaxes with a rate that is identical to that predicted by the continuum expression. Also, the Larsen-Borgnakke model with Abe's modification satisfies detailed balance.

The new model is also applied to the 5 km/s flight of the BSUV-2 space vehicle at altitudes of 80 km and

*Abstract 2366 submitted to the 21st International Symposium on Rarefied Gas Dynamics, Marseilles, France, July 26-31, 1998

†Graduate Research Assistant

‡Associate Professor

90 km. DSMC results are obtained with the new model and with a code that employs a temperature-dependent energy exchange probability. This comparison points out some inadequacies of the latter approach, especially for modeling vibrational relaxation processes in the region ahead of the bow shock wave. Figure 2 shows the comparison of probabilities of vibrational energy exchange obtained by the two models, along a row of cells adjacent to the stagnation stream line.

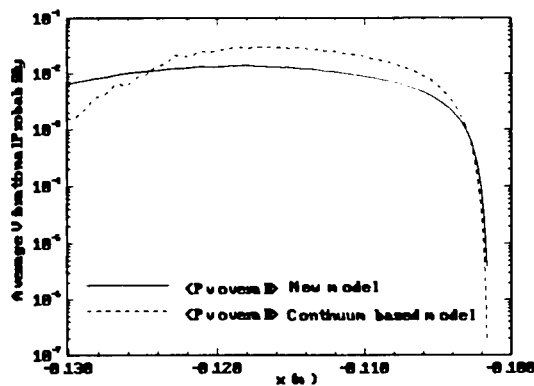


Figure 2: Comparison of probabilities of vibrational energy exchange, along stagnation stream line, at 80km altitude

The translational temperature values used by the continuum based model are very low in the region just ahead of the bow shock wave. Consequently, this model gives very low probability values in this region. However, some high energy collisions occur in this region which is reflected in the comparatively high values given by the velocity-dependent model. Figure 3 shows the comparison of vibrational temperatures along the stagnation stream line.

Though the vibrational probabilities are lower in the relaxation region behind the shock for the new model, the temperature values agree quite well, especially in the shock layer. This is because only collision pairs with large translational energy are accepted for vibrational energy exchange in this case.

Figure 4 gives the distribution of the vibrational energy among the energy levels for a cell located next to the stagnation stream line and close to the bow shock. The two DSMC results display a distinct bimodal distribution.

More extensive computations will be presented in the final paper and the performance of the velocity-dependent model will be compared to other models.

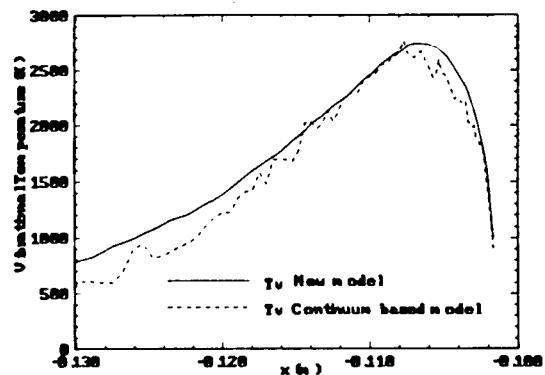


Figure 3: Comparison of vibrational temperature, along stagnation stream line, at 80km altitude

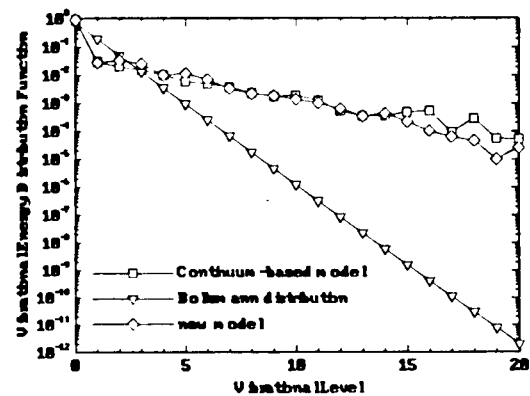


Figure 4: Vibrational Energy distribution at a cell located immediately after the shock and next to the stagnation stream line.

References

- [1] Borgnakke, C., and Larsen, P.S., J. Comp. Phys., 18, 1975, p. 405.
- [2] Boyd, I.D., Phys. Fluids A, 3, 1991, p. 1785.
- [3] Park, C., Prog. Astronautics and Aeronautics, Vol. 96, AIAA, New York, 1985, p. 511.
- [4] Abe, T., Prog. Astronautics and Aeronautics, Vol. 159, AIAA, Washington, 1993, p. 103.
- [5] Lumpkin, F.E., Haas, B.L. and Boyd, I.D., Phys. Fluids A, 3, 1991, p. 2282.

Analyses on Vibrational Mode in DSMC Calculations *

H. K. Park, D. D. Lee

Dept. of Mechanical Engineering, Chonnam National University, Korea

1 Introduction

Hypersonic aerospace vehicles fly under rarefied atmospheric conditions which lie outside the regime of applicability of the traditional continuum equations such as Navier-Stokes equation. In this situation, we have used particle simulation methods like DSMC [1](Direct Simulation Monte Carlo) for the flow field analysis. DSMC method used for this paper is known as the most efficient numerical scheme for analyzing the flow field in rarefied gas regime and is being modified in upgrading the calculation speed and accuracy by many researchers.

The results obtained by using DSMC method may be significantly different according to what kinds of calculation models are used in the simulation programs. Some examples of important things to consider in DSMC calculations are statistical selection rules of possible collision partners, the forms of collision mechanics, and gas-surface interaction models.

In this paper, we examined the characteristics and accuracies of the computational models used for handling vibrational mode [2] in DSMC calculations. Comparisons of the accuracies of results have been made between harmonic and anharmonic oscillator models such as Morse potential model by solving vibrational relaxation problem of nitrogen [3]. In those calculations we examined anharmonic effects in high temperatures. And we also studied how the vibrational model is linked with the dissociation model which must be considered in hypersonic rarefied gas flow calculations. Normal shock waves are used to examine the high temperature effects including dissociation [4].

2 Methods

The DSMC used for the paper is based on the Bird's NTC(No Time Counter) method. And for collision mechanics we adopted the VHS(Variable Hard

Sphere) model which has the same scattering rule as the HS model. But the collision cross-section of the VHS model is a function of the relative translational energy in the collision. For the anharmonic model, the vibrational energy at level i is given by the following empirical equation by Herzberg [1].

$$\epsilon_{v,i} = k[3395((i + 1/2) - 0.006126(i + 1/2)^2 + 0.00000318(1 + 1/2)^3) - 1692.3]$$

In a strong normal shock wave problem, a molecule dissociates when the Larsen-Borgnakke selection of energy [5] into the vibrational mode leads to a level above the maximum level. And the dissociation rate is consistent with the theory of the equilibrium collision theory.

3 Results

Figs. 1 and 2 show anharmonicity of vibrational model and variation of vibrational energy with levels, respectively. Fig. 1 shows that the spacing between adjacent levels is becoming narrower as the level goes higher. In Fig. 2 the values of vibrational energy divided by Boltzmann constant are plotted up to 113,200K of the N_2 dissociation limit.

Fig. 3 shows the profiles of translational, rotational, vibrational and overall temperatures. This calculation was made for a normal shock wave with an upstream Mach number of 20 in nitrogen whose number density is 10^{21} to examine vibration-linked dissociation effects on flow field variables. From the results shown in Fig. 3 it is observed that at the near equilibrium state the temperatures at the downstream region is lower than those of no dissociation cases. The reason is that the dissociation is an endothermic chemical reaction. Also we can see an overshoot of translational temperature near the shock center where the contribution of internal energy out of total energy is small.

The results which are not shown in this abstract will be shown in the full paper.

*Abstract 4706 submitted to the 21st International Symposium on Rarefied Gas Dynamics, Marseille, France, July 26-31, 1998

4 Conclusions

From the results obtained we recognize that the anharmonic oscillator model whose energy levels are not uniformly distributed over all energy levels but densely distributed in high energy levels must be used to describe the problems related with fully-excited vibration mode and high temperature effects including dissociation correctly.

References

- [1] G. A. Bird, *Molecular Gas Dynamics and the Direct Simulation of Gas Flows*, Clarendon Press, 1994.
- [2] B. L. Haas and I. D. Boyd, *Models for Vibrationally-Favored Dissociation Applicable to a Particle Simulation*, 29th Aerospace Sciences Meeting, 1991
- [3] C. F. Hansen, *Theoretical Estimates of Vibrational Relaxation in Nitrogen up to 40,000K*, AIAA Journal, Vol. 31, No. 6, June 1993
- [4] G. A. Bird, *Direct Molecular Simulation of a Dissociating Diatomic Gas*, Journal of Computational Physics, Vol. 25, 1977
- [5] C. Borgnakke and P. S. Larsen, *Statistical Collision Model for Monte Carlo Simulation of Polyatomic Gas Mixture*, Journal of Computational Physics, Vol. 18, 1975

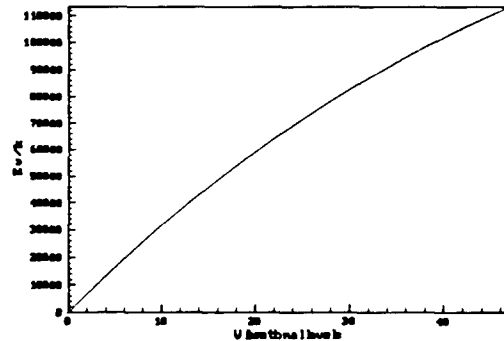


Figure 2: Variation of vibrational energy with levels

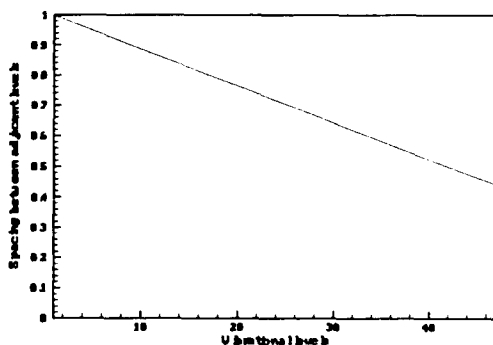


Figure 1: Anharmonicity of vibrational model

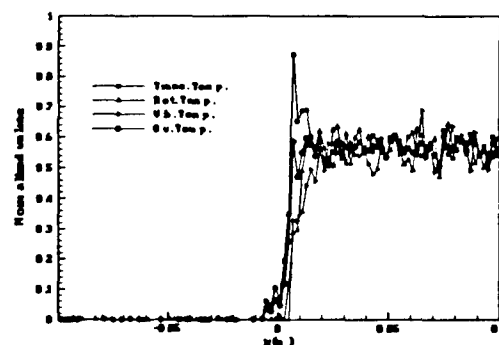


Figure 3: Temperature distributions

Mathematical modelling and numerical simulation of vibrationally nonequilibrium flows of a pure diatomic gas *

Yu. Gorbachev¹, M. Ivanov², E. Kustova³, F. Mallinger⁴

¹ IHPPCDB, St Petersburg, Russia

² ITAM, Novosibirsk, Russia

³ University of St. Petersburg, Russia

⁴ INRIA, Rocquencourt, France

1 Introduction

In simulations of hypersonic flows, one temperature or multi-temperature models are commonly used [1], [4]. These models assume an existence of steady-state distributions, at the gas temperature in the case of equilibrium between all the degrees of freedom, or at the vibrational temperature in the case of vibrational nonequilibrium. But this assumption is not always valid. In particular, in a short relaxation zone behind a shock wave, where the vibrational distribution is strongly disequibrated and cannot be described by a steady-state distribution. Such flows are characterized by a mean vibrational collision time of the same order as the characteristic time of the flow and much greater than the mean translational and rotational collision times. It is important therefore to consider the population of each vibrational energy level as an unknown and to use the state-to-state approach.

We use a mathematical model of transport processes developed in [5]. Furthermore, we present a new model for the vibrational relaxation based on the quasi-classical theory. Yet, numerical results are available considering the Euler approximation and in a very next future, we will propose numerical results for the Navier-Stokes case.

2 Level kinetic approach

We restrict ourself in the case of a pure diatomic gas and we suppose a strong vibrational nonequilibrium. The kinetic equations for this case are written in [3]. The corresponding system of macroscopic equations contains the equations for the vibrational level populations n_i , momentum and total energy

conservation equations.

$$\frac{\partial n_i}{\partial t} + \nabla \cdot (n_i \mathbf{v} + n_i \mathbf{V}_i) = R_i^{(0)VT-VV} + R_i^{(1)VT-VV}, \quad (1)$$

$$\frac{\partial \rho \mathbf{v}}{\partial t} + \nabla \cdot (\rho \mathbf{v} \mathbf{v} + \mathbf{P}) = 0, \quad (2)$$

$$\frac{\partial \rho E}{\partial t} + \nabla \cdot (\rho \mathbf{v} E + \mathbf{P} \mathbf{v} + \mathbf{q}) = 0. \quad (3)$$

Here ρ is the density, \mathbf{v} is the macroscopic gas velocity, E is the total energy per unit mass, R_i^{VT-VV} are the production terms due to VV and VT vibrational energy exchange. The transport terms in the first order approximation of the generalized Chapman-Enskog method are obtained in [3]. Thus, the stress tensor may be written

$$\mathbf{P} = (p - p_{rel}) \mathbf{I} - 2\mu \mathbf{S} - \eta \nabla \cdot \mathbf{v} \mathbf{I}, \quad (4)$$

the diffusion velocity

$$\mathbf{V}_i = - \sum_l D_{il} \mathbf{d}_l - D_{Ti} \nabla \log T, \quad (5)$$

and the heat flux

$$\mathbf{q} = -\lambda' \nabla T - p \sum_i D_{Ti} \mathbf{d}_i + \sum_i \left(\frac{5}{2} kT + \langle \epsilon_j^i \rangle_r + \epsilon_i \right) n_i \mathbf{V}_i, \quad (6)$$

Using a method described in [5], [3] the diffusion coefficients D_{ik} , the thermal diffusion coefficients D_{Ti} , the pressure of relaxation p_{rel} , the bulk viscosity η , the shear viscosity μ and the coefficient of thermal conductivity λ' may be expressed in terms of the rotational relaxation time and the elastic collision integrals. They are computed and tabulated in order to be used in a hydrodynamic solver.

3 A quasi-classical model for VT and VV rate constants

To compute the zero order vibrational relaxation term in (1), we propose new formulas for VT and

*Abstract 6921 submitted to the 21st International Symposium on Rarefied Gas Dynamics, Marseille, France, July 26-31, 1998

VV rate constants, for a pure diatomic gas with discrete vibrational energy [2]. Formulas were obtained using the quasi-classical multidimensional scattering theory for polyatomic gases developed by Gorbachev. Potentials including both attractive and repulsive part are considered. Anharmonicity effects are taken into account.

Figure (1) shows, as an example, a comparison between VT rate constant, for the reaction $N_2(1) + N_2 \rightarrow N_2(0) + N_2$, computed by Billing-Fisher and with your new model.

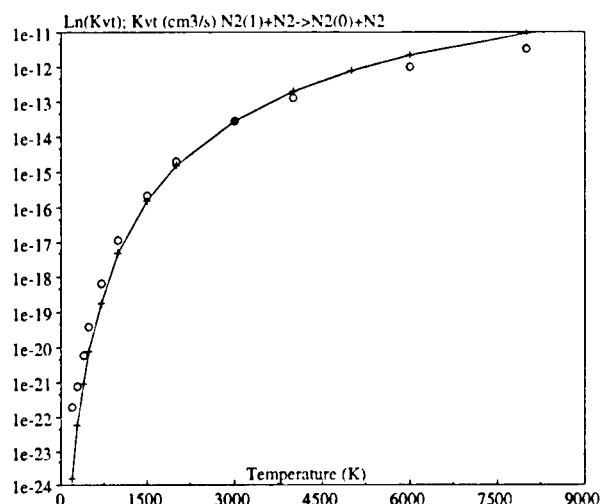


Figure 1: VT rate constants: circles (Billing-Fisher), continuous line (Gorbachev).

Figure (2) shows the profiles of the vibrational and translation-rotational temperature along the stagnation line of a flow around an infinite cylinder at Mach number 10 for a nitrogen. Here, the system (1)–(3) is solved in the Euler approximation. The Gorbachev and Adamovich models of VT and VV rate constants are used for the calculation of the production terms in Eqs.(1) [6]. For each case, we consider 20 energy levels and one and four level transitions.

4 Conclusions

The level kinetic approach is required to compute flows with strong vibrational nonequilibrium. In our case, we have not considered dissociation and recombination processes. They may be important for high temperatures.

References

- [1] S. Pascal, R. Brun, *Transport properties of*

STAGNATION LINE

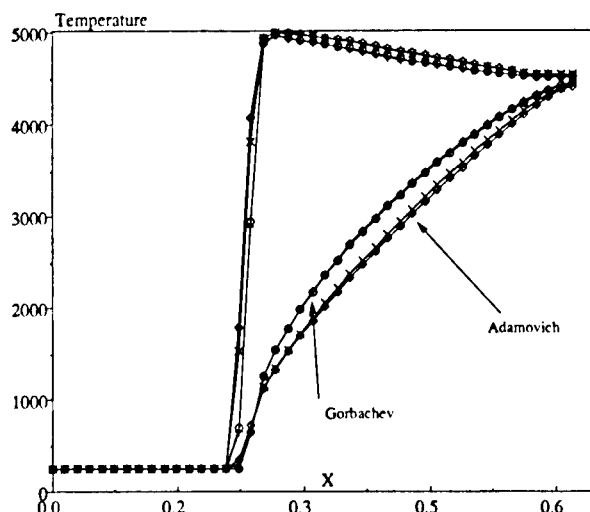


Figure 2: Temperatures profiles along the stagnation lines. Upper lines: translational temperatures, lower lines: vibrational temperatures

nonequilibrium gas mixtures, Physical Review E, Vol. 47, N. 5, may 1993.

- [2] Yu. E. Gorbachev, F. Mallinger, *A quasi-classical model for VT and VV rate constants* RR INRIA, No 3331, Janvier 1998.
- [3] E. V. Kustova, F. Mallinger, *Level Kinetic approach in the case of strong vibrational nonequilibrium for a pure diatomic gas*, in preparation.
- [4] E.V. Kustova and E.A. Nagnibeda, *New kinetic model of transport processes in the strong nonequilibrium gas*, Rarefied Gas Dynamics 19, volume 1, Oxford Univ. Press, 1995.
- [5] E.V. Kustova and E.A. Nagnibeda, *Transport properties of a reacting gas mixture with strong vibrational and chemical nonequilibrium*, Accepted in Chem. Physics, 1998.
- [6] F. Mallinger, *Numerical analysis of different vibrational relaxation models for master equations*, RR INRIA, No 3263, September 1997.

Monte Carlo Simulation of Evolution of Tails of Velocity Distributions for Gas Mixtures in the Front of a Shock Wave *

S.V. Koulikov

Inst. of Chem. Phys. (Chernogolovka) of Rus. Acad. of Sci.
Chernogolovka, Moscow Region, 142432, Russia

Studies of translational nonequilibrium in the front of a shock wave propagating in a gas is particularly important for understanding peculiarities of the threshold physicochemical processes initiated by the shock wave. Previously it was shown what in the front the distribution of relative velocities g exceeded weakly its equilibrium values behind the shock wave for a one-component gas [1]. An analogous effect of superequilibrium was more considerable for the case of a two-component gas when the concentration of impurity was small and the impurity had a much higher molecular mass in comparison with the main gas [2]. In the front, the distributions of g for pairs of light and heavy molecules and for pairs of only heavy molecules exceeded stronger their equilibrium values behind the shock wave in the region of high g . A three-component gas containing two very heavy impurities in a light gas was considered in [3]. It was shown that the strong effect of superequilibrium was revealed for the distribution of g for pairs of heavy molecules of different sorts. The studies were performed in all considered above cases by the Monte Carlo method of unstationary statistical simulation with constant weighting factors [2]. The number of model particles used in these simulations wasn't very large. So, the mean number N of model particles in a cell ahead of the wave was less than 100.

The presented below results were also obtained by above mentioned method. Only values of N were much higher. This permitted to study in more details evolution of tails of velocity distributions. Except one case, molecules were considered as hard spheres. In every case internal structure of molecules didn't take into account. The collision stage was simulated using the sophisticated ballot-box scheme [4]. The modeling of a planar stationary shock wave was carried out in a one-dimensional coordinate space and a three-dimensional velocity

space.

At first, simulation has been performed for the case of a one-component gas at Max numbers $M = 5$ and $M = 7$. It was shown that increase of N up to 3000 didn't affect the calculated distribution of velocities though the distribution of g were obtained up to $g/a = 20$ for $M = 5$ and up to $g/a = 30$ for $M = 7$. (Here a is the velocity of sound in the gas mixture ahead of the wave.)

Next, a two-component gas has been considered. Simulation was carried out for a mixture of helium and xenon with the molecular mass ratio 1 : 33 and the numerical density ratio 1 : 500. The shock Mach number M was set to 5 and $N = 900$. It was shown that in the front, the distribution of g for pairs of only heavy particles (Xe) exceeded significantly its equilibrium values behind the shock wave in the region of high g . The maximum obtained overshoot was about 10^5 at $g/a = 4.5$. The effect of superequilibrium for the distributions of g for pairs of light and heavy molecules was not so high. The maximum obtained overshoot was about 40 at $g/a = 17$. Calculations performed with the use of the model of point centers of repulsion interacting with the force $F \sim r^{-9}$ [2] have given close results. Analogous simulation was carried out for a mixture of helium and oxygen with the molecular mass ratio 1 : 8 and the numerical density ratio 1 : 500, $M = 5$, and $N = 750$. It was found, as previously, that, in the front, the distribution of g for pairs of only of molecules of oxygen exceeded strongly its downstream equilibrium values behind the shock wave in the region of high g . The maximum obtained overshoot was about 100 at $g/a = 7.9$ and about 200 at $g/a = 8.6$. (It should be noted that the threshold of dissociation of oxygen by collisions with helium corresponds to $g/a = 7.9$ if the temperature ahead of the wave is equal to 293K. Moreover, The effect of superequilibrium for the distributions of g for pairs of molecules of oxygen must rise with increase of g .) The maximum obtained overshoot for the distributions of g for pairs of light and heavy molecules was

*Abstract 4956 submitted to the 21st International Symposium on Rarefied Gas Dynamics, Marseille, France, July 26-31, 1998

only about 20 at $g/a = 16.3$.

Next, translational nonequilibrium in the front of a shock wave was investigated for the case of a three-component gas. Mixture of helium, oxygen and xenon with the molecular mass ratio 1 : 8 : 33 and the numerical density ratio 1 : 1 : 200 was considered. The shock Mach number M was set to 4 and $N = 432$. If the temperature ahead of the wave is equal to 293K then the threshold of dissociation of oxygen by collisions with xenon corresponds to $g/a = 6.7$. Obtained maximum overshoot for the distributions of g for pairs containing one molecule of oxygen and one molecule of xenon was about 10^6 at threshold velocity. Similar obtained maximum superequilibria were equal to 50, 30 and 70 for the distributions of g for pairs of molecules of helium and xenon, for pairs of molecules of oxygen and helium and for pairs of molecules of oxygen in the region of high g , respectively. They were not so high as superequilibrium for the distributions of g for pairs of molecules of oxygen and xenon. Decrease in concentrations of high additives increased effect of superequilibrium. So, maximum overshoot for the distributions of g for pairs containing one molecule of oxygen and one molecule of xenon was about 10^7 at $g/a = 6.1$ for the mixture with density ratio 1 : 1 : 4000. The overshoot must be higher at threshold velocity. But, unfortunately values of the distribution weren't obtained in this region of g . The simulation was repeated at $M = 2.5$. Qualitative picture hasn't changed.

Thus, the number of collisions of oxygen molecules with xenon molecules or with oxygen molecules in the region of great g must be considerably higher in the front than behind the shock wave for the considered cases. Consequently, the reaction of dissociation of oxygen by collisions with xenon or with oxygen may have a considerably higher rate in the front than the total dissociation behind the wave. And some amount of atoms of oxygen may appear in the front of wave.

Introduction of small amount of molecules of hydrogen in the considered mixtures of helium, oxygen and xenon or of helium and oxygen can't visibly change translational relaxation in the front of a shock wave. And appearing atoms of oxygen, in the wave front, may decrease a period of induction of interaction of oxygen and hydrogen behind the shock wave. Influence of the atoms of oxygen on the period of induction is stronger at low temperatures (less than 1000K) [5]. The period of induction of interaction of oxygen and hydrogen behind the shock wave was experimentally investigated in [6]. And it was shown that the period of induction decreased

at low temperatures when argon was substituted for helium. This is explained by the considered above effect of translational nonequilibrium in the front of a shock wave.

References

- [1] Kulikov S.V., Ternovaia O.N., Chereshev S.L., *Peculiarity of Evolution of Distributions of Relative Velocities for One-Component Gas in the Front of SW*, Fiz. Gor. Vzd., Vol.30, No.4, pp.140-144, 1994 (in Russian).
- [2] Genich A.P., Kulikov S.V., Manelis G.B., Chereshev S.L., *Thermophysics of Translational Relaxation in Shock Waves in Gases*, Sov. Tech. Rev. B Therm. Phys. Vol.4, Part 1, pp.1-69, 1992.
- [3] Kulikov S.V., *Possibility of Acceleration of the Threshold Processes for Multi-Component Gas in the Front of a Shock Wave*, Shock Waves, Vol.7, No.1, pp.25-28, 1977.
- [4] Kulikov S.V., Serikov V.V., *Weighting Algorithms for the Monte Carlo Simulation of Multicomponent Reactive Gas Flows and Their Application to the Shock-Wave Problem*, Rus. J. Comput. Mech., Vol.1, No.3, pp.49-69, 1993.
- [5] Ivanova A.N., Koulikov S.V., Manelis G.B., Tarnopolskii B.L., Ternovaia O.N., *Influence of Additives of Atomic Oxygen on Interaction of Mixture of $H_2 - O_2 - He$ behind the Shock Wave*, Chemical Physics of Processes Combustion and Exploen. XI Symposium on Combustion and Exploen. Chernogolovka 1996, Vol.1, Part 2, pp.324-325, 1996 (in Russian).
- [6] Eremin A.V., Velikodny A.V., Ziborov V.S., *Nonequilibrium Ignition of H_2/O_2 Mixtures in the Weak Shock Wave Front*, 16th Inter. Colloquium on the Dynam. of Esplos. and React. Syst. (16th ICDERS), Cracow 1997, Conference Proceedings, p.597, 1997.

NON-EQUILIBRIUM FLOWS - NE 3

ROOM MARION

FRIDAY, JULY 31, 1998

16:10

Shock Wave Relaxation for VRS Molecules*

S.L. Gorelov, S.V. Rusakov.

Moscow Institute of Physics and Technology, Russia.

1 Introduction.

The model of molecules being modernization of a model of rough spheres is put in a basis of the given work which on the one hand it is possible to simulate collisions of 2-nd atomic molecules, and on the other hand selection of parameters achieved the correspondence of a functional association of model factor of viscosity from temperature and experimental values. It is a VRS -model (variable rough sphere-model).

2 VRS -model.

The model of rough spheres of a variable diameter differs from a classical model of absolutely rough spheres [1] in two items:

a) the mass of a molecule is concentrated in some isolated points inside an sphere that corresponds to a disposition of atoms in a molecule,

b) the diameter of an sphere is some function from a relative velocity of molecules at the moment of collision, the choice of which determined an association of factors of transposition (for example, factor of viscosity) from temperature.

The molecules represent impenetrable spheres by a diameter $-d$ and mass $-M$. The magnitude and direction of principal moments of inertia depend on a disposition of atoms in a molecule. Let's assume, that the center of a mass of a molecule coincides with a center of an sphere. The magnitude d in each collision is fixed, but depends on a relative velocity of centers of masses of colliding molecules. The absolute rough of spheres assumes, that the relative velocity of spheres in a point of their touch changes own sign on inverse.

We shall designate angular velocities of molecules before collision as ω_1 , ω_2 , and ω_1' , ω_2' and V_1 , V_2 and V_1' , V_2' -velocity of their centers of masses. Let k is unit vector along a line of centers of spheres directed from a center of a 2-nd molecule to a center 1-st. at the moment of collision. Then the relative velocity $-S$ of points of a touch of spheres at the moment of collision will be equal:

$$\begin{aligned} S &= V_1 - V_2 + [k \times (\omega_1 + \omega_2)](d/2) \\ -S' &= -V_1' + V_2' - [k \times (\omega_1' + \omega_2')](d/2) \end{aligned} \quad (1)$$

J -the impulse transmitted to a 2-nd molecule from 1-st molecule then from a conservation law of impulse can be noted:

$$V_{1,2}' = V_{1,2} \pm J/M \quad (2)$$

This impulse is transmitted along direct taking place through a point of a touch of spheres. The atoms are located symmetrically concerning a center of an sphere on a distance- d_1 from each other.

For a moment of molecules concerning points of their touch before collision it is possible to note:

$$M'_{1,2} = M_{1,2} - [k \times J](d/2)$$

Taking into account, that the projection of a moment on an axes of a molecule is equal 0 (vector of an angular velocity is in a plane of a perpendicular axes of a molecule), we obtain for angular velocities after collision:

$$\omega'_{1,2} = \omega_{1,2} - [l_{1,2} \times ([k \times J] \times l_{1,2})](d/2I) \quad (3)$$

Where l_1 and l_2 (unit vectors, defining direction of axes of molecules. From the equations (2), (3) with the help of (1) is obtained expression for impulse:

$$J/M = \{[S + k(k, S) + f[k \times l_2](A/2) + f[k \times l_1](B/2)]\} / (1+f) \quad (4)$$

In this expression scalars A and B are equal:

$$\begin{aligned} A &= (a_1 c - c_1 b) / (a_1 a - b^2); \quad B = (a c_1 - c b) / (a_1 a - b^2); \\ a_1 &= -1 - f + (1 - (k, l_1)^2) / 2; \quad a = -1 - f + (1 - (k, l_2)^2) / 2; \\ c_1 &= (l_1, [k \times S]); \quad c = (l_2, [k \times S]); \quad b = ((l_1, l_2) - (k, l_1)(k, l_2)) / 2 \end{aligned}$$

where $f = (d_1/d)^2$ is dimensionless parameters of a model.

Substituting (4) in (2) and (3), we obtain unknown quantities translational and angular velocities of molecules after collision. Is converted attention, that as $d_1 < d$, the parameter f should vary from 0 up to 1.

In the VRS (model two parameters enter: a diameter of an sphere d and parameter f . These parameters are determined from a comparison of calculated factors of viscosity and parameter Z_R (ratio of time of rotational relaxation to time of translational relaxation) with the appropriate experimental values.

*Abstract 5293 submitted to the 21st International Symposium on Rarefied Gas Dynamics, Marseille, France, July 26-31, 1998.

The diameter of a model sphere $-d$ is calculated on the base of VHS -model in case of a degree potential with an exponent $-\nu$. Under a numerical research of a model was obtained, that the parameter f depends on a relative velocity as:

$$f(1+f)^2 \sim 1/g^{1/4-\nu} Z_R$$

where the expression for Z_R is taken from [2].

The model was checked on a task about a homogeneous relaxation of 2-nd atomic gas [3].

3 Shock wave structure.

The task of the shock structure for 2-nd gas was solved with the use of the VRS-model by DSMC method. The simulated gas was nitrogen, the Mach number of a filling stream -10 , temperature 300 K , $\nu=9.1$, $Z_{R\infty}=15.7$ was taken. The obtained results were compared to experiment [4]- Fig.1, where

$$n^*(x^*) = (n(x^*) - n_1(+\infty)) / (n_2(-\infty) - n_1(+\infty)),$$

$$T^*(x^*) = (T(x^*) - T_1(+\infty)) / (T_2(-\infty) - T_1(+\infty)), \text{ and } x^* = x/\lambda_\infty,$$

$\lambda_\infty = 16\mu_1/5\rho_1(2\pi RT_1)^{1/2}$. The divergence with the experiment is explained by a lack nowadays of exact experimental data on a measurement of factor of viscosity and Z_R from temperature. Last renders significant influence on structure of a shock wave (with a modification $Z_{R\infty}$

from 20 up to 15.7 (25 %), distance between profiles of a density and translational temperature, defined as a position $n^*(x^*) = 0.5$ and $T^*(x^*) = 0.5$, varied on 7 %. The problem on a choice Z_R is basic, because the range of modifications Z_R during a solution of a task coincides with a scatter of experimental data. The influence of an inaccuracy of measurements of viscosity and therefore the definition $-\nu$ (appears negligible).

The work is carried out with the financial help of Russian fund of fundamental researches (code of the project 96-01-01244) and grant of support of conducting scientific schools (code of the project 96-15-96063).

References.

- [1]. Chapman S., Caugling T. *The Mathematical theory of inhomogeneous gases*. // M. IL., 1960.
- [2]. Parker J.G. *Rotational and vibrational relaxation in diatomic gases*. // Phys. Fluid, 1969, N4.
- [3]. S.L.Gorelov, S.V.Rusakov. *A model of rough spherical molecules of a variable diameter*. // Mathematical simulation. N9,1997,Russia.
- [4]. Alsmeyer H. *Density profiles in argon and nitrogen shock waves measured by the absorption of an electron beam*. // J. Fluid Mech., 1976, v.74, part 3, p.p. 497-513.

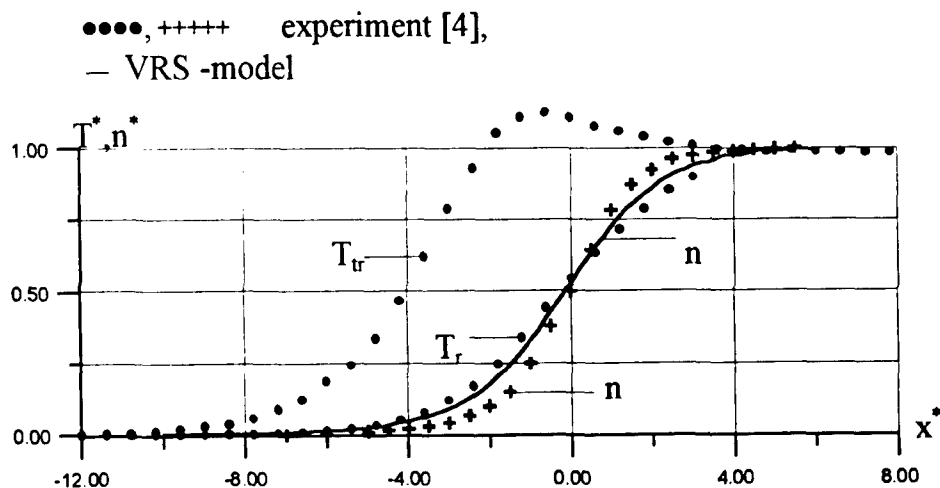


Figure 1: Shock wave structure.

Bulk Viscosity of a Gas Mixture with Bimolecular Reactions *

G.M. Kremer

Departamento de Física UFPR, Curitiba, Brasil

Chemical reactions by using the Boltzmann equation were investigated by several authors. Among others we cite the works of Prigogine and Xhrouet [1], Ross and Mazur [2], Present [3], Shizgal and Karplus [4], Eu and Li [5], Xystriis and Dahler [6]. In none of these works it was found that chemical reactions in gases of structureless particles there is a non-zero bulk viscosity due to the heat of reaction, i. e. due to the binding energy difference between the products and reactants. This result was obtained recently by Kremer and Müller [7, 8] from an extended thermodynamic theory of relativistic gases [7] and from an extended thermodynamic theory of classical gases [8].

The aim of this work is to calculate the bulk viscosity of a gas mixture with bimolecular reactions by using the Boltzmann equation.

We consider a mixture of ideal gases of four constituents of structureless particles A, B, C and D undergoing a simple reversible bimolecular reaction of the type $A + B \rightleftharpoons C + D$.

A state of the mixture is characterized by the set of one-particle distribution functions

$$f_\alpha \equiv f(\mathbf{x}, \mathbf{c}_\alpha, t) \quad (\alpha = A, B, C, D), \quad (1)$$

such that $f_\alpha d\mathbf{x} d\mathbf{c}_\alpha$ gives, at time t , the number of α particles in the volume element $d\mathbf{x} d\mathbf{c}_\alpha$ around the position \mathbf{x} and the velocity \mathbf{c}_α . The one-particle distribution function f_α is assumed to satisfy a Boltzmann equation of the form

$$\frac{\partial f_\alpha}{\partial t} + c_i^\alpha \frac{\partial f_\alpha}{\partial x_i} = \sum_{\beta=A}^D \int (f'_\alpha f'_\beta - f_\alpha f_\beta) g_{\beta\alpha} \sigma_{\alpha\beta} d\Omega_{\beta\alpha} dc_\beta + R_\alpha \quad (2)$$

In the above equation we have neglected external body forces. Also, $\sigma_{\alpha\beta}$ is the differential elastic cross section, the primes denote functions of velocities after collision and $d\Omega_{\beta\alpha}$ is an element of solid angle that specifies the orientation of the relative

velocity after collision $\mathbf{g}'_{\beta\alpha} = \mathbf{c}'_\beta - \mathbf{c}'_\alpha$ relative to the relative velocity before collision $\mathbf{g}_{\beta\alpha} = \mathbf{c}_\beta - \mathbf{c}_\alpha$. R_α is the collision term due to chemical reactions, its form for the constituent A is given by [4]

$$R_A = \int \left[f'_C f'_D \left(\frac{m_{AB}}{m_{CD}} \right)^3 - f_A f_B \right] \sigma_{AB}^* g_{BA} d\Omega_{DC} dc_B \quad (3)$$

where σ_{AB}^* is the differential reactive cross section and $m_{AB} = m_A m_B / (m_A + m_B)$, $m_{CD} = m_C m_D / (m_C + m_D)$ are reduced masses (we note that $m_A + m_B = m_C + m_D$). Similar expressions are valid for the other constituents.

The conservation laws of linear momentum and total energy for a reactive collision are given by

$$m_A \mathbf{c}_A + m_B \mathbf{c}_B = m_C \mathbf{c}'_C + m_D \mathbf{c}'_D, \quad (4)$$

$$\begin{aligned} e_A + \frac{1}{2} m_A c_A^2 + e_B + \frac{1}{2} m_B c_B^2 \\ = e_C + \frac{1}{2} m_C c_C'^2 + e_D + \frac{1}{2} m_D c_D'^2, \end{aligned} \quad (5)$$

where $E = e_A + e_B - e_C - e_D$ is the heat of reaction. The affinity \mathcal{A} for the forward reaction measured in units of kT is defined by

$$\mathcal{A} = \frac{\mu_A + \mu_B - \mu_C - \mu_D}{kT} = \ln \left(\frac{n_A n_B n_C^{eq} n_D^{eq}}{n_C n_D n_A^{eq} n_B^{eq}} \right), \quad (6)$$

where μ_α is the chemical potential, and n_α is the particle number density of the constituent α .

To get explicit expressions for the transport coefficients we have assumed that the differential elastic cross section is that of rigid spheres

$$\sigma_{\alpha\beta} = \frac{1}{4} a_{\alpha\beta}^2, \quad a_{\alpha\beta} = \frac{1}{2} (a_\alpha + a_\beta), \quad (7)$$

where a_α and a_β are the diameters of the colliding spheres. For the reactive cross section we have used the line-of-centers energy model proposed by Present [3]

$$\sigma_{AB}^* = \begin{cases} 0 & \epsilon < \epsilon^*, \\ \frac{1}{4} a_{AB}^2 \left[1 - \frac{\epsilon^*}{\epsilon} \right] & \epsilon > \epsilon^*, \end{cases} \quad (8)$$

*Abstract 2677 submitted to the 21st International Symposium on Rarefied Gas Dynamics, Marseille, France, July 26-31, 1998

where ϵ^* is the activation energy in units of kT and $\epsilon = m_{AB}g_{BA}^2/2kT$ the initial relative translational energy.

We have applied the combined method of Chapman-Enskog and Grad [9] and obtained the following system of equations for the partial dynamic pressures ϖ_α , i.e. for the non-equilibrium part of the trace of the pressure tensor:

$$-\frac{E^{*2}}{\Delta} n_\alpha^{eq} n_A^{eq} n_B^{eq} n_C^{eq} n_D^{eq} \frac{\partial v_i}{\partial x_i} + M_\alpha A = \sum_{\beta=A}^D \frac{N_{\alpha\beta}}{p_\beta} \varpi_\beta, \quad (9)$$

where $E^* = E/kT$, and Δ , M_α , $N_{\alpha\beta}$ are known coefficients.

By solving the system of equations (9) and by considering that the dynamic pressure of the mixture is the sum of the partial dynamic pressures, we get the coefficient of bulk viscosity, which depends on the square of the heat of reaction. This result was obtained previously by [7, 8].

References

- [1] Prigogine, I.; Xhrouet, E., *On the Perturbation of Maxwell Distribution Function by Chemical Reaction in Gases*, Physica, Vol. 15, pp. 913-932, 1949.
- [2] Ross, J.; Mazur, P., *Some Deductions from a Statistical Mechanical Theory of Chemical Kinetics*, J. Chem. Phys., Vol. 35, pp. 19-28, 1960.
- [3] Present, R. D., *Chapman-Enskog Method in Chemical Kinetics*, J. Chem. Phys., Vol. 48, pp. 4875-4877, 1960.
- [4] Shizgal, B.; Karplus, M., *Nonequilibrium Contributions to the Rate of Reaction. I. Perturbation of the Velocity Distribution Function*, J. Chem. Phys., Vol. 52, pp. 4262-4278, 1970.
- [5] Eu, B. C.; Li, K. W., *Kinetic Theory of Reacting Systems*, Physica, Vol. 88A, pp. 135-157, 1977.
- [6] Xystris, N.; Dahler, J. S., *Mass and Momentum Transport in Dilute Reacting Gases*, J. Chem. Phys., Vol. 68, pp. 354-373, 1978.
- [7] Kremer, G. M.; Müller, I., *Thermal Conductivity and Dynamic Pressure in Extended Thermodynamics of Chemically Reacting Gases*, to appear in Ann. Inst. Henri Poincaré, 1998.
- [8] Kremer, G. M.; Müller, I., *On the Effect of a Chemical Reaction on Heat Conduction and Dynamic Pressure*, to appear in Acta Mech., 1998.
- [9] Bezerra Jr., A. G.; Reinecke, S.; Kremer, G. M., *A Combined Chapman-Enskog and Grad Method. I. Monatomic Gases and Mixtures*, Continuum Mech. Thermodyn., Vol. 6, pp. 149-160, 1994.

Nonequilibrium Distributions in CO_2 and their Influence on the Transport and Thermodynamic Properties *

E. Kustova, E. Nagnibeda

Math. and Mech. Dept., St. Petersburg University, 198904, St. Petersburg, Russia

Some questions of the kinetic theory of mixtures containing CO_2 are considered in this paper. The major attention is focused on the nonequilibrium quasi-stationary distributions and their influence on the transport and thermodynamic properties of carbon dioxide.

The development of the kinetic theory methods for gases consisting of three-atomic and more complex molecules is very important in nonequilibrium gas dynamics, laser physics, chemical technology. The joint consideration of the vibrational kinetics and transport processes in such gases as CO_2 , NO_2 , N_2O is needed for the prediction of the flow parameters near the space vehicle entering the planet atmosphere, in expanding flows, in the high enthalpy facilities. At the present time the kinetic theory of polyatomic gases is much less advanced compared to the theory of diatomic molecules due to some additional difficulties. In fact the existence of several vibrational modes and energy exchanges between them have to be taken into account and may influence essentially the vibrational kinetics and dissipative properties.

The theoretical models of the vibrational kinetics of strongly excited polyatomic gases were developed in [1], [2], [3] where it was shown that the anharmonic effects appear to be much more important for the vibrational kinetics of three-atomic molecules than for the diatomic ones. Transport properties of polyatomic molecules in the weak nonequilibrium conditions, when all characteristic times of relaxation processes are much less than the macroscopic time, were considered in [4], [5]. The kinetic models of the vibrational kinetics and transport phenomena taking into account the exchange of vibrational energy within and between internal modes were developed in [6], [7], [8], [9].

In this paper the kinetic equations for the distribution functions in a polyatomic gas under various nonequilibrium conditions are considered. On

the basis of eigenfunctions of the linearized integral collision operator the new nonequilibrium quasi-stationary distributions over vibrational levels of different modes are derived. The anharmonism of molecular vibrations as well as the different rates of various energy exchanges are taken into account. Three nonequilibrium distributions are found for carbon dioxide with strongly excited vibrational degrees of freedom: the four-temperature, three-temperature and two-temperature ones. In each case the distribution functions deviate from the Maxwell-Boltzmann ones.

For a strongly excited linear three-atomic molecule the nonresonant vibrational energy exchange within modes appears to be more probable than the exchange of the vibrational energy between various modes. Under this condition the four-temperature distribution function in CO_2 is valid and is obtained in such a form [6]:

$$f_{ij}^{(0)} = \frac{ns_{ij}}{Z} \exp\left(-\frac{mc^2}{2kT} - \frac{\varepsilon_{ij}}{kT}\right) \exp\left(\sum_{m=1}^3 \vartheta_m i_m\right), \quad (1)$$

where i, j are the vibrational and rotational level, the indices $m = 1, 2, 3$ indicate the symmetric, bending and asymmetric vibrational modes correspondingly, c is the peculiar velocity, ε_{ij} is the internal energy, s_{ij} is the statistical weight, m is the molecular mass, n is the number density, Z is the partition function, T is the gas temperature, the parameters ϑ_m are connected with the vibrational temperature of the different modes:

$$\vartheta_m = \frac{\varepsilon_1^{(m)}}{k} \left(\frac{1}{T} - \frac{1}{T_1^{(m)}} \right), \quad m = 1, 2, 3$$

$$\varepsilon_1^{(1)} = \varepsilon_{10^00}, \quad \varepsilon_1^{(2)} = \varepsilon_{01^10}, \quad \varepsilon_1^{(3)} = \varepsilon_{00^01}$$

The wave numbers of CO_2 satisfy to the condition of Fermi-resonance. This fact results in the increase of the probability of the near-resonant exchange between the symmetric and bending modes and strong coupling between them. In this case the

* Abstract 4997 submitted to the 21st International Symposium on Rarefied Gas Dynamics, Marseille, France, July 26-31, 1998

three-temperature distribution takes into account rapid vibrational energy exchange between the first and the second modes [6]:

$$f_{ij}^{(0)} = \frac{n s_{ij}}{Z} \exp \left(-\frac{mc^2}{2kT} - \frac{\varepsilon_{ij}}{kT} \right) \times \exp (\vartheta_{12}(2i_1 + i_2) + \vartheta_3 i_3). \quad (2)$$

The parameter ϑ_{12} is defined in terms of the temperature $T_1^{(12)}$ of the combined Fermi-resonance mode:

$$\vartheta_{12} = \frac{\varepsilon_1^{(2)}}{k} \left(\frac{1}{T} - \frac{1}{T_1^{(12)}} \right)$$

A number of experiments on laser fluorescence and measurements of vibrational temperatures in laser mixtures containing polyatomic gases show that the symmetric and bending modes can be often considered in equilibrium with the rotational and translational degrees of freedom. In this case the two-temperature distribution is valid [9]:

$$f_{ij}^{(0)} = \frac{n s_{ij}}{Z} \exp \left(-\frac{mc^2}{2kT} - \frac{\varepsilon_{ij}}{kT} \right) \times \exp \left(-\frac{\varepsilon_i - i_3 \varepsilon_1^{(3)}}{kT} - \frac{i_3 \varepsilon_1^{(3)}}{kT_1^{(3)}} \right) \quad (3)$$

In the frame of these models the formulas for the pressure tensor, heat flux and transport coefficients are derived using the generalized Chapman-Enskog method. The structure of the heat flux depends on the zero order distribution functions (1), (2), (3) and corresponding first order distribution functions. It differs for the three cases considered. The procedure of the calculation of the transport coefficients is also different in various nonequilibrium conditions.

The practical algorithm for the calculation of the heat conductivity and viscosity coefficients are given. The heat conductivity coefficients are expressed in terms of the elastic collision integrals and the nonequilibrium specific heats which should be found on the basis of the strong nonequilibrium non-Boltzmann distribution. It is shown that the contribution of the inelastic collision integrals to the heat conductivity is small. On the contrary, for the calculation of the bulk viscosity coefficient, relaxation pressure and microscopic rate constants the inelastic cross-sections are very important. The non-Boltzmann distributions influence strongly the specific heats and transport coefficients, especially in the case of essential excitation more than one vibrational mode. Anharmonic effects on the specific heats and transport coefficients increase with

the gas temperature. The contribution of the vibrational degrees of freedom to the thermal conductivity coefficients is much more for polyatomic gases than for diatomic ones.

Acknowledgement.

The authors are grateful to ESA ESTEC for the support of this work.

References

- [1] A.A. Likalter. On the vibrational distribution of polyatomic molecules. *Prikl. Mekh. Tekn. Fiz.*, 4:3, 1976. (in Russian).
- [2] B.F. Gordiets, A.I. Osipov, and L.A. Shelepin. *Kinetic Processes in Gases and Molecular Lasers*. Gordon and Breach Science Publishers, Amsterdam, 1988.
- [3] V.D. Rusanov, A.A. Fridman, and G.V. Sholin. Vibrational Kinetics and Reactions of Polyatomic Molecules in Nonequilibrium Systems. In M. Capitelli, editor, *Nonequilibrium vibrational kinetics*, Berlin, Heidelberg, New York, Tokyo, 1986. Springer-Verlag.
- [4] W.F. Ahtye. Thermal conductivity in vibrationally excited gases. *Journ. of Chem. Phys.*, 57:5542, 1972.
- [5] R.M. Thomson. The thermal conductivity of gases with vibrational internal energy. *Journal Phys. D: Applied Phys.*, 11:2509, 1978.
- [6] E.A. Nagnibeda and M.A. Rydalevskaya. Vibrational relaxation in mixtures with rapid exchange between vibrational modes. In *Trudy TSAGI*, Moscow, 1982, p.17-29. (in Russian)
- [7] E.A. Nagnibeda and T.N. Baburina. Transport processes in polyatomic gases with vibrational relaxation. In A.E. Beylich, editor, *Rarefied Gas Dynamics 17*, New York, Basel, Cambridge, 1991. VCH, Weinheim.
- [8] E.V. Kustova and E.A. Nagnibeda. The effect of strong vibrational nonequilibrium on transport phenomena in polyatomic gases. In *Nonequilibrium Processes and their Applications 3*, Minsk, 1996.
- [9] A. Chikhaoui and E.V. Kustova. Effect of strong excitation of CO_2 asymmetric mode on transport properties. *Chemical Physics*, 216:297-315, 1997.

AEROSPACE APPLICATIONS - AA 1

ROOM PÉRÈS

FRIDAY, JULY 31, 1998

9:15

DSMC Simulation of Normal and Parallel Jet Impingements on a Flat Plate *

T. Hyakutake and M. Nishida

Department of Aeronautics and Astronautics, Kyushu University
Fukuoka 812-81, Japan

1 Introduction

A plume issuing from a thruster of a satellite to space may impinge on the satellite body, antennas and solar panels. This impingement causes problems of contamination, heat load and disturbance torque, and so on. Therefore, more detailed studies of this problem are required.

The flowfield of the impingement covers a wide range from continuum to a free molecular regime. The impingement situation therefore is a typical rarefied problem, and the continuum theory isn't applicable to such flow fields. On the other hand, the DSMC method introduced by Bird [1] has been widely used in calculating rarefied gas flow with the development of computers.

In the present paper, we have simulated normal and parallel jet impingements on a flat plate by using the DSMC method. The simulated results have been compared with the experiments of the jet impingement done by Legge [2] [3], and in additions, we have examined the influences of Knudsen number and a distance from a nozzle exit to a flat plate on the structure of the jet impingement flow field.

2 Numerical Method

In this study, two types of impingement were considered, normal and parallel impingements. The normal impingement was considered as an axisymmetric problem, and the parallel as a three dimensional problem. Molecules impinging on a flat plate suffer diffuse reflection or specular reflection. In the case of the diffuse reflection, the temperature on the flat plate is assumed as equal to the reservoir temperature. We could exactly determined the nozzle exit conditions by calculating from the upstream of the nozzle exit. Downstream conditions

are assumed to be vacuum conditions. In the case of axisymmetric problem, molecules cross the axially symmetric line suffer specular reflection.

The range of z_N/r^* , where z_N is the distance from the nozzle exit to the flat plate and r^* the radius of the nozzle exit (see Fig.1), is from 5 to 20, and the range of the Knudsen number is from 5.0×10^{-2} to 6.04×10^{-3} in order to compare with Legge's experiments. [2] [3]

The collisions of molecules are simulated using the variable hard sphere (VHS) model [4] for nitrogen. Energy exchange between translational and rotational modes is controlled by the Borgnakke-Larsen statistical model. [5]

3 Results and Discussion

In the case of a normal impingement, a good agreement between the present DSMC results and Legge's experiments was obtained for the wall pressure and shear stress distributions at $Kn=6.04 \times 10^{-3}$ and $z_N/r^*=20$. However, as becoming far from the axis, it was seen a discrepancy between the present results and Legge's experiments for the pressure distribution. That means Legge's experimental condition is non-zero background pressure, whereas the present downstream conditions are vacuum conditions. Compared with Legge's empirical law [3], the maximum of the pressure was larger than that of the empirical law, and came close to the free molecular theory. In the case of $z_N/r^*=5, 10$, the calculated results also were same as the results of $z_N/r^*=20$ (not shown in this abstract).

Next, a parallel impingement was calculated. The comparison of the present results with Legge's experiments and empirical law for pressure distribution on the flat plate is shown in Fig.2, where P_0 is the reservoir pressure and P_i the pressure on the flat plate. As shown in Fig.2, even in a more rarefied regime, the DSMC result agrees well with Legge's experiments and empirical law, and the

*Abstract 4496 submitted to the 21st International Symposium on Rarefied Gas Dynamics, Marseille, France, July 26-31, 1998

maximum of the pressure on the flat plate is found at $x/z_N \approx 0.8$. The pressure, however, comes close to the free molecular theory for $x/z_N < 0.1$. It is also seen that $P_i/P_0(z_N/r^*)^2$ is independent of the distance from the nozzle exit to the flat plate. Therefore, we may mention that the Legge's empirical law can be applied in a wide range.

Figure 3 illustrates the shear stress distribution on the flat plate in the case of the parallel impingement. Since the present DSMC calculation used more rarefied flow conditions than Legge's experimental conditions, the present result is close to the free molecular theory. And the maximum of the shear stress on the flat plate is found at $x/z_N \approx 1.0$.

4 Conclusions

The DSMC simulation of normal and parallel jet impingements on a flat plate yielded the following conclusions: The present results agreed well with Legge's experiments and empirical law for the pressure distributions on the flat plate, whereas the present result and Legge's ones show a qualitatively good agreement for the shear stress distributions.

It may be mentioned based on the present results that the Legge's empirical law is applicable in wide ranges of $z_N/r^* = 5$ to 20 for the normal impingement and $z_N/r^* = 5$ to 10 for the parallel impingement.

References

- [1] Bird G.A., *Molecular Gas Dynamics and the Direct Simulation of Gas Flows*, Clarendon Oxford, 1994.
- [2] Legge, H., *Shear Stress and Pressure in Plume Impingement Flow*, Rarefied Gas Dynamics, Vol.I, pp.523-538, 1986.
- [3] Legge, H., *Plume Impingement Forces on Inclined Flat Plate*, Rarefied Gas Dynamics, pp.955-962, 1990.
- [4] Bird G.A., *Monte-Carlo Simulation in an Engineering Context*, Progress in Astronautics and Aeronautics, Vol.74, pp.239-255, AIAA, 1981.
- [5] Borgnakke, C. and Larsen, P. S., *Statistical Collision Model for Monte Carlo Simulation of Polyatomic Gas Mixture*, Journal of Computational Physics, Vol.18, pp.405-420, 1975.

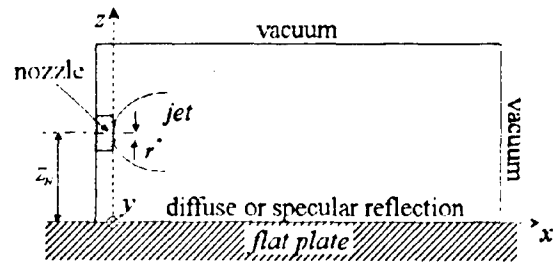


Figure 1: Calculation field

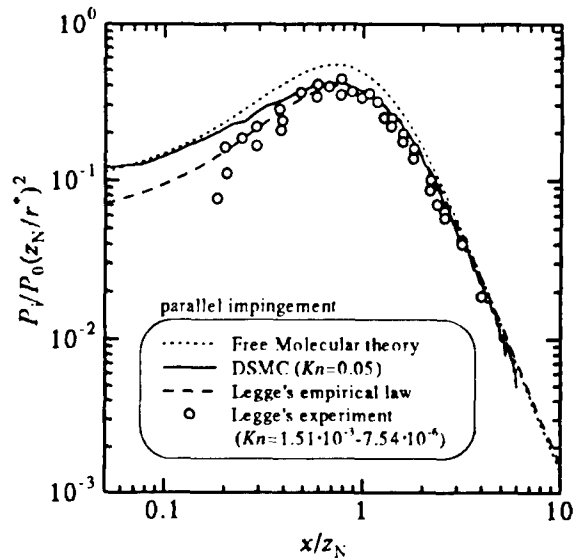


Figure 2: Pressure distributions on a flat plate

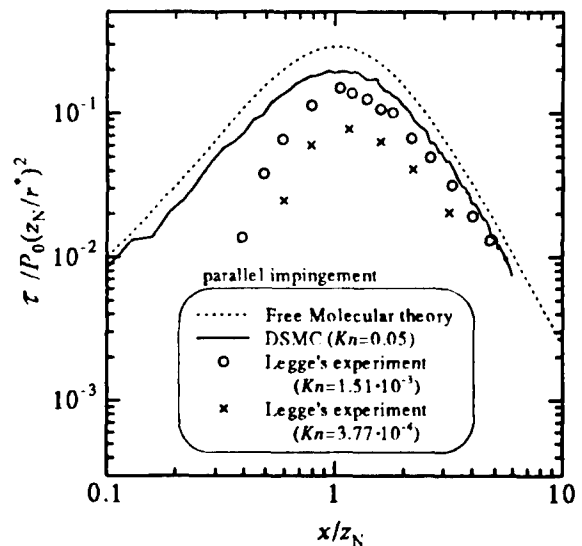


Figure 3: Shear stress distributions on a flat plate

Characteristics of Supersonic Expansion from Polygonal Orifices with Convex and Concave Corners *

K. Teshima

Dept. Industrial Arts Ed., Kyoto Univ. of Education, Kyoto, Japan

1 Introduction

Although the axisymmetric expansion from a circular orifice has been studied well, literatures of expansion from non-axisymmetric orifices are still limited. Dupeyrat[1] made experiments with long slit orifices and showed the non-isotropic expansion in two- and three-dimensional spaces. Beylich[2] measured three dimensional density profiles of jets issuing from rectangular orifices with small aspect ratios. The present author[3,4,5] showed detailed three dimensional structure of jets from a triangular and a square orifice as well as from rectangular orifices by visualization of different jet cross sections using a laser induced fluorescence (LIF) technique.

In the present study in order to deduce general characteristics of the expansion from non-axisymmetric orifices, regular n -polygonal orifices with $n=6,8,12$ are examined. In addition to these polygons which have convex corners, regular polygons with both convex and concave corners, such as pentagram, hexagram and octagram are tested.

2 Experimental

Room temperature nitrogen was expanded through sonic orifices with the polygonal shapes. The stagnation pressure p_0 was ranged from 50 to 400 Torr and the expansion chamber pressure p_∞ was adjusted so as the pressure ratio p_0/p_∞ was kept 10 to 200. Various jet cross sections were visualized using the LIF technique[6].

The orifices were made of 1 mm thick brass plate and were manufactured using a normal lace. However, the accuracy were rather good and the roundness of the corners was less than 1/100 of the side length. The equivalent orifice diameter ranged 2 - 3 mm.

3 Results and Discussion

In Fig.1 jet cross sections with regular n -polygonal orifices with $n=3,4,6,8,12$ are shown. Projections in the directions normal to the sides of the orifice geometry can be seen for all the orifices. These projections are gas jets directed outward and split into two. Each of this outward jet forms a vortex pair with the jet from the neighboring side. These vortex pairs seem to be strong enough to stabilize the shear flow in the jet boundary. Due to the expansion normal to the orifice sides the jet cross section is seen as if the jet axis has rotated. The rotation angle is π/n for all the polygons. Since for rectangular orifices it was 90° [5], then if we define $n=2$ for the rectangular shape the formula for the rotation angle can be also applicable.

In Fig.2 jet cross sections with a hexagram orifice are shown. The expansion at the concave corners is faster and the expansion at the convex corners is slower than other regions; the gas expands along the exit wall of the orifice at the convex corners as can be seen in the photograph at $x = 0$. Due to the faster expansion of the jets outward in the directions of the concave corners the jet cross section becomes hexagonal with its axis rotated 30° . The outward jet projection does not split and interact stronger with either of neighbors and forms a vortex pair. The side length of the jet core between the vertices from which the vortex pair originates becomes shorter than the other; the jet core has three long sides and three short sides. Due to the geometrical symmetry the pairing of the vortices changes time to time with a slight fluctuation in the flow condition. Since the photograph was taken as a time-integrated image, these two different cross sections are exposed in Fig.2. The similar phenomena were observed with the pentagram and octagram orifices. The rotation angle of the jet cross section can be also described by π/n , if we define n is the number of the concave corners.

*Abstract 4641 submitted to the 21st International Symposium on Rarefied Gas Dynamics, Marseille, France, July 26-31, 1998

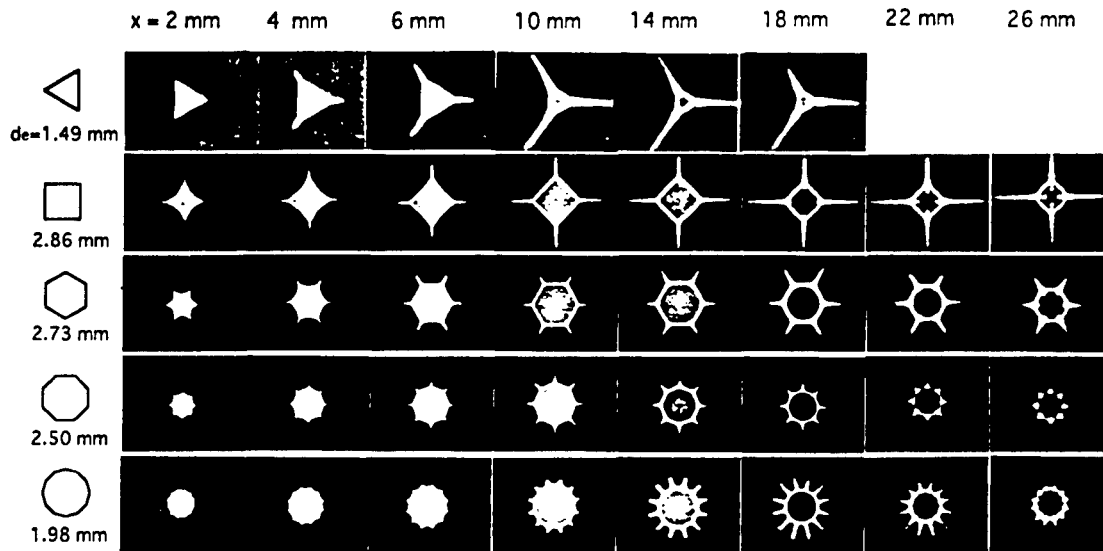


Figure 1: Visualized cross sections of jets issuing from regular n -polygonal orifices with $n=3,4,6,8,12$. x is distance from the exit of orifice.

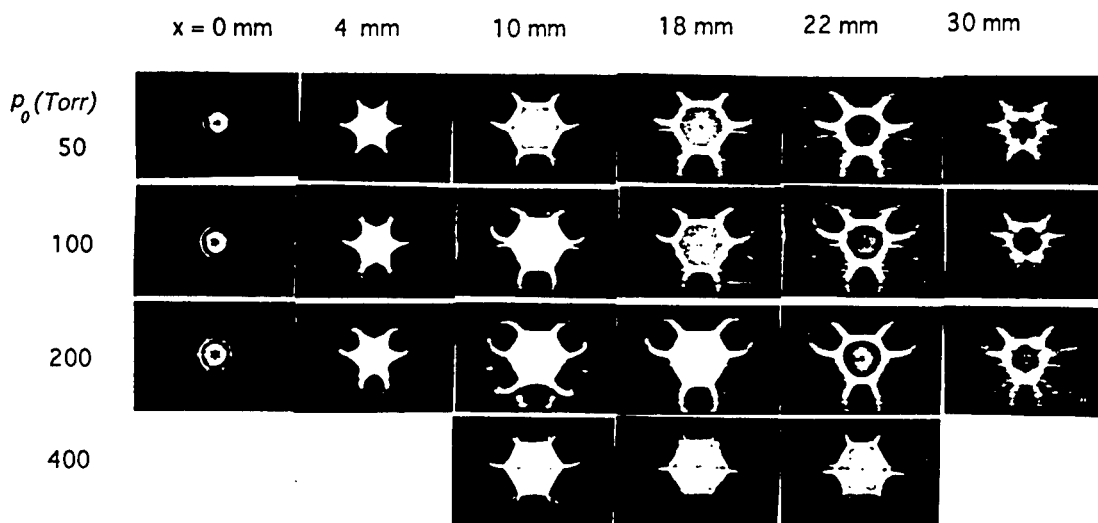


Figure 2: Visualized cross sections of jets issuing from a hexagram orifice.

References

- [1] Dupeyrat G., *Two-and Three-Dimensional Aspects of a Freejet Issuing from a Long Rectangular Slit*, Rarefied Gas Dynamics, AIAA, New York, 1979.
- [2] Beylich A., *Struktur von Überschall-Freistrahlen aus Schlitzblenden*, Zeit Flugwiss. Weltraumforsch. 3 1979.
- [3] Teshima K. and Nakatsuji H., *Structures of Freejets from Slit Orifices*, Rarefied Gas Dynamics, Teubner, Stuttgart, 1986.
- [4] Teshima K., *Two-Dimensional Focusing of a Supersonic Free Jet by a Rectangular Orifice*, Phys. Fluids 30 1987.
- [5] Teshima K., *Three-Dimensional Characteristics of Supersonic Jets*, Rarefied Gas Dynamics, Beylich A ed. VCH Verl. 1991.
- [6] Teshima K., Moriya T. and Mori T., *Visualization of a Free Jet by a Laser Induced Fluorescence Method*, Tran. J. Jpn. Soc. Aeron. & Space Sci. 1984.

Three Dimensional DSMC Calculation of Interacting Flowfield in Two Parallel Underexpanded Jets *

M. Usami¹, K. Teshima²

¹ Mie University, Tsu, Japan

² Kyoto University of Education, Kyoto, Japan

The three dimensional interacting flowfield in two parallel axisymmetric underexpanded jets is simulated by the DSMC method. The single free jet has been already calculated by the authors in an axisymmetric flowfield[1] where a cell volume is set larger as its radial distance increases from the jet axis so that each cell includes an enough number of molecules to calculate intermolecular collisions. In the three dimensional flowfield, on the other hand, every volume of cell is very small and it is not easy to obtain the optimum cell network for the DSMC method in the condition of limited computer resource. In the present calculation the upstream flowfield of each orifice is assumed to be axisymmetric, and only the downstream of the orifice is managed to be three dimensional, although the downstream flowfield is restricted one fourth of the full flowfield by a symmetrical assumption as shown in Fig.1. Before calculation of the plume-plume in-

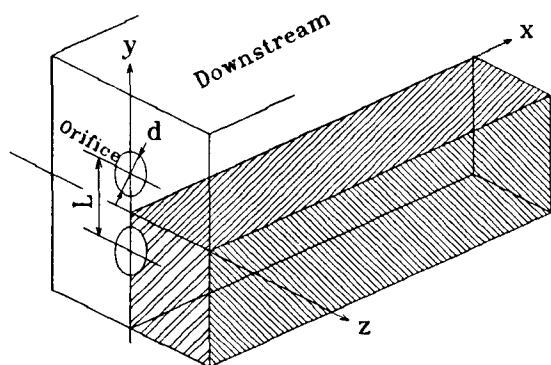


Figure 1: Downstream region of calculation

teraction, a single free jet is simulated both in an axisymmetric flowfield and in a three dimensional flowfield in order to confirm whether a satisfying three dimensional cell network is attained or not.

* Abstract 4672 submitted to the 21st International Symposium on Rarefied Gas Dynamics, Marseille, France, July 26-31, 1998

The conditions of calculation are: $1/Kn = 2500$, where Kn is the Knudsen number based on the mean free path λ of the upstream stagnation and the orifice diameter d ; $p_0/p_1 = 50$, where p_0 is the stagnation pressure and p_1 is the background pressure; and distance between centers of two orifices $L = 2d$. The VHS molecular model for argon and the null-collision scheme for intermolecular collisions are adopted. The typical size of the upstream domain is $0.75d \times 0.75d$ (axisymmetric) and that in the $1/4$ downstream is $15d \times 4d \times 4d$ (Fig.1). The diffuse reflection is assumed on the surface of the orifice. Large cell dimensions independent of the local mean free path are used in order to simulate the whole jet structure in this study. Molecules entering through the upstream boundary are generated using the Maxwell distribution with some flow velocity normal to the boundary. On the other hand, those through the downstream boundary are generated by the Maxwellian at the background pressure without flow velocity. The number of simulated molecules, dealt with simultaneously in a computer, is about 5×10^6 and the number of cells is also about 5×10^6 .

Figures 2 to 6 indicate the DSMC results for the interaction of two circular parallel jets for argon, where two orifices through which each jet flows out have the same diameter. Figure 2 is a profile of density normalized by the stagnation density ρ/ρ_0 observed on the $x-y$ plane ($z = 0$). Figures 3, 4, and 5 are profiles of axial flow velocity u/c_{m0} , temperature T/T_0 , and Mach number M on the plane, respectively, where c_{m0} is the most probable molecular speed in the stagnation and T_0 are the stagnation temperature. The secondary jet-cell that is formed with two barrel shocks of the two primary jets can be seen clearly in the middle between the jets in Fig.6 (Mach number contour). These two jets approach each other as they proceed to the downstream and finally they merge into one jet. This fundamental flow structure is well simulated in comparison with the flow visualization in Fig.7,

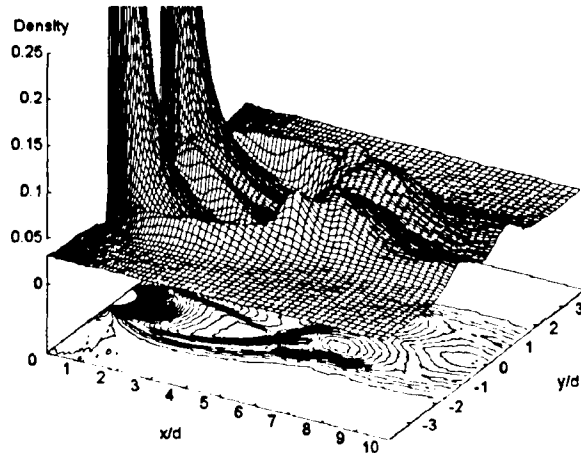


Figure 2: Density

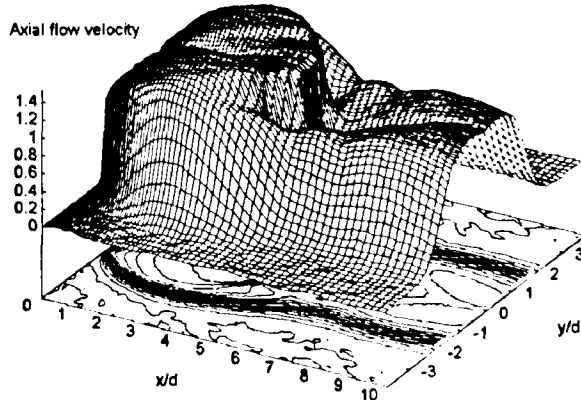


Figure 3: Axial flow velocity

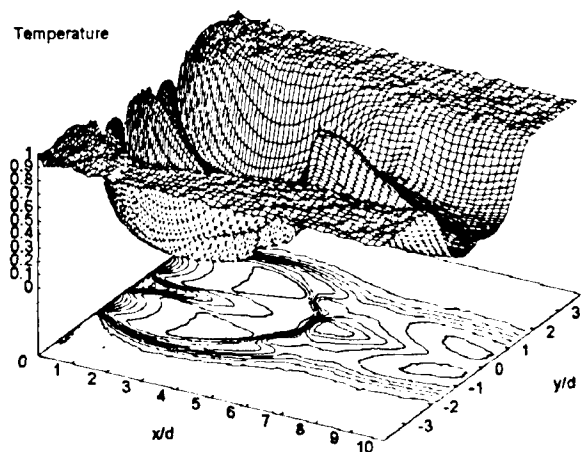


Figure 4: Temperature

which is obtained by the laser induced fluorescence technique in the same condition of the DSMC calculation.

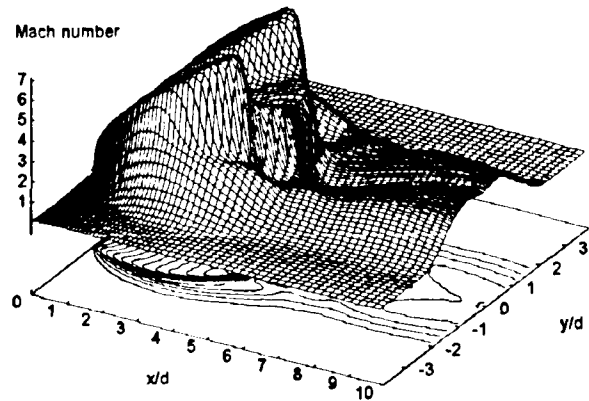


Figure 5: Mach number

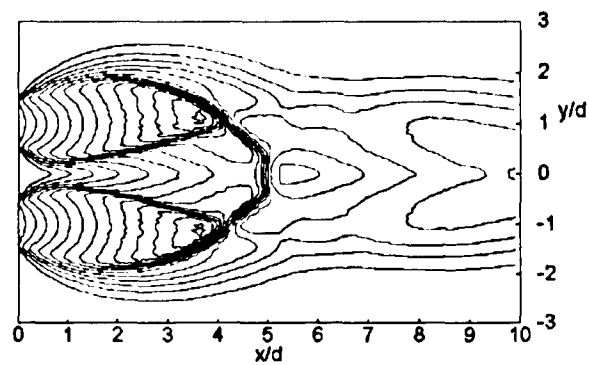


Figure 6: Mach number contour

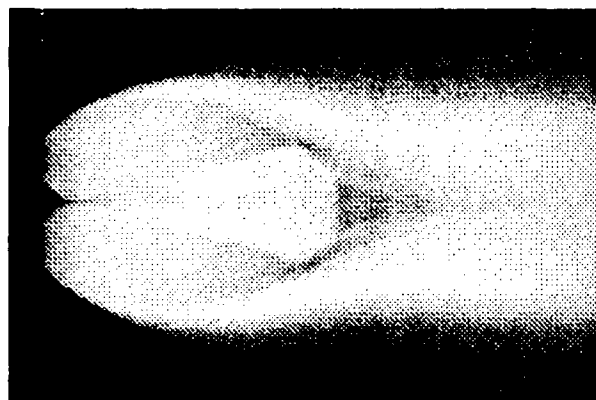


Figure 7: Flow visualization by LIF

References

- [1] Teshima K., Usami M., An Experimental Study and DSMC Simulation of Rarefied Supersonic Jets, *Rarefied Gas Dynamics* 20, pp.567-572, 1997.

Influence of the Angle between Nozzle Axis upon Flow pattern of Two Equally Initially Opposing Underexpanded Jets *

I.V. Shatalov¹, E.I. Sokolov¹, V.S. Favorsky²,

¹ Baltic State Technical University, Saint - Petersburg, Russia

² Siberian Aerospace Academy, Krasnojarsk, Russia

Some regimes of the interaction of two equal opposite underexpanded rarefied jets were described in [1]. Boundaries of their existence were determined as functions of nozzle-to-nozzle distance L and jet rarefaction criterion Re_L with M_e , n and γ fixed. In this paper, angle between nozzle axis is added into the range of controlled flow parameters. Experiments were conducted in the vacuum chamber equipped with balance mechanisms, density and pressure probes and spark visualization. This facility was described in details in [1]. Jets of cold air were investigated in the following range of parameters: $M_e = 1$, $D_e = 2.8 \text{ mm}$, $Re_L = Re_c(P_o/P_\infty)^{-1/2} = 100 \div 900$, $n = P_e/P_\infty = 71.28$, $L/2 = 0.5l/q = 0.5 \div 2.0$; $q = M_e r_e \sqrt{\gamma n}$; labels o, c, e, ∞ correspond to stagnation, critical, exit and ambient parameters respectively. One of nozzles was mounted on turning mechanism equipped with limb (angle measurements accuracy $\pm 0.5^\circ$). Angle between axis $180^\circ \pm \alpha$ was varied in the range of $180^\circ \pm 135^\circ$. Center of rotation was situated in the middle of the distance between nozzles. Distances from this point and each nozzle were fixed.

Experiments were conducted in the following way. Initially opposing nozzles were placed at few fixed distances correspond to some regime described in [1] at Re_L and n chosen, then variations of angle α at constant speed were made.

As example of data obtained, some results for the case $Re_L = 150$ are described here. Opposite interaction at distance $L/2 = 0.57$ corresponds to longitudinally symmetrical regime with flat interface. During small variations of α (up to 30°) one may observe structure with symmetry related to the plane interface inclined at bisector angle to the initial axis (Fig.1, A). Then, jump-wise transition to non-symmetrical structure was realised. Visible form of central shock of one jet is changed near

triple point situated more closely to bisector plane; wave structure of another jet seems not disturbed and has the same form as at smaller angles (regime A, Fig.1, B). Fan jet originated in interaction of two axisymmetric ones has an inclination of approximately 45° towards undisturbed jet. The interface is not already plane. Deformations of wave structures described above are not stable: non-regular jump-wise transition to "mirror structure" is realised with period between part of second to tens seconds. It must be mentioned experiments with rigid flat plate placed into the jet at the equivalent conditions does not manifest any unsteady effects.

When α became to the value near 45° , period of the described above changes in wave structure decreased and become regular. One may see two limit positions of shock inside both jets and fan resulting jet. Central shock in far position looks like Mach disk of undisturbed jet. In this case, oscillations of whole flow pattern seems are quite different from observed in axially symmetrical opposing jets. In this last case, interface is stable, both shocks moves simultaneously off and to the interface at equal but opposite speeds (counterphase oscillations). In described case of inclined axis, both shocks and the interface move at the same side with same speed (sinphase oscillations, Regime B; Fig.1, C). Period of self - oscillations decreases with angle growing. When α is about 80° , stable wave structure with planar symmetry is observed (Fig.1, D).

When initially opposing jets are placed at distance corresponds to self-oscillations ($L/2 = 0.73$, [1]) they are observed up to angles about $20^\circ - 30^\circ$, then stable structure with planar symmetry is observed. It replaced by regime A at angles between $29^\circ - 48^\circ$, and regime B at angles $48^\circ - 69^\circ$. Finally, stable wave structure with planar symmetry is observed.

When initially opposing jets were placed at larger distance, regime A disappeared in the range of ones observed with angle α growing. Sequence of regimes

* Abstract 5176 submitted to the 21st International Symposium on Rarefied Gas Dynamics, Marseille, France, July 26-31, 1998

is following: stable skew-symmetric flow exists at angles $0^\circ - 11^\circ$, counterphase oscillations of decreasing frequency exist at angles between $11^\circ - 30^\circ$, stable wave structure with planar symmetry is observed when angle α lays in the range $30^\circ - 41^\circ$, then regime B realyses ($\alpha = 41^\circ - 59^\circ$). Stable wave structure with planar symmetry exists at all lower angles.

Flow with weak self - oscillations studied in details in jet-flat plate interaction [2] ($L/2 = 1.73$) exists at corresponding distances and angles up to 30° ; regime B realyses at angles between $30^\circ - 60^\circ$. Except it, some other non- stationary flow pattern may occur at these angles. This flow looks like type C1 inside opposite jets [1] when first cell of one jet is undisturbed but central shock of other jet oscillates; disturbed and undisturbed cells may suddenly change in non-regular way.

The last flow pattern described in [1] is one with longitudinal asymmetry. In this flow the interface may also suddenly replace from one to another nozzle. This type of flow exists at appropriate L values and angles up to $4^\circ - 5^\circ$. When angle growing, period of replacement decreases with transition to regime B. At angles of $40^\circ - 42^\circ$ and more stable wave structure with planar symmetry is observed.

All named above regimes replaced each other in described order at all rarefactions investigated, but quantitative boundaries of them are depend on Re_L . All they were observed at negative but equal by absolute values of angle α . It prove that effects observed at low angles are not a result of non-accuracy of nozzle position.

Data of investigations of wave structures generated in opposing inclined supersonic jets are compared with described earlier in [3].

The data of an influence of rarefaction upon amplitudes and frequencies for some regimes are presented in comparison with similar results in jet-plate interaction. Some reasons related to the problem of interface stability are discussed, too.

References

- [1] Sokolov E.I., Shatalov I.V., *Skew - Symmetric Wave Structures in Two Opposing Coaxial Rarefied underexpanded jets*, Proceedings of the 20-th Int. Symposium on Rarefied Gas Dynamics, Beijing, 1996 (to be published).
- [2] Favorsky V.S., Savin A.V., Shatalov I. V., Sokolov E. I., *Rarefaction Effect on the*

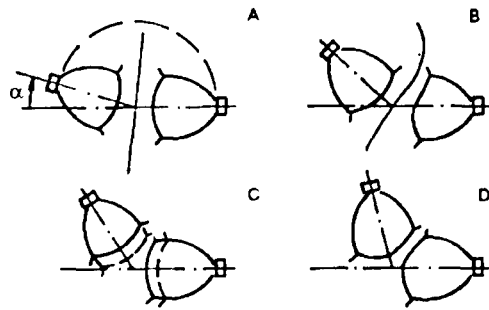


Figure 1:

Non - Stationary Underexpanded Supersonic Jet/Infinite Flat Plate Interaction, Proceedings of the 17-th Int. Symposium on Rarefied Gas Dynamics, Aachen, pp. 979-986, 1990.

- [3] Fujimoto T., Ni-Imi T., *Three - Dimensional structures of interacting free jets*, Proceedings of the 16-th Int. Symposium on Rarefied Gas Dynamics, Pasadena, CA, Progress in Astronautics and Aeronautics, V.116, pp. 391-406, 1988.

Flow Properties of a Free Molecule Micro-Resistojet for Small Spacecraft Applications *

A.D. Ketsdever¹, D.C. Wadsworth², S.E. Vargo³, E.P. Muntz³

¹Propulsion Directorate, ²Hughes STX,

Air Force Research Laboratory, Edwards AFB, CA USA

³Dept. of Aerospace Eng., Univ. of Southern California, Los Angeles, CA USA

1 Introduction

Interest in low cost space operations and exploration has encouraged the investigation of small satellite constellations which enhance the performance of tasks previously performed by a few much larger spacecraft. Satellite constellations consisting of several spacecraft with masses between 0.01 and 100 kg will be used for various missions [1]. The growing trend towards the use of large numbers of small spacecraft operating in local clusters or constellations has created a critical requirement for low power, efficient propulsion systems.

There is a growing realization that, in many cases, microthrusters will not be simply scaled down versions of present thruster systems. For example, to maintain efficiency at small scales for chemical thrusters requires a significant increase in operating pressure to maintain equivalent levels of frozen flow and viscous losses which may be incompatible for MEMS valves. Typical nozzle expansions require throat diameters on the order of tens of microns which are easily plugged by particulates [2]. Therefore, there is a viable requirement for novel microthrusters which, from a systematic point of view, offer several benefits over conventional, scaled down versions of existing thrusters.

A free molecule micro-resistojet (FMMR) thruster concept has been developed which offers several distinct advantages over conventional microthruster concepts for attitude control and station keeping maneuvers. The FMMR combines microelectromechanical systems (MEMS) fabrication techniques with simple, lightweight construction as shown schematically in cross section in Fig.1. The FMMR consists of a polysilicon thin film heating element at a temperature T_w and a long expansion slot. A

slot is chosen as an advantage over a small nozzle expansion because of the possibility of catastrophically plugging a small orifice (typically on the order of 10 μm in diameter) by contaminants.

In the case of the FMMR, the characteristic dimension defining free molecule flow is taken as the slot width, w . The design requirement is to arrange that the last surface contact by a molecule before it exits through the slot is with the heated surface. Although the free molecule condition sacrifices thruster performance over an ideal continuum expansion, the added benefits of simple construction, reduced risk of nozzle plugging, reduced propellant storage pressure, and simplified valve requirements make the FMMR attractive for several mission requirements.

The figure of merit for thruster performance is the specific impulse (I_{sp}) or generated thrust per unit propellant mass flow [3]. In free molecule flow, the specific impulse varies as $(T_o/m)^{1/2}$ where T_o is the propellant gas stagnation temperature and m is the propellant molecular mass. The ratio of the specific impulse for limit expansion through an ideal nozzle to that for free molecule flow through a slot depends on the propellant but is approximately two.

In the present problem, we use parametric, direct simulation Monte Carlo (dsMC) [4] numerical simulations to measure the enhancement of thrust made possible by local / differential surface heating of the rarefied propellant gas in a relatively easily-fabricated and robust MEMS structure. The simple one-dimensional, stationary gas, free-molecular results used in this study are expected to be useful in basic design, however, the actual micro-resistojet involves multidimensional transitional rarefied gas flow, and more sophisticated analysis methods are required for accurate performance predictions.

*Abstract 6031 submitted to the 21st International Symposium on Rarefied Gas Dynamics, Marseille, France, July 26-31, 1998

2 Results

Fig. 2 shows typical flowfield results for the nominal case ($T_w = 600\text{K}$, $T_o = 300\text{K}$) oriented in the horizontal direction. The contours consist of raw data, with each pixel corresponding to a flowfield cell, and give an indication of grid resolution. The upper half of the figure shows translational temperature contours. At this rarefaction, slip phenomena are expected to be large. This feature is confirmed by the peak temperature in the gas near the pedestal remaining much lower than the pedestal wall surface temperature. The lower half of the figure shows axial velocity contours. The acceleration of the gas due to the slot expansion is evident, while near the slot wall large velocity slip occurs. These results assume that all thruster walls are fully accommodating.

A parametric study has shown the effect of the slot divergence angle on performance or specific impulse. Comparison of the axial components of slot surface pressure and shear forces indicate that the slot expansion provides net positive increment to performance for the smaller angles (40 to 60 degrees) and lengths ($250\text{ }\mu\text{m}$) considered. The relatively large shear losses indicate that for these highly rarefied flows, small expansion ratios (or short slot heights) are preferable. The limiting case of 90 degrees results in a constant width slot, where only shear losses arise, leading to poor performance. A maximum in the specific impulse is achieved near 60 degrees for a Knudsen number of approximately one, indicating a maximum in the difference between the slot surface pressure and the shear force along the slot expansion wall.

3 Conclusions

The scope of this research addresses the FMMR flowfield properties as a function of several parameters including the gas/surface interaction model, FMMR geometry, propellant stagnation temperature and pressure, and slot divergence angle. Of particular interest will be the effect of the slot expansion on thruster performance. A complete parametric evaluation of thruster performance will be presented in the final manuscript.

References

- [1] Janson, S., Helvajian, H., Robinson, E., *The Concept of Nanosatellite for Revolutionary Low-Cost Space Systems*, paper IAF-93-

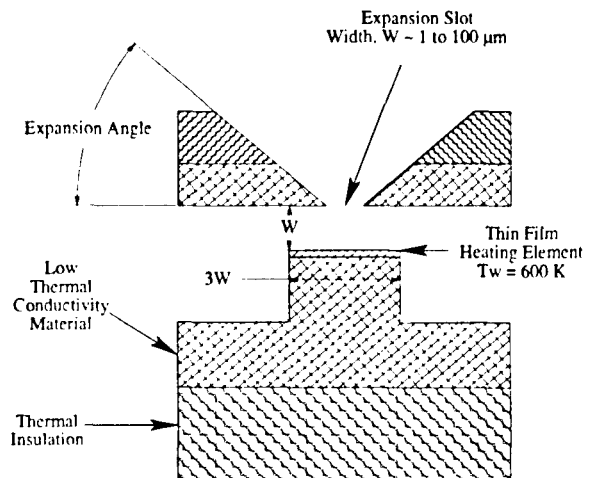


Figure 1: Free Molecule Micro-Resistojet (FMMR) conceptual design schematic

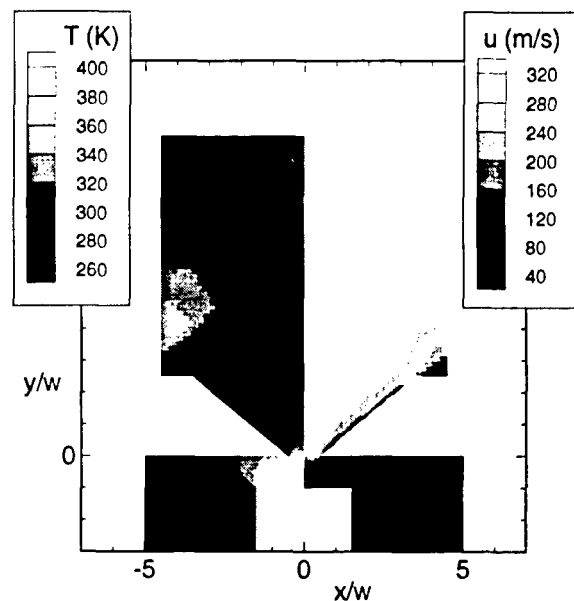


Figure 2: Translational temperature and axial velocity contours for $T_w = 600\text{ K}$ and $T_o = 300\text{ K}$

U.5.573, 44th Congress of the International Astronautics Federation, Graz, Austria, 1993.

- [2] Bayt, R., Ayon, A., Breuer, K., *Performance Evaluation of MEMS-based Micronozzles*, paper AIAA-97-3169, 1997.
- [3] Sutton, G., *Rocket Propulsion Elements*, 6th Ed., Wiley and Sons, New York, 1992.
- [4] Bird, G., *Molecular Gas Dynamics and the Direct Simulation of Gas Flows*, Clarendon Press, Oxford, 1994.

AEROSPACE APPLICATIONS - AA 2

ROOM PÉRÈS

FRIDAY, JULY 31, 1998

11:10

Trailing Edge Flow on the Leaside of a Flat Plate at Incidence in Low Density Supersonic Stream *

S.L. Gai, J.F. Milthorpe

University College, UNSW, The Australian Defence Force Academy
Canberra, Australia

It is well known that when a flat plate is at incidence in supersonic or hypersonic flow, depending on the flow Mach number and Reynolds number, the flow on the expansion side can separate because of the shock wave at the trailing edge. For example, Klineberg *et al.* [5] have shown that the phenomenon of separation on the expansion side is very sensitive to both Mach number and Reynolds number and that the angle at which separation starts gets larger, the smaller the Reynolds number.

Even though Klineberg *et al.* [5] discuss separation and its effects, they do not suggest any method of calculating the angle at which separation would begin. However, Brown and Stewartson [1], in their discussion of trailing edge stall, give an analytical expression for this critical angle of incidence. The expression given by Brown and Stewartson is

$$\alpha^{\dagger} \approx \left(\frac{C(M_{\infty}^2 - 1)}{Re_l} \right)^{1/4}$$

where C = Chapman-Rubesin viscosity constant

M_{∞} = Free stream Mach number

Re_l = Reynolds number based on the length of the plate

α^{\dagger} = critical angle of incidence at which separation first occurs

To check the validity of the above equation, calculations were made for the separation angle for the experimental conditions of Hulcher and Behrens [4]. The Reynolds number and Mach number in their experiments were 186000 and 6 respectively. For these conditions, the Brown-Stewartson equation above gives $\alpha^{\dagger} \approx 7^{\circ}$. In fact, Hulcher and Behrens [4] state that they found first indication of separation when the plate incidence was 8° . This is not altogether surprising because of the reasonably high Reynolds number of their experiments.

Gottesdiener [3] has shown that the expression for the upstream influence of the trailing edge derived by Stewartson [6], based on the triple deck theory, is valid at low Reynolds numbers such as are encountered in supersonic and hypersonic low density flows. It was, therefore of interest to examine the validity of the Brown-Stewartson expression above in low Reynolds number low density supersonic flow.

Experiments were therefore conducted in an open jet continuous flow low density wind tunnel which provided supersonic flow through axi-symmetric contoured nozzles. A flat plate model was designed which was relatively free from both leading and trailing edge thickness effects and was free from interference of extraneous disturbances such as pressure tubes and support sting. The plate incidence could be varied between $\pm 12^{\circ}$. Surface pressures were measured with a bank of thermistor manometers and corrected for both tube and orifice effects (Gai [2]). The flow field data were obtained by combining pitot and hot wire measurements.

The test conditions were:

$M_{\infty} = 4.02$; $p_{\infty} = 44 \text{ mTorr}$; $Re_l = 1050$;

$\lambda_{\infty} = 0.144 \text{ mm}$. The stagnation temperature was approximately equal to the room temperature.

The results showed that the flow was dominated by both leading and trailing edge interactions. Over the rear part of the plate, for both compression and expansion surfaces, close to the trailing edge, the pressures tended to approach free stream values. On the compression side, the inviscid pressures are higher than the free stream static pressure so that the trailing edge effect produces a reduction in pressures. On the expansion side, the pressure in the absence of any trailing edge interaction, is lower than the free stream static pressure so that the trailing edge effect causes an increase in pressures toward the trailing edge. These experimental results are then compared with computational results. The computer code is based on convection of

* Abstract 2541 submitted to the 21st International Symposium on Rarefied Gas Dynamics, Marseille, France, July 26-31, 1998

properties (mass, momentum, and energy) across the cells of the computational grid. The code also predicts the angle of incidence at which separation on the expansion side will first begin. This is then compared with the Brown-Stewartson prediction as well as the Klineberg *et al.* [5] data.

References

- [1] Brown S. N. and Stewartson K. , *Trailing edge stall*, J. Fluid Mech., Vol.42, p.561, 1970.
- [2] Gai S.L., *Surface pressures and their corrections for the flow past a finite length plate in supersonic low density flow*, J. Fluid Mech. , Vol.95, p.177, 1979.
- [3] Gottesdiener L. , *Experimental study of the Reynolds Number effect on the length of the trailing edge region*, Proc. 12th RGD Symp., p.1055, 1980.
- [4] Hulcher, G. D. , and Behrens, W. , *Viscous hypersonic flow over a flat plate at angle of attack with leeward boundary layer separation*, Proc. Heat Trans. & Fluid Mech. Inst. , p.108, 1972.
- [5] Klineberg, J. M. , Kubota, T. , Lees, L. , *Theory of exhaust-plume/boundary-layer interactions at supersonic speeds*, AIAA J. , Vol.10, No.5, p. 581, 1972.
- [6] Stewartson, K. , *Multi-structured boundary layers on flat plates and related bodies*, Advances in Applied Mechanics, Academic Press, Vol. 17, p. 146. 1974.

Study of the Shock Wave/Boundary Layer Interactions in Low Density Hypersonic Flow : Comparisons between flowfield measurements and numerical results *

B. Chanetz¹, R. Bur¹, T. Pot¹, D. Pigache¹, N. Gorchakova², J. Moss³, D. Schulte⁴

¹ Office National d'Etudes et de Recherches Aéronautiques, Châtillon, France

² Institute of Thermophysics, Novosibirsk, Russia

³ NASA, Langley, USA

⁴ DLR, Köln, Germany

1 Introduction

The communication deals with both experimental and numerical studies of the laminar shock wave/boundary layer interaction occurring past a hollow cylinder flare model without incidence in a Mach 10 flow. This test-case was presented at the first Europe-US High Speed Flow Field Database Workshop [1]. Thirteen numerical contributions were presented using this test-case. Indeed comparisons with wall properties constitute an important step in the validation process of any solver, since the surface pressure and heat transfer distributions are often the ultimate and main target of a predictive method. However, the sole inspection of the wall properties and some fragmentary visualizations are not sufficient to elucidate the cause of discrepancies between experiments and calculations.

Therefore this test-case is now completed by flow-field measurements performed by X-Rays detections thanks to a cooperation with the Institute of Thermophysics in Novosibirsk

Three different methods have been used to compare with the experimental results :

- a research two-dimensional Naviers-Stokes solver (NASCA) from ONERA using a finite volume approach
- a two dimensional Navier-Stokes solver (FLOW) from DLR using a finite element approach

- a Direct Simulation Monte-Carlo Solver (DSMC) from NASA, using the variable hard sphere (VHS) molecular model

2 Condition of the experiment

The experiments have been performed in the R5Ch blow-down wind tunnel at ONERA Meudon center. The contoured nozzle of revolution gives an uniform Mach 10 flow in the outlet plane under the following nominal conditions : stagnation pressure $p_{st} = 2.5 \cdot 10^5 Pa$ and stagnation temperature $T_{st} = 1050 K$ which leads to an upstream Mach number equal to $Mo = 9.91$ and a unit Reynolds number : $Re_u = 186000 m^{-1}$

The model used Fig.1 is constituted by a hollow cylinder, with a sharp leading edge, followed by a flare terminated by a cylindrical part.

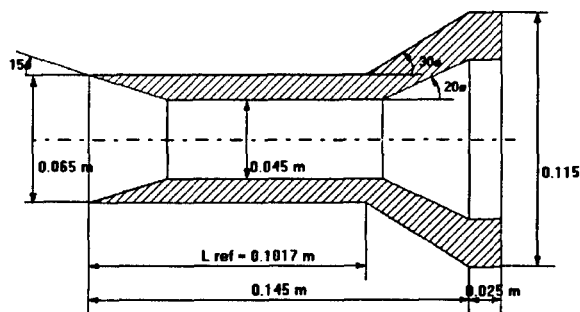


Figure 1: Hollow cylinder flare

* Abstract 6312 submitted to the 21st International Symposium on Rarefied Gas Dynamics, Marseille, France, July 26-31, 1998

3 Wall results

The surface flow was qualified by viscous coating visualizations. The separation line was detected at $X/L = 0.76 \pm 0.01$ and the attachment line at $X/L = 1.34 \pm 0.015$. The separation domain is in agreement with numerical results. Experimental pressure coefficients are also very close to numerical results. Heat-fluxes have also been measured and compared with numerical results in Fig.2. We note a slight decrease on the heat-flux evolution appearing just at the abscissa where the separation begins, which is the sign of a laminar separation.

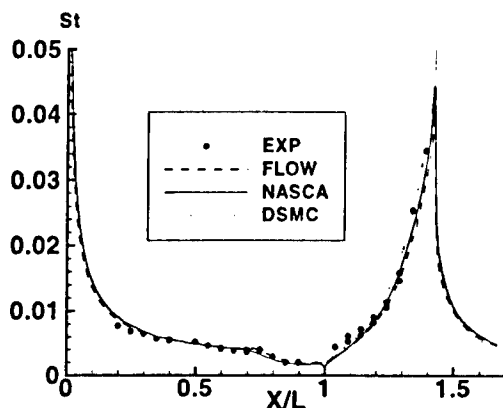


Figure 2: Longitudinal evolution of heat flux number

4 Density measurements by X-Ray detection

This technique uses an electron beam which produces electrons. The detection of the brehmstrahlung and characteristic X-rays was here employed. We used two detectors, one measuring the density reference in the free stream flow outside the boundary layer and another detector moving inside the boundary layer.

Three density profiles have been probed in September and October 1997 in the R5Ch wind tunnel. The profile $X/L = 0.3$ shown in Fig.3 is located before the separation line. At this station, the increase of density is due to the shock generated by the sharp leading edge. It is very satisfactory to observe a good agreement between numerical results and experimental ones, as far as the density peak intensity is concerned. However the shock position in altitude depends with the simulation used. It

may be a slip effect, this point will be discussed in the paper.

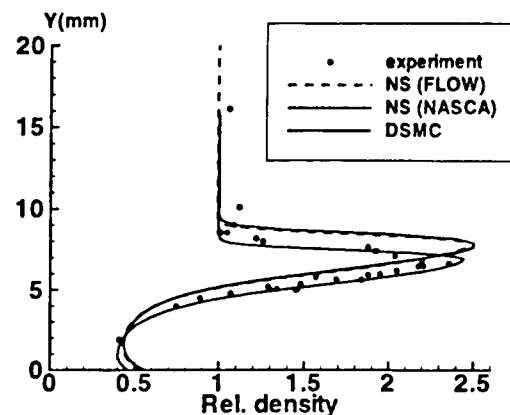


Figure 3: Density profile $X/L = 0.3$

5 Conclusion

We have devised an experiment which constitutes a precious entirely laminar test-case for the validation of computational codes without lateral effects.

Furthermore, the density in the flow field has been probed thanks to an X-rays detection technique, developed by the Thermophysics Institute of the Siberian Branch of the Russian Academy of Sciences in Novosibirsk. This technique has been used successfully on this model with the help of scientists from that Institute [see joint paper Gorchakova et al. - abstract a6311].

References

- [1] Chanetz B., Benay R., Bousquet J.M., Bur R., Oswald J., Pot T., Grasso F., and Moss J., *Study of a laminar shock/wave layer interaction in hypersonic flow : Experimental and numerical aspects.*, First Europe US High Speed Flow Field Database Workshop, Napoli 12-14 November 1997.

Fundamental Study of Shock/Shock Interference in Low Density Hypersonic Flow *

B. Chanetz¹, T. Pot¹, M. Lefebvre², P. Bouchardy²

¹ ONERA, Department of Fondamental Aerodynamics, France

² ONERA, Department of Physics, France

1 Introduction

Experimental measurements of shock/shock interactions in a hypersonic flow environment are presented in this paper. These results are obtained by using optical diagnostic techniques like Electron Beam Fluorescence visualisations (EBF) and Dual-Line Coherent Anti-Stokes Raman Scattering (DL-CARS) [1]. Besides, pressure and heat-flux measurements have been executed at the model wall. Three configurations have been tested, the reference case without interaction, with the cylinder alone and the type III and IV interaction according to Edney's classification.

2 Experimental set up

The experimental arrangement is constituted by a shock generator with a sharp leading edge located in front of a cylinder (diameter $D = 16.10^{-3}m$, spanwise length $L = 0.1 m$) lying perpendicular to the free stream flow delivered by the ONERA blow-down wind tunnel R5Ch. The facility, where stagnation temperature and pressure are 1070 K and $2.5.10^5 Pa$ respectively, produces a uniform flow at Mach number 10. The free stream static conditions are : $p_o = 6.3Pa$, $T_o = 52K$ and $\rho_o = 4.3kg.m^{-3}$. It's a full laminar flow.

3 Results

In a first step, the reference case without interferences has been considered. The detached shock region in front of the cylinder alone has been probed by DLCARS. Rotational temperature and nitrogen number density have been measured along the stagnation line in front of the cylinder. These results

are presented in figs.1 and 2 compared to a Navier-Stokes calculation.

The good agreement between calculation and experiment leads to two conclusions :

- the validity of the measurement technique
- the accuracy of the continuum approach used to solve the conservation equations for mass, momentum and energy (Navier-Stokes equations)

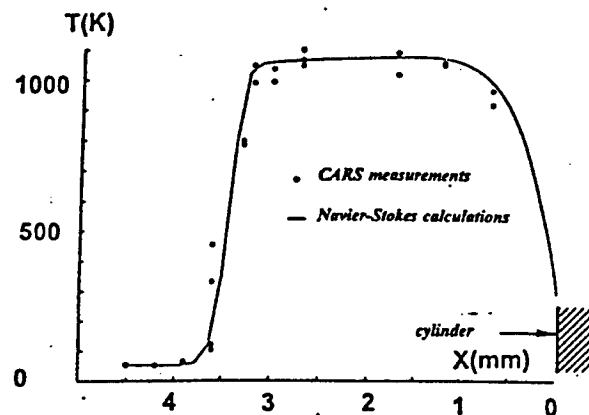


Figure 1: Evolution of temperature along the stagnation line in front of the cylinder.

In a second step, a type III shock/shock interference (fig. 3) has been studied. A slip line results from this interference. The impact of the slip line on the cylinder causes an intense pressure peak showed in Fig.5. The maximum p/p_{ref} rises up to 2.6 (p_{ref} being the pressure measured at the stagnation point in the reference case). A heat-flux peak is also measured at this location, the peak value of the ratio Φ/Φ_{ref} being also close to 2.6 (Φ_{ref} the heat-flux measured at the stagnation point in the reference case).

The third part of this work is relative to a type IV shock/shock interference. Fig.4 shows the shocks

* Abstract 6314 submitted to the 21st International Symposium on Rarefied Gas Dynamics, Marseille, France, July 26-31, 1998

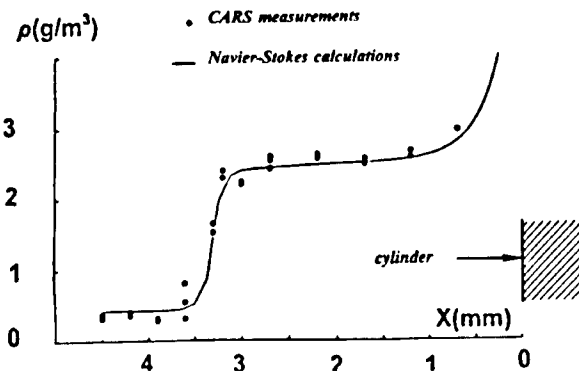


Figure 2: Evolution of specific mass along the stagnation line in front of the cylinder.

system revealed by EBF visualization. In this type IV pattern, the reattachment of the slip line is impossible on the cylinder and a supersonic jet emanates from the slip line surrounded by subsonic flows. This interference type leads to very high pressure and heat-flux peaks. As shown in Fig.5, the pressure peak measured at the impact of the supersonic jet on the model wall rises up to 6.6. The same value is obtained for the heat-flux peak. Besides

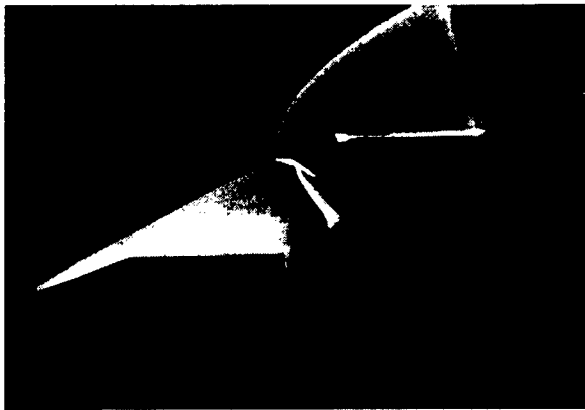


Figure 3: Visualization by E.B.F. of a type III shock/shock pattern.

wall measurements, DLCARS technique has been used to qualify the flow. Rotational temperature and nitrogen number density have been measured along 9 lines in front of the cylinder. More than 100 points were probed with DLCARS technique in the shock/shock interference region.

4 Conclusion

The complete results of the study of a type II and IV shock/shock interaction in full laminar flow will



Figure 4: Visualization by E.B.F. of a type IV shock/shock pattern.

be presented for the first time in this paper. This paper has been accepted for the ISSW21 Symposium in July 96, but not presented because of a lack of money. This experiment constitutes a well documented test-case very useful for validation of Navier-Stokes solvers and for a good understanding of the heat-transfer phenomena that take place during the reentry of hypersonic vehicles into the upper atmosphere.

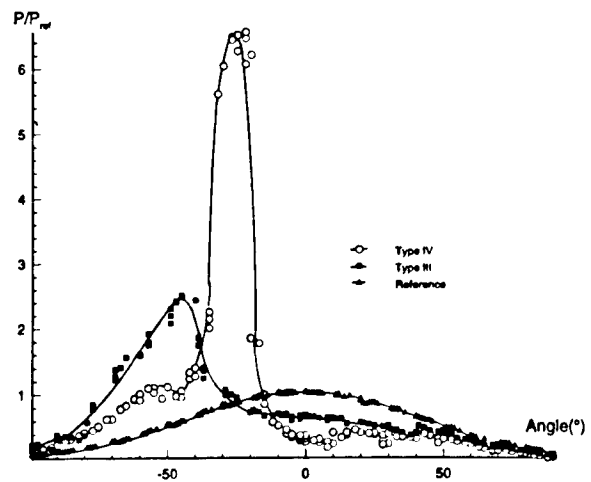


Figure 5: Evolution of pressure along the cylinder in the reference case and the type III and IV patterns.

References

- [1] Grisch F., Bouchardy P., Péalat M., Chanetz B., Pot T. and Coët M.C. *Rotational temperature and density measurements in a hypersonic flow by dual line CARS*. (1993) Appl. Phys. B56 : 14-20

Rarefied Transitional Bridging of Blunt Body Aerodynamics *

R. G. Wilmoth, R. C. Blanchard, J. N. Moss
NASA Langley Research Center, Hampton, VA, USA

Introduction

Mission analysis of high-speed planetary entry vehicles requires an extensive aerodynamic database to provide accurate analysis of trajectory dynamics, vehicle stability and landing footprint. In the rarefied transitional regime, computational methods are required to generate the database, but it is common to perform full flow simulations for only a relatively small number of conditions and then use curve-fitting techniques to provide a means for enriching the database. This is especially true in the rarefied transitional flow regime, where the flow simulations require three-dimensional Direct Simulation Monte Carlo (DSMC) analyses that may be quite expensive to perform. Therefore, rarefied transitional bridging relations are used to provide an analytical description for aerodynamic quantities that can then be used to supplement the original database [1, 2].

This paper presents results for several blunt-body entry vehicles in the rarefied transitional flow regime where bridging relations have been constructed to describe the transition from free-molecular to continuum flow aerodynamics. Predictions are given for the Viking, Stardust, and Pathfinder vehicles under entry conditions appropriate to each vehicle. A schematic showing the geometry and relative size of the aeroshell for each vehicle is shown in Fig. 1. Both Viking and Pathfinder are 70-deg half-angle blunt cone forebodies with biconic and truncated conical afterbodies, respectively, designed for direct entry to Mars at velocities of 4.5 and 7.5 km/s, respectively. Stardust is a comet sample return vehicle with a 60-deg half-angle blunt cone forebody designed for direct entry to Earth at 12.6 km/s. Viking is of particular interest because flight data exists for comparison, and good agreement is shown between DSMC predictions and the flight data for the measured drag and the measured ratio of normal-to-axial force [3]. Both Stardust and Pathfinder are statically unsta-

ble in the free-molecular regime but become stable as they approach the continuum regime, thereby posing difficulties in using conventional bridging techniques to describe the aerodynamic moments with the transitional regime [4, 5].

Computational Methods

Both axisymmetric and full three-dimensional free-molecular, DSMC, and continuum methods are used to compute the flowfields and aerodynamics for all three vehicles. Axisymmetric DSMC calculations are performed using the G2 code of Bird [6] while three-dimensional free-molecular, DSMC and Newtonian calculations are performed using the DSMC Analysis Code (DAC) and companion free-molecular/Newtonian codes described in Ref. [7].

Results

Sample predicted results for the ratio of normal-to-axial force are shown in Fig. 2 for the Viking 1 lander. Included on the figure are the measured flight data and results from a standard sine-squared bridging relation. The bridging relation fits the DSMC predictions extremely well using values of 25 and 0.002 as the Knudsen number limits for free-molecular and continuum flow respectively. Although the flight data is somewhat noisy at the higher Knudsen number, the overall agreement with the DSMC predictions and bridging relation is excellent. The full paper will present similar computational results for the Stardust and Pathfinder vehicles with emphasis on aerodynamic quantities such as pitching moment that do not always follow such simple bridging relationships (see Fig. 3). Alternate methods for bridging these quantities will be presented.

References

- [1] Blanchard, R. C., *Rarefied Flow Lift-to-Drag Measurements of the Shuttle Orbiter*, ICAS

*Abstract 6467 submitted to the 21st International Symposium on Rarefied Gas Dynamics, Marseille, France, July 26-31, 1998

Proceedings 1986, edited by P. Santini and R. Staufenbiel, Vol. II, London 1986, pp. 1421-1430.

- [2] Ivanov, M. S., Markelov, G. N., Gimelshein, S. F. and Antonov, S. G., *DSMC Studies of High-Altitude Aerodynamics of Reentry Capsule*, 20th International Symposium on Rarefied Gas Dynamics, Beijing, China, 1996.
- [3] Blanchard, R. C., Wilmoth, R. G., and Moss, J. N., *Aerodynamic Flight Measurements and Rarefied-Flow Simulations of Mars Entry Vehicles*, Journal of Spacecraft and Rockets, Vol. 34, No. 5, 1997, pp. 687-690.
- [4] Wilmoth, R. G., Mitcheltree, R. A., and Moss, J. N., *Low-Density Aerodynamics of the Stardust Sample Return Capsule*, AIAA Paper 97-2510, June 1997.
- [5] Moss, J. N., Blanchard, R. C., Wilmoth, R. G., and Braun, R. D., *Mars Pathfinder Rarefied Aerodynamics: Computations and Measurements*, AIAA Paper 98-0298, Jan. 1998.
- [6] Bird, G. A., *The G2/A3 Program Users Manual*, G.A.B. Consulting Pty Ltd, Killara, N.S.W., Australia, Mar. 1992.
- [7] Wilmoth, R. G., LeBeau, G. J., and Carlson, A. B., *DSMC Grid Methodologies for Computing Low-Density Hypersonic Flows About Reusable Launch Vehicles*, AIAA Paper 96-1812, June 1996.

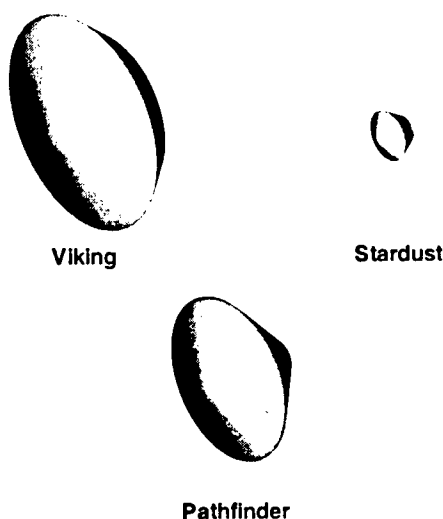


Figure 1: Blunt-Body Entry Vehicles.

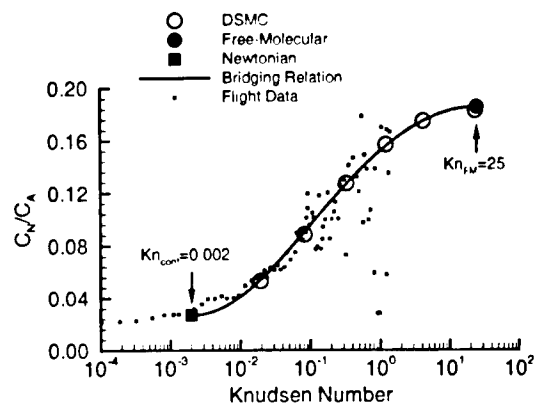


Figure 2: Comparison DSMC, Bridging Relation, and Flight Data for Viking 1.

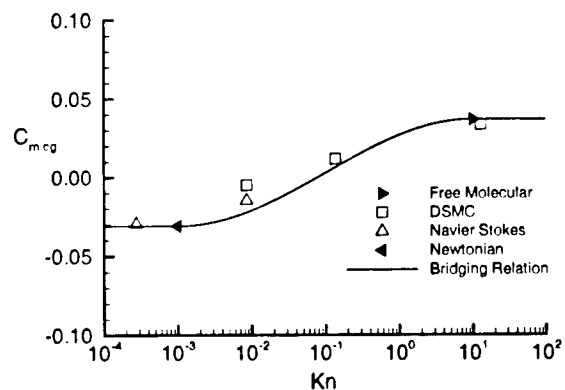


Figure 3: Comparison of Pitching Moment Bridging Relation to DSMC for Stardust Sample Return Capsule.

AEROSPACE APPLICATIONS - AA 3

ROOM PÉRÈS

FRIDAY, JULY 31, 1998

14:35

The Influence of Relaxation on the Transition from Regular to Mach Reflection *

S. F. Gimelshein, M.S. Ivanov

Computational Aerodynamics Lab., ITAM SB RAS, Novosibirsk, Russia

1 Introduction

Two types of shock wave reflection are possible in steady flows, regular and Mach reflection. There are two principal criteria of the transition between these reflections. The first is the detachment criterion that determines the upper boundary of existence of regular reflection (RR), and the second is the von Neumann criterion that states the bottom limit where Mach reflection (MR) may exist. For an angle of incident shock wave, α , that lies between these boundaries, in a so-called dual solution domain, both Mach and regular reflections are theoretically possible. The difference between the transition angles, corresponding to the detachment, α_D , and von Neumann, α_N , criteria, is rather large and approaches 10 degrees when the Mach number is more than 5.

The dependence of transition angle on the direction of shock angle variation was actively studied from mid 70s to mid 80s, mostly by experimental methods. The results of such experimental investigation were summarized in [1] as follows: transition from RR to MR and back in steady flows takes place according to von Neumann criterion; in the dual-solution domain RR is unstable and a hysteresis effect, i.e. a dependence of reflection type on the direction of the incidence angle variation, was not observed. However, new numerical studies [2] revealed a possibility of such a hysteresis to exist. Moreover, the hysteresis was experimentally established [3], though under conditions different from experiment [1]. Further numerical investigations of the hysteresis phenomenon were performed in [4] where this effect has been examined by kinetic (DSMC) and continuum (Euler equations) methods.

The numerical studies that were carried out in the field of steady shock wave reflection phenomena are limited to the case of one-species non-reactive gas.

As for the flow of chemically reactive gas mixture, this topic presently has not been studied yet. This paper will therefore fill the lack of information and knowledge on steady shock wave reflection in reactive flows.

2 Objective and approach

The principal goal of this work is to study the impact of high-temperature real gas effects, i.e. excitation of vibrational mode and chemical reactions, on regular and Mach configurations and on the transition between two reflection types. A detailed comparison of results with and without real gas effects will be presented. The study of the problem of shock wave reflection in steady reactive flows has an obvious theoretical as well as practical interest that is connected to hypersonic flight of spacecraft. In fact, the paper is a first attempt to examine this problem.

The main approach used here is the Direct Simulation Monte Carlo (DSMC) method. An important advantage of this method is that it takes account of viscosity, and the thickness of the shock waves is physically grounded. Lately this method has been commonly used for calculating near-continuum flows as an alternative for the finite-difference approach. Moreover, the DSMC models for real gas effects proposed lately, enable us to obtain reliable data on high-temperature flows in the near-continuum regime.

A special numerical approach combining cell and free cell majorant frequency schemes [5] of the DSMC is used in computations in order to provide an adequate space resolution in the entire computational domain. The transitions between the translational and vibrational molecular modes are simulated with the model [6] based on the quasiclassical approach, one of the most effective techniques to describe the energy exchanges between the translational and internal modes. Both vibration-translation and vibration-vibration en-

*Abstract 4831 submitted to the 21st International Symposium on Rarefied Gas Dynamics, Marseille, France, July 26-31, 1998

ergy exchanges are considered in this model. Chemical reactions are treated with the model [6] which includes the effect of vibration-dissociation coupling by using specific chemical reaction rate constants for each vibrational level.

3 Scope and results

The main topics of the work are the following.

1. *The determination of the angle of transition from RR to MR.* The computations of both one- and diatomic non-reactive gases (specific heat ratio, γ , was 1.66 and 1.4) showed that in these flows the reflection type depends on the direction of the incidence angle variation, coming from below and from above the dual solution domain. When increasing the angle, the transition from RR to MR occurs in accordance with the detachment criterion. The computed transition angles of the wedge-generated shock wave were found to be corresponding to its theoretical value α_D obtained from the inviscid gas-dynamics.

Meanwhile, vibrational excitation and chemical reactions cause a decrease of the specific heat ratio γ , and therefore a reduction of the incident shock wave angle. Relaxation effects cause curving the incident shock wave, and the transition from RR to MR is determined by the local angle of the incident shock wave near the reflection point.

2. *The problem of hysteresis phenomena* is closely connected with the first topic. As was mentioned above, a hysteresis and a dependence of the final reflection type on the initial condition was observed in the DSMC simulations of non-reactive gases. The results of computations for a gas with high-temperature real effects will be presented in the full-length paper.

3. *The influence of flow rarefaction on the shock configuration* (in particular, on the Mach stem height) is an important problem. The computations manifested a decrease of the Mach stem and an earlier transition from MR to RR when increasing the Knudsen number for non-reactive gases. Real gas effects complicate considerably this phenomenon, since the size of relaxation zone is comparable with the characteristic size of the flow even for very small Knudsen numbers.

To investigate the hysteresis effect, the incident shock angle α was changed by the wedge rotation around its trailing edge during the calculations. This was achieved by the following procedure. First, the calculation was performed for some α_0 . After the flow became stationary, the wedge

was rotated around the trailing edge so that the new wedge position generated a shock wave with the incidence angle α . When the flow became stationary in this position, the wedge was rotated again.

The studies have been performed for Mach number $M = 7.5$ and Knudsen numbers $Kn = 10^{-3}$ and $3.5 \cdot 10^{-4}$. The DSMC studies support the presence of the hysteresis effect in chemically reacting flows, i.e. of the reflection type dependence on the direction of the incidence angle variation. Real gas effects increase the angle of the transition from regular to Mach reflection. It is shown also that the dissociation reactions as well as the excitation of vibrational degrees of freedom cause a decrease of the Mach stem height; the influence of vibrations is more pronounced. More detailed data regarding all three above mentioned topics will be given in the full-length paper.

References

- [1] Hornung H.G., Robinson M.L. *Transition from regular to Mach reflection of shock waves*, Part 2. The steady-flow criterion. J. Fluid Mech., 123, 1982, 155-164.
- [2] Ivanov M.S., Gimelshein S.F., Beylich A.E. *Hysteresis effect in stationary reflection of shock waves*, Phys. Fluids 7(4), 1995, 685-687.
- [3] Chpoun A., Passerel D., Li H., Ben-Dor G. *Reconsideration of oblique shock wave reflections in steady flows*, J. Fluid Mech., 301, 1995, 19-35.
- [4] Ivanov M., Zeitoun D., Vuillon J., Gimelshein S., Markelov G. *Investigation of the hysteresis phenomena in steady shock reflection using kinetic and continuum methods*, Shock Waves 5(6), 1996, 341-346.
- [5] Ivanov M.S., Antonov S.G., Gimelshein S.F., Kashkovsky A.V. *Computational Tools for Rarefied Aerodynamics. Proc. of 17-th Symp. on RGD. Vancouver, Canada, 1994, Vol.160, 115-126.*
- [6] Gimelshein S., Gorbachev Yu., Ivanov M., Markelov G. *Statistical Simulation of Nonequilibrium Rarefied Flows with Quasiclassical VVT Transition Models*. Atlanta, 1997, AIAA Paper 97-2585.

High - Altitude Aerothermodynamics *

V.N. Gusev

Central Aerohydrodynamic Institute (TsAGI)

1, Zhukovsky str., 140160 Zhukovsky, Russia

Hypersonic high-altitude flight can be conventionally divided into the continuum, the free-molecule and the transitional regimes. In general, each of these regimes differs with respect to both the structure of the flow and the method of determining the aerodynamic and thermal characteristics. The analysis of these investigations include determination of aerodynamic and thermal characteristics of vehicles and their components, study of the interaction between hypersonic flows and surface, and jets, investigation of non-equilibrium processes, heat transfer, etc.

Interrelations between the similarity criteria and advisability of their utilization in different combinations are established while simulating hypersonic flows in wind tunnels. The possibilities of using a numerical experiment to solve the problems of simulation and determination of aerodynamic and thermal characteristics of hypersonic vehicles at flight conditions have been considered. Analysis and generalization of the experimental and calculating data have been performed, their comparison with the flight data has been given. Peculiarities of the hypersonic vehicle configurations, their launch and reentry trajectories result in a considerable augmentation of heat fluxes applied to the whole vehicle and especially to its separate components. The presence of different physico-chemical processes in the air and on the vehicle surface complicates considerably a problem to simulate the heat transfer. The numerical experiment takes much time when such investigations are performed. Local simulation is widely used while studying the local peculiarities of the flow during the experiment which can not be determined when hypersonic flows are simulated as a whole. The examples of such investigations related to the Buran orbiter are given in the work. Investigations of a streamlined body in the near-the-wall areas take an important place at hypersonic velocities. Such physical phenomena as gas

slip, its interaction with the surface at the molecular level, catalytic and emission properties of a streamlined surface and others become important. One of the objectives of the investigations is to determine correctly the boundary conditions for the Navier-Stokes and Boltzman equations followed by their integration. Data on the characteristics obtained during the experiment, their systematization and classification for different materials are given in the work.

The work was carried out at support of the Russian Foundation for Basic Research (Grant 97-01-00577)

* Abstract 4871 submitted to the 21st International Symposium on Rarefied Gas Dynamics, Marseille, France, July 26-31, 1998

The Interaction of Opposite Supersonic Flows in Vacuum and a Background Gas *

A.A. Morozov, M.Yu. Plotnikov, A.K. Rebrov
Institute of Thermophysics, 630090 Novosibirsk, Russia

1 Introduction

The aim of this investigation was the study of collisions of opposite parallel-plane flows in vacuum and a background gas. The essential part of this work was the simulation on the molecular level of the transient structures of resulting shock waves and compressed layers in the region of the collision. The direct simulation Monte Carlo method [1] was used as an effective instrument for the study of processes with any degree of nonequilibrium. The analysis was performed for impacts of identical monatomic gases. The symmetry of the problem allowed to consider the interaction of a flow with a specular wall. The flow formed from a simultaneously started plane source. The VHS model was employed for the description of intermolecular collisions. As the units of measure, there were used the density and the temperature of the source gas at rest n_0 and T_0 , the mean free path $\lambda_0 = 1/(n_0\sigma\sqrt{2})$, and the most probable molecular thermal speed $c'_m = \sqrt{2kT_0/m}$. The computation was performed in a region of length L between the initial boundary of the source and the specular wall.

The DSMC calculation of the beginning of the molecular expansion has shown that the thermodynamic equilibrium is settled and the gas macroscopic properties remain invariable in the plane of the source after approximately 50 normalized time units. So if the computation time and the region size L are sufficiently large, one can use constant values of gas parameters at the source plane as the boundary conditions.

2 Calculations

Fig.1 shows the evolution of normalized density and temperature profiles with time for $L = 5450\lambda_0$ when gas expands into vacuum. The high temperature re-

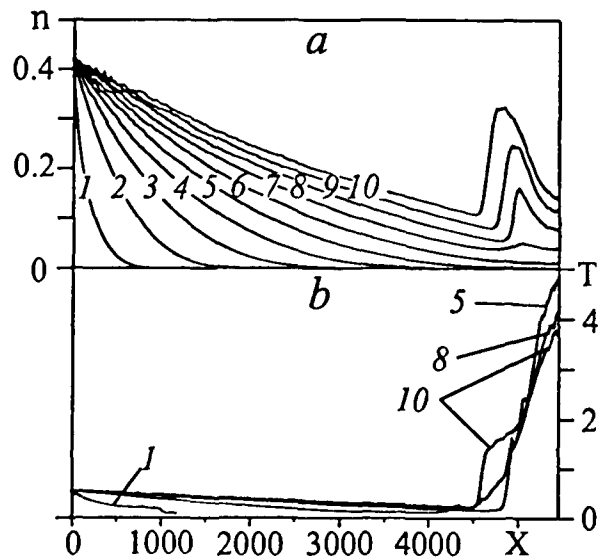


Figure 1: The profiles of the density (a) and the temperature (b) when gas expands into vacuum. Numbers 1 - 10 correspond to time moments $t = 240, 710, 1190, 1660, 2130, 2610, 3080, 3560, 4030, 4500$.

gion appeared close to the wall is due to the formed shock wave and subsequent compression on the condition of very high heat-conductivity. The transient picture of the compressed layer is characterized by strong translational nonequilibrium, which can be illustrated by temperature anisotropy.

Also, the investigation was performed when the region between the source and the specular wall is filled by the same gas as the source one with a density $n_b \ll n_0$ and a temperature $T_b = T_0$. Fig.2 presents the density and the temperature profiles for $L = 5450\lambda_0$ and $n_b = (1/230)n_0$. In this case the process of diffusion (mixing the source gas and the buffer gas) is superimposed on the process of formation of the shock waves and the compressed layer. The high temperature arisen in the vicinity of the wall is a result of the prime compression of the buffer gas enhanced by the consequent compression behind the reflected shock wave in the source gas.

*Abstract 5066 submitted to the 21st International Symposium on Rarefied Gas Dynamics, Marseille, France, July 26-31, 1998

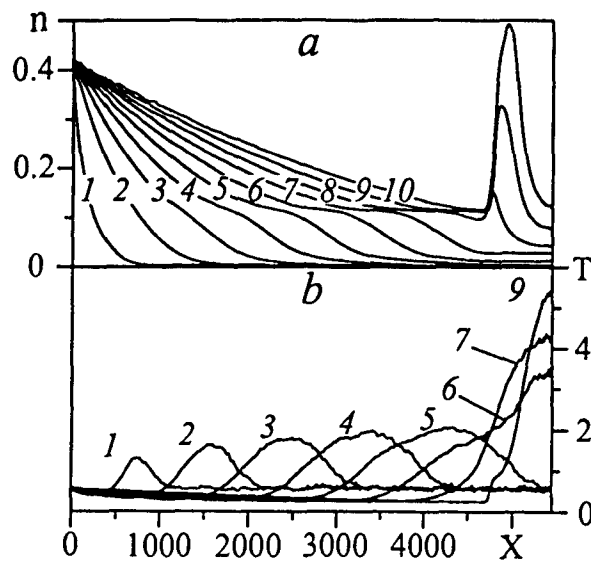


Figure 2: The profiles of the density (a) and the temperature (b) when gas expands into a background gas with $n_b = (1/230)n_0$. Numbers 1 - 10 correspond to time moments $t = 240, 710, 1190, 1660, 2130, 2610, 3080, 3560, 4030, 4500$.

The zone adjacent to the wall contains the mixture of the source and background gases at translational nonequilibrium.

3 Results and discussion

Fig.3 shows the correlation between the temperature and the density at the specular wall from the beginning of the collision up to the time when the reflected shock wave in the buffer gas comes apparently back. These calculations were performed for $n_b = (1/230)n_0$ and for different distances between the source plane and the wall. The temperature peak for $n_b = 0$ should not be taken into account because it corresponds to collisionless mixing the opposite flows at very low densities. When the density is high enough for the temperature to be considered, the temperature increase in the vicinity of the wall is much higher for the collision in a background gas than one in vacuum.

This study presents details of nonstationary formation of the shock wave structures of colliding flows and shows that it is possible to obtain very high temperatures by the collision of flows in a low density background gas.

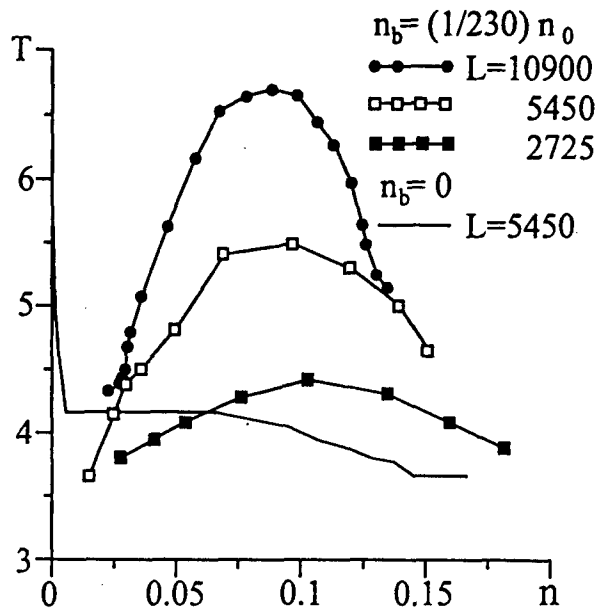


Figure 3: The correlation between the temperature and the density in the vicinity of the specular wall for the constant background gas density $n_b = (1/230)n_0$.

4 Acknowledgements

This work was supported by the Russian Foundation for Basic Research through Grant 97-01-00878.

References

- [1] Bird G.A., *Molecular Gas Dynamics and the Direct Simulation of Gas Flows*. Clarendon Press, Oxford, 1994.

Laminar-Turbulent Transition of Hypersonic, Chemically Reacting Boundary Layers *

J. Perraud, D. Arnal, F. Thivet
ONERA CERT, DMAE, Toulouse, France

1 Introduction

Laminar-turbulent transition of hypersonic boundary layers in high enthalpy flows requires the modelling of real gas effects within the boundary layer. We consider two cases, of chemical equilibrium and non-equilibrium, assuming thermal equilibrium.

2 Stability Analysis Method

The gas mixture is composed of five species (N₂, O₂, N, O, NO). The transition prediction process is based on a local, linear stability calculation. The aim is to study the propagation and development of small perturbations (order 1), added to the boundary layer stationary flow (order 0). Perturbations are of the form:

$$f = \hat{f}(y) e^{i(\alpha x + \beta z - \omega t)} e^{-\alpha_i x}, \quad (1)$$

where α_i is the local amplification rate. The mathematical model results from the linearization of the Navier Stokes, energy and species conservation equations, and equation of state. Existence of non trivial solutions is obtained pending verification of a dispersion relation $\mathcal{R}(\alpha, \beta, \omega) = 0$.

With the assumption of chemical equilibrium, transport coefficients and species concentrations are only function of two parameters, temperature and pressure. The use of a Mollier interpolating table is then possible. In this case, the stability formulation only modifies terms in the system of differential equations, without changing the rank (8) of the system. The usual resolution technique based on a fourth order Runge-Kutta integrator, which we use in case of ideal compressible flow [1], can still be used.

In case of chemical nonequilibrium, the species conservation equation is added to the system. This brings the concentration perturbations into the set

of variables, assuming that concentration fluctuations have no effect on the chemistry rates. The rank of the first order system of differential equations then rises to 16. Hopefully, extension of the previous resolution method is possible.

At chemical equilibrium, the stationary boundary layer is calculated using the code EQUI [2]. For nonequilibrium flow, the code REBECA [3] is used. Chemical reactions are represented using non-Arrhenius laws with coefficients from Gardiner's model [4]. Transport coefficients are obtained following the method by Hirschfelder *et al.* [5].

3 Results

The stability results presented on figure 1 relates to a classical Mach 10 case, with a static temperature of 350K, over an adiabatic infinitely thin flat plate. Several publications have addressed this case in the past for ideal and equilibrium flow [6], chemical nonequilibrium [7, 9] and thermochemical nonequilibrium [8].

Ideal and equilibrium gas results compare well with published data [6]. For nonequilibrium flow, our results confirms the second mode to be the most unstable. They also show the existence of an unstable third mode, as in equilibrium, which was not found in [7] and [8]. Existence of a third mode is confirmed in [9], using nonlocal stability theory. The first mode, of an oblique nature, is also computed. While it was reduced for equilibrium conditions, it is now close to the ideal gas curve. Comparisons are presented at a given X station, as in the published results. Spatial integration of these amplification rates gives the N factor, at any given frequency. Maximum value over frequency of the N factor is then used for transition prediction. These N factor curves for the two main modes will show what contribution these modes can be expected to have at transition. An original analysis of the real gas effects on transition will thus be presented in the final paper.

*Abstract 6515 submitted to the 21st International Symposium on Rarefied Gas Dynamics, Marseille, France, July 26-31, 1998

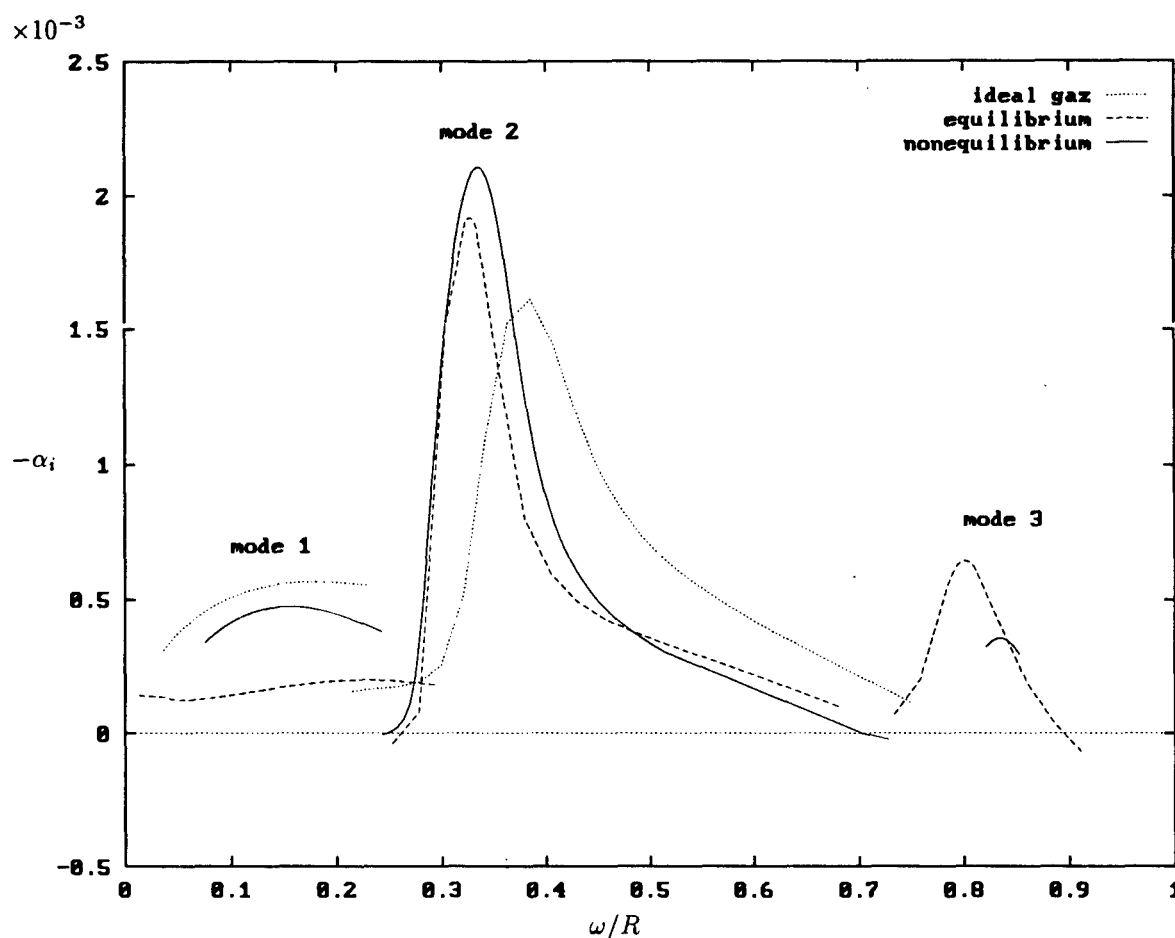


Figure 1: Spectrum of the amplification rate for a Mach 10 adiabatic flat plate ($R = 2000$, $T_e = 350$ K)

References

- [1] Arnal D., *Three-dimensional Compressible Stability Computations Using the Spatial Theory*, 5th Symposium on Numerical and Physical Aspects of Aerodynamic Flows, Long Beach, CA, USA, 1992.
- [2] Aupoix B., *Calcul des couches limites compressibles bidimensionnelles. Programmes CLIC et EQUI*, ONERA/DERAT Report No.42/5005.34, 1991.
- [3] Leclère F., Aupoix B., *Hypersonic Turbulent Nonequilibrium Reactive Flow Calculations*, ICAS 94 - 16th Congress of the Int. Council of the Aeronautical Sciences, Anaheim, CA, USA, 1994.
- [4] Gardiner W.C. Jr., *Combustion Chemistry*, Springer-Verlag, 1984.
- [5] Hirschfelder J. O., Curtiss C.F., Bird R.B., *Molecular Theory of Gases and Liquids*, John Wiley and Sons, 1954.
- [6] Malik M. R., Anderson E. C., *Real Gas Effects on Boundary Layer Stability*, Physics of Fluids A, Vol.3, No.5, 1991.
- [7] Stuckert G.K., Reed H. L., *Linear Disturbances in Hypersonic, Chemically Reacting Shock Layers*, AIAA Journal, Vol.32, No.7, 1994.
- [8] Hudson M. L., Chokani N., Candler G.V., *Linear Stability of Hypersonic Flow in Thermochemical Nonequilibrium*, AIAA Journal, Vol.35, No.6, 1997.
- [9] Chang C.L., Vinh H., Malik M.R., *Hypersonic Boundary Layer Stability with Chemical Reactions using PSE*, AIAA Paper 97-2012, 1997.

AEROSPACE APPLICATIONS - AA 4

ROOM PÉRÈS

FRIDAY, JULY 31, 1998

16:10

Ion flow in Stationary Plasma Thruster *

K. Makowski¹, Z. Peradzynski¹, N. Gascon², P. Lasgorceix², M. Dudeck²
 Institute of Fundamental Technological Research - PAS, Warsaw, Poland
 Laboratoire d'Aérodynamique - CNRS, Orléans, France

Introduction

In modelling plasma discharges the different, characteristic scales e.g. geometric and collisional have to be taken into account. A hybrid approach (see[1]) is currently used as a compromise between quality of results and time calculations for the description of the Stationary Plasma Thruster (S.P.T.) discharges. However, a purely fluid model describing the discharge can be also written [2,3] with the goal of global parameter analysis and sensibility as a function of running parameters. In this paper, this last approach is used to investigate the plasma properties by the quasi-1D formulation taking into account the azimuthal electron drift velocity. Assuming stationary conditions for all the plasma parameters a set of two equations has been deduced to describe the ion flow distribution along the thruster channel. These equations show the necessity of appearance the discontinuities of ion velocity if we are going to obtain a supersonic ion flow at the channel exit.

Stationary Plasma Thruster (S.P.T.)

Actually, Stationary Plasma Thruster are under intensive investigations because of its application for the position keeping of geostationary satellites. A schematic view of a Hall-type ion thruster (S.P.T.) is shown in Fig.1. Electrons are emitted by the hollow cathode and focussed in the annular cylindrical channel of the thruster by an external magnetic field sustained by the system of coils. Then, the ions created in the electron-atom collisions are axially accelerated by the electric field and produce the thrust. The xenon gas inlet is performed at the bottom of the channel and the gas injection system is currently used as an anode.

Discharge parameters

The typical values are: 250G for the maximum radial magnetic field, a discharge voltage of 300V, a

discharge current of 5A and a xenon mass flow rate of 5 mg/s. In this case the maximum value of the electron density is of order of $5 \cdot 10^{11} \text{ cm}^{-3}$, the azimuthal electron velocity is of the order of 10^6 m/s , the electron cyclotron frequency is up to $\approx 10^9 \text{ s}^{-1}$ and the electron-wall collision frequency is $\approx 10^8 \text{ s}^{-1}$. The latter frequency is large enough to explain the observed plasma electric conductivity. The working gas is xenon and its inlet velocity at the anode is $\approx 500 \text{ m/s}$.

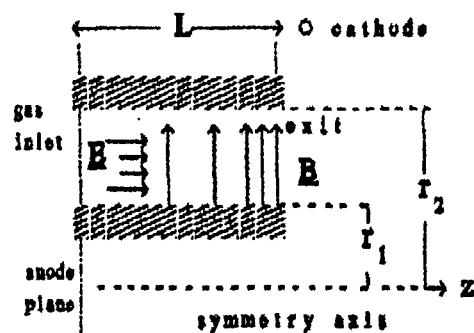


Fig.1 Schematic view of a SPT thruster channel.

Fluid model

The presented quasi-1D model of S.P.T. plasma consist of: - the ion and electron continuity equations, - the ion and electron momentum equations and electron energy equation, where we have introduced the ionization rate β and the electron collisions with other particles as well as their collisions with the channel wall v_{eff} . The meaningful simplification can be achieved by assuming: - constant electron temperature T_e , - electric neutrality (except the

* Abstract 3207 submitted to the 21st International Symposium on Rarefied Gas Dynamics, Marseille, France, July 26-31, 1998

possible double layers), and - that only the electrons are magnetized. These assumptions allow us to reduce the model to:

- ion continuity equation

$$\frac{d(NW)}{dz} = \beta N_a N$$

- ion momentum equation

$$W \frac{dW}{dz} = E - \beta N_a (W - V_0)$$

where the electric field E is determined from the neutrality condition as

$$E = \frac{\beta N_a (2W - V_0) - v_{eff} (1/eNW - 1)W}{1 - MW^2/T_e}$$

Here I denotes the discharge current density. The boundary conditions are:

$$W(0) = W_0; \quad N(0) = N_0; \quad \Phi_{avod\epsilon} = \int_0^L Edz$$

It can be easily observed that the electric field E has a singularity at

$$W^2 = (T_e / M) = C_s^2$$

Moreover, the general analysis of these equations shows that on the trajectory $W(z)$, $N(z)$ starting from the initial values (at $z = 0$) such that: $N_0 < N_0(0)$ and $W_0 < C_s$, the value of $W(z)$ will never exceed the ion sound velocity C_s . But from the other hand we can always find also such trajectory, that for every z ($0 \leq z \leq L$): $W(z) > C_s$ and $N(z)W(z) > J_0$, where J_0 is the characteristic for this plasma minimal value of ionic current in case of supersonic flow. Consequently we can not fulfill the boundary conditions. Therefore we can pass to the supersonic ion flow only allowing the discontinuous solutions connecting these separate trajectories. Such discontinuity physically corresponds to appearance of a double layer. From the governing equations written in the conservative form we deduce the unique relation between the N -, W -values behind and before double layer discontinuity. It turns out that introducing these type of solutions we find such a position of double layer, that the potential drop between the anode and the exit will be equal to the prescribed value (in the example presented below 300V). The numerically determined ion velocity axial distributions with discontinuities located at various z are presented in the Fig.2.

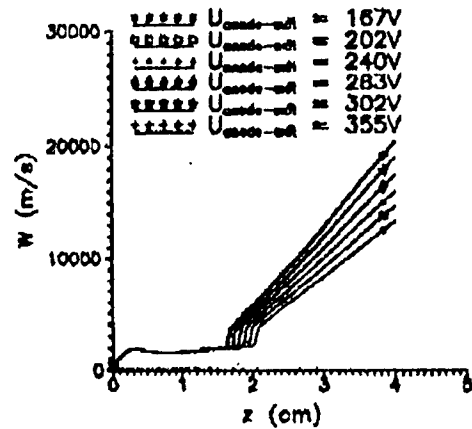


Fig.2 Ion velocity along the channel
($T_e = \text{cste} = 10\text{eV}$).

References

- [1] J.P.Boeuf, *Moteurs ioniques*, Actes du Workshop commun GDR SPARCH-PPSO, Nice, France, avril 1997, p.1.
- [2] K.Makowski, M.Dudeck, *Transition to supersonic ion flow in stationary plasma thruster*, XIIth ICPIG, Toulouse, France, July 1997, vol.V-100.
- [3] M.Dudeck, K.Makowski, Z.Peradzynski *Transition to supersonic ion flow in stationary plasma thruster*, International Symposium Plasma'97, June 1997, Opole, Poland, vol.1, p.21.

Spatial Parameters of a Glow near Space Objects in Free Molecular Flow *

O. G. Friedlander¹, V. D. Perminov¹, G. F. Carabadgak², U. A. Plastinin²

¹ Central Aerohydrodynamic Institute (TsAGI), Zhukowsky, Russia

² Central Research Institute of Machine Building (TsNIIMASH), Korolev, Russia

1 Introduction

To process space objects observation data at shady side of the Earth it is necessary to know a spatial intensity distribution of glow that arises as a result of an interaction of atmosphere molecules with surfaces of both the object observed and the object where the inspection is carried out from. According to data available today [1] [2]

1. the glow is more often observed near parts of object surface whose normal vector is collinear to velocity vector;
2. for object with reference size from 1 to 30 m the glow reference size is from 0.2 to 1.0 m;
3. the glow's intensity at altitudes above 160 km is proportional to oxygen atoms concentration in the atmosphere and
4. the glow's intensity decreases exponentially with moving away from the object surface.

Assuming these facts as a basis one can suppose that

- the glow is generated by shining out of metastable molecules which form on the object surface and
- a flow of such molecules is proportional to molecular flow incident at the surface element.

In this paper the spatial distributions of glow intensity near different space objects are investigated for different values of mean life time of metastable molecules.

*Abstract 5096 submitted to the 21st International Symposium on Rarefied Gas Dynamics, Marseille, France, July 26-31, 1998

2 Mathematical models, limit case and computational algorithm

The simplest group of mathematical models can be constructed if one uses the abovementioned supposition that the flow of metastable molecules from the surface element j_r is proportional to the incoming flow to the same element j_∞ .

$$j_r = A j_\infty, \quad A = \text{Const} < 1,$$

$$j_\infty = \frac{n_\infty}{2(\pi h_\infty)^{1/2}} \chi(S_\theta)$$

$$\chi(S_\theta) = \exp(-S_\theta^2) + \pi^{1/2} S_\theta (1 + \text{erf}(S_\theta))$$

$$S_\theta = S_\infty \cos \theta, \quad S_\infty = V h_\infty^{1/2}$$

$$h_\infty = \frac{m}{2kT_\infty}, \quad \text{erf}(x) = \frac{2}{\pi^{1/2}} \int_0^x \exp(-t^2) dt$$

Here V , T_∞ , S_∞ are the velocity of object, temperature of undisturbed atmosphere and velocity ratio correspondingly, m is mass of gas molecules, k is Boltzmann constant and θ_∞ is an angle between the object velocity vector and the surface normal vector. If $S_\infty \gg 1$, $j_\infty = n_\infty V \cos \theta$ and $j_\infty(\theta = 0) = n_\infty V$.

Designate the mean life time of metastable molecules by τ . The probability of a molecule to be shined out during time interval dt subsequent to time t after its start from surface is $dp = \exp(-t/\tau) dt/\tau$. Let us suppose that the metastable molecules start from the surface with Maxwellian velocity distribution function. The temperature of this distribution T_r can differ from the wall temperature T_w . The parameter n_r of this distribution function depends on the flow from the surface j_r : $n_r = 2j_r(\pi h_r)^{1/2}$. A number of molecules shining out at unit time in unit volume near a point \vec{x} is equal to

$$N(\vec{x}) = \iiint f_r(\vec{\xi}) \frac{dp}{dt} d\vec{\xi}$$

Here the integration extends through all values of $|\vec{\xi}|$ and only through the directions of $\vec{\xi}$ that lie inside of solid angle based on the object.

In a case when $\tau c_r \ll R$ (R is object reference size) it is possible to get for $N(\vec{x})$ a closed formula which is the first term of expansion in a series at small parameter $\varepsilon = \tau c_r / R$. Glow's intensity for this approximation is equal to one for a very narrow layer near a flat plate each element of which emits the same flow of metastable molecules j_r .

Equally with a natural model of Maxwellian velocity distribution it is possible to use for assessments more crude models based on motion of molecules with constant velocity [3]. In the paper a correlation between different models proposed is analysed.

The calculation of spatial distribution of glow intensity near geometrically complex objects (or, in other words, the calculation of multiple integrals with complex integration region) was carried out by Monte Carlo method. Fulfillment of the condition $j_r \propto j_\infty$ was provided with the following procedure. A control surface (parallelepiped) was drawn up around the object. From sides of the parallelepiped molecules were thrown in with the probabilities that were proportional to molecular flows through these sides. The velocity distribution function of these molecule was Maxwellian one. The molecules either flew without a collision with the object surface or collided with it. In the latter case they started from the surface with velocity distribution function $f_r(\vec{\xi})$.

The object surface was presented as a set of pieces of the second order surfaces. The calculation region, i.e. the volume limited by control surface, was divided by an orthogonal grid into a set of cells. Each of them had a summator of number of the metastable molecules shined out inside the cell. The reference size of the calculation region and, therefore the number of cells, depends on a value of mean life time τ of metastable molecules.

In this paper the calculation results for the glow intensity near sphere, cone and cylinder with spherical blunt nose at four values of $\varepsilon = \tau c_r / R = 0.1, 0.5, 1.0, 2.0$ are presented and discussed. An angular intensity distribution of the glow incoming to onboard sensing elements was calculated for the blunted cylinder with a ratio of bluntness to cylinder radius equal to 2.5. In all calculation cases $S_\infty = 10$.

3 Acknowledgement

This work has been supported by the State Program of Leading Scientific Schools Support, the Grant 96-15-96063 and partly by BMDO/IST through The Army Research Office and managed by The Air Force Arnold Engineering and Development Center.

References

- [1] Mende S. B., Swenson G. R., *Vehicle Glow Measurements on the Space Shuttle*, Proc. of the Second Workshop on Spacecraft Glow, NASA CD-2391, 1985.
- [2] Green B. D., Caledonia J. E., Wilkerson T. D., *The Shuttle Environment: Gases, Particles and Glow*, J. of Spacecraft and Rockets, Vol.23, No.5, pp.500-512, 1985.
- [3] Yee J.-H., Dalgarno A., *Radiative Lifetime Analysis of the Shuttle Glow*, J. of Spacecraft and Rockets, Vol.23, No.6, pp.635-640, 1986.

Type III and Type IV Shock/Shock Interferences : Theoretical and Experimental Aspects *

B. Chanetz¹, F. Grasso², C. Purpura²

¹ Office National d'Etudes et de Recherches Aéropatiales, France

² Università di Roma "La Sapienza", Italy

1 Introduction

This study of shock/shock interference has been undertaken in the framework of the "program of research and technology for hypersonic propulsion" (PREPHA) decided by the French Ministry of Defence. The aim of this program is to conceive a scramjet for hypersonic applications. For this project -as far as external aerodynamics is concerned- one of the most challenging problem is the definition of air intakes. The shocks produced by the compression ramp intersect the shock forming ahead of the cowl, whose profile is blunt so as to limit the heat flux. The shock/shock interferences can produce locally spectacular heat flux and pressure increases. Edney, by analysing his own experiments, has defined six types of basic interferences which have been universally accepted. The present paper is divided in two parts. The first part is devoted to the theoretical presentation of an original method to determine -in two-dimensional flow around a large spanwise cylinder- the interference type produced versus the characteristics of the incident shock. This method identifies the transition locations between the different interference types. A second part of this paper concerns type III and type IV interference analysed in the hypersonic wind tunnel R3CH ($M = 10$) at the ONERA Meudon center. Additionally, the cylinder alone in the free stream without incident shock has been studied in order to constitute the reference case.

2 Transition prediction of the six interference types

We here consider an oblique shock (C_1) propagating from below and meeting the detached shock (C_2) which forms ahead of a blunt obstacle. The method

presented is based on the hypothesis of perfect fluid without viscosity [1]. The theory of shock waves and shock polars is used to detect the transition between the different types. The transition between type I-II and V-VI are obtained by using the graphical method of shock polar representations. Physically, the transition between type I and type II is consecutive to the appearance of two slip lines instead of one downstream of the shock/shock interferences. The determination of the transition between type III and type IV requires the calculation of the flow characteristics downstream of the intersection. The hypothesis used to distinguish the two types is an angular criterion. We determine the limit angle to have an attached shock when the shear layer strikes the wall. Indeed if it is possible to have an attached shock, type III is obtained. If it is impossible, type IV occurs. The transition between type II-IV and IV-V are given by the determination of the sonic lines, the type III and IV occurring when the flow behind the detached shock is subsonic. Thanks to this method, a precise classification of the six interference domains has been performed for different incident shock values comprised between 10° and 30° degrees. For example, it has been found that for an incident shock angle equal to 20° , the type III interference situation was not possible. These results have to be confirmed by comparison with experimental work.

3 Experimental results

Some results have been obtained testing a cylindrical model with a circular section (diameter $D = 0.0040m$, spanwise $L = 0.120m$) and compared with the theoretical prediction of Fay-Ridell and formulas proposed by Borovoy et al. [2], which takes in account corrections due to the wind tunnel disturbances. The experimental arrangement is constituted by a shock generator with a sharp leading edge located in front of a cylinder lying perpendic-

* Abstract a6313 submitted to the 21st International Symposium on Rarefied Gas Dynamics, Marseille, France, July 26-31, 1998

ular to the free stream flow delivered by the R3CH wind tunnel. The facility, whose stagnation temperature and pressure are $1050K$ and $126 \cdot 10^5 Pa$ respectively, produces an uniform flow at Mach number 10. The freestream static conditions are: $p = 3.1 \cdot 10^2 Pa$, $AT = 50K$, $\rho = 0.021 kg/m^3$. Three configurations have been tested. In a first step, the reference case without interference (fig.1) shows for different stagnation pressure values that the comparison between the experimental stagnation point heat flux and Fay-Ridell determination is in agreement in the domain of low Reynolds numbers but not at higher Reynolds numbers. This discrepancy has been pointed out in other experiments performed at TsAGI [2] and attributed to an effect of acoustic free stream disturbances generated by the nozzle boundary layer. This phenomenon has been taken into account and corrected formulae have been proposed [2], and have been used here (see fig.1). But the over estimated experimental heat flux may be due to three dimensional effects, resulting from the small model span. This point will be elucidated by increasing the model span.

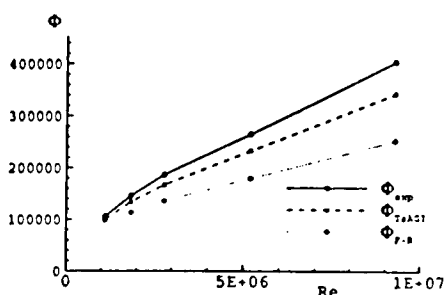


Figure 1: Comparison between experimental results and theoretical predictions

In a second step, a type III shock/shock interaction has been studied. In this case, (fig.4) the impact of the slip line with the cylinder surface causes a pressure peak 2.5 times higher than in the case of the cylinder only (P_{ref} being the pressure measured at the stagnation point in the experimental reference case). Moreover (fig.4) the heat flux peak is 5 times higher than Φ_{ref} (reference case). The type IV has also been studied. In this case the reattachment of the slip line on the cylinder surface is impossible, and a supersonic jet emanates from the slip line surrounded by subsonic flows. With this type of interference one sees that the peak of pressure is 4 times higher than P_{ref} (fig.4), and the heat flux peak is 7 times higher than Φ_{ref} (fig.4).

4 Conclusion

Other experiments will be done to investigate about the discrepancy between the experimental and theoretical approach for the determination of heat flux peaks at the stagnation point in the reference case (cylinder only). The effect of incident shock angle variation on the pressure and heat flux peaks will be studied. The effect of the incident shock variation on the interference nature will be studied in depth and analyzed in comparison with the theoretical approach. A Reynolds number effect in the type III interaction will be achieved in order to determine the influence of the shear layer nature -laminar or turbulent- on the wall heat-flux peak.

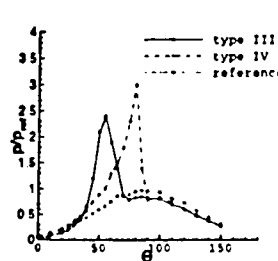


Figure 2: Evolution of pressure around the cylinder

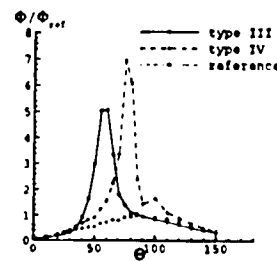


Figure 3: Evolution of heat flux around the cylinder

References

- [1] Chanetz B., *Mémoire d'Habilitation à Diriger des Recherches (HDR)* soutenu le 15 décembre 1997 à l'Université Claude Bernard (Lyon I)
- [2] V.Ya.Borovoy, A.Yu.Chilinov, V.N.Gusev, I.V.Struminskaya, J.Délery, B.Chanetz, *Interference Between a Cylindrical Bow Shock and a Plane Oblique Shock*, AIAA Journal, Vol.35, No.11, pp.1721-1728.

ASTROPHYSICS AND ENVIRONMENT - AE 1

ROOM MARION

FRIDAY, JULY 31, 1998

11:10

Application of the Fluid/Kinetic Approach to Io's Atmosphere *

M.L. Marconi¹, M.C. Wong², W.H. Smyth²¹ Fresh Pond Research Institute, Cambridge Ma., USA² Atmospheric and Environmental Research Inc., Cambridge Ma., USA

A planet atmosphere may be generally viewed as consisting of three regions: a region where gas densities are high enough for collisions to impose a Maxwellian and hydrodynamics applies, a quasi-collisional transition region where self-collisions are important but not frequent enough to impose a Maxwellian so that the solution of the full nonlinear Boltzmann equation must be undertaken to properly describe the atmosphere, and an exospheric region where the gas is self-collisionless and a linear Boltzmann equation provides a suitable description of the atmosphere. A primary challenge of atmospheric theory is the consistent modeling of the planet atmosphere, particularly the theoretically difficult transition region (Merryfield and Shizgal [1]). As reported in RGD-20 by Marconi and Smyth [2] and in Marconi et al [3] we have developed a hybrid fluid/kinetic model of a planetary atmosphere which can self-consistently describe a single species spherical atmosphere with a heating layer through all levels of collisionality. We have recently extended the fluid/kinetic model to a spatially 2 D multispecies model with chemistry. Presently we have begun to apply our new version of the hybrid fluid/kinetic model to a highly challenging problem, i.e. the moon of Jupiter, Io.

Io has long been recognized as having a unique and physically most interesting atmosphere. Io's atmosphere, believed to be mainly SO₂, derives from a combination of volcanic sources, sublimation of surface SO₂ ices on the sunward side of Io, and probably to a smaller extent from sputtering by energetic charged particles. Such a spatially and temporally inhomogeneous distribution of sources leads to a dynamic and highly nonspherically symmetric atmosphere quite unlike any other in the solar system. This spatially complex atmosphere is heated and chemically processed by the dense ($n \approx 1000 \text{ cm}^{-3}$ of ionized O and S) and highly magnetized ($B \approx 0.018 \text{ Gauss}$) plasma of the Io plasma torus which

corotates with Jupiter and strikes Io's atmosphere with a speed of 57 km s^{-1} (plasma energies of a few hundred electron volts). This collision between atmosphere and plasma results in substantial atmospheric heating with profound consequences for atmospheric structure and plasma flow near Io. In addition, there is the production of a highly non-Maxwellian distribution of neutral species (S, O, SO, etc.) in the transition and exospheric regions of the atmosphere, many of which escape Io and give rise to the various extended neutral clouds. We will describe our initial attempts to model this highly complex atmosphere with our new 2 D hybrid fluid/kinetic model.

References

- [1] Merryfield W.J. and Shizgal B.D., Planet Space Sci., 42, 409, 1994.
- [2] Marconi M.L. Proceedings of RGD-20, 1997.
- [3] Marconi M.L., Dagum L., and Smyth W.H., Ap. J., 469, 393, 1996.

* Abstract 4466 submitted to the 21st International Symposium on Rarefied Gas Dynamics, Marseille, France, July 26-31, 1998

Direct Numerical Simulation of Supersonic Rarefied Atmospheric Flows on Io *

J. V. Austin, D. B. Goldstein
Computational Fluid Physics Laboratory
University of Texas at Austin

1 Introduction

Low-density supersonic flows in the atmosphere of Jupiter's moon Io are modeled using the direct simulation Monte Carlo (DSMC) method, a rarefied gas computational technique. Two cases of rarefied atmospheric flow are studied. The first case is the sublimation/condensation driven SO₂ winds where large vapor pressure differences can cause the flow to become supersonic. The supersonic, condensing flow produces a sloping standing shock near the terminator. The second case is the flow produced by a supersonic exhausting SO₂ volcanic plume. The volcano creates two shocks; a hemispherical canopy shock located above the plume and a re-entry shock located near the ground. The effects of the presence of a non-condensable gas on Io's atmosphere are also explored.

2 Methodology

The basic DSMC method as presented by Bird [1], has been expanded for this effort. Modifications include: use of a gravitational body force, introduction of an adaptive weighting factor distribution and collision limiters to handle the huge density variations, the use of quasi-spherical geometry, the use of a novel semi-structured grid as well as a multi-grid approach to enhance spatial resolution, and the use of progressive ensemble averaging to speed the approach to steady state.

3 Sublimation driven winds

The transplanetary SO₂ winds on Io were modeled. Gas sublimates from SO₂ frost in the warm subsolar region and flows towards the colder nightside where it condenses. The model is axi-symmetric about the

sub-solar point and the day-side azimuthal surface temperature distribution (in kelvins) is described by

$$T_{\text{surface}} = (T_{\text{subsolar}} - 50) \times \cos^{1/4} \Theta + 50$$

where Θ is the solar zenith angle. The temperature on the night-side is assumed to be 85 K. The resulting surface pressure due to the vapor pressure of SO₂ frost ranges from over 10⁻⁴ Pa at the subsolar point to 10⁻¹⁰ Pa on the night-side. SO₂ molecules sublimate from the lower boundary due to the vapor pressure and SO₂ molecules which strike the surface condense. Any non-condensable molecules are diffusively reflected from the surface with the appropriate temperature.

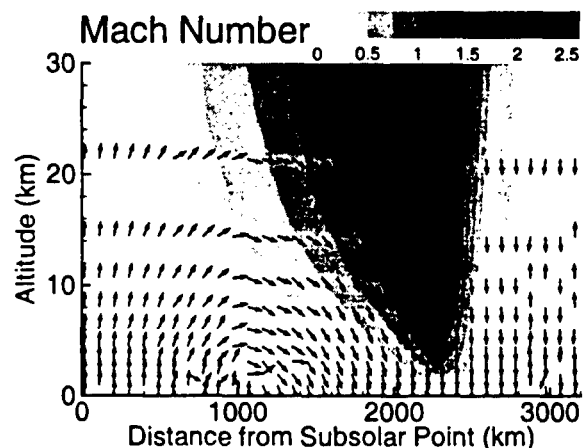


Figure 1: Mach number contours of sublimation driven winds with velocity vectors. Note exaggerated vertical scale.

The acceleration of the flow due to the large vapor pressure difference and the cooling due to expansion causes the flow to become supersonic. A boundary layer grows along the surface, decelerating the flow, until the gas passes through a standing shock about 70 degrees away from the subsolar point (≈ 2200 km). This differs from the results

*Abstract 6327 submitted to the 21st International Symposium on Rarefied Gas Dynamics, Marseille, France, July 26-31, 1998

of [2], [3], and [4] which do not find a shock because viscosity is neglected. The shock produces high temperatures and pressures in the vicinity of the terminator, which may explain large ionospheric densities found by Pioneer 10 and Galileo.

A range of subsolar temperatures were investigated using the model. The strength of the shock was found to vary greatly with the subsolar temperature. The shock strength also had a significant effect on the surface deposition pattern of SO_2 frost. Molecules of O_2 were added to study the effect of the presence of a gas that is non-condensable at the expected surface temperatures. However, the range of non-condensable gas pressures that were tried had a negligible effect on the SO_2 deposition.

4 Volcanic atmospheres

The near-field atmosphere produced by a night-side volcanic plume on Io was also explored. The model is axi-symmetric about the centerline of the plume. Sulfur-dioxide gas is exhausted vertically at Mach 3 from a volcanic vent 8km in radius. The lower boundary of the domain models the cold, night-side of Io, and SO_2 molecules which strike the surface condense with a sticking factor of 0.2. Non-condensable molecules, when present, are diffusively reflected from the surface with the appropriate temperature.

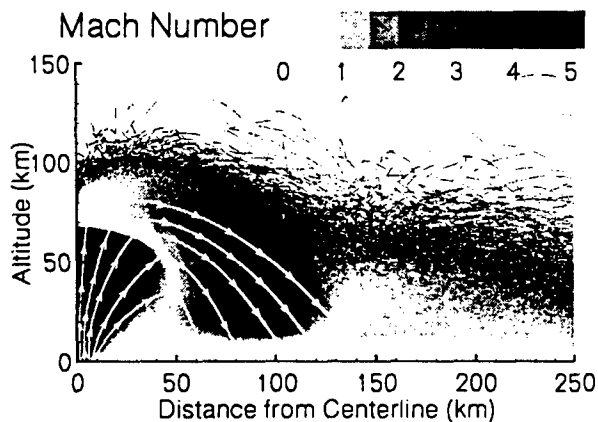


Figure 2: Mach number contours of a SO_2 volcano with streamlines.

As the plume rises gravity slows the flow and a canopy-shaped shock ($\approx 75\text{km}$ altitude) then turns the flow outward. The outward moving gas continues to cool due to expansion as it accelerates toward the surface, causing the flow to again become supersonic. The re-entry shock then slows

the falling gas and turns it outward again. The flow then undergoes a weak "bounce" at a radius of approximately 175km, possibly caused by an increase in scale height due to the heating of the gas in the re-entry shock or by specular collisions with the surface of Io.

A non-condensable background gas was also added to simulate the possible presence of O_2 or H_2S . The ratio of background gas pressure to plume SO_2 mass flow rate was varied to study the effect on SO_2 transport. The results show that large non-condensable gas pressures will constrain the SO_2 gas to the region near the plume and limit its extent. However, smaller background gas pressures were found to actually enhance the transport of SO_2 away from a local source when compared to a model with no background gas. The warm SO_2 plume gas rides on top of a layer of non-condensable gas and is buffered from the cold, condensing surface, so the SO_2 gas may reach farther from the vent.

References

- [1] Bird G.A., *Molecular Gas Dynamics and the Direct Simulation of Gas Flows*, Oxford University Press, 1994.
- [2] Ingersoll A.P., *Io Meteorology: How Atmospheric Pressure is Controlled Locally by Volcanos and Surface Frosts*, *Icarus* **81**, 298-313, 1989.
- [3] Moreno M.A., Schubert G., Baumgardner J., Kivelson M.G. and Paige D.A., *Io's Volcanic and Sublimation Atmospheres*, *Icarus* **93**, 63-81, 1991.
- [4] Wong M.C. and Johnson R.E., *The Effect of Plasma Heating on Sublimation-Driven Flow in Io's Atmosphere*, *Icarus* **115**, 109-118, 1995.

Mutual Influence of Nonequilibrium Condensation and Radiative Excitation of Water Molecules on the Structure of a Cometary Coma. Kinetic Model *

A.L. Itkin

Inst. High-Performance Compt. and Data Bases, Moscow Branch, Russia &
Inst. Problems of the Asteroid Hazard, Moscow, Russia

We report a study devoted to investigation of nonequilibrium processes in a cometary coma and their influence on the coma structure which have been started by [1, 2]. Here we bring into consideration condensation of water vapor in the coma which realizes against a background of radiative excitation of water molecules. New microscopic kinetic model of coupled nonequilibrium condensation and radiative excitation of water molecules effusing from a nucleus surface is developed. The method in strong degree is based on the microscopic theory of nonequilibrium condensation (MTC) developed by the author [3, 4]. To analyze vibrational and rotational excitation of the H_2O molecule model [5] has been used which includes infrared rovibrational pumping by the solar radiation flux, thermal excitation by collisions and radiation trapping in the rotational and rovibrational lines. The kinetic equations for cluster concentrations and populations of their energetic levels are solved analytically that permits one to reduce initially coupled balance equations of the condensation and radiative kinetics to a closed system of differential equations with respect to only rotational populations of the water molecule.

When developing this theory the main physical assumption is made that the rotationally excited molecule has a smaller cross-section than non-excited. This problem was theoretically investigated in [6] with the purpose to explain experiments on rotational-selective condensation of water and heavy water molecules [7]. A multistep mechanism of the resonant capture of molecules through the formation of an intermediate complex was considered which was illustrated by system $\text{He}-\text{H}_2\text{O}$. It was found in these works that ratio η of the rate constant of capture of water molecules being in the ground ortho and para states is $8.4 \leq \eta \leq 12.3$ as

the temperature is ranged in the limits $30\text{K} \leq T \leq 50\text{K}$. Thus these data testify to an opportunity of the rotational selectivity of condensation already at the stage of capture. It is clear that as the rotational energy of molecule increases its rate constant of capture decreases. Therefore in this work we use a model where the only molecules being in a ground para state are able to condense while the probability of the formation of molecular complexes by attaching the water molecule being in another rotational state is neglected.

The structure of the work is the following. First, we derive new kinetic equations to describe the coupled processes of condensation and radiative excitation of water molecules. Then we propose an asymptotic method to get analytical solutions of these equations. It gives rise to the closed system of differential equations only for supersaturation S_0 of the ground para state and populations $x_1(k)$ of the rotational states of the water molecule. Solving this system one can further analytically restore the cluster size distribution function as well as populations of the internal states of the clusters. Some new features of this solution, in particular, an appearance of singularities at a certain S_0 are discussed. Finally, results of simulation of a water vapor flow effusing from the nucleus surface performed with the help of the present model and prospects of our model usage when studying an influence of the indicated processes on the structure of the inner coma are discussed.

Some conclusions as applied to physical processes in the inner coma can be made based on the results obtained. First we consider a weak comet with a small production rate of the water vapor from the cometary nucleus. It means, that the numerical density of the vapor is small enough that results in a low value of the collision relaxation rate C_c . For these conditions the radiative processes dominates the collisional relaxation ($\Omega_k^r \ll \Omega_k^c$), and the steady

*Abstract 4883 submitted to the 21st International Symposium on Rarefied Gas Dynamics, Marseille, France, July 26-31, 1998

distribution of populations is largely determined by the external radiation, i.e. by the interaction of water molecules with the radiative flux from the Sun. As the result the populations of the rotational levels of monomer are nonequilibrium. They can be expressed through supersaturation S by solving the system of equations derived in the paper. Then substituting these solutions into the equation for S we arrive to the closed equation for S .

Another situation takes place for active comets with a high production rate. Here the increase in initial vapor density results in more frequent collisions, which reduce the rate of the collisional relaxation C_c so, that it becomes more than the rate of the radiative processes ($\Omega_k^c \gg \Omega_k^r$). As a result, at all times the equilibrium distribution over the energy of rotational sublevels has time to be established. Hence, once again we arrive to the closed equation for S but the difference with the previous situation is that R.H.S. of this equation in the last case depends upon S rather than in the first case (generally speaking, more simply).

At the intermediate distances both terms Ω_k^c and Ω_k^r could be of the same order of magnitude therefore quasisteady populations $x_1(k)$, $k = 0, \dots, M$ are nonequilibrium and should be found by solving the full system of kinetic equations, given in the paper. Note also that the correlation between Ω_k^c and Ω_k^r can vary from one rotational sublevel to another in accordance with the value of the Einstein coefficients.

The gas production rate of the comet increases as the distance between the comet and the Sun decreases. On the other hand the decrease of this distance results also in the increase of radiation intensity (see [1]) therefore these two processes are competitive. For concrete estimations simulation is needed.

References

- [1] Itkin A.L., Bockelee-Morvan D, and Rodionov A.V. Nonequilibrium processes and their influence on the structure of the inner coma. I. Radiative excitation of water molecules. Space Researches, Vol.35, N1, p.18, 1997.
- [2] Kolesnichenko E.G., and Itkin A.L. Nonequilibrium processes and their influence on the structure of an inner cometary coma. II. Models of a dusty gas flow. Space Researches, Vol.36, N2., 1998, (in press).
- [3] Itkin A. L., and Kolesnichenko E.G., Calculation of condensing gas flows by means of the monomolecular condensation theory. Fluid Dynamics, Vol.25, p.765, 1990.
- [4] Itkin A.L., and Kolesnichenko E.G., Microscopic theory of condensation in gases and plasma, World Scientific, New York, London, HongKong, 1997.
- [5] Bockelee-Morvan D., A model for the excitation of water in comets. Astronomy & Astrophysics, 181, p.169, 1987.
- [6] Epifanov S.Y., and Faizullaev, V.N., Multistep model of capture at molecular association in vapor. Technical Report 4, Inst.Gen.Phys., RAS, 1992.
- [7] Konuchov V.K., et al., Letters in Soviet JETP, Vol.43, p.65, 1986.

ASTROPHYSICS AND ENVIRONMENT - AE 2

ROOM MARION

FRIDAY, JULY 31, 1998

14:35

A Quantised Approach to the Chemistry of the Atmosphere Using DSMC*

P. Marriott, 20 Larkfield Rd., Farnham, Surrey, U.K., GU9 7DB

A state specific chemistry model for use in DSMC simulations which have quantised vibrational energy information has been used to simulate the rate behaviour of the non-ionic Zeldovich exchange and dissociation reactions considered important in the atmosphere. There are certain situations where chemistry takes place at low temperatures caused by the presence of excited states such as that arising from the absorption of radiation. As an example, regions of the upper atmosphere are translationally cold but cosmic and solar radiation produce sufficient excited molecules to cause ionisation and dissociation. Rarefaction effects may also cause local thermodynamic non-equilibrium and, in those cases where higher temperatures are present, chemical reactions can occur. In all these cases it is important to treat the chemistry in a state related way, that is the probability of a chemical reaction is related to the quantum state of the reacting molecules and the disposal of energy post reaction is also non-equilibrium. This paper uses a chemistry method based on ideas which have already been described¹ both for energy disposal and energy exchange. The Semi-Quantum Maximum Entropy (SQME) approach method is based on the ideas of Statistical Thermodynamics (ST) applied to the available states of the molecules in a volume of gas. The *prior* distributions of rate and energy disposal² and are based on the assumption that all available quantum states are equally likely. The Maximum Entropy (ME) method extends the ST treatment for those cases where rate and post collision disposal of energy are of a non-equilibrium nature. The method has been used in the treatment of chemistry reaction rate determination and disposal in DSMC³. In the case of chemical rates, if the prior probability of reaction from every vibrational quantum level, n , is p_0 then the ME extension to the method introduces an exponential term so that the probability is given by the expression $p_n = p_0 \exp(-\lambda n)$ where λ is a disposable parameter determined by the type of reaction considered. As an example, if the reaction takes place

preferentially from higher vibrational levels then λ is negative.

The energy disposal post collision is also disposed using the same methods except in this case every possible vibrational level has large number of associated translational and rotational levels. The prior probability of a particular level must take this into account. In this case $p_0 = f(n)$ where $f(n)$ depends on the molecularity of the colliding molecules. This is generally formulated in terms of E_n , the energy of the level, for convenience.

The chemical behaviour of reacting species varies considerably. The presence or absence of an energy barrier to reaction has a large effect on the rate of reaction. Those reactions which proceed in the absence of an activation barrier tend to exhibit the same type of behaviour. The rate of reaction tends to be constant over large temperature range and to be independent of vibrational level. Figure 1 shows the published data for the reaction $\text{NO} + \text{N} \rightarrow \text{N}_2 + \text{O}$. As is usual for all reactions there is a large range of the value of rate constant and of behaviour with increasing temperature. Figure 2 shows the results of a single cell simulation of an equilibrium reacting mixture of NO and N. It can be seen that various values of the disposable parameters which are used in the method, λ and n_{max} , (the vibrational level above which the probability of reaction is one,) can be chosen so as to mimic any of the published rate behaviour. If λ equals zero then every collision has the same probability of reaction regardless of the vibrational level of the NO molecule which can be seen to be very close to the rates given in references 6 and 7. If λ is negative then the rate enhanced for higher values of the vibrational quantum number. Reactions with an energy of activation exhibit a rate behaviour which is largely determined by the number of molecules which have sufficient energy to surmount the energy barrier. Reference 3 describes this behaviour in more detail. The new chemistry method was tested using a reacting cell of 50000 N_2

* Abstract 5631 submitted to the 21st International Symposium on Rarefied Gas Dynamics, Marseille, France, July 26-31, 1998

and O₂ molecules set up to simulate a pressure of one atmosphere. The cell was set up with the molecules in equilibrium at an initial translational/rotational temperature of approximately 5000K and the quantised vibrational occupancy consistent with Cv at that temperature. The species concentrations of the products of reaction, N, O, and NO were followed as the reactions proceeded. The same cell was then set up with the same overall energy but with a higher vibrational excitation and lower translational temperature. The reactions simulated are:

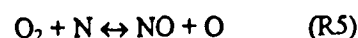
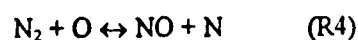
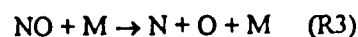
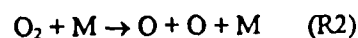
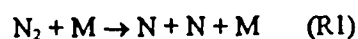


Figure 3 shows the results of the simulations plotted on the same scale. It is clear that both simulations are similar, showing an initial production of atomic oxygen produced from reaction R2 which then reacts to produce NO and N via reactions R4 and R5. Since the probability of reaction is greater from higher vibrational for the reactions above, there is a much greater initial production of the species shown in the second case than in the first.

This paper will include a survey of the available estimates for the rate constants of the above reactions and a discussion leading to a recommendation for the 'best value'. A sensitivity study of the effect of using different rate data and energy disposal in a simple reacting cell such as that described above will also be included.

References

- [1] Marriott, P.M. 'Non-equilibrium chemical reactions in the simulation of hypersonic rarefied flows', Ph.D. Thesis, ICSTM, University of London, U.K., 1994
- [2] Marriott, P.M. Harvey J.K. 'Non-equilibrium chemical effects in hypersonic rarefied flow using the Direct Simulation Monte Carlo method', 18th RGD symposium, Progress in Aeronautics and Astronautics, 1992
- [3] Marriott, P.M. 'Fully coupled approach to chemical reactions and energy exchange in DSMC', AIAA 97-2506, 1997
- [4] NSRDS 'Table of recommended rate constants for chemical reactions occurring in combustion. US department of commerce. National Bureau of Standards 1980
- [5] Park C. Menees G.P. 'Odd nitrogen production of meteoroids', J. Geophys. Res., 83-4035, 1978
- [6] Kang S.W., Dunn M. T., 'Theoretical and measured electron density distribution for RAM vehicles at high altitudes' AIAA 72-689, 5th fluid and plasma conference, Boston Ma. 1972
- [7] Park C., Yoon S., 'Calculation of real gas effects on blunt body trim angles.' AIAA 30(4), 999, 1992
- [8] Oertel H jr. 'Regular shock reflectors used for study in nitrogen dissociation' Modern developments in shock tube research, Proceedings of the 10th International shock tube symposium ed. Kamimoto, 605, 1975
- [9] Evans J et al. 'Effect of non-equilibrium ablation chemistry on Viking radio blackout' AIAA 73-260

ASTROPHYSICS AND ENVIRONMENT - AE 2

Figure 1: Published Arrhenius rates for NO + N exchange reaction

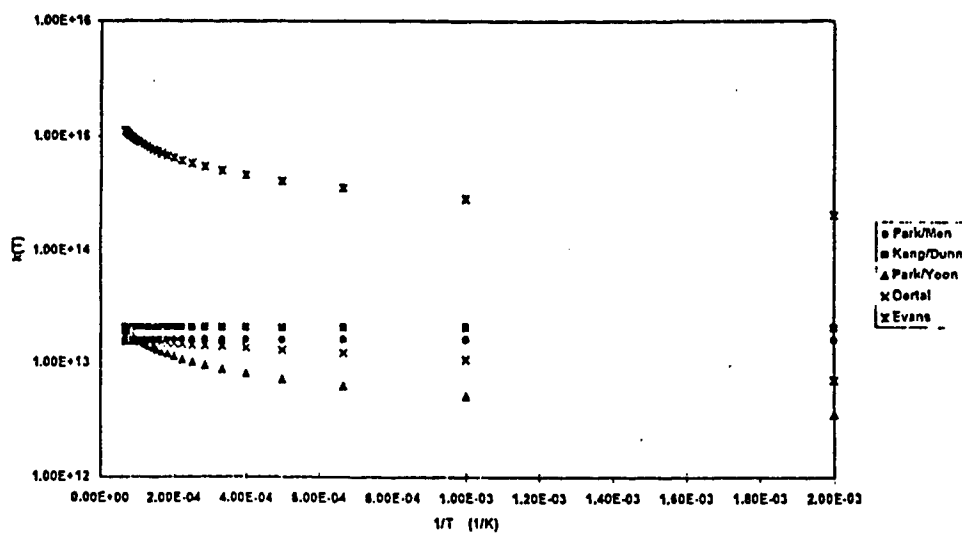


Figure 2: Simulations of NO + N exchange reaction

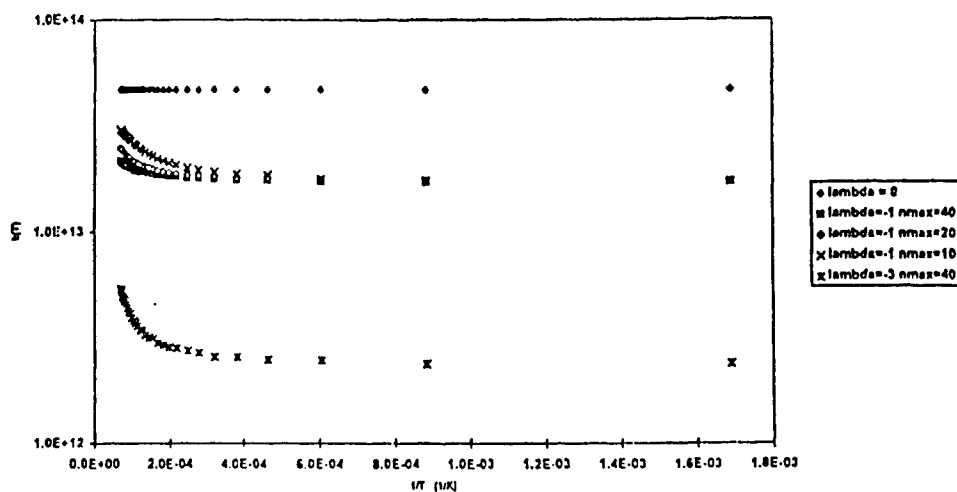
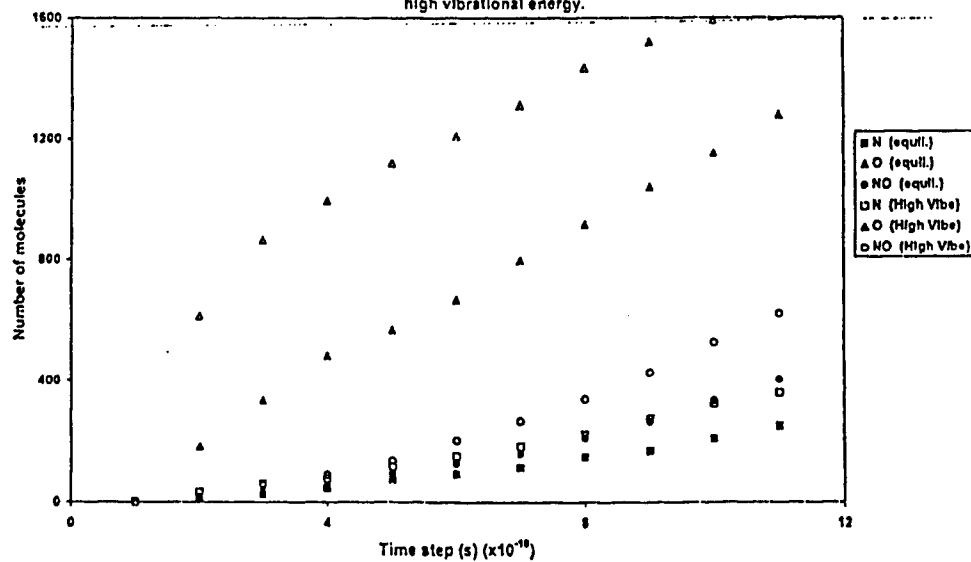


Figure 3: Product concentrations in a reacting cell of N2 and O2 under conditions of equilibrium and high vibrational energy.



A Reexamination of the Atmospheric Explorer Data Using the DSMC Technique *

V.D. Dogra¹, R.J. Collins², D.A. Levin³

¹Science and Technology Corporation, Hampton, USA

²Department of Electrical Engineering, University of Minnesota, Minneapolis, USA

³Science and Technology Division, Institute for Defense Analyses, Alexandria, USA

Spacecraft-induced glow optical measurements have been made from the Atmospheric Explorer and the Space Shuttle.[1, 2] Various models have been developed to explain the shuttle glow spectroscopic observations,[3]-[6] which were made in contaminated environment of a large spacecraft. The clean environment of a small spacecraft such as Atmospheric Explorer (AE) makes it a better candidate for modeling the glow and comparing with data. Almost all models of visible spacecraft glow attribute the glow to emission from excited NO₂ formed at the surface. Until the recent Direct Simulation Monte Carlo (DSMC) modeling of efforts of Karpides[7] and ourselves[8] none of the spacecraft glow models resolved the question of the source of NO, an important precursor.

Our work[8] has shown that there is sufficient NO formed due to chemical reactions in the flowfield to explain NO as a precursor of the glow phenomena. The number density of NO in the freestream is less than the number density of other species by several orders of magnitude at high altitudes. Also the production rates of NO in the flowfield are low due to rarefaction effects. Thus NO is classified as a trace species, and a new DSMC technique has been developed.[8] In this new technique the simulations are performed in two steps. First, the DSMC calculations are performed with a reasonable number of simulated particles so that the major species are represented appropriately in the computational domain. Then the second DSMC calculations are performed where trace species simulated particles are represented properly and it is assumed that trace species particles do not affect the major species particles. The flow conditions and the body configuration of the Skipper satellite[9] was used for these calculations. The altitude range used is that from 130 to 200 km which encompasses moderate to high

rarefied conditions. Freestream velocity of about 8 km/s is considered for these simulations. The freestream conditions for major species are from the work of Jacchia[10] and for trace species are from a sounding rocket experiment.[11]

In recent work[12] we proposed the development of a new surface model for the formation of excited NO₂ at the surface using the DSMC method[13] for the study of the surface glow phenomena. In previous calculations[8] it was assumed, as a lower bound, that all the NO molecules that strike the surface recombine with O atoms at the surface to form NO₂. The surface model assumes that the spacecraft is completely covered with a few monolayers of atomic oxygen; i.e., an oxide surface exists. The atomic oxygen that bond to the surface to form the surface oxide are chemisorbed and are not available to react with incoming NO. Additional surface bombardment by O and NO will result in those species being physisorbed to the surface, as long as there are available sites. Our surface model assumes that any O colliding with surface, physisorbed NO will form NO₂. The physisorption process implies a weaker bond than chemisorption as seen by the data of Somorjai[14] which gives a typical heat of absorption of 5 instead of 30 kcal/mole. The measurements of Sonnenfroh and Caledonia[15] also indicate that the NO is physisorbed on a Ni oxide surface. The surface processes that have been modeled are O and NO gases impinging on the surface and sticking, the reverse process (desorption), and an Eley-Rideal form of chemiluminescence whereby an impinging O atom releases NO from the surface to form NO₂ and light. Since the conditions deviate so strongly from thermochemical equilibrium the relationship between the absorption and desorption rates used in other DSMC calculations[17] has been re-evaluated in terms of the sticking coefficient.[19, 20] The gas phase measurements of Fontijn[18] are used to estimate the chemiluminescent rate.

* Abstract 6121 submitted to the 21st International Symposium on Rarefied Gas Dynamics, Marseille, France, July 26-31, 1998

Our work have emphasized DSMC axisymmetric calculations for the Skipper satellite configuration, a vehicle with a base diameter of 0.772 m and a nose radius of 1.0 m. It is reasonable to compare the results for this geometry with Atmospheric Explorer (AE) data since the nose radii of both geometries is on the order of 1.0 m and less than the mean free path for the altitudes of interest. Comparison of computed flux levels show them to be identical within the accuracy of the calculations for both geometries. However, the results presented in this paper will concentrate on the AE geometry. The present surface model will be used to demonstrate an apparent asymmetry in the AE radiance data.[22] Data taken from selected elliptical orbits will be analyzed and compared with calculations. The effect of vehicle spinning motion will be discussed.

Acknowledgments

We would like to acknowledge the help and discussions of Dr. Yee of the Applied Physics Laboratory and Dr. Mark Burrage at the University of Michigan for his help in accessing and using the data on the VAE web site.

References

- [1] Yee, J. H., Abreu, V. J., "Visible Glow Induced by Spacecraft-environment Interaction," *Geophysical Research Letters*, Vol. 10., NO. 2, 1983.
- [2] Caledonia, G. E., Holtzclaw, K. W., Green, B. D., and Kreech, R. H., "Laboratory Investigation of Shuttle Glow Mechanism," *Geophysical Research Letters*, Vol. 17, NO. 11, pp 1881-1884, October 1990.
- [3] Caledonia, G. E., *et al* "Mechanistic Investigations of Shuttle Glow," *J. Geoph. Res.*, Vol. 98, No. A3, 3725-3730, Mar. 1. 1993.
- [4] Viereck, R. A., *et al* "Special Characteristics of Shuttle Glow," *Geoph. Res. Lett.*, Vol. 19, No. 12, pp. 1219-1222, June 19, 1993.
- [5] Orient, and Murad, E. "Recombination of 5-eV $O(^3P)$ atoms on Surface adsorbed NO," *Physical Review A* Vol. 45, No. 51, Mar 1992.
- [6] Swenson, et .al, *Geophy. Res. Lett.* Vol. 12, 97 (1985).
- [7] Karipides, D. P., Boyd, I. D., and Caledonia, G. E., "Development of a Monte Carlo Overlay Method with Application to Spacecraft Glow," *AIAA Paper 96-1847*, June 1996.
- [8] Collins, R. J., Dogra, V. K., and Levin, D. A., "Modeling of High Altitude Spacecraft Environments," *AIAA Paper No. 97-0987*, January 1997.
- [9] Levin, D., Finke, R., Candler, G., Boyd, I., Howlett, L., and Erdman, P., "In-Situ Measurements of Transitional and Continuum Flow UV Radiation from Small Satellite Platforms," *AIAA Paper No. 94-0248*, January, 1994, presented at the 32nd Aerospace Sciences Meeting.
- [10] Jacchia, L. C., "Thermospheric Temperature, Density, and Composition: New Models," *Research in Space Science, SAO Special Report No. 375*, March 1977.
- [11] McCoy, R. P., "Thermospheric nitrogen 1. NO, $N(^4S)$, and $O(^3P)$ densities from rocket measurements of the NO δ and γ bands and the O_2 Herzberg I bands," *Journal of Geophysical Research*, Vol.1. 88 No. A4, 1983, pp. 3197-3205.
- [12] Collins, R. J., Dogra, V. K., and Levin, D. A. "Simulations of Spacecraft Rarefied Environments Using a Proposed Surface Model," paper to be presented at the Reno Aerospace Sciences Meeting January 1998.
- [13] Bird, G. A., *Molecular Gas Dynamics and the Direct Simulation of Gas Flows*, Clarendon Press, Oxford, England, 1994.
- [14] Somorjai, G. A., *Principles of Surface Chemistry*, Prentice-Hall, Inc., New Jersey, 1972.
- [15] Sonnenfroh, D. M. and Caledonia, G. E., "Collisional Desorption of NO by Fast O Atoms," *Journal of Geophysical Research*, Vol. 98, No. A12, pp. 21,605-21,610, December, 1993.
- [16] Hamza, A. V., Ferm, P.M., Budde, F., and Ertl, G., "The dynamics of NO scattering from NO- and Co-covered Ni(100)," *Surf Sci.*, Vol. 199, pp. 13-27, 1988.
- [17] Bergemann, F., "A Detailed Surface Chemistry Model for the DSMC Method," *Rarefied Gas Dynamics*, edited by John Harvey and Gordon Lord, Oxford University Press, 1995.

- [18] Fontijn, A., Meyer, C. B., and Schiff, H. I., "Absolute Quantum Yield Measurements of the NO-O Reaction and Its Use as a Standard for Chemiluminescent Reactions," *The Journal of Chemical Physics*, Vol. 40, No. 1, Jan. 1964.
- [19] Vattuone, L, Rocca, M, Boragno, C., and Valbusa, U., "Initial sticking coefficient of O₂ on Ag(110)," *The Journal of Chemical Physics*, Vol. 101, No. 1, July 1994, pp. 713-725.
- [20] Insepov, Z., A. and Zhankadamova, A. M., "Molecular dynamics calculation of the sticking coefficient of gases to surface," *Z. Phys. D - Atoms, Molecules and Clusters*, Vol. 20, 1991, pp. 145-146.
- [21] Baulch, D. L., D. D. Drysdale, D. G. Home, and A. C. Lloyd, *Evaluated Kinetic Data for High Temperature Reactions, 2, Homogeneous Gas Phase Reactions of the H₂-N₂-O₂ System*, Butterworth, 1972, ISBN 0 408 70346 6.
- [22] VAE - Visible Air Glow Experiment, <http://www.sprl.umich.edu/VAE/>

Multimoment and Multispecies Model Adapted to the Expansion of the Proton in the Solar and Polar Terrestrial Winds *

F. Leblanc, D. Hubert
Observatoire de Paris/DESPA Meudon, France

1 Introduction

We construct a new approach to model the Velocity Distribution Function (VDF) for the expansion of planetary polar winds and solar winds. Our model is a polynomial expansion based on an asymmetric weight function and associated with a set of transport equations following the generalized Grad's method. The generalized model is well adapted to reproduce the long tail features of a majority of the proton VDF in planetary or stellar winds. Moreover our model supports normalized heat flux larger than unity. A 16-moment approximation allows us to provide an associated set of generalized transport equations for the density n_p , the velocity V_p , the pressure tensor P_p and two heat flows q_p^{\parallel} and q_p^{\perp} and to determine the deriving conductivity law.

2 The generalized model

Our weight function is defined as

$$f_G^o(c_{\parallel}, c_{\perp}) = n_p \frac{m_p}{2k_B \pi T_{\perp p}} \exp\left\{-\frac{m_p}{2k_B T_{\perp p}} c_{\perp}^2\right\} \times \frac{1}{2D^*} \exp\left\{-\frac{c_{\parallel} + D^*}{D^*} + \frac{1}{E^*}\right\} \times \operatorname{erfc}\left\{E^{*1/2} \left(\frac{1}{E^*} - \frac{c_{\parallel} + D^*}{2D^*}\right)\right\}, \quad (1)$$

where n_p , m_p and $T_{\perp p}$ are respectively the proton density, the proton mass and the perpendicular temperature. D^* and T^* depend on the heat flux value q_p^{\parallel} and of the parallel temperature $T_{p\parallel}$. c is the thermal velocity ($c = v - u$, with v the velocity and u the average drift velocity) and k_B is Boltzmann's constant. The VDF is then defined as:

$$f(c_{\parallel}, c_{\perp}) = f^o(c_{\parallel}, c_{\perp}) \sum_{i=1}^{\infty} a_i(r, t) M_i(r, v, t), \quad (2)$$

where the M_i are polynomials constructed following orthonormalization rules associated with the weight function. We separate the velocity space into two parts because of the gyrotropic state of the charged particles along the magnetic field line as it is observed in the terrestrial polar wind and in the solar wind. In Figure 1 we show typical profile of the weight function along the magnetic field direction.

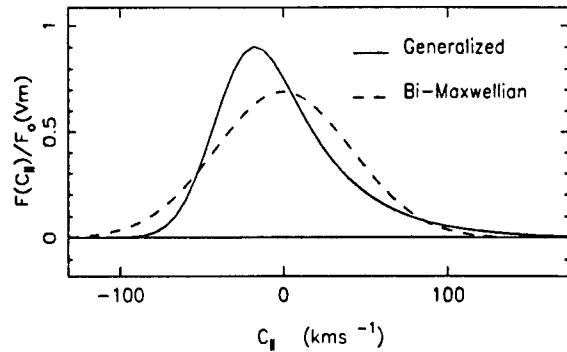


Figure 1: Typical profile of the weight function of the generalized model and of the bi-Maxwellian model.

The definition 1 and 2 depends on the macroscopic parameters which represent the unknowns of our model and could be easily associated with the velocity moments of the VDF. We determine them by solving an associated set of transport equations which is determined by multiplying the Boltzmann equation by the corresponding velocity tensor and by integrating over the velocity space. In the case of applications to the solar and terrestrial polar winds we only keep the first 16 velocity moments which correspond to the following macroscopic parameters: n_p , u_p , $T_{\parallel p}$, $T_{\perp p}$, τ_p , q_p^{\parallel} and q_p^{\perp} where τ_p is the stress tensor and $q_p^{\perp} = n_p m_p \langle c_{\perp}^2 c_p \rangle$. We notice $\langle c^p \rangle$ the velocity moments of order p . This number of unknowns reduce to 6 in the case of a 1D geometry. The right terms of the equations derive from the Fokker Planck collisional terms. We will analyse in those terms different forces which act on

*Abstract 3211 submitted to the 21st International Symposium on Rarefied Gas Dynamics, Marseille, France, July 26-31, 1998

the expansion of the particles, as for instance the friction forces, the thermal forces and the magnetohydrodynamic mirror forces. We extract the conductivity law associated with the generalized model.

3 Comparison with others multimoment models

The main progress of our model in comparison with the previous multimoment models derive from our choice of model of velocity distribution function. The choice of an asymmetric weight function depending on the heat flux along the magnetic field direction allows us to better truncate the set of transport equations and to better evaluate the collisional terms for far from equilibrium state associated with high values of the heat flux. The model of Demars and Schunk (1979) for instance is based on a weight function defined as a bi-Maxwellian function that is a product of two Maxwellian functions at the parallel and perpendicular temperatures. These authors have determined a set of transport equations of the same order of development (the third one) as we did. In order to compare both models we use two approaches. In the first one, we consider the microscopic description of each model.

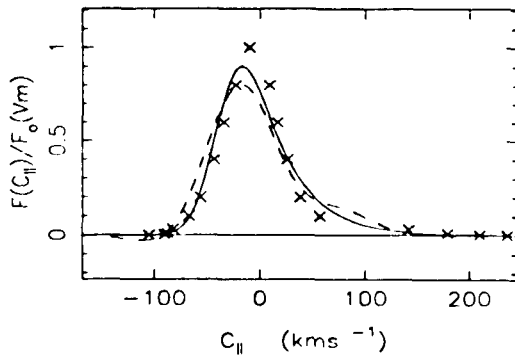


Figure 2: Comparisons of the generalized model (solid line) and of the bi-Maxwellian model (dashed line).

In Figure 2, we have plotted the third order of development for values of the velocity moments for a typical measurement (crosses) of the Helios 2 probe (Marsch 82) in the solar wind for both models. The model based on a bi-Maxwellian weight function developed unphysical behaviors as negative values of the VDF whereas our model is well adapted to the measurement.

The second way of analysis corresponds to the study of the macroscopic part of our model. We have

studied the hyperbolicity properties of our model that is the conditions to verify in order that the set of transport equations be hyperbolic. In a 1D application without collisional terms, this condition reduced to a limitation of the heat flux: $q_{||p} \leq 2(P_{||} \times V_{th||})_p$ where $(P_{||} \times V_{th||})_p$ is the free streaming flux, when for the bi-Maxwellian model this condition is $q_{||p} \leq (P_{||} \times V_{th||})_p$. This condition corresponds roughly also to the realizability criterion that is the condition under which the velocity moments which are determined by our model could be associated with a physical VDF. The realizability criterion is more exactly a criterion on the closure assumption of the system of transport equations.

4 Conclusion

We will explain in details the technic of construction of the multimoment and multispecies model and show that our model is a generalization of the magnetohydrodynamic ones and of the 16 moment bi-Maxwellian model. In fact we chose a model of VDF in order to be able to better reproduce the high values of the heat flux observed in the solar wind and terrestrial polar wind and to construct better suited conductivity law. We will illustrate our points of view by comparisons with an other multimoment model, the Demars and Schunk model. These works corresponds to real efforts to adapt the classical models for ionized gas to far from equilibrium states.

References

- [1] Demars, H. G., & Schunk, R. W. 1979, J. Phys. D: Appl. Phys., 12, 1051
- [2] Grad, H., 1958 Principles of the kinetic theory of gases, Hand. der Phys., 12
- [3] Leblanc, F., & Hubert, D., Astrophys. J., 483, 464, 1997
- [4] Leblanc, F., & Hubert, D., Astrophys. J., Submitted, 1998
- [5] Marsch, E., Mulhauser, K. H., Schwenn, R., Rosenbauer, H., Pillip, W., & Neubauer, F. M. 1982, J. Geophys. Res., 87, 52

On the Modeling of the Solar Wind Interaction with Non - Magnetic Planets *

M.D. Kartalev, V.I. Nikolova
Institute of Mechanics, BAS, Sofia, Bulgaria

Introduction

The problem of quantitative modeling of the interaction of the solar with plasma with non-magnetic planets (like Venus and Mars) remains till now one of the unresolved astrophysical tasks. This interaction is characterized by a formation of: *planetosheath (ionosheath or magnetosheath), containing solar plasma, and planetosphere (mantle), containing plasma with planetary origin*. These regions are bounded by: *bow shock wave, ionosheath boundary (ionopause or planetopause), and dense planetary atmosphere*.

Several basic issues need further quantitative explanations: (i) the mechanisms of creation of the ionized planetospheric gas; (ii) the cause of its dynamic behavior - especially the flow toward the night-side region; (iii) the self-consistent determination of the shape and position of the planetopause; (iv) the mechanism of the interplanetary magnetic field (IMF) penetration into the planetosphere. There are possibly two basic hypotheses in the literature (e.g. Nagy et al., 1990 [7]) explaining the existence of the planetosphere: Vaisberg and Zeleny, 1984 [10] suggested that the photoionization is responsible for the ions' creation and both magnetic pressure gradient and magnetic tension are causing the convection toward the wake. Sagdeev et al., 1990 [9] suggest that the planetopause is resulted by escape of planetary ions into the magnetosheath region, caused by turbulent diffusion.

It was shown in the paper [8], focusing the consideration on the Venusian case, that unexpectedly adequate quantitative explanation of the planetosphere creation, as well of its size and dynamics, could be done in the frame of a single-fluid gasdynamics with introduced appropriate mass-loading (photo-chemical) processes. The numerical consideration had excluded the wake region. A modified form of the magnetic field induction equation was derived in [2]

as a consequence of taking into account the finite time for assimilating the new born ions into mass-loaded plasma. As a result, the magnetic field is not frozen in the fluid substance, which is applied in [2] for qualitative explanation of the penetration of IMF into the planetosphere.

The present study is generalizing and extending the investigations in [8] and [2]. The results of these papers are presented here from common point of view, solving numerically the problem for the IMF penetration into the planetosphere. The self-consistent solution for the flow in all the regions is extended to the wake domain.

Model description and numerical

Modified Euler equations with included mass-loading effects are applied in both considered regions (planetosheath and planetosphere):

$$\begin{aligned}\partial\rho/\partial t + \nabla^k \rho v_k &= S, \\ \partial(\rho v)/\partial t + \nabla^k \rho v v_k + \nabla p &= 0, \\ \partial(\rho E)/\partial t + \nabla^k \rho E v_k + \nabla^k p v_k &= S U_0\end{aligned}\quad (1)$$

where $\rho = m_i n_i$ is density, p is pressure, v_i ($i = 1, 2, 3$) are the Cartesian coordinates of the velocity \mathbf{v} ; $E = v^2/2 + U$ is the total energy; $U_0 = kT_0/(m_0(1 - \gamma))$ is the density of the internal energy of the neutrals with mass m_0 , k is the Boltzmann constant; γ is the specific heat ratio. In the source term $S = \sigma m_0 N_0$ with ionization frequency $\sigma = 10 \times 10^{-6} \text{ s}^{-1}$ in this paper.

A neutral oxygen exosphere around the planet is supposed with distribution of the number-density N_0 (r is the distance from the planet center): $N_0 = N_{ex} \exp[-(r - r_{ex})/H_0]$, where: N_{ex} is the density at the exobase (for r_{ex}), and H_0 is the scale height of hot oxygen. The neutrals affect the flows in both region only indirectly - as a source "reservoir" for photo-ions. In addition to the case of the static exosphere, considered in [8], here a nonstatic

* Abstract 6891 submitted to the 21st International Symposium on Rarefied Gas Dynamics, Marseille, France, July 26-31, 1998

exosphere is also considered, leading to the IMF penetrating.

Grid characteristic first order scheme, described in Magomedov and Holodov, 1988 [5] in axial symmetry is used for numerical solving the problem simultaneously in both above defined domains. This numerical scheme was applied in astrophysical task earlier in [3].

Some numerical results

The geometries of the planetosheath and the planetosphere, their dynamic behavior, as well the IMF penetration are examined for different values of the solar wind Mach number M_∞ , dynamic pressure D_p , thermal pressure p , and magnetic field B_∞ . The parameters in the presented here several numerical examples correspond to the case of Venusian planetosphere.

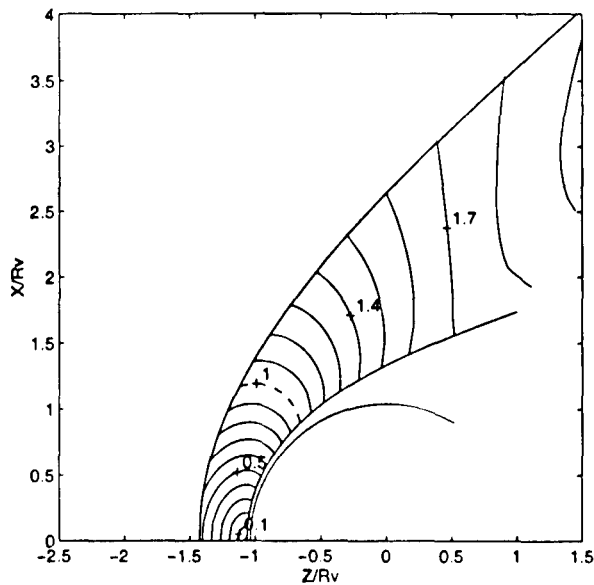
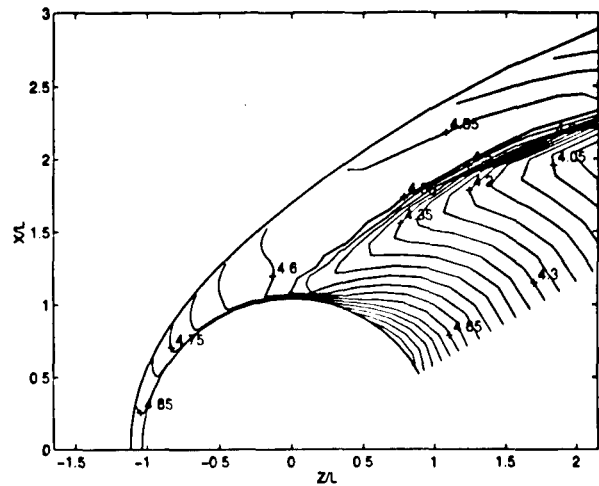


Figure 1: A typical computational result for the planetosphere and planetosheath (with drawn Mach number isolines in the planetosheath). Here $D_p = 4$ and $p = 0.11$ nPa.

Acknowledgements – This research was supported by the Bulgarian National Foundation "Scientific Research" under grant NZ 522.

References

- [1] Brace, L.H., Hartle, R.E., and Theis, R.F. The nightward ion flow scenario at Venus revisited. *Adv. Space Res.*, **16**, (6)99-(6)112, 1995.



Reviews, 55, 201-274, 1991.

- [5] Magomedov K.M., and Holodov A.S. Grid characteristic numerical methods. Moscow, Nauka, 1988.
- [6] Phillips, J.L. and McComas D.J. The magnetosheath and magnetotail of Venus. Space Science Reviews, 55, 1-80, 1991.
- [7] Nagy, A.F., Gombosi, T.I., Szego, K, Sagdeev, R.Z., Shapiro, V.D., and Shevchenko, V.I. Venus mantle - Mars planetosphere: What are similarities and differences? Geoph. Res. Lett., 17, 865-868, 1990.
- [8] Nikolova V.I. and Kartalev M.D., On the numerical modeling of the Venus planetosphere/mantle, Journal of Theoretical and Applied Mechanics, in press, 1998.
- [9] Sagdeev, R.Z., et al. Wave activity in the neighborhood of the bow shock of Mars, Geophys. Res. Lett., 17, 1990.
- [10] Vaisberg, O.L., and Zeleny, L.M. Formation of the plasma mantle in the venusian magnetosphere, Icarus, 58, 412, 1984.

Index

Author	Paper	Vol	Session	Author	Paper	Vol	Session
Abe T.	1817	I	IR1	Beresnev S.A.	4902	II	TP-P
Abe T.	1816	I	MCM3	Beskok A.	6021	I	RF3
Abramov A.A.	5039	II	NS-P	Beylich A.E.	1627	I	GS-P
Abramovskaja M.G.	2282	I	RF3	Beylich A.E.	1660	II	ID-P
Abramovsky E.R.	2282	I	RF3	Beylich A.E.	1628	I	Invited
Adamovich I.V.	2286	I	NE2	Beylich A.E.	1626	II	NS-P
Agrawal H.	4016	II	IP-P	Billing G.D.	1771	I	GS2
Aksyutenko A.N.	2069	II	GS-P	Bird G.A.	1006	I	MCM1
Alder B.J.	5821	I	NS1	Bityurin V.A.	1976	II	NE-P
Aleksandrov O.E.	6526	II	IP-P	Blanchard R.	2351	I	Invited
Alexandrychev I.P.	6527	II	GS-P	Blanchard R.C.	6467	I	AA2
Alexandrychev I.P.	6528	II	GS-P	Blömer J.	1627	II	GS-P
Alexeev B.V.	1918	II	KTM-P	Bobylev A.V.	1871	I	Invited
Alfyorov V.I.	5002	II	AA-P	Bobylev A.V.	4111	I	KTM4
Ambroso A.	6776	II	KTM-P	Boeuf J.P.	1226	I	Invited
Amouroux J.	1106	II	GS-P	Bogdanov A.V.	4842	II	AE-P
Anolik M.V.	1921	II	GS-P	Bogdanov A.V.	5235	I	GS3
Anolik M.V.	1922	II	NS-P	Borisov S.F.	6736	II	GS-P
Aoki K.	4361	I	NS1	Borisov S.F.	6737	II	GS-P
Aoki K.	4586	I	RF3	Boubert P.	6724	II	ID-P
Aoki K.	4621	I	TP1	Boubert P.	6725	II	ID-P
Aristov V.V.	1931	I	MCM3	Bouchardy P.	6314	I	AA2
Aristov V.V.	1932	II	NS-P	Bourdon A.	6721	I	NE1
Arkhipov Yu.Y.	4286	I	KTM4	Bowden R.L.	5866	II	KTM-P
Armenise M.	1946	I	NE1	Boyd I.D.	2369	I	IP2
Arnal D.	6515	I	AA3	Boyd I.D.	2367	I	MCM2
Asadzadeh M.	2100	I	NS2	Boyd I.D.	2366	I	NE2
Asano K.	1831	I	KTM1	Boyd I.D.	2368	I	RF4
Aspect A.	7106	I	Invited	Brazinsky V.I.	2281	II	AE-P
Aufrère L.	3291	I	GS2	Brun R.	1551	II	NE-P
Austin J.V.	6327	I	AE1	Brun R.	3292	II	NE-P
Autric M.	6811	I	IP2	Buet C.	1466	I	IR2
Autric M.	6812	II	IP-P	Buet C.	1431	I	KTM4
Azarova O.A.	5276	I	MCM2	Bulgakova N.M.	5101	II	IP-P
Babu R.S.P.	4013	II	AA-P	Bur R.	6312	I	AA2
Badie J.M.	1141	I	GS4	Buzykin O.G.	5087	II	KTM-P
Bakanov S.P.	5132	II	TP-P	Buzykin O.G.	5088	II	NE-P
Bakker P.	5456	I	MPT	Bykov N.Y.	4842	II	AE-P
Balakrishnan J.	2369	I	IP2	Bykov N.Y.	4843	II	IP-P
Balat M.	1141	I	GS4	Cabannes H.	1301	I	KTM2
Barantsev R.G.	1922	II	NS-P	Cacciatore M.	1771	I	GS2
Bartel T.	2336	I	IP1	Cacciatore M.	1946	I	NE1
Bartel T.	5966	I	IP1	Cai C.-P.	2368	I	RF4
Bartel T.	2337	I	MCM4	Capitelli M.	1776	I	Invited
Baryshnikov A.S.	1971	II	IR-P	Capitelli M.	1801	I	NE1
Baryshnikov A.S.	1972	II	NE-P	Capitelli M.	1946	I	NE1
Bass V.P.	2281	II	AE-P	Carabadgak G.F.	5096	I	AA4
Bass V.P.	2069	II	GS-P	Cattolica R.	2426	II	ID-P
Bass V.P.	2282	I	RF3	Cavadias S.	1106	II	GS-P
Béchu S.	3208	II	AE-P	Celenligil M.C.	2171	I	IP2
Bell J.B.	5821	I	NS1	Cercignani C.	4111	I	KTM4
Belouaggadia N.	3292	II	NE-P	Cercignani C.	4112	I	MCM3
Belyi V.V.	1986	II	IR-P	Cercignani C.	2697	I	RF3
Benazzouz T.	6826	II	IR-P	Chanetz B.	6312	I	AA2
Beresnev S.	4901	II	TP-P	Chanetz B.	6314	I	AA2

<i>Author</i>	<i>Paper</i>	<i>Vol</i>	<i>Session</i>	<i>Author</i>	<i>Paper</i>	<i>Vol</i>	<i>Session</i>
Chanetz B.	6211	II	AA-P	Elizarova T.G.	3237	II	KTM-P
Chanetz B.	6313	II	AA-P	El-Shall M.S.	2622	II	TP-P
Chanetz B.	6311	II	ID-P	Emelianov A.V.	6621	II	NE-P
Chapovsky P.L.	5456	I	MPT	Ender A.Ya.	6837	I	KTM3
Charrier P.	1521	I	KTM3	Ender I.A.	6837	I	KTM3
Charrier P.	3301	I	KTM4	Eremin A.V.	6623	I	NE1
Chen J.	5866	II	KTM-P	Eremin A.V.	6621	II	NE-P
Chernyak V.G.	2041	II	IR-P	Erofeev A.I.	4874	II	AA-P
Chernyak V.G.	4902	II	TP-P	Erofeev A.I.	2068	I	KTM6
Cheron B.G.	6724	II	ID-P	Erofeev A.I.	4941	I	RF2
Chikhaoui A.	1536	II	KTM-P	Erofeev A.I.	4942	II	TP-P
Chikhaoui A.	6752	II	NE-P	Erofeev A.I.	4943	II	TP-P
Chikhaoui A.	1401	II	NE-P	Esposito F.	1776	I	Invited
Ching Shen	2846	II	NS-P	Fan J.	2847	I	NS2
Chirokov I.A.	2056	II	KTM-P	Farley D.R.	2426	II	ID-P
Choquet I.	1406	I	GS3	Fateeva E.I.	5156	I	NE1
Ciurea-Borcia R.	6882	II	AE-P	Ferreira C.M.	4785	II	IR-P
Clapp L.H.	2426	II	ID-P	Feugeas J.L.	1521	I	KTM3
Collins R.J.	6121	I	AE2	Fisenko S.P.	2621	II	TP-P
Colonna G.	1801	I	NE1	Fisenko S.P.	2622	II	TP-P
Cook S.	5876	II	GS-P	Flèche J.L.	2951	II	IP-P
Cook S.R.	2471	I	GS1	Frezzotti A.	4081	I	MCM4
Cordier S.	1431	I	KTM4	Friedlander O.G.	5096	I	AA4
Crutchfield Wm.Y.	5821	I	NS1	Friedlander O.G.	2069	II	GS-P
Cumin L.M.G	2676	II	NS-P	Friedlander O.G.	2068	I	KTM6
Dam N.J.	2156	I	RF4	Friedlander O.G.	4941	I	RF2
Danckert A.	1640	I	GS1	Friedlander O.G.	4942	II	TP-P
Dankert C.	1656	I	GS1	Friedlander O.G.	4943	II	TP-P
Dankert C.	1660	II	ID-P	Fritsche B.	3801	II	AE-P
de Boer J.	2706	II	IR-P	Frolova A.	6626	II	AA-P
de Socio L.M.	1766	II	NS-P	Fujita K.	1817	I	IR1
Dellacherie S.	1466	I	IR2	Funabiki K.	1816	I	MCM3
Desvilletes L.	4532	I	KTM1	Furukawa T.	4266	II	TP-P
Dettleff G.	1666	I	RF4	Gai S.L.	2541	I	AA2
Dmitriev L.M.	5002	II	AA-P	Galkin V.S.	5087	II	KTM-P
Dogra V.K.	6121	I	AE2	Gallis M.A.	5711	I	IR2
Doi T.	4541	II	TP-P	Gallis M.A.	5712	I	MCM3
Domingo P.	6826	II	IR-P	Garcia A.L.	5821	I	NS1
Domingo P.	6721	I	NE1	Garrigues L.	1226	I	Invited
Dubroca B.	1521	I	KTM3	Garzío V.	5341	II	IR-P
Dubroca B.	3301	I	KTM4	Garzo V.	5376	I	MPT
Dudeck M.	3208	II	AE-P	Gascon N.	3207	I	AA4
Dudeck M.	3209	II	ID-P	Gascon N.	3208	II	AE-P
Dudeck M.	3166	I	IP2	Gatignol R.	3001	II	KTM-P
Dudeck M.	3167	I	IR1	Gatignol R.	3002	I	KTM5
Dudeck M.	1536	II	KTM-P	Gatsonis N.	6021	I	RF3
Dudeck M.	3207	I	AA4	Gatsonis N.A.	6601	II	AA-P
Dudon J.P.	1536	II	KTM-P	Gatsonis N.A.	6602	I	IR2
Dumitrescu M.-P.	1551	II	NE-P	Genieys S.	1401	II	NE-P
Duruisseau P.	3001	II	KTM-P	George M.A.	5876	II	GS-P
Ebinuma Y.	1817	I	IR1	Gevorkyan A.S.	5235	I	GS3
Economou D.	2336	I	IP1	Gillet D.	3041	I	Invited
Egorov B.V.	5002	II	AA-P	Gimelshein S.F.	5039	II	NS-P
Egorov B.V.	5001	II	TP-P	Gimelshein S.F.	4831	I	AA3
Elizarova T.G.	2057	I	KTM2	Gimelshein S.F.	4832	I	IR2
Elizarova T.G.	2056	II	KTM-P	Gimelshein S.F.	4890	I	NS1

Author	Paper	Vol	Session	Author	Paper	Vol	Session
Gimelshein S.F.	5041	I	RF3	Honda T.	4361	I	NS1
Giordano D.	1801	I	NE1	Honma H.	5581	I	IR1
Giurini M.C.	2697	I	RF3	Hubert D.	3211	I	AE2
Glass C.E.	6741	I	RF1	Hudson M.	2336	I	IP1
Gochberg L.A.	6916	II	IP-P	Hudson M.	5966	I	IP1
Godard R.	2706	II	IR-P	Hudson M.	2337	I	MCM4
Goldstein D.	6326	I	NS1	Hyakutake T.	4496	I	AA1
Goldstein D.B.	6327	I	AE1	Ianiro N.	1766	II	NS-P
Golse F.	4532	I	KTM1	Ibraguimova L.B.	6396	II	NE-P
Gopinath A.	6056	I	RF4	Igarashi S.	4321	II	AA-P
Gorbachev Yu.	6921	I	NE2	Ignat M.	6882	II	AE-P
Gorbachev Yu.E.	4842	II	AE-P	Ignatiev A.A.	5232	II	AA-P
Gorchakova N.G.	6312	I	AA2	Ishida T.	4486	II	ID-P
Gorchakova N.G.	6311	II	ID-P	Ishikawa H.	3830	I	KTM4
Gordiets B.F.	4785	II	IR-P	Itina T.E.	6811	I	IP2
Gordillo-Vasquez F.J.	6651	I	MPT	Itina T.E.	6812	II	IP-P
Gorelov S.L.	5293	I	NE3	Itina T.E.	6813	II	IP-P
Gorelov V.A.	4851	II	AE-P	Itkin A.I.	4883	I	AE1
Gorse C.	1776	I	Invited	Itkin A.I.	4881	II	TP-P
Gorshkov G.F.	4810	II	AA-P	Ivanov A.G.	6529	II	NS-P
Grachyov I.A.	6737	II	GS-P	Ivanov M.S.	4831	I	AA3
Grasso F.	6313	II	AA-P	Ivanov M.S.	5232	II	AA-P
Graur I.A.	2057	I	KTM2	Ivanov M.S.	4832	I	IR2
Greber I.	5861	I	NS2	Ivanov M.S.	6921	I	NE2
Greenberg W.	5866	II	KTM-P	Ivanov M.S.	4890	I	NS1
Gregory J.C.	5876	II	GS-P	Ivanov M.S.	5039	II	NS-P
Grigoryan A.G.	5235	I	GS3	Ivanov M.S.	5041	I	RF3
Grigoryev Yu.N.	6631	II	KTM-P	Iwagami H.	6690	II	NE-P
Grmela M.	2651	II	KTM-P	Iwayama Y.	6866	II	AA-P
Gromov V.G.	5156	I	NE1	Jing Fan	2846	II	NS-P
Guarrigues L.	1226	I	Invited	Johannes J.	2336	I	IP1
Guerra V.	4781	I	IR1	Kaltz T.L.	6146	I	TP2
Guilbaud D.	2951	II	IP-P	Kandemir I.	5861	I	NS2
Gundlach G.	1656	I	GS1	Kane D.B.	2622	II	TP-P
Gusev V.N.	4871	I	AA3	Karniadakis G.E.	6021	I	RF3
Gusev V.N.	4874	II	AA-P	Karsten V.M.	5216	I	RF3
Gusev V.N.	4873	II	NS-P	Kartalev M.D.	6891	I	AE2
Hadjadj A.	6856	II	NS-P	Kartalev M.D.	6892	II	AE-P
Hanser F.	2601	I	KTM6	Katasonov A.A.	6811	I	IP2
Harvey J.K.	5711	I	IR2	Katasonov A.A.	6813	II	IP-P
Harvey J.K.	5712	I	MCM3	Kato S.	4601	II	IP-P
Harvey J.K.	5713	I	IP2	Kawamoto S.	4576	I	NS2
Hash D.B.	5921	I	IP1	Kawashima S.	6911	I	Invited
Hatakeyama M.	3830	I	KTM4	Kazmierczak B.	4756	I	TP2
Hauser A.	3208	II	AE-P	Ketsdever A.D.	6031	I	AA1
Hayashi A.K.	6690	II	NE-P	Khabalov V.D.	1921	II	GS-P
Hayashi S.	4486	II	ID-P	Khalidov I.A.	1921	II	GS-P
He C.	2848	II	IR-P	Khanlarov G.O.	4842	II	AE-P
Heinrich S.	7111	I	MCM4	Khisamutdinov A.I.	4916	I	MCM2
Hermans L.J.F.	5456	I	MPT	Khisamutdinov A.I.	4917	II	NS-P
Hiraoka M.	6690	II	NE-P	Khlopkov Yu.I.	5292	II	NS-P
Hirose K.	4601	II	IP-P	Khlopkov Yu.I.	5294	II	NS-P
Hirose N.	6866	II	AA-P	Kim B.G.	6866	II	AA-P
Hoffbauer M.A.	2471	I	GS1	Kireev A.Yu.	4926	II	IR-P
Hoffbauer M.A.	5876	II	GS-P	Kloimboeck C.J.	6766	II	NE-P
Hollis B.R.	6211	II	AA-P	Koch D.L.	6056	I	RF4

<i>Author</i>	<i>Paper</i>	<i>Vol</i>	<i>Session</i>	<i>Author</i>	<i>Paper</i>	<i>Vol</i>	<i>Session</i>
Kogan M.N.	4941	I	RF2	Lengrand J.C.	2056	II	KTM-P
Kogan M.N.	4942	II	TP-P	Lengrand J.C.	3237	II	KTM-P
Kogan M.N.	4943	II	TP-P	Leroux A.	6721	I	NE1
Kolesnick R.E.	2906	II	NE-P	Levdansky V.V.	2626	II	IP-P
Koppenwallner G.	3801	II	AE-P	Levin D.A.	6121	I	AE2
Kortsenstein N.M.	6666	I	AA4	Liming Chen	2846	II	NS-P
Kortsenstein N.M.	6667	II	TP-P	Lions P.L.	3246	I	Invited
Kotake S.	4392	I	GS3	Liu F.	6021	I	RF3
Koulidiati J.	3167	I	IR1	Long L.N.	6146	I	TP2
Koulikov S.V.	4956	I	NE2	Longo S.	2367	I	MCM2
Koura K.	4396	I	MCM1	Longo S.	1802	II	NS-P
Kovach E.A.	5166	II	NE-P	Lord G.	5621	I	Invited
Kovalev F.D.	6847	II	TP-P	Lord R.G.	5622	II	NE-P
Kovalev V.L.	4966	I	GS4	Losev S.A.	5166	II	NE-P
Kovalev V.L.	4967	I	GS4	Loureiro J.	4781	I	IR1
Kowalczyk P.	4741	II	NS-P	Lucquin-Desreux B.	3256	I	KTM6
Krasnolutskii S.	5138	II	KTM-P	Lucquin-Desreux B.	3257	II	KTM-P
Kremer G.M.	2677	I	NE3	Lukianov G.A.	4842	II	AE-P
Kremer G.M.	2676	II	NS-P	Lukianov G.A.	4843	II	IP-P
Krishnan A.	6916	II	IP-P	Lukshin A.V.	1931	I	MCM3
Krupnov A.A.	4966	I	GS4	M.K. Gladyshev	4851	II	AE-P
Kryukov A.P.	4981	I	TP2	Maeno K.	5581	I	IR1
Kryukov A.P.	4982	II	TP-P	Makashev N.K.	5088	II	NE-P
Kudryavtsev A.N.	5041	I	RF3	Makashev N.K.	5039	II	NS-P
Kukhareenko Yu.A.	1986	II	IR-P	Makihara Y.	4531	I	TP1
Kunc J.A.	6651	I	MPT	Makowski K.	3207	I	AA4
Kurian J.	4013	II	AA-P	Mallinger F.	6921	I	NE2
Kurian J.	4015	II	AA-P	Manoj Kumar V.	4016	II	IP-P
Kurzyna J.	3209	II	ID-P	Marconi M.L.	4466	I	AE1
Kustova E.	4996	I	MPT	Mariage E.	1141	I	GS4
Kustova E.	1946	I	NE1	Marín C.	5341	II	IR-P
Kustova E.	6921	I	NE2	Marine W.	6811	I	IP2
Kustova E.	4997	I	NE3	Marine W.	6812	II	IP-P
Kuznetsov L.I.	6311	II	ID-P	Marino L.	1766	II	NS-P
Kuznetsova I.	5006	II	TP-P	Markachev Yu.E.	5002	II	AA-P
Kuzyakin D.V.	5294	II	NS-P	Markachev Yu.E.	5001	II	TP-P
Lago V.	3209	II	ID-P	Markelov G.A.	5232	II	AA-P
Lago V.	3166	I	IP2	Markelov G.N.	4890	I	NS1
Lago V.	3167	I	IR1	Markelov G.N.	5041	I	RF3
Lampis M.	4112	I	MCM3	Markoff Yu.G.	5046	II	GS-P
Larina I.N.	5016	II	NS-P	Markoff Yu.G.	5047	II	IP-P
Lasgorceix P.	3207	I	AA4	Marriott P.	5631	I	AE2
Lasgorceix P.	3208	II	AE-P	Matsui J.	3861	II	GS-P
Lazarev A.V.	5135	II	NE-P	Matsumoto Y.	4432	II	AA-P
Lebeau G.J.	6601	II	AA-P	Matsumoto Y.	3861	II	GS-P
Lebéhot A.	3209	II	ID-P	Matsumoto Y.	4431	II	GS-P
Leblanc F.	3211	I	AE2	Matsumoto Y.	4646	II	NE-P
Lebon G.	2651	II	KTM-P	McDaniel J.C.	6686	I	RF1
Leborgne L.	6723	I	IR1	Méhats F.	6776	II	KTM-P
Lécot C.	2381	II	NS-P	Memnonov V.P.	5057	I	NS1
Lee D.D.	4706	I	NE2	Méolans J.G.	3291	I	GS2
Lefebvre M.	6314	I	AA2	Meyyappan M.	5921	I	IP1
Legge H.	1640	I	GS1	Micci M.M.	6146	I	TP2
Lemou M.	6926	II	NS-P	Mieussens L.	3301	I	KTM4
Lengrand J.C.	3238	II	GS-P	Mikhailov V.V.	1918	II	KTM-P
Lengrand J.C.	2057	I	KTM2	Milthorpe J.F.	2541	I	AA2

<i>Author</i>	<i>Paper</i>	<i>Vol</i>	<i>Session</i>	<i>Author</i>	<i>Paper</i>	<i>Vol</i>	<i>Session</i>
Miroshin R.N.	5062	II	KTM-P	Park H.K.	4706	I	NE2
Mohamed A.	1656	I	GS1	Parsons T.L.	5712	I	MCM3
Moiseev M.M.	5292	II	NS-P	Pellerin S.	3167	I	IR1
Mokhov V.A.	5002	II	AA-P	Peradzynski Z.	3207	I	AA4
Molinari V.G.	4136	II	IR-P	Perminov V.D.	5096	I	AA4
Monaco R.	2601	I	KTM6	Pérot C.	3208	II	AE-P
Montanero J.M.	5377	I	MPT	Perraud J.	6515	I	AA3
Mori H.	4486	II	ID-P	Petrova V.N.	5062	II	KTM-P
Morimoto T.	4476	I	MCM2	Pettersson R.	5386	I	KTM1
Morioka T.	5581	I	IR1	Piechor K.	4756	I	TP2
Morozov A.A.	5066	I	AA3	Pigache D.	6312	I	AA2
Morozov A.A.	5067	II	NS-P	Pigache D.	6311	II	ID-P
Morozov A.A.	5102	II	NS-P	Plähn K.	1657	I	RF2
Moss J.N.	6312	I	AA2	Plähn K.	1666	I	RF4
Moss J.N.	6467	I	AA2	Plastinin U.A.	5096	I	AA4
Moss J.N.	6211	II	AA-P	Plastinin Yu.A.	6666	I	AA4
Muntz E.P.	6031	I	AA1	Platkowski T.	4741	II	NS-P
Muntz E.P.	6216	I	Invited	Plekhanov E.A.	5001	II	TP-P
Muntz E.P.	6032	I	IP1	Plotnikov M.Yu.	5066	I	AA3
Murakami M.	4266	II	TP-P	Plotnikov M.Yu.	5101	II	IP-P
Nagata K.	4501	I	KTM5	Plotnikov M.Yu.	5067	II	NS-P
Nagels B.	5456	I	MPT	Plotnikov M.Yu.	5102	II	NS-P
Nagnibeda E.	4996	I	MPT	Plotnikov M.Yu.	5121	I	TP1
Nagnibeda E.	1946	I	NE1	Polyckarpov Ph.J.	6737	II	GS-P
Nagnibeda E.	4997	I	NE3	Polyckarpov Ph.J.	6736	II	GS-P
Nakakita M.	3861	II	GS-P	Popken L.	7101	II	KTM-P
Nanbu K.	4476	I	MCM2	Popov S.A.	5187	II	AA-P
Nanbu K.	4576	I	NS2	Popov S.P.	5246	I	RF2
Nanson R.	6601	II	AA-P	Popov V.V.	5292	II	NS-P
Napier D.G.	2776	I	KTM2	Porodnov B.T.	6526	II	IP-P
Nazarenko A.I.	2069	II	GS-P	Porodnov B.T.	6529	II	NS-P
Nazari B.K.	1660	II	ID-P	Pot T.	6312	I	AA2
Nebbache A.	6752	II	NE-P	Pot T.	6314	I	AA2
Nicodin I.	3001	II	KTM-P	Pot T.	6211	II	AA-P
Niimi T.	4486	II	ID-P	Pot T.	1656	I	GS1
Nikiforov A.P.	2069	II	GS-P	Pot T.	6311	II	ID-P
Nikolova V.I.	6891	I	AE2	Powell A.	2171	I	IP2
Nikolova V.I.	6892	II	AE-P	Prettyman T.	5876	II	GS-P
Nishida M.	4496	I	AA1	Provotorov V.P.	4874	II	AA-P
Nishide T.	4673	II	NS-P	Purpura C.	6313	II	AA-P
Nishigori T.	4501	I	KTM5	Pyarnpuu A.A.	5111	I	GS4
Nosik V.I.	5087	II	KTM-P	Qian Y.H.	3002	I	KTM5
Nosik V.I.	5088	II	NE-P	Raines A.A.	5116	I	NS2
Novopashin S.	1656	I	GS1	Ramjaun D.	1551	II	NE-P
Nyeland C.	2916	I	GS2	Rathakrishnan E.	4016	II	IP-P
Ogawa S.	6961	I	MCM4	Rault D.F.G.	6466	II	AA-P
Oguchi H.	4516	I	KTM5	Raviart P.A.	6776	II	KTM-P
Ohwada T.	4531	I	TP1	Rebrov A.K.	5066	I	AA3
Okuyama M.	4601	II	IP-P	Rebrov A.K.	5101	II	IP-P
Onishi Y.	4541	II	TP-P	Rebrov A.K.	5218	II	NS-P
Ooshida T.	4541	II	TP-P	Rebrov A.K.	5121	I	TP1
Ota M.	2698	II	IP-P	Reitshammer C.	2602	I	IR2
Ota M.	4471	II	IP-P	Reshetin A.G.	5126	II	AA-P
Oualid S.	3238	II	GS-P	Rich J.W.	2286	I	NE2
Paklin B.L.	6901	II	IP-P	Rjasanow S.	3971	I	MCM1
Pandolfi Bianchi M.	4146	II	KTM-P	Robin L.	6724	II	ID-P

<i>Author</i>	<i>Paper</i>	<i>Vol</i>	<i>Session</i>	<i>Author</i>	<i>Paper</i>	<i>Vol</i>	<i>Session</i>
Robin L.	6725	II	ID-P	Serikov V.V.	4576	I	NS2
Robinson C.D.	5713	I	IP2	Shakhmistov V.M.	2069	II	GS-P
Röck W.	3166	I	IP2	Shakhov E.M.	5173	II	AA-P
Röck W.	3167	I	IR1	Shakhov E.M.	5172	II	GS-P
Rodulghin V.I.	5132	II	TP-P	Shakhov E.M.	5171	II	TP-P
Roldughin V.I.	5131	I	KTM3	Shane R.W.	6466	II	AA-P
Rosenhauer M.	1657	I	RF2	Sharafutdinov R.G.	5216	I	RF3
Rossani A.	2602	I	IR2	Sharipov F.M.	2686	II	KTM-P
Rossani F.	2601	I	KTM6	Sharipov F.M.	2676	II	NS-P
Rouminsky A.N.	6811	I	IP2	Sharipov F.M.	2687	II	NS-P
Rousseau P.	1106	II	GS-P	Shatalov I.V.	5176	I	AA1
Roussinov V.	2697	I	RF3	Shatalov O.P.	6396	II	NE-P
Roveda R.	6326	I	NS1	Shematovich V.I.	5186	II	AE-P
Rudyak V.	5136	I	KTM6	Shematovich V.I.	5111	I	GS4
Rudyak V.	5138	II	KTM-P	Shen C.	2848	II	IR-P
Ruminsky A.N.	6813	II	IP-P	Shen C.	2847	I	NS2
Runkov V.A.	6847	II	TP-P	Shilenkov S.V.	4926	II	IR-P
Rusakov S.V.	5293	I	NE3	Shiliu Peng	2846	II	NS-P
Rutigliano M.	1771	I	GS2	Shiota T.	4702	I	GS3
Rutigliano M.	1946	I	NE1	Shishkova I.N.	4981	I	TP2
Ryabicova T.V.	5147	II	NE-P	Shishkova I.N.	4982	II	TP-P
Rydalevskaya M.A.	5146	II	NE-P	Shizgal B.D.	2776	I	KTM2
Rydalevskaya M.A.	5147	II	NE-P	Shkarupa E.V.	5191	II	NS-P
Rykov V.A.	5016	II	NS-P	Shugaev F.V.	5196	II	IR-P
Rymarchuk A.V.	5111	I	GS4	Shumova V.V.	6623	I	NE1
Sabelfeld K.K.	2511	I	MCM4	Shvedov F.	6529	II	NS-P
Saito T.	4551	II	NS-P	Sidorenko L.L.	4917	II	NS-P
Sakai K.	4476	I	MCM2	Sijtsema N.M.	2156	I	RF4
Sakamoto M.	4471	II	IP-P	Simonin O.	3003	II	KTM-P
Sakharov V.I.	5156	I	NE1	Singayevskaya G.I.	5196	II	IR-P
Sakiz M.	3003	II	KTM-P	Skovorodko P.A.	5217	II	NS-P
Sakurai A.	4561	I	RF4	Skovorodko P.A.	5218	II	NS-P
Sakurai N.	5581	I	IR1	Skovorodko P.A.	5216	I	RF3
Samuilow E.W.	6666	I	AA4	Skrynnikov A.V.	5216	I	RF3
Samuilow E.W.	6667	II	TP-P	Smekhov G.D.	6396	II	NE-P
Sankovitch V.	5367	I	GS4	Smith A.	1141	I	GS4
Sankovitch V.	5366	II	NE-P	Smyth W.H.	4466	I	AE1
Santos A.	5377	I	MPT	Snegursky A.V.	5766	II	ID-P
Santos A.	5376	I	MPT	Soares A.J.	4146	II	KTM-P
Sato S.	1817	I	IR1	Söderholm L.H.	5396	I	KTM3
Saunois P.	2951	II	IP-P	Soga T.	6866	II	AA-P
Saveliev V.L.	6761	II	KTM-P	Soga T.	4520	I	KTM5
Savin A.V.	5231	I	RF1	Sokolov E.I.	5176	I	AA1
Sazhin O.V.	6737	II	GS-P	Sokolov E.I.	5232	II	AA-P
Schneider J.	6801	II	KTM-P	Sokolov E.I.	5231	I	RF1
Schram D.C.	6906	I	Invited	Sokolova I.A.	6791	II	NE-P
Schuerrer F.	2602	I	IR2	Sone Y.	4361	I	NS1
Schuerrer F.	2601	I	KTM6	Sone Y.	4586	I	RF3
Schulte D.	6312	I	AA2	Sone Y.	4531	I	TP1
Schweigert V.A.	4832	I	IR2	Sreekanth A.K.	4026	II	IP-P
Seleznev V.D.	6527	II	GS-P	Starikov S.A.	4902	II	TP-P
Seleznev V.D.	6528	II	GS-P	Starinov A.	4901	II	TP-P
Seleznev V.D.	6526	II	IP-P	Stark J.	5731	II	KTM-P
Seleznev V.D.	6529	II	NS-P	Stefanov S.	2698	II	IP-P
Sentis R.	1466	I	IR2	Stefanov S.	2697	I	RF3
Sergievskaia A.L.	5166	II	NE-P	Stefanov S.K.	2368	I	RF4

<i>Author</i>	<i>Paper</i>	<i>Vol</i>	<i>Session</i>	<i>Author</i>	<i>Paper</i>	<i>Vol</i>	<i>Session</i>
Struckmeier J.	4112	I	MCM3	Vervisch P.	6724	II	ID-P
Struckmeier J.	2697	I	RF3	Vervisch P.	6725	II	ID-P
Suetin P.	4901	II	TP-P	Vervisch P.	6723	I	IR1
Suetin P.E.	6847	II	TP-P	Vervisch P.	6721	I	NE1
Sugimoto H.	4586	I	RF3	Vijayakumar P.	2366	I	NE2
Sumini M.	4136	II	IR-P	Vilisova E.A.	2041	II	IR-P
Suslov O.N.	4967	I	GS4	Vizcaino A.	3166	I	IP2
Svirschevsky S.B.	5187	II	AA-P	Vlasov V.I.	4873	II	NS-P
Szymanski Z.	3209	II	ID-P	Vodovozova J.F.	5232	II	AA-P
T. Hayashi T.	4471	II	IP-P	Voronich I.V.	5292	II	NS-P
Takaada A.	3830	I	KTM4	Wadsworth D.C.	6031	I	AA1
Takata S.	4621	I	TP1	Wadsworth D.C.	6506	II	NE-P
Takayama F.	4561	I	RF4	Wagner W.	3971	I	MCM1
Takayama K.	4551	II	NS-P	Walenta Z.A.	4771	I	RF2
Taran J.P.	6311	II	ID-P	Wallenborn J.	1986	II	IR-P
Tarhov E.L.	5187	II	AA-P	Walus W.	4741	II	NS-P
Taylor J.C.	6406	II	NS-P	Watanabe Y.	6690	II	NE-P
Tchebureev V.G.	4851	II	AE-P	Wilmoth R.	2351	I	Invited
Tcheremissine F.G.	5247	II	NS-P	Wilmoth R.G.	6467	I	AA2
Tcheremissine F.G.	5246	I	RF2	Wilmoth R.G.	6466	II	AA-P
ter Meulen J.J.	2156	I	RF4	Wilmoth R.G.	6916	II	IP-P
Teshima K.	4641	I	AA1	Wong M.C.	4466	I	AE1
Teshima K.	4672	I	AA1	Woo M.	5861	I	NS2
Tessarotto M.	4241	II	NS-P	Wysong I.	6507	I	Invited
Thivet F.	6515	I	AA3	Wysong I.J.	6506	II	NE-P
Tij M.	5376	I	MPT	Yalamov Yu.	5006	II	TP-P
Tirskiy G.A.	5251	II	AA-P	Yamamoto K.	4701	I	GS2
Titarev V.A.	5173	II	AA-P	Yamamoto K.	4702	I	GS3
Titarev V.A.	5172	II	GS-P	Yamanishi N.	4431	II	GS-P
Titulaer U.M.	6766	II	NE-P	Yanitskii V.E.	5276	I	MCM2
Toennies J.P.	2916	I	GS2	Yarygin V.N.	6311	II	ID-P
Tokmantsev V.I.	6529	II	NS-P	Yasuhara M.	6866	II	AA-P
Tokumasu T.	4646	II	NE-P	Yigiter O.	2171	I	IP2
Tokunaga T.	6690	II	NE-P	Yin X.	6602	I	IR2
Tolboom R.A.L.	2156	I	RF4	Yonemura S.	4476	I	MCM2
Tolson R.H.	6466	II	AA-P	Yoshida N.	5396	I	KTM3
Tomoeda M.	4656	II	NS-P	Yoshimoto M.	4361	I	NS1
Trapaga G.	2171	I	IP2	Ytrehus T.	4731	I	TP1
Trubnikov D.N.	5135	II	NE-P	Yumashev V.L.	5001	II	TP-P
Tsuboi N.	4432	II	AA-P	Yurasov V.S.	2069	II	GS-P
Tuttafesta M.	1801	I	NE1	Yushkanov A.	5006	II	TP-P
Usami M.	4672	I	AA1	Zabelok S.A.	1931	I	MCM3
Usami M.	4673	II	NS-P	Zakharov V.V.	4842	II	AE-P
Uskov V.N.	4810	II	AA-P	Zastenker N.N.	5135	II	NE-P
Van Ootegem B.	6724	II	ID-P	Zhdanov V.M.	5131	I	KTM3
Van Ootegem B.	6723	I	IR1	Zhdanov V.M.	5296	I	NE2
Vandromme D.	6856	II	NS-P	Zhdanov V.M.	5135	II	NE-P
Varghese P.	6326	I	NS1	Zmievskaaya G.I.	5306	II	NE-P
Vargo S.E.	6031	I	AA1	Zmievskaaya G.I.	5307	II	TP-P
Vargo S.E.	6032	I	IP1	Zolotoukhina T.N.	4392	I	GS3
Velicodny V.Yu.	6621	II	NE-P	Zorat R.	4241	II	NS-P
Velikodny V. Yu.	1976	II	NE-P				